Nonlinear spring modelling approach for the evaluation of anchor groups

Von der Fakultät Bau- und Umweltingenieurwissenschaften der Universität Stuttgart
zur Erlangung der Würde einer Doktor-Ingenieurin (Dr.-Ing.)
genehmigte Abhandlung

Vorgelegt von

Boglárka Bokor

aus Sopron, Ungarn

Hauptberichter:	Prof. Dr.-Ing. Jan Hofmann
Mitberichter:	Jun.-Prof. Dr.-Ing. Akanshu Sharma
	prof. Ing. František Wald, CSc.

Tag der mündlichen Prüfung: 26. April 2021

Institut für Werkstoffe im Bauwesen der Universität Stuttgart

2021

OUTLINE

Keywords:	Nonlinear spring model Displacement-based concept Experimental investigations Anchorages in concrete Concrete breakout failure Tension, shear and interaction Arbitrary configuration of anchors Base plate stiffness Crack pattern Hole clearance pattern

Author:	Boglárka Bokor (Sopron, Ungarn)

Title (English):	Nonlinear spring modelling approach for the evaluation of anchor groups
Title (German):	Nichtlinearer Federmodellansatz für die Berechnung von Gruppenbefestigungen

Institution:	University of Stuttgart Faculty of Civil and Environmental Engineering Institute of Construction Materials (IWB)

Bibliography:	2021, 384 Pages, 217 Figures, 56 Tables

Eigenständigkeitserklärung

Ich erkläre, dass ich die vorliegende Arbeit selbstständig verfasst und keine anderen als die angegebenen Quellen und Hilfsmittel benutzt habe. Alle Stellen der Arbeit, die wörtlich oder sinngemäß aus Veröffentlichungen oder aus anderweitigen Äußerungen entnommen wurden, sind als solche gekennzeichnet.

Ostfildern, im Januar 2021

Boglárka Bokor

ABSTRACT (English)

This thesis presents a nonlinear spring model based approach for the realistic assessment of anchorages loaded in tension, shear or combined tension-shear in the case of concrete breakout failure modes. First, the nonlinear spring model was conceptualised for anchor groups subjected to (1) tension loads, (2) shear loads, (3) combined tension-shear. The concept of the spring model for tension is based on the assumption that within an anchor group, anchors resist the tension forces, while the compression forces are transferred directly by the base plate to the concrete. Nonlinear tension-only springs are used for modelling the anchor behaviour in order to account for the distribution of forces among the anchors of the group. While defining the characteristics of the nonlinear anchor springs, due consideration is given to the vicinity of the edge and the neighbouring anchors through a tributary area approach. The contact between the base plate and concrete is modelled using compression-only springs, while the base plate is modelled using finite shell or solid elements to realistically consider the base plate stiffness. An analogous model was conceptualised for shear loaded anchorages. However, the tributary area approach was replaced by a tributary volume approach to enable the consideration of different edge distances within an anchor group. The model for interaction is a superposition of the nonlinear spring model for tension and shear. A comprehensive experimental program was designed and performed to verify the postulates made during the conceptualisation of the nonlinear spring model. The aim of this experimental program was to investigate the behaviour of tension and shear loaded anchor groups of various configurations undergoing concrete cone and concrete edge breakout failure, and to understand the load-displacement behaviour of single anchors and anchors as a part of an anchor group. The tension tests on anchor groups were aimed to investigate the following influences: (i) different geometric configurations, (ii) varying stiffness of the base plate, (iii) loading eccentricity, (iv) vicinity of concrete edge and (v) crack pattern. The shear tests were carried out on single anchors and anchor groups of different configurations to obtain information on (i) the group behaviour, (ii) the crack initiation and propagation, (iii) the influence of the displacement behaviour of single anchors on the behaviour of anchor groups (iv) the influence of hole clearance pattern and (v) the influence of crack pattern. The nonlinear spring models for tension, shear and interaction were verified against a vast number of experimental results on diverse anchor groups performed within the framework of this thesis and those available from the literature. The results of the experiments and the spring model display excellent agreement in terms of ultimate loads as well as load-displacement behaviour due to considering the change in stiffness and the corresponding redistribution of forces among the anchors of a group. Recommendations for the calculation of resistances of anchorages are given for using the nonlinear spring modelling approach including the field of application, the safety concept, the modelling rules and the verification of the results for Ultimate Limit State (ULS) and Serviceability Limit State (SLS).

KURZFASSUNG (Deutsch)

Im Rahmen dieser Dissertation wurde ein nichtlinearer Federmodellansatz für die realitätsnahe Berechnung und Bewertung von Gruppenbefestigungen bei Betonversagensarten unter Zug-, Quer- oder kombinierten Zug- und Querbeanspruchung entwickelt. Zunächst wurde das nichtlineare Federmodell für Gruppenbefestigungen konzipiert, die (1) Zug-beanspruchungen, (2) Querbeanspruchungen oder (3) deren Interaktion ausgesetzt sind. Das Konzept des nichtlinearen Federmodells basiert auf der Annahme, dass innerhalb einer Gruppenbefestigung die Zugkräfte von den einzelnen Befestigungsmitteln aufgenommen werden, während die Druckkräfte direkt durch das Anbauteil in den Beton eingeleitet werden. Zur Modellierung des Dübelverhaltens werden nichtlineare Federn verwendet, um eine realistische Kraftverteilung und -umverteilung innerhalb einer Gruppe in Abhängigkeit der Ankerplattensteifigkeit und der sonstigen Randbedingungen zu berücksichtigen. Um den Einfluss eines Bauteilrandes und benachbarter Befestigung zu berücksichtigen, wird im nichtlinearen Federmodell ein neuer Ansatz für die Berücksichtigung der Flächenverhältnisse bei der Ermittlung der Federkennlinien der Einzelbefestigungen verwendet. Der Kontakt zwischen der Ankerplatte und dem Beton wird mit reinen Druckfedern modelliert, während die Ankerplatte mit finiten Schalen- oder Solidelementen modelliert wird, um die Steifigkeit der Ankerplatte realistisch zu berücksichtigen. Ein analoges Modell wurde für querbeanspruchte Gruppenbefestigungen entwickelt. Allerdings wurde der Ansatz der projizierten Flächen durch einen Ansatz der Volumen ersetzt, um die Berücksichtigung unterschiedlicher Randabstände innerhalb einer Gruppenbefestigung zu ermöglichen. Das Modell für Interaktion ist die Kombination der nichtlinearen Federmodelle für Zug- und Querbeanspruchung. Ein umfassendes Versuchsprogramm wurde konzipiert und durchgeführt, um die bei der Konzeptualisierung des nichtlinearen Federmodells aufgestellten Postulate zu verifizieren. Ziel dieses experimentellen Programms war es, das Verhalten von zug- und querbeanspruchten Gruppenbefestigungen verschiedener Anordnungen zu untersuchen, und das Lastverschiebungsverhalten von Einzelbefestigungen und Befestigungen als Teil einer Gruppenbefestigung bei den Versagensarten Betonausbruch und Betonkantenbruch zu verstehen. Die Zugversuche an Dübelgruppen zielten darauf ab, die folgenden Einflüsse zu untersuchen: (i) unterschiedliche geometrische Anordnungen, (ii) unterschiedliche Steifigkeiten der Ankerplatte, (iii) exzentrische Belastung, (iv) Nähe der Betonkante und (v) Einfluss des Rissbildes. Die Querzugversuche wurden an Einzel- und Gruppenbefestigungen unterschiedlicher Anordnungen durchgeführt, um Information über (i) das Gruppenverhalten, (ii) die Rissinitiierung und -ausbreitung, (iii) den Einfluss des Verschiebungsverhaltens von Einzelbefestigungen auf das Verhalten von Gruppenbefestigungen, (iv) den Einfluss des Lochspiels und (v) den Einfluss des Rissbildes zu erhalten. Die nichtlinearen Federmodelle für Zug, Querzug und Interaktion wurden anhand einer Vielzahl von Versuchsergebnissen an verschiedenen Gruppenbefestigungen verifiziert, die im Rahmen dieser Dissertation durchgeführt wurden und aus der Literatur vorliegen. Die Ergebnisse der experimentellen Untersuchungen und des Federmodells zeigen eine sehr gute Übereinstimmung sowohl hinsichtlich der Tragfähigkeiten als auch des Lastverschiebungsverhaltens unter

Berücksichtigung der Steifigkeitsänderungen und der entsprechenden Kraftverteilung und Kraftumverteilung zwischen den Befestigungen einer Gruppe. Es werden Empfehlungen für die Berechnung des Widerstandes von Verankerungen unter Verwendung des nichtlinearen Federmodellansatzes gegeben, die das Anwendungsgebiet, das Sicherheitskonzept, die Modellierungsregeln und die Verifizierung der Ergebnisse für den Grenzzustand der Tragfähigkeit (GZT) und den Grenzzustand der Gebrauchstauglichkeit (GZG) umfassen.

I would like to thank everyone who believed in me and supported me.

The research work presented in this Ph.D. thesis was funded by fischerwerke GmbH & Co. KG.
The support received from fischerwerke is greatly acknowledged.

TABLE OF CONTENTS

NOTATION

a_{cl}	hole clearance
$A^0_{c,N}$	reference projected area of a tension loaded single anchor
$A^i_{c,N}$	projected area of an ith individual anchor of a tension loaded group
$A_{c,N}$	actual projected area of a tension loaded anchor or anchor group considering the member thickness, the spacing and edge distance from all sides
$A^0_{c,V}$	reference projected area of a shear loaded single anchor
$A^i_{c,V}$	projected area of an ith individual anchor of a shear loaded group
$A_{c,V}$	actual projected area of a tension loaded anchor or anchor group considering the member thickness, the spacing and edge distance from all sides
c	edge distance
c_1	edge distance in direction 1
c_2	edge distance in direction 2
$c_{1,i}$	edge distance of the individual anchors of a shear loaded group, in direction 1 (loading direction)
$c_{2,i}$	edge distance of the individual anchors of a shear loaded group, in direction 2 (direction perpendicular to loading)
c_{cr}	characteristic edge distance to ensure the characteristic resistance of a single anchor
cv_{k1}	coefficient of variation of initial anchor stiffness
d	diameter of anchor bolt or thread diameter, diameter of the stud or shank of headed anchors
d_f	diameter of clearance hole in fixture
d_{nom}	nominal anchor diameter
E_d	design action
e_N	eccentricity of resultant tension force of tensioned anchors with respect to the centre of gravity of the tensioned anchors
e_V	eccentricity of resultant shear force of shear loaded anchors with respect to the centre of gravity of shear loaded anchors
f_{cc}	concrete compressive strength of a cube with a side length of 150 mm
$f_{cc,200}$	concrete compressive strength of a cube with a side length of 200 mm
f_{ck}	characteristic concrete compressive strength of a cylinder of 150 mm diameter by 300 mm height
f_{cm}	mean cylinder compressive strength of concrete
f_t	tensile strength of concrete
G_f	fracture energy of concrete

h	thickness of concrete member in which the anchor is installed
h_{ef}	effective embedment depth of the anchor
k_1, k_2, k_3, k_4	secant stiffness values of the anchor (idealised load-displacement curve)
$k_{individual}$	secant stiffness of an individual anchor of a group
k_{group}	secant stiffness of the anchor group
l	base plate length
l_f	effective load transfer length
n	number of anchors within a group
n_1 (n_2)	number of anchors in a group in direction 1 (direction 2)
N_{Ed}	tension component of the design action
N_{Rd}	design tension resistance of the anchorage
$N_{Rd,c}$	design resistance in case of concrete cone failure under tension load
$N^0_{Rk,c}$	characteristic resistance of a single anchor placed in concrete and not influenced by adjacent anchors or edges of the concrete member in case of concrete cone failure
$N_{Rk,c}$	characteristic resistance of an anchor or an anchor group in case of concrete cone failure
N_{Rm}	mean tension resistance of the anchorage
$N^0_{Rm,c}$	mean resistance of a single anchor placed in concrete and not influenced by adjacent anchors or edges of the concrete member in case of concrete cone failure
$N^i_{Rm,c}$	mean resistance of an ith individual anchor of an anchor group in case of concrete cone failure
$N_{Rm,c}$	mean tension resistance of the anchorage in case of concrete cone failure
N_u	measured ultimate tension load
$N_{u,m}$	mean measured ultimate tension load
$N_{u,spring\ model}$	ultimate tension load obtained from the spring model
$P_{Ed}(\theta)$	design action in the direction with the θ vertical
$P_{Rd}(\theta)$	design resistance of the anchorage loaded at an angle θ with the vertical
$P_{Rk,c}(\theta)$	characteristic resistance of the anchorage loaded at an angle θ with the vertical for concrete breakout failure
$P_u(\theta)$	measured ultimate load of an anchorage loaded under combined tension and shear under loading angle θ with the vertical
R_d	design value of resistance
R_k	characteristic value of resistance
s	anchor spacing
s_1	anchor spacing in direction 1
s_2	anchor spacing in direction 2

$s_{1,i}$	spacing of the individual anchors of a shear loaded group, in direction 1 (loading direction)
$s_{2,i}$	spacing of the individual anchors of a shear loaded group, in direction 2 (direction perpendicular to loading)
s_{cr}	characteristic spacing for to ensure the characteristic resistance of a single anchor
t	base plate thickness
$V_{c,V}^{0,j}$	reference tributary volume of a single anchor with an edge distance equal to the edge distance of an anchor of a jth row of a shear loaded group
$V_{c,V}^{i,j}$	tributary volume assigned to an ith anchor of a jth row considering the distance from the adjacent anchors, edge distance and member thickness
V_{Ed}	shear component of the design action
V_{Rd}	design shear resistance of the anchorage
$V_{Rd,c}$	design resistance in case of concrete edge failure under shear load
$V_{Rk,c}^{0}$	characteristic resistance of a single anchor in case of concrete edge failure not affected by neighboring anchors or edge or member thickness
$V_{Rk,c}$	characteristic resistance of an anchorage in case of concrete edge failure
V_{Rm}	mean shear resistance of the anchorage
$V_{Rm,c}^{0}$	mean basic resistance of a single anchor in case of concrete edge failure
$V_{Rm,c}^{0,j}$	mean basic resistance of a single anchor in case of concrete edge failure corresponding to the edge distance of an anchor of a jth row
$V_{Rm,c}^{i,j}$	mean resistance of an ith individual anchor of a jth row of an anchor group in case of concrete cone failure
$V_{Rm,c}$	mean resistance of an anchorage in case of concrete edge failure
V_{u}	measured ultimate shear load
$V_{u,m}$	mean measured ultimate shear load
$V_{u,num}$	ultimate shear load obtained from numerical analysis
$V_{u,spring\ model}$	ultimate shear load obtained from the spring model
w	base plate width
α	exponent for the interaction equation, which depends on the failure mode
β_{w}	compressive strength of concrete measured on cubes with a side length of 200 mm
γ_{Mc}	partial safety factor for concrete cone, concrete edge, concrete blow-out and concrete pry-out failure modes
γ_{Ms}	partial safety factor for steel failure
δ	displacement of anchor
Δw	crack width
$\psi_{\alpha,V}$	factor taking into account the influence of a shear load inclined to the edge in case of concrete edge failure
$\psi_{ec,N}$	factor taking into account the group effect when different tension loads are acting on the individual anchors of a group in case of concrete cone failure

$\psi_{ec,V}$	factor taking into account the group effect when different shear loads are acting on the individual anchors of a group in case of concrete edge failure
$\psi_{h,V}$	factor taking into account the fact that concrete edge resistance does not increase proportionally to the member thickness
$\psi_{M,N}$	factor taking into account the effect of a compression force between the fixture and concrete in case of bending moments with or without axial force
$\psi_{re,N}$	shell spalling factor
$\psi_{re,V}$	factor taking into account the effect of reinforcement located on the edge in case of concrete edge failure
$\psi_{s,N}$	factor taking into account the disturbance of the distribution of stresses in the concrete due to the proximity of an edge in the concrete member in case of concrete cone failure
$\psi_{s,V}$	factor taking into account the disturbance of the distribution of stresses in the concrete due to the proximity of further edges in the concrete member in case of concrete edge failure
σ_{Ns}	steel stress of the highest tension loaded anchor
σ_{Vs}	steel stress of the highest shear loaded anchor
θ	loading angle with the vertical

1 INTRODUCTION

1.1 MOTIVATION AND PROBLEM STATEMENT

Anchor groups consisting of cast-in headed studs or post-installed anchors are widely used in engineering practice to form connections between structural elements or to fasten non-structural elements to structures. Examples for structural applications include i.a. connections between steel columns to concrete foundations (base plate connections) or beam to column connections. Typical non-structural applications are for example pipe hangers, façade installations and suspended ceilings.

In general, the design of anchorages offers a flexible application in terms of anchor size, anchor spacing, edge distance, embedment depth and concrete strength. However, the scope of the configurations covered by the current design provisions is rather limited due to the semi-empirical nature of the concepts and due to the force-based methods where the highest loaded anchor governs the design. These limitations restrict the design to a maximum of 3×3 anchor group with anchors arranged in a rectangular pattern in all loading directions, and using a sufficiently stiff base plate is required for tension loaded anchorages. In the case of shear loading, in general, the base plate stiffness is not critical. However, the hole clearance pattern and the crack pattern cannot be explicitly considered in the recent design approaches, leading to over-conservative design solutions in certain cases. Currently, for anchorage under shear, a pre-decision on the failure crack initiation should be made in the sense of whether the crack will appear from the front row or the back rows. Influences such as the vicinity of concrete edge(s) or loading eccentricity are accounted for by different empirical factors, which have been determined based on the available test data on mostly single anchors and 2×2 anchor groups and might not be directly applicable to larger than 3×3 anchor groups. For anchorages beyond the scope of the design guidelines, which are used due to technical, functional or architectural requirements, the design requires special considerations based on finite element modelling and engineering judgement.

Introducing a displacement-based (or performance-based) method for the design of anchorages in the fastening technology could eliminate the restrictions of the current methods leading to reliable design solutions considering arbitrary anchor group configurations, base plate geometries, base plate stiffness and the influence of loading eccentricity, crack pattern and hole clearance pattern with accounting for realistic load distribution and redistribution. Further benefit of a displacement-based approach is that a step-by-check performance check is available for the designed anchorage.

In this thesis, a new displacement-based approach referred to as the nonlinear spring model is developed, verified and proposed for the design of anchorages in the case of concrete breakout failure modes under tension, shear and interaction thereof. The information obtained by performing a nonlinear analysis with the nonlinear spring model can be used for the performance-based assessment of reinforced concrete structures.

The main goals of this dissertation are:

I. To understand and summarise the limitations of the currently applicable provisions for the design of anchorages in the case of concrete breakout failure modes under tension, shear and interaction loading.
II. To generate a test database for both tension and shear loaded anchor groups, that goes beyond the scope of the current regulations such as non-rectangular anchorages, anchorages with more than three anchors in a row, anchorages with flexible base plate and anchorages with hole clearance.
III. To develop a generally applicable model for the concrete breakout failure of anchor groups, which accounts for influences such as different arrangement of anchors, eccentricity of loading, base plate stiffness, cracked concrete condition, multiple anchor rows, hole clearance pattern and is able to consider a realistic load distribution and redistribution within anchor groups. The model is referred to as the nonlinear spring model.

1.2 CONTEXT FOR THE RESEARCH

The overall goal of this thesis was to develop a displacement-based approach for the design of anchorages in concrete, which is applicable irrespective of the arrangement of the anchors, the stiffness of the base plate, the loading case and can explicitly consider the influence of crack pattern and the hole clearance pattern. A nonlinear spring model was developed, verified and proposed for the design of anchorages in the case of concrete breakout failure modes under tension, shear and inclined loads (interaction).

First, the nonlinear spring model was conceptualised for anchorages under tension, shear and inclined (interaction) loading considering several aspects to reach the ultimate aim i.e. to reflect the behaviour of anchor groups of arbitrary configuration realistically, and to give a good estimate about the performance of the anchorage.

To reach that goal and to obtain the information required for the development of the model while understanding the behaviour of anchor groups better, an extensive test program was designed for tension- and shear loaded anchorages. The well-designed and well-instrumented experimental program was carried out to generate a new test database, with special emphasis on load-distribution and redistribution among the anchors within an anchor group.

The tests were performed on different rectangular and non-rectangular anchor group configurations with varying the base plate stiffness, crack pattern, edge distance, loading case (concentric/eccentric), hole clearance pattern and the combination of the mentioned parameters under tension and shear loads. The focus of the experiments was to obtain the required information about the load-displacement behaviour of the anchor group and the behaviour of the individual anchors of the group, and their comparison with the load-displacement behaviour of the corresponding single anchor. Therefore, the measurement of the load and displacement values was of particular importance when generating new results. Only with careful measurement of loads and displacements in the ascending branch, plateau and descending branch, it is possible to

evaluate the load distribution and redistribution (if any) among the anchors of a group. Furthermore, in this way, the parameters influencing (or not influencing) the axial and shear stiffness of the anchors can be determined or confirmed.

The careful evaluation of the test results enabled to establish the principles of the new displacement-based method (nonlinear spring model). The basic principles in the development of the nonlinear spring model include the consideration of virtual edges between the neighbouring anchors through the tributary area or tributary volume approach and the consideration of realistic distribution and redistribution of forces among the anchors by performing nonlinear analysis in displacement control, taking into account the anchor stiffness and the change in stiffness under tension and shear.

The nonlinear spring model for tension, shear and interaction was verified against a vast number of experiments carried out within the framework of this thesis and from the literature. The results of experiments and the spring model display excellent agreement in terms of ultimate loads as well as load-displacement behaviour. The verified approach was associated with a general safety concept in order to make the approach suitable for the design of anchorages in concrete.

1.3 ORGANISATION OF THE WORK

The work carried out within the framework of the thesis is organized as follows:

I. Development of spring models
   a. Development of a nonlinear spring model for tension loaded anchor groups in the case of concrete cone failure mode
   b. Development of a nonlinear spring model for shear loaded anchor groups in the case of concrete edge breakout failure mode
   c. Development of a nonlinear spring model for tension-shear interaction in the case of concrete breakout failure

II. Experimental and numerical investigations
   a. Experimental investigations on tension loaded single anchors and anchor groups in case of concrete cone failure mode
   b. Experimental and numerical investigations on shear loaded single anchors and anchor groups in case of concrete edge failure mode

III. Verification of models
   a. Verification of the nonlinear spring model for tension against experiments from this work and from the literature
   b. Verification of the nonlinear spring model for shear against experiments from this work and from the literature
   c. Verification of the nonlinear spring model for tension-shear interaction against experiments from the literature

IV. Recommendations for the calculation of resistances
   a. Recommendations for applying the nonlinear spring model for anchorages undergoing concrete breakout failure modes

2 GENERAL BEHAVIOUR OF ANCHORAGES IN CONCRETE

This chapter discusses the behaviour of anchorages in concrete. Section 2.1 focuses on the behaviour of anchorages under tension loading, whereas Section 2.2 on the behaviour of anchorages under shear loading with explaining the basics of the load-transfer mechanisms and failure modes. Special emphasis is placed on the concrete breakout failure modes such as concrete cone failure under tension and concrete edge failure under shear loads in Sections 2.1.2 and 2.2.2, respectively.

Anchorages are used to transfer loads into concrete structures while connecting structural or non-structural elements with structural components. The components of an anchorage include the fixture or base plate usually made of structural steel, which distributes the loads to the anchors, the attachment and the anchors that transfer the load from the base plate to the concrete and the concrete base material surrounding the anchorages. The side view of a typical anchorage with headed studs having one anchor row in a crack is depicted in *Figure 2.1*.

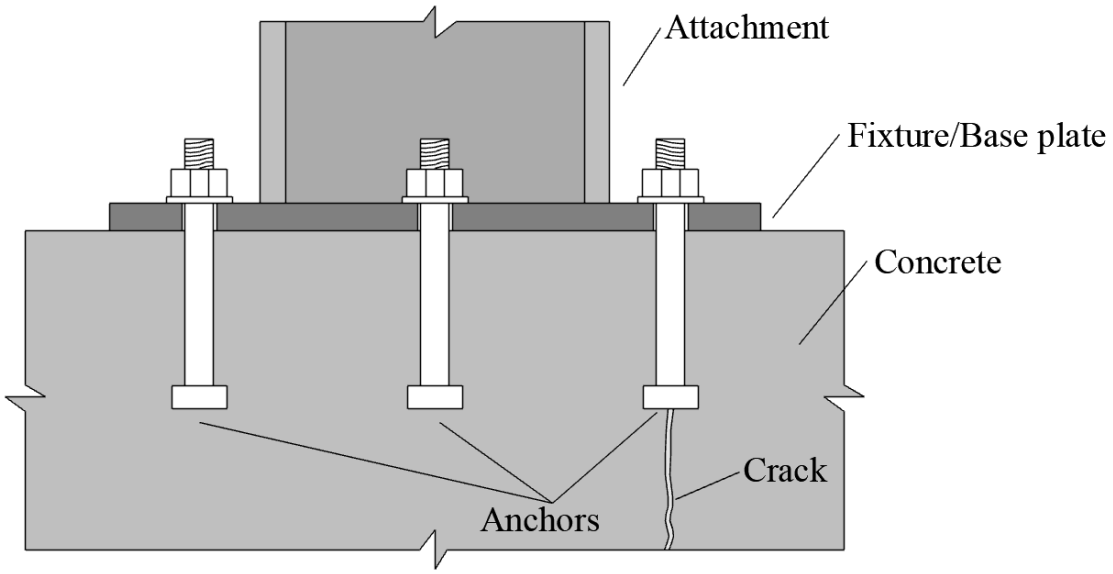

Figure 2.1. Nomenclature of a typical anchorage

In this thesis, the terms anchor, anchor group, anchorage are used to describe the "connections". However, these terms are considered equivalent to the terms fastener and group of fasteners used according to the European Standard EN 1992-4. *Figure 2.2* gives an overview of the definitions related to concrete member dimensions used.

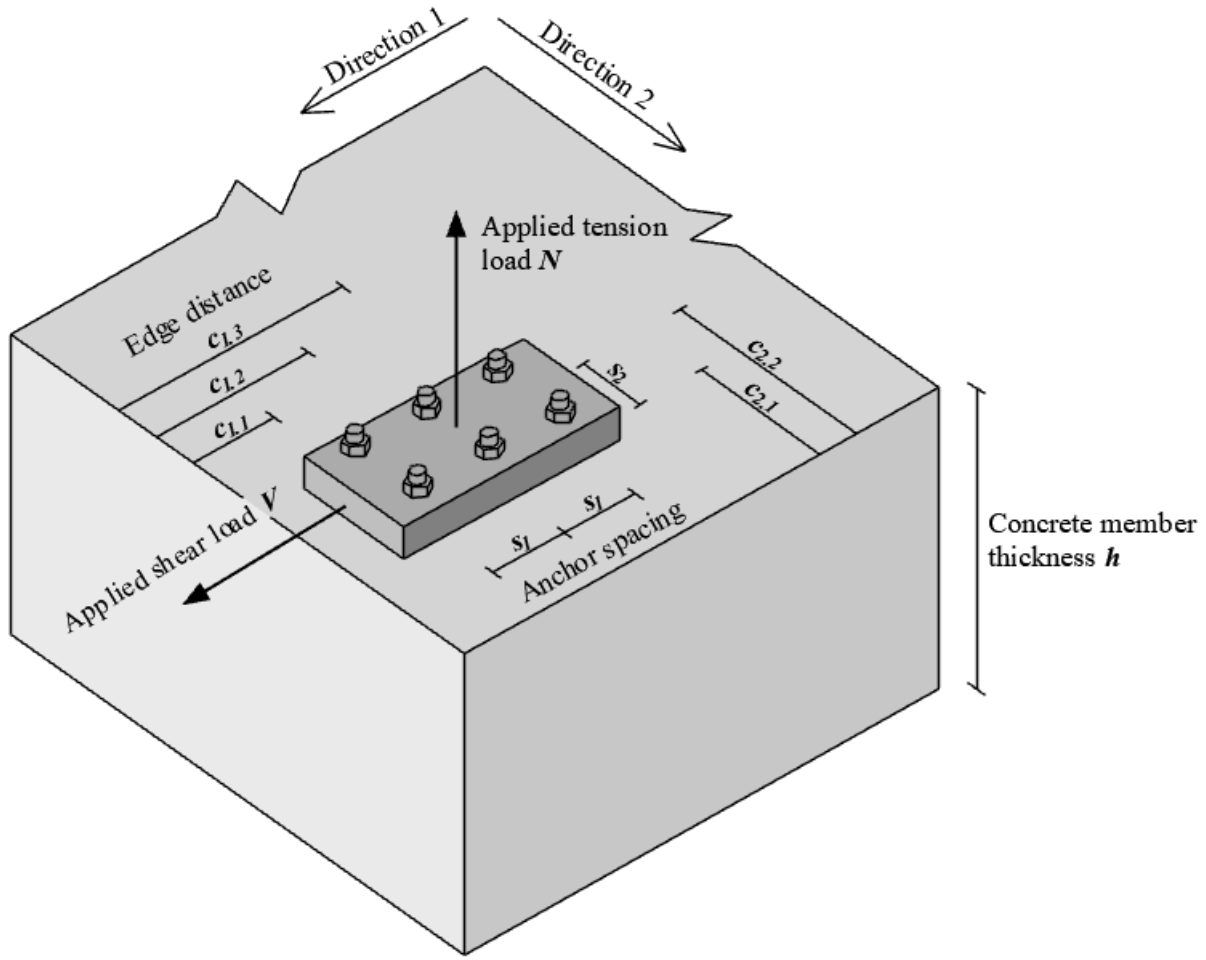

Figure 2.2. Definitions related to concrete member dimensions and loading directions

2.1 BEHAVIOUR OF TENSION LOADED ANCHORAGES

2.1.1 Load-transfer mechanism and failure modes

Depending on the anchor type, tension loads applied on anchorages are transferred into the concrete by mechanical interlock, friction, or bond or by a combination of these load-transfer mechanisms as depicted in *Figure 2.3* (Eligehausen et al., 2006). Examples for anchor systems using mechanical interlock as load-transfer mechanism include headed studs, undercut anchors, concrete screws and anchor channels. In the case of mechanical interlock, the load transfer is ensured by a bearing interlock between the fastening system and the concrete. The load-transfer mechanism friction is employed by expansion anchors, which generate high expansion forces during installation (pressing the expansion sleeve of the anchor against the wall) leading to high frictional forces between the anchor. The resistance is provided by the frictional force, which is in equilibrium with the externally applied tension force. In the case of adhesive anchors, the tension load is transferred into the concrete by means of bond, which is a combination of adhesion and micro keying.

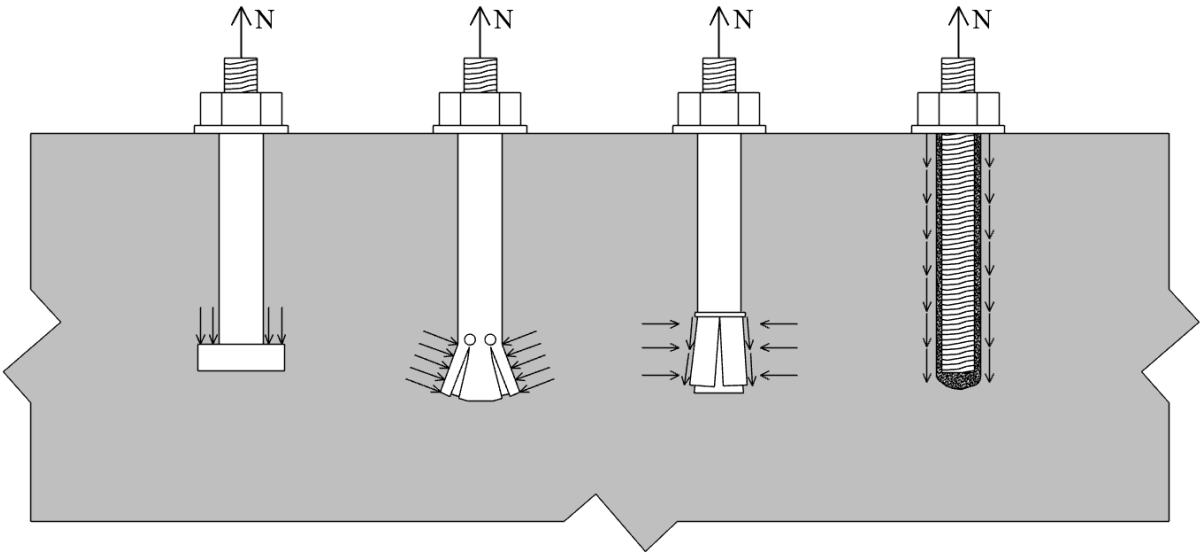

Figure 2.3. Load transfer mechanism of anchors under tension, from left to right: mechanical interlock, mechanical interlock, friction, bond (reproduced based on Eligehausen et al. 2006)

Anchorages in concrete subjected to tension loads may fail due to anchor steel failure, pull-out failure, concrete cone failure, splitting of the concrete component or side face blow-out failure (Eligehausen et al., 2006). Which failure mode is governing, depends on a number of parameters such as anchor size, anchor embedment depth, anchor spacing (in the case of anchor groups), edge distance, concrete strength and the combination of the installation parameters. Note that the decisive failure mode of an anchor group might differ from the decisive failure mode of the corresponding single anchor.

The anchor steel failure is associated with the ductile failure of the steel, which represents the upper limit of the load-bearing capacity of a single anchor (*Figure 2.4a*). The pullout failure as shown in *Figure 2.4b* in case of headed studs occurs when the mechanical interlock is inadequate and the anchor can be pulled out of the concrete causing concrete crushing at the anchor head (Furche, 1994), however, without leading to the breakout of the concrete. In the case of post-installed anchors, pull-out failure corresponds to the failure mode where the anchor is being pulled out of the drilled hole. This can be due to insufficient expansion forces in the case of displacement-controlled expansion anchors or due to the lack of a proper follow-up expansion in the case of torque-controlled expansion anchors (Eligehausen & Pusill-Wachtsmuth, 1982). Furthermore, bonded anchors may fail due to pullout failure at the mortar-concrete or threaded rod-mortar interface in case of an insufficient bond (Meszaros, 1999, Kunz et al., 1998). *Figure 2.4c* and *d* show a single anchor and an anchor group failing due to concrete cone breakout. In the case of a single anchor, a cone-shaped breakout body develops, which in the case of anchor groups might result in the development of a common breakout body depending on the anchor spacing (Fuchs et al., 1995). *Figure 2.4d* refers to the combined concrete cone-pullout failure of bonded anchors, where the concrete cone forms at the top end of the anchor, and the bond fails along the embedment depth (*Figure 2.4e)* (Lehr & Eligehausen, 1998, Appl, 2009). The splitting failure occurs either due to limited dimensions of the concrete specimen (*Figure 2.4f)* or due to the installation of the anchor close to an edge or when a line of anchors are installed close to each other (Asmus, 1999). Side face blow-out failure might be decisive in

case of tension loaded headed studs having small edge distances in combination with large embedment depths (Furche & Eligehausen, 1991) generating a local blowout failure in the vicinity of the head (*Figure 2.4g)*.

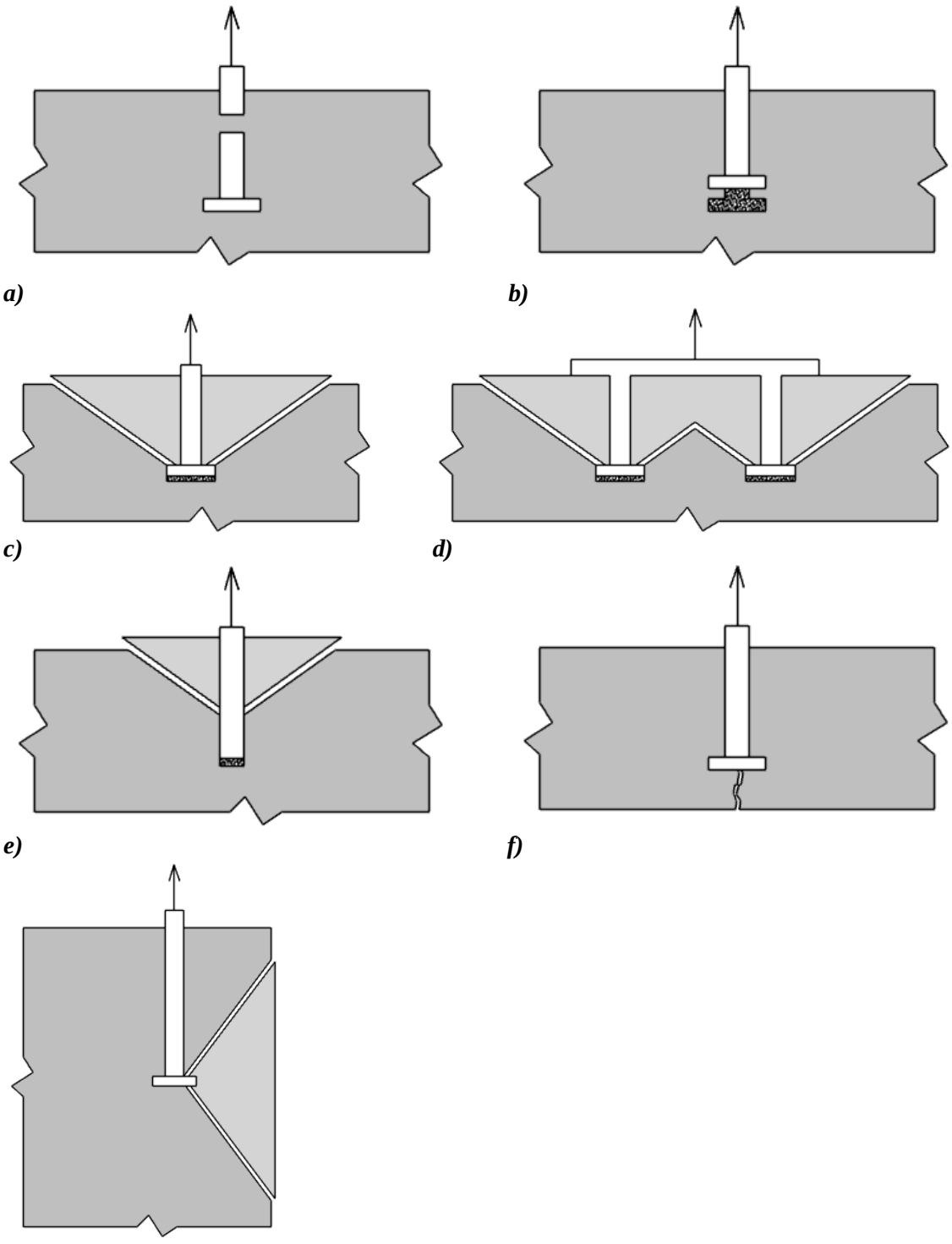

Figure 2.4. Failure modes of anchors under tension: a) steel failure, b) pull-out failure, c) concrete cone failure of a single anchor, d) concrete cone failure of an anchor group, e) combined concrete cone and pull-out failure, f) concrete splitting failure, g) side blow-out failure

Note that in the case of steel failure and pull-out failure, the resistance of the anchors is not influenced by the adjacent anchors or by the vicinity of the edge of the concrete member. Therefore, the verification of these failure modes for anchor groups should be carried out only for the most loaded single anchor. However, in the case of concrete cone failure and splitting failure of anchor groups, the anchor spacing and the concrete edge distance have a significant influence on the load-bearing capacity of the group, which have to be considered in the design. Further details about the behaviour of anchorages failing due to concrete cone breakout are given in Section 2.1.2.

2.1.2 Concrete cone failure of tension loaded anchorages

When a single headed stud embedded in concrete is loaded in tension, the load is transferred to the concrete by the bearing of the head against the concrete. During the initial loading phase, the stiffness of the load-displacement curve (*Figure 2.5*) is determined primarily by the elastic elongation of the steel shaft. If the steel shaft of the anchor is smooth, then the frictional resistance along the anchor shaft is negligible. On further increasing the applied tensile force, the concrete crushing takes place locally around the head, which results in the change in stiffness of the load-displacement curve.

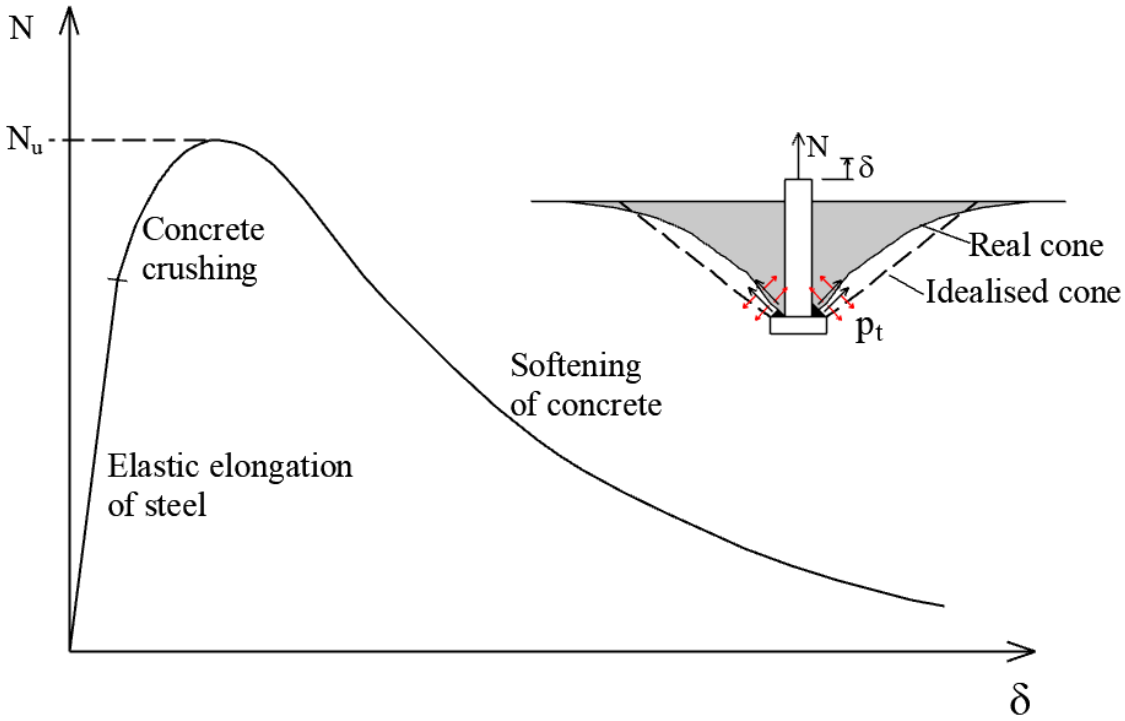

Figure 2.5. Nonlinear behaviour of a single headed stud failing due to concrete cone failure

The local crushing of the concrete leads to the formation of a wedge that results in the development of radial tensile stresses in the concrete. Once the tensile strength of the concrete is exceeded, the radial crack develops (concrete cone) typically from the edge of the head due to stress concentration. Experimental investigations by Eligehausen and Sawade (1989) showed that when the ultimate resistance of the anchor is reached, the crack length *a* is approximately

30-40 % of the side length l_c of the radial crack (*Figure 2.6*). After reaching the peak load, the crack growth becomes unstable and the softening in the load-displacement curve can be observed.

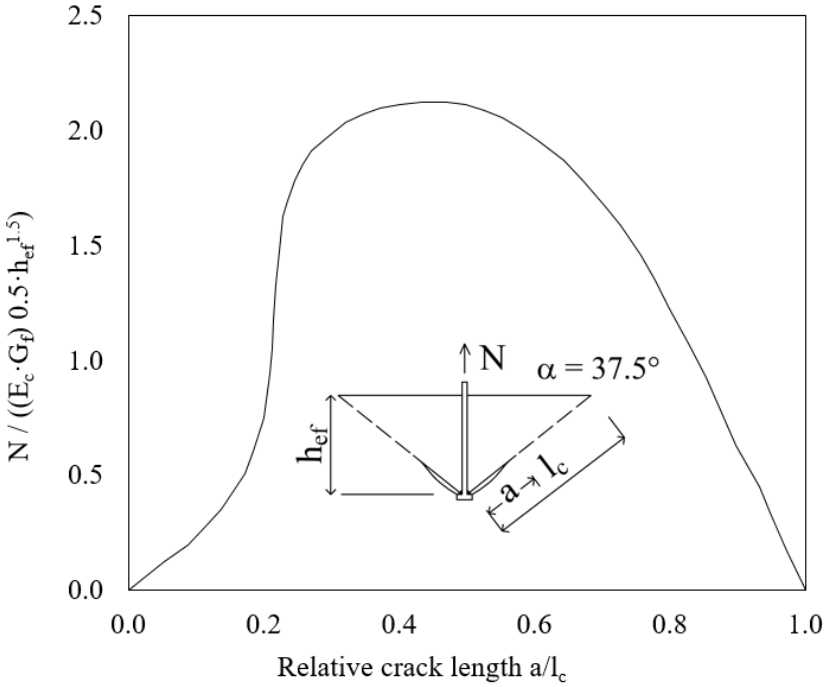

Figure 2.6. Relative tension load as a function of relative crack length (reproduced based on Eligehausen & Sawade, 1989)

The tensile behaviour of post-installed anchors in the case of concrete cone failure is, in general, similar to the behaviour of a cast-in place headed stud as described above. However, the actual load-displacement behaviour might be different depending on the anchor type/product. Generally, the initial stiffness is governed by the anchor type. For example, bonded anchors or concrete screws display higher stiffness than the expansion anchors or the undercut anchors of the corresponding size and embedment depth. The change in stiffness and the length of the plateau are dominated by the stress concentration at the unloaded end of the anchor, which in turn, depends on the anchor type. The descending branch of the load-displacement curve is controlled by the concrete strength, concrete type, aggregate type (crushed or round gravel) and size.

Tests by Eligehausen et al. (1992) showed that the average angle of the failure cone measured with respect to the surface of the concrete member corresponds to ca. a slope of 1:1.5. This means that the diameter of the projected concrete cone at the concrete surface is ca. 3-times the anchor embedment depth.

If a neighbouring anchor is placed at a distance of smaller than 3-times the anchor embedment depth, and the anchors are connected by a common base plate, then the connection is referred to as an anchor group. In this case, the concrete cone breakout bodies of the individual anchors intercept, and a common breakout body develops. An example is shown in *Figure 2.7*.

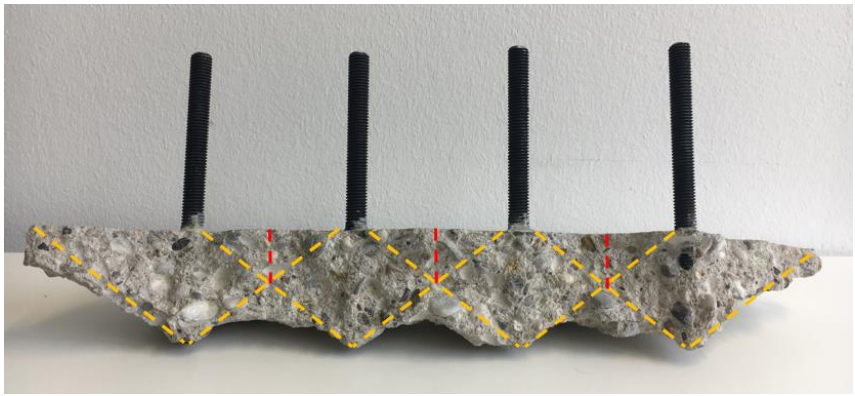

Figure 2.7. Photo of a 1×4 anchor group failed due to concrete cone failure

However, the behaviour of anchor groups and the force distribution among the anchors of a group is significantly influenced by the base plate stiffness. In the case of an anchor group having a stiff base plate subjected to a concentric tension force, the displacement of the individual anchors is equal (*Figure 2.8a)*. Assuming the same anchor axial stiffness for the anchors of the group, the load carried by the individual anchors is equal. However, if the same anchor group configuration is connected by a flexible (or not sufficiently stiff) base plate, due to the unequal displacement of the individual anchors, the tension force taken up by the individual anchors depends on the base plate stiffness (*Figure 2.8b*). The current force-based design provisions (on the basis of CCD Method, such as EN 1992-4) are valid only in the case of anchor groups with sufficiently stiff base plates. The necessary but not sufficient condition to consider the base plate as stiff is that under design actions it must remain elastic. Additionally, the deformations of the base plate should be significantly smaller than the displacement of the anchors. This implies that the requirement of a sufficiently stiff base plate depends on the anchor stiffness and therefore, the relative flexural rigidity of the base plate to the stiffness of the anchors should be considered. However, there is no specific guidance given to ensure that the base plate is sufficiently stiff.

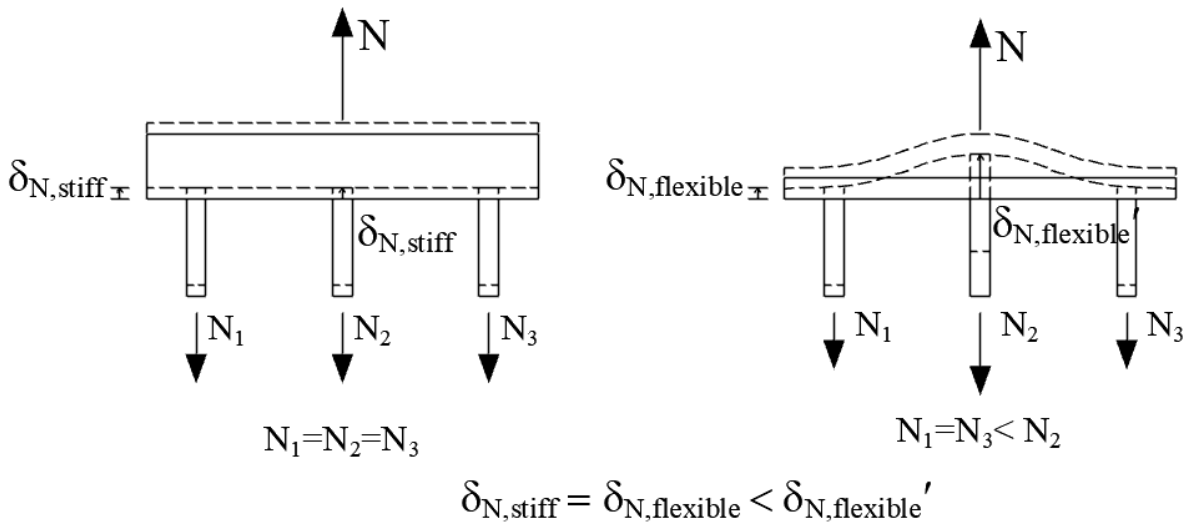

Figure 2.8. Influence of the base plate stiffness on the load distribution among the anchors of an anchor group

The requirement of a stiff base plate is, however, contradictory to the approach followed in the design of the base plates for steel structures where the plasticisation of the base plate is one of the desirable failure mechanisms. In particular, in the case of column bases subjected to bending moments, the anchor bolts are considered to take up the tension forces, while the bearing of the base plate on the concrete surface provides the internal equilibrium (Wald et al., 2008a). Generally, two cases are considered for the column bases. In the first case, the bolts are flexible and the base plate is stiff, and the plate is separated from the concrete. In the second case, the base plate is in contact with the concrete resulting in prying action, and the bolts are loaded by additional prying force. Alternatively, the component method can be used for the design of steel-column bases (Wald et al., 2008b).

In the case of tension loaded anchors in uncracked concrete, the rotationally symmetric stress distribution is generated by the anchor, where the hoop stresses in the concrete provide the equilibrium (*Figure 2.9a*). However, if an anchor loaded in tension is intercepted by a crack, the distribution of stresses in the anchorage zone changes compared to the anchor in uncracked concrete because the tension force cannot be transferred across the crack plane (Eligehausen et al., 2006). This leads to a reduction in the stiffness and the load-carrying capacity of the anchor depending on the anchor type and size, embedment depth, crack width, etc. *Figure* 2.9 shows a schematic from (Rehm et al., 1988) for consideration of force distribution in uncracked and cracked concrete. Two independent cones are considered for cracked concrete (*Figure 2.9b*). However, in reality, the shape of the concrete fracture surface in cracked concrete is not different from that in uncracked concrete except that the cone is separated by the crack. Further information on the behaviour of anchorages under tension loads can be obtained from Eligehausen et al. (2006).

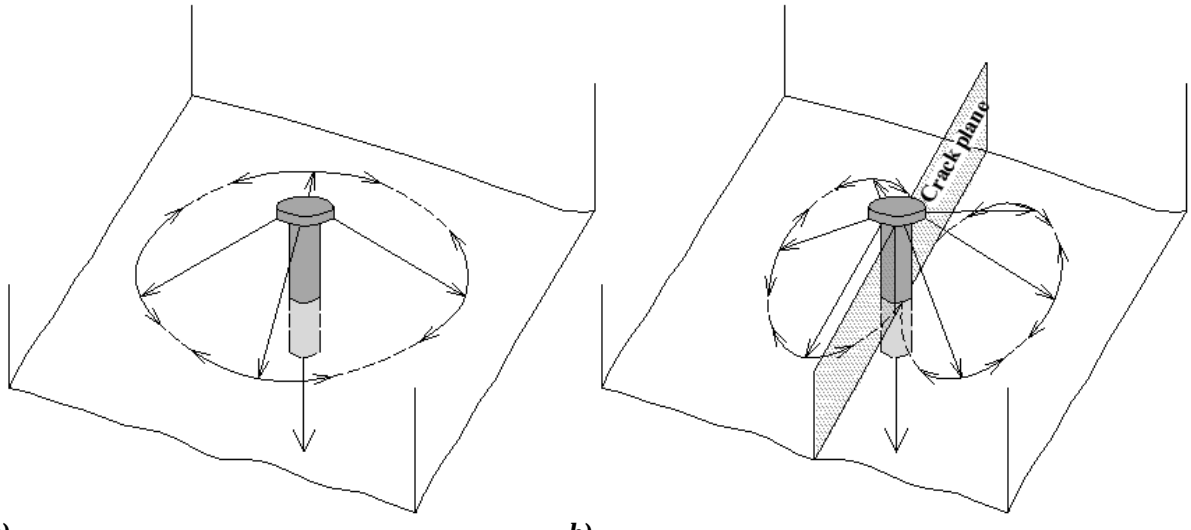

a) ***b)***

Figure 2.9. Force distribution in the concrete anchorage zone of a tension loaded headed stud in a) uncracked concrete, b) cracked concrete (reproduced based on Rehm et al., 1988)

2.2 BEHAVIOUR OF SHEAR LOADED ANCHORAGES

2.2.1 Load-transfer mechanism and failure modes

When anchorages are loaded in shear, it is assumed that the behaviour of post-installed anchors is the same as the behaviour of cast-in-place anchors and that the same failure modes can occur for both post-installed and cast-in anchors (Hofmann, 2005).

When an anchorage is subjected to shear loads, the shear load is transferred to the anchors via the base plate or fixture. In the beginning, the shear load is transferred between the concrete and the base plate via friction generated by the preload in the anchor (if any). When the applied shear load exceeds the frictional resistance of the base plate, the anchors start to take up the shear forces and the resistance is provided by the bearing of the anchor shaft against the concrete (*Figure 2.10*). In the initial loading phase, beyond frictional resistance, the stiffness is primarily governed by the anchor diameter, which in turn governs the bearing pressure. As the load is increased, concrete spalling in front of the anchors take place leading to a loss of stiffness. The shear behaviour beyond this point is decided by the dominant failure mode, which is controlled by the installation parameters such as anchor type and size, steel grade, anchor embedment depth, concrete strength, edge distance, anchor configuration, anchor spacing and loading direction (*Figure 2.11*).

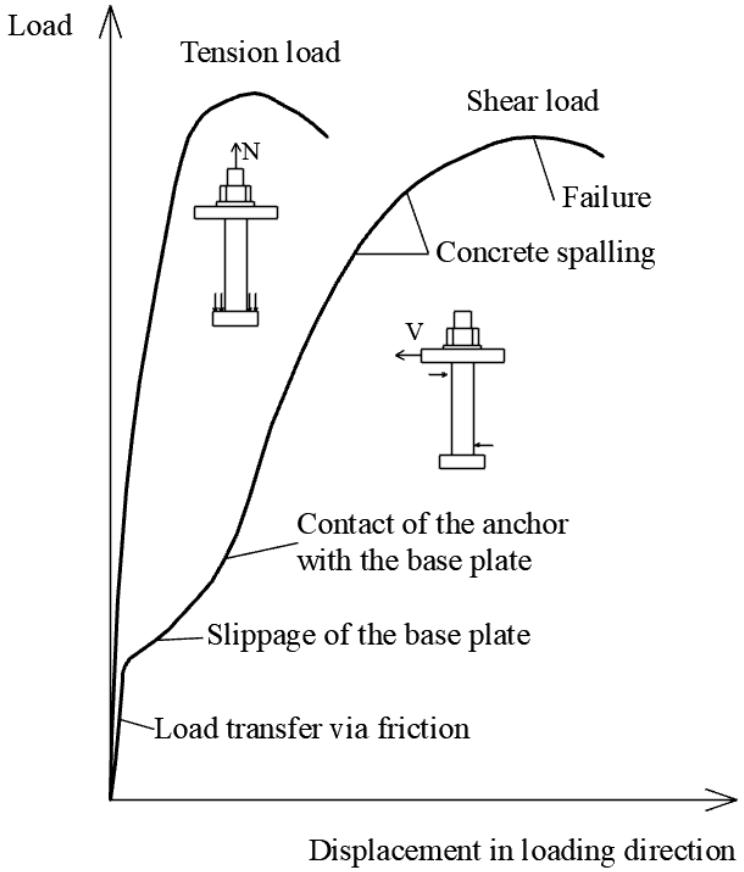

Figure 2.10. Comparison of idealised load-displacement curves for anchors subjected to tension and shear with no edges in proximity (Rehm, Eligehausen, Mallée, 1988, reproduced on the basis of Eligehausen et al., 2006)

If the anchor is placed far from the concrete edge and the embedment depth is sufficiently large, it might fail due to steel failure of the anchor with a concrete spalling in front of the anchor in case the load is applied without lever arm (*Figure 2.11a*) (Fuchs, 1990). If the shear load is applied with a lever arm (*Figure 2.11b)*, the failure occurs due to the bending of the anchor (Scheer et al., 1987). Pryout failure is governing when the anchor embedment depth is short and the anchor is placed far from the edge, or located close to the edge but the shear force is applied in the direction away from the edge (*Figure 2.11c*) (Zhao, 1993, Anderson & Meinheit, 2005, Jebara, 2018). Anchorages loaded in shear close to one or more edges and loaded towards the edge may fail by the breakout of the concrete (*Figure* 2.11*c*) (Fuchs, 1990, Hofmann, 2005, Unterweger, 2008, Grosser, 2012, Bokor et al., 2020, Bokor et al., 2021).

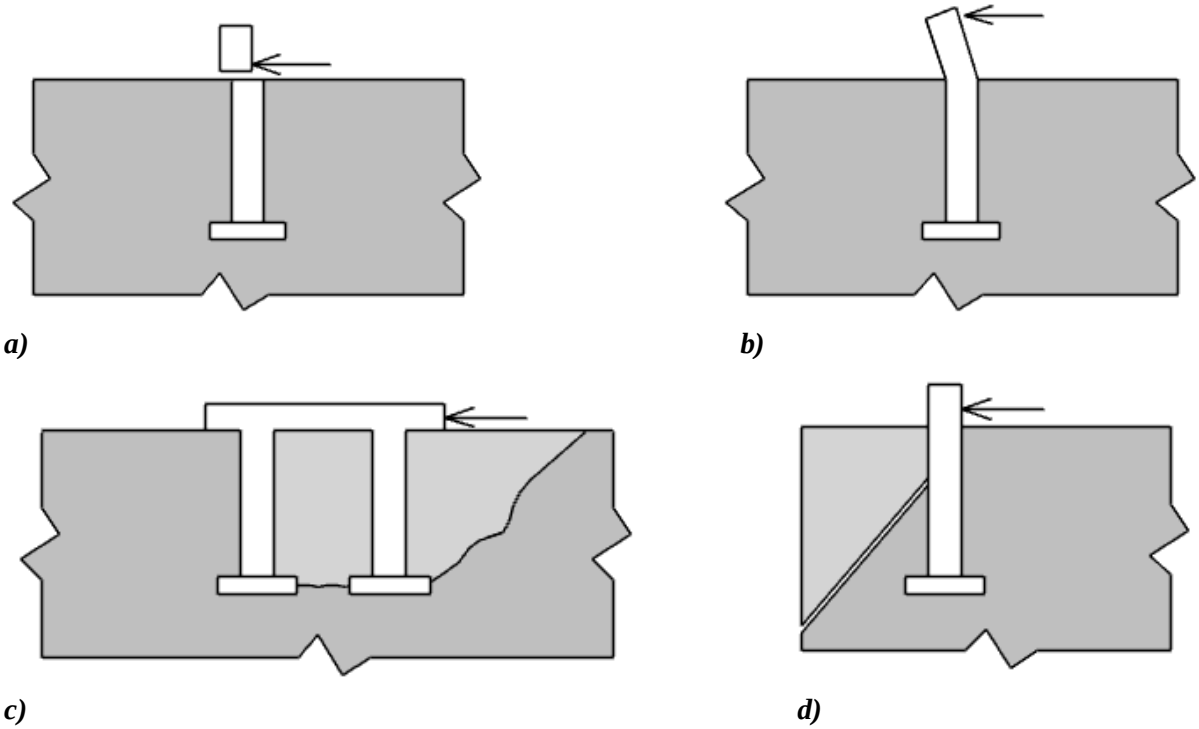

Figure 2.11. Failure modes of anchorages under shear-loading: a) steel failure, b) steel failure with a lever arm, c) pryout failure, d) concrete edge failure

2.2.2 Concrete edge failure of shear loaded anchorages

The concrete edge breakout failure of shear loaded anchorages, just as the concrete cone failure in the case of tension loaded anchorages, is a concrete tensile failure, which occurs when the tensile strength of the concrete is exceeded by the tensile stresses generated by the applied shear load. In the case of post-installed anchors, an annular gap exists between the hole in the base plate and the anchor rod to enable installation and construction tolerances. If this gap is not filled, first the base plate might displace in order to close this gap before the force can be transferred by the plate to the anchor (*Figure 2.12*). The resistance up to this point is provided only by friction and is rather small (Cook, 1989). Once the base plate starts pushing the anchor and the anchor rod bears against concrete resulting in compression force in the front of the anchor shaft, the resistance rises steeply with the displacement (*Figure 2.12*). High bearing stresses in this zone result in concrete spalling in the front of the anchor and the radial tensile stresses

develop in the half-space continuum, which are analogous to the radial tensile stresses developed under the tensile forces in case of anchors under tension (Section 2.1.2). The direction of the tensile cracks is perpendicular to the direction of the tensile stresses developing in the concrete. Once these stresses exceed the tensile resistance of concrete, failure crack develops forming a semi-conical shaped concrete edge breakout body. As *Figure 2.12* shows, the angle subtended by the failure crack with the concrete edge is typically ca. 35° and develops to a depth at the face of the concrete edge equal to approximately 1.5 times the edge distance (Stichting Bouwresearch, 1971, Fuchs & Eligehausen, 1986/2). This is analogous to the development of the failure crack in the case of tension loading, where the average angle of the failure cone with respect to the concrete surface corresponds to ca. 35° (Section 2.1.2).

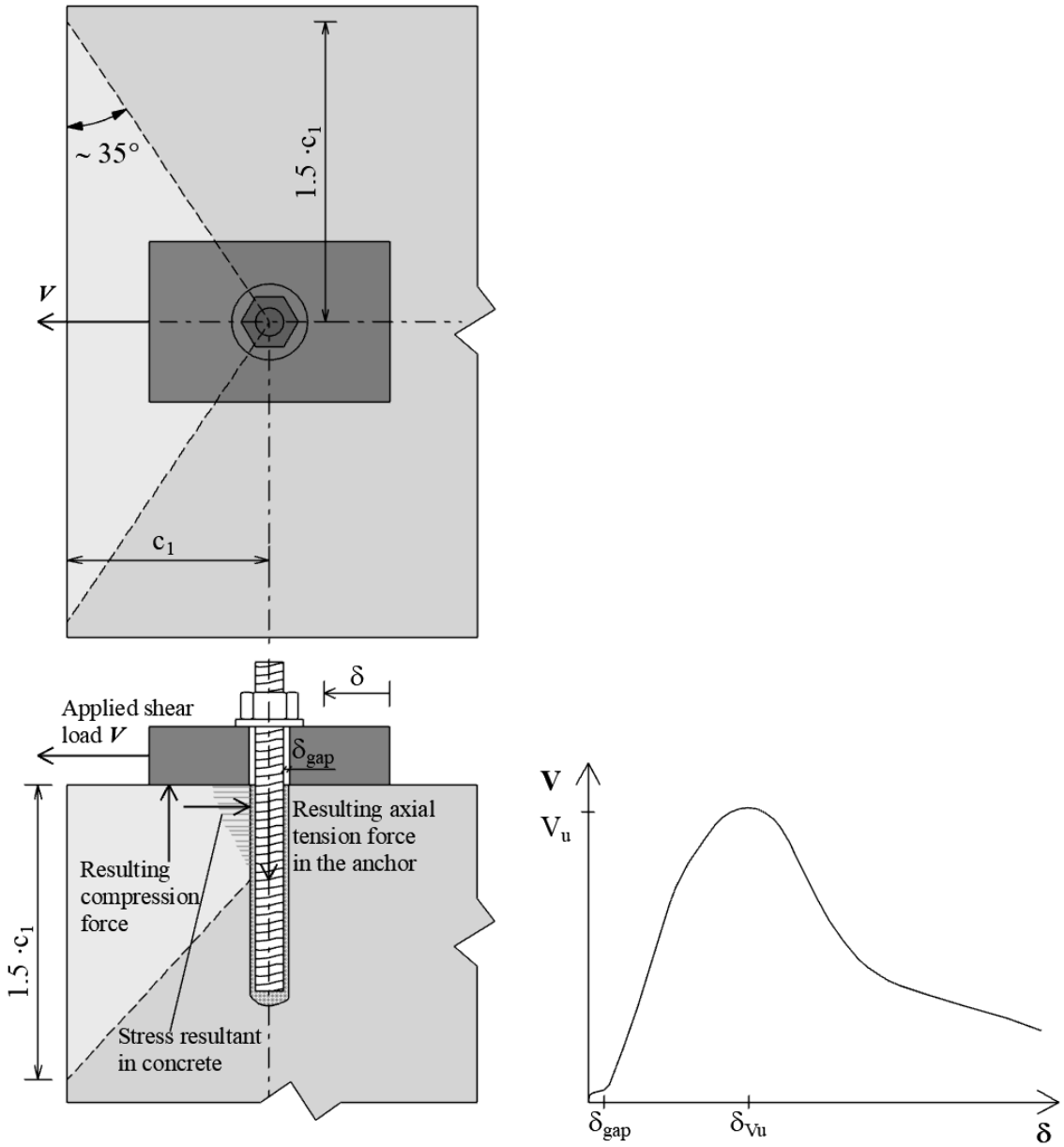

Figure 2.12. Single anchor loaded in shear towards a close edge: load-bearing mechanism and idealised load-displacement curve

The stress distribution along the anchor length depends on the embedment depth to anchor diameter ratio of the individual anchors; consequently, also the depth of the concrete breakout body depends on this ratio. This is because stiff anchors distribute the stresses more evenly and deeper into the concrete, whereas for anchors with lower stiffness, stress concentration takes place rather in the area of the concrete surface (Hofmann, 2005).

In the case of anchor groups failing due to concrete edge breakout, the base plate stiffness is not critical because the in-plane stiffness of the base plate is generally sufficient to allow equal displacement under concentric loading. The concrete edge breakout under shear is analogous to the concrete cone breakout under tension. However, unlike anchor groups loaded in tension, where the anchors always have equal embedment depth as per design, the shear loaded anchorages with multiple anchor rows are associated with different edge distances. Therefore, under tension, the projection of the concrete cone breakout bodies can be used to determine the group capacity (CCD Method, projected area, 2D problem). However, in the case of shear loaded anchorages with multiple anchor rows, the problem is essentially three-dimensional. Therefore, currently, for anchor groups having multiple anchor rows under shear, a pre-decision on the failure crack initiation should be made in the sense of whether the crack will appear from the front row or the back rows. This pre-decision is required in order to enable the 3D problem to be simplified to a 2D problem. *Figure 2.13* depicts the theoretical crack pattern of a 1×3 anchor group in the case of concrete cone and concrete edge breakout failure

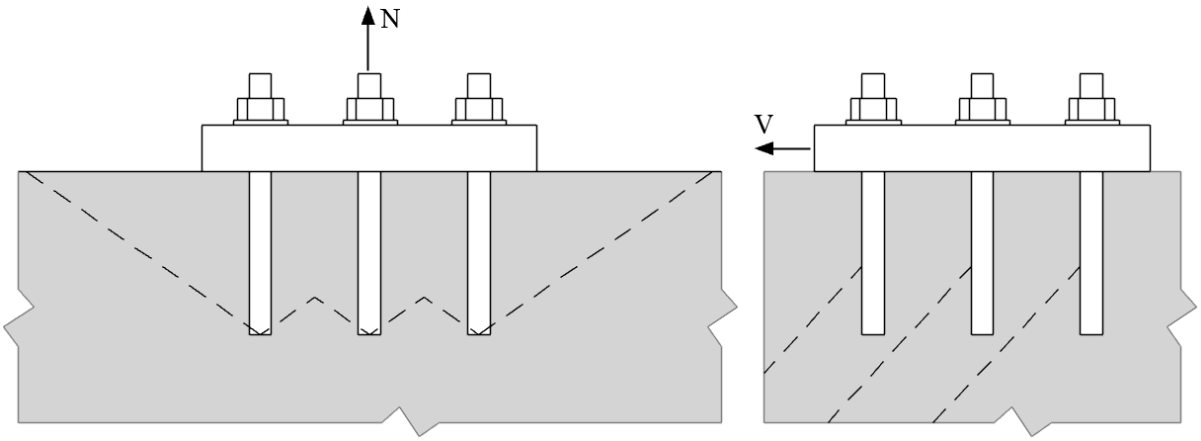

a) ***b)***

Figure 2.13. Theoretical crack pattern of a 1×3 anchor group in case of a) concrete cone and b) concrete edge failure

When anchorages are loaded in shear, the force distribution depends on the effectiveness of the anchors resisting shear loads, which is among others influenced by the hole clearance pattern. For anchor groups without hole clearance, the shear load is initially distributed to all anchors. For anchor groups with hole clearance, the entire shear load is initially distributed only to the front anchors in case of unfavourable anchor configuration or only to the back anchors in case of favourable anchor configuration as shown in *Figure 2.14.* The formation of a crack at the front anchors may negatively influence the group capacity, depending on the hole clearance, anchor spacing to edge distance ratio, anchor type etc. (Fuchs & Eligehausen, 1986, Hofmann, 2005, Unterweger, 2008, Grosser, 2012, Bokor, 2020). The influence of hole clearance pattern

on the load-displacement behaviour of an anchorage with two anchor rows is schematically explained in *Figure 2.14*. If the hole clearance of the back anchor row is zero (case 1), the shape of the load-displacement curve is similar to that obtained for the case of the corresponding anchorage with a single anchor row. However, if the front anchor row has no hole clearance ($a_{cl,front} = 0$) while the back row does ($a_{cl,back} > 0$) as in case 2, then the shear load is initially taken up by the front anchor row only. Assuming that the shear stiffness is independent of the edge distance, the initial stiffness of the curves for case 1 and case 2 would be the same. In case 2, the cracking would first occur at the front anchor row and the load-displacement curve would display a drop in the capacity with increasing displacements until the base plate displaces by $a_{cl,back}$, and the back anchor row gets activated. Once the back anchor row gets activated, the load-displacement curve starts to rise again and depending on the displacement behaviour of the anchors and the hole clearance ($a_{cl,back}$), the same anchorage capacity for case 1 and case 2 might be reached.

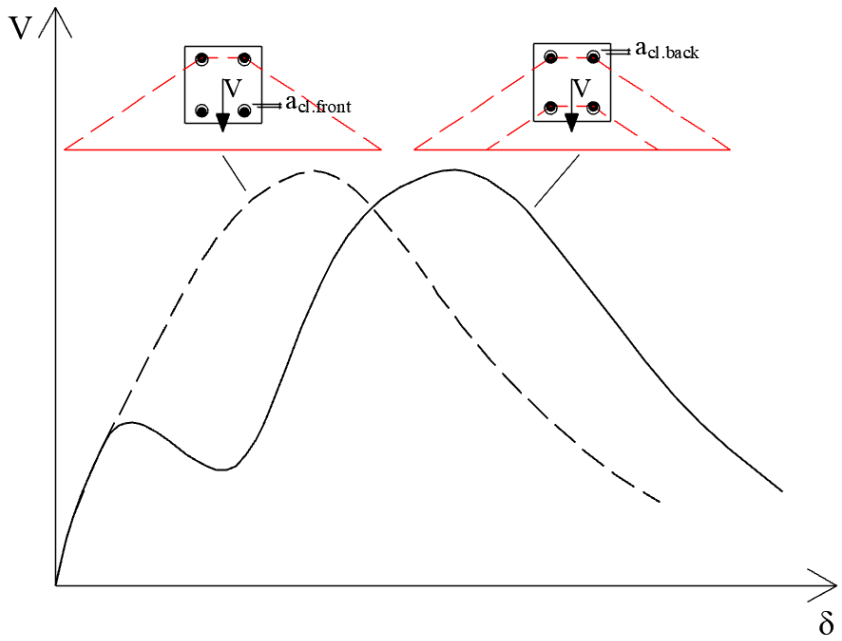

Figure 2.14. Load-displacement behaviour of a 2×2 anchor group having favourable and unfavourable hole clearance pattern

The behaviour of anchor groups with different spacing to front row edge distance ratios ($s_{1.1}/c_{1.1}$) failing due to concrete edge breakout, was investigated by Grosser (2012). It was summarised that for anchor groups without hole clearance, the crack formation at the front anchor may be neglected for the ultimate limit state (ULS) verification, however, the performance of the group should be checked for the serviceability limit state (SLS) verification. In the case of tests with hole clearance, the focus of the study was on the displacement at the failure of the corresponding single anchor to the hole clearance ratio. It was reported that if the activation of the back anchor is possible before the failure of the front anchor occurs, then the shear load can be redistributed to the back anchor and the anchors are loaded equally. The approach, to not only focus on the failure loads, but also on the displacement behaviour of the different anchor rows is deemed appropriate, and concurrently highlights the importance of the evaluation of the

complete load-displacement behaviour of anchorages. However, to presume whether a crack at the front anchor row will form or not, Grosser (2012) evaluated the resistance of the front row compared to the resistance of the back row for the corresponding $s_{1.1}/c_{1.1}$ (anchor spacing in the loading direction to edge distance of the front anchor) ratios.

2.3 BEHAVIOUR OF ANCHORAGES UNDER INCLINED LOADS (INTERACTION)

The behaviour of anchorages subjected to combined tension-shear loads (interaction) is a combination of the behaviour of the anchorage under concentric tension and shear loading and is dependent on the loading angle. The failure modes associated individually with tension or shear loads are possible in different combinations under inclined loads: for example, steel-steel, concrete-steel, concrete-concrete, steel-concrete (tension-shear). For large embedment depths and large edge distances, typically, the combination of steel-steel failure is dominant. For medium embedment depths and large edge distances, the concrete-steel failure combination is typical. The combination of concrete-concrete failure mode is governing in the case of anchorages placed close to the concrete edge having relatively small embedment depths. The failure combination steel-concrete is theoretically associated with anchorages placed close to the concrete edge, having large embedment depths in a combination with small anchor diameters. The actual influence of the tension component to the shear capacity and vice-versa is dependent on the failure mode. The interaction between the tension and shear capacity of an anchorage is typically considered through a so-called interaction equation (see ***Eq. 1***). The influence of the failure mechanism on the interaction between tension and shear capacity is considered through the exponent α.

$$\left(\frac{N_u}{N_{Rm}}\right)^{\alpha} + \left(\frac{V_u}{V_{Rm}}\right)^{\alpha} \leq 1.0 \qquad \textbf{\textit{Eq. 1}}$$

Where

N_u is the tension component of the applied ultimate load

N_{Rm} is the mean tension resistance of the anchorage

V_u is the shear component of the applied ultimate load

V_{Rm} is the mean shear resistance of the anchorage

α is the exponent for interaction equation, which depends on the failure mode (α = 1.5 for concrete breakout failure mode according to EN 1992-4 assuming rigid base plate)

The behaviour of anchorages under inclined loads in the case of concrete-concrete failure combination was investigated by Zhao & Eligehausen (1992/1). For tension loaded anchorages undergoing concrete cone breakout, the concrete fracture is initiated at approximately 30 - 40% of the ultimate load. Similar behaviour is associated also for shear loaded anchorages in case of concrete edge breakout. For anchor groups with multiple anchor rows, placed close to the concrete edge and subjected to inclined loads towards the edge, the crack initiation from the front anchor row due to the shear component of the applied load might occur at relatively low load level compared to the ultimate shear capacity of the group (*Figure 2.15*). This crack might have

a negative influence on the group capacity under the tension component of the applied load. Zhao & Eligehausen (1992/1) provide this behaviour as an explanation why the exponent α assumes a value of 1.5 in case of concrete-concrete breakout failure, while a value of 2.0 is valid in case of steel-steel failure. Relatively recent tests performed by Sharma et al. (2019) confirmed the validity of the exponent $\alpha = 1.5$ in case of anchor groups formed by headed studs welded on the base plate.

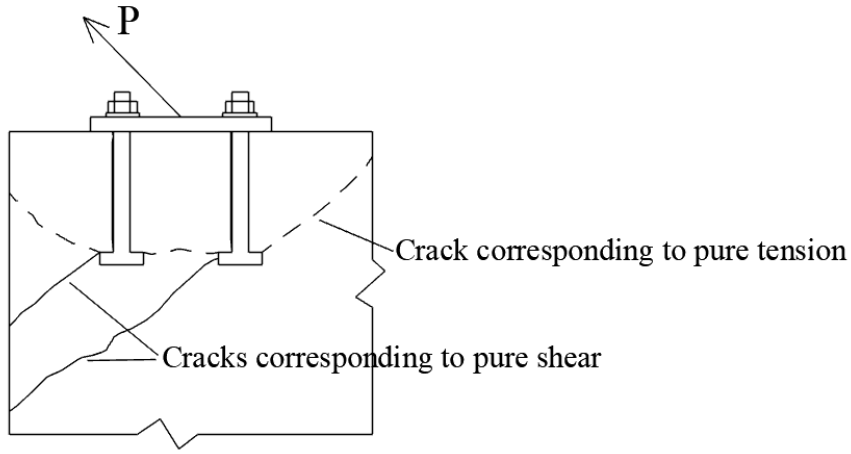

Figure 2.15.Schematic of a crack pattern of an anchor group close to an edge subjected to inclined loading (reproduced based based on Zhao, Eligehausen 1992/1)

Lachinger (2012) investigated the behaviour of 2×2 anchor groups placed close to the edge and installed with the most unfavourable hole clearance pattern. He explained that the behaviour of anchor groups with unfavourable hole clearance pattern under inclined loads is significantly affected by the ratio of anchor embedment depth to edge distance of the front anchor row. In the case of anchor groups with relatively short embedment depth, the failure cracks developing from the front anchor row (*Figure 2.16.a*) would have a much stronger negative influence on the tension capacity of the anchorage compared to the corresponding anchorage with larger embedment depth (*Figure 2.16.b*). Therefore, the consideration of the hole clearance pattern is essential for the assessment of anchorages under inclined loads.

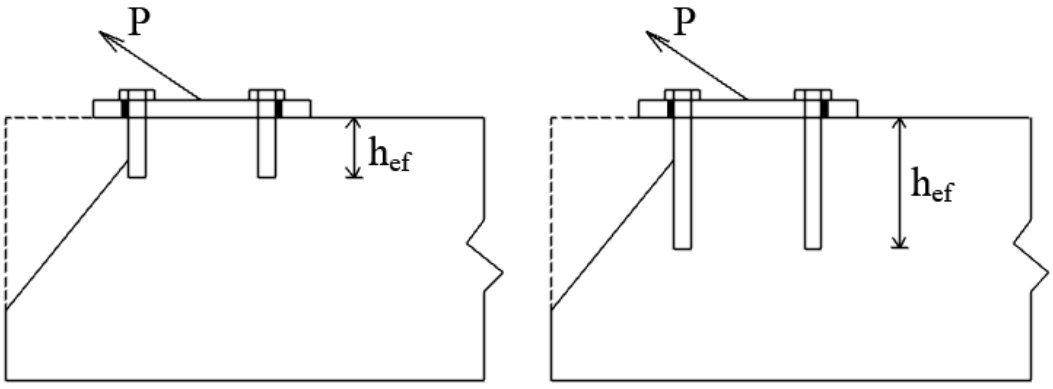

a) ***b)***

Figure 2.16. Influence of embedment depth on the interaction behaviour of 2×2 anchor groups placed close to an edge and installed with most unfavourable hole clearance pattern: a) small embedment depth, b) large embedment depth (reproduced based on Lachinger, 2012, Lachinger & Bergmeister, 2014)

Another important aspect that must be considered while evaluating the performance of anchorages under inclined loads is the base plate stiffness. The base plate stiffness influences the behaviour of the anchorage under the tension component of the applied load significantly. The behaviour under the shear component, however, remains largely uninfluenced by the base plate stiffness. Therefore, the influence of base plate stiffness would be more pronounced for the cases with lower values of loading angle with respect to the vertical. Therefore, the exponent $\alpha = 1.5$ used in the interaction equation for concrete-concrete breakout failure mode is valid provided a sufficiently stiff base plate is used and might not be applicable in case of anchor groups with flexible base plates.

Based on the above discussion it is clear that the behaviour of anchor groups placed close to the concrete edge subjected to inclined load towards the edge is influenced by the following parameters and the combination thereof: edge distance, anchor spacing, anchor embedment depth, anchor size, anchor stiffness, base plate stiffness, hole clearance pattern. Therefore, for realistic and reliable design of anchorages, it is essential to consider the load-displacement behaviour of the anchors under tension and shear.

2.4 SUMMARY

In this chapter, the behaviour of anchorages in concrete, in general, is briefly summarized. The load transfer mechanism of anchorages under tension, shear and inclined load (interaction) is discussed, and the typical failure modes are described. The importance of a realistic consideration of base plate stiffness, anchor stiffness, hole clearance pattern and crack pattern is discussed. Special emphasis is placed on the load-displacement behaviour of anchors and anchor groups in the case of concrete breakout failure modes to highlight the fact that for the realistic and reliable design of anchorages the load-displacement behaviour of the anchors under tension and shear should be considered.

3 APPROACHES FOR THE DESIGN AND ASSESSMENT OF ANCHORAGES

The design of anchorages is, in general, performed according to force-based approaches, which are implemented in various standards such as the European Standard EN 1992-4 or the standard of the American Concrete Institute, ACI 318. However, depending on the application, anchorage configuration and the complexity of the design task, displacement-based or research-based approaches, as well as the Finite Element Method, might be necessary to apply to ensure a reliable, safe and realistic design of the anchorage. In Section 3.1, the development of force-based approaches is summarized, on which the current design provisions are based. Section 3.2 gives an overview of possible design solutions based on displacement-based approaches such as the component method and the equivalent spring model for anchorages. In Section 3.3, the design based on using the Finite Element Method is discussed.

3.1 FORCE-BASED APPROACHES

3.1.1 General safety concept

The design of anchorages, in general, is performed by considering all the possible failure modes that an anchor may undergo under applied action and evaluating the resistance of the anchorage against each failure mode. The failure modes for an anchorage loaded in tension are steel failure, concrete cone failure, pull-out, side face blow-out and splitting failure (Section 2.1.1). The failure modes, shear loaded anchorages can undergo are steel failure, pryout failure and concrete edge failure (Section 2.2.1). In the case of anchorages under inclined loading (interaction), failure modes associated individually with tension or shear loads are possible in different combinations as described in Section 2.3.

The design load is determined as the minimum value of the resistances calculated for each failure mode after applying the appropriate partial safety factors. The verification for tension, shear and interaction is to be performed separately. Following the design philosophy of EN 1990, when using the partial factor method, it shall be verified that, in all relevant design situations, no relevant limit state is exceeded when design values for actions or effects of actions and resistances are used in the design models (EN 1990). The design values are typically obtained by using the characteristic values, in combination with partial factors. Correspondingly, the following requirement must be fulfilled: $E_d \leq R_d$ (Design action ≤ Design resistance).

In this dissertation, the focus is placed on the concrete breakout failure modes, under tension, shear and inclined loads. Therefore, in the following, only failure modes associated with concrete breakout are discussed in detail. Further information on the design approaches for anchorages can be obtained from Eligehausen et al. (2006).

3.1.2 Concrete cone breakout failure of anchorages under tension loading

For the calculation of the failure load for anchorages undergoing concrete edge breakout under tension loading, numerous analytical approaches, based on various assumptions have been developed in the past (Courtois, 1969, Braestrup et al., 1976, Cannon et al., 1981, Pusill-Wachtsmuth, 1982, Rehm et al., 1992, Fuchs et al., 1995). Two general philosophies exist to predict the concrete cone failure load of a tension loaded anchorage: the 45° cone method (Courtois, 1969) and the concrete capacity design (CCD) method (Fuchs et al., 1995). For the 45° cone method, the concrete breakout resistance of an anchor is calculated assuming a conical surface taking the slope between the failure surface and concrete surface as 45°(*Figure 3.1a*). In the case of the CCD method, a four-sided pyramid failure surface, with a slope between the failure surface and the surface of the concrete member of approx. 35 ° (1:1.5) is assumed to calculate the concrete breakout resistance of an anchor (*Figure 3.1b*).

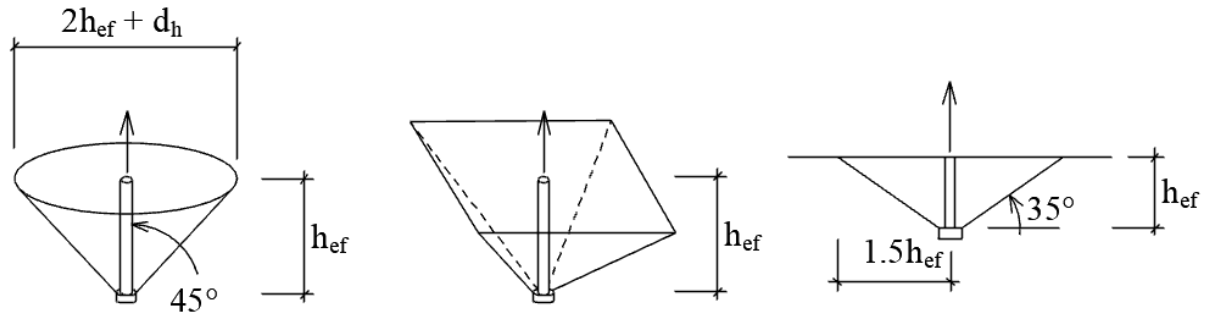

a) ***b)***

Figure 3.1. Concrete cone idealisation a) conical failure surface. b) four-sided pyramid failure surface (reproduced from Pallarés & Hajjar, 2009)

The first guides to calculate the resistance of anchors subjected to tension, shear and combined loads were proposed by Cannon et al. (1981). For tension loaded single anchors, the 45° failure cone was assumed in the formulations. The recommendations by Cannon et al. were adopted by the American Concrete Institute, ACI 349 (1980).

In the approach according to the American Concrete Institute, ACI 349 (1980 to 1997), the concrete cone was assumed to be a 45° cone for embedment depth higher than or equal to 5 inches (127 mm) initiating at the bearing edge of the anchor (anchor head) and radiating toward the free surface of the concrete member, and constant tensile stress over the projected failure surface was recommended (*Figure 3.2*). The nominal tensile strength of the anchorage, T_e, is determined by applying a nominal tensile strength to the projected area, A_p, of the pullout cone at the surface (***Eq. 2***).

$$T_e = 4 \cdot \sqrt{f_c'} \cdot A_p \text{ (lb)} \qquad \textbf{Eq. 2}$$

Where

$\sqrt{f_c'}$ is the square root of specified compressive strength of concrete, psi

A_p is the total projected area of the failure surface as described above, in^2

The projected area of the pullout cone is limited by the intersection of the cone with any free edge of the concrete *Figure 3.2*). To calculate the concrete cone resistance of a group, the projected area of the group, A_p, should be calculated, which is limited by the overlap of the individual anchor concrete cones, by the intersection with free edges and by the member thickness. The exact calculation of the projected area of the groups is difficult. Therefore, Marsh & Burdette (1985) and Siddiqui & Beseler (1989) provided an approximate method for calculating the projected area with overlapping failure cones in a simplified way.

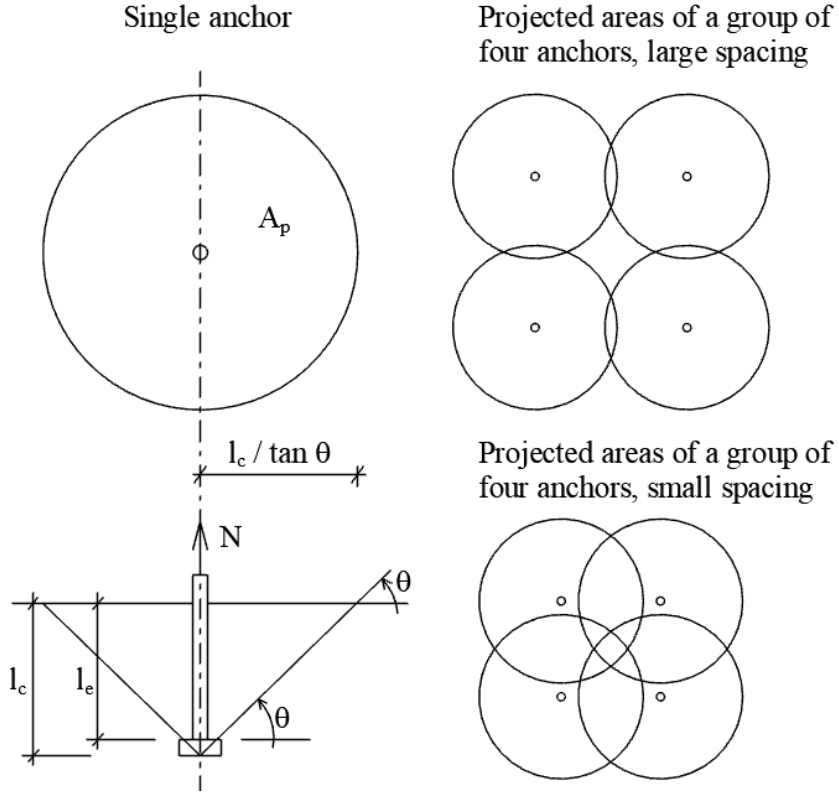

Figure 3.2. Shape of concrete cone according to ACI 349 (1990) and projected areas

However, the limitation of this approach is that it becomes unconservative for large embedment depths since the size effect is neglected. Ožbolt (1990) investigated numerically the influence of considering size effect on the capacity of an anchorage. He showed that it is reasonable to consider the highest possible size effect according to the Bažant´s size effect law (Bažant, 1994) while calculating the concrete cone breakout capacity of an anchorage. *Figure 3.3* gives a comparison of the failure load calculated following different approaches. It can be seen that neglecting the influence of size effect might lead to rather unconservative estimates of the failure loads for embedment depth larger than ca. 300 mm). Note that the recent versions of the ACI standards adopted the CCD method to calculate the concrete breakout resistance of anchorages (ACI 318, versions 2002 onwards).

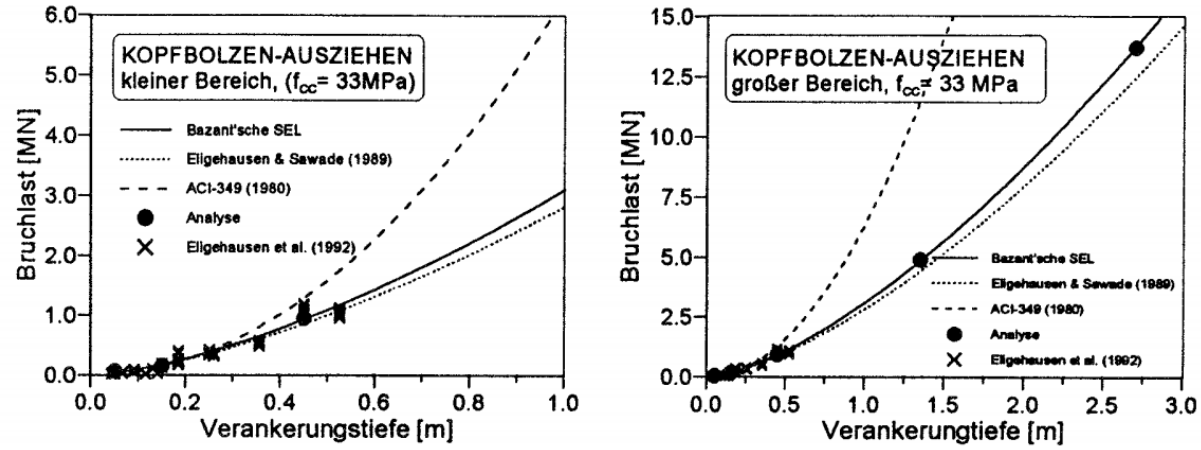

Figure 3.3. Comparison of failure loads calculated following different approaches: Vertical axis = Failure load in MN, Horizontal axis = Effective anchor embedment depth in m, (importance of considering size effect), (taken from Ožbolt, 1995)

Furthermore, the results of experimental and numerical investigations showed that the angle of the concrete cone breakout corresponds to approximately 35° instead of 45° as assumed earlier. To account for these two phenomena, a modified approach that came to be known as CCD Method was introduced (Fuchs et al., 1995). In principle, the CCD Method is based on the mechanical model used in the so-called κ-Method by Rehm et al. (1992). However, due to visualising the various influencing factors (known as κ-factors) used in the κ Method, the CCD Method is more user friendly. In the CCD Method, to include the size effect, the equation for concrete cone breakout was modified for a single anchor as follows:

$$N_{u,c}^{0} = k_1 \cdot {f_{cc,200}}^{0,5} \cdot k_2 \cdot {h_{ef}}^{2} \cdot \frac{k_3}{{h_{ef}}^{0,5}} \qquad \textbf{Eq. 3}$$

$$N_{u,c}^{0} = k \cdot {f_c}^{0,5} \cdot {h_{ef}}^{1.5} \qquad \textbf{Eq. 4}$$

Where,

$f_{cc,200}$ is the concrete compressive strength of a cube with a side length of 200 mm, N/mm^2

f_c is the cylinder compressive strength of concrete, N/mm^2

h_{ef} is the effective embedment depth of the anchor, mm

k, k_2 and k_3 are constants

${k_1 \cdot f_{cc,200}}^{0,5}$ specifies the concrete tensile capacity

${k_2 \cdot h_{ef}}^{2}$ considers the surface area of the failure cone

$\frac{k_3}{{h_{ef}}^{0,5}}$ considers the largest possible size effect of on failure load (Bažant 1984, Sawade & Eligehausen 1989, Eligehausen & Ožbolt 1990, Ožbolt 1995)

Recognizing the angle of the failure cone as approx. 35°, the projected area of the breakout body for a single anchor without any influence of a nearby edge or other anchors is defined as

the area of the square circumscribing an idealised projection of the concrete cone to the concrete surface (*Figure 3.4a*), which can be calculated according to ***Eq. 5***.

$$A_{c.N}^{0} = 9 \cdot (h_{ef})^2 \qquad \textbf{Eq. 5}$$

If the anchors are installed in a group with a common fixture with spacing larger than or equal to three times the embedment depth ($s \geq 3h_{ef}$), the developing adjacent concrete cones are not overlapping and for each anchor, a full-size concrete breakout body can form (*Figure 3.4b*). Consequently, the resistance of the group corresponds to "n"-times the concrete cone resistance of a single anchor. If, however, the anchors within a group are installed with spacing less than three times the embedment depth ($s < 3h_{ef}$), the adjacent concrete cones are intercepting and a common failure cone develops (*Figure 3.4c*). According to the CCD Method, the influence of the spacing on the group resistance is taken into account by the ratio $A_{c,N}/A_{c,N}^{0}$. The failure load of an anchor group away from the concrete edge and loaded in concentric tension is calculated according to ***Eq. 6***.

$$N_{u,c} = N_{u,c}^{0} \cdot \frac{A_{c,N}}{A_{c,N}^{0}} \qquad \textbf{Eq. 6}$$

$A_{c,N}^{0}$ is the reference projected area of a single anchor with a distance from all the edges equal to or greater than the critical edge distance $c_{cr,N} = 1.5h_{ef}$ (see ***Eq. 5***)

$A_{c,N}$ is the actual projected area for the group of anchors considering the spacing and edge distance from all sides

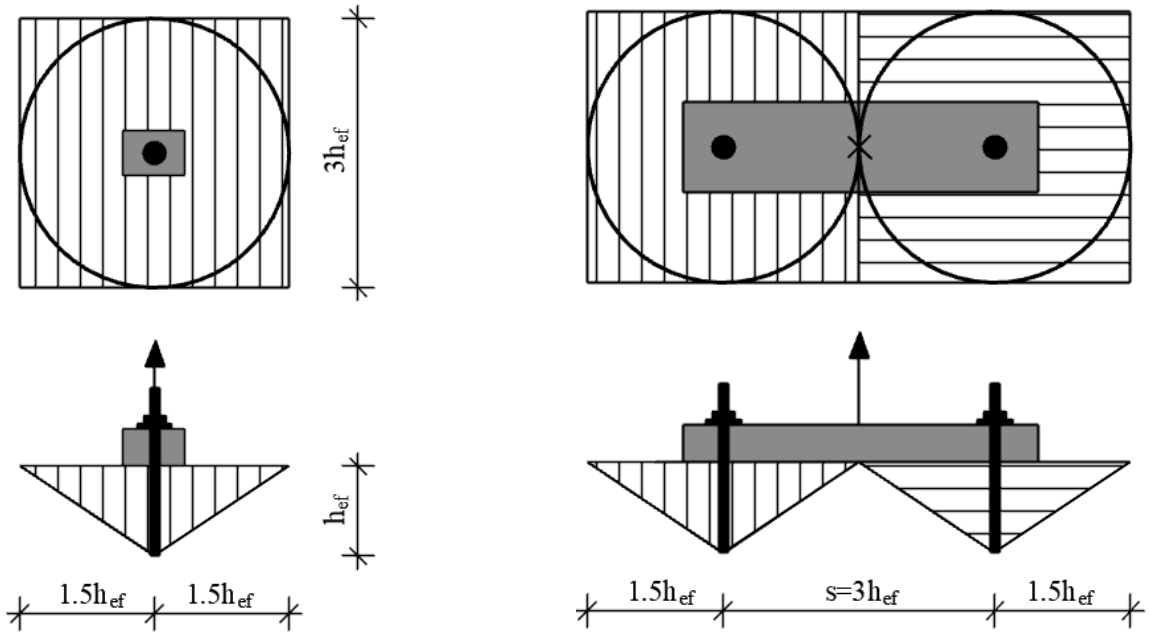

a) ***b)***

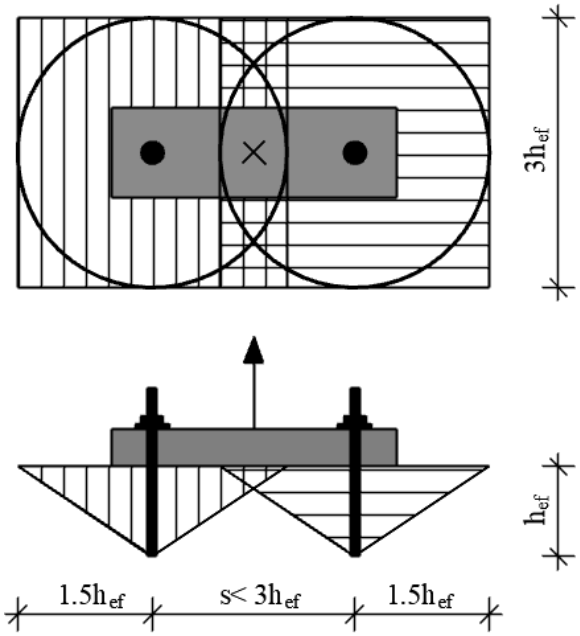

c)

Figure 3.4. a) Idealised concrete cone failure surface of a tension loaded a) single anchor, b) anchor group with $s \geq 3h_{ef}$, c) anchor group with $s < 3h_{ef}$ (reproduced based on Fuchs et al., 1995)

Figure 3.5 gives a comparison of analytical failure loads obtained for single anchors and for anchor groups with up to 36 headed studs following the CCD Method and the 45° cone method approach (ACI 349-1990) along with experimental values. The failure load is plotted as a function of the anchor spacing between outermost anchors. It can be seen that the failure load estimated by the CCD method follows the experimental values closely, while the 45° cone method generally overestimates the strength of the anchorages. This overestimation increases with increasing embedment depth due to size effect (Bažant 1984, Sawade & Eligehausen 1989, Ožbolt & Eligehausen 1990).

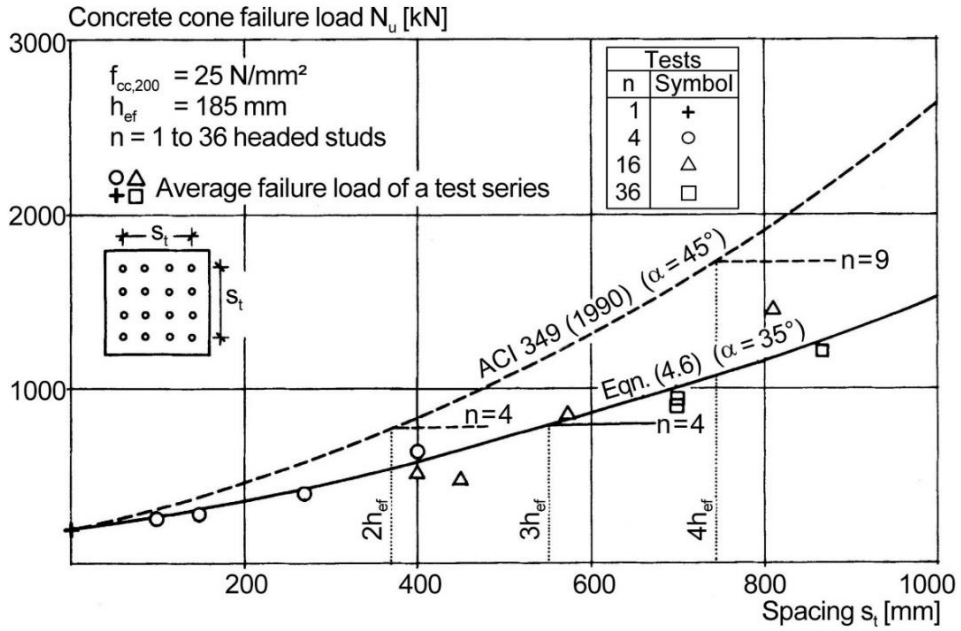

Figure 3.5. Comparison of failure loads calculated according to the 45° cone method and the CCD Method with test results (taken from Eligehausen et al., 2006)

If the free edge of the concrete member is located at a distance of less than the critical edge distance, ($c_{cr,N} < 1.5h_{ef}$) from the anchorage, it has a two-fold effect that leads to the reduction of concrete cone breakout resistance (Fuchs et al., 1995). On one hand, the complete concrete cone breakout body cannot form leading to a reduced projected area ($A_{c,N}$), while on the other hand, the state of stresses is disturbed compared to the rotationally symmetric case (compare *Figure 3.6* with *Figure 3.4c*). The geometric influence of reduced projected area is accounted for by the ratio $A_{c,N}/A^{0}_{c,N}$, whereas the influence due to disturbed stress state is considered by the multiplication factor $\psi_{s,N}$ defined by ***Eq. 7***.

$$\psi_{s,N} = 0.7 + 0.3\frac{c}{c_{cr,N}} \leq 1.0 \qquad \textbf{Eq. 7}$$

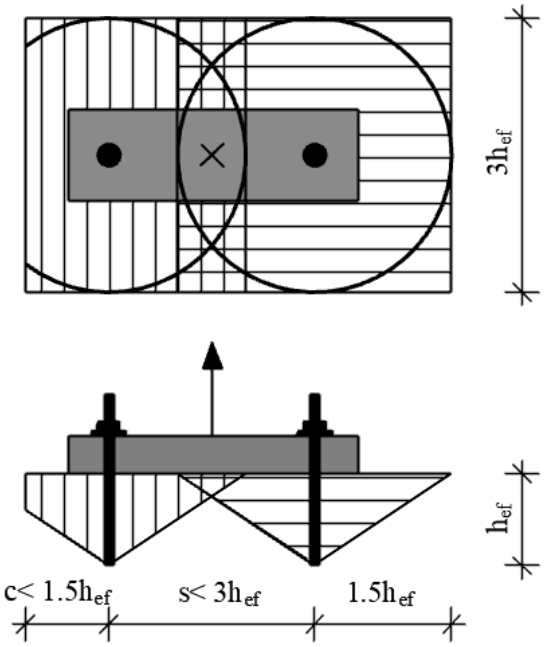

Figure 3.6. Influence of edge distance on the shape of the concrete breakout body

Note that the limiting value of $\psi_{s,N} = 0.7$, for $c = 0$ represents a theoretical case, where the free edge is considered equivalent to a crack passing through the anchor axis resulting in a reduction in the capacity by 30% (Eligehausen et al. 2006). Furthermore, according to the CCD Method, for anchor groups influenced by more than one close edges, the factor $\psi_{s,N}$ should be calculated for every close edge, and the minimum value should be applied in ***Eq. 7***. Interestingly, according to the κ-Method by Rehm et al. (1992), the corresponding κ-factor accounting for the influence of the vicinity of the concrete edge $\kappa_{ar,I}$ should be determined for every close edge and the product of the factors should be applied in ***Eq. 7***.

The point of application of the resultant tension loads on the anchorage may not coincide with the centre of gravity of the anchorage leading to an eccentric load situation. The eccentricity of the load alters the load-distribution on the anchors of a group with certain anchors being more loaded than the others and therefore results in a reduction in the load-carrying capacity of the anchorage. The influence of eccentricity on the concrete cone resistance under tension loads is

considered in the CCD Method through a reduction factor, $\psi_{ec,N}$ applied to the group capacity according to ***Eq. 8*** (Riemann, 1985).

$$\psi_{ec,N} = \frac{1}{1 + 2 \cdot e_N / 3 \cdot h_{ef}} \qquad \textbf{Eq. 8}$$

Where e_N is the eccentricity of resultant tension force of tensioned fasteners with respect to the centre of gravity of the tensioned fasteners. For anchorages loaded with a tension load eccentrically about both the orthogonal axis, 1 and 2 (biaxial eccentricity), the factor $\psi_{ec,N}$ is calculated in the two directions and multiplied. The product of the factors ($\psi_{ec,N} = \psi_{ec,N1} \cdot \psi_{ec,N2}$) should be applied in ***Eq. 8***.

Note that according to the CCD method, in the case of an anchor group with two anchor rows subjected to uniaxial eccentricity, if the loading is applied directly in line with one anchor row, the failure load of the group corresponds to the failure load of a single anchor irrespective of the spacing. This can be explained by the fact the factor $\psi_{ec,N}$ becomes equal to $A_{c,N}/A^0_{c,N}$ for $e_N = s/2$.

The general formulation of the CCD Method to calculate the concrete cone capacity of an anchorage in unreinforced concrete accounting for the influence of anchor embedment depth, concrete strength, anchor arrangement and spacing, vicinity of concrete edge, eccentric load application is given as ***Eq. 9***.

$$N_{u,c} = N^0_{u,c} \cdot \frac{A_{c,N}}{A^0_{c,N}} \cdot \psi_{s.N} \cdot \psi_{ec.N} \qquad \textbf{Eq. 9}$$

The CCD Method forms the basis of design procedures for anchors in various international codes and standards (EN 1992-4, ACI 318, ACI 349, fib Bulletin 58).

3.1.2.1 Design for concrete cone failure according to EN 1992-4

The design of anchorages for concrete cone failure under tension loads according to the European Standard EN 1992-4 is based on the CCD Method. The design is applicable if the following requirements are met:

(i) Within one anchor group, only anchors of the same type, size and embedment depth are used.

(ii) Only rectangular anchor groups with a maximum of three anchors in a row are allowed. The possible configurations are categorized according to anchor groups with or without hole clearance, edge distances and loading directions. *Figure 3.7* shows the permissible configurations of anchorages (post-installed and cast-in headed anchors).

(iii) The base plate should be sufficiently stiff.

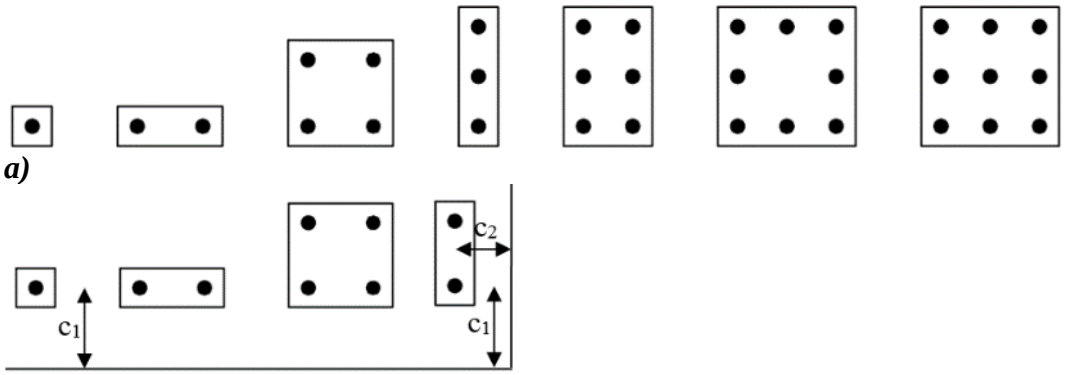

a)

b)

Figure 3.7. Permissible configurations according to EN 1992-4: a) fastenings without hole clearance for all edge distances and fastenings with hole clearance situated far from edges ($c_i \geq max\{10h_{ef}; 60d_{nom}\}$) for all load directions and fastenings with hole clearance situated near to an edge ($c_i < max\{10h_{ef}; 60d_{nom}\}$) loaded in tension only; b) fastenings with hole clearance situated near to an edge ($c_i < max\{10h_{ef}; 60d_{nom}\}$) for all load directions

According to EN 1992-4, the characteristic resistance of an anchor or an anchor group in case of concrete cone failure is calculated according to the following formula (***Eq. 10***):

$$N_{Rk,c} = N^0_{Rk,c} \cdot \frac{A_{c,N}}{A^0_{c,N}} \cdot \psi_{s,N} \cdot \psi_{ec,N} \cdot \psi_{re,N} \cdot \psi_{M,N} \qquad \textbf{Eq. 10}$$

Where, $N^0_{Rk,c}$ is the characteristic resistance of a single anchor placed in concrete and not influenced by adjacent anchors or edges of the concrete member

$$N^0_{Rk,c} = k_1 \cdot {h_{ef}}^{1,5} \cdot {f_{cm}}^{0,5} \qquad \textbf{Eq. 11}$$

k_1 is the empirical coefficient taken from the technical approval ($k_1 = k_{cr,N}$ for cracked concrete and $k_1 = k_{ucr,N}$ for uncracked concrete). Indicative values for $k_{cr,N}$ and $k_{ucr,N}$ are $k_{cr,N} = 7.7$ and $k_{ucr,N} = 11.0$ for post-installed and $k_{cr,N} = 8.9$ and $k_{ucr,N} = 12.7$ for cast-in headed fasteners

f_{ck} is the characteristic cylinder compressive strength of concrete in N/mm^2

h_{ef} is the effective embedment depth of the anchor in mm

The geometric effect of axial spacing and edge distance on the characteristic resistance is taken into account by the value $A_{c,N}/A^0_{c,N}$

$A^0_{c,N}$ see ***Eq. 5***

$A_{c,N}$ is the actual projected area for the group of anchors considering the spacing and edge distance from all sides

$\psi_{s,N}$ see ***Eq. 7***

$\psi_{ec,N}$ see ***Eq. 8***

$\psi_{re,N}$ shell spalling factor considering the influence of the presence of surface reinforcement

$\psi_{M,N}$ moment loading factor that takes into account the effect of a compression force between the fixture and concrete in case of bending moments with or without axial force

3.1.3 Concrete edge breakout failure of anchorages under shear loading

In general, the models for concrete edge breakout failure (pushout-cone failure) for shear loaded anchorages are analogous to the models for concrete cone failure of anchorages under tension. Some of the early works that focused on the concrete edge breakout failure mechanism were performed by Bailely & Burdette (1977), Swirsky et al. (1977), Cannon et al. (1981), Klinger et al. (1982) and Armstrong et al. (1985). Probably the first recognised method to calculate the concrete edge breakout resistance of anchorages was the 45° method, which was also incorporated in ACI 349 (1990). According to this method, the concrete edge breakout body (referred to as pushout-cone) is considered to initiate from the intersection point of the top concrete surface with the anchor longitudinal axis. The base angle, θ, of the pushout cone is taken as 45° (*Figure 3.8*). Constant tensile stress proportional to the square root of the concrete compressive strength is assumed over the breakout surface. The concrete edge resistance is obtained according to ***Eq. 12*** (see example in *Figure 3.8*). The projected area of the pushout cone is limited by the intersection of the cone with any other free edge of the concrete. The projected area of the group, A_p, is limited by the overlap of the individual anchor pushout cones and by the intersection with any other free edges.

$$V_e = 4 \cdot \sqrt{f_c'} \cdot A_p \text{ (lb)} \qquad \textbf{Eq. 12}$$

Where

$\sqrt{f_c'}$ is the square root of specified compressive strength of concrete, psi

A_p is the total projected area of the failure surface, in^2

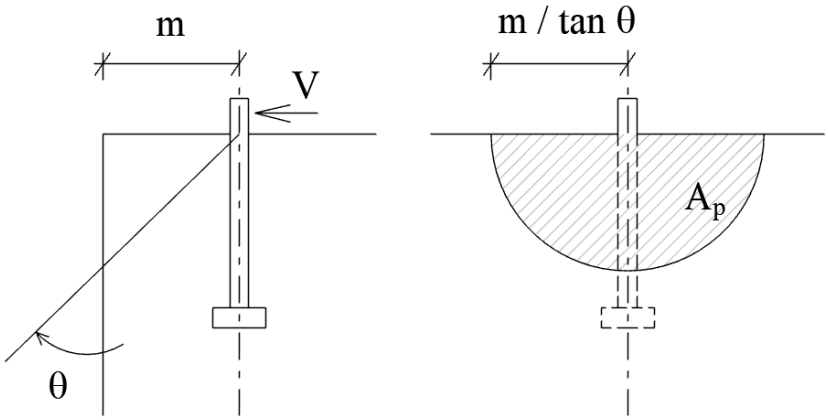

Figure 3.8. Shape of concrete pushout cone according to ACI 349 (1990) and projected area (reproduced based on Cook, 1989)

A similar approach was suggested by Klingner et al. (1982), where the concrete edge resistance of a single anchor is calculated as follows:

$$F_{uR} = 0.48 \cdot \sqrt{\beta_w} \cdot {a_r}^2 \text{ (N)} \qquad \textbf{Eq. 13}$$

Where

β_w is the compressive strength of concrete measured on cubes with a side length of 200 mm, N/mm^2

a_r is the edge distance, mm

Cannon et al. (1981) studied the variation of the angle of the breakout body as a function of edge distance. He proposed a linear variation of the failure cone angle from $\alpha = 25°$ for the theoretical value of $a_r = 0$ to an angle of $\alpha = 45°$ for $a_r = 127$ *mm* (5 inches). This was considered in the calculation of the projected area of the breakout body modifying ***Eq. 13*** to ***Eq. 14***.

$$F_{uR} = 0.48 \cdot \sqrt{\beta_w} \cdot (a_r + 0.5 \cdot d_B / \tan\alpha)^2 \text{ (N)} \qquad \textbf{Eq. 14}$$

Where

d_B is the diameter of anchor shaft, mm

Fuchs et al. (1995) extended the application of the CCD Method for anchorages under shear loads undergoing concrete edge breakout failure. Analogous to the tension model, the breakout angle was considered as approximately 35° (1:1.5), and the projected area of the breakout body was considered through a rectangle circumscribing the theoretical breakout body projected to the front edge (*Figure 3.9a*).

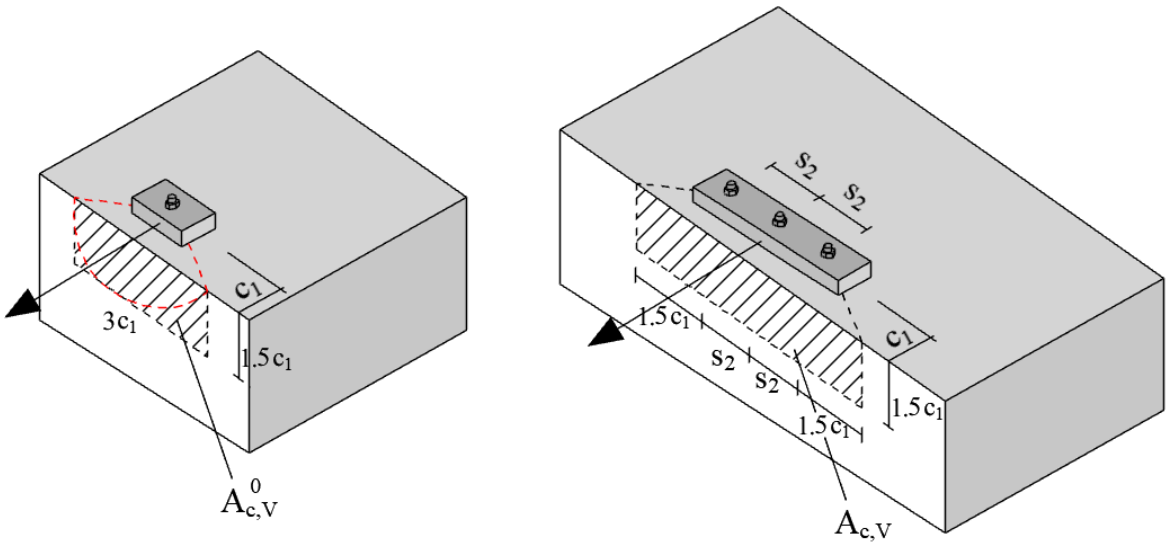

a) ***b)***

Figure 3.9. Shape of concrete breakout body and projected area of a single anchor and a 1×3 anchor group according to the CCD Method

The basic concrete edge breakout resistance of a single anchor not influenced by further edges or neighbouring anchors or by the limited thickness of the concrete specimen is given as:

$$V_{u,c}^0 = 0.9 \cdot \sqrt{d_{nom}} \cdot \sqrt{f_{cc,200}} \cdot \left(l_f / d_{nom}\right)^{0.2} {c_1}^{1.5} \ (N) \qquad \textbf{Eq. 15}$$

d_{nom} is the nominal anchor diameter, mm

l_f is the effective load transfer length, mm, $\leq 8 \cdot d_{nom}$

c_1 is the edge distance, mm

Note that the size effect in case of concrete edge breakout failure is considered in a similar way as in the case of tension loaded anchorages.

Based on a large number of experimental and numerical investigations, Hofmann (2005) showed that ***Eq. 16*** leads to an overestimation of the influence of anchor diameter, specifically for anchors with $d_{nom} > 25\ mm$. He proposed a modified equation to calculate the basic concrete edge breakout resistance:

$$V_{u,c}^{0} = 3.0 \cdot {d_{nom}}^{\alpha} \cdot {l_f}^{\beta} \cdot \sqrt{f_{cc,200}} \cdot {c_1}^{1.5} \qquad \textbf{Eq. 16}$$

$$\alpha = 0.1 \cdot (^{l_f}/_{c_1})^{0.5} \qquad \textbf{Eq. 17}$$

$$\beta = 0.1 \cdot (^{d_{nom}}/_{c_1})^{0.2} \qquad \textbf{Eq. 18}$$

If the anchors are installed in a group with a common base plate with spacing larger than or equal to three times the edge distance ($s_1 \geq 3c_1$), the developing adjacent concrete breakout bodies do not intercept and for each anchor, a full-size concrete breakout body can form and the resistance of the group corresponds to "n"-times the concrete edge breakout resistance of a single anchor. However, if the anchors within a group are installed with spacing less than three times the edge distance ($s_1 < 3c_1$), the adjacent concrete breakout bodies intercept and a common failure breakout body develops (*Figure 3.9b*). The influence of the spacing, as well as of further edge distances and partly the effect of thickness of the concrete member on the resistance on the group resistance is taken into account by the ratio $A_{c,V}/A_{c,V}^{0}$. The failure load of an anchor group loaded concentrically in shear towards the free edge is calculated according to ***Eq. 19***.

$$V_{u,c} = V_{u,c}^{0} \cdot \frac{A_{c,V}}{A_{c,V}^{0}} \qquad \textbf{Eq. 19}$$

Where,

$A_{c,V}^{0}$ is the reference projected area of a single anchor calculated as:

$$A_{c,V}^{0} = 4.5 \cdot {c_1}^{2} \qquad \textbf{Eq. 20}$$

$A_{c,V}$ the projected area of the idealised concrete breakout body, limited by the overlapping concrete breakout bodies of adjacent anchors ($s \leq 3c_1$) as well as by edges parallel to the loading direction ($c_2 \leq 1.5c_1$) and by member thickness ($h \leq 1.5c_1$)

In the case of shear loaded anchorages placed in the corner of a concrete member or in a narrow component, the concrete breakout body (that develops in the case of one close edge) cannot fully develop, and the concrete fracture surface may be restricted leading to further stress disruptions (Rehm et al., 1992, Fuchs, 1990, Paschen & Schönhoff, 1983, Zhao et al., 1989). This applies when the distance to the edge parallel to the load direction is smaller than 1.5-times the edge distance in the loading direction ($c_2 < 1.5c_1$). The critical value $c_2 < 1.5c_1$ corresponds to a fracture angle of 35° assumed in the CCD Method. The geometric influence of reduced projected area is accounted for by the ratio $A_{c,V}/A_{c,V}^{0}$ with the limit condition $c_2 = 0$ representing a theoretical case, where the breakout cone associated with a shear loaded anchor in a corner is reduced by 50%. Furthermore, the disrupted stress state leads to further capacity reduction,

which is considered in a manner similar to that adopted for tension loads by the multiplication factor $\psi_{s,V}$ defined by ***Eq. 21***.

$$\psi_{s,V} = 0.7 + 0.3\frac{c_2}{1.5 \cdot c_1} \leq 1.0 \qquad \textit{Eq. 21}$$

When anchorages are installed in a concrete member with limited thickness, the formation of the concrete breakout body is restricted leading to a reduction in the anchorage capacity (Eligehausen et al., 2006). The geometric influence of the limited thickness is accounted for by the ratio $A_{c,V}/A_{c,V}^0$. However, the concrete edge resistance does not decrease proportionally to the member thickness as assumed by the ratio $A_{c,V}/A_{c,V}^0$ (Hofmann, 2004, Zhao & Eligehausen, 1992/2, Zhao et al., 1989, Eligehausen et al. 2003). To account for this influence, ***Eq. 19*** should be multiplied by the factor $\psi_{h,V}$.

$$\psi_{h,V} = (\frac{1.5 \cdot c_1}{h})^{0.5} \geq 1.0 \qquad \textit{Eq. 22}$$

In the case of anchor groups placed close to the free edge and loaded in eccentric shear towards the edge, the influence of the eccentric load application on the concrete breakout resistance can be calculated in a manner similar to that proposed by Riemann (1985) for the tension case (see ***Eq. 8***). The reduction factor accounting for the influence of eccentric shear loading is $\psi_{ec,V}$, that takes into account a group effect when different shear loads are acting on the individual anchors of a group.

$$\psi_{ec,V} = \frac{1}{1 + {2 \cdot e_V}/{3 \cdot c_1}} \qquad \textit{Eq. 23}$$

Where,

e_V is the eccentricity of the resulting shear load acting on the anchors relative to the centre of gravity of the anchors loaded in shear, mm

Several research activities have been done to investigate the influence of the loading angle of shear loaded anchorages close to the edge. If the anchorage is subjected to a shear force acting parallel to the free concrete edge, a splitting force acting perpendicular to the edge is generated corresponding to ca. 50% of the applied shear force (Stichting Bouwresearch, 1971, Fuchs, 1990). This means that the resistance of the anchorage placed close to the free edge and is loaded parallel to the free edge is two times the capacity of the corresponding anchorage loaded perpendicular towards the edge. The influence of inclined loading is considered by the factor $\psi_{\alpha,V}$, in the CCD Method. However, note that the formulation was not verified loading angles other than 0 and 90°.

$$\psi_{\alpha,V} = 1.0 \qquad \text{for } 0° \leq \alpha_V \leq 55° \qquad \textit{Eq. 24}$$

$$\psi_{\alpha,V} = 1/(cos\alpha_V + 0.5 \cdot sin\alpha_V) \qquad \text{for } 55° \leq \alpha_V \leq 90°$$

$$\psi_{\alpha,V} = 2.0 \qquad \text{for } 90° \leq \alpha_V \leq 180°$$

α_V is the angle between design shear load and a line perpendicular to the verified edge.

Based on a large number of experimental and numerical investigations, Hofmann (2004) showed that the concrete pressure generated by the anchor influences the ratio concrete breakout load of an anchor loaded in shear parallel to the edge to the value valid for loading perpendicular to the edge. The concrete pressure generated by the anchor depends on the size of the compressed concrete area and is proportional to the square of the anchor diameter. According to Hofmann (2004) the linear interaction equation ***Eq. 24*** is conservative and a more accurate prediction is given by a quadratic interaction equation:

$$\left(\frac{V_u^{\alpha} \cdot cos\alpha}{V_{u,perpendicular}}\right)^2 + \left(\frac{V_u^{\alpha} \cdot sin\alpha}{V_{u,parallel}}\right)^2 = 1.0 \qquad \textit{Eq. 25}$$

The general formulation of the CCD Method to calculate the concrete edge breakout resistance of an anchorage in unreinforced concrete accounting for the influence of concrete edge distance, anchor embedment depth, anchor diameter, concrete strength, anchor arrangement and spacing, vicinity of further concrete edges, eccentric load application, the influence of limited member thickness and influence of inclined load application is given as ***Eq. 26***.

$$V_{u,c} = V_{u,c}^0 \cdot \frac{A_{c,V}}{A_{c,V}^0} \cdot \psi_{s,V} \cdot \psi_{h,V} \cdot \psi_{ec,V} \cdot \psi_{\alpha,V} \qquad \textit{Eq. 26}$$

3.1.3.1 Design for concrete edge failure according to EN 1992-4

The design of anchorages for concrete edge breakout failure under shear loads according to the EN 1992-4 is based on the CCD Method. The design is applicable if the following requirements are met:

(i) Only rectangular anchor groups are permissible. For anchorages without hole clearance, the maximum permissible anchor pattern is with three anchors in a row, and for anchorages with hole clearance, a maximum of only two anchors in a row is allowed (see *Figure 3.7*)

(ii) Only anchors closest to the free edge loaded in shear are assumed to be effective for the verification of concrete edge failure if the anchor is located close to the free edge ($c < max\{10h_{ef}; 60d_{nom}\}$) and loaded perpendicular towards the edge

(iii) The minimum spacing of the anchors in a group should be $s_{min} \geq 4d_{nom}$

(iv) For anchorages with more than one edge, the verification shall be carried out for all edges.

According to the EN 1992-4, the characteristic shear resistance of an anchorage in case of concrete edge failure is calculated according to the following equations:

$$V_{Rk,c} = V_{Rk,c}^0 \cdot \frac{A_{c,V}}{A_{c,V}^0} \cdot \psi_{s,V} \cdot \psi_{h,V} \cdot \psi_{ec,V} \cdot \psi_{\alpha,V} \cdot \psi_{re,V} \qquad \textit{Eq. 27}$$

Where,

$V_{Rk,c}^0$ is the characteristic resistance of a single anchor in case of concrete edge failure in uncracked concrete without any influences and is calculated according to ***Eq. 28***.

$$V_{Rk,c}^{0} = k_9 \cdot {d_{nom}}^{\alpha} \cdot {l_f}^{\beta} \cdot \sqrt{f_{ck}} \cdot {c_1}^{1.5} \qquad \textbf{Eq. 28}$$

k_9 is the empirical coefficient, $k_9=1.7$ for cracked concrete and $k_9=2.4$ for uncracked concrete

$l_f = h_{ef}$ in case of uniform diameter of the shank of the headed fastener and a uniform diameter of the post-installed fastener, $l_f \leq 12 d_{nom}$ if $d_{nom} \leq 24\ mm$
and $l_f \leq max\ (8d_{nom}, 300\ mm)$ if $d_{nom} > 24\ mm$

$A_{c,V}^{0}$ see ***Eq. 20***

$A_{c.V}$ is the actual projected area for the group of anchors considering the spacing, edge distance from all sides and geometric influence of member thickness, mm^2

$\psi_{s,V}$ see ***Eq. 21***

$\psi_{h,V}$ see ***Eq. 22***

$\psi_{ec,V}$ see ***Eq. 23***

$\psi_{\alpha,V}$ see ***Eq. 24***

$\psi_{re,V}$ factor takes account of the effect of the reinforcement located on the edge.

Note that in case of anchor groups with multiple anchor rows, according to the approach given in EN 1992-4, the failure load corresponding to the concrete edge failure is calculated by assuming the failure crack originating from the front anchor row, whereas according to the approach followed by the fib Bulletin 58 and ACI 318-19, the failure crack initiation can be assumed from the front, middle or back anchor row. However, if the failure crack is considered to appear from the back or mid anchor row, only the anchors not located in the theoretical breakout body can be considered to resist shear loads for the verification for steel failure.

3.1.4 Concrete breakout failure of anchorages under inclined loading (tension-shear interaction)

The behaviour of anchorages subjected to inclined loads (tension-shear interaction) was studied by McMakin et al. (1973) through performing experimental tests on headed stud anchors and an elliptical interaction equation was proposed. Further tests were done by Bode & Hanenkamp (1985) to investigate the load-bearing behaviour of headed studs with a large edge distance subjected to combined tension and shear loads. Bode & Roik (1987) proposed a tri-linear equation to describe the behaviour of anchors under inclined loads. Zhao & Eligehausen (1992/1) evaluated the results of interaction tests performed on single anchors as well as on groups of 2 and 4 anchors. They segregated the tests based on the failure modes such as steel-steel, steel-concrete, concrete-steel and concrete-concrete failure under tension-shear combination. Lotze & Klinger (1997) studied the load-bearing behaviour of torque-controlled expansion anchors and undercut anchors.

The verification of anchorages subjected to combined tension and shear loading (interaction) is performed through a so-called interaction equation. In general, two types of interaction equations are recommended in the design provisions for anchorages, namely a tri-linear or an elliptical equation. In the case of a tri-linear interaction curve, the anchorage need not be verified for interaction if the tension or shear load applied to the anchor is smaller than 20% of the ultimate strength in tension or shear, respectively. If the tension component, *N*, of the applied load is larger than 20% of the tension capacity, N_u, and the shear component, *V*, of the applied load is larger than 20% of the shear capacity, V_u, then the following equation should be satisfied to verify the anchorage for interaction:

$$\frac{N}{N_u} + \frac{V}{V_u} \leq 1.2 \qquad \textit{Eq. 29}$$

Alternatively, the elliptical interaction can be used, as given in ***Eq. 30***. The influence of the failure mechanism on the interaction between tension and shear capacity is considered through the exponent α.

$$\left(\frac{N}{N_u}\right)^{\alpha} + \left(\frac{V}{V_u}\right)^{\alpha} \leq 1.0 \qquad \textit{Eq. 30}$$

An exponent equal to 5/3 on both the tensile and shear strength was proposed by McMakin et al. (1973) for the elliptical interaction equation irrespective of failure modes. Zhao & Eligehausen (1992/1) suggest using an exponent $\alpha = 2.0$ (circular interaction) for steel-steel combined failure mode, $\alpha = 1.5$ for concrete-steel combined failure mode, $\alpha = 1.5$ for concrete-concrete combined failure mode (anchorage far from edge) and $\alpha = 1.2$ for concrete-concrete combined failure mode (anchorage close to edge) under tension and shear loads.

3.1.4.1 Design for concrete breakout failure of anchorages under inclined loading according to EN 1992-4

The design for concrete breakout failure of anchorages under combined tension and shear loading according to EN 1992-4 is performed by verifying the following equation.

$$\left(\frac{N_{Ed}}{N_{Rd,i}}\right)^{\alpha} + \left(\frac{V_{Ed}}{V_{Rd,i}}\right)^{\alpha} \leq 1.0 \qquad \textit{Eq. 31}$$

Where

N_{Ed} is the tension component of the design action

$N_{Rd,i}$ is the design tension resistance of the anchorage for ith failure mode

V_{Ed} is the shear component of the design action

$V_{Rd,i}$ is the design shear resistance of the anchorage for ith failure mode

The subscript "*i*" represents a particular failure mode.

α is the exponent for the interaction equation, which depends on the failure mode

$\alpha = 2.0$ for anchor steel failure

α = *1.5* for failure modes other than anchor steel failure

Alternatively, EN 1992-4 allows to use a tri-linear interaction relationship for verification of failure modes other than steel failure:

$$\left(\frac{N_{Ed}}{N_{Rd,i}}\right)+\left(\frac{V_{Ed}}{V_{Rd,i}}\right)\leq 1.2 \qquad \textit{Eq. 32}$$

with $\frac{N_{Ed}}{N_{Rd,i}}\leq 1.0$ and $\frac{V_{Ed}}{V_{Rd,i}}\leq 1.0$

3.2 DISPLACEMENT-BASED METHODS

3.2.1 Component method for the design of steel-to-concrete joints

The component method proposed by Kuhlmann et al. (2014) for the design of steel to concrete joints uses a network of springs to represent the behaviour of headed studs embedded in concrete under tension loads. For a headed stud without supplementary reinforcement, three springs connected in series represent the anchor load-displacement behaviour (see *Figure 3.10*). The first spring simulates the steel elongation (component S), the second spring captures the pullout behaviour (component P) and the third spring considers the displacements due to concrete cone breakout (component CC).

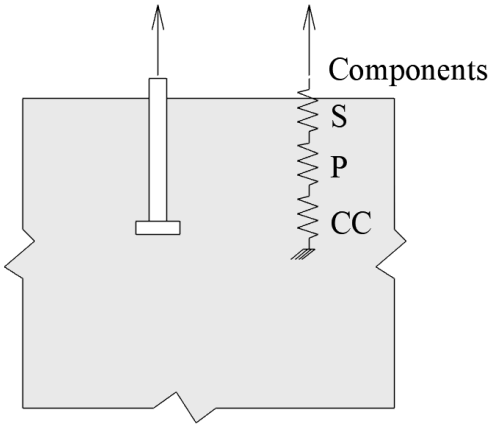

a)

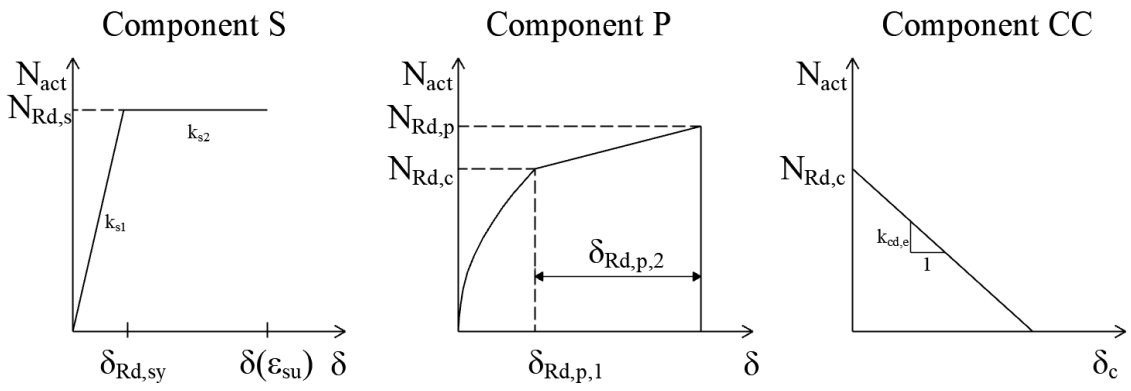

b) ***c)*** ***d)***

Figure 3.10. Components of anchorages embedded in concrete, a) spring component model, b) component S, c) component P, d) component CC according to Kuhlmann et al. (2014)

The steel component assumes an elastic-perfectly plastic behaviour to simulate the elongation of the shaft headed stud (see *Figure 3.10b*). The design yield load can be calculated as:

$$N_{Rd,s} = A_{s,nom} \cdot \frac{f_{uk}}{\gamma_{Ms}} = \pi \cdot \left(\frac{d_{s,nom}^2}{4}\right) \cdot \frac{f_{uk}}{\gamma_{Ms}} \qquad \textit{Eq. 33}$$

Where

$A_{s,nom}$ is the cross-sectional area of the shaft of the headed stud, mm^2

f_{uk} is the characteristic ultimate strength of the shaft material, N/mm^2

γ_{Ms} is the partial safety factor for steel

Until design yield strength, the anchor elongates with its elastic properties. Displacement corresponding to yield load is given as

$$\delta_{Rd,sy} = \frac{N_{Rd,s} \cdot L_h}{A_{s,nom} \cdot E_s} = \frac{\sigma_{Rd,s} \cdot L_h}{E_s} \qquad \textit{Eq. 34}$$

L_h is the length of the anchor shaft measured from the point of loading to the top of the anchor head, mm

E_s is the elastic modulus of the steel, E_s = 210 000 N/mm²

To consider the deformations due to the local crushing, the spring simulating the pullout component is represented by the nonlinear load-displacement curve, which is divided into two range of loads (see *Figure 3.10c*). The design failure load corresponding to pull-out failure is determined as:

$$N_{Rd,p} = p_{uk} \cdot \frac{A_h}{\gamma_{Mc}} \qquad \textit{Eq. 35}$$

p_{uk} is the characteristic ultimate bearing pressure at the headed of the stud in N/mm^2 $\mathrm{p_{uk}} = 12 \cdot \mathrm{f_{ck}}$

A_h is the bearing area on the head of the headed stud, mm^2 $\mathrm{A_h} = \frac{\pi}{4} \cdot (\mathrm{d_h^2} - \mathrm{d_s^2})$

d_h is the diameter of the head of a headed stud, mm

d_h is the diameter of the shaft of a headed stud, mm

γ_{Mc} = 1.5 partial safety factor for concrete

Until the concrete cone breakout initiates, the stiffness of the stud is high and later it reduces. Two load ranges are considered: $N_{act} \leq N_{Rd,c}$ and $N_{Rd,c} < N_{act} \leq N_u$

For the first range ($N_{act} \leq N_{Rd,c}$ and $\delta \leq \delta_{Rd,p,1}$), the load-displacement relationship is defined as:

$$\delta = k_p \cdot \left(\frac{N}{A_h \cdot f_{ck}}\right)^2 \leq \delta_{Rd,p,1} \qquad \textit{Eq. 36}$$

For the second range ($N_{Rd,c} < N_{act} \leq N_u$), the load-displacement relationship is defined as

$$\delta = 2k_p \cdot \left(\frac{N}{A_h \cdot f_{ck}}\right)^2 - \delta_{Rd,p,1} \qquad \textit{Eq. 37}$$

Where k_p considers the influence of the head size and the concrete condition (uncracked or cracked)

For the concrete cone component, no deformation is considered until the failure load is reached (see *Figure 3.10d*). This is reasonable since until the concrete cone capacity is reached (***Eq. 4***), the deformations are caused by the steel elongation or local crushing of concrete around the head, which are considered in the steel component and the pullout component, respectively. However, component CC is assuming a linear descending branch to take into account the deformations coming due to the concrete cone breakout failure in the post-peak phase. The degrading stiffness is given by the following equation:

$$k_{c,de} = \alpha_c \cdot \left[f_{ck} \cdot h_{ef}\right]^{0,5} \cdot \psi_{A,N} \cdot \psi_{s,N} \qquad \textit{Eq. 38}$$

α_c = - 537 is an empirical factor of component "concrete break out in tension"

h_{ef} is embedment depth of the anchorage, mm

f_{ck} is characteristic concrete compressive strength, N/mm²

At any load level N_{act}, the stiffness is calculated and the corresponding displacement can be determined.

3.2.2 Component model for the pull-out behaviour of a headed anchored blind bolt within concrete-filled circular hollow section by Oktavianus et al. (2017)

To model the behaviour of a headed anchored blind bolt (HABB) within concrete-filled circular hollow section (CFCHS), a component model for pull-out was proposed by Oktavianus et al. (2017). The approach was developed based on a multi-linear component spring model that is able to represent the behaviour of the components of a blind bolt such as the shank of the bolt, the embedded head and the washer, which is bearing on the inside of the tube wall (*Figure 3.11*). To develop and calibrate the nonlinear behaviour of each component for monotonic loading, in which the yield and ultimate strength and the initial and secant stiffness of each component were taken into account, Oktavianus et al. performed extensive finite element analyses using ABAQUS. The component spring model of a HABB connection proposed by Oktavianus et al. (2017) is shown in *Figure 3.11* that assumes the tensile behaviour of each component as a spring and ignores the bond between the bolt shank and the concrete. The ultimate pull-out strength of an individual HABB within a CFCHS is either determined by the strength of the free blind bolt or the combined strength of the tube wall and the headed anchor, therefore the springs in the model are connected as follows: The springs for the embedded bolt shank (3) and for the embedded head (4) are modelled in series corresponding to local concrete crushing or concrete cone failure and are modelled parallel to the spring accounting for the steel tube wall (2), and finally, the system of springs 2-3-4 is in series with the free blind-bolt spring (1). The pull-out behaviour of the HABB in CFCHS is modelled by assembling the springs provided

that the corresponding load-displacement curve of each spring is determined. Further details of the model can be taken from Oktavianus et al. (2017).

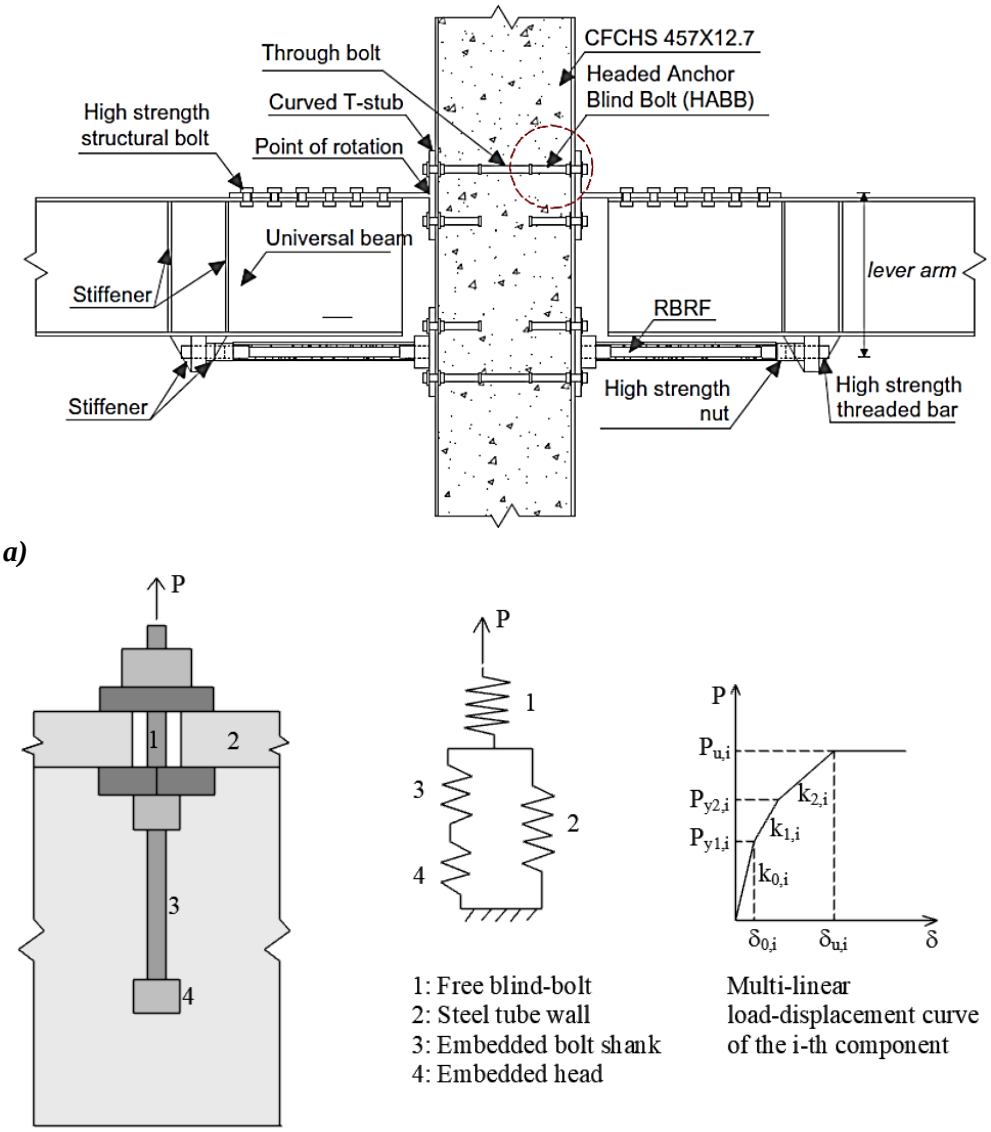

Figure 3.11. a) application of blind bolted T-stub connections, b) components of the spring component model (taken from and reproduced based on Oktavianus et al., 2017)

3.2.3 Equivalent spring model by Sharma (2013)

Sharma (2013) developed an equivalent spring model considering the anchor stiffness and anchor deformations over the complete linear-nonlinear range to describe the behaviour of anchor groups under tension loading. The equivalent spring model was then included in an assessment model to evaluate the seismic performance of joints retrofitted with fully fastened haunch retrofit solution (FFHRS) (*Figure 3.12*).

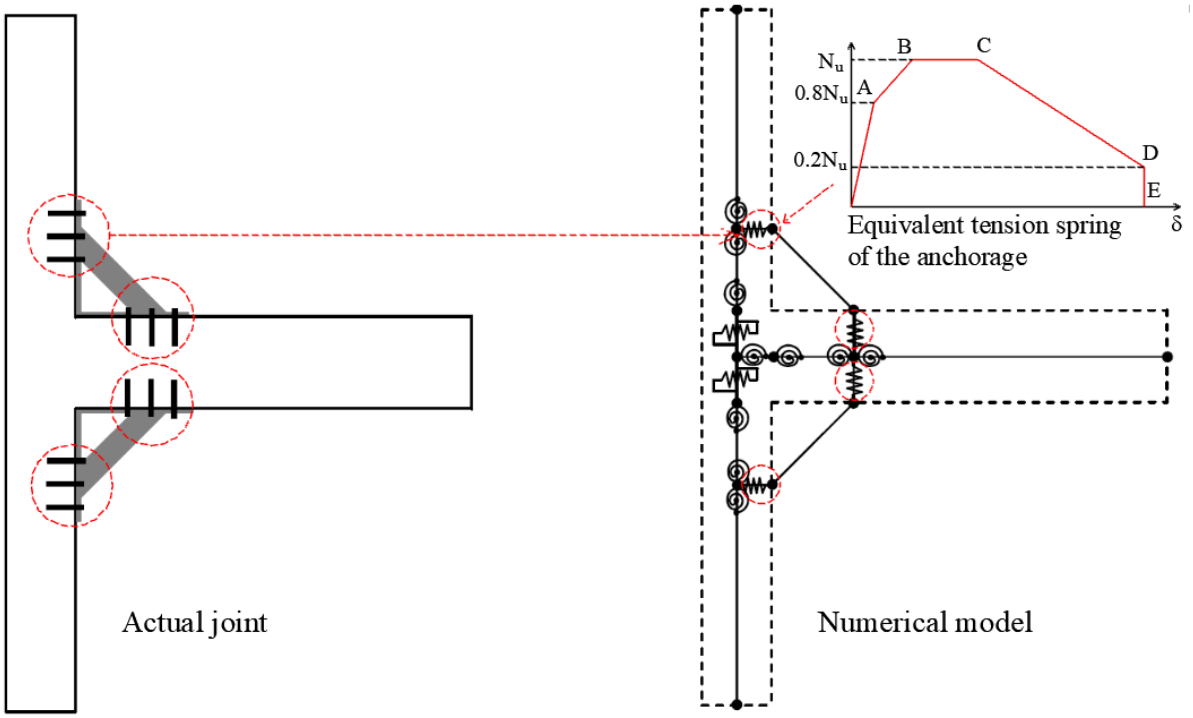

Figure 3.12. Equivalent spring model proposed to consider the anchorage behaviour for FFHRS (reproduced based on Sharma, 2013)

The anchor group behaviour is modelled by a single spring (circled in *Figure 3.12*), which offers a good solution for a relatively simplified model and can also predict the concrete cone/bond-slip behaviour of the group with sufficient accuracy. Several assumptions were taken to consider the anchorage behaviour realistically. The anchorage is modelled as axial spring because only tension loads are critical in the case of the designed anchorage. The axial spring representing the anchorage system is considered as stiff and linear elastic when loaded in compression to simulate that the developing compression is transferred through the bearing of the base plate on the concrete member. The possible failure modes for anchorages under tension loading are considered in the model such as steel failure, concrete cone failure and pull-out failure. The concrete cone breakout strength for anchor group, which is considered as the most critical failure mode for the anchors, is calculated using the formulations of the CCD Method at mean level (***Eq. 9***). Furthermore, due to the nature of the problem of seismic retro-fitting, cracked concrete should be assumed and the model is only applicable for anchors approved for the use in cracked concrete.

The characteristics for the equivalent spring to model anchorage behaviour are described by the nonlinear load-displacement behaviour of the anchor group (L-δ curve in *Figure 3.12*). For idealisation of the load-displacement response of the anchorage, a penta-linear format was used by Sharma, offering a good balance between accuracy and simplicity. The coordinates of load-displacement data-pairs A, B, C and D as shown in *Figure 3.12* are dependent on the failure mode of the anchor group. To consider the corresponding estimated failure mode in the model, the distance between points B and C as well as between points C and D should be varied. Furthermore, typical displacement values are recommended for anchors in uncracked and cracked concrete undergoing steel failure, pullout and pull-through failure, bond failure and concrete cone failure to consider the load-displacement behaviour reasonably.

The stiffness values of individual anchors are suggested to take from technical approvals or better from test results evaluating the stiffness of the anchors. To determine the group stiffness, further recommendations are given. In the case of steel failure, pull-out failure, pull-through and bond failure, the resistance of the anchors is not influenced by the adjacent anchors or by the vicinity of the edge of the concrete member. Therefore not just the resistance ($N_{group} = n \cdot N_{individual}$) but also the stiffness of the group can be obtained as n-times the stiffness of the individual anchor ($k_{group} = n \cdot k_{individual}$), where n corresponds to the number of anchors within the group. In the case of concrete cone failure, similar philosophy is proposed to estimate the group stiffness ($k_{0.5Nu}$ or k_{Nu}) as to consider the geometric influence of group effect: $k_{group} = A_{c,N}/A^{0}_{c,N} \cdot k_{individual}$. Once the equivalent model for the tension loaded anchorage is established, it can be used to model the anchorage behaviour in the proposed joint model (*Figure 3.12, right*).

The principle concept of the model was retained and used by other researchers for the idealisation of the load-displacement response of the anchorage as it is or with slight modifications to the format (Hofmann et al., 2015, Dwenger et al., 2016, Dwenger, 2019, Hofmann et al., 2020).

3.3 FINITE ELEMENT MODELLING

In the case where no standard rules for the design of anchorages are available, the Finite Element (FE) method can be used for the assessment and design of anchorages. However, as FE modelling is a powerful tool, it requires a careful understanding of the assumptions, the modelling rules and problem definition. For simulating concrete breakout failure modes, the FE analysis must be performed using FE codes incorporating constitutive laws and fracture criteria that can reasonably simulate the concrete behaviour under predominant tension failure. Note that the applied FE code should be well-proven and validated against experiments. Such codes were used, for example, in the work of Elfgren et al. (1989), Ožbolt & Eligehausen (1990), Cervenka et al. (1990), Hofmann (2005), Schmid (2010), Fichtner (2011), Grosser (2012), Nilforoush (2017), Jebara (2018), Tian (2019), Tóth (2020). For axisymmetric cases, 2-dimensional analysis can be performed to reduce the problem size and the computational time. However, performing a 3-dimensional analysis is always the best option to capture the behaviour of the anchorage.

The following components for anchorages in unreinforced concrete should be modelled carefully: (i) concrete specimen, (ii) anchors, (iii) contact or bond between anchor and concrete, (iv) base plate and attachments, (v) contact between the base plate and concrete, (vi) boundary conditions, (vii) loading scenario.

(i) Concrete specimen: The concrete specimen should be meshed in a way to enable the crack initiation and propagation to be captured in a reasonable way. The concrete can be meshed using solid finite elements. Generally, 4-node tetrahedral elements are considered appropriate for modelling the concrete as base material for anchorages because it allows for a relatively random orientation of the mesh. Typically, a relatively finer mesh is required in the critical zones where the crack might initiate and propagate from. To reduce the computational time, the zones away from the critical zones can be

meshed with a relatively coarse mesh. The choice of the mesh size depends on the overall dimensions of the problem such as anchor size and anchor spacing, edge distance, detailing of the base plate and attachment. To model the crack, a discrete crack approach (Ngo & Scordelis, 1967, Nilson, 1968) or a smeared crack approach (Rashid, Y: R., 1968, Bažant & Oh, 1983) may be followed with the latter being more popularly used because it does not require re-meshing after a crack has developed and therefore, this approach is computationally inexpensive. To ensure mesh objectivity, methods such as crack-band method (Bažant & Oh, 1983) can be employed. The concrete constitutive law should interact well with the analysis method used. Microplane model for concrete with relaxed kinematic constraint (Ožbolt et al., 2001) has been shown to be capable of a realistic assessment of anchorages in concrete under different loading conditions. The same model has been utilised to simulate the anchorage behaviour in this work (Section 9.3). The crack initiation is generally decided by the attainment of critical stress limits in the finite elements, while the fracture behaviour of the concrete is typically simulated through fracture energy-based criteria.

(ii) Anchors: The model of the anchor should be able to represent the load-transfer mechanisms under tension, shear and combined (tension-shear interaction) loading appropriately. The anchors should be modelled using 3-dimensional solid (tetrahedral or hexahedral) elements. The mesh should replicate the geometric features of the anchors depending on the anchor type. The material behaviour assumed for steel depends on the expected behaviour of the anchorages. If no yielding of the anchors is expected, a linear-elastic material behaviour can be used. Alternatively, to capture the material nonlinearity, an appropriate constitutive law, such as elastic-perfectly plastic or trilinear stress-strain curve can be used. A yield criterion such as von-Mises is generally associated with the constitutive law for steel. Furthermore, recent studies have shown the appropriateness of the microplane model for steel to capture the nonlinear as well as fracture behaviour of steel (Ožbolt et al., 2015).

(iii) Contact or bond between anchor and concrete: Depending on the type of the anchor, which is modelled, and the loading direction, the contact between the anchor and concrete should be modelled such that the load-transfer mechanism is considered appropriately. For example, in general, in the case of headed studs, the contact between the anchor and the concrete should be simulated using compression-only elements that do not take up any tension or shear forces. In the case of bonded anchors, the load-transfer is activated by the bond between the anchor and concrete. Therefore, bond elements that can transfer both compression and shear should be modelled between the anchor and concrete. This approach is used in this work, and further details are given in Section 9.3.

(iv) Base plate and attachments: The base plate and attachments should be modelled in a way that the model represents the geometric properties such as area, the moment of inertia, shear area, etc. as realistically as possible. The base plate should be modelled

using 3-dimensional solid (tetrahedral or hexahedral) elements. The material behaviour can be modelled in a similar way as for anchors, either as linear-elastic or, preferably, by associating the stress-strain law and yield criteria.

(v) Contact between the base plate and concrete: In the design of anchorages, the base plate is assumed to take up compression forces only, which develop between the base plate and the concrete. To account for this in the model, the contact between the base plate and the concrete should be simulated using compression-only elements that do not take up any tension or shear forces.

(vi) Boundary conditions: The boundary conditions should represent the actual support conditions of the test specimen and the anchorage. Note that since the anchorage is a local problem, the boundary conditions might have a strong influence on the predicted behaviour of the anchorage. Therefore, the realistic modelling of the boundary conditions is essential.

(vii) Loading conditions: The loading conditions should represent the actual loading scenario. Unless otherwise required, the analysis should be performed in displacement control to obtain the overall response, including the post-peak behaviour of the anchorage.

The results of the FE analyses can be evaluated in terms of load-displacement behaviour of the anchorage and the single components, crack propagation, stress-state, deformations, strut mechanisms etc. Through careful post-processing, the performance of the anchorage can be checked at each loading step in different directions at any location of the model

3.4 SUMMARY

This chapter provides an overview of the approaches used for the design and assessment of anchorages in concrete. In Section 3.1, the development of force-based approaches is summarized. Section 3.2 gives an overview of possible design solutions based on displacement-based approaches such as the component method and the equivalent spring model for anchorages. In Section 3.3, the design based on using the Finite Element Method is discussed.

4 OPEN QUESTIONS AND OBJECTIVES

Over the past several decades, researchers have worked towards the understanding of anchorage behaviour and the development of design rules and recommendations for them. An overview of the state of the art is discussed in Chapters 2 and 3. However, several questions remain open, which limit the application of the current design rules for anchorages in concrete. This Chapter aims at summarizing some of the open questions, which are targeted to be solved by the non-linear spring modelling approach for anchor groups developed within the framework of this thesis.

The following open questions are addressed:

(i) Geometric configuration and anchor pattern
(ii) Consideration of cracked concrete condition
(iii) Influence of loading eccentricity
(iv) Requirements on base plate stiffness
(v) Assumption of failure crack initiation for anchorages placed close to the concrete edge.

4.1 GEOMETRIC CONFIGURATION AND ANCHOR PATTERN

The current design approaches explicitly address the design of rectangular anchor groups with anchors with a maximum of three anchors in a row, where the group consists of anchors of same type and size. Consequently, it is assumed in the design that all anchors within a group exhibit the same stiffness. However, due to technical, functional or architectural requirements, anchorages with more than three anchors in a row and non-rectangular anchorage configurations such as circular, triangular, trapezoidal, L- shaped are also used in the industry (*Figure 4.1*). These restrictions are primarily due to the semi-empirical nature of the CCD method, which relies heavily on the available test data. Note, however, in the case of anchor channels, the number of anchors is not limited. This is because the verification for anchor channels is performed for the most unfavourable anchor accounting for uneven load distribution among the anchors.

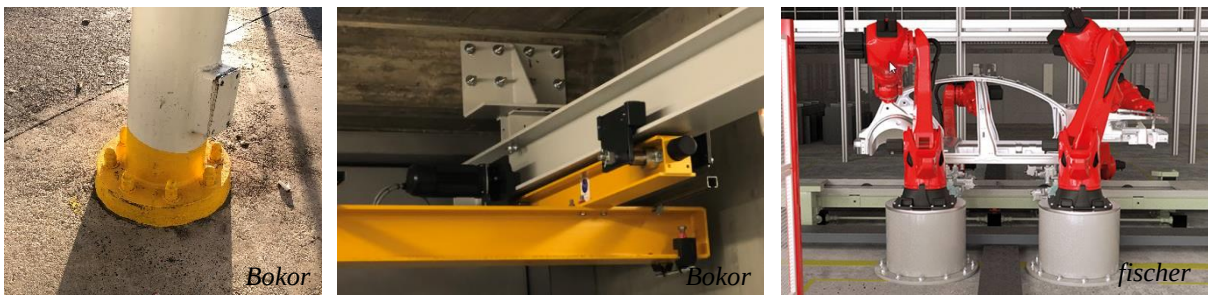

Figure 4.1. Anchorages used in practice possibly not covered by the current design provisions

The existing test database is mostly based on investigations on single anchors and anchor groups of regular rectangular configurations with a maximum of three anchors in a row. Rather limited tests are available on anchor groups with more than three anchors in a row in unreinforced

concrete, but these investigations are primarily carried out under shear or shear and moment loads (Grosser, 2012, Sharma et al., 2016, Ruopp & Kuhlmann, 2017). Further tests available on anchor groups with multiple rows were mostly carried out either far from the concrete edge or in heavily reinforced specimens or failure modes other than concrete edge breakout were governing (Cook & Klingner, 1992, Buia et al., 2018, Epackachi et al., 2015). Extremely limited tests exist on the tension behaviour of anchor groups with more than three anchors in a row (Eligehausen et al., 2006, Eligehausen et al., 1992, Zhao, 1992). Nevertheless, all the existing tests are performed on the anchorages with anchors arranged in a rectangular and regular pattern and no tests on other geometrical configurations (e.g. circular) are not known to the author. The possible configurations are categorised according to anchor groups with or without hole clearance, edge distances and loading directions (see *Figure 3.7*).

4.2 CRACKED CONCRETE CONDITION

According to the current force-based design approaches, the concrete condition (cracked or uncracked) must be determined by the design engineer. If the crack initiation in the concrete member cannot be ruled out in the anchorage zone, all anchors are assumed to be intercepted by cracks and the design of the anchor group must be carried out for cracked concrete condition. For anchorages, the concrete cone or concrete edge resistance in cracked concrete is considered as 70% of the corresponding anchorage resistance in uncracked concrete, with all the other parameters remaining same. Furthermore, for all the anchors of the group, it is assumed that the stiffness goes down by the same amount and therefore, the relative stiffness of the anchorage does not change. This assumption of considering all the anchors intercepted by a crack is deemed conservative according to the current design philosophy.

However, due to the geometric and reinforcement detailing of the anchorage base (structural member) for anchorages with multiple anchor rows, it is possible that not all the anchors of the group are intercepted by a crack. This leads to a significant difference in the stiffness of the anchors of the same group (anchors not intercepted by a crack having significantly stiffer response than the anchors intercepted by a crack). The difference in the stiffness of the anchors causes the anchors in uncracked concrete to be loaded more than the anchors in cracked concrete, which in certain conditions might result in a group resistance that is lower than the resistance obtained assuming all the anchors intercepted by a crack.

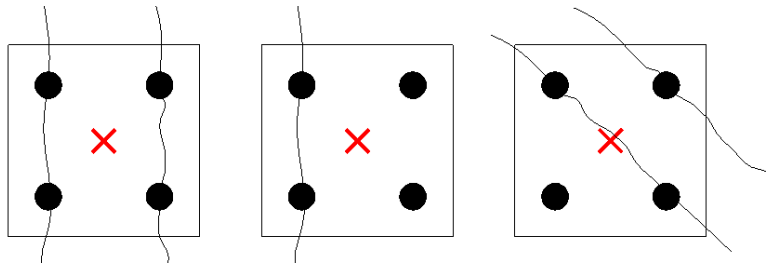

a) ***b)*** ***c)***

Figure 4.2. Quadruple anchor group with different crack pattern loaded in concentric tension a) design case, b) normal case, c) most unfavourable case

This aspect has been addressed with limited experimental, analytical and numerical investigations on quadruple anchor groups with applying the tension load concentrically on a stiff base plate and varying the crack pattern according to *Figure 4.2* (Mayer & Eligehausen, 1984, Okelo, 1996, Periskic, 2009, Mahrenholtz, 2012, Di Nunzio & Muciaccia, 2019). No tests were found, where the load was applied with eccentricity or/and a flexible base plate was used.

Considering only cases from the literature, where the anchor spacing was equal to the critical anchor spacing, it was found that assuming all anchors to be located in cracks is conservative since the ultimate load of the group was higher than four times the ultimate load of one single anchor in cracked concrete. However, it was found that when three out of four anchors are located in cracks, the group resistance is smaller than four times the capacity of a single anchor in crack. In this case, the cracked concrete assumption would yield unconservative. The ultimate load of anchor groups in cracked concrete is strongly influenced by the number of anchors located in cracks and by the load-displacement behaviour of the anchors in cracked and uncracked concrete. It should be noted that all the reported investigations were carried out with stiff base plates and on 2×2 anchor groups. However, the base plate stiffness and the relative stiffness (base plate to anchor stiffness) have a significant influence on the load distribution and on the behaviour of the anchor groups (Cook & Klinger 1992, Malleé, 2004/1, Malleé, 2004/2, Bokor et al., 2019). Furthermore, the influence of crack pattern might be more pronounced in case of larger anchorages, in particular in the case of groups with a single anchor row having multiple anchors.

The influence of crack pattern on the behaviour of anchor groups placed close to the concrete edge, loaded in shear towards the edge failing due to concrete edge breakout failure has not been investigated. A limited number of tests are available on single anchors. Fuchs & Eligehausen (1989) performed tests on post-installed anchors placed close to the concrete edge failing due to concrete edge breakout. The results showed a reduction of approximately 30-40% in terms of ultimate load and a reduction in terms of anchor stiffness (not quantified) due to the presence of the crack. Experimental investigations were carried out by Vintzeleou & Eligehausen (1991) on the influence of crack width ($\Delta w = 0.1\ mm \div 0.8\ mm$) on the single anchor shear resistance using undercut and expansion anchors. For the tested cases, the anchors with small edge distances, the anchor failed due to concrete edge breakout showing a reduction in failure load with increasing crack width (see *Figure 4.3a*). For crack widths greater than 0.3 mm, the failure load decreased approximately by 30% compared to the failure load measured in uncracked concrete. *Figure 4.3b* depicts typical shear load-displacement curves from tests on expansion anchors with 80 mm edge distance and different crack widths failing due to concrete edge breakout. The curves display a reduction in anchor stiffness; however, since not all load-displacement curves are reported in Vintzeleou & Eligehausen (1991), the stiffness reduction due to the presence of the crack cannot be evaluated quantitatively. No tests were found that show the dependence of crack width on the behaviour of anchors with different diameters. However, depending on various parameters for individual anchors and the crack pattern of the group, the specified reduction of 30% due to crack ($\Delta w = 0.3\ mm$) on the anchorage capacity might not be generally applicable for all cases.

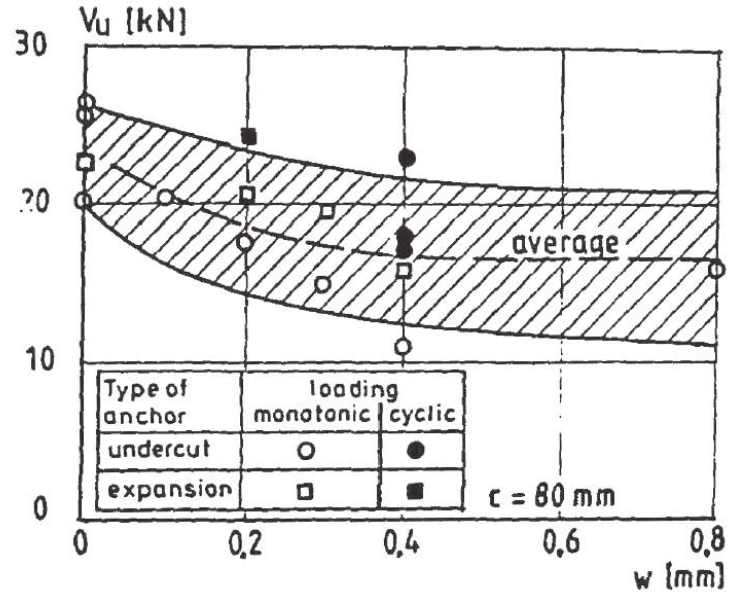

a)

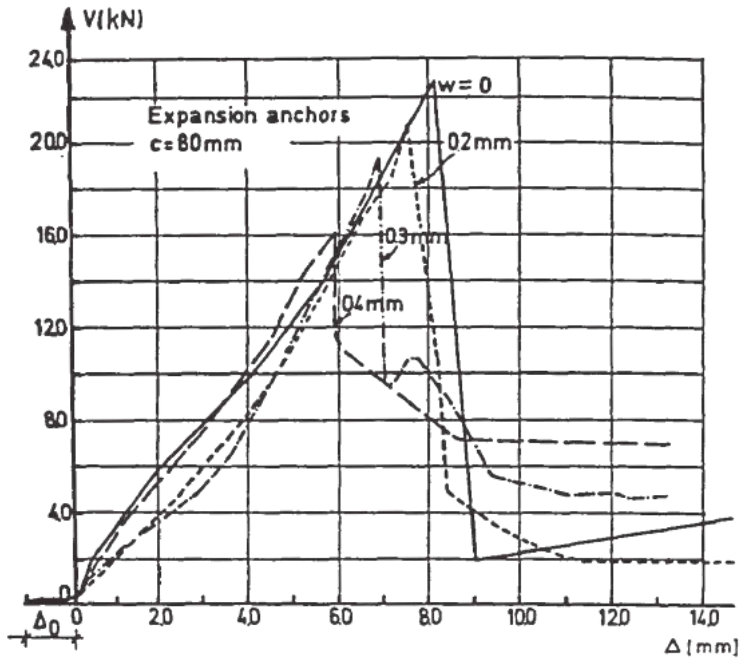

b)

Figure 4.3. a) Influence of crack width on the anchor shear resistance, b) Typical shear load-displacement curves from tests on expansion anchors with 80 mm edge distance failing due to concrete edge breakout (taken from Vintzeleou & Eligehausen, 1991)

4.3 CONSIDERATION OF THE ECCENTRICITY OF LOAD

If the point of application of the resultant loads on the anchorage does not coincide with the centre of gravity of the anchor group, it leads to an eccentric load situation due to which, the load-distribution on the anchors of a group is altered. Due to the loading eccentricity, certain anchors are loaded more than the others resulting in a reduction in the load-carrying capacity

of the anchorage. The influence of eccentricity on the concrete breakout resistance under tension and/or shear loads is considered in the design through a reduction factor, $\psi_{ec,N}$ (***Eq. 8***) or $\psi_{ec,V}$ (***Eq. 23***) applied on the calculated group capacity.

The factor, $\psi_{ec,N}$, was proposed by Riemann (1985), for anchorages under eccentric tension loads and was analogously adopted and applied to anchorages under eccentric shear loads ($\psi_{ec,V}$). The eccentricity factor is defined as a function of the eccentricity (distance between the point of application of the load and the centre of gravity of the group) and the critical spacing of the anchor. It is valid only if the base plate can be considered rigid, and the eccentricity is uniaxial. For anchorages loaded with a tension load under biaxial eccentricity, the factor $\psi_{ec,N}$ is calculated in the two directions and multiplied (*Figure 4.4a*) leading to significantly conservative results (Zhao, 1993, Bokor et al., 2019/1). In general, the factor $\psi_{ec,N}$, to consider the influence of eccentricity on group capacity, is deemed conservative (Eligehausen et al., 2006). However, all the eccentric tension tests available in the literature have been performed on the groups away from an edge.

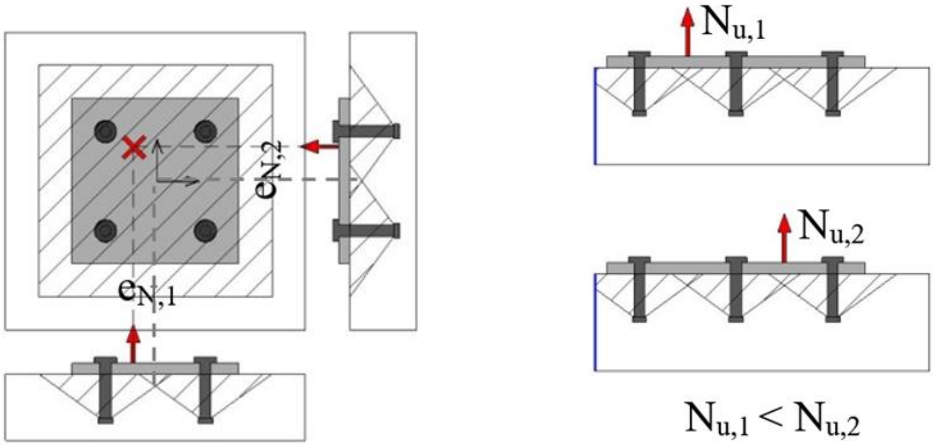

a) ***b)***

Figure 4.4. a) Influence of biaxial eccentricity on a 2×2 anchor group, b) Influence of eccentric tension loading on an anchor group placed close to an edge

No tests are currently available verifying the superposed influence of eccentric loading and vicinity of the concrete edge. When an anchorage is placed close to an edge such that edge distance is less than the critical distance and the load is applied eccentrically, there is a significant difference in the behaviour of the anchorage whether the eccentricity is applied towards or away from the free edge. In such a case, if the eccentricity of the applied load lies towards the edge, it should be expected for the anchorage to provide lower resistance compared to the case when the eccentricity of the applied load lies away from the edge. An example of a tension loaded anchor group loaded eccentrically close to an edge is given in *Figure 4.4b*.

The loading eccentricity and the uneven load distribution among the anchors of a group placed close to the concrete edge and loaded in shear towards the edge is considered in the design analogous to the corresponding eccentrically loaded anchorage under tension through the reduction factor, $\psi_{ec,V}$, applied to the calculated group capacity. When an anchor group is placed close to an edge and is loaded in shear eccentrically towards the edge, some anchors of the

group might be subjected to shear loads acting away from the edge. This effect was shown by Mallée (2002), Hofmann (2005) and Grosser (2012). Based on these findings, the current design provisions for anchorages neglects the component of a shear load acting away from the verified concrete edge in the calculation of the shear forces on the anchors close to the verified edge. However, it may not be reasonable to exclude this effect for general cases.

4.4 REQUIRED STIFFNESS OF THE BASE PLATE

For the application of the CCD Method for the design of anchorages, one of the most important requirements is that the base plate, which transmits the loads into the single anchors, must be sufficiently stiff. The requirement of the sufficiently stiff base plate is currently not quantified, and only qualitative guidelines are given such that the base plate should remain linear elastic and the deformations of the base plate should be small compared to the vertical displacement of the single anchors.

If the requirement for the rigid base plate is not fulfilled, the elastic deformation behaviour (e.g. prying effect) of the base plate shall be adequately taken into account to determine the tension loads acting on individual anchors. However, no explicit guidelines or methods are described to consider the deformation behaviour of the non-rigid base plate. Since the deformations of the base plate can have a significant influence on the lever-arm of the internal forces (Bokor et al., 2019/1), the verification of the rigid base plate assumption is of particular importance for the safety of anchorages designed according to EN 1992-4. If the base plate is not sufficiently stiff, the assumption of using a rigid base plate when determining the anchor forces can lead to unsafe results. This is explained in *Figure 2.8*. In the case of a rigid base plate, the forces are distributed linearly among the anchors within a group, but the assumed linear force distribution is not valid if the base plate is not rigid and therefore certain anchors would carry higher forces than calculated using a linear force distribution. Relatively few experimental investigations were performed to verify the influence of base plate stiffness on the anchor forces (Cook & Klingner, 1992, Mallée, 2004, Fichtner, 2011). Based on the evaluation of these tests, the influence of the base plate thickness on the anchor forces is highlighted (Fichtner, 2011, Li, 2017, Bokor et al., 2019/1). A reliable analytical method for evaluating the anchor forces in case of non-rigid base plates is still under discussion in scientific committees. Two approaches are possible: (i) to ensure through an analysis that the base plate is sufficiently stiff and the CCD Method is applicable, or (ii) for the given base plate, the analysis is performed considering the actual stiffness of the base plate and its influence on the force distribution on the anchors.

(i) The first approach requires direct comparison of the flexural rigidity of the base plate with the axial stiffness of the anchors. In such an approach, it is required to appropriately account for the thickness of the base plate, arrangement of the anchors, anchor stiffness, overhang of the base plate beyond the anchor rows, arrangement of stiffeners and attachment. Currently, no such quantitative guidelines are available, which include all the aforementioned parameters. Certain simplified guidelines are proposed by researchers (Cook & Klingner, 1992, Fichtner, 2011) but their scope of application is rather limited (mostly to 2×2 anchorages).

(ii) Alternatively, the distribution of anchor forces can be calculated by explicitly modelling the actual base plate stiffness, anchor stiffness and anchorage configuration. Some of such methods that try to consider some of the aforementioned parameters have been proposed in the past, and are included in the work of Stork (1998), Li (2017), Trautner & Hutschinson (2017), Fitz et al. (2018). Although some of these approaches consider the influence of base plate and anchor stiffness, one of the major limitations of these methods is that the analysis is performed within the force domain. Therefore, accounting for the anchor force redistribution is not possible and consequently, various influences cannot be captured automatically, and an indirect approach is needed for the evaluation of the obtained results. Furthermore, the group effect in case of anchorages failing due to concrete cone failure mode is not explicitly considered in these methods.

4.5 CONSIDERATION OF FAILURE CRACK INITIATION FOR CONCRETE EDGE BREAKOUT

In the case of anchor groups placed close to a concrete edge, the failure is often governed by concrete edge breakout. The design of anchorages loaded in shear against concrete edge failure is performed according to the CCD Method (see Section 3.1.3). For anchor groups with only one anchor row (anchors placed parallel to the edge), the design provisions given in various standards are, in principle, unified since the failure crack appears from the location of the anchor row. However, in case of anchor groups with multiple anchor rows, the failure load corresponding to the concrete edge failure may be calculated either by assuming the failure crack originating from the front anchor row (approach given in EN 1992-4) or by assuming the failure crack originating from the front, middle or back anchor row (approach followed by fib Bulletin 58, ACI 318-19). However, if the failure crack is considered to appear from the back or mid anchor row, only the anchors not located in the theoretical breakout body can be considered to resist shear loads for the verification of steel failure (*Figure 4.5*). The approach to consider the failure crack originating from the first anchor row was included in EN 1992-4 because in many cases, it is not obvious whether the redistribution of the shear load to the back anchor row can take place after the crack (if any) has formed at the front anchor row (Bokor et al., 2020). This approach is deemed conservative for anchorages with multiple anchor rows since the force redistribution to the back anchor rows is completely neglected (see e.g. in Grosser, 2012, Sharma et al., 2017). If the failure crack is assumed to initiate from the back anchor row, then due to the larger edge distance, the calculated failure load is significantly higher than the failure load obtained by assuming the failure crack originating from front anchor row. *Figure 4.5* highlights that according to the current rules, if the failure crack is assumed from the front anchor row, the design is resulting in the same failure load for a group having a single anchor row or multiple anchor rows if the edge distance for the first anchor row and all other installation parameters are the same (Bokor et al., 2020).

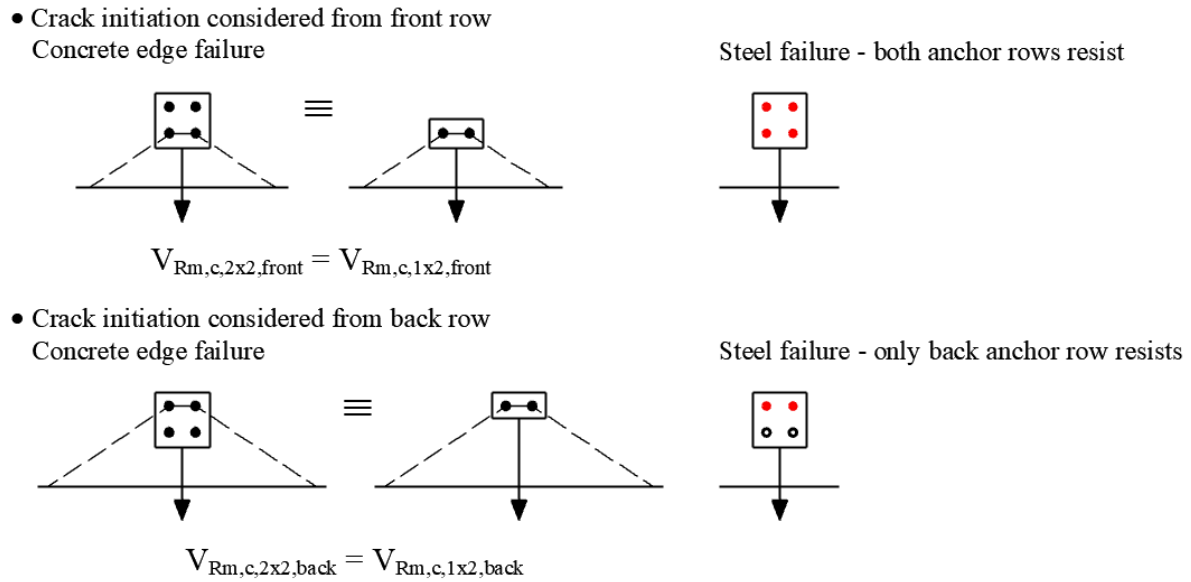

Figure 4.5. Possible approaches to consider the failure crack initiation for concrete edge failure in case of groups with two anchor rows without hole clearance

The requirement of a pre-decision on the initiation of the failure crack for concrete edge failure comes from the fact that the CCD Method utilizes the projected areas (Section 2.2.2), the calculation of which requires a specific edge distance. However, with this approach, it is difficult to account for the influence of anchor spacing in loading direction, hole clearance pattern and to account for different limit states. Furthermore, it is not possible to consider the load redistribution among the anchors of different anchor rows. In case of anchorages with multiple anchor rows, the approach to assume the failure crack originating from the front anchor row can be rather conservative (Grosser, 2012, Sharma et al., 2017, Bokor et al., 2020). On the contrary, assuming the failure crack from back anchor row might be unconservative depending on the spacing to edge distance ratio or hole clearance pattern (Hofmann, 2005, Unterweger, 2008, Grosser & Cook, 2009). Therefore, an approach that can consider the displacement behaviour, different edge distances, anchor pattern, hole clearance pattern and the load distribution and redistribution, is essential to minimize the assumptions and pre-decisions currently required for the design of anchorages under shear loads.

4.6 NEED FOR A NEW CONCEPT

Cast-in place and post-installed anchorages are used for decades to form connections between structural components or between structural and non-structural components. Typically, to connect structural members, base plate connections (e.g. column base plates) are applied, whereas to connect non-structural elements to structures, fixture attachments including a base plate and the anchors are used (Morgan, 2018). The design of anchorages according to the “fastening technology” is limited to strict boundaries. The main reason for the limitations can be attributed to the semi-empirical and force-based nature of the design provisions, which are generally sufficient for the design of non-structural connections.

With vast progress in the manufacturing technology, better, heavy-duty and robust anchor systems are developed. At the same time, the development of code provisions and approval procedures allow extended applications of the anchors to structural connections. However, frequently in structural applications, and in particular, for anchorages used for strengthening, innovative solutions are required because the anchorage cannot be designed following the standard provisions due to the relatively high demand placed on anchorages in structural and strengthening applications (Sharma, 2019).

The improvement of computational power allows higher-level analysis methods such as displacement-based analysis, nonlinear analysis, pushover analysis, etc. for the assessment of the structures. With such methods, the interaction between the structure, connected component and the anchorage can be accounted for over the complete range of interest (for example SLS, ULS; loading until failure). Furthermore, through performing such an analysis, detailed information about the components of the structure can be obtained, and a step-by-step performance check can be made.

However, to include an anchorage as a component in such a nonlinear analysis of the structure, the nonlinear load-displacement behaviour of the anchorage should be provided. A few models exist that can consider the nonlinear behaviour of anchorages (refer to Section 3.2). However, they are either overly complex to be included in a global structural model (refer to Section 3.2.1), or simpler but based on several assumptions (refer to Section 3.2.3). An optimum solution would be to combine the strength of the two approaches such that the load-displacement behaviour of individual anchors, as well as other influences (group effect, base plate stiffness, crack pattern, hole clearance pattern, edge influences etc.) of an arbitrary anchor group are considered, and the model yields a resultant load-displacement curve that can be implemented as equivalent spring characteristics in a global structural model. Such a model is highly advantageous not only to simulate structural connections but also the calculate the capacity and load-displacement response of non-structural connections.

4.7 OBJECTIVES OF THE WORK

The overall aim of this work is to develop a nonlinear spring model that is able to predict the load-displacement behaviour of anchorages. The model should consider arbitrary anchor pattern, base plate geometry and stiffness, the influence of parameters such as eccentricity, edge distance, crack pattern, hole clearance pattern realistically. To account for all these aspects, a displacement-based approach is needed that can consider the load distribution considering the relative stiffness (base plate stiffness/anchor stiffness) and load redistribution among the anchors considering the nonlinear behaviour of the anchorage. To realise the overall aim, the following objectives were targeted:

(i) to conceptualise and develop the nonlinear spring model for anchorages subjected to tension, shear and combined tension-shear (interaction) loads,
(ii) to design, execute and evaluate an optimum and well-instrumented test program to extract the information required for the development of basic postulates and to understand the load-displacement behaviour of anchor groups,

(iii) to design, execute and evaluate a well-instrumented test program for the verification of the model against anchorages of various configurations,
(iv) to associate the verified model with a general safety concept in order to make the approach suitable for the design of anchorages in concrete.

4.8 SUMMARY

This chapter summarises several open questions that are aimed to answer within the framework of this thesis. The following open questions are addressed: Extension of the scope of application to arbitrary geometric configuration and anchor pattern, consideration of cracked concrete condition, the influence of loading eccentricity, requirements on base plate stiffness, assumption of failure crack initiation for anchorages placed close to the concrete edge. The need for a new displacement-based concept is emphasized and the objectives of the work are summarised.

5 CONCEPT OF THE NONLINEAR SPRING MODEL FOR CONCRETE CONE FAILURE

In Chapter 5, the concept and the development of the nonlinear spring model for evaluation and design of tension loaded anchor groups in the case of concrete cone failure are discussed. Section 5.1 summarises the most important assumptions made to develop the concept and defines the components used for the nonlinear spring modelling approach. Detailed discussion on the nonlinear spring modelling approach is given in Section 5.2-5.5.

5.1 INTRODUCTION

Several aspects need to be considered for the development of the spring model for concrete cone failure of tension loaded anchor groups. The ultimate aim is to reflect the behaviour of tension loaded anchor groups of arbitrary configuration realistically and to give a good estimate about the performance of the anchorage. For that, first, assumptions for the modelling were made and the components, which should be considered in the model, were fixed. These are the nonlinear anchor behaviour in uncracked and cracked concrete, the geometry and stiffness of the base plate, the contact between the concrete surface and the base plate (to consider prying action), possible steel stiffeners, the position and geometry of connecting profile and the loading.

The assumption, on which the concept of the nonlinear spring model for tension is primarily based, is that within an anchor group only the anchors resist the tension forces, while the compression forces are transferred directly by the base plate to the concrete. Anchors suitable for resisting compression forces are beyond the scope of this dissertation and they are not considered by the spring modelling approach. To realise the assumption, the real behaviour of the anchors is modelled using tension-only springs, while the contact between the base plate and concrete is modelled using compression-only springs (see details in Section 5.2 and Section 5.4, respectively). The base plate is modelled using finite shell or solid elements to consider the base plate geometry, and consequently, the base plate stiffness realistically (Section 5.3).

Furthermore, the complete nonlinear anchor behaviour is considered in the model by the tension-only anchor springs to enable a realistic force distribution and force redistribution among the anchors of the group. In this way, it is possible that the anchors, which lose stiffness by reaching high forces, redistribute the forces to the other anchors of the group. However, in order to do that, it is essential to perform a displacement-controlled nonlinear analysis according to Section 5.5.

The components of the spring model are schematically depicted in *Figure 5.1* for an anchor group of 1×4 configuration, which are:

i. Anchor springs: nonlinear tension-only axial springs to model the nonlinear load-displacement behaviour of individual anchors in uncracked and cracked concrete,
ii. Contact springs: compression-only axial springs for modelling the bearing of the base plate on concrete

iii. Base plate: Finite shell or solid elements to model the base plate inclusive stiffener and profile (if any) realistically.

The details about (i) the procedure for the determination of the anchor spring characteristics, (ii) the modelling of the base plate, (iii) the modelling of the contact springs and (iv) the displacement-controlled nonlinear analysis are described in the following Sections 5.2-5.5.

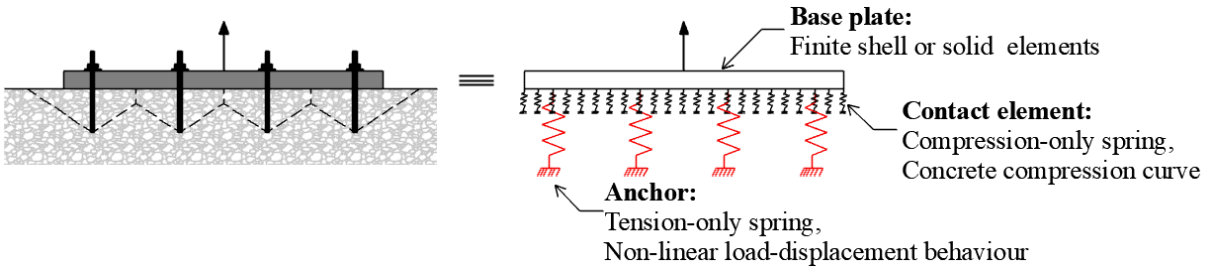

Figure 5.1. Conceptual representation of the spring model of tension loaded anchor groups in case of concrete cone failure

5.2 DETERMINATION OF THE CHARACTERISTICS FOR SPRINGS TO MODEL THE ANCHOR BEHAVIOUR

In this section, the determination of the characteristics for springs to model the anchor behaviour is discussed. The nonlinear spring modelling approach is a displacement-based approach, where the spring characteristics are used to define the nonlinear load-displacement behaviour of a tension loaded single anchor. As defined in Section 5.1, the anchor behaviour in case of tension loading is considered in this thesis by tension-only nonlinear axial springs derived based on the idealised load-displacement curves obtained from tension test on single anchors away from the edge or neighbouring anchors. The question is how to determine the springs and how to consider different failure modes and influences such as edge distance and anchor spacing.

The load-displacement behaviour, and consequently the spring characteristics depend on the anchor type and failure mode of the anchor, i.e. steel failure, pullout failure or concrete cone failure. Note that splitting failure or combined concrete cone and pullout failure modes are out of the scope of this work. However, an approach similar to given here can be developed in future to cover these failure modes as well. The load-displacement curves for the targeted failure mode of the anchors can be determined from the tension tests performed on single anchors as it is schematically shown in *Figure* 5.2. The targeted failure mode should be ensured by the appropriate combination of the geometric and material parameters (h_{ef}, d_{nom}, f_c, etc.).

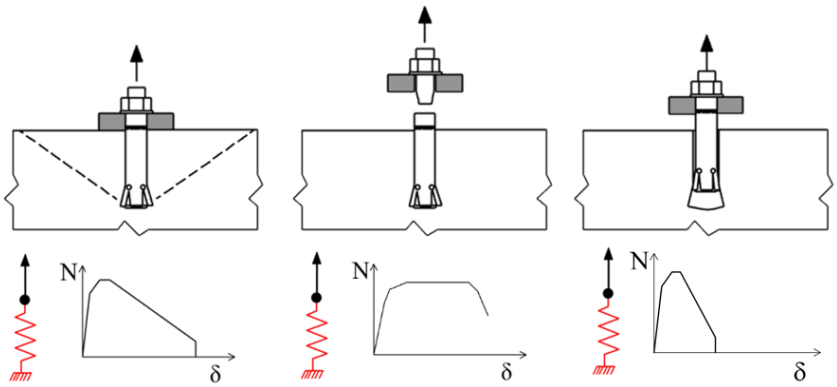

Figure 5.2. Schematic of the failure modes of a single anchor with the idealised load-displacement behaviour (typical) represented as spring characteristics: concrete cone, steel, pullout

In the case of steel failure and pullout failure, the resistance and behaviour of the anchors are not influenced by the adjacent anchors or by the vicinity of the edge of the concrete member. Consequently, for the failure modes steel failure and pullout failure, the load-displacement curves obtained for single anchors can be directly used as the spring characteristics for the individual anchors of an anchor group (*Figure 5.3*). Note that for different anchor types and pullout failure types, different types of curves are possible (Eligehausen et al., 2006). A detailed discussion of failure modes other than concrete cone failure is beyond the scope of this dissertation. However, recommendations for the application of the proposed approach for steel failure and pullout failure are given in Section 14.2.1.

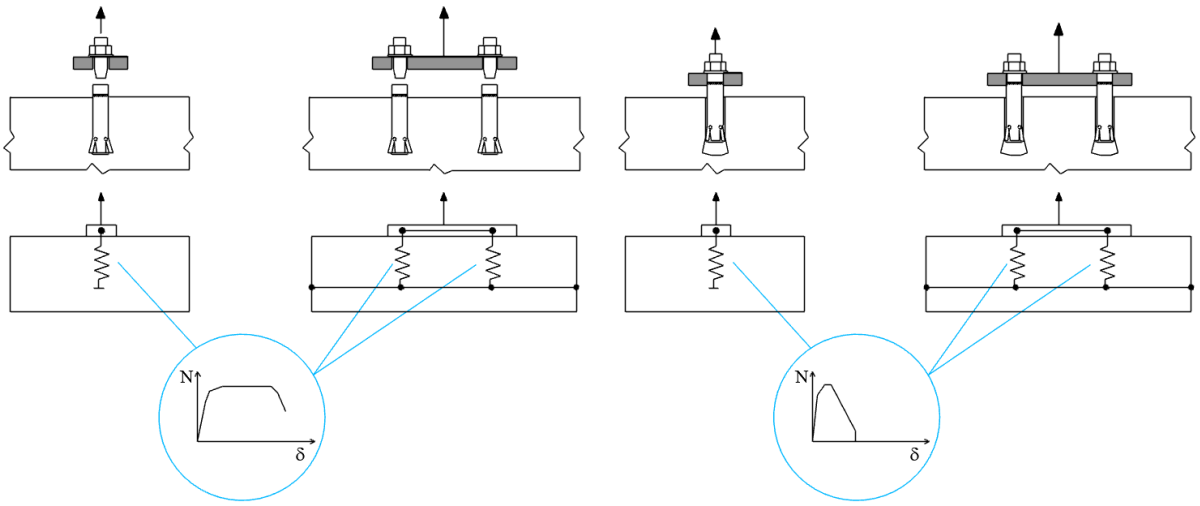

a) ***b)***

Figure 5.3. Spring properties (typical) for individual anchors of a group in case of a) steel failure, b) pullout failure

The relatively brittle concrete cone failure mode occurs if the capacity of the anchorage ground is less than the pullout capacity and the steel failure load of the anchorage, and the full tensile capacity of the concrete is utilised (Eligehausen et al., 2006). The resistance of a single anchor, which fails due to concrete cone failure is mainly influenced by the anchor embedment depth,

the concrete fracture energy, the concrete Young´s Modulus and the cracked or uncracked concrete condition (Eligehausen et al., 2006). However, if we are talking about anchor groups, the geometric arrangement of the anchors, the anchor spacing, the concrete edge distance and the base plate stiffness also have a significant influence on the concrete cone resistance of the group. Therefore, it is intuitive that in many cases, when the single anchor would fail by, for example, pullout failure, the decisive failure mode of the group will be concrete cone failure.

An anchor group (or group of fasteners) by the definition of EN 1992-4 is a "number of fasteners with identical dimensions and characteristics acting together to support a common attachment, where the spacing of the fasteners does not exceed the characteristic spacing". If the spacing between the n number anchors of a group is equal to the critical spacing ($3h_{ef}$), and the anchor group is loaded concentrically in tension with a rigid base plate, then the capacity of the group is n-times the capacity of a single anchor in case of concrete cone failure. However, if the spacing between the anchors is less than the critical spacing, then the capacity of the group will be less than n-times the capacity of a single anchor. This means that the spring characteristics obtained from the load-displacement curves of single anchors cannot directly be used in the model, but must be modified to account for the influence of anchor spacing and/or the vicinity of concrete edge (*Figure 5.4*). This method is discussed in Section 5.2.2.

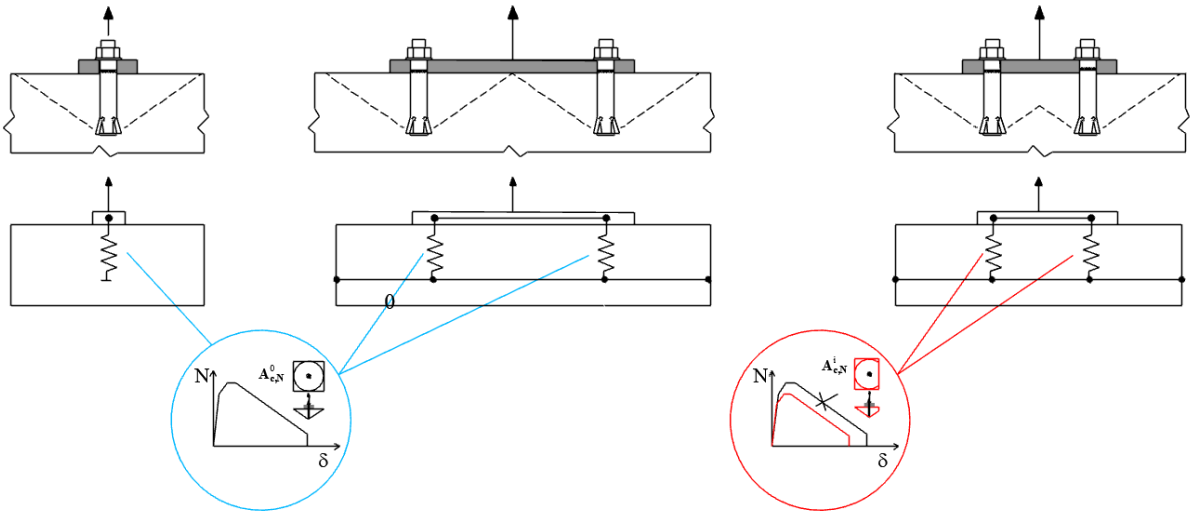

Figure 5.4. Spring properties (typical) for individual anchors of a group in case of concrete cone failure

5.2.1 Idealisation of the anchor springs for concrete cone failure

This section gives information about how to generate the spring characteristics from load-displacement curves on single anchors, which can be then assigned to the spring model as shown in *Figure 5.1*. For the development of the concept and the verification, the spring model and the test results are considered and evaluated at the mean value level. This allows the best comparison and plausibility. Recommendations for a method for conversion to characteristic level is explained in Chapter 13.

Load-displacement curves obtained from tension tests on single anchors should be used to generate the spring characteristics for a single anchor failed due to concrete cone failure. The anchor spring properties should be evaluated on the basis of tension tests performed on single anchors in cracked and uncracked concrete according to the recommendations given by EAD 330499 and EAD 330232 or ACI 355.2 and ACI 355.4. However, in order to describe the spring characteristics with a limited number of parameters, the load-displacement curves should be idealised by generating load-displacement data pairs (*Figure 5.5*).

For idealisation of the load-displacement response of the single anchor, a penta-linear format was chosen (*Figure 5.5b*) because it offers a good balance between accuracy and simplicity, and because the software used in this dissertation (SAP2000) supports this format when defining the nonlinear behaviour of the corresponding component. It is recommended to characterize the nonlinear anchor behaviour using the penta-linear format. However, more number of segments may be used for the idealization of the load-displacement curve if the curve progression of a certain anchor behaviour requires that. A minimum of tri-linear curve should be used having an ascending branch, a plateau and a descending branch.

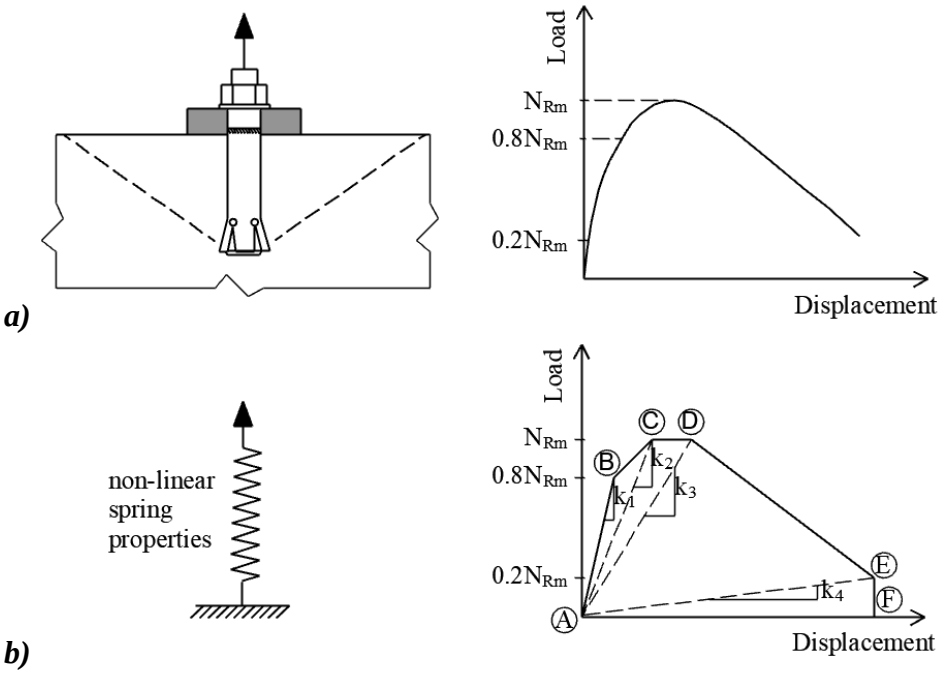

Figure 5.5. Nonlinear spring properties of a tension loaded single anchor: a) Load-displacement curve of a single anchor failed by concrete cone – "reference" load-displacement curve; b) Idealisation of the "reference" L-d curve to the penta-linear format

This dissertation supports using the penta-linear format for which six characteristic points should be defined. Data pairs of load (N) and displacement (δ) values define the characteristic points A-F. Point A is at the origin located at $N = 0\ kN$ and $\delta = 0\ mm$. Points C and D correspond to the maximum load, and their displacement coordinates define the extent of the plateau in the peak region, which depends on the type of the anchor and failure mode (Sharma, 2013 and 2017). Point B corresponds to the end of the idealised initial stiffness range, which can be defined as 80% of the maximum load. The transition point (point B) for the initial stiffness range of 80% was chosen because it was shown by authors in the past, based on the evaluation of a

large number of tests, that for most of the anchors the initial stiffness is valid up to 80% of the maximum load. The initial stiffness is defined as the secant stiffness corresponding to 50% of peak load sustained by the anchor. Point E is used to idealise the descending branch and corresponds to 20% of the ultimate load in the post-peak region. Note that here also, the displacement depends on the type of anchor and failure mode. Point F is located at $N = 0\ kN$ and $\delta_F = \delta_E$. In *Figure 5.5*, the spring characteristics are defined using the load and secant stiffness values (k_1-k_4) corresponding to each point (Sharma, 2013).

If n number of tests were carried out in one test series, all load-displacement curves should be idealised separately, and the mean value of load and stiffness values should be taken for the spring characteristics ($N_{i,m} = (\Sigma N_i^g)/n$, where $g = 1 \rightarrow n$ and $k_{i.m} = (\Sigma k_i^g)/n$, where $g = 1 \rightarrow n$).

Table 5.1. Salient points of the idealised load-displacement curve: spring properties

Point	Load	Stiffness	Displacement
A	0	0	$\delta_A = 0$
B	$0.8 \cdot N_{Rm}$	k_1	$\delta_B = 0.8 \cdot N_{Rm}/k_1$
C	N_{Rm}	k_2	$\delta_C = N_{Rm}/k_2$
D	N_{Rm}	k_3	$\delta_D = N_{Rm}/k_3$
E	$0.2 \cdot N_{Rm}$	k_4	$\delta_E = 0.2 \cdot N_{Rm}/k_4$
F	0	0	$\delta_F = \delta_E$

Note that different anchor systems may display different load-displacement behaviour, therefore the definition of points A- F of the idealised curve may be altered depending on the shape of the load-displacement curve (for example B at $0.5N_{Rm}$ or $0.6N_{Rm}$ in case of some anchors), provided that the idealised curve offers a reasonably good representation of the original load-displacement curve. Based on the description above, the load-displacement curves obtained from the tests can be idealised and used as spring characteristics of a single anchor failed by concrete cone failure.

In addition, based on the evaluation of a vast number of test results (from tests of this thesis and from approval tests) on single anchors, recommendations were worked out for a method to idealise the obtained load-displacement curves with sufficient accuracy and safety, which can be used for the design. It should be noted that the results from the approval tests are not published. Those test results were made available by fischerwerke GmbH & Co. KG for scientific purposes in order to develop a method for idealisation, which can be automated. Details are given in Section 13.3.2.1.

5.2.2 Consideration of anchor spacing and vicinity of the concrete edge

As it is accentuated in Section 5.2 that a method should be developed to consider the influence of anchor spacing and concrete edge distance on the behaviour of individual anchors within a group. This is essential for the nonlinear spring model, where the individual springs represent the nonlinear behaviour of the neighbouring anchors in the group. In this section, examples are

given and assumptions and postulates are made based on theoretical and practical considerations.

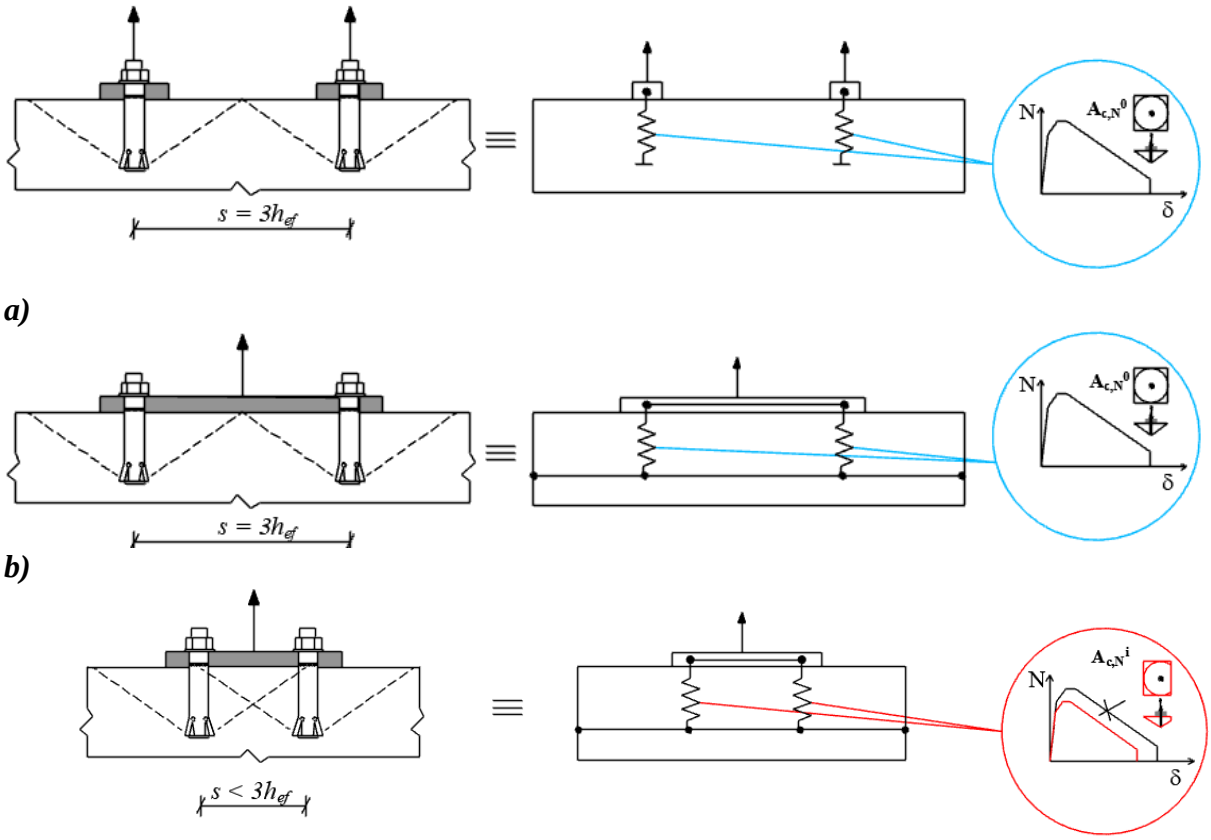

Figure 5.6. Modelling of anchorages using nonlinear springs: a) two single anchors with $s = 3h_{ef}$, b) anchor group with $s = 3h_{ef}$ and c) anchor group with $s < 3h_{ef}$

If two single anchors having the same installation parameters are placed with a spacing equal or larger than the critical spacing ($s \geq 3h_{ef}$), two separate concrete cones can develop and the behaviour of each anchor can be described by the load-displacement curve obtained from tension tests on single anchors. These load-displacement curves can be used as spring characteristics in an idealised format (according to Section 5.2.1) for each anchor (*Figure 5.6a*). It is intuitive, however, that it is not necessary to use a spring model to describe the behaviour of a single anchor loaded concentrically in tension far from a concrete edge because the result of the model would be the same as the spring characteristics. However, the same spring characteristics of the single anchor can be assigned to the individual anchors connected by a common base plate if the anchor spacing is larger or equal the critical anchor spacing ($s \geq 3h_{ef}$) (*Figure 5.6b*). Under concentric tension loading, the theoretical anchor group capacity will be twice the capacity of the corresponding single anchors because in this case, sufficient volume of concrete is available for each anchor to develop its full capacity. The overall displacement of the group, which is measured at the point of load application, will depend on the stiffness of the individual anchors and on the stiffness of the base plate. However, if the anchor spacing within the group is smaller than the critical spacing (*Figure 5.6c*), then the theoretical concrete cones of the neighbouring anchors are partly intersecting and a common failure cone develops leading to a group capacity, which is less than twice the capacity of the corresponding single anchor. Consequently, the

spring characteristics applied in *Figure 5.6a* and *b* cannot directly be used for the case depicted in *Figure 5.6c* but the spring characteristics of the individual anchors must be modified to account for the reduced capacity due to group effect and the overlapping concrete cones.

The question is how to modify the spring characteristics of a single anchor to account for group effect and/or vicinity of the concrete edge. The examples shown in *Figure 5.7* and *Figure 5.8* should help to explain the assumptions and postulates made for the non-linear spring model.

According to the CCD Method, the influence of the spacing on the group resistance is taken into account by the factor $A_{c,N}/A^{0}_{c,N}$ where the concrete cone resistance is increasing in proportion to the projected area of the group (Fuchs et al., 1995, Eligehausen et al., 2006). The projected area of a single anchor that is not influenced by the concrete edge and neighbouring anchors is calculated according to ***Eq. 5***, and the projected area of an example anchor group depicted in *Figure 5.7* is calculated according to ***Eq. 39***, respectively.

$$A_{c,N} = (3 \cdot h_{ef}) \cdot (c + 2 \cdot s + 1{,}5 \cdot h_{ef}) \qquad \textbf{Eq. 39}$$

$$N_{Rm,c} = N^{0}_{Rm,c} \cdot n \qquad \text{if } s \geq 3 \cdot h_{ef} \qquad \textbf{Eq. 40}$$

$$N_{Rm,c} = N^{0}_{Rm,c} \cdot \frac{A_{c,N}}{A^{0}_{c,N}} \qquad \text{if } s < 3 \cdot h_{ef} \qquad \textbf{Eq. 41}$$

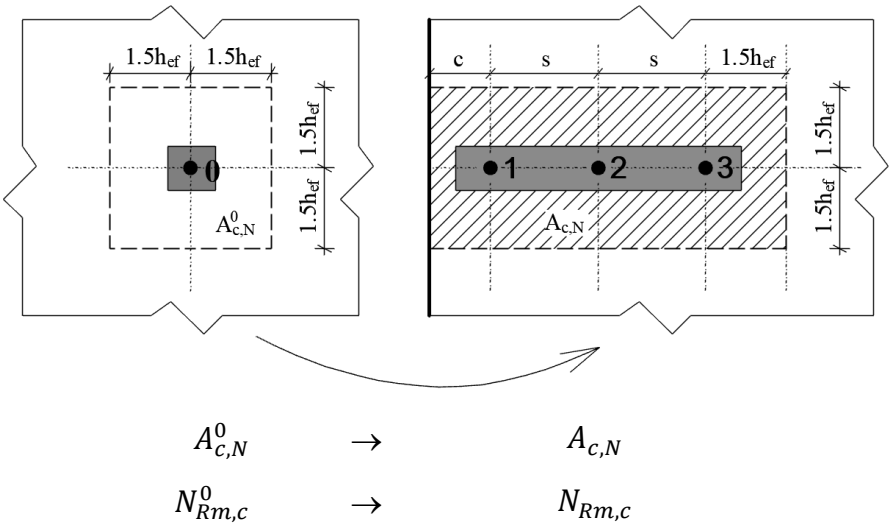

Figure 5.7. Definition of the projected area of a single anchor (left) and of an anchor group of 1×3 configuration close to the concrete edge (right) according to the CCD Method

In the spring model, the focus is on the resistance and load-displacement behaviour of the individual anchors of the group so that the spring properties can be assigned to the individual anchors in the model (*Figure 5.1*). According to the current design provisions, anchors within an anchor group must have the same type, size and embedment depth so that it can be assumed that the stiffness conditions within the group are approximately the same. In the nonlinear spring modelling approach, anchor groups having the same embedment depth are considered. However, it is possible to consider anchors having different stiffness such as for example the same anchor type but in cracked or in uncracked part of the concrete (see Section 5.2.3). Having equal embedment depth for all anchors means also that the tension loaded anchor groups can

be simplified to a 2D problem (just like according to the CCD Method). The intersection of the conical breakout bodies can be converted into the overlapping of the projected areas. Therefore, in the spring model, the projected tributary area of the individual anchors and the resistance of the individual anchors are of interest. The same example group (1×3 configuration close to the edge) as for the CCD Method is taken to explain the procedure used in the spring model, to highlight the similarities and point out the differences (compare *Figure 5.7* with *Figure 5.8*). The assumptions taken are explained in the following. It is assumed in the nonlinear spring model that the failure load of an ith anchor of an anchor group (compared to the failure load of a single anchor) is influenced by the neighbouring anchors and/or by a close edge and it decreases in proportion to the projected area. The influence of the spacing and vicinity of concrete edge on the individual anchor resistance compared to the single anchor resistance is taken into account by the factor $A^i_{c,N}/A^0_{c,N}$. This is similar to how the CCD Method accounts for the geometric influence of the vicinity of the concrete edge in the case of a single anchor. However, here, a virtual edge instead of a real edge is assumed between the neighbouring anchors.

Postulate 1:

The first postulate made in the spring model for the individual properties: The mean failure load of an ith anchor, $N^i_{Rm,c}$, influenced by neighbouring anchors or close edge can be calculated as

$$N^i_{Rm,c} = N^0_{Rm,c} \cdot \frac{A^i_{c,N}}{A^0_{c,N}} \qquad \textbf{Eq. 42}$$

Where,

$N^0_{Rm,c}$ is the basic concrete cone breakout strength of the anchor not influenced by the neighbouring anchors or close edge, given by ***Eq. 4*** or obtained from single anchor tests, kN

$A^i_{c,N}$ is the tributary projected area assigned to the anchor considering the distance from the adjacent anchors and the edge distance, mm

$A^0_{c.N}$ is the reference projected area of a single anchor with a distance from all the edges equal to or greater than the critical edge distance $c_{cr,N} = 1.5h_{ef}$, mm, given by ***Eq. 5***

The tributary projected area assigned to an ith anchor is limited either by the real concrete edge c in case of the vicinity to the edge, or by a virtual edge c_{virt} considered at a distance of half the spacing to the neighbouring anchor, but not more than $1.5h_{ef}$. This is explained with the help of the example in *Figure 5.8*. For a 3×1 anchor group depicted in *Figure 5.8*, both the close edge and the neighbouring anchor limit the tributary area. Thus, for anchor 1, the tributary area can be calculated as

$$A^1_{c,N} = (c + 0.5 \cdot s) \cdot (3 \cdot h_{ef}) = (c + c_{virt}) \cdot (3 \cdot h_{ef}) \qquad \textbf{Eq. 43}$$

For anchor 2 (middle anchor), the tributary projected area is limited by both the neighbouring anchors but not by the real concrete edge. The tributary area can be calculated as

$$A^2_{c,N} = 2 \cdot (0.5 \cdot s) \cdot (3 \cdot h_{ef}) = (2 \cdot c_{virt}) \cdot (3 \cdot h_{ef}) \qquad \textbf{Eq. 44}$$

For anchor 3, the tributary area is limited by the neighbouring anchor on one side but not by the concrete edge. Therefore, the tributary area can be calculated as

$$A_{c,N}^{3} = \left(0.5 \cdot s + 1.5 \cdot h_{ef}\right) \cdot \left(3 \cdot h_{ef}\right) = \left(c_{virt} + 1.5 \cdot h_{ef}\right) \cdot \left(3 \cdot h_{ef}\right) \qquad \textbf{Eq. 45}$$

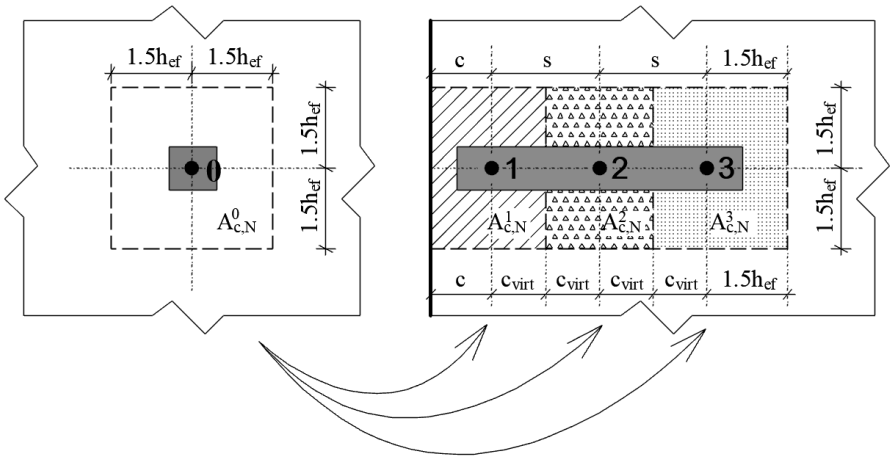

$$A_{c,N}^{0} \rightarrow A_{c,N}^{1} \quad A_{c,N}^{2} \quad A_{c,N}^{3}$$

$$N_{Rm,c}^{0} \rightarrow N_{Rm,c}^{1} \quad N_{Rm,c}^{2} \quad N_{Rm,c}^{3}$$

Figure 5.8. Definition of the tributary areas and anchor resistances associated with individual anchors

$$\begin{aligned} A_{c,N} &= A_{c,N}^{1} + A_{c,N}^{2} + A_{c,N}^{3} \\ &= \left(3 \cdot h_{ef}\right) \cdot \left[\left(c + 0.5 \cdot s\right) + s + \left(0.5 \cdot s + 1{,}5 \cdot h_{ef}\right)\right] \\ &= \left(3 \cdot h_{ef}\right) \cdot \left(c + 2 \cdot s + 1.5 \cdot h_{ef}\right) \end{aligned} \qquad \textbf{Eq. 46}$$

Eq. 46 shows that if the individual tributary areas used in the spring model are summed up, the area is equal to the area considered for the group according to the CCD Method. However, the nonlinear spring modelling approach is a displacement-based approach, and the tributary areas are only used to determine the resistances of the individual anchors based on results on single anchors, so the force ($N_{Rm,c}^{i}$) value becomes known, but here, data pairs of load and displacement values are required for the analysis and consequently, stiffness values. Therefore, the rules for the stiffness should be set.

Postulate 2:

The second postulate made in the spring model for the individual properties: The tributary area assigned to an ith anchor of the group does not influence the stiffness of the anchor (k_1 - k_4 in *Figure 5.9*) and the stiffness values remain unchanged compared to the stiffness values determined for the corresponding single anchor.

This means that when the tributary area, which belongs to an ith anchor is ascertained, the spring characteristics for the ith anchor can be determined by scaling the basic spring characteristics of the single anchor by following the postulates 1 and 2 stated above. The failure load is reduced using ***Eq. 42***, while the stiffness values for each characteristic point is maintained. This is explained in *Figure 5.9*. Note that no further modification due to the vicinity of a real or virtual edge is required. The virtual edge does not lead to the disruption of hoop stresses. The negative

effect caused by the disruption of hoop stresses in case of anchors placed close to the edge, which is accounted for by $\psi_{s,N}$ factor in the CCD Method, is taken into account automatically in the spring model by performing a displacement-controlled nonlinear static analysis.

It can be summarised that the spring characteristics can be determined provided that the load-displacement curves of single anchor tests are available. Finally, the dashed-curve in *Figure 5.9* can be directly used as spring characteristics for anchor 1 in the group depicted in *Figure 5.8*.

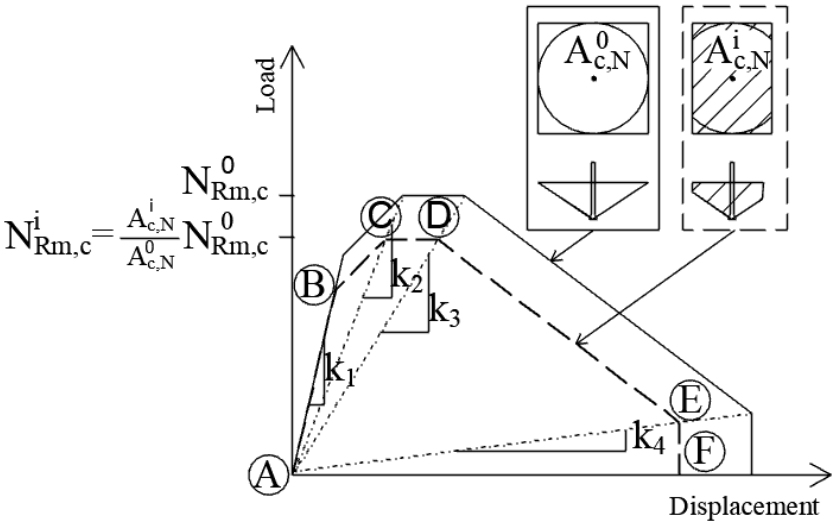

Figure 5.9. Scaling of the idealised curve of a single anchor

5.2.2.1 Non-rectangular configurations

The tributary approach can be extended to rectangular anchor groups up to a large number of anchors if the rules are followed. However, one of the biggest advantages of the nonlinear spring modelling approach for concrete cone failure is that the input parameters (nonlinear spring properties) are defined for each individual anchor within the group. Consequently, if a rule for assigning the tributary areas can be set for anchor groups of non-rectangular configurations, then any anchor configuration can be calculated or evaluated by means of the approach. For that, the method for the assignment of the tributary area for an individual anchor should be extended, and certain extra considerations are necessary. The concept for assigning the tributary area for the individual anchors, so that the spring characteristics for the individual anchors arranged in a non-rectangular pattern can be determined, is explained with the help of a triangular anchor group in the following.

As depicted in *Figure 5.10a*, first, a theoretical reference tributary area given by a square of side length equal to $3h_{ef}$ is assigned to each anchor of the triangular group. Then, as *Figure 5.10b* shows, keeping the anchor axis as the axis for rotation, the reference theoretical tributary areas ($3h_{ef} \cdot 3h_{ef}$) are rotated until the highest amount of overlap between the reference tributary areas of neighbouring anchors is achieved. Once the condition of the maximum overlap is reached, the individual tributary area is given by the non-overlapping area belonging to the anchor and half of the overlapping area with the neighbouring anchors (see *Figure 5.10b*).

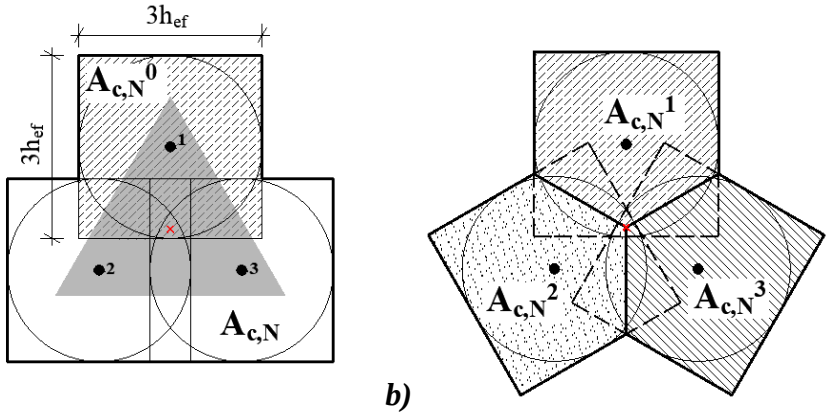

a) *b)*

Figure 5.10. (a) Possible consideration of the projected area with reference projected area of a single anchor; (b) actual projected area of the group based on the considerations below

In other words, the tributary area of an ith anchor within a group can be obtained by subtracting half of the overlapping area with the neighbouring anchors from the reference projected area according to ***Eq. 47***. These tributary areas are identified by the pentagons hatched with different patterns in *Figure 5.10b*. This method is supported by the least energy principle: The highest overlap leads to the lowest total projected area, which in turn leads to the least force required for the breakout.

$$A_{c,N}^{i} = A_{c,N}^{0} - 0.5 \sum A_{c,N}^{p} \qquad \textbf{Eq. 47}$$

Where,

$A_{c,N}^{i}$ is the tributary projected area assigned to the i^{th} anchor

$A_{c,N}^{0}$ is the reference projected area of a single anchor = $9(h_{ef})^2$

$\sum A_{c,N}^{p}$ is the total overlapping area of the i^{th} anchor with all the neighbouring influencing anchors

Note that the method for determining the tributary areas for anchors arranged in a rectangular pattern is a special case of the method for determination of tributary areas for anchors arranged in an arbitrary (non-rectangular) configuration. The definition of the virtual edge at the middle of the adjacent anchors automatically accounts for the maximum overlap or minimum total projected area of the anchor group.

The postulates taken for the consideration of anchor groups of non-rectangular configurations are verified by the experimental results discussed in Section 8.3.2.2, and the verification is given in Section 10.

5.2.3 Considering cracked concrete condition

As it is discussed in Section 4.2, according to the current design of anchorages, the anchor group is to be considered in cracked concrete if the crack initiation cannot be ruled out in the anchorage zone. This is valid even if only one or some of the anchors are intercepted by a crack. If the cracked concrete condition is determined, all anchors of an anchor group are considered to be

intercepted by a crack, and it is assumed that the stiffness of all the anchors go down by the same percentage as that for a single anchor due to the interception by the crack and, therefore, the relative stiffness of the anchor group does not change. However, due to the anchor configuration, crack spacing and loading condition, the requirement that all anchors within a group are intercepted by the crack and therefore have approximately the same stiffness may not always be valid. The assumption that all the anchors are intercepted by the crack is not necessarily conservative (Okelo, 1996). In reality, the stiffness of the anchor group is highly dependent on the real crack pattern. Therefore, conservatively, the worst possible crack pattern and its influence on the group behaviour should be considered in the design. This is possible by using the nonlinear spring modelling approach, since the load-displacement behaviour, and consequently, the stiffness characteristics of each individual anchor within the group is considered explicitly. The question is, how should the spring characteristics be modified to account for the cracked concrete condition at individual anchor level. Note that the method described below is valid only for the anchors that are approved for use in cracked concrete.

First, the spring characteristics should be determined for the individual anchors of the group as it is explained in Sections 5.2.1 and 5.2.2, and the dashed curve depicted in *Figure 5.9* should be obtained. After this, the cracked concrete condition should be accounted for by reducing the failure load and the stiffness in case of concrete cone failure according to ***Eq. 48*** and ***Eq. 49*** (see *Figure 5.11*). This can be done because it is assumed that for static cracks of limited crack widths, which are typically less than 0.3 mm, the concrete cone resistance of the anchors reduces by ca. 30% compared to the concrete cone resistance of the anchors in uncracked concrete. Based on the evaluation of the tests performed in this work on bonded anchors using a high strength epoxy mortar, it appears reasonable to assume that the stiffness of anchors in cracked concrete is also approximately 30% lower than the stiffness of anchors in uncracked concrete. The actual values of reduction in stiffness may vary from one product to another. The typical values of the stiffness of anchors in cracked concrete lie within 30 % to 70 % of the stiffness in uncracked concrete (Mahrenholtz, 2013, Sharma et al., 2014). The tributary area, which is assigned to the individual anchors, is assumed to remain the same as earlier. This is based on the considerations of the CCD Method, where the cracked concrete condition is simply accounted for by 0.7 factor on the group capacity. Furthermore, experimental investigations were performed on single anchors and anchor groups of different configurations to verify the assumptions. The test results are discussed in Section 8.3.3, and the verification is given in Section 10.

$$N^{i}_{Rm,c,cracked} = \alpha_N \cdot N^{0}_{Rm,c} \cdot \frac{A^{i}_{c,N}}{A^{0}_{c,N}} \qquad \textbf{Eq. 48}$$

$$k^{i}_{1-4,cracked} = \alpha_{k,N} \cdot k^{i}_{1-4} \qquad \textbf{Eq. 49}$$

Finally, when the spring characteristics for the individual anchors of a group are ascertained (see *Figure 5.11)*, the particular springs can be assigned to the group. A simple example is given in *Figure 5.12*, where one anchor of a 1×2 anchor group is placed in the uncracked part of the concrete, whereas the other anchor is placed in such a way that it is intercepted by a crack. In this case, the tributary area, which can be assigned for the individual anchors is the same due

to symmetry reasons, whereas the failure load and stiffness of the anchor located in a crack is 30% lower. Although the external tension load is applied concentrically on the group, the different stiffness conditions and load-displacement behaviour of the two anchors result in an eccentricity of internal forces. This behaviour is, however, automatically taken into account by the displacement-controlled non-linear static analysis, which is explained in Section 5.5.

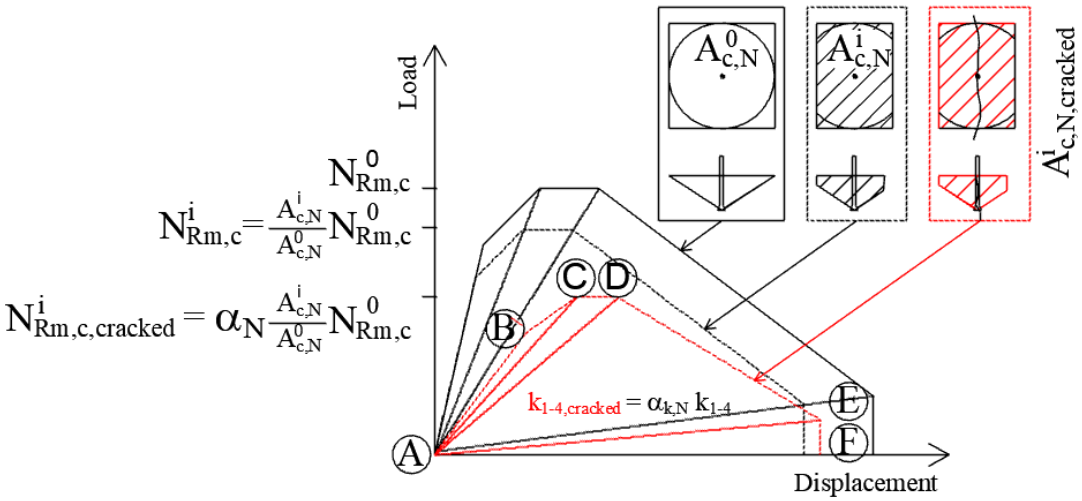

Figure 5.11. Scaling of the idealised curve of a single anchor accounting for cracked concrete condition

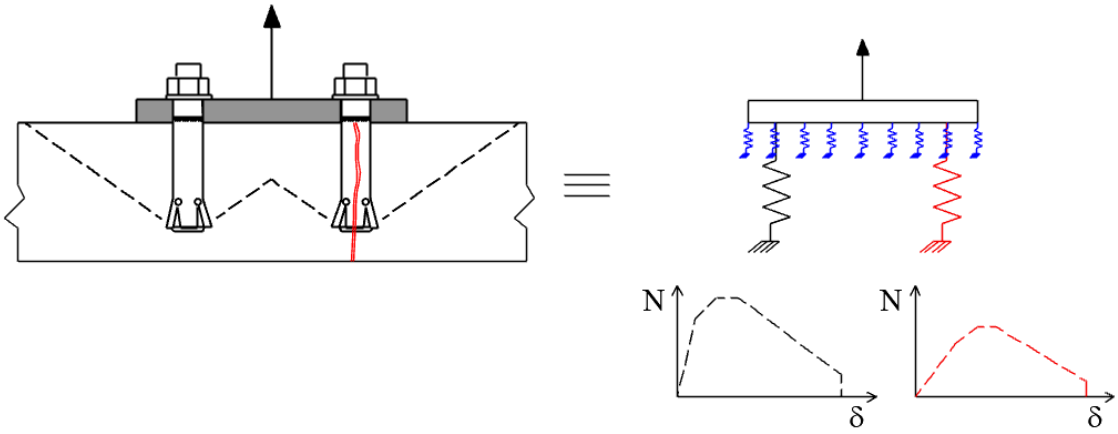

Figure 5.12. Spring properties for an anchor group of 1×2 configuration with one anchor in a crack, one anchor in uncracked concrete

5.3 MODELLING OF THE BASE PLATE

In this section, the requirements on the modelling of the base plate are summarised. The forces acting on an anchor group are transferred to the anchors and concrete via the base plate. Therefore, it should be modelled in such a way that a realistic load transfer and load distribution among the anchors is ensured.

The geometry and the stiffness of the base plate have a significant influence on the force distribution among the anchors of an anchor group and on the load-displacement behaviour of the

group. Therefore, it is essential to consider the base plate geometry as realistically as possible. The current design provisions require the use of a rigid base plate to consider the assumptions made in the CCD Method valid. However, assuming and modelling a rigid base plate in every condition may not be conservative. Having a flexible base plate might result in nonlinear force distribution and high prying forces on the anchors.

Furthermore, different anchor types have different load-displacement behaviour and different stiffness values. This means that for some anchor types, the base plate could be considered as rigid by definition, but for a different type of anchor having very high stiffness values, the same base plate could be considered as flexible. This is because the behaviour of the anchor group depends on the relative stiffness of the base plate, which is the ratio of the anchor stiffness to the base plate stiffness, and not on the absolute value of the stiffness of the base plate (Sections 4.4 and 8.3.2.1). This means that the stiffness of the base plate is rather relative by definition. Therefore, the exact base plate geometry and the material properties should be modelled in the spring model to account for the base plate deformations and stresses automatically, which develop due to the applied loading. The base plate may be modelled by using finite solid elements or shell elements applying thick-plate formulation following the Mindlin-Reissner plate theory.

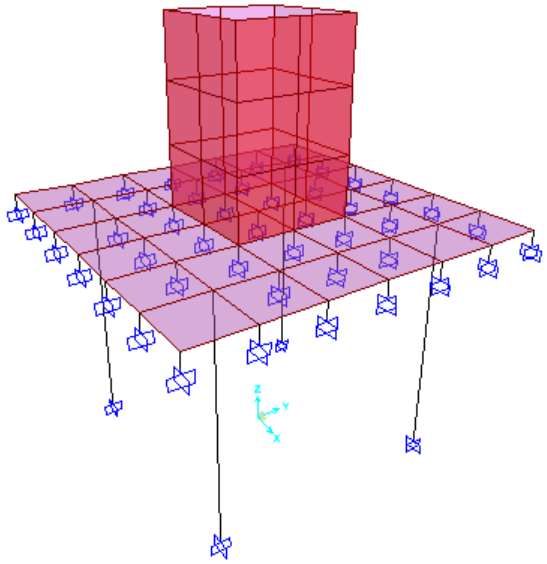

Figure 5.13. Example of modelling of an anchorage with attachment using finite shell elements

The model should also consider the welded profile and the stiffeners or any additional parts, which belong to the base plate and might influence the stiffness conditions. In the case, when the base plate and the profile are modelled with finite shell elements, the attachments should be modelled orthogonal to the base plate while connecting all the corresponding nodes (see example in *Figure 5.13*). Correspondingly, the meshing of the base plate should consider the shape of the attached profile etc. and the anchor location. Within the frame of this dissertation, shell elements applying thick-plate formulation following the Mindlin-Reissner plate theory were used. Alternatively, instead of modelling the attached profile with shell or solid elements, the adequate constraining of the corresponding nodes of the base plate can be modelled (Master-

slave constraint). In a system, where each node has six degrees of freedom, the rotation about all three axes should be constrained, so that all the constrained nodes are rotating equally, whereas the translation in all three directions should be free for all nodes.

Note that the nonlinear spring modelling approach does not aim to define the quantitative requirement of a rigid base plate, where a linear strain profile assumption is valid. It is targeted to analyse the anchor group behaviour for the given base plate geometry. However, the nonlinear spring modelling approach can be used for the optimisation of the base plate geometry or optimisation of anchor type. In this work, the material behaviour of the steel base plate is considered as linear-elastic with an elasticity modulus of $E_s = 200\ GPa$. However, if required, a yield criterion, e.g. von-Mises may be assigned to consider the nonlinear behaviour of the base plate as well. In the nonlinear analysis, the load-displacement behaviour of the group is obtained considering the anchor springs, contact springs and the base plate deformations in every loading step.

5.4 CONTACT BETWEEN THE BASE PLATE AND CONCRETE GROUND

It is clear from Section 5.1 that the concrete as anchorage ground is not modelled discretely in the spring modelling approach. This makes modelling relatively simple and timesaving. The concrete tensile behaviour in case of concrete cone failure of the anchors is considered by the anchor spring characteristics (as discussed in Section 5.2).

However, when anchor groups are loaded eccentrically in tension and/or non-rigid base plate is used, compression forces below the base plate can develop, which may influence the load distribution and hence the anchor group behaviour.

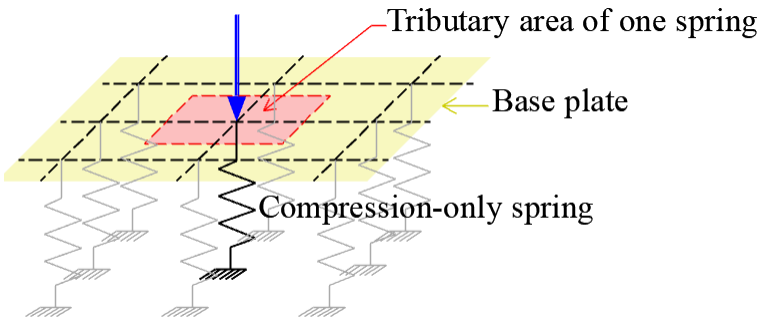

Figure 5.14. Representation of a compression-only contact spring

The developing compression forces between the base plate and concrete surface should be accounted for and therefore, are modelled with contact springs. This is done by modelling elastic bedding below the baseplate using uniformly distributed compression-only springs as shown in *Figure* 5.14.

These springs get active in case the base plate deformations result in compression between the base plate and concrete surface. The compression-only springs are calculated according to the Winkler spring characteristics assuming a modulus of elasticity $E_{cm} = 30\ GPa$. Note that the Winkler spring method is originally an idealization representing the soil medium as a system

of identical but mutually independent, closely spaced, discrete, linear-elastic springs. It is used for modelling the interaction between the structure and soil assuming that a mat foundation sits on vertical linear springs representing the deformable (linear elastic) soil. In the nonlinear spring model, similar springs are used but instead of modelling the interaction between the structure and soil, the developing compressive stresses between the base plate and the concrete (which is not modelled discretely) are accounted for by the compression-only axial springs.

5.5 DISPLACEMENT-CONTROLLED NONLINEAR STATIC ANALYSIS

When the model of an anchorage under tension is developed using (i) the nonlinear tension-only springs for considering nonlinear anchor behaviour (taking into account the tributary areas), (ii) base plate modelled with solid/shell elements and (iii) compression-only springs to model the contact between base plate and concrete; a displacement-controlled nonlinear static analysis is performed. It is essential to perform a displacement-controlled nonlinear static analysis to account for an accurate force distribution and redistribution among the anchors of the group considering their nonlinear behaviour and to account for the base plate deformations. This analysis can be done theoretically by hand calculation for certain simple configurations. However, to use the benefits offered by the approach (arbitrary anchor configuration and base plate stiffness etc.), the analysis is best done by a structural analysis software that is capable of performing nonlinear static analysis.

Displacement-controlled analysis

The displacement-controlled analysis is required in order to capture the influence of stiffness change on the load-distribution and re-distribution among the anchors and to obtain the post-peak branch of the load-displacement curve for the anchorage. It is, however, an iterative process, so the displacement should be increased iteratively until the entire anchorage fails. Alternatively, the analysis can be performed by incrementing the load and following a secant stiffness method to obtain the descending branch. Note that during the entire analysis, the applied load and/or the combination of applied loads (e.g. different forces on different locations or a tension force and a moment) is maintained.

Consideration of nonlinearity

It is required to perform nonlinear analysis to be able to consider the material nonlinearities to account for the anchor group behaviour realistically. The nonlinear anchor behaviour is a material nonlinearity and is considered with tension-only nonlinear (in this work penta-linear) springs. The equation of equilibrium $\{F\} = [k_g]\cdot\{\delta\}$ is solved and the global stiffness matrix is updated in each loading step (*Figure 5.15*). The spring stiffness value $k_{sp,i}$ is updated in each step.

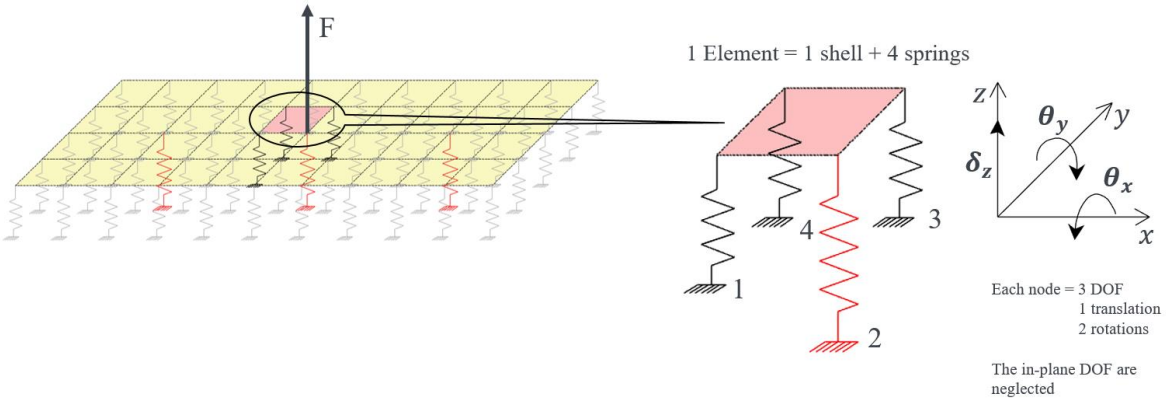

a)

System of equations to be solved: $\{F\} = [k_g]\{\delta\}$

Applied Force Vector

$$\{F\} = \begin{Bmatrix} N_{z,1} \\ M_{x,1} \\ M_{y,1} \\ N_{z,2} \\ M_{x,2} \\ M_{y,2} \\ N_{z,3} \\ M_{x,3} \\ M_{y,3} \\ N_{z,4} \\ M_{x,4} \\ M_{y,4} \end{Bmatrix}$$

Global stiffness matrix of one element for shell + springs

$$[k_g] = \begin{bmatrix} k_{1,1}+k_{sp,1} & k_{1,2} & k_{1,3} & k_{1,4} & k_{1,5} & k_{1,6} & k_{1,7} & k_{1,8} & k_{1,9} & k_{1,10} & k_{1,11} & k_{1,12} \\ k_{2,1} & k_{2,2} & k_{2,3} & k_{2,4} & k_{2,5} & k_{2,6} & k_{2,7} & k_{2,8} & k_{2,9} & k_{2,10} & k_{2,11} & k_{2,12} \\ k_{3,1} & k_{3,2} & k_{3,3} & k_{3,4} & k_{3,5} & k_{3,6} & k_{3,7} & k_{3,8} & k_{3,9} & k_{3,10} & k_{3,11} & k_{3,12} \\ k_{4,1} & k_{4,2} & k_{4,3} & k_{4,4}+k_{sp,2} & k_{4,5} & k_{4,6} & k_{4,7} & k_{4,8} & k_{4,9} & k_{4,10} & k_{4,11} & k_{4,12} \\ k_{5,1} & k_{5,2} & k_{5,3} & k_{5,4} & k_{5,5} & k_{5,6} & k_{5,7} & k_{5,8} & k_{5,9} & k_{5,10} & k_{5,11} & k_{5,12} \\ k_{6,1} & k_{6,2} & k_{6,3} & k_{6,4} & k_{6,5} & k_{6,6} & k_{6,7} & k_{6,8} & k_{6,9} & k_{6,10} & k_{6,11} & k_{6,12} \\ k_{7,1} & k_{7,2} & k_{7,3} & k_{7,4} & k_{7,5} & k_{7,6} & k_{7,7}+k_{sp,3} & k_{7,8} & k_{7,9} & k_{7,10} & k_{7,11} & k_{7,12} \\ k_{8,1} & k_{8,2} & k_{8,3} & k_{8,4} & k_{8,5} & k_{8,6} & k_{8,7} & k_{8,8} & k_{8,9} & k_{8,10} & k_{8,11} & k_{8,12} \\ k_{9,1} & k_{9,2} & k_{9,3} & k_{9,4} & k_{9,5} & k_{9,6} & k_{9,7} & k_{9,8} & k_{9,9} & k_{9,10} & k_{9,11} & k_{9,12} \\ k_{10,1} & k_{10,2} & k_{10,3} & k_{10,4} & k_{10,5} & k_{10,6} & k_{10,7} & k_{10,8} & k_{10,9} & k_{10,10}+k_{sp,4} & k_{10,11} & k_{10,12} \\ k_{11,1} & k_{11,2} & k_{11,3} & k_{11,4} & k_{11,5} & k_{11,6} & k_{11,7} & k_{11,8} & k_{11,9} & k_{11,10} & k_{11,11} & k_{11,12} \\ k_{12,1} & k_{12,2} & k_{12,3} & k_{12,4} & k_{12,5} & k_{12,6} & k_{12,7} & k_{12,8} & k_{12,9} & k_{12,10} & k_{12,11} & k_{12,12} \end{bmatrix}$$

Displacement vector

$$\{\delta\} = \begin{Bmatrix} \delta_{z,1} \\ \theta_{x,1} \\ \theta_{y,1} \\ \delta_{z,2} \\ \theta_{x,2} \\ \theta_{y,2} \\ \delta_{z,3} \\ \theta_{x,3} \\ \theta_{y,3} \\ \delta_{z,4} \\ \theta_{x,4} \\ \theta_{y,4} \end{Bmatrix}$$

b)

Figure 5.15. a) Finite element representation of an anchorage using spring model, b) Equation of equilibrium

Output

The following output is obtained from the analysis: the load-displacement curve of the anchor group (the global displacement of the anchorage), which is the result of the displacement and deformation of the individual components), the load-displacement curves of individual anchors, deformed shape of the base plate and the stresses developed in the base plate. Furthermore, a step-by-step performance check for every component of the model is available. It is intuitive that the accuracy of the nonlinear analysis depends on how well the anchor spring characteristics are determined. The better the characterisation of anchor springs and the estimate of stiffness values, the better the estimate on the anchor group performance. Once a nonlinear analysis

has been performed on the anchorage, its final stiffness matrix and load-displacement behaviour can be used as an input to represent an anchorage component (one equivalent spring) in the structural analysis of a structure.

An indicative example showing seven analysis steps for a concentric loaded 1×3 anchor group located close to a concrete edge is given in *Figure 5.16*. The spring characteristics corresponding to Anchor A, B and C are given as load-displacement curves in the graphs (Spring A, Spring B and Spring C).

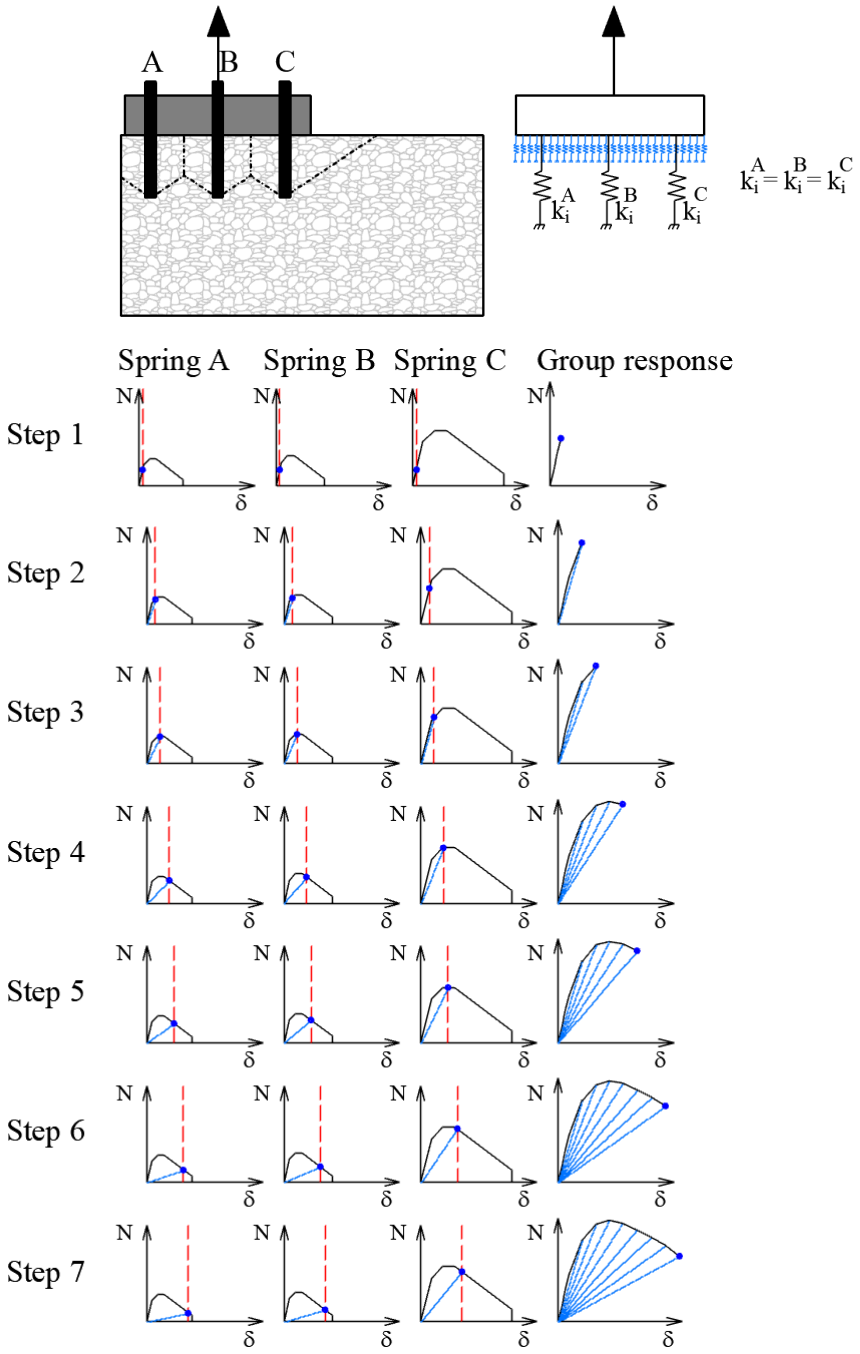

Figure 5.16. Nonlinear static analysis steps using the spring model – a representative example (N and δ correspond to Tension load and Displacement of the anchor or anchor group)

During the analysis, the anchor group is loaded in displacement control by incrementally applying the load until failure. This procedure is shown by the Group response load-displacement curves in every step. The graphs of the contact springs accounting for the developing compression between the base plate and concrete surface were neglected in this example, for the reason of simplicity. *Figure 5.17* shows the step-by-step procedure of the spring model for tension loaded anchor groups. Note that the analysis can be performed following a tangent stiffness matrix approach or a secant stiffness matrix approach. Due to the fact that secant stiffness is always positive, the secant stiffness method provides a more robust method of solution.

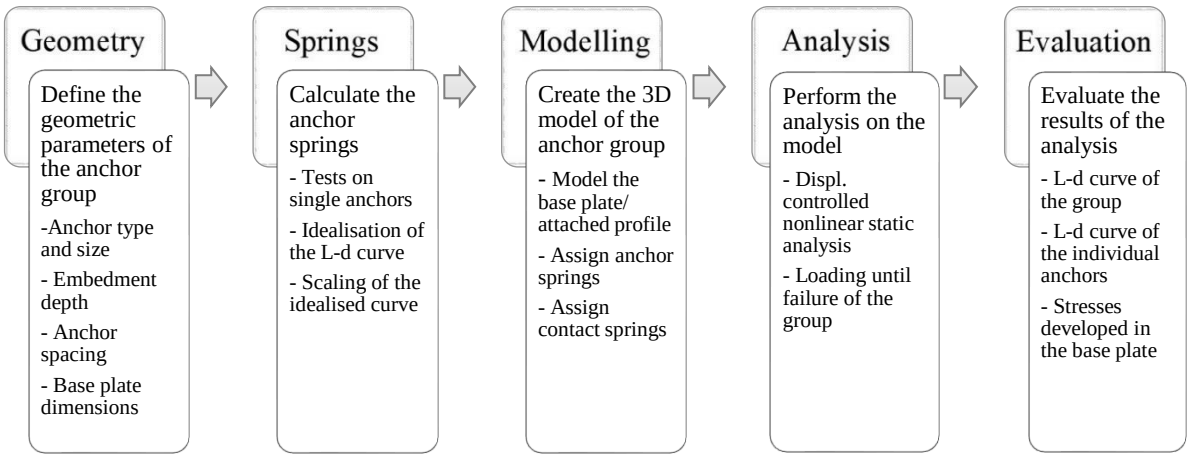

Figure 5.17. Step-by-step procedure of the nonlinear static analysis using spring model for tension loaded anchor groups

5.6 SUMMARY

In Chapter 5, the concept of the nonlinear spring modelling approach for tension loaded anchorages in case of concrete cone failure in uncracked and cracked concrete is discussed. The basic components of the model such as the nonlinear tension-only anchor spring, the compression-only contact springs and the base plate are introduced, and it is explained how to determine them. Furthermore, the modelling principles are described, and recommendations for the modelling of the base plate, modelling of the contact springs and performing an appropriate displacement-controlled nonlinear static analysis are given.

The most essential part to apply the spring model for anchor groups in the case of concrete cone failure is the derivation of the anchor springs from load-displacement curves obtained from single anchor tests. The approach is discussed in detail, and a new tributary area approach is introduced to consider the edge distance and anchor spacing on the load-displacement behaviour of individual anchors of a group of rectangular and non-rectangular configurations. The concept required to set two postulates: The first postulate made in the spring model for the individual anchor properties is the calculation of the mean failure load of an ith anchor, $N^{i}_{Rm,c}$, which is influenced by neighbouring anchors or close edge, and it can be calculated based on the tributary area available for this anchor compared to the projected area of a single anchor ($A^{i}_{c,N}/A^{0}_{c,N}$). The second postulate made in the spring model for the individual anchor properties

is that the tributary area assigned to the i^{th} anchor of the group does not influence the stiffness of the individual anchor and therefore, the stiffness values remain unchanged compared to the stiffness values determined for the corresponding single anchor. The postulates are verified by experimental investigations. The verification of the postulates and the verification of the entire concept of the nonlinear spring modelling approach for the failure mode concrete cone failure is discussed in Chapter 10.

6 CONCEPT OF THE NONLINEAR SPRING MODEL FOR CONCRETE EDGE FAILURE

In Chapter 6, the concept and the development of the nonlinear spring model for evaluation and design of shear loaded anchor groups in the case of concrete edge breakout failure mode are discussed. Section 6.1 summarises the major assumptions made to develop the concept and defines the components used for the nonlinear spring modelling approach. Detailed discussion on the nonlinear spring modelling approach is given in Section 6.2-6.5.

6.1 INTRODUCTION

The behaviour of shear loaded anchor groups is rather complex due to various parameters, which influence the failure mode, the load distribution and the load-displacement behaviour of the anchorage. The anchorages subjected to shear loads might fail due to anchor steel failure, concrete edge failure, pryout failure or pullout failure. Which failure mode is decisive, depends on the anchor type and size, steel grade, anchor embedment depth, concrete strength, edge distance, anchor configuration, anchor spacing and loading direction (Eligehausen et al., 2006). In addition, for more than one anchor rows, the load taken up by different anchor rows and the location of initiation of critical failure crack makes the assessment of anchor groups in shear rather complicated. Furthermore, the load distribution is significantly influenced by the hole clearance pattern in case of anchor groups. Within the frame of this dissertation, a nonlinear spring modelling approach for the concrete edge failure mode of shear loaded anchorages is developed.

The influencing parameters, the basic failure mechanisms and the open questions regarding the load-displacement behaviour of shear loaded anchor groups in case of concrete edge failure are discussed in Sections 2.2.2 and 3.1.3 and Chapter 4, which serve as basis for developing the concept of the nonlinear spring modelling approach for shear loaded anchorages. Furthermore, the knowledge gained during the development of the spring model for the concrete cone failure mode of tension loaded anchorages is applied. It should be highlighted that the concrete edge breakout failure, just like the concrete cone failure, is a concrete tensile failure, which occurs when the tensile strength of the anchorage ground is exceeded. However, it is important to define the similarities and differences between the behaviour and modelling of anchor groups, which fail due to concrete cone failure under tension and concrete edge failure under shear.

The spring model for shear aims to describe the realistic behaviour of shear loaded anchor groups, which fail due to concrete edge failure. However, it is not aimed to divide the concrete edge failure into the particular components or mechanisms leading to failure but it is aimed to use the load-displacement behaviour corresponding to concrete edge failure mode. Furthermore, it is not aimed to pre-decide, where the failure crack initiates. It is described in Section 4.5 that the current design approaches handle the problem of the crack initiation differently, but rather conservatively. To avoid the need for preliminary decisions on the failure pattern, it is essential to use a displacement-based approach.

In the nonlinear spring modelling approach for shear loading, it is assumed that the shear forces acting on a group are transferred from the base plate directly to the anchors. The forces acting in the loading direction are resisted by the anchors (concrete edge breakout resistance), and the forces that might develop on the anchor shaft in the direction opposite to the loading in case of eccentric loading, are transferred also by the anchor; however, considering a resistance in the direction opposite to the loading. In this thesis, this is referred to push-back effect and is explained in *Figure 6.1*. Furthermore, the hole clearance pattern and crack pattern (if any) should be accounted for.

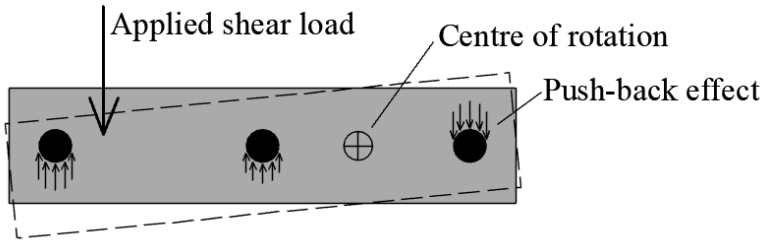

Figure 6.1. Schematic of the bearing actions on the anchors under eccentric shear load

To realise the assumption, the behaviour of the anchors, including the hole clearance, is modelled using uni-directional shear springs active in the loading direction (equivalent to a tension-only spring), while the push-back effect, which is equivalent to the prying action in case of tension loads is modelled using uni-directional shear springs active in the direction opposite to loading (equivalent to a compression-only spring). This latter component is important to consider when an anchor group is subjected to eccentric shear loading or to torsional loading and the shaft of certain anchors is pressing against the concrete in the direction opposite to the loading (far from edge), contributing to the anchorage capacity positively (see *Figure 6.1*). However, this is not considered in the current force-based design provisions, leading to a conservative estimate of the group resistance. The influences such as edge distance and anchor parameters are included in the nonlinear anchor characteristics in case of concrete edge failure and are discussed in detail in Section 6.2. The base plate is modelled using finite shell or solid elements to consider the base plate dimensions realistically (Section 6.4).

Like in the tension model, the complete nonlinear anchor behaviour is considered in the shear model by the anchor springs to enable a realistic force distribution and force redistribution among the anchors of the group and to account for the load redistribution from row-to-row in case of anchorages with multiple anchor rows. However, to consider a realistic load distribution and redistribution among the anchors and to avoid the need of any preliminary decision or assumption on the developing crack pattern, it is essential to perform a displacement-controlled nonlinear static analysis according to Section 6.5.

The components of the spring model are schematically depicted in *Figure 6.2* for an exemplary anchor group of 3×2 configuration, which include:

i. Anchor springs: uni-directional shear springs active in the loading direction (equivalent to a tension-only spring) to model the nonlinear load-displacement behaviour of individual anchors in case of concrete edge failure,

ii. Anchor springs: uni-directional shear springs active in the direction opposite to loading (equivalent to a compression-only spring) to model the pressure on the anchors in the direction opposite to the direction of loading (push-back effect),
iii. Base plate: Finite shell or solid elements to model the base plate realistically.

Note: In this approach, the friction between the base plate and the concrete surface is conservatively ignored. However, it is straightforward to extend the model to consider the influence of friction by using friction elements below the base plate.

The details about the procedure for the determination of the anchor spring characteristics, the modelling of the base plate and the displacement-controlled nonlinear analysis are described in the following Sections 6.2 - 6.5.

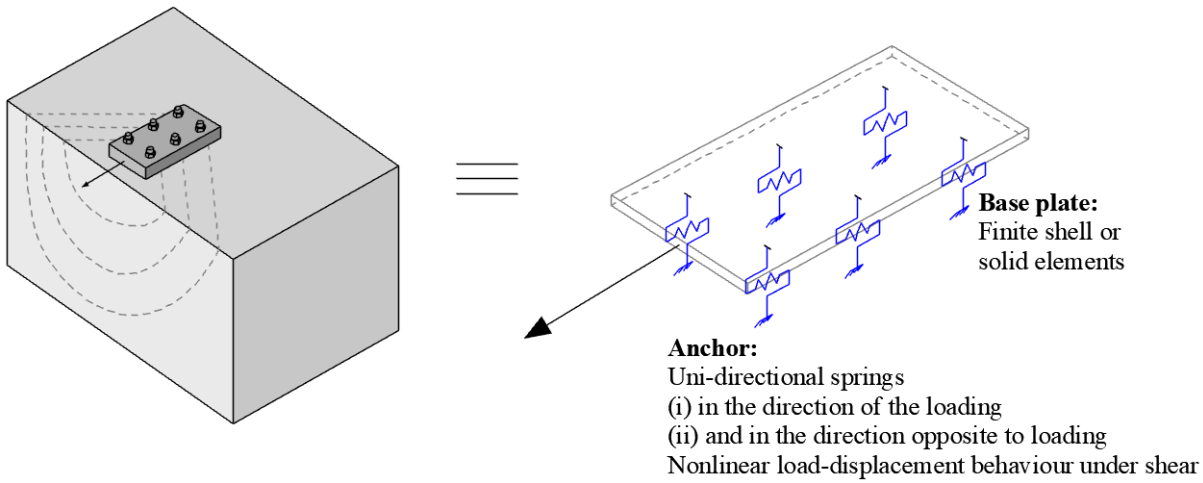

Figure 6.2. Conceptual representation of the spring model for shear loaded anchor groups in case of concrete edge breakout failure

6.2 DETERMINATION OF THE CHARACTERISTICS FOR SPRINGS TO MODEL THE ANCHOR BEHAVIOUR

This section discusses the determination of the spring characteristics to model the anchor behaviour in the case of concrete edge failure of anchor groups. The anchor behaviour in case of shear loading is considered in this thesis by uni-directional shear springs active in the loading direction (equivalent to a tension-only spring) derived from load-displacement curves from shear test on single anchors, which failed due to concrete edge failure.

In the following, it is discussed how the spring characteristics can be derived, and how to consider the influences edge distance in the loading direction (c_1), influence of a further edge parallel to the loading direction (c_2) and anchor spacing in loading direction (s_1) and in the direction perpendicular to loading (s_2). Note that in accordance with the current design provisions, only anchor groups having anchors of the same type, size and embedment depth are covered.

The spring characteristics of a single anchor are, basically, nothing else but the idealised load-displacement curve of the single anchor failed due to a particular failure mode. *Figure 6.3* depicts a schematic drawing of the concrete edge failure of a single anchor with the assumed load-displacement behaviour represented as spring characteristics. This failure can occur, when the

concrete edge fails before the load-bearing capacity of the steel is reached. Similar springs can be derived for other failure modes such as steel failure or pryout failure of shear loaded anchorages. However, that is beyond the scope of this dissertation.

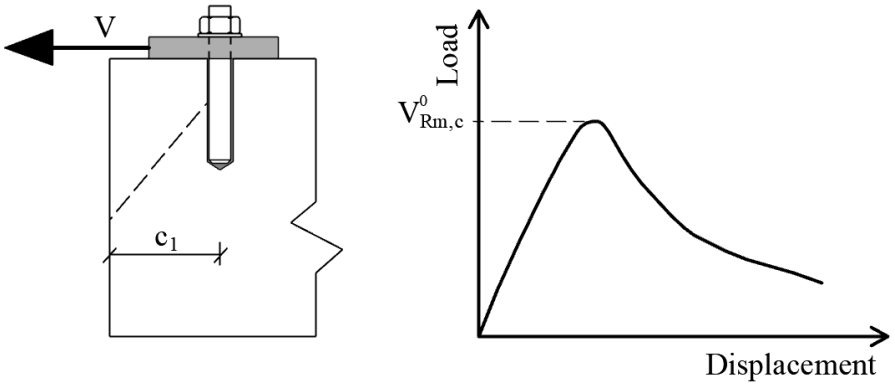

Figure 6.3. Schematic of the concrete edge failure mode of a single anchor with the assumed load-displacement behaviour represented as spring characteristics

It is well known that in the case of anchor groups, the geometric arrangement of the anchors, the anchor spacing and the hole clearance pattern have a significant influence on the concrete edge resistance of the group. Therefore, it is logical that in some cases, even though the shear loaded single anchor would fail by for example steel failure, the anchor group might fail by concrete edge failure depending on the anchor spacing and arrangement. This is due to the group effect. When the anchor spacing is smaller than the critical spacing, then the concrete edge breakout bodies are intersecting leading to a group resistance smaller than *n*-times the single anchor resistance because the concrete tensile strength is utilised before the steel failure of would happen. A simple example having only one anchor row with two anchors is given in *Figure 6.4*.

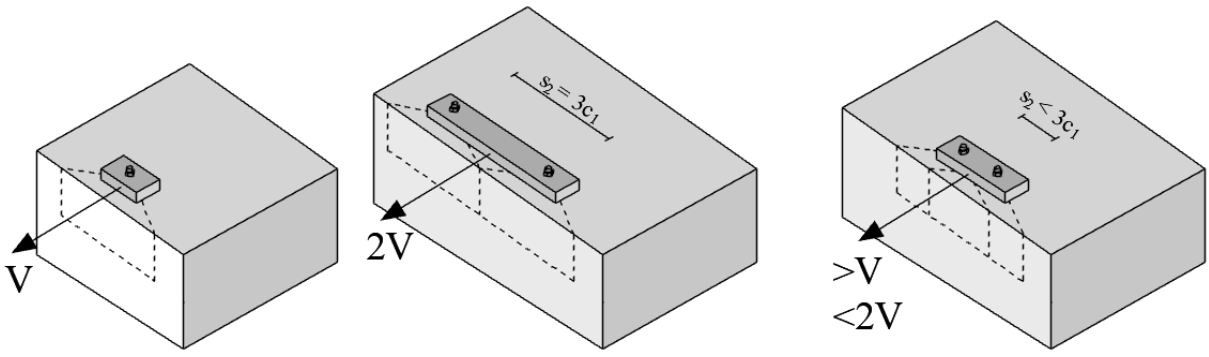

Figure 6.4. Influence of the anchor spacing on the anchorage resistance

6.2.1 Idealisation of the anchor springs for concrete edge failure

The idealisation of the anchor springs can be done, in general, for all kind of failure modes of a single anchor the same way, as it is described for the concrete cone failure of a tension loaded single anchor in Section 5.2.1. Accordingly, in case of concrete edge failure, the spring characteristics should be generated from load-displacement curves of single anchors, which failed due to concrete edge failure.

The idealisation should be done as it is described in Section 5.2.1, however, of course, instead of $N_{Rm,}$ V_{Rm} should be applied. If n number of tests were carried out in one test series, all load-displacement curves should be idealised separately, and the mean value of load and stiffness values should be taken for the spring characteristics ($V_{i,m}=(\sum V_i^g)/n$, where $g = 1 \rightarrow n$ and $k_{i,m}=(\sum k_i^g)/n$, *where* $g = 1 \rightarrow n$). Note that it is also possible that the mean failure load values (V_{Rm}) of the particular single anchor at the corresponding edge distance are calculated on the basis of the CCD Method, and the load-displacement curves are used to define the stiffness values k_1 - k_4. The stiffness values k_1 - k_4 can be used for more edge distances of a particular product if it is assumed that the shear stiffness of the single anchors does not depend on the edge distance, provided all other parameters such as anchor type, size and embedment depth are the same at room temperature (see e.g. in Grosser, 2012, Tian et al., 2018, Bokor et al., 2020). The salient points of the idealised spring properties for the recommended penta-linear format are given in *Figure 6.5* and *Table 6.1*.

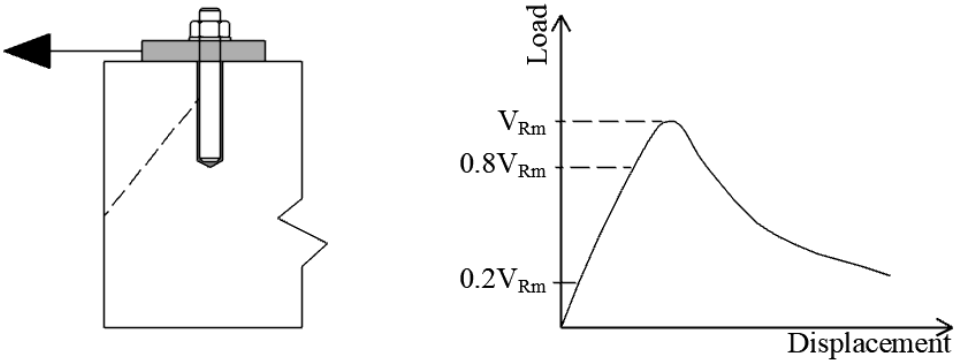

a)

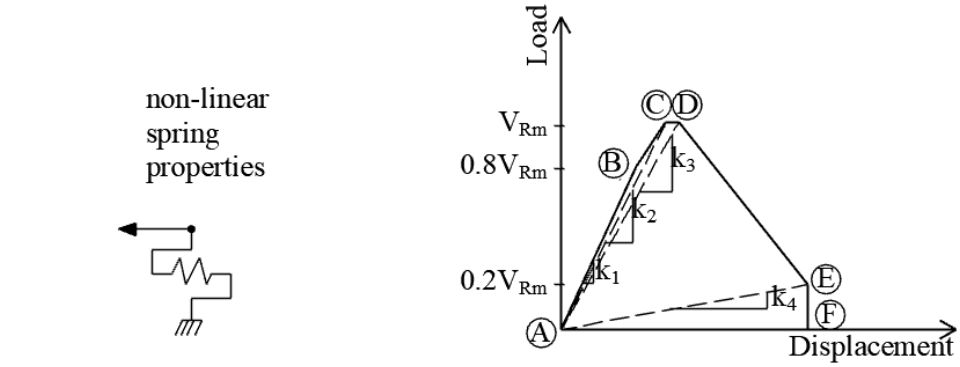

b)

Figure 6.5. Nonlinear spring properties of a shear loaded single anchor: a) Load-displacement curve of a single anchor, which failed by concrete edge failure a_{cl} = 0, "reference" load-displacement curve; b) Idealisation of the "reference" L-d curve to the penta-linear format

Table 6.1. Salient points of the idealised load-displacement curve: spring properties of a single anchor without hole clearance

Point	Load	Stiffness	Displacement
A	0	0	$\delta_A = 0$
B	$0.8 \cdot V_{Rm}$	k_1	$\delta_B = 0.8 \cdot V_{Rm}/k_1$
C	V_{Rm}	k_2	$\delta_C = V_{Rm}/k_2$
D	V_{Rm}	k_3	$\delta_D = V_{Rm}/k_3$
E	$0.2 \cdot V_{Rm}$	k_4	$\delta_E = 0.2 \cdot V_{Rm}/k_4$
F	0	0	$\delta_F = \delta_E$

However, if the hole clearance pattern of the anchors within a group should be considered, then the hole clearance (gap) should be considered in the individual anchor spring properties with an additional segment A-A´, as it is shown in *Figure 6.6* and *Table 6.2*. The hole clearance can be modelled using a gap element (*Figure 6.6b*).

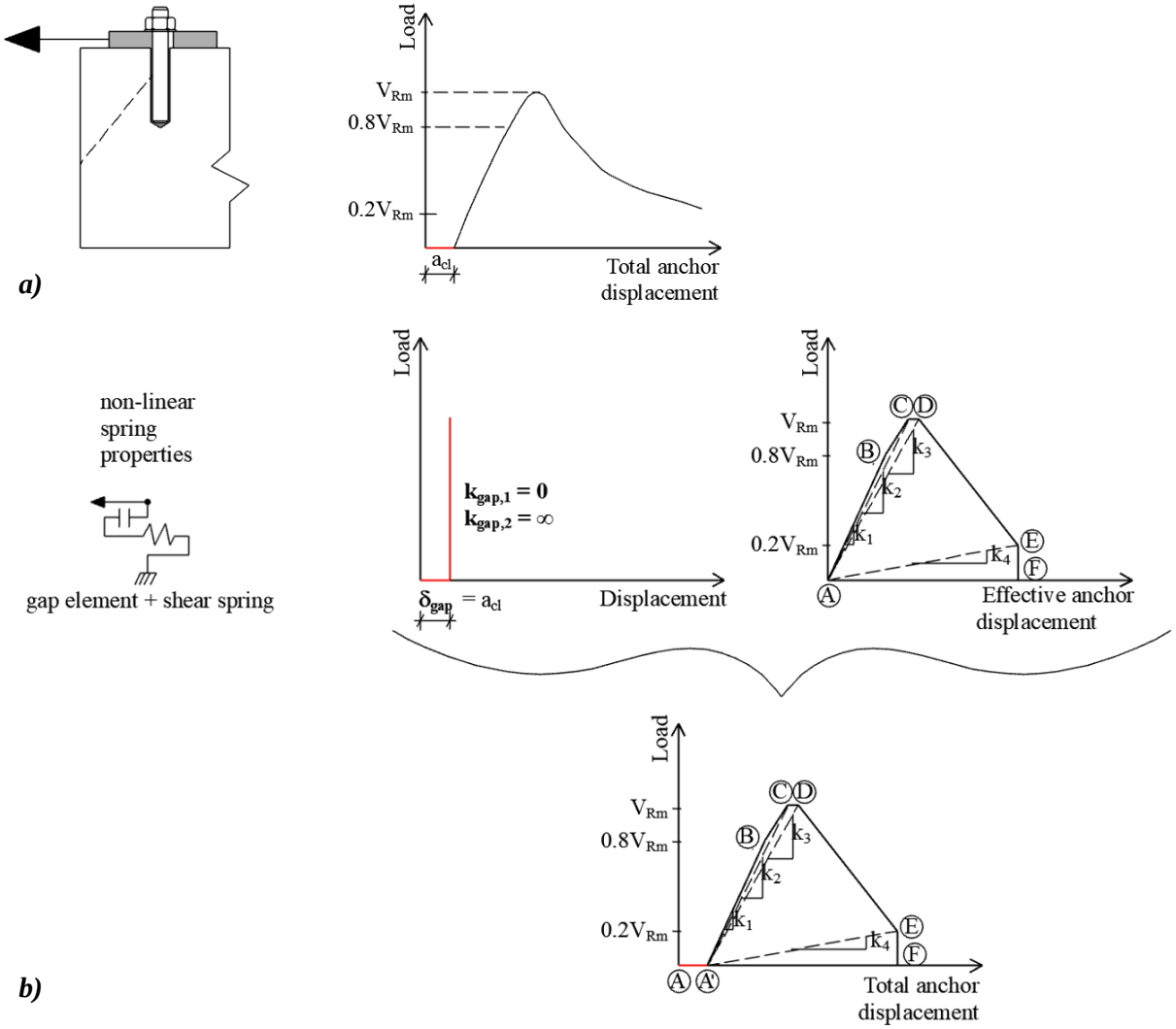

Figure 6.6. Nonlinear spring properties of a shear loaded single anchor: a) Load-displacement curve of a single anchor, which failed by concrete edge failure $a_{cl} > 0$ mm, "reference" load-displacement curve; b) Idealisation of the "reference" L-d curve to the penta-linear format using gap element and shear spring

Table 6.2. Salient points of the idealised load-displacement curve: spring properties of a single anchor with hole clearance "a_{cl}"

Point	Load	Stiffness	Displacement
A	0	0	$\delta_A = 0$
A´	0	0	$\delta_{A'} = a_{cl}$
B	$0.8 \cdot V_{Rm}$	k_1	$\delta_B = \delta_{A'} + 0.8 \cdot V_{Rm}/k_1$
C	V_{Rm}	k_2	$\delta_C = \delta_{A'} + V_{Rm}/k_2$
D	V_{Rm}	k_3	$\delta_D = \delta_{A'} + V_{Rm}/k_3$
E	$0.2 \cdot V_{Rm}$	k_4	$\delta_E = \delta_{A'} + 0.2 \cdot V_{Rm}/k_4$
F	0	0	$\delta_F = \delta_{A'} + \delta_E$

6.2.2 Consideration of anchor spacing

6.2.2.1 Anchor groups with one anchor row

For an anchor group having one anchor row only, the shear spring model for concrete edge failure is rather analogous and can be generated in a similar manner as the tension spring model for concrete cone failure. Because in this case the edge distance c_1 is equal for all anchors just like the embedment depth h_{ef} in the tension model. Therefore, the only influence to account for the group effect are the anchor spacing s_2 in the direction perpendicular to the loading direction and the member thickness h. However, this is not valid for the case for anchor groups of multiple anchor rows (Section 6.2.2.2).

In *Figure 6.7*, four cases are shown, which are, basically, analogous to the case for concrete cone failure (compare *Figure 5.6*). *Figure 6.7a* depicts the spring characteristics for a single anchor, which fails due to concrete edge breakout. It is intuitive that the same spring characteristics can be assigned to the two single anchors if they are placed at a spacing s_2 equal to or greater than $3c_1$ (*Figure 6.7b)*. In this case, two separate breakout bodies can develop and the behaviour of each anchor can be described by the load-displacement curve obtained from shear tests on single anchors. The same spring characteristics can be applied, when two individual anchors with $s_2 \geq 3c_1$ are connected by a common base plate (*Figure 6.7c*). Under concentric shear loading, the resistance of the anchor group against concrete edge failure will be twice the resistance of the corresponding single anchor since sufficient volume of concrete is available for each anchor to develop its full capacity. However, if the spacing between the anchors is less than the critical spacing ($s_2 < 3c_1$), the capacity of the group will be smaller than 2-times the capacity of the single anchor. This requires the modification of the spring characteristics to account for the influence of anchor spacing (*Figure 6.7d*).

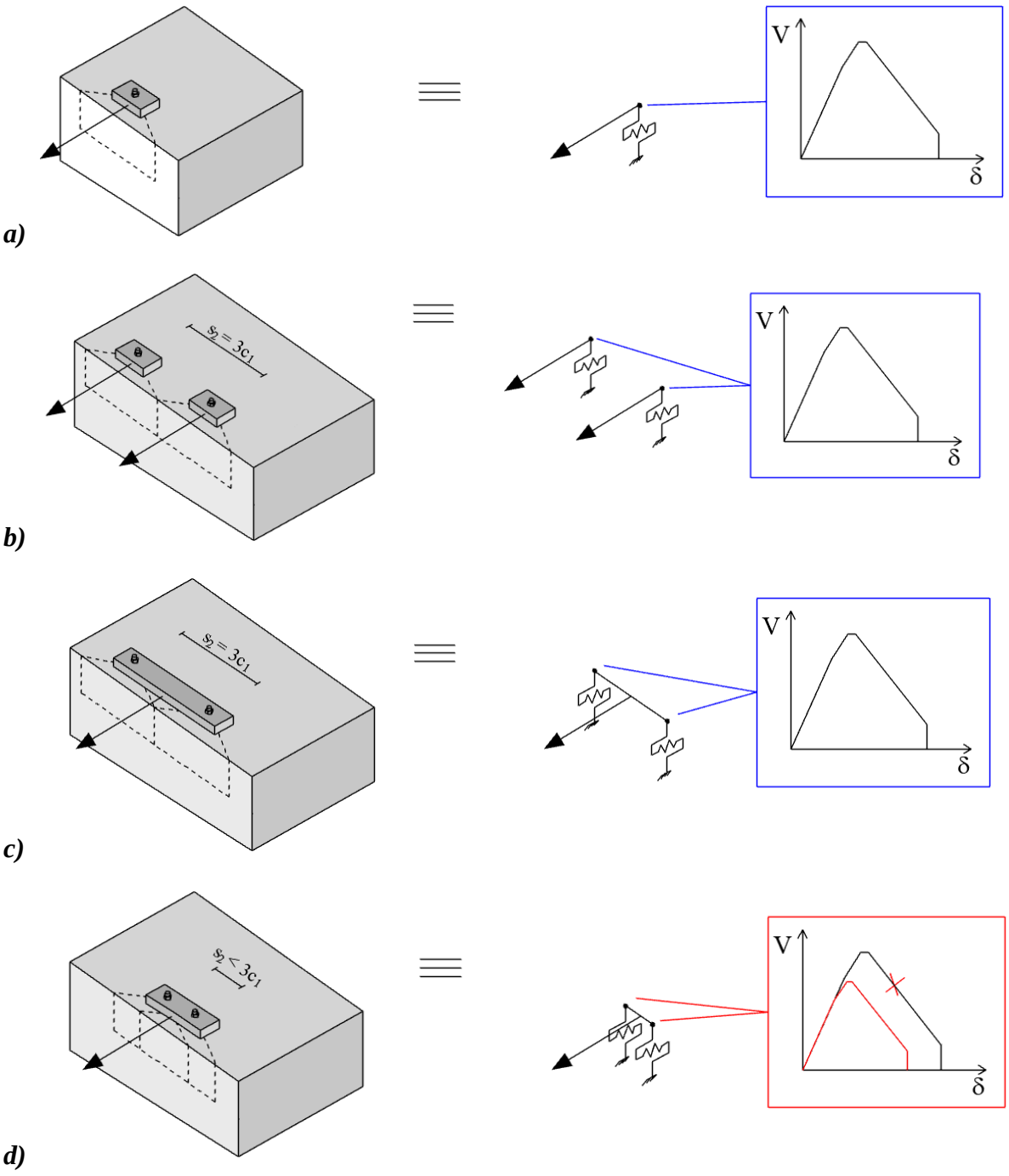

Figure 6.7. Modelling of anchorages using nonlinear springs: a) a single anchor b) two single anchors with $s_2 = 3c_1$, c) anchor group with $s_2 = 3c_1$ and d) anchor group with $s_2 < 3c_1$

According to the CCD Method, the failure load of a shear loaded anchor group in case of concrete edge failure can be evaluated in a similar manner as for tension loaded anchors in case of concrete cone failure, namely by means of projected areas. However, in this case, the projection is on the front surface (see *Figure 3.9*, *Figure 6.8*). According to the CCD Method, the influence of the spacing on the group resistance is taken into account by the factor $A_{c,V}/A^{0}_{c,V,}$ where the concrete edge breakout resistance is increasing in proportion to the projected area of the group (Fuchs et al., 1995, Eligehausen et al., 2006). The projected area of a single anchor that is not

influenced by a further concrete edge and adjacent anchors is calculated according to ***Eq. 20*** and the projected area of an example anchor group depicted in *Figure 6.8* is calculated according to ***Eq. 50***, respectively.

$$A_{c,V} = (1.5 \cdot c_1) \cdot (3 \cdot c_1 + 2 \cdot s_2) \qquad \textbf{Eq. 50}$$

$$V_{Rm,c} = V^0_{Rm,c} \cdot n \qquad \text{if } s \geq 3 \cdot c_1 \qquad \textbf{Eq. 51}$$

$$V_{Rm,c} = V^0_{Rm,c} \cdot \frac{A_{c,V}}{A^0_{c,V}} \qquad \text{if } s < 3 \cdot c_1 \qquad \textbf{Eq. 52}$$

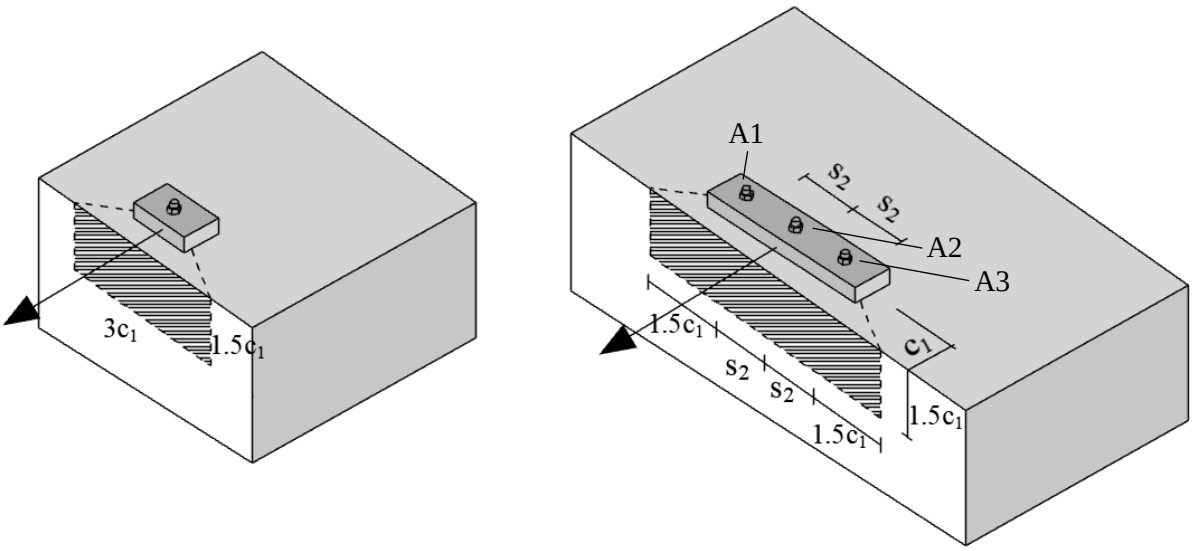

$A^0_{c,V} \rightarrow A_{c,V}$

$V^0_{Rm,c} \rightarrow V_{Rm,c}$

Figure 6.8. Definition of the projected area of a single anchor (left) and of an anchor group of 1×3 configuration close to one concrete edge (right)

By the analogy of the tension model, the projected tributary area of the individual anchors and the resistance of the individual anchors within the group having only one anchor row should be defined. The group of 1×3 configuration is taken to explain the procedure that is used in the spring model to define the tributary areas of individual anchors within the group. It is assumed that the concrete edge failure load of an ith anchor of a group is influenced by the adjacent anchors, and it decreases in proportion to the projected tributary area. The influence of the spacing on the individual anchor resistance compared to the single anchor resistance is taken into account by the factor $A^i_{c,V}/A^0_{c,V}$. Furthermore, in case of anchorages installed in thin members, besides the consideration of the geometric influences by the projected areas, the individual anchor resistance should be multiplied by the factor $\psi_{h,V}$, to account for the fact that the concrete edge resistance does not decrease proportionally to the member thickness, *h* as assumed by the ratio $A^i_{c,V}/A^0_{c,V}$.

Postulate 1:

For the individual anchor properties in the spring model for concrete edge failure, the same postulate is made as for the tension model: The mean failure load of an i^{th} anchor, $V^i_{Rm,c}$, influenced by neighbouring anchors or limited member thickness can be calculated as

$$V^i_{Rm,c} = V^0_{Rm,c} \cdot \frac{A^i_{c,V}}{A^0_{c,V}} \cdot \psi_{h,V} \qquad \textit{Eq. 53}$$

Where,

$$V^0_{Rm,c} = 1.33 \cdot k_9 \cdot {d_{nom}}^{\alpha} \cdot {l_f}^{\beta} \cdot \sqrt{f_{cm}} \cdot {c_1}^{1.5} \qquad \textit{Eq. 54}$$

$$\psi_{h,V} = (\frac{1.5 \cdot c_1}{h})^{0.5} \geq 1 \qquad \textit{Eq. 55}$$

$V^0_{Rm,c}$ is the basic concrete edge breakout strength of the anchor not influenced by the neighbouring anchors or further edge, given by ***Eq. 54*** or obtained from single anchor tests, kN

$A^i_{c,V}$ is the tributary projected area assigned to the anchor considering the distance from the adjacent anchors and thin member when applicable, mm^2

$A^0_{c,V}$ is the reference projected area of a single anchor with, given by ***Eq. 20***.

The tributary projected area assigned to an ith anchor is limited either by a virtual edge considered at a distance of half the spacing to the neighbouring anchor, but not more than $1.5c_1$ or by the member thickness if $h < 1.5c_1$. This is explained with the help of the examples in *Figure 6.9* and *Figure 6.10* without and with the influence of member thickness, respectively.

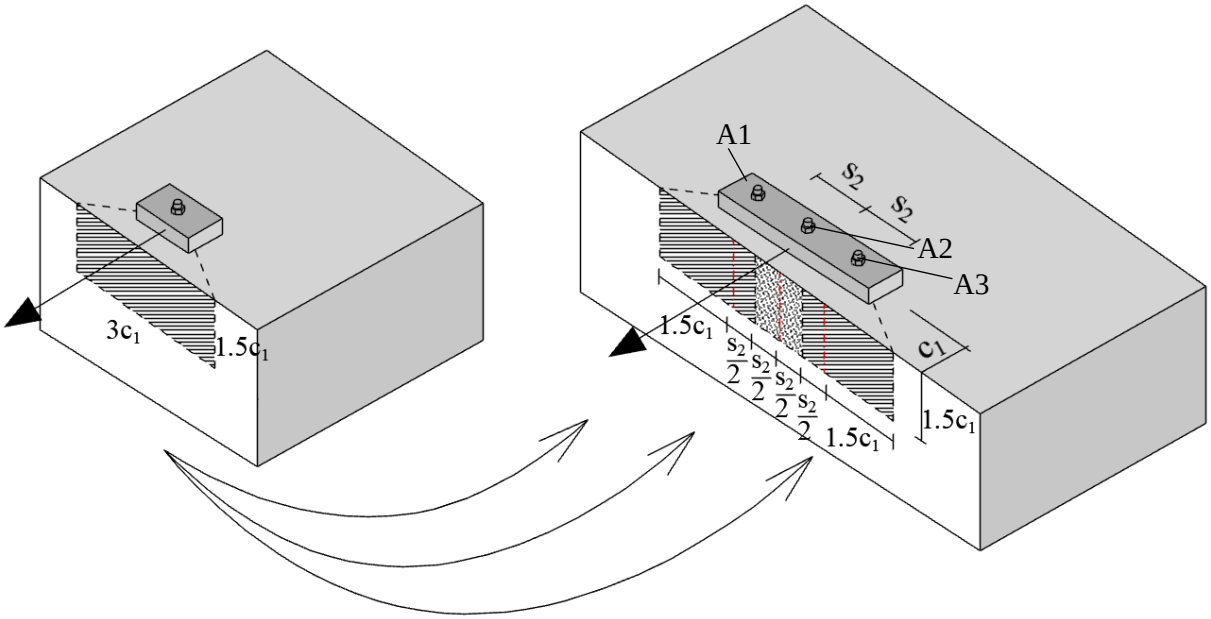

$A^0_{c,V} \rightarrow A^1_{c,V} \quad A^2_{c,V} \quad A^3_{c,V}$

$V^0_{Rm,c} \rightarrow V^1_{Rm,c} \quad V^2_{Rm,c} \quad V^3_{Rm,c}$

Figure 6.9. Definition of the tributary areas and anchor resistances associated with individual anchors in case of concrete edge failure of an anchor group having one anchor row

For the 1×3 anchor group without influence of member thickness (*Figure 6.9*), only the adjacent anchors limit the tributary area. For anchor 1 and 3, the tributary area can be calculated as

$$A_{c,V}^{1} = A_{c,V}^{3} = \left(1.5 \cdot c_1 + \frac{s_2}{2}\right) \cdot (1.5 \cdot c_1) = (1.5 \cdot c_1 + c_{virt}) \cdot (1.5 \cdot c_1) \qquad \textbf{Eq. 56}$$

For anchor 2 (middle anchor), the tributary projected area is limited by both the adjacent anchors. The tributary area can be calculated as

$$A_{c,V}^{2} = (s_2) \cdot (1.5 \cdot c_1) = (2 \cdot c_{virt}) \cdot (1.5 \cdot c_1) \qquad \textbf{Eq. 57}$$

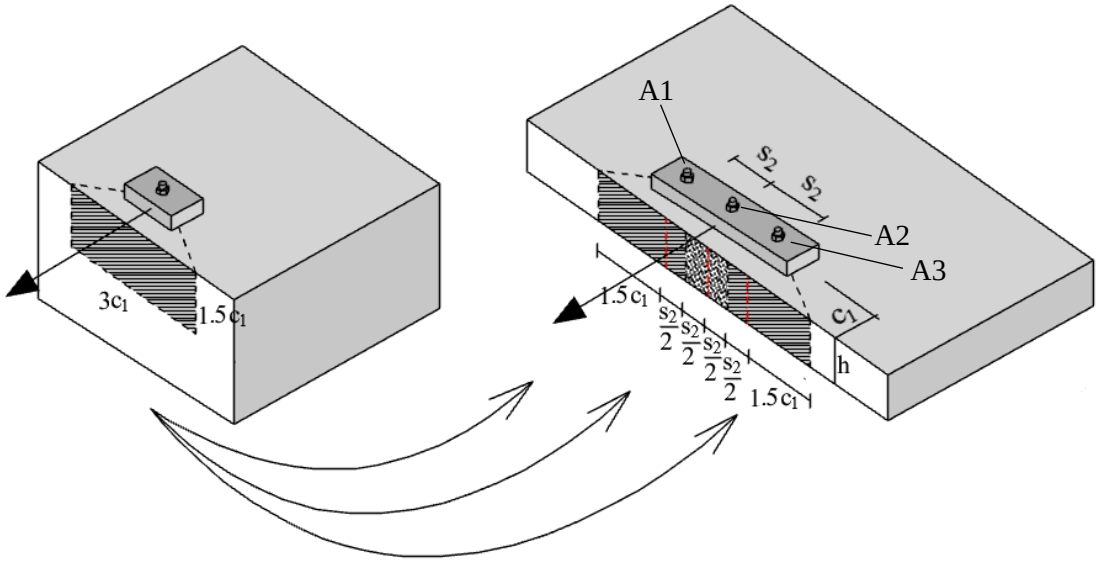

$$A_{c,V}^{0} \rightarrow A_{c,V}^{1} \quad A_{c,V}^{2} \quad A_{c,V}^{3}$$

$$V_{Rm,c}^{0} \rightarrow V_{Rm,c}^{1} \quad V_{Rm,c}^{2} \quad V_{Rm,c}^{3}$$

Figure 6.10. Definition of the tributary areas and anchor resistances associated with individual anchors in case of concrete edge failure of an anchor group having one anchor row in a thin member

For the 1×3 anchor group with the influence of member thickness as shown in *Figure 6.10*, the adjacent anchors, and the member thickness limit the tributary area. For anchor 1 and 3, the tributary area can be calculated as

$$A_{c,V}^{1} = A_{c,V}^{3} = \left(1.5 \cdot c_1 + \frac{s_2}{2}\right) \cdot h = (c_2 + c_{virt}) \cdot h \qquad \textbf{Eq. 58}$$

For anchor 2 (middle anchor), the tributary projected area is limited by both the adjacent anchors. The tributary area can be calculated as

$$A_{c,V}^{2} = (s_2) \cdot h = (2 \cdot c_{virt}) \cdot h \qquad \textbf{Eq. 59}$$

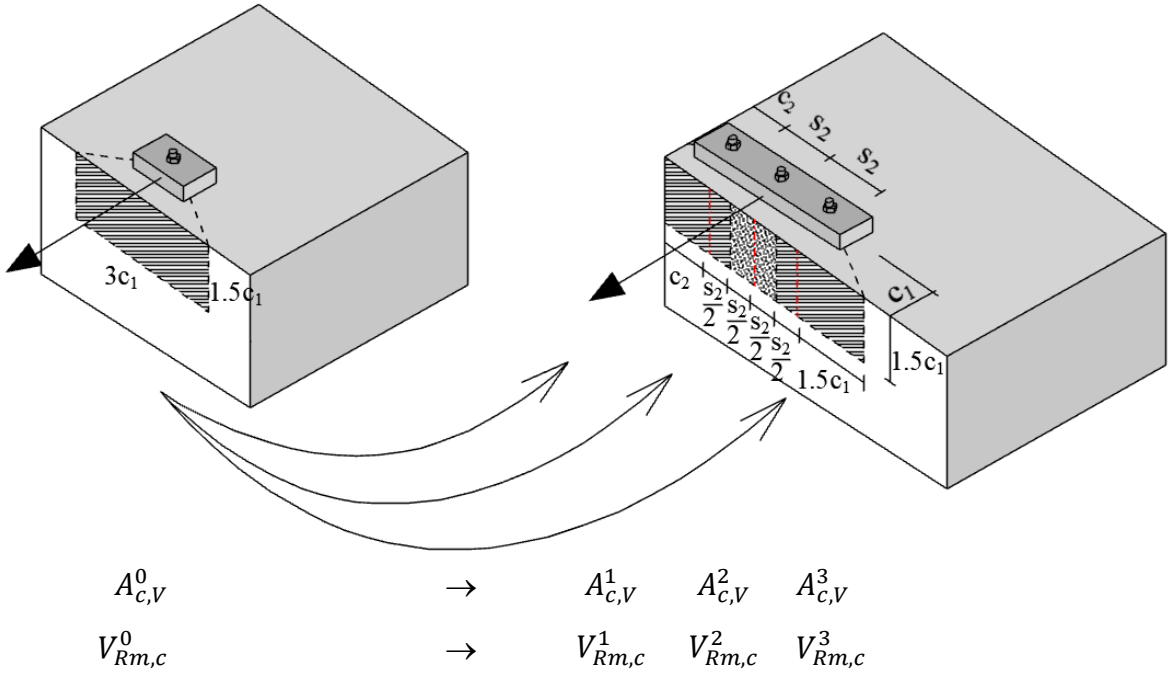

Figure 6.11. Definition of the tributary areas and anchor resistances associated with individual anchors in case of concrete edge failure of an anchor group influenced by a further edge parallel to the loading direction

For the 1×3 anchor group influenced by a further edge parallel to the loading direction as shown in *Figure 6.11*, the adjacent anchors, and a second close edge limit the tributary area for the anchor closest to the further edge. For anchor 1, the tributary area can be calculated as

$$A^1_{c,V} = \left(c_2 + \frac{s_2}{2}\right) \cdot (1.5 \cdot c_1) = (c_2 + c_{virt}) \cdot (1.5 \cdot c_1) \qquad \textbf{Eq. 60}$$

For anchor 2 (middle anchor), the tributary projected area is limited by both the adjacent anchors. The tributary area can be calculated as

$$A^2_{c,V} = (s_2) \cdot (1.5 \cdot c_1) = (2 \cdot c_{virt}) \cdot (1.5 \cdot c_1) \qquad \textbf{Eq. 61}$$

For anchor 3, the tributary area can be calculated as

$$A^3_{c,V} = \left(1.5 \cdot c_1 + \frac{s_2}{2}\right) \cdot (1.5 \cdot c_1) = (1.5 \cdot c_1 + c_{virt}) \cdot (1.5 \cdot c_1) \qquad \textbf{Eq. 62}$$

Postulate 2:

The second postulate for the individual properties of shear loaded anchors is the same as for the tension model: The tributary area assigned to an ith anchor of the group does not influence the anchor stiffness (k_1 - k_4 in *Figure 6.5*) and the stiffness values remain unchanged from the stiffness values determined for the corresponding single anchor away from other influences. Furthermore, the determined stiffness values can be applied for different edge distances, provided that the other installation parameters are the same. This assumption is based on the conclusions given in the literature (Grosser, 2012, Tian et al., 2018, Bokor et al., 2020).

Finally, if the tributary area, which belongs to an ith anchor of a group, is determined and the further influence of the member thickness is accounted for by the factor $\psi_{h,V}$, then the spring characteristics for the ith anchor can be determined by scaling the reference spring characteristics of the single anchor by following the postulates stated above. This is done by calculating the failure load for individual anchor according to ***Eq. 53*** while maintaining the stiffness values for each characteristic points of the curve unchanged. The method to derive individual anchor spring characteristics represented by the dashed-curve from the original spring characteristics valid for a single anchor away from all influences, depicted by the solid line is illustrated in *Figure 6.12* can be directly used as spring characteristics for an ith anchor in the group depicted e.g. in *Figure 6.9*.

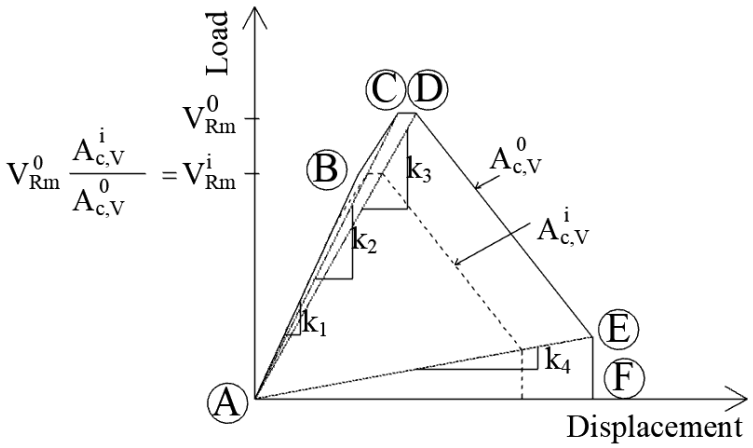

Figure 6.12. Scaling of the idealised curve of a single anchor failed by concrete edge breakout considering tributary areas

Note that the method for considering the group effect with projected areas in case of concrete edge failure is valid only if the anchor group consists of a single anchor row (anchors arranged parallel to the edge). As the sum of individual tributary areas is equal to the total projected area and the stiffness of all anchors is equal, in case of concentric shear and a rigid base plate (rigid perpendicular to the loading direction), the spring model should result in the same concrete edge resistance as the calculated concrete edge resistance based on the CCD method. In the case of concentric shear, the spring model should result in the same concrete edge resistance as the calculated concrete edge resistance based on the CCD Method. Verifications for such cases are shown in Section 9.4.3. However, under eccentric loading, due to the possible rotation of the baseplate about the vertical axis, some of the anchors of the group might push the concrete

in the direction opposite to the direction of loading (push-back effect) that is analogous to the prying action of the base plate under tension loading. Therefore, to consider the behaviour of the group in case of eccentric loading appropriately, the compression forces developing in the direction opposite to loading direction should be accounted for. This is explained in Section 6.3.

The benefits offered by the spring model are much more pronounced in case of anchorages with multiple anchor rows since the spring model can account for a realistic force distribution and redistribution among the anchors within one anchor row and multiple rows. To consider these, however, further development of the model is required, which is explained in the following Section 6.2.2.2.

6.2.2.2 Anchor groups with multiple anchor rows

The behaviour of anchor groups with multiple anchor rows (more than one anchor row arranged one behind the other parallel to the edge) is rather complex and it is strongly influenced by the force distribution and redistribution among the anchors. In Section 6.2.2.1 it is explained, why the tributary area approach used for the tension model can analogously be applied to shear loaded anchor groups having one anchor row only. This is because the edge distance of all anchors is the same. However, in the case of anchor groups having multiple rows, every anchor row has a different edge distance. This leads to the fact that the tributary area approach cannot be simply overtaken for this case because it cannot be simplified to a 2D problem. Instead, it is a 3D problem, where the load-displacement behaviour of the anchor group depends on the activation order of the anchors, and the amount of activated concrete by the individual anchors. The current design approaches based on the CCD method utilize the projected area method to calculate the concrete edge failure capacity of the group. Therefore, it is required to make a prejudgement regarding the appearance of the failure crack for the anchorage, namely, either from the front row (EN 1992-4) or possibly from the middle or back row (fib Bulletin 58, ACI 318). However, in any case, from one particular anchor row, and no force redistribution is accounted for. However, to allow a realistic force distribution and redistribution, which is aimed by the spring model, the failure crack pattern should not be assumed or decided in advance, but the task is to determine the resistance and the load-displacement behaviour of individual anchors within a group, which are influenced by the adjacent anchors.

In the spring modelling approach for shear, due to the 3-dimensional framework of the problem, the tributary area approach is extended into a tributary volume approach to consider all the dimensions necessary for a realistic evaluation of anchor groups. However, it is not straightforward how much volume of concrete can be attributed to a particular anchor of a group. In the following, the developed tributary volume approach and the assumptions taken are explained through an example of a 2×3 anchor group (*Figure 6.13)*. By extension of the shear model for anchor groups having one anchor row and calculating using tributary areas, the tributary volume of the individual anchors and the resistance of the individual anchors within the group is determined. It is taken into account that the concrete edge failure load of an i^{th} anchor of a j^{th} row of a group is influenced by the adjacent anchors both orthogonal direction. The resistance of this particular i^{th} anchor of j^{th} row decreases in proportion to its tributary volume compared to the tributary volume of a single anchor having the same edge distance and with all the other conditions remaining same. The influence of the spacing s_1 and s_2 on the individual anchor resistance,

compared to the single anchor resistance (of the same edge distance), is taken into account by the factor $V_{c,V}^{i,j}/V_{c,V}^{0,j}$.

Furthermore, in case of anchorages installed in thin members, besides the consideration of the geometric influences by the projected volumes, the individual anchor resistance should be multiplied by the factor $\psi_{h,V}$ to account for the fact that the concrete edge resistance does not decrease proportionally to the member thickness h as assumed by the ratio $V_{c,V}^{i,j}/V_{c,V}^{0,j}$. Thus, for the individual anchors within an anchor group, the mean failure load of an ith anchor of a jth row, $V_{Rm,c}^{i,j}$, influenced by neighbouring anchors or an edge or limited member thickness can be calculated as

$$V_{Rm,c}^{i,j} = V_{Rm,c}^{0,j} \cdot \frac{V_{c,V}^{i,j}}{V_{c,V}^{0,j}} \cdot \psi_{h,V} \qquad \textbf{\textit{Eq. 63}}$$

The following dimensions are considered for a single anchor without the influence of neighbouring anchors as it is shown in *Figure 6.13a* and *b* for two edge distances, namely for the front row and back row, respectively: (i) $3c_1$ projected to the front in the horizontal direction, (ii) $1.5c_1$ projected to the front in vertical direction and (iii) c_1 projected to the top, which results in a volume equal to $4.5c_1^3$. Note that this volume is nothing else but the projected area in accordance with the CCD Method multiplied by c_1. Thus, for groups with a single anchor row, the tributary volume approach automatically reduces down to the tributary area approach as given by ***Eq. 53***. The tributary volume assigned to an i^{th} anchor of a j^{th} row of a group is limited either by a virtual edge considered at a distance of half the spacing to the neighbouring anchor, but not more than $1.5c_1$ projected to the front in horizontal direction or by the member thickness if $h < 1.5c_1$ projected to the front in vertical direction.

Note: The actual volume of the theoretical breakout body would be less than the volume of the parallelepiped formed by extruding the projected area. However, since ***Eq. 63*** utilizes the ratio of the volume of an anchor to the reference volume rather than the actual volume itself, it does not result in any inaccuracy since the reference volume is also calculated based on the reference parallelepiped. It is clear that calculating the volume of a parallelepiped is much simpler than calculating the volume of an actual breakout body. The primary reason to utilise a tributary volume approach instead of a tributary area approach is the fact that for groups with more than one anchor rows, the problem becomes 3-dimensional. One of the major concerns in the case of groups with more than one anchor row is, what is the influence of the presence of front anchors on the resistance/behaviour of the group? It is known from the past research (Grosser, 2012, Sharma et al., 2017) that in case of anchor groups without hole clearance if the ratio of the anchor row spacing to edge distance is neither too large nor too small, the initial cracks appear from the front anchor rows but the failure crack appears from the back anchor row. Even though the initial stiffness for all the anchors would be same (if the stiffness is assumed to be independent of the edge distance), due to the onset of cracking at the front anchor row, the stiffness of the front rows would go down and the load will be taken up by the anchors in the back rows. To take this aspect into account realistically, in the spring model, in case of anchors having another anchor in the front, the tributary volume of the front anchor is deducted from the tributary volume of the anchor in the back row (see *Figure 6.13d* and ***Eq. 66*** and ***Eq. 67***).

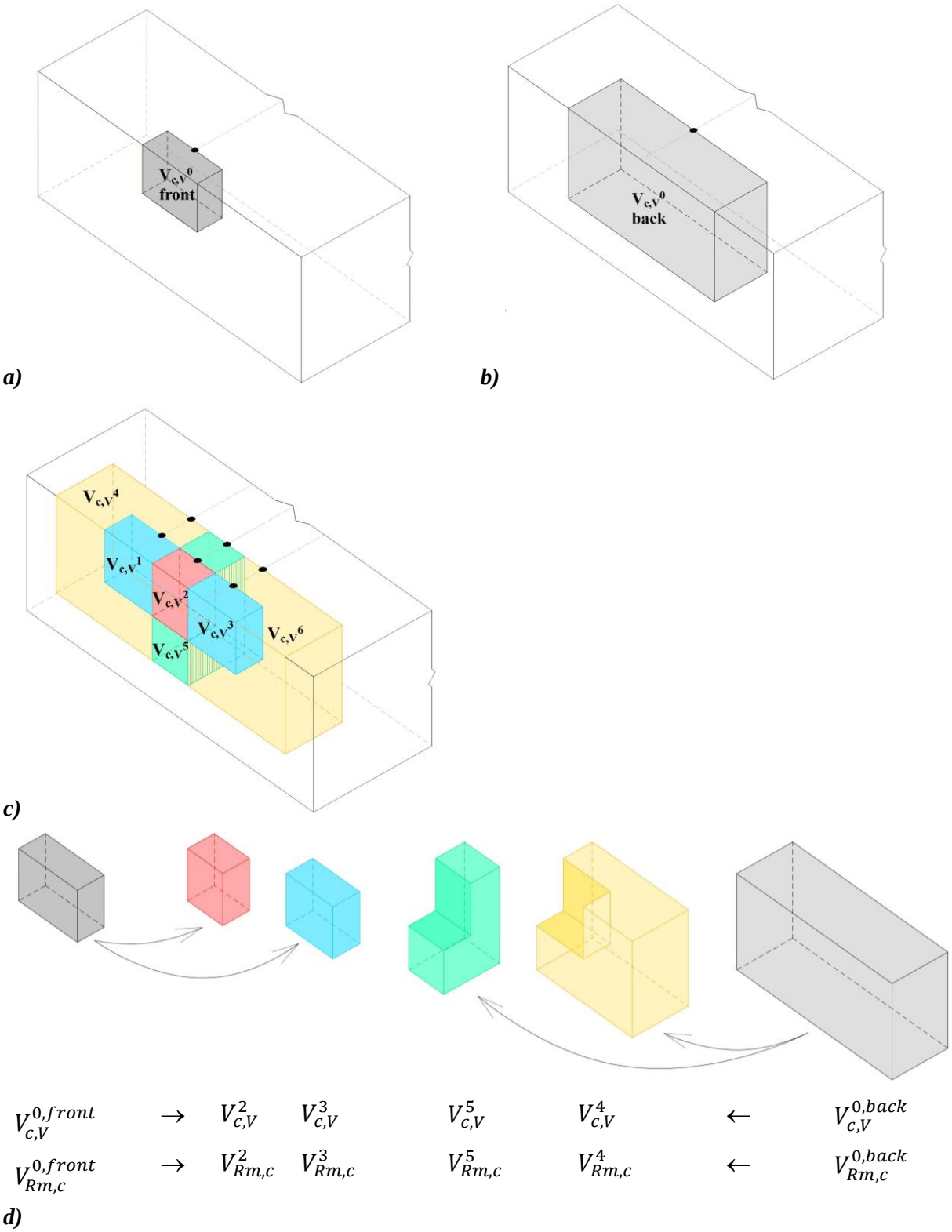

a) *b)* *c)* *d)*

Figure 6.13. a)Tributary volume of the front single anchor, b) tributary volume of the back single anchor, c) tributary volumes $V_{c,V}^1$ to $V_{c,V}^6$, d) tributary volumes and anchor resistances associated with individual anchors in case of concrete edge failure of an anchor group of 2×3 configuration

As mentioned before, the breakout body formed by the front anchor or the back anchor is typically in the shape of a half cone (cone split vertically), since we work with the ratio of volumes, using the volume of a parallelepiped that would circumscribe the half cone leads to equally good results. The considerations made here with respect to the tributary volume of the front anchors is also verified by tests and finite element analysis that will be discussed later in Section 9.

Figure 6.13c depicts the volumes $V_{c,V}^{1}$ to $V_{c,V}^{6}$, which can be assigned to the individual anchors of a group of six anchors (two anchor rows with three anchors in each row) based on the tributary volume approach. The edge distance of the front row is $c_{1.1}$ and the edge distance of the back row is $c_{1.2}$. The anchor spacing in the loading direction is s_1 and in the direction perpendicular to the loading is s_2. Intuitively, $s_1 = c_{1.2} - c_{1.1}$. Note that the symbols for spacing and edge distance are not given in *Figure 6.13* to avoid the overcrowding of the drawings. The tributary volumes can be calculated according to ***Eq. 64*** - ***Eq. 67***.

$$V_{c,V}^{1} = V_{c,V}^{3} = \left(1.5 \cdot c_{1.1} + \frac{s_2}{2}\right) \cdot (1.5 \cdot c_{1.1}) \cdot c_{1.1} \qquad \textbf{Eq. 64}$$

$$V_{c,V}^{2} = (s_2) \cdot (1.5 \cdot c_{1.1}) \cdot c_{1.1} \qquad \textbf{Eq. 65}$$

$$V_{c,V}^{4} = V_{c,V}^{6} = \left(1.5 \cdot c_{1.2} + \frac{s_2}{2}\right) \cdot (1.5 \cdot c_{1.2}) \cdot c_{1.2} - V_{c,V}^{1} \qquad \textbf{Eq. 66}$$

$$V_{c,V}^{5} = (s_2) \cdot (1.5 \cdot c_{1.2}) \cdot c_{1.2} - V_{c,V}^{2} \qquad \textbf{Eq. 67}$$

The second postulate made for the shear loaded individual anchor properties is again the same as according to Section 6.2.2.1: The tributary volume assigned to an i^{th} anchor of a j^{th} row of a group does not influence the anchor stiffness (k_1 - k_4 in *Figure 6.5*), and the stiffness values remain unchanged compared to the stiffness values determined for the corresponding single anchor. Of course, the determined stiffness values for a particular edge distance can be applied for different edge distances if the other installation parameters (anchor type, size, concrete grade, steel grade etc.) remain same.

Once the tributary volume of an i^{th} anchor of a j^{th} row of a group is determined, and the influence of the member thickness is accounted for by the factor $\psi_{h,V}$ (if applicable), then the spring characteristics for the i^{th} anchor of a j^{th} row can be defined by scaling the reference spring characteristics of the single anchor (having edge distance equal to that in the j^{th} row) by following the two postulates above. The failure load should be reduced according to ***Eq. 63***, while the stiffness values k_1 - k_4 of the curve remain unchanged. The dashed curve in *Figure 6.14* can be directly used as spring characteristics for an i^{th} anchor in the group depicted in *Figure 6.13*. *Figure 6.15* shows the springs of the model for the discussed group schematically.

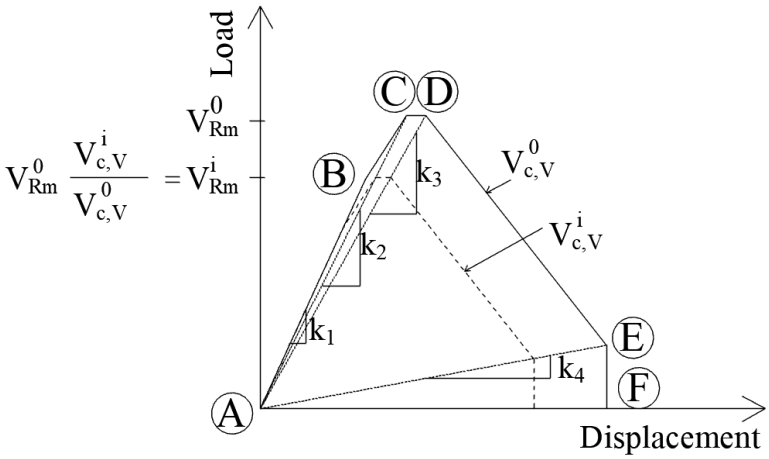

Figure 6.14. Scaling of the idealised curve of a single anchor failed by concrete edge breakout considering tributary volumes

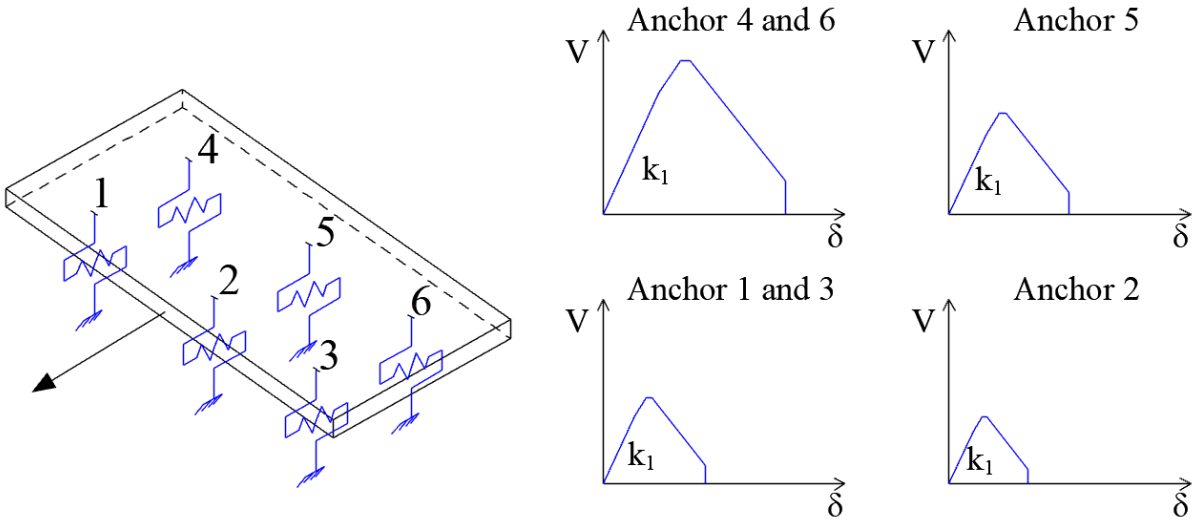

Figure 6.15. Spring model of an anchor group of 2×3 configuration loaded in concentric shear with the corresponding spring properties in the direction of the loading in case of concrete edge failure

This approach was verified against a vast number of tests on different anchor group configurations and specimen geometries, conducted within the framework of this thesis and against test results from the literature. The details about the test program are described in Sections 9.1.1 and 9.2, respectively. The test results are discussed in detail in Chapter 9. To consider the behaviour of anchor groups in case of eccentric loading, the compression forces developing in the direction opposite to loading direction should be accounted for. This is explained in Section 6.3.

6.2.2.3 Anchor groups of arbitrary configuration anchor rows

One of the biggest advantages the spring model has to offer is that the evaluation and design of anchor groups of arbitrary configurations is possible. This is due to the fact that in the nonlinear spring modelling approach, the load-displacement behaviour of the individual anchors is taken into account. Following the approach for anchor groups with multiple rows presented in Section 6.2.2.2, the evaluation of anchor groups of arbitrary configurations is also possible. The tributary volumes for each individual anchor should be determined starting from the front row and proceeding from row to row just like in *Figure 6.13*. Finally, the tributary volume of each

anchor should be compared to the tributary volume of the single anchor with the corresponding edge distance, and the individual anchor resistance can be determined according to ***Eq. 63***. Then, the reference spring properties (idealised load-displacement curve) should be scaled for each anchor. Note that the developed approach can also be used if the concrete specimen is arbitrary, and the edge distance is variable in the front due to considering tributary volumes instead of areas projected to the front. To verify that the approach also works for anchor groups of arbitrary configurations and for anchorages placed in specimens with non-regular geometries, shear-loading tests were carried out on triangular and hexagonal configurations. Furthermore, tests were done on 1×3 configuration in a specimen with a step in front of the middle anchor (different edge distance for outer anchors). The test results are presented in Sections 9.4.2 and 9.4.3, and the verification of the model is summarised in Section 11.

6.2.3 Considering cracked concrete condition

Section 5.2.3 describes how to consider the cracked concrete condition in case of concrete cone failure of tension loaded anchor groups. The similar procedure applies for the concrete edge breakout of shear loaded anchorages as well. First, the spring characteristics should be determined for the individual anchors of the group as according to Section 6.2.2, and the dashed curve shown in *Figure 6.12* should be obtained. After this, the cracked concrete condition is to be considered by reducing the failure load and the stiffness by factor α_V and $\alpha_{k,v}$ respectively, according to ***Eq. 68*** and ***Eq. 69*** (see *Figure 6.16*). The factor for stiffness reduction, α_{Kv} is considered to be equally applicable to the initial stiffness as well as the secant stiffness corresponding to each salient point of the idealised load-displacement curve.

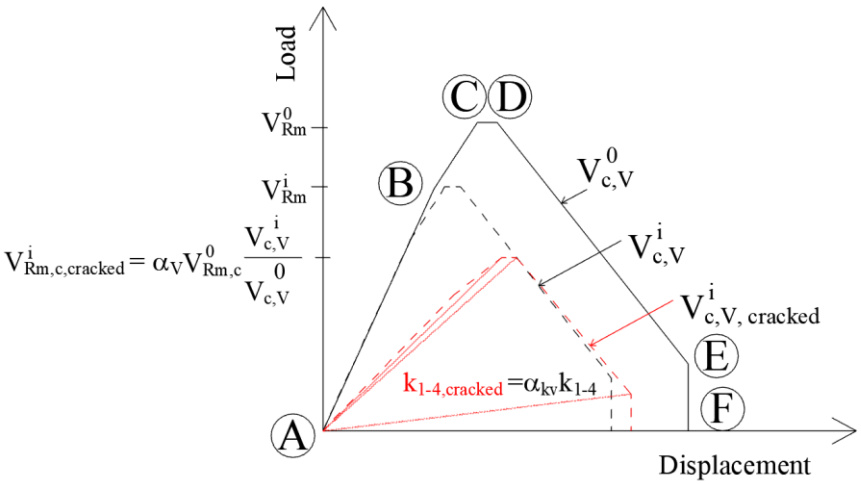

Figure 6.16. Scaling of the idealised curve of a single anchor accounting for cracked concrete condition

$$V^i_{Rm,c,cracked} = \alpha_V \cdot V^0_{Rm,c} \cdot \frac{V^i_{c,V}}{V^0_{c,V}} \qquad \textbf{Eq. 68}$$

$$k^i_{1-4,cracked} = \alpha_{k,V} \cdot k^i_{1-4} \qquad \textbf{Eq. 69}$$

Note that in the current design of anchorages, the recommended value of the strength reduction factor $\alpha_V = 0.7$ for considering cracked concrete condition for shear (for $\Delta w = 0.3$ *mm*) is primarily based on the test results on tension loaded anchors (Eligehausen et al., 2006) and the analogy between the concrete edge and concrete cone failure. To verify the validity also for the concrete edge breakout failure of anchors, a test program was carried out within the frame of this dissertation. A special concrete specimen was designed to investigate the influence of crack, without the influence of member geometry or reinforcement of the test specimen. The tests are evaluated in Section 9.4.3. Based on the test results, a value of the reduction factors $\alpha_V = 0.7$ and $\alpha_{Kv} = 0.7$ is found to be appropriate to consider the influence of cracked concrete for the anchors used in these tests and for concrete edge breakout failure. However, different anchor types might result in different values of α_V and α_{Kv}, and therefore the actual values should be determined based on the tests on anchors under consideration in uncracked and cracked concrete, which fail by concrete edge breakout. No influence of the presence of crack is considered on the tributary volume assigned to the individual anchors within the group (analogous to the tension model). This is based on the evaluation of the test results (see in Section 9.4.3).

For the reason of simplicity, an anchor group of 1×2 configuration is presented as an example, where one anchor is placed in the uncracked part of the concrete, whereas the other anchor is placed in a crack (*Figure 6.17*). When the spring characteristics for the individual anchors of a group are ascertained (see *Figure 6.16)*, the corresponding springs can be assigned to the anchors of the group. In this case, the tributary volume, which can be assigned for the individual anchors is the same for both anchors due to symmetry, whereas the failure load and stiffness of the anchor located in a crack is reduced by 30%. Although the external shear load is applied concentrically on the group, the different stiffness conditions and load-displacement behaviour of the two anchors result in an eccentricity of internal forces. This behaviour is, just like in the tension model, automatically taken into account by the displacement-controlled non-linear static analysis, which is explained in Section 6.5.

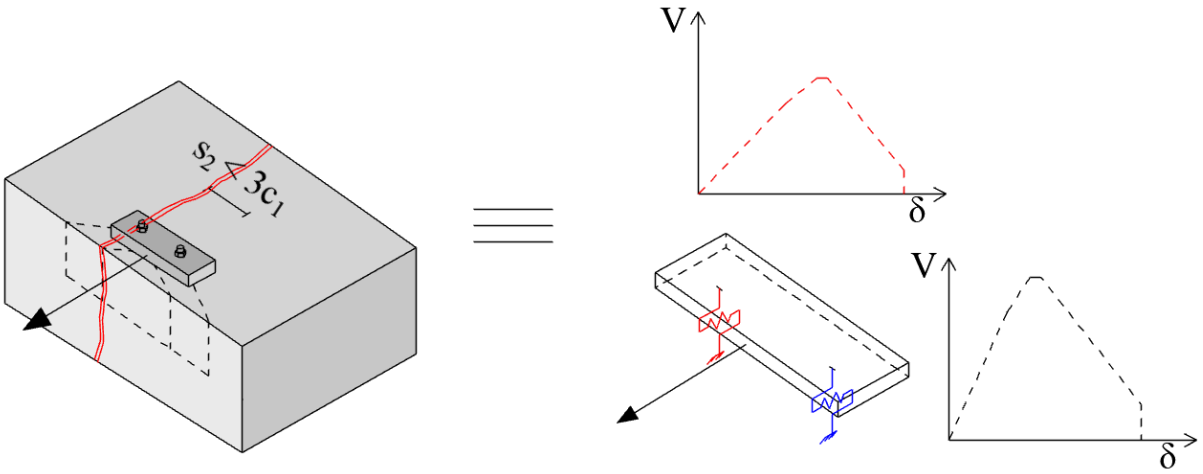

Figure 6.17. Spring properties for an anchor group of 1×2 configuration with one anchor in crack, one anchor in uncracked concrete

6.3 Modelling of the compression between anchor shaft and concrete (The push-back effect)

In case of anchor groups under eccentric shear loading or torsional loading, or in case of arbitrary anchor configurations, when the applied concentric shear load results in an eccentricity, the shaft of some of the anchors might press the concrete in the direction opposite to the direction of loading. For realistic evaluation, this effect should be accounted for within the framework of the nonlinear spring model. For the anchor placed close to an edge, the resistance under loading towards the edge is always smaller than its resistance under shear loading away from the edge. Furthermore, since it is postulated and confirmed by the tests, the stiffness of the anchor is independent of the edge distance and hence also of the loading direction. In this work, the load-displacement behaviour of the anchors placed close to an edge but loaded in the direction away from the edge was not investigated. Therefore, to be realistic yet conservative, it is assumed that the same load-displacement behaviour is valid for the anchor in the direction of the applied load (towards the edge) and in the direction opposite to the direction of the applied load (away from the edge). This assumption is not overly conservative since, even if a higher capacity would be considered in the direction opposite to loading, it could not be utilised, since the highest loaded anchors would fail in the loading direction leading to a group failure.

To consider this behaviour in the model, uni-directional shear springs, which are active only in the direction opposite to loading (equivalent to a compression-only spring) are assigned to the model at the anchor locations. However, an even simpler way, which seems to be sufficient on the basis of the verifications (see Chapter 11), is to define symmetric anchor spring properties in the shear plane while following the modelling details described. *Figure 6.18* depicts the modelling of a 2×3 anchor group loaded eccentrically in shear. Note that the symmetric springs can be used in every case because even if there is concentric loading, the springs in the opposite direction remain inactive.

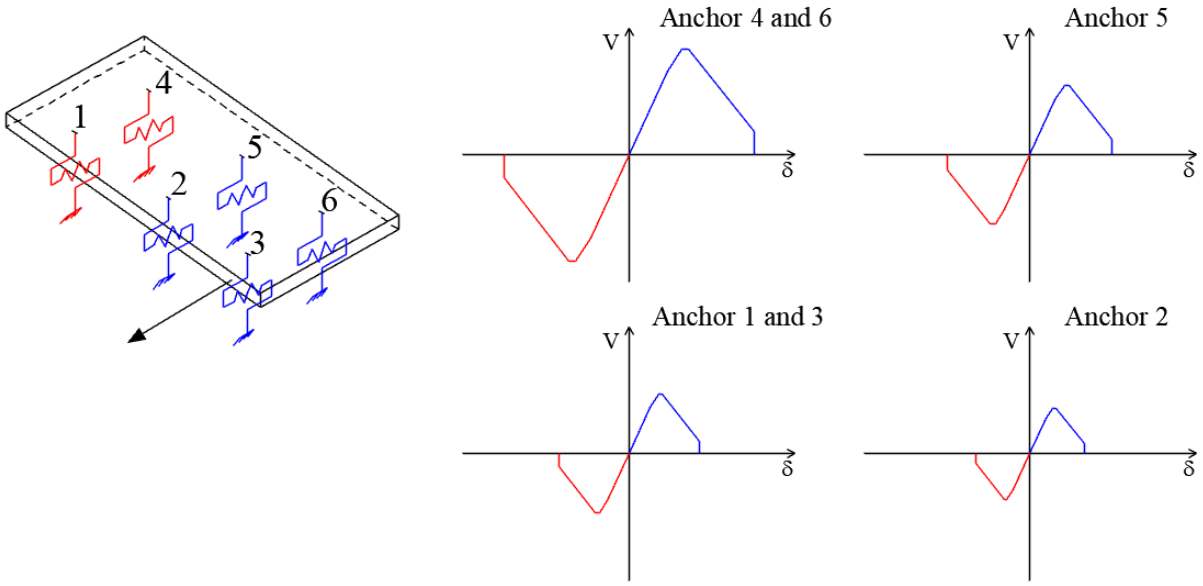

Figure 6.18. Spring model of an anchor group of 2×3 configuration loaded in eccentric shear with the corresponding symmetric spring properties in case of concrete edge failure

6.4 MODELLING OF THE BASE PLATE

This section summarises the requirements of the base plate modelling for shear spring model. In general, the modelling of the base plate should be performed the same way as for the tension model according to Section 5.3. However, there are some additional aspects to consider to model the anchorage behaviour when subjected to pure shear loading.

The current design requires that the base plate is constructed in such a way that the shear forces can be transferred to the anchors without considerable deformations of the base plate. In the model, the base plate geometry should be modelled as realistically as possible. The base plate may be modelled by using finite solid elements or shell elements applying thick-plate formulation following the Mindlin-Reissner plate theory. The mesh of the base pate should consider the position of the anchors and/ or possible attachments or stiffeners and of course, the loading position. In this thesis, the base plate is modelled with finite shell elements and the material behaviour of the base plate is considered as linear-elastic with an elasticity modulus of $E_s = 200\ GPa$. However, just like for the tension model, for example, the von-Mises yield criterion may be assigned to account for the nonlinear behaviour of the base plate if required. The friction between the base plate and the concrete surface is neglected and is not modelled.

The hole clearance pattern has a big influence on the load distribution and consequently, on the load-displacement behaviour of the anchor group. Therefore, it is essential to consider it in the spring model for concrete edge failure. However, it is accounted for by the anchor spring properties, and it is not modelled explicitly as a part of the base plate (see Section 6.2).

6.5 DISPLACEMENT-CONTROLLED NONLINEAR STATIC ANALYSIS

To perform the displacement-controlled nonlinear static analysis in case of concrete edge breakout failure of an anchor group, the guidance given Section 5.5 applies.

6.6 SUMMARY

In Chapter 6, the concept of the nonlinear spring modelling approach for shear loaded anchorages in case of concrete edge breakout failure in uncracked and cracked concrete is presented and discussed. The basic components of the model such as the uni-directional shear springs active in the loading direction (equivalent to a tension-only spring), uni-directional shear springs active in the direction opposite to loading (equivalent to a compression-only spring) and the modelling of the base plate are explained. Furthermore, the modelling principles are described and differences from the tension model are highlighted.

It is explained in detail how to derive the anchor springs from load-displacement curves obtained from single anchor tests, which fail by concrete edge breakout to apply them in the spring model. To consider the influence of anchor spacing, vicinity of an edge, member thickness, anchor configuration and load eccentricity, a general tributary volume approach is proposed that is applicable for general anchor groups including groups with multiple rows and arbitrary

configurations. For the case of anchor groups with a single anchor row, the tributary volume approach simplifies to the tributary area approach.

The concept(s) is based on two postulates: The first postulate made in the spring model for the individual anchor properties is the calculation of the mean failure load of an ith anchor, $V^i_{Rm,c}$, which is influenced by neighbouring anchors or thin member, and it can be calculated based on the tributary volume available for this anchor compared to the tributary volume of a single anchor having the same edge distance ($V^i_{c,V}/V^0_{c,V}$). The second postulate made in the shear spring model for the individual anchor properties is that the tributary volume assigned to an ith anchor of jth row of the group does not influence the stiffness of the individual anchor and therefore, the stiffness values remain unchanged compared to the stiffness values determined for the corresponding single anchor. These postulates are verified by experimental investigations. The verification of the postulates and the entire concept of the nonlinear spring modelling approach for the failure mode concrete edge failure is discussed in a separate chapter, in Chapter 11.

7 CONCEPT OF THE NONLINEAR SPRING MODEL FOR TENSION-SHEAR INTERACTION FOR CONCRETE BREAKOUT FAILURE MODE

In Chapter 7, the concept of the nonlinear spring model for tension-shear interaction for concrete breakout failure is discussed. The failure modes other than the combination of concrete cone failure under tension and concrete edge failure under shear (concrete-concrete) such as steel-steel, steel-concrete, concrete-steel, are beyond the scope of this dissertation. Only the cases, where the shear component of the applied load acts perpendicular and towards the edge is considered. However, the principles of the model should be extendable to other loading directions as well.

7.1 INTRODUCTION

The behaviour of anchorages subjected to combined tension-shear loads (interaction) is a combination of the behaviour of the anchorage under concentric tension and shear loading, and is dependent on the loading angle θ. An anchor group placed close to the concrete edge and subjected to combined tension-shear loading P at a loading angle of θ with the vertical is depicted in *Figure 7.1*. The failure load of the group is equal to P_u, whereas the tension N_u ($\theta = 0°$) and shear V_u ($\theta = 90°$) components can be derived using the following equations:

$$N_u = P_u \cdot Cos\theta \qquad \textbf{Eq. 70}$$

$$V_u = P_u \cdot Sin\theta \qquad \textbf{Eq. 71}$$

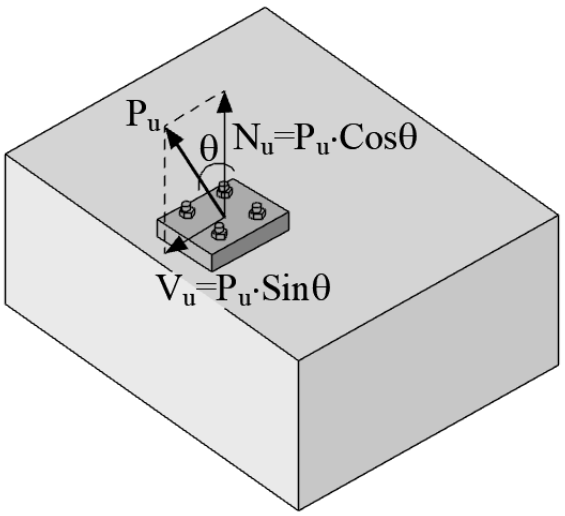

Figure 7.1. Anchor group subjected to combined tension-shear loading at a loading angle of θ with the vertical, force components

According to the current force-based design approaches, the verification of anchorages subjected to combined tension and shear forces in case of concrete breakout failure is carried out by satisfying the interaction equation given in ***Eq. 72***.

$$\left(\frac{N_u}{N_{Rm}}\right)^{\alpha} + \left(\frac{V_u}{V_{Rm}}\right)^{\alpha} \leq 1.0 \qquad \textit{Eq. 72}$$

Where

N_u is the tension component of the applied ultimate load

N_{Rm} is the mean tension resistance of the anchorage

V_u is the shear component of the applied ultimate load

V_{Rm} is the mean shear resistance of the anchorage

α is the exponent used in the interaction equation, which depends on the failure mode ($\alpha = 1.5$ for concrete breakout failure mode according to EN 1992-4 assuming rigid base plate)

It is clear that to perform the verification for interaction, the calculations for pure tension and pure shear must be done first to obtain the values of N_{Rm} and V_{Rm}, respectively so that ***Eq. 72*** can be solved. The resistances N_{Rm} and V_{Rm} - considering the influences such as base plate stiffness, vicinity of concrete edge, loading eccentricity, arbitrary anchor pattern, crack pattern and hole clearance pattern - can be obtained by using the non-linear spring modelling approach for tension and shear, respectively. In this case, two analyses should be carried out separately: (1) the nonlinear analysis on the tension loaded anchorage and (2) the nonlinear analysis on the shear loaded anchorage considering the geometric and material parameters, spring characteristics etc., and following the procedures explained in Chapters 6 and 7.

However, note that the behaviour of anchor groups placed close to the concrete edge with unfavourable hole clearance pattern under inclined loads might be significantly influenced by the formation of the cracks at the front row (refer to Lachinger 2012 and *Figure 2.16*). The damage at the front anchor row depends on the ratio of anchor embedment depth to edge distance of the front anchor row. Therefore, the verification for tension-shear interaction in case of concrete cone – concrete edge breakout by satisfying ***Eq. 72*** should only be used for the anchorages with no hole clearance, or where the most favourable hole clearance pattern can be ensured to avoid crack development at the front row(s). Further discussion of the problem and recommendations are given in Section 12.2.

Furthermore, to verify the anchorage under combined tension-shear (interaction) loads, the interaction equation according to ***Eq. 72*** may be used, if and only if a sufficiently stiff base plate is used (EN 1992-4). Consequently, if the base plate is not sufficiently stiff (or it is flexible), the interaction equation cannot be applied since it might yield unconservative results. This is because the deformations of the base plate caused by the tension component are not considered accurately if the tension and shear analyses are performed separately since they are just accounted for in the tension model and are neglected in the shear model.

In *Figure 7.2*, the assumed deformations of a stiff and a flexible base plate for an anchor group with two anchor rows under concentric tension, concentric shear and combined tension and shear loading (interaction) are depicted. It can be seen that under concentric tension loading, if

a stiff base plate is used, the vertical displacements are equal at every section and the forces are distributed uniformly among the anchors within the group. However, if a flexible base plate is used, the deformation profile of the base plate, as well as the force distribution are nonlinear. This means that if a stiff base plate is assumed in the calculations, but in reality a flexible base plate is used, due to the prying action of the base plate, the anchors might be subjected to larger forces than anticipated.

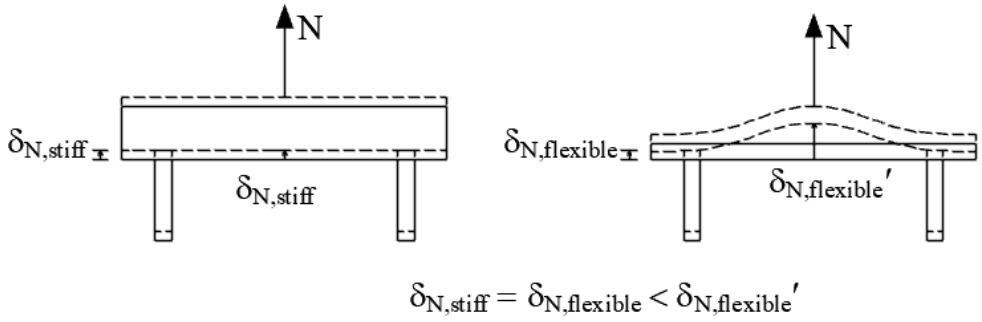

a)

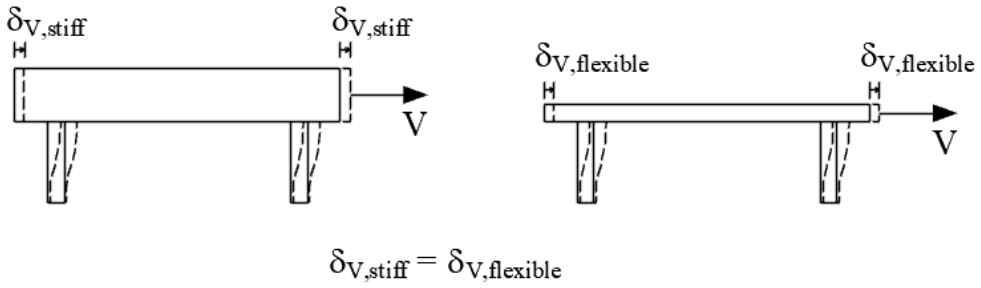

b)

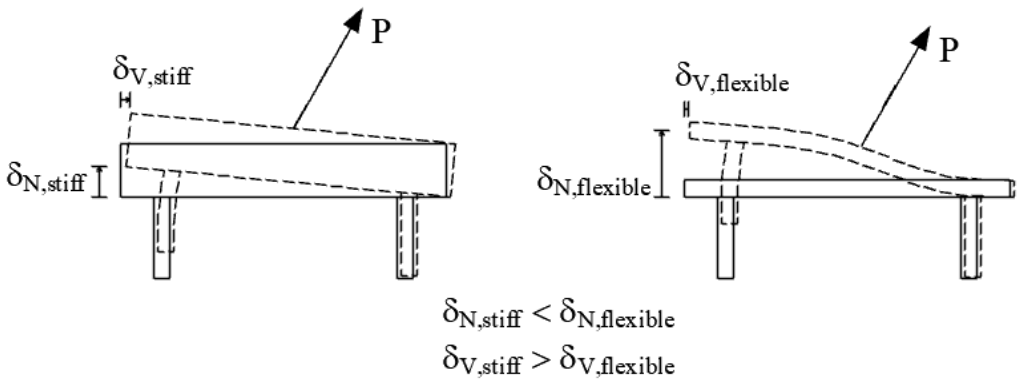

c)

Figure 7.2. Deformations of a stiff and a flexible base plate under a) concentric tension loading, b) concentric shear loading, c) combined tension and shear loading (interaction)

For groups with more than two anchors, certain anchors would take up higher forces than calculated using a linear force distribution, which leads to unsafe results (*Figure 7.2a)*. In the case of shear loading, the base plate is considered to be sufficiently stiff to transfer the loads in the shear direction without considerable deformations. Consequently, the horizontal displacements

(δ_V) of a stiff and flexible (under tension) base plate, which are loaded with the same amount of force (V) will be the theoretically the same (*Figure 7.2b)*. However, when the anchor group with not sufficiently stiff or flexible base plate is subjected to combined tension and shear loading and fails due to concrete breakout failure, the force distribution, the anchor displacements and the base plate deformations are even more complicated because of the interactional influence (*Figure* 7.2*c)*. Therefore, it is not obvious that the ultimate load and displacement at ultimate load obtained from the tension (N_{Rm}, $\delta(N_{Rm})$) and shear (V_{Rm}, $\delta(V_{Rm})$) spring models are equal to the tension ($P_{R,model}\cdot Cos\theta$, $\delta(P_{R,model})\cdot Cos\theta$) and shear ($P_{R,model}\cdot Sin\theta$, $\delta(P_{R,model})\cdot Sin\theta$) components obtained from an interaction equation, where all influences are considered at the same time. In such cases, to consider the influences with sufficient accuracy and to avoid an unsafe design, the nonlinear spring model for tension-shear interaction should be used, which is described in the following.

7.2 THE CONCEPT

The nonlinear spring model for tension-shear interaction of anchor groups, which fail due to concrete cone-concrete edge breakout failure, is a combination of the nonlinear spring model (tension) for concrete cone failure of an anchorage placed close to the concrete edge (Chapter 5) and the nonlinear spring model (shear) for concrete edge failure (Chapter 6). The assumptions and postulates made for the tension and shear models are valid for the interaction model as well.

The influence of combined tension and shear loading on the load-displacement behaviour of the anchor group is taken into account automatically by applying the corresponding spring characteristics for anchors in tension and shear and for the concrete contact springs, as well as by realistic modelling of the base plate and performing displacement controlled nonlinear analysis.

However, note that the behaviour of anchor groups placed close to the concrete edge with unfavourable hole clearance pattern and loaded under inclined loads might be significantly influenced by the formation of the cracks at the front row. The influence of cracking with respect to shear resistances is accounted for by the shear spring characteristics by considering the influence of hole clearance pattern explicitly. However, the influence of this cracking at the front is not automatically considered for the tension component with the tension springs. Neglecting this influence might yield unconservative results. Therefore, the spring model – without modifications- should only be used for anchor groups without hole clearance, or when the most favourable hole clearance pattern can be ensured. Based on evaluation of test results from Lachinger (2012), further discussion of the problem and recommendations for applications with most unfavourable hole clearance pattern are given in Section 12.2.

The components of the spring model for interaction are schematically depicted in *Figure 7.3* for an exemplary anchor group of 2×2 configuration without the influence of hole clearance, which include:

i. Anchor tension springs: the nonlinear tension-only springs for considering the nonlinear anchor behaviour in case of concrete cone failure
ii. Anchor shear springs: uni-directional shear springs active in the loading direction (equivalent to a tension-only spring) to model the nonlinear load-displacement behaviour of individual anchors in case of concrete edge failure,
iii. Anchor shear springs: uni-directional shear springs active in the direction opposite to loading (equivalent to a compression-only spring) to model the pressure on the anchors in the direction opposite to the direction of loading (push-back effect – if any),
iv. Base plate: finite shell or solid elements to model the base plate realistically,
v. Contact springs: compression-only springs to model the contact between base plate and concrete.

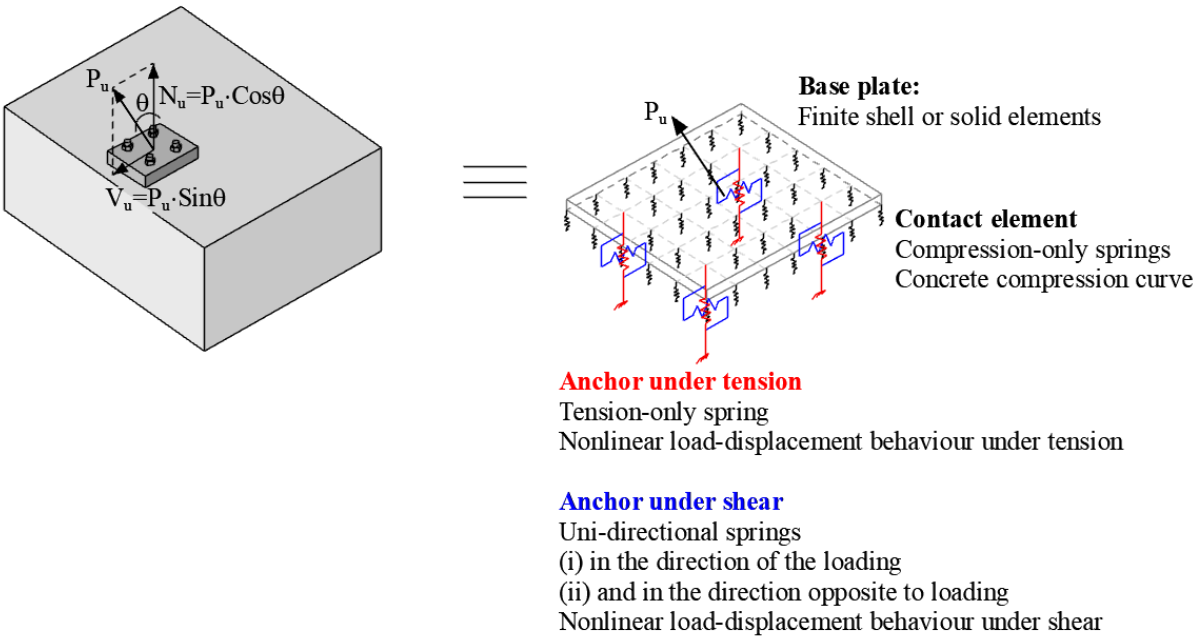

Figure 7.3. Components of the spring model for combined tension-shear (interaction) in case of concrete breakout failure

7.3 DETERMINATION OF THE SPRING CHARACTERISTICS TO MODEL THE ANCHOR BEHAVIOUR

For determining the anchor spring characteristics for tension and shear, Sections 5.2 and 6.2, respectively apply. *Figure 7.4* depicts the spring characteristics of an exemplary anchor group of 2×2 configuration without hole clearance. To each anchor, one tension and one shear spring should be assigned considering the geometric and concrete conditions (cracked or uncracked) according to the rules given in the corresponding sections.

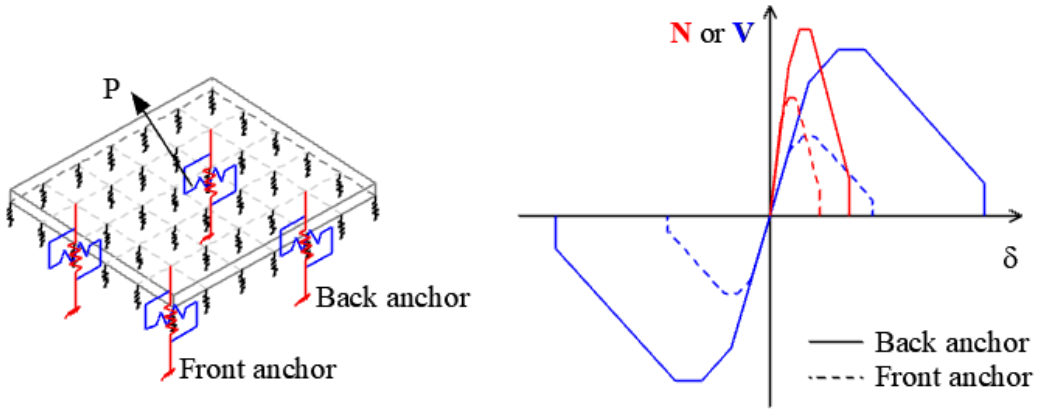

Figure 7.4. Anchor spring characteristics for tension and shear

7.4 MODELLING OF THE BASE PLATE

The modelling of the base plate should be performed as described in Section 5.3.

7.5 CONTACT BETWEEN THE BASE PLATE AND CONCRETE GROUND

When anchor groups are subjected to combined tension-shear loading, compression (prying) forces below the base plate might develop, which would influence the load distribution and thus the anchor group behaviour. The developing compression forces between the base plate and concrete surface should be accounted for in the nonlinear spring model and therefore, are modelled with contact springs. The contact between the base plate and concrete ground should be modelled according to Section 5.4.

7.6 DISPLACEMENT-CONTROLLED NONLINEAR STATIC ANALYSIS

It is essential to perform a displacement-controlled nonlinear analysis on the anchorage subjected to combined tension-shear to account for an accurate force distribution and redistribution among the anchors of the group considering their nonlinear behaviour in tension and shear, and to account for the base plate deformations. The behaviour in case of interaction is automatically considered by assigning the corresponding springs in tension and shear loading directions as

described in Section 7.3. The components given in *Figure* 7.3 should be modelled before proceeding with the analysis. In general, the description given in Section 5.5 applies for the displacement-controlled nonlinear static analysis if an anchor group is loaded in combined tension-shear failing due to concrete breakout failure (concrete cone and concrete edge breakout).

Load application and monitoring

In case of interaction, the load is applied on the anchor group at an angle θ (measured from the vertical) as shown in *Figure 7.1*. The best way to perform the analysis is if the load can be applied in the polar coordinate system, and the monitoring of forces $P(\theta)$ and displacements $\delta(\theta)$ is also done directly in the direction of loading. This way, the load-displacement curve obtained from the analysis corresponds to the behaviour of the group that is loaded at an angle of θ. The obtained ultimate load of the group corresponds to $P_{R,model}(\theta)$ and the displacement at failure load corresponds to $\delta(P_{R,model}(\theta))$. If in the used structural analysis software the load application is only possible in a Cartesian coordinate system, then the load should be applied on the anchorage as tension and shear components. Furthermore, in this case, the results of the analysis are also obtained as components in tension (N, $\delta(N)$) and shear (V, $\delta(V)$) directions and these components should be combined through vector addition to obtain the load-displacement behaviour in the direction of the loading.

7.7 SUMMARY

In Chapter 7, the concept of the nonlinear spring modelling approach for anchor groups subjected to combined tension-shear loading (interaction) is described. The model for interaction is a combination of the spring models for concrete cone failure in tension and concrete edge failure in shear. Besides the application of the interaction model, it is discussed that in cases, where using of a sufficiently stiff base plate can be ensured and the anchor group is without hole clearance, the interaction verification of the anchorage according to ***Eq. 72*** can be done using the analysis results from the tension (N_u) and shear (V_u) models. However, in all other cases it is recommended to use the nonlinear spring model for interaction to account for the realistic behaviour of the anchor group. The verification of the concept of the nonlinear spring modelling approach for interaction in case of concrete breakout failure mode is discussed in Chapter 12.

8 EXPERIMENTAL INVESTIGATIONS ON TENSION LOADED ANCHORAGES

8.1 SCOPE

The experimental investigations carried out on tension loaded anchorages to investigate their behaviour in case of concrete cone breakout are described and discussed in this chapter. The program overview is given in the following sub-sections (8.1.1, 8.1.2, 8.1.3 including all test parameters.

The experimental investigations on tension loaded anchorages aimed to generate a test database on anchor groups of various configurations, to investigate different influences, to obtain information about the load distribution, and most importantly to validate the concept of the nonlinear spring model for tension (Chapter 5). The tests included rectangular and non-rectangular anchor group configurations within and beyond the scope of EN 1992-4. The test parameters were the anchor configuration, anchor spacing, edge distance, anchor type and size, the base plate thickness (stiffness), the eccentricity of the loading, the concrete compressive strength and the concrete condition (cracked or uncracked). Within the scope of this dissertation, 143 tension loading tests were carried out on single anchors and different anchor group configurations with up to eight anchors in a group in uncracked and cracked concrete. In *Table 8.1* to *Table 8.3*, the pictogram of the particular anchor group along with the most important installation and test parameters are given.

Reference single anchor tests were performed to the corresponding anchor groups to verify the postulates made for the tributary area approach (Section 5.2.2), and to monitor the distribution and redistribution of forces (if any) within a group. Furthermore, the load-displacement behaviour of single anchors and individual anchors of an anchor group with the same installation parameters were compared to verify the behaviour of the individual anchors as a part of the anchor group.

The test parameters, such as concrete strength, anchor diameter, embedment depth and anchor spacing were chosen through pre-calculations in a way that failure modes other than concrete cone failure, i.e. steel failure, pullout failure or bond/mixed failure were not decisive neither in single anchor tests nor in the anchor group tests.

Three to five tests were performed for each test series. The details about the testing procedure such as the description of the used concrete specimens, anchor types, anchor installation and test setups are described in Sections 8.2.1 to 8.2.3.

The test results are evaluated in Section 8.3. Section 8.3.1 provides information about the load-displacement behaviour of anchor groups within the scope of EN 1992-4. Section 8.3.2.1 discusses the results on the influence of base plate stiffness. The test series beyond the scope of EN 1992-4 are discussed in Section 8.3.2.2 and the results of tests performed in cracked concrete are given in Section 8.3.3.

8.1.1 Anchor groups in uncracked concrete within the scope of EN 1992-4

Table 8.1 includes the test parameters for regular rectangular anchorages of 1×3 and 2×2 configurations that are within the scope of the current design provisions of EN 1992-4. It was aimed to investigate the influence of loading eccentricity, edge distance, base plate stiffness and their superposed influence on the behaviour of the anchor groups. For this reason, the tests included concentric and eccentric tension test away from the concrete edge and close to the concrete edge using base plates with varying thickness. Through this test program, it could be shown, which of the influences are considered with sufficient accuracy according to the current force-based design provisions. Furthermore, these configurations enabled direct comparison with the CCD Method, since the CCD Method is accepted and verified to be accurate for anchor groups up to 2×2 configuration having a stiff base plate and applying concentric or eccentric loading about one axis, and it is permitted to use up to 3×3 anchor configurations (acc. to EN 1992-4). In *Table 8.1*, the eccentricities, e_1 and e_2 are defined as distances between the point of the load application and the centre of gravity of all anchors within the group in two perpendicular directions 1 and 2, respectively, and the point of load application on an anchor group is marked by the symbol 'x'.

Table 8.1. Test program for anchor groups in uncracked concrete within the scope of EN 1992-4

Anchor system	Test series ID	Test type	Base plate dimensions	Mean concrete cube compr. strength	Embedment depth	Anchor spacing	Edge distance	Eccentricity of loading	No. of tests
			l*w*t	$f_{cc,m}$	h_{ef}	s_1/s_2	c	e_1/e_2	
			[mm*mm*mm]	[N/mm²]	[mm]	[mm/mm]	[mm]	[mm/mm]	[-]
Torque-controlled expansion anchor – M12	R1	Ref. single	-	25.8	55	-	>c_{cr}	0/0	3
	G11R	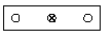	270*50*30	25.8	55	98/-	>c_{cr}	0/0	3
	G12	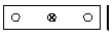	270*50*30	25.8	55	98/-	50	0/0	3
	G13	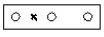	270*50*30	25.8	55	98/-	>c_{cr}	-49/0	3
	R2	Ref. single	-	30.3	55	-	>c_{cr}	0/0	3
	G22	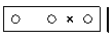	270*50*30	30.3	55	98/-	50	49/0	3
	G23	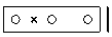	270*50*30	30.3	55	98/-	50	-49/0	3
	R3	=R1	-	25.8	55	-	>c_{cr}	0/0	-
	G31R		160*160*30	25.8	55	98/98	>c_{cr}	0/0	3
	G32		160*160*30	25.8	55	98/98	>c_{cr}	-25/+25	3
	R4	=R2	-	30.3	55	-	>c_{cr}	0/0	-
	G43		160*160*30	30.3	55	98/98	50	-25/+25	3
Bonded anchor – M16	R5	Ref. single	-	66.6	70	-	>c_{cr}	0/0	3
	G51R	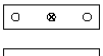	400*120*50	66.6	70	120/-	>c_{cr}	0/0	3
	G52	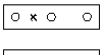	400*120*50	66.6	70	120/-	>c_{cr}	-60/0	3
	G53	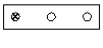	400*120*50	66.6	70	120/-	>c_{cr}	-120/0	3
	G54	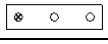	400*120*25	66.6	70	120/-	>c_{cr}	-120/0	3

8.1.2 Anchor groups of rectangular and non-rectangular configurations beyond the scope of EN 1992-4

Table 8.2 tabulates the test parameters for rectangular and non-rectangular anchor groups, which are currently beyond the scope of the design provisions of EN 1992-4. The tests included concentric and eccentric tension test away from the concrete edge using rigid and flexible base plates of different geometry.

Table 8.2. Test program for anchor groups in uncracked concrete beyond the scope of EN 1992-4

Anchor system	Test series ID	Test type	Base plate dimensions	Mean concrete cube compr. strength	Embedment depth	Anchor spacing	Edge distance	Eccentricity of loading	No. of tests
			l*w*t	$f_{cc,m}$	h_{ef}	s_1/s_2	c	e_1/e_2	
			[mm*mm*mm]	[N/mm²]	[mm]	[mm/mm]	[mm]	[mm/mm]	[-]
Bonded anchor – M12	R8	Ref. single	-	31.4	60	-	>c_{cr}	0/0	4
	G81	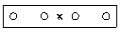	350*60*40	31.4	60	90/-	>c_{cr}	0/0	3
	G82		350*60*40	30.3	60	90/-	>c_{cr}	-90/0	3
	G83	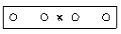	350*60*10	31.4	60	90/-	>c_{cr}	0/0	3
	G84	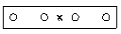	350*60*5	30.3	60	90/-	>c_{cr}	0/0	3
Bonded anchor – M16	R9	Ref. single	-	37.0	60	-	>c_{cr}	0/0	3
	G91		Side length: 220,140, 140, 220, 360, 360, t=50	37.0	60	s=140	>c_{cr}	Position B1	3
	G92		Side length: 220,140, 140, 220, 360, 360, t=50	37.0	60	s=140	>c_{cr}	Position B2	3
	R10	= R9	-	37.0	60	-	>c_{cr}	0/0	-
	G101		D=210 t=25	37.0	60	s=140	>c_{cr}	0/0	3
	R20	Ref. single	-	70.0	60	-	>c_{cr}	0/0	3
	G201		D=210 t=25	70.0	60	s=140	>c_{cr}	0/0	3
Bonded anchor – M12	R30	=R8	-	31.4	60	-	>c_{cr}	0/0	-
	G301		D=300 t=40	30.3	60	s=120	>c_{cr}	0/0	3
	R40	=R8	-	31.4	60	-	>c_{cr}	0/0	-
	G401		D=300 t=40	31.3	60	s=120	>c_{cr}	Position P	2

In *Table 8.2,* the eccentricities, e_1 and e_2 are defined as distances between the point of the load application and the centre of gravity of all anchors within the group in two perpendicular directions 1 and 2, respectively, and the point of load application on an anchor group is marked by the symbol 'x'.

The tested configurations were the 1×4 anchor group, L-shaped anchor groups including 8 anchors, triangular anchor group with round base plate, hexagonal anchor group with round base plate and trapezoidal anchor group with round base plate. Testing such configurations was necessary to show that using the nonlinear spring model approach, not only rectangular anchor groups with stiff base plate can be designed but the model can be generalised to arbitrary anchor group configurations. It was aimed to generate a test database and to validate the spring model against experiments with different installation parameters, anchor configurations, and base plate stiffness. This section reports and discusses the test results, whereas the verification of the model is given in Chapter 10.

8.1.3 Anchor groups installed in cracked or partly-cracked concrete

Table 8.3 includes the test program for anchorages in cracked concrete within and beyond the scope of the current design provisions of EN 1992-4. The tests aimed to investigate the influence of the crack pattern, and the superposed influence of crack pattern and loading eccentricity on the load-displacement behaviour of anchorages, and to verify the spring modelling approach for cracked concrete (Section 5.2.3). The tests included concentric and eccentric tension tests away from the concrete edge and relatively thick base plates that were assumed to be rigid were used. The crack width was $\Delta w = 0.3$ *mm* in all cases. In *Table 8.3,* the eccentricities, e_1 and e_2 are defined as distances between the point of the load application and the centre of gravity of all anchors within the group in two perpendicular directions 1 and 2, respectively, and the point of load application on an anchor group is marked by the symbol 'x'.

Due to a relatively low tensile strength, the concrete members may experience cracking due to mechanical or thermal loads during its lifetime, unless the section is designed to resist these actions as an uncracked section. Due to the notch effect of the anchor hole and the high tensile stresses caused by the pre-stressing force applied to the anchor, there is a high probability that fasteners are intercepted by a crack unless special reinforcement is provided to arrest the formation of the crack. According to the current design procedure, unless otherwise proven, the design of the anchorage must be carried out assuming cracked concrete. In case of an anchor group, it is assumed that all the anchors are intercepted by the crack; however, this may not always be true and also may not lead to the most conservative case. To investigate, how the anchor group behaviour is influenced if only some of the anchors are being intercepted by a crack, tension tests were performed on single anchors, anchor groups with a single row of three anchors (1×3 configuration), on quadruple anchor groups (2×2 configuration) and on hexagonal anchor groups in cracked and uncracked concrete according to *Table 8.3*.

Table 8.3. Test program for anchor groups in cracked concrete

Anchor system	Test series ID	Test type	Base plate dimensions l*w*t [mm*mm*mm]	Mean concrete cube compr.strength $f_{cc,m}$ [N/mm^2]	Embed-ment depth h_{ef} [mm]	Anchor spacing s_1/s_2 [mm/mm]	Eccen-tricity of loading e_1/e_2 [mm/mm]	No. of tests [-]
Bonded anchor – M12	R6-ncr	Ref. single uncracked	-	23	60	-	0	5
	R6-cr	Ref. single cracked	-	23	60	-	0	3
	G61		400*120*50	23	60	120/-	0	4
	G62R		400*120*50	23	60	120/-	0	4
	G62	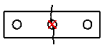	400*120*50	23	60	120/-	0	3
	G63	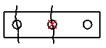	400*120*50	23	60	120/-	0	2
	G64	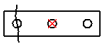	400*120*50	23	60	120/-	0	3
	G65		400*120*50	23	60	120/-	-60/0	3
	G66		400*120*50	23	60	120/-	60/0	3
	G67		400*120*50	23	60	120/-	0	3
	G68	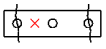	400*120*50	23	60	120/-	-60/0	3
Under-cut an-chor – M12	R7-ncr	Ref. single uncracked	-	18	80	-	0	4
	R7-cr	Ref. single cracked	-	18	80	-	0	4
	G71		220*220*50	18	80	160/160	0	3
	G72		220*220*50	18	80	160/160	0	3
	G73		220*220*50	18	80	160/160	+40/-40	3
	G74		220*220*50	18	80	160/160	+40/+40	3
Under-cut an-chor – M12	R50-ncr	= R7-ncr	-	18	80	-	0/0	-
	R50-cr	= R7-cr	-	18	80	-	0/0	-
	G501	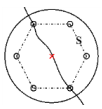	D=300 t=40	18	80	s=120	0/0	3

8.2 TESTING

8.2.1 Test specimens for tension tests

The tension tests on single anchors and anchor groups in uncracked concrete were carried out using plain concrete slabs as the anchorage material (Specimen I and II). The dimensions of the concrete specimens were designed in a way that during the testing, the formation of the full-size concrete breakout bodies was ensured without the influence from or to the adjacent anchorages. The clear distance between the outermost anchors of the neighbouring anchor groups was always greater than four times the effective embedment depth (h_{ef}) of the anchors to prevent any influence from one group to another. The thickness of the concrete specimen was maintained greater than $2h_{ef}$ to have negligible flexural deformations and no splitting of concrete. The drawing of the typical test specimens is given in Appendix A.

Special concrete specimens were cast for the tests in cracked concrete, where all anchors or some anchors of the group were intercepted by cracks (see Specimen III, Appendix A). Steel plates of 2 mm thickness were used as crack inducers in the design of the concrete specimens that enabled the crack formation by hammering wedges into the pre-formed holes in the concrete members. The pattern of the crack inducers in the specimens was designed in a way that the crack pattern of the corresponding anchor configurations could be ensured. Note that the same specimens could be used for anchorages in uncracked concrete provided that the cracks were not induced. The economic design and the casting direction of the specimens allowed using two sides of the specimen for the anchorage testing. However, once a crack was induced in one side, the same position of the other side had to be considered as cracked concrete. The thickness of the concrete specimen was 440 mm. The plain concrete depth available for the anchors was 205 mm due to the steel plates cast in the concrete, which is greater than 2.5 - times the embedment depth of the largest anchor embedment depth (80 mm) of the test program (see *Table 8.3*). The dimensions of the concrete specimens enabled the formation of the full-size concrete breakout bodies without influencing the adjacent groups during testing.

The tension loading tests were carried out in the following types of test specimens:

- Specimen I: concrete slab with edge reinforcement at the top and bottom (Appendix A)
- Specimen II: concrete slab with edge reinforcement only at the bottom (Appendix A)
- Specimen III: concrete specimen for tests in cracked concrete (Appendix A)

The concrete mix of the corresponding concrete batches was designed according to DIN EN 206, with a maximum grain size of 8 mm for the Series R5-G54 and 16 mm for all other tests, respectively. In all tests, round gravel aggregates were used. The influence of concrete mix composition and aggregate type (crushed or rounded) was beyond the scope of this dissertation. The compressive strength of the concrete batches was measured on standard concrete cubes ($a = 150\ mm$) according to DIN EN 12390-15. The concrete compressive strength in the performed tests was in the range of $f_{cc,150,m} = 18\ N/mm^2 – 70\ N/mm^2$. The exact values at the day of the testing are given in *Table 8.1 - Table 8.3* for the corresponding test series.

8.2.2 Tested fasteners and installation

Within the scope of this dissertation, three different types of post-installed anchor systems were used according to *Table 8.1* - *Table 8.3*:

- Torque-controlled expansion anchor of size M12,
- Adhesive anchor with a bond strength of ca. 30-35 MPa (Epoxy mortar + 12.9 threaded rod of size M12 and M16)
- Undercut anchor of size M12.

Note that the most of the experiments were carried out with bonded anchors because this anchor system allows flexible combination of test parameters such as embedment depth, anchor diameter, steel strength and no installation torque is required, which is beneficial when testing close to the concrete edge.

- **Anchor installation in uncracked concrete:**

The anchors were installed according to the corresponding Manufacturer´s Installation Instructions. Accordingly, the holes were drilled perpendicular to the concrete surface. In the case of anchor groups, steel templates with pilot-holes were built with an accurate hole spacing to ease the precise vertical drilling process since an accurate positioning of the anchors within the group was necessary to investigate the influences with sufficient accuracy. After the drilling and cleaning process, the anchors were set, and the fixture or the base plate was positioned on the anchor(s), respectively. In the case of the expansion anchor and undercut anchor, the prescribed installation torque was applied, which resulted in the expansion (in case of expansion and undercut anchors) and pre-stressing of the anchors. The torque was set back to 0 Nm after 10 minutes, and the nuts were only hand-tightened to ensure the same initial conditions for all anchors during the testing since the different stiffness conditions within a group would influence the load-displacement behaviour of the group. In the case of bonded anchors, no installation torque was applied, and the nut was only hand-tightened after the prescribed curing time of the epoxy mortar.

- **Anchor installation in cracked concrete:**

In the case of the tests in cracked concrete, an initial crack (hairline crack) was created first to ensure that the crack passes the anchor location. After that, the hole was drilled through the crack using steel templates with pilot-holes to ensure accurate positioning of the anchors within the group, according to the steps given in *Figure 8.1*. After drilling, the boreholes were cleaned according to the corresponding Manufacturer´s Installation Instructions, the borehole depth was measured, and it was verified with an endoscope that the crack is present over the complete depth and goes diametrically across the borehole. Only boreholes with a diametrically passing crack over the full depth were accepted as cracked condition to ensure the same initial conditions for each test in cracked concrete. After the drilling and cleaning process, the anchors were set and the base plate was positioned on the anchors, respectively. For the anchor groups with bonded anchors, no installation torque was applied and the nut was only hand-tightened after

the prescribed curing time of the epoxy mortar. In the case of the undercut anchors, the prescribed installation torque was applied and after 10 minutes the torque was set back to 0 Nm and the nuts were only hand-tightened.

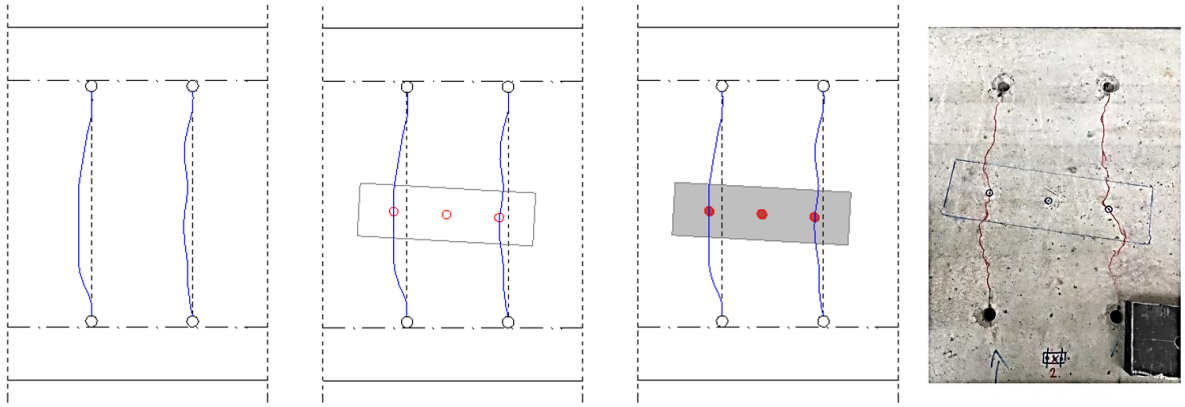

a) ***b)*** ***c)*** ***d)***

Figure 8.1. Installation steps of anchor groups in cracked concrete: a) formation of hairline cracks; b) drilling the holes using steel template and checking the presence of the cracks in the holes; c) installation of the anchors, d) photo of the first installation step

8.2.3 Test setup and test procedure

This section provides information about the test setups, which were used for the experiments. *Figure 8.2* depicts a schematic drawing of a test setup for anchor groups, which can be used for testing in cracked and uncracked concrete applying the tension load concentrically or eccentrically.

The test setup consisted of the following major components:

- a tension test rig with adequate support distance to allow the formation of an unrestricted concrete cone,
- a hydraulic cylinder and high strength threaded rod for load application,
- a calibrated load cell,
- displacement transducers for measuring anchor and base plate displacement and crack width,
- a data acquisition system with computer interface to record the test data.

The tension load was applied to the anchors through the base plate. The load was actuated using the hydraulic test cylinder of the expected load range. A high strength M24 threaded rod was used to transfer the load from the hydraulic cylinder into the base plate. In the case of tests with eccentrically applied loads and tests in cracked concrete, a hinge was built in between the base plate and the threaded rod to allow the free rotation of the base plate (*Figure 8.2* and *Figure 8.3c*). Thus, the load acting on the group could be distributed among the individual anchors of the group based on their stiffness. The tension load applied to the anchor group was measured using a calibrated load cell with respect to the expected load range.

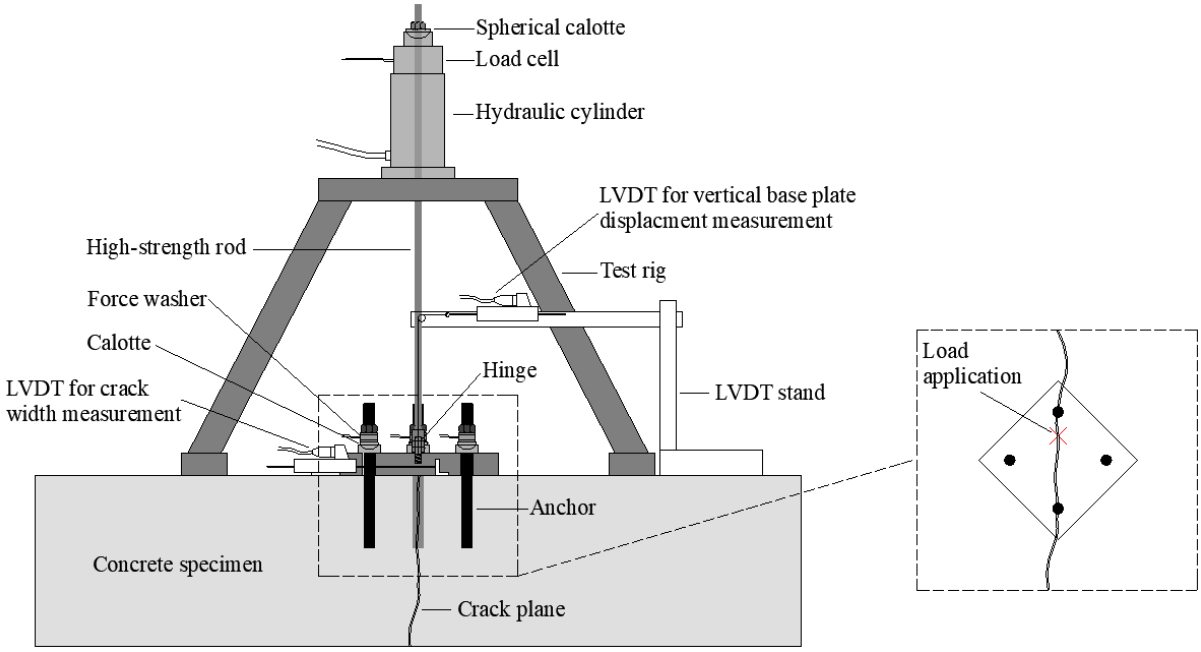

Figure 8.2. Typical test setup for tension loaded anchor group - eccentric loading in cracked concrete

To measure the axial anchor forces in the group, Strain Gauge-Based force washer (*Ø26.5 mm*, clearance hole *12.7 mm/16 mm*, *t = 20 mm* incl. hardened washer) and a spherical calotte (*Ø32 mm*, *t = 10 mm*) were placed between the nut and the base plate (*Figure 8.3d*) where it was possible. The vertical displacements were measured using displacement transducers (LVDT with a measuring range of 0.01 – 75.00 mm) directly at the point of load application on the base plate, and in case of tests with non-rigid base plates also on individual anchors (*Figure 8.3d*).

For the case of tests where the plane of rotation of the anchor plate was not obvious, e.g. anchor groups with L-configuration (test series G91 and G92), to allow free rotation of the plate, a double hinge system as shown in *Figure 8.3e* was used. In the case of tests in cracked concrete, the crack width was measured as the average of two LVDTs placed perpendicular to the crack on both sides of the group (*Figure 8.4*). For the tests with more than one crack, e.g. test series G67 and G68, both the cracks were set to a width of 0.3 mm and both the cracks were monitored during the test. The total load, the individual anchor axial forces and the total vertical displacement of the group were recorded continuously during the tests. The tension tests on single anchors were carried out according to the recommendations given in ETAG 001, Annex A, Section 4 with a setup in *Figure 8.3a* having the same major components as the group tests. Photos of the setups used for the tests in uncracked and cracked concrete are shown in *Figure 8.3* and *Figure 8.4*, respectively.

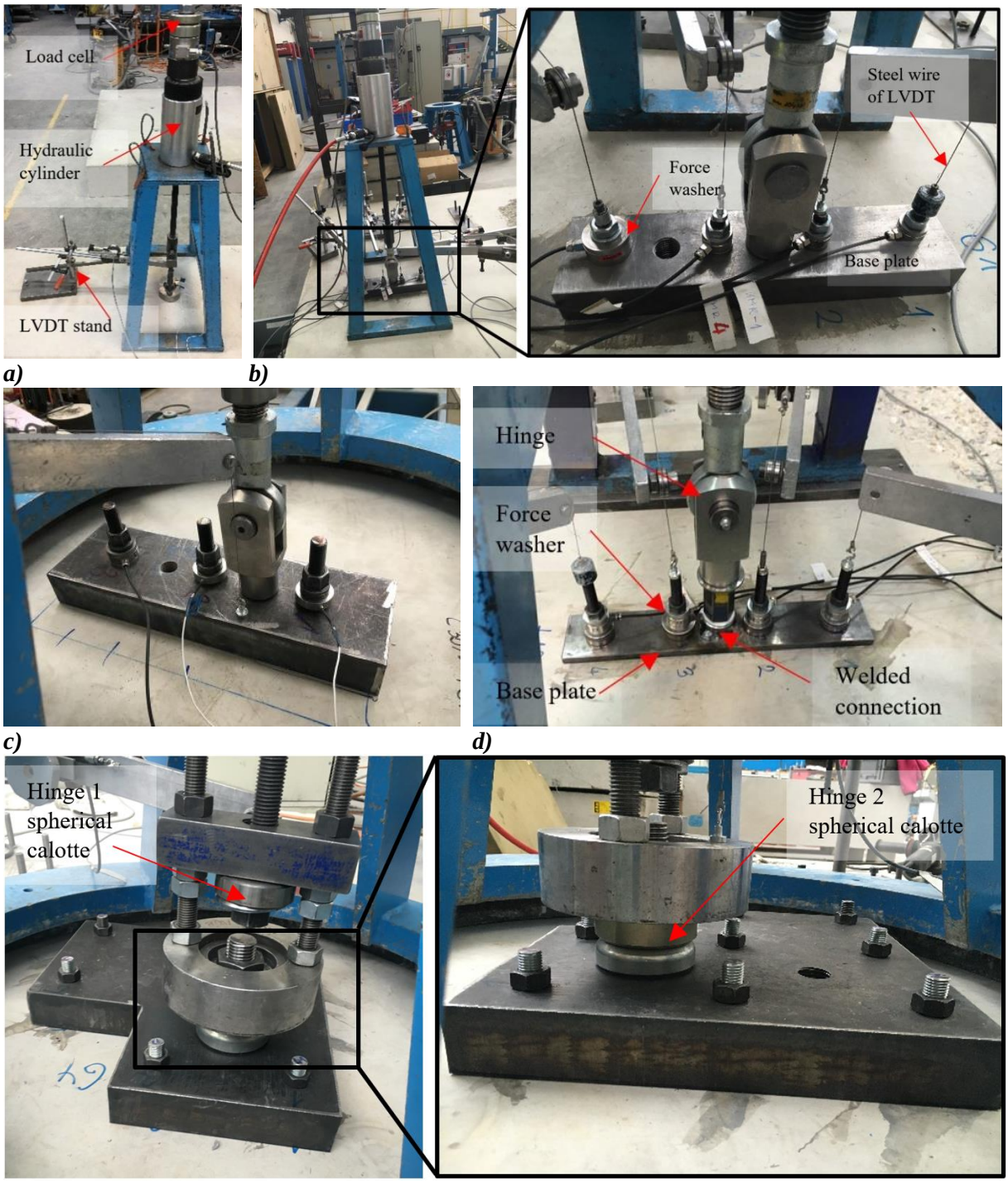

Figure 8.3. Typical test setup in uncracked concrete a) for reference tension tests on single anchors; b) for tension tests on anchor groups with stiff base plate; c) for eccentric tension tests; d) for tension tests on anchor groups with non-rigid base plate; e) for tension test on anchor groups of L-shaped configuration

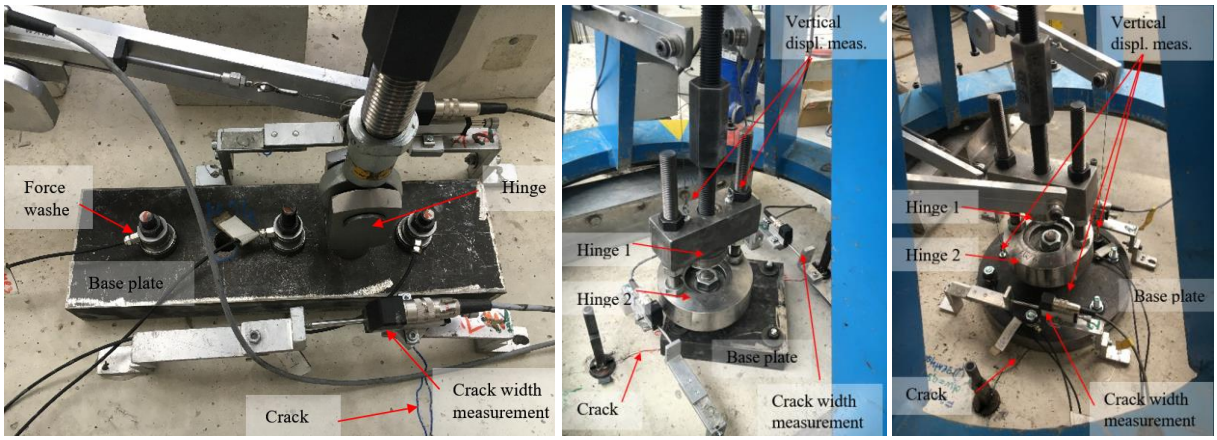

a) ***b)*** ***c)***

Figure 8.4. Typical test setup for tension tests on anchor groups in cracked concrete: a) 1×3 configuration, b) 2×2 configuration, c) hexagonal configuration

8.3 TEST RESULTS AND DISCUSSION ON TENSION LOADED ANCHORAGES

The results of the experimental investigations carried out on tension loaded anchorages are discussed in this section. The results were obtained from performing the programs on anchorages, according to *Table 8.1 - Table 8.3.* Furthermore, the results are compared with calculations based on the recommendations given in EN 1992-4, where applicable. The summary of the experimental results in terms of the mean value of the ultimate tension loads $N_{u,m}$ for the particular test series is given in *Table 8.4 - Table 8.6.* The load-displacement curves and the failure modes are given in the following, in the corresponding subsections. Note that for the cases, where the group tests (e.g. G82, G84, G301 and G401) were performed in a different concrete batch than the batch of the reference single anchor test, the mean ultimate load of the groups was normalised with respect to the concrete compressive strength using the following expression:

$$N_{um} *= N_{um} \cdot \left(\frac{f_{cc,ref}}{f_{cc,test}}\right)^{0.5} \qquad \textit{Eq. 73}$$

Where,

N_{um}* is the mean failure load obtained after normalisation due to concrete strength

N_{um} is the mean failure loads obtained from the group tests

$f_{cc,ref}$ is the cubic compr. strength of concrete in which ref. single anchor tests were performed

$f_{cc,test}$ is the cubic compressive strength of concrete in which the anchor groups were tested

8.3.1 Anchorages of rectangular configurations in uncracked concrete within the scope of EN 1992-4

The tension tests discussed in this section were carried out on anchor groups of rectangular configurations in uncracked concrete within the scope of EN 1992-4. *Table 8.4* summarises the results obtained on anchor groups of 1×3 and 2×2 configurations. The tests listed in *Table 8.4* aimed to generate test data on anchor groups with the corresponding reference tests, which are covered by the current standards. Through this, it is possible to verify the spring model for tension not just against experiments but also to compare the results directly with calculation results. Adhesive anchors and torque controlled expansion anchors were used in the tests. All the tests were designed to achieve the concrete cone failure, which was also the failure mode observed in all the tests on single anchors and anchor groups.

Table 8.4. Summary of the test results of anchorages of rectangular configurations within the scope of EN 1992-4 tested in uncracked concrete

Anchor system	Test series ID	Test type	Mean ultimate load	Calc. mean concrete cone resistance	
			$N_{u,m}$	$N_{u,EN1992-4}$	$N_{u,m} / N_{u,EN1992-4}$
			[kN]	[kN]	[-]
Torque-controlled expansion anchor – M12	R1	Ref. single	27.2	27.1	1.00
	G11R	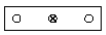	56.1	59.3	0.94
	G12		48.1	47.5	1.01
	G13		40.7	37.2	1.09
	R2	Ref. single	29.5	29.3	1.01
	G22		33.1	32.2	1.03
	G23	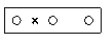	41.6	32.2	1.29
	R3	=R1	27.2	27.1	1.00
	G31R		63.4	68.8	0.92
	G32		46.4	40.6	1.14
	R4	=R2	29.5	29.3	1.01
	G43		49.2	33.9	1.45
Bonded anchor – M16	R5	Ref. single	58.5	62.4	0.94
	G51R	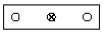	103.9	133.5	0.78
	G52	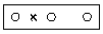	83.3	84.9	0.98
	G53		70.4	65.1	1.08
	G54		61.8	-	-

8.3.1.1 Anchor groups of 1×3 configuration – Influence of loading eccentricity and influence of vicinity of the concrete edge

The test series G11R, G11 and G12 were performed to investigate the influence of the eccentricity and the vicinity of concrete edge separately. The effective embedment depth of the used torque-controlled expansion anchors was $h_{ef} = 55\ mm$, and the anchor spacing was $s = 98\ mm$. The test series G11 was carried out on anchor groups of 1×3 configuration away from the concrete edge. The anchorages were subjected to concentric tension loads. The obtained failure load was 56.1 kN (see *Table 8.4*). The series G12 was performed on the same anchor configuration, however, the anchorage was installed close to the concrete edge to verify the influence of the vicinity of the edge. In the tests, the load application was maintained as concentric. In test series G13, it was targeted to investigate and verify the influence of load eccentricity on anchor groups having large edge distance. The influences of the vicinity of concrete edge and eccentricity led to a reduction in the failure load of the corresponding groups, which was also expected, and confirm the well-known phenomena on the behaviour of anchorages (Eligehausen et al., 2006). Compared to the concentric-loaded anchor group, the mean ultimate loads decreased by 26% due to an eccentricity of $e = 49\ mm$ and by 14% due to the vicinity of the edge. The load-displacement curves obtained from the individual tests are depicted in *Figure 8.5a*. Note that negative displacements shown in the graph are due to measuring errors and not due to anchor behaviour. The influence of the close edge or the eccentricity on the failure loads is clear, however, not that much pronounced on the displacement behaviour in pre- or post-peak. *Figure 8.5b-d* depicts typical failure modes of the performed tests.

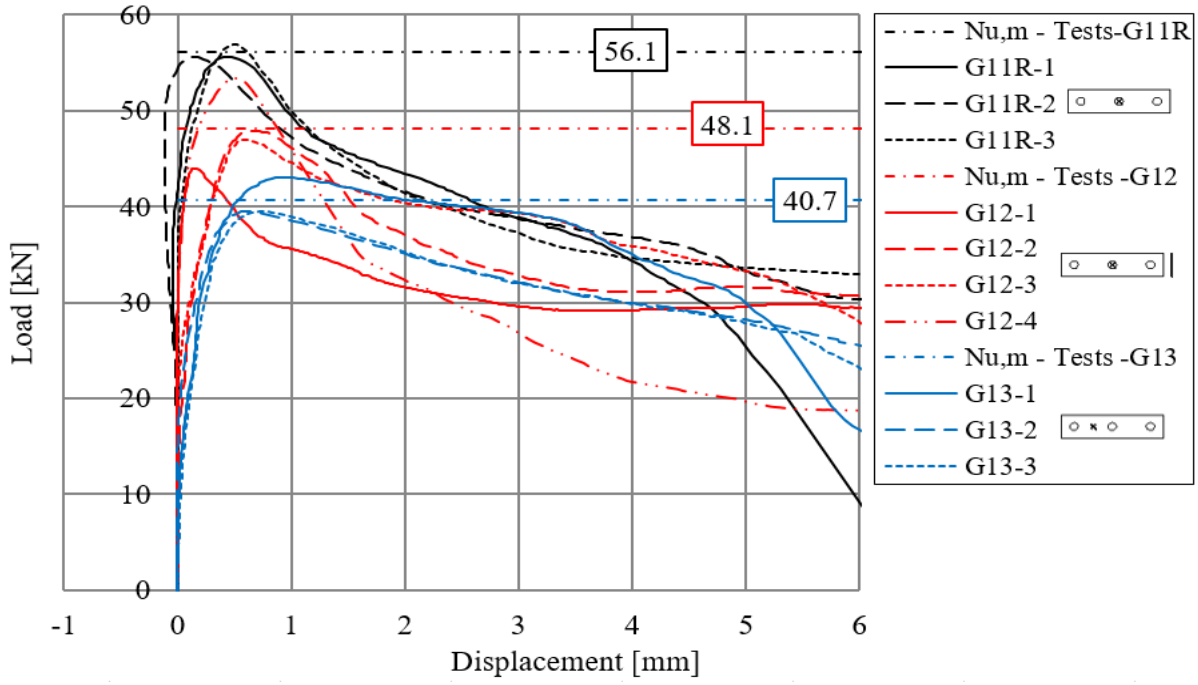

a)

b) *c)* *d)*

Figure 8.5. a) Load-displacement curves of test series G11R, G12 and G13; Typical failure modes of test series: b) G11R; c) G12; d) G13

8.3.1.2 Anchor groups of 1×3 configuration – Superposed influence of loading eccentricity and vicinity of the concrete edge

The test series G22 and G23 were performed to investigate the superposed influence of the vicinity of the edge and the eccentricity. The effective embedment depth of the used torque-controlled expansion anchors was $h_{ef} = 55$ *mm*, and the anchor spacing was $s = 98$ *mm*. The tests results show that when anchor groups are located close to the concrete edge and are loaded eccentrically in tension, it makes a considerable difference whether the eccentricity of the load is away or close the edge (*Figure 8.6*). For the same value of load eccentricity, $e = 49$ *mm*, the measured mean ultimate load for the group loaded with eccentricity close to the edge (series G22) was obtained as 33.1 kN, while the mean failure load for the group loaded with eccentricity away from the edge (series G23) was 41.6 kN. This shows that even with the same eccentricity, the resistance of the anchor group against concrete cone failure was 21% lower when the eccentricity was measured towards the edge. This behaviour is because anchors, which are closer to the load application, have to take up higher forces than the other anchors within the group. However, if the higher-loaded anchors are close to the concrete edge, their resistance is limited due to the influence of the concrete edge, and therefore, the group capacity is also reduced. The load-displacement curves corresponding to series G21 and G22 are plotted in *Figure 8.6a*. Furthermore, a typical failure pattern obtained in test series G22 is depicted in *Figure 8.6b*.

The calculated mean ultimate group resistance according to EN 1992-4 is given in *Table 8.4* along with the measured mean ultimate loads. The calculated mean ultimate load agrees well with the mean ultimate load of series G22, while it is conservative with respect to the mean ultimate load obtained for the test series G23. This is in agreement with the statements by Zhao (1993) and Eligehausen et al. (2006), which say that the model for considering the influence of loading eccentricity on the failure loads of tension loaded anchor groups is, in general, conservative. However, it should be noted that with the model given in EN 1992-4 might not be always conservative for certain cases, e.g. the case where the eccentricity is measured towards

the edge. Therefore, to maintain a uniform safety margin for all cases, the exact loading position should be considered in the calculations.

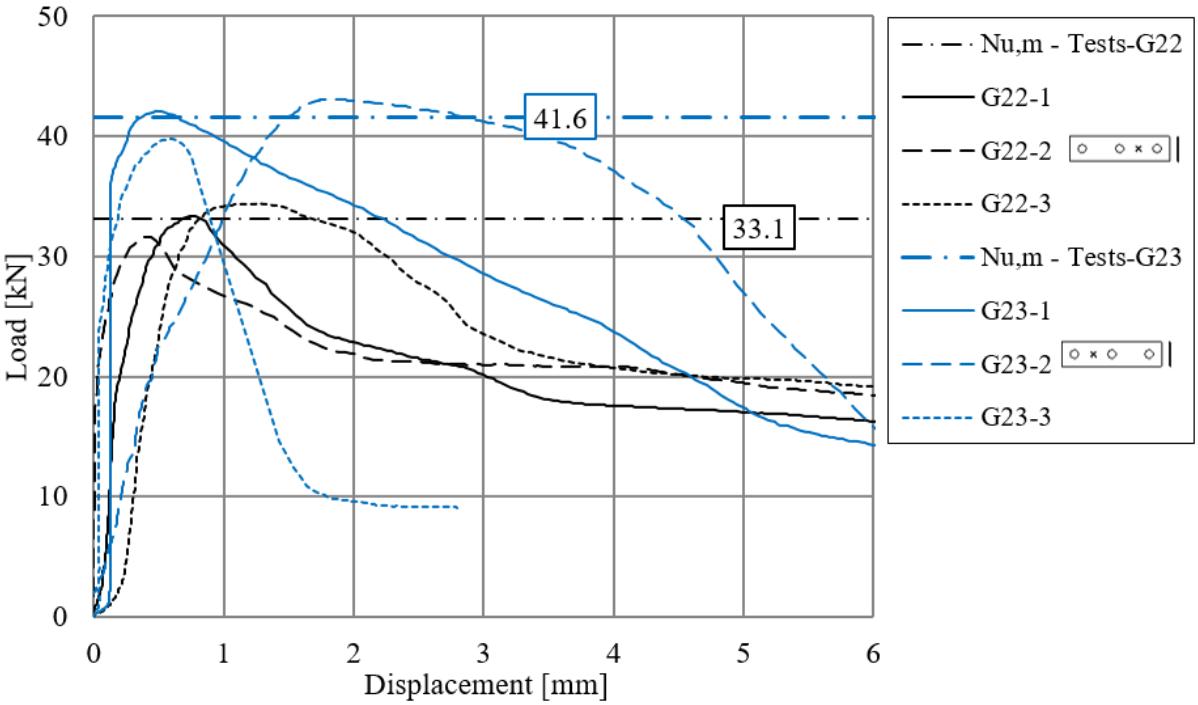

a)

b)

Figure 8.6. a) Load-displacement curves of test series G22 and G23; b) failure mode of series G22

8.3.1.3 Anchor groups of 2×2 configuration – Influence of loading eccentricity about two axes

The test series G31R, G32 and G43 were performed on quadruple to investigate the influence of biaxial eccentricity (eccentricity about two orthogonal axes). The tests aimed to highlight that the current standards consider this influence rather conservatively. According to EN 1992-4, in case of biaxial eccentric loading (*Figure 4.4b*), the factor $\psi_{ec,N}$ (***Eq. 8***) to account for eccentric loading is to be determined separately for the loading directions as $\psi_{ec,N,,1}$ and $\psi_{ec,N,2}$. After that, the multiplication of the factors shall be inserted in the equation to determine the resistance of the anchorage.

In test series G31R, the anchor group was installed far from the concrete edge and the load was applied in the centre, whereas in series G32, the loading was eccentric about two orthogonal axes. The effective embedment depth of the used torque-controlled expansion anchors was $h_{ef} = 55$ *mm*, and the anchor spacing was $s = 98$ *mm*. The mean failure load reduced by 27% due to the biaxial eccentricity (*Table 8.4*). However, according to the calculations of EN 1992-4, the reduction in the mean failure load was 41% for the eccentric case compared to the concentric case, which is significantly more than that was measured in the tests. The load-displacement curves and typical failure patterns are given in *Figure 8.7*. The conservatism in the current design approach is clear by comparing the test results with the calculated failure loads for the anchorage subjected to eccentric tension loads. Note that the conservatism increases with increasing level of eccentricity.

Test series G43 was carried out to investigate the superposed influence of biaxial eccentricity on quadruple anchor groups and the vicinity of the concrete edge. The anchor group was installed parallel to the edge and was loaded with biaxial eccentricity away from the edge as it can be seen in *Figure 8.7d*. The measured mean ultimate load was 49.2 kN and the calculated mean ultimate load according to EN 1992-4 was 33.9 kN, which is 31% lower than the measured value. The difference between the measured and calculated resistances is rather big and highlights the conservatism of the current approach for cases where the eccentric load is applied about two axes. Furthermore, the current approach does not consider the exact loading position (eccentricity towards or away from the edge) when calculating the concrete cone resistance of groups located near to the concrete edge, which again leads to further differences. The load-displacement curves obtained from the tests are depicted in *Figure 8.7b*.

To express the influence of biaxial eccentricity on anchor groups located near the concrete edge, it is necessary to compare tests performed on the anchorage loaded in eccentric tension far from the edge and on anchorages loaded in eccentric tension close to the edge. Since there were no eccentric tests carried out far from the edge in the concrete batch of series G43, the influence of the vicinity of the concrete edge is shown by comparing the series G43 to series G32 after normalising the failure loads according to ***Eq. 73***. The ultimate load decreased by only 2% if the group with biaxial eccentricity was placed near to concrete edge with the eccentricity away from the edge (G43). According to the model of EN 1992-4, the reduction for the eccentric loaded group due to the concrete edge is 23%. This again indicates that there is a significant difference in the capacity of the anchorages placed close to an edge depending on whether the eccentricity of the load is towards or away from the edge. If the eccentricity is towards the edge, the current approach seems reasonable for the cases tested here, while if the eccentricity of the load is away from the edge, then the current approach appears to be rather conservative.

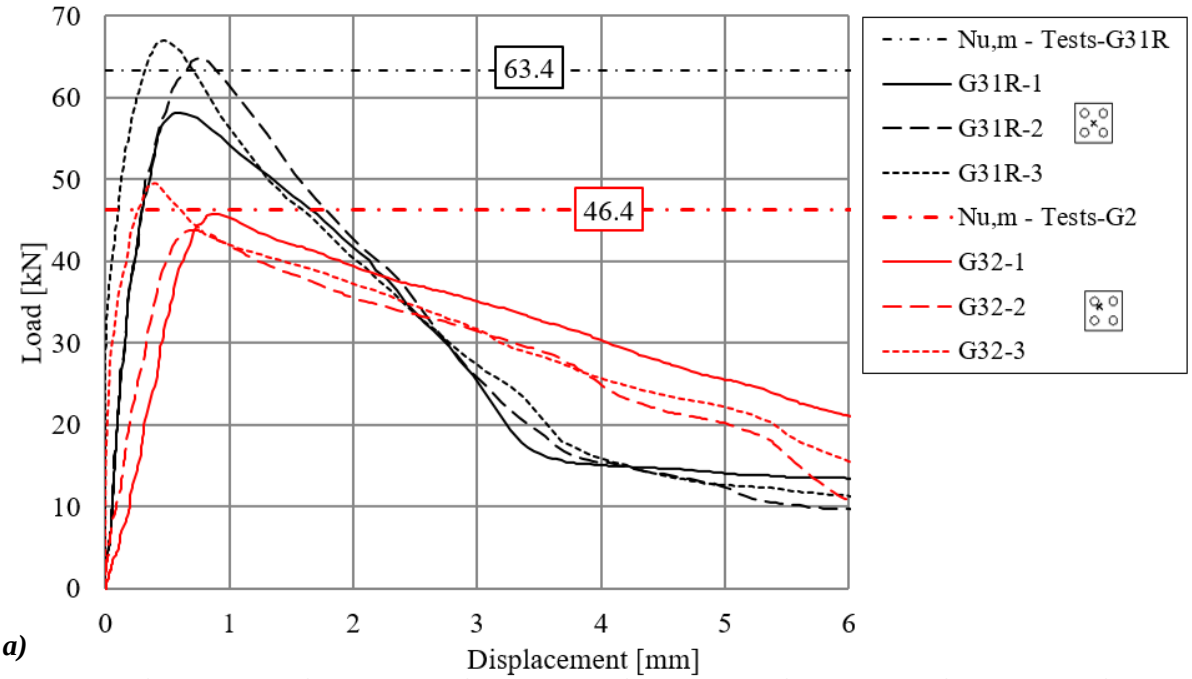

a)

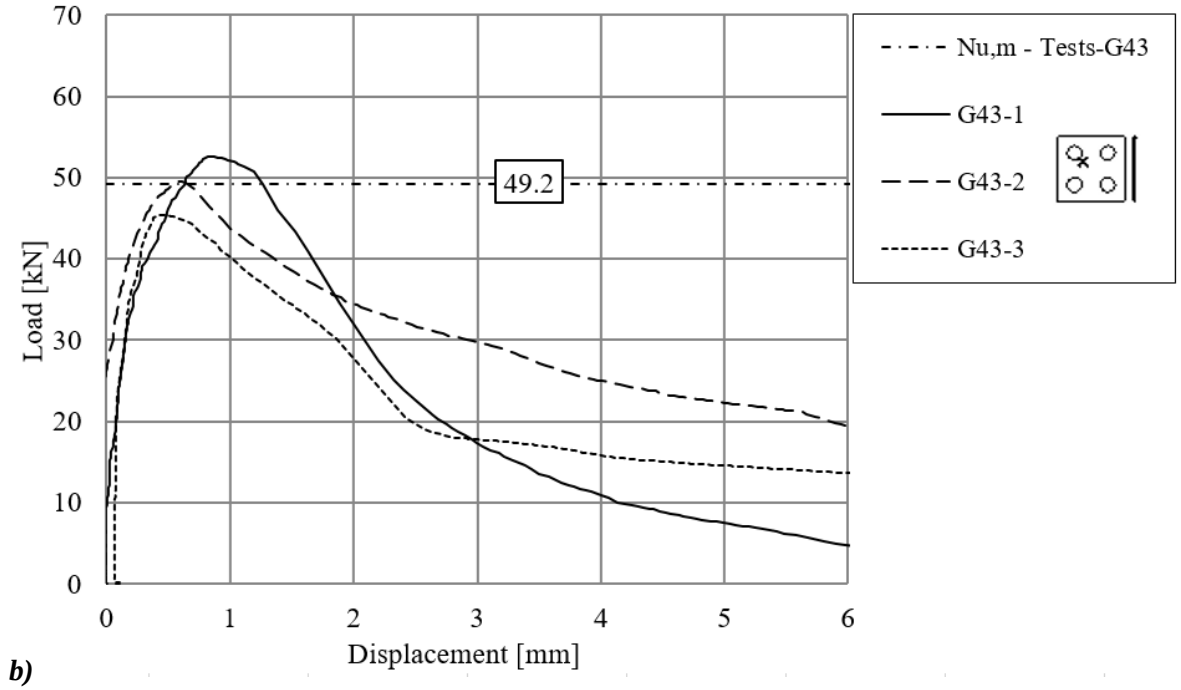

b)

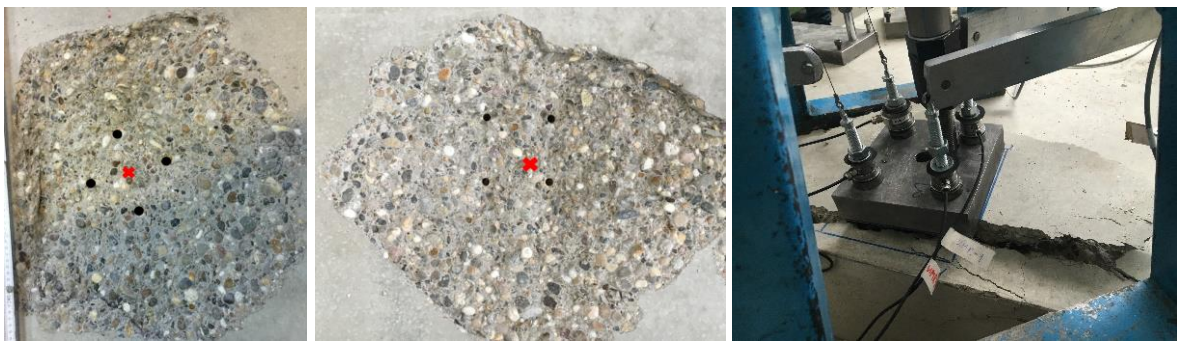

c) *d)* *e)*

Figure 8.7. Load-displacement curves of test series a) G31R and G32; b) G43; Typical failure modes of series: c) G31R; d) G32; e) G43

8.3.1.4 Anchor groups of 1×3 configuration – Influence of loading eccentricity

The test series G51R, G52 and G53 were performed to investigate the influence of the eccentricity on anchor groups of 1×3 configuration. The tests were carried out in normal-strength concrete using bonded anchors away from the edge, under concentric and eccentric loading. The effective embedment depth of the anchors was $h_{ef} = 70$ *mm*, and the anchor spacing was $s = 120$ *mm*. The base plate was 50 mm thick, which can be considered as relatively stiff. Three levels of load eccentricity were investigated. The first level is the concentric-loaded case with e = 0 mm in series G51R, the second level is with medium eccentricity $e = s/2 = 60$ *mm* in series G52, and the third level is with extreme eccentricity e = s = 120 mm with the tension load applied directly on the outermost anchor in series G53. The test results clearly show the negative influence of the eccentric loading (see *Table 8.4*).

Compared to series G51R with concentric load application, the measured mean ultimate load decreased by 20%, when the load was applied eccentrically $e = s/2 = 60$ *mm* (G52). By applying the load with $e = s = 120$ *mm* eccentricity (G53), the reduction compared to the concentric case was 32%. The influence of the eccentricity on the failure loads is clear, however, the displacement behaviour did not change significantly. *Figure 8.8a* shows that the displacements at failure load increased only slightly due to the base plate rotation. The typical failure breakout bodies are depicted in *Figure 8.8e-g* for series G51R, G52 and G53. In all three cases, a common breakout body developed. However, for the eccentric cases, a crack between the lesser-loaded anchors can be observed. This indicates the load redistribution among the anchors of the group.

Besides evaluating the load-displacement behaviour of the anchor groups, also the individual anchor axial forces were measured during the experiments to get information about the load distribution and redistribution among the individual anchors within an anchor group. In *Figure 8.8b-d*, the axial anchor forces and the measured group force are plotted as a function of time for selected tests of series G51R, G52 and G53. *Figure 8.8b* shows that in the case of concentric tension loading with a 50 mm thick base plate (series G51R), the middle anchor reached its peak load just before also the outer anchors reached their peak load. Due to a smaller tributary area of the middle anchor, the resistance of the middle anchor is lower compared to the outer anchors. At the time, when the ultimate load of the group was reached, the middle anchor was already in its post-peak phase, and consequently, the maximum possible group capacity could not be fully utilised. In *Figure 8.8c*, the anchor axial forces and the overall group force are plotted as a function of time for the group with eccentric tension loading $e = s/2 = 60$ *mm* (series G52). The anchors A1 and A2, which are closer to the point of load application reached their peak load nearly at the same time with a contribution based on the activated concrete (tributary area approach – see Section 5.2.2), whereas anchor A3 contributed to the ultimate group resistance only with a small amount. Anchor A3 reached its peak load when A1 and A2 already failed and this way the resistance of anchor A3 only influenced the post-peak behaviour of the group. Furthermore, the force-time graph is supported by the crack pattern on the concrete breakout body shown in *Figure 8.8f*. It can be seen that anchors A1 and A2 form a common fracture body, whereas anchor A3 is separated by a crack between anchors A2 and A3, which is attributable to the rotation of the base plate due to eccentric loading and the prying forces generated thereby. In the case of series G53, the tension load was applied on

the group with extreme eccentricity, where the load is applied directly on the outermost anchor. The graph in *Figure 8.8d* shows that the most loaded anchor A1 reached approximately 58 kN at the peak, which is almost the capacity of the reference single anchor without any influences (series R5 *Table 8.4*). In addition, anchor A2 also contributed to the ultimate load of the group, and consequently, a higher ultimate load (70.4 kN) could be reached. The anchor A3 was activated only after the anchors A1 and A2 have already failed. However, the resistance of anchor A3 is also not negligible because it influences the post-peak behaviour of the group. It can be seen in *Figure 8.8g* that anchors A1 and A2 form a common fracture surface, while anchor A3 is forming a breakout body, which is similar to a breakout body of a single anchor loaded in concentric tension.

The mean ultimate load was calculated for the tested configurations according to EN 1992-4 (see *Table 8.4*). The calculated ultimate load compared to the concentrically loaded group (G51R) decreased by 36% due to an eccentricity of $e = s/2 = 60$ *mm* and by 51% due to an eccentricity of $e = s = 120$ *mm*, respectively. This shows that for anchor groups with three anchors in a row the current approach estimates more conservative results with increasing the eccentricity.

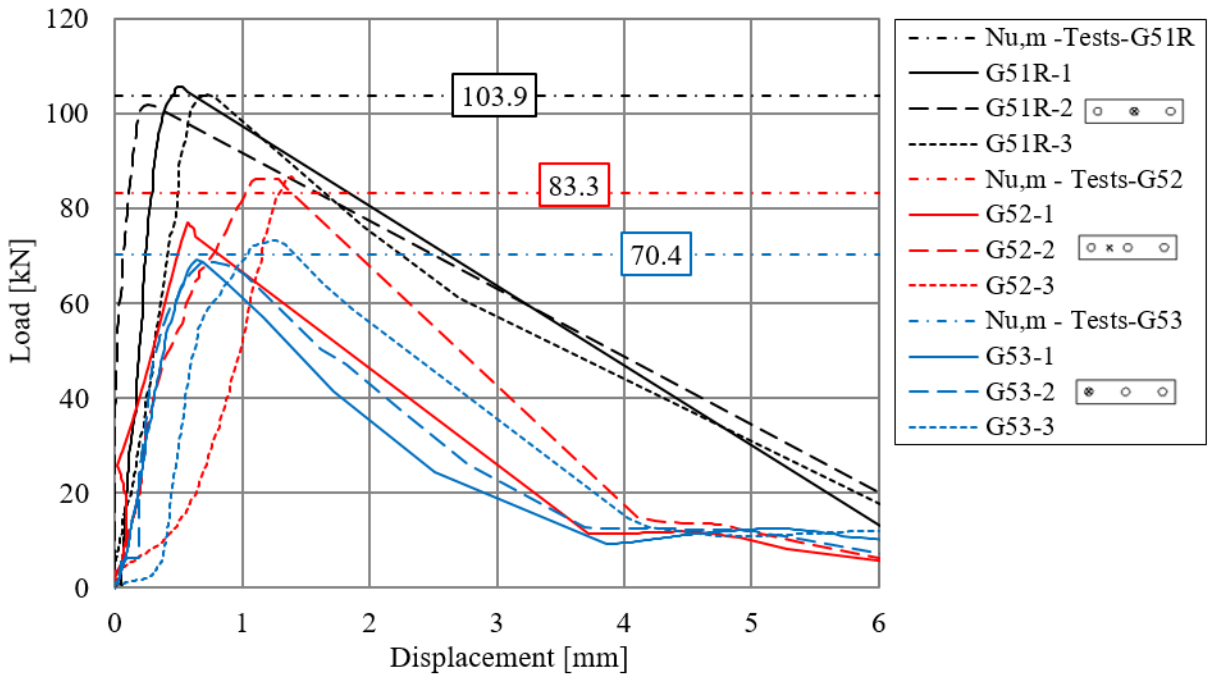

a)

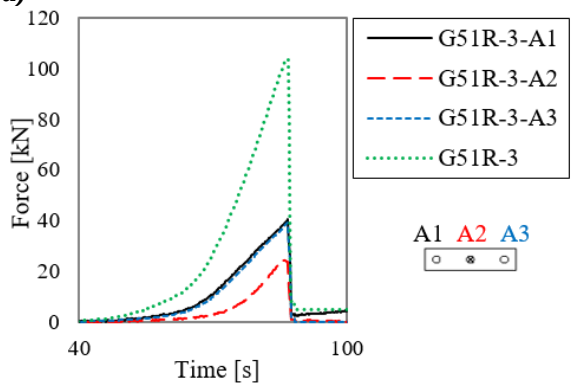

b)

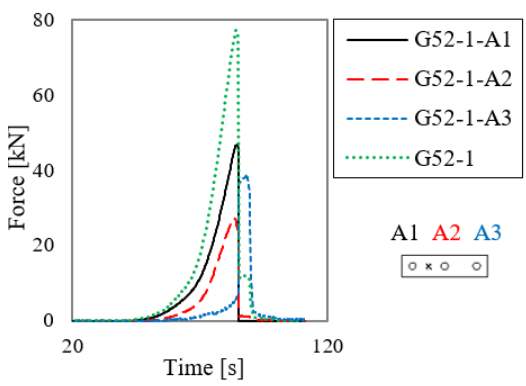

c)

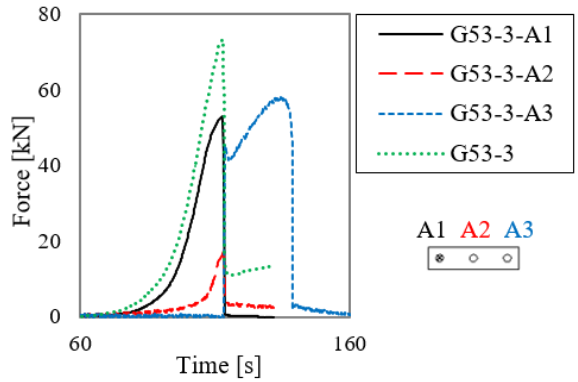

d)

e)

f)

g)

Figure 8.8. a) Load-displacement curves of test series G51R-G53; Axial anchor forces and group force in function of elapsed time for test series: b) G51R; c) G52; d) G53; Typical failure modes of test series: e) G51R; f) G52; g) G53

8.3.2 Anchorages of rectangular and non-rectangular configurations in uncracked concrete

This section discusses the tests, which were carried out on rectangular and non-rectangular anchor groups that are currently beyond the scope of EN 1992-4. Special emphasis was placed on the behaviour of anchorages with non-rigid base plate to evaluate the influence of base plate stiffness. *Table 8.5* summarises the results obtained from the experiments. The tests aimed to generate test data on anchor groups with the corresponding reference tests, which are beyond the scope of the current standards and to verify the tension spring model for anchor groups of arbitrary configurations. Bonded anchors of size M12 and M16 were used in the experiments. All tests were designed to achieve the concrete cone failure, which was also the failure mode observed in all the tests on single anchors and anchor groups.

Table 8.5. Test results of anchorages of rectangular and non-rectangular configurations in uncracked concrete

Anchor system	Test series ID	Test type	Mean ultimate load $N_{u,m}$ [kN]	Normalised mean ultimate load $N_{u,m*}$ [kN]
Bonded anchor – M12	R8	Ref. single	34.3	34.3
	G81	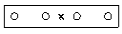	73.5	73.5
	G82		48.8	49.7
	G83	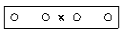	51.6	51.6
	G84	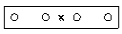	46.1	46.9
Bonded anchor – M16	R9	Ref. single	39.5	39.5
	G91		105.4	105.4
	G92		113.4	113.4
	R10	= R9	39.5	39.5
	G101		89.8	89.8
	R20	Ref. single	52.5	52.5
	G201		128.9	128.9
Bonded anchor – M12	R30	=R8	34.3	34.3
	G301		127.3	129.6
	R40	=R8	34.3	34.3
	G401		70.5	70.6

Note that the results of test series G53 and G54 on 1×3 anchor groups from Section 8.3.1.4 are used when discussing the influence of base plate stiffness. However, the test results are not repeated in *Table 8.5*.

8.3.2.1 Influence of the base plate stiffness

Test series G53-G54 and G81-G84 were performed to investigate the influence of the base plate stiffness on the load-displacement behaviour of anchor groups away from the concrete edge. For this reason, tension tests were carried out on anchor groups with a single row of three anchors and on anchor groups with a single row having four anchors in uncracked concrete with varying the base plate thickness according to *Table 8.1* and *Table 8.2*.

Anchor groups of 1×3 configuration

Test series G53 and G54 were performed on 1×3 anchor groups applying the tension load with a loading eccentricity of $e = s = 120$ *mm*. The base plate thickness was 50 mm and 25 mm for test series G53 and 54, respectively. By reducing the base plate thickness by 50%, the measured mean ultimate load decreased by 12%. The corresponding load-displacement curves from the test series G53 and G54 are depicted in *Figure 8.9a*, which show a similar behaviour but with reduced capacity for the 25 mm base plate. It may be noted that the results obtained from test series G51R highlighted that even a base plate thickness of $t = 50$ *mm* is not sufficiently stiff. The results on series G54 show that a base plate with $t = 25$ *mm* thickness is rather flexible. However, a base plate thickness of 25 mm for similar spacing of anchors is often used in practice and the design of anchorage is performed assuming a rigid response, which might be unconservative.

To understand better how the force distribution and redistribution takes place among the anchors of a group with a flexible base plate, the individual anchor axial forces were measured during the tests. These results are evaluated by plotting the anchor axial forces in the function of time to see the anchor activation order. *Figure 8.9b* shows the force distribution within the group G54. Anchor A1 is immediately active because the load is applied at the location of this anchor. In the initial stages of loading, the load-time curve for the group is the same as the load-time curve of the anchor A1. The participation of anchor A2 is very limited until the anchor A1 fails, and the anchor A2 takes up the load. This explains that the group ultimate load was only 6% higher compared to the resistance of one single anchor (compare series R5). Anchor A3 is activated after both anchor A1, and A2 fail and therefore, it does not contribute to an increased resistance of the group G54-3. It can be seen that the load applied on the group drops after failure. This is because due to the lever arm and the prying action of the flexible base plate, the force measured in the anchor is significantly higher than the external load applied to the group. The evaluation shows that the forces were not distributed linearly among the anchors within a group due to the flexible base plate, which highlights that the base plate stiffness highly influences the nonlinear behaviour of the anchor group. The crack pattern in *Figure 8.9c* confirms the order of anchor activation of the graph in *Figure 8.9b*. The cracks between the anchors indicate that the load distribution took place from anchor to anchor and the anchor force contribution seems to be in accordance with the tributary area, which can be assigned to the group according to Section 5.2.2.

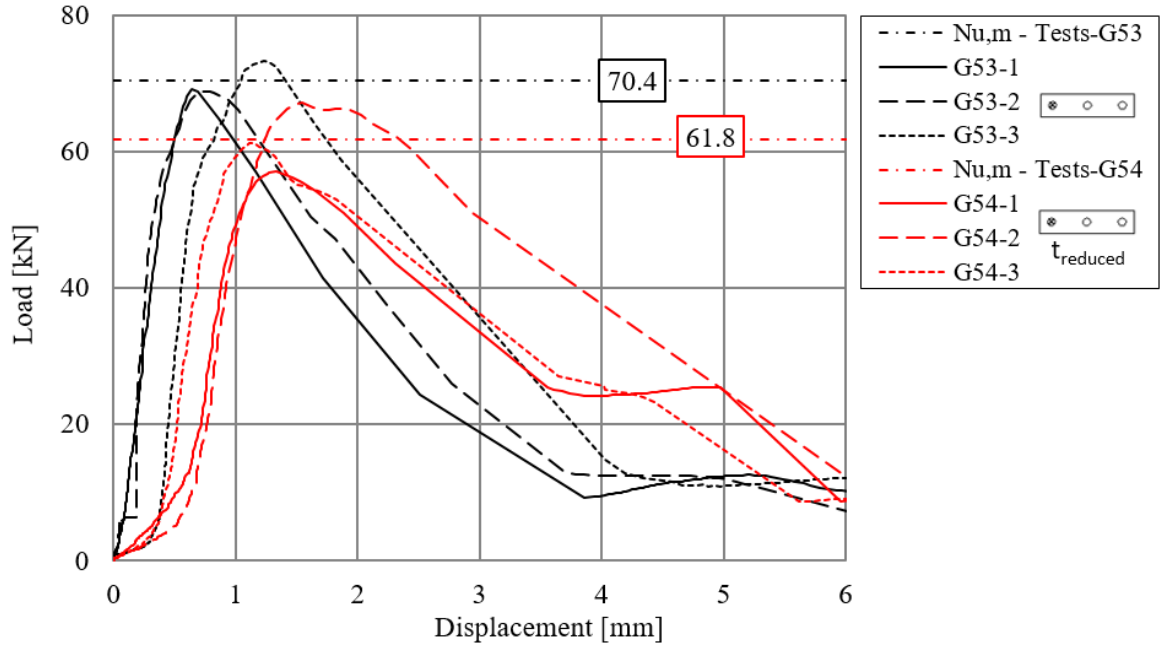

a)

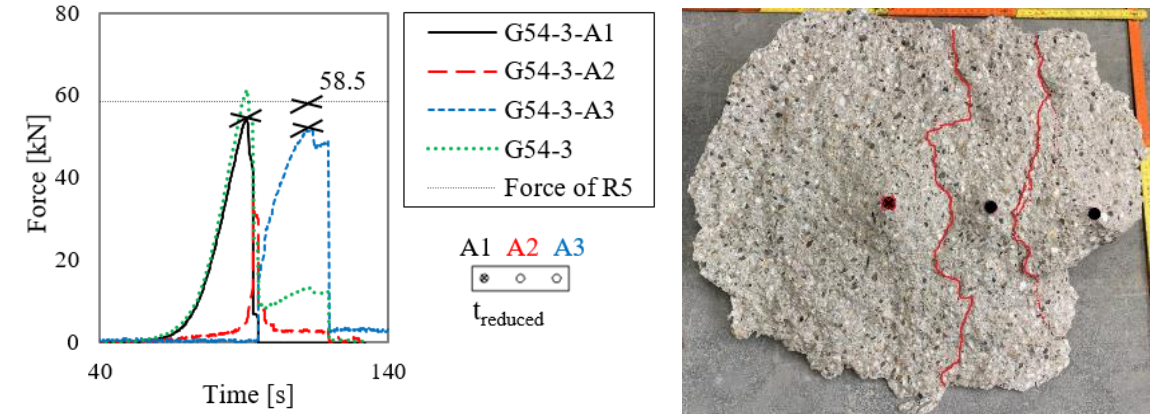

b)

c)

Figure 8.9. Influence of the base plate stiffness: a) Load-displacement curves of test series G53 and G54; b) Axial anchor forces and group force in function of elapsed time for test series G54; c) Typical failure mode of test series G54

Anchor groups of 1×4 configuration

The influence of base plate stiffness on the behaviour of tension loaded anchorages was further investigated by test series G81, G83 and G84. In this case, the concentric tension load was applied on a 1×4 anchor group with a base plate thickness of *t = 40 mm*, which was assumed to be rigid; *t = 10 mm* and *t = 5 mm*, which may be considered as flexible elastic and flexible inelastic base plates, respectively. This anchor configuration is not covered according to the current regulations of EN 1992-4. However, according to ACI 318, the CCD method is capable of extension to different layouts. The load-displacement curves obtained from the tests on the anchor groups are depicted in *Figure 8.10a* for the three investigate base plate thicknesses. The failure pictures are given in *Figure 8.11* for one representative test per series.

The test results confirmed the negative influence of the reduced base plate thickness (and consequently stiffness) for the investigated cases (*Figure 8.5*). The measured mean ultimate load decreased by 30% when the base plate thickness was 10 mm in series G83 instead of 40 mm in series G81. An even bigger influence was observed in the displacement behaviour: the mean displacement at ultimate load increased from 0.52 mm to 2.38 mm highlighting the base plate deformations. If the first peak load of the tests on groups G83 is considered instead of the peak load, then the decrease in ultimate load is 33%. When the base plate with 5 mm thickness was used in series G84, the measured mean ultimate load decreased by 37% compared to G81, and the mean displacement at ultimate load increased from 0.52 mm to 8.20 mm. However, this large vertical base plate displacement can be attributed to the large base plate deformations. In the tests G84-1 and G84-2, yielding of the base plate was observed which is shown by the curve progression in *Figure 8.11e*.

The influence of the base plate stiffness on the anchor group behaviour is verified by the anchor axial force versus time curves in *Figure 8.10b-d* as well. In the case of the 40 mm thick base plate (*Figure 8.10b*), which was assumed to be sufficiently stiff, a common breakout body developed (see *Figure 8.11b*). However, it can be seen in *Figure 8.10b* that the anchorage capacity was not fully utilised. This is because the outer anchors reached their peak load just after the group reached its ultimate load, so the four anchors were not loaded simultaneously. This indicates that the 40 mm thick base plate was not sufficiently stiff and therefore, the equal load distribution among the anchors of the group was not valid. In addition to the experiments, numerical investigations were carried out on the same anchor group configuration in another work (Bokor et al., 2018) to verify the assumption. The results of the numerical investigation confirmed that the 40 mm thick base plate is not sufficiently stiff and an equal force distribution within this particular anchor group could only be reached if the base plate was at least 80 mm thick. However, note that this is only valid for the investigated configuration and might be different for other anchorages.

In the case of the groups with thinner base plates, the anchor activation order is related to the base plate deformations as it can be observed from the load-displacement curves in *Figure 8.10a*. The force-time curves in *Figure 8.10c* show that in case of the 10 mm thick base plate in series G83, first, the two inner anchors took up the loads and only after their failure the outer anchors were activated and contributed. However, the contribution of the outer anchors affected mostly the post-peak behaviour of the group. *Figure 8.11d* depicts the concrete

breakout body of one representative test of series G83, which verifies that the middle anchors were loaded first and only after their failure, the outer anchors were utilised. The same evaluation was done for series G84 with $t = 5\ mm$ base plate thickness. The anchor forces are plotted in function of time in *Figure 8.10d*. The two middle anchors reached ca. 80% of their capacity when the outer anchors started to contribute to the group capacity. For further clarification, the anchor axial force – anchor vertical displacement curves of series G84 are plotted in *Figure 8.10e* presents. The graph shows that the outer anchors reached their resistance by less than 1 mm vertical anchor displacement in contrast to the inner anchors, which exceeded 2 mm. The influence of the base plate deformations on the anchor group behaviour is confirmed by *Figure 8.10d* and *e* and explain the large displacements measured on the group. Furthermore, *Figure 8.10c* and *d* show that the measured group ultimate load is smaller than the sum of the axial anchor forces at the time of reaching the peak load. The difference between the sum of the axial anchor forces and the ultimate load of the group is equal to the compressive reaction forces below the base plate, which develop due to the prying action of the non-rigid base plate.

The results of test series G53 and G54, as well as series G83 and G84, showed that the base plate deformation has a significant influence on the nonlinear behaviour of the anchor group and the force distribution within the anchors of the group. Therefore, the particular base plate stiffness should be taken into account when calculating the group resistance and anchor forces as it is done using the nonlinear spring model (see Section 5).

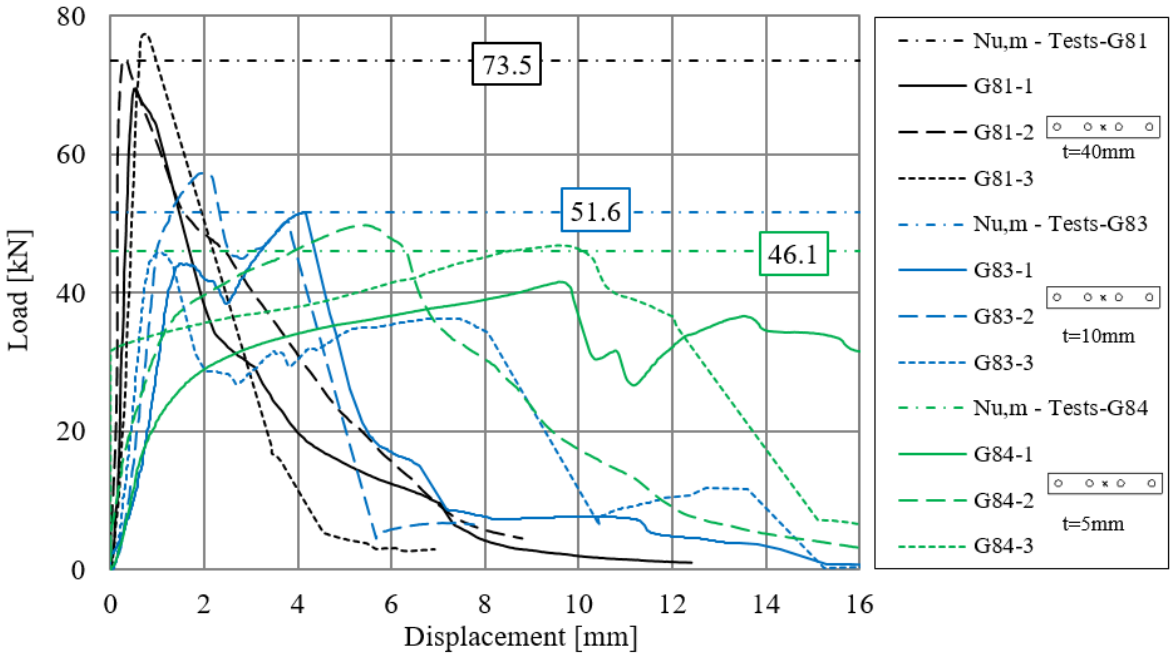

a)

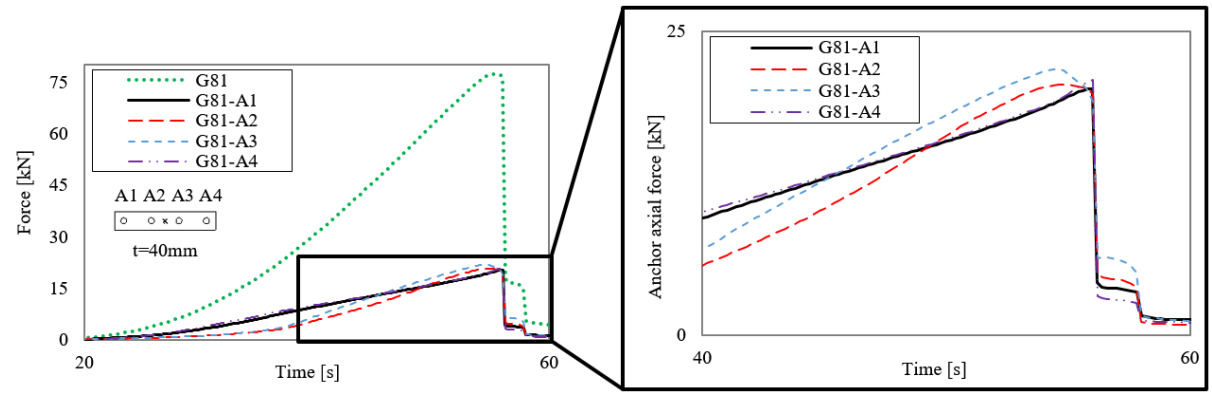

b)

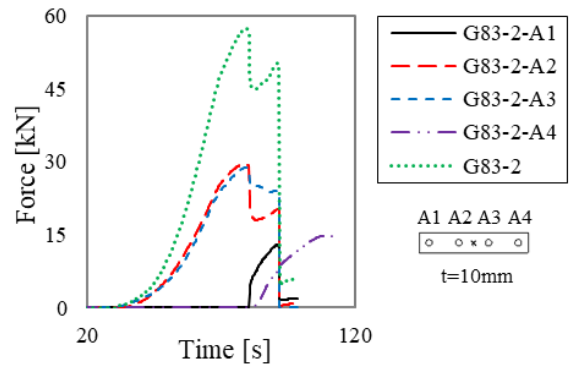

c)

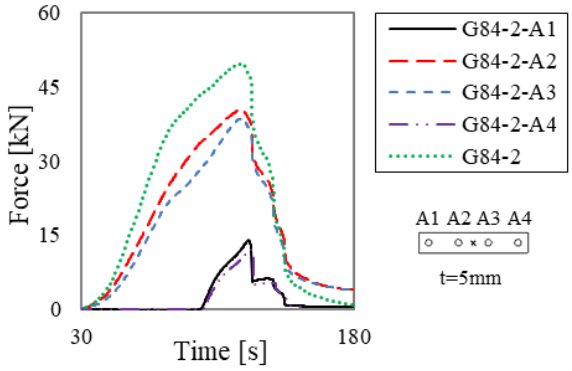

d)

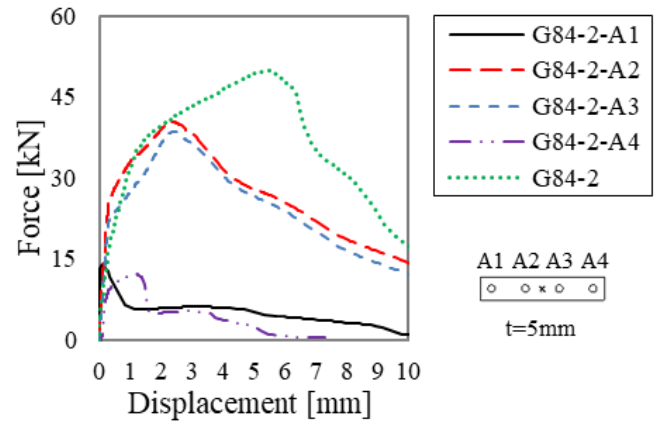

e)

Figure 8.10. Influence of the base plate stiffness: a) Load-displacement curves of test series G81-G84; Axial anchor forces and group force in function of elapsed time for test series: b) G81; c) G83; d) G84; e) Axial anchor forces and group force plotted against the individual and group displacement (G84-2)

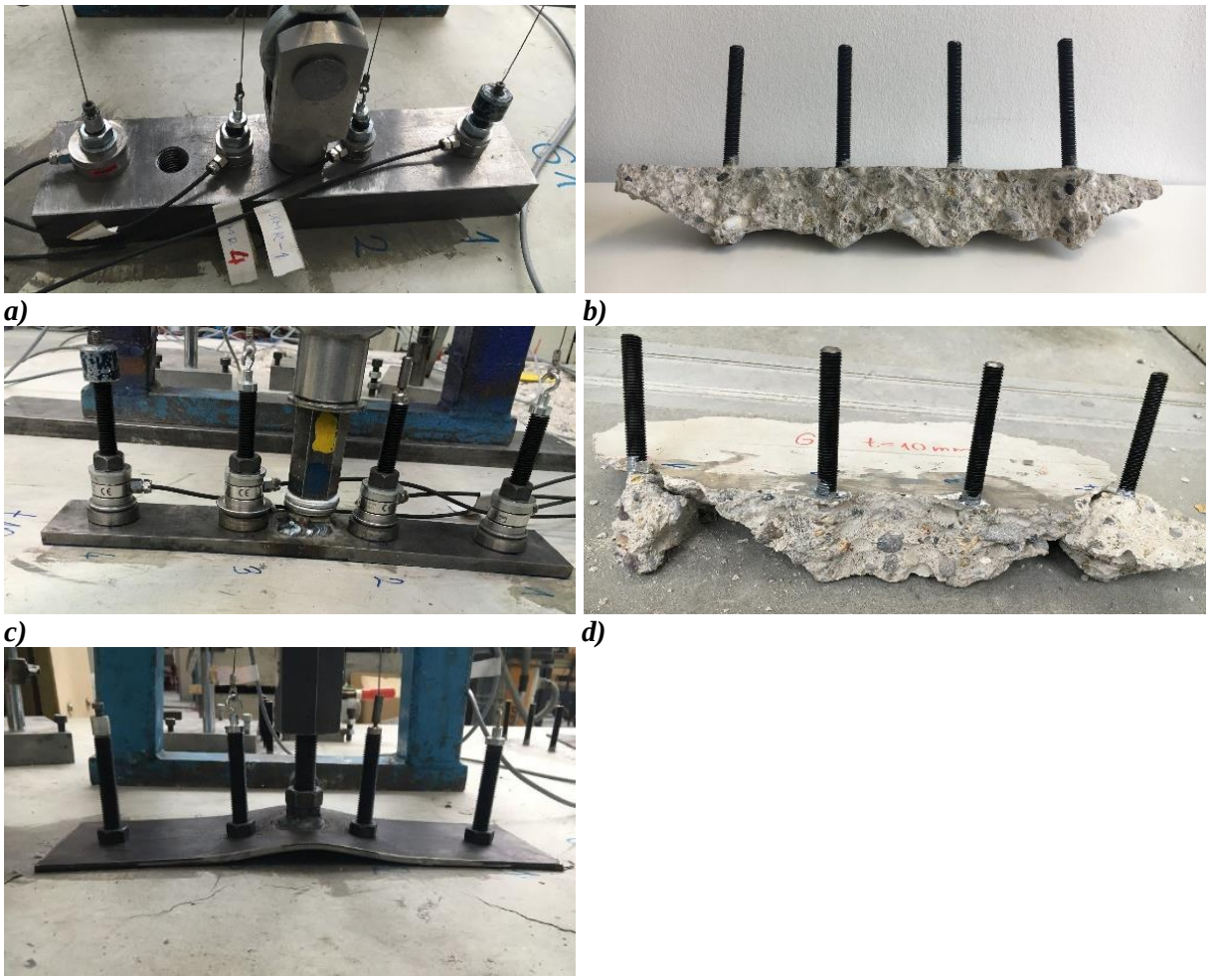

a) *b)* *c)* *d)* *e)*

Figure 8.11. Influence of base plate stiffness: a) anchor group G81 with rigid base plate during testing; b) concrete breakout body of G81 (t = 40 mm); c) anchor group G83 with non-rigid base plate during testing; d) concrete breakout body of G83 (t =10 mm); e) anchor group G84 with thin base plate during testing

8.3.2.2 Test results on anchor groups of arbitrary configurations

To generate a test database and to verify the tension spring model for anchor groups, which are beyond the scope of the current design provisions, tension tests were carried out on anchor groups of 1×4, L- shaped, triangular, hexagonal and trapezoidal configurations.

Anchor groups of 1×4 configuration

Test series G81-G82 were carried out on anchor groups of 1×4 configurations subjected to concentric and eccentric tension loads with having 40 mm thick base plate. These series aimed to show that the tributary area approach can be extended to configurations having more than one anchor per anchor row. Furthermore, the influence of loading eccentricity was investigated. The anchor embedment depth was $h_{ef} = 60\ mm$ and the external force was applied with an eccentricity of $e = s = 90\ mm$. The influence of the eccentric loading led to a reduction of the failure loads as it was expected. Compared to the concentric test series G81, the measured mean ultimate load decreased by 34% due to the eccentricity, whereas the displacement at peak load remained almost unchanged (see *Figure 8.12a*). In *Figure 8.12b,* the anchor axial forces and

the applied tension force are plotted in function of the time showing the contribution and the activation order of the individual anchors within the group G82. The anchors A1, A2, which are closest to the point of load application were loaded the most, and their contribution is related to the concrete area that they can activate. Anchor A3 contributed with ca. 50% of its resistance to the group ultimate resistance. However, the graph shows that anchors A3 and A4 reached their maximum load only after the group ultimate load. This way, their performance was influencing only the post-peak behaviour of the group.

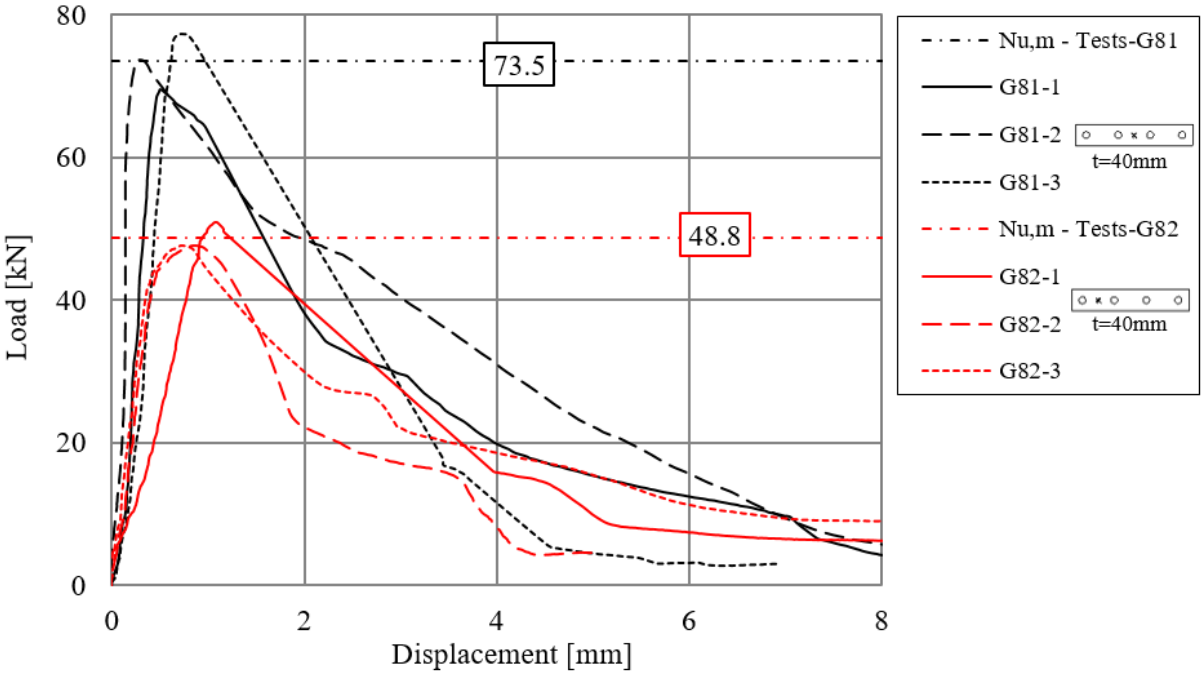

a)

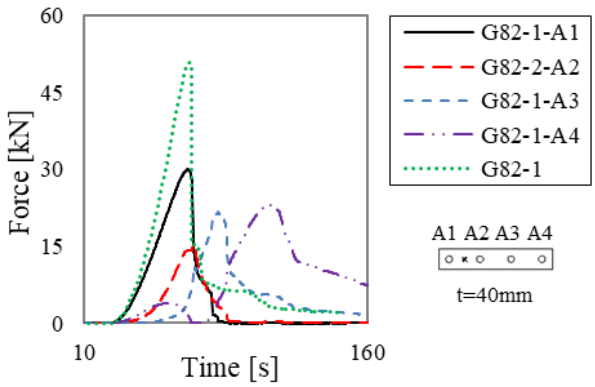

b)

Figure 8.12. a) Load-displacement curves of test series G81 and G82; b) Axial anchor forces and group force in function of elapsed time of test series G82

Anchor groups of L - shaped configuration

Tension tests were carried out in test series G91 and G92 on anchor groups with L - shaped base plate geometry and with regularly spaced, $s = 140$ *mm*, L - shaped anchor pattern. The base plate with $t = 50$ *mm* thickness was assumed to be rather stiff. This anchor group configuration is beyond the scope of the current design provisions. The point of load application, B1

for G91 and B2 for G92, is shown in *Table 8.5* and *Figure 8.13*. Bonded anchors of size M16 with an embedment depth of h_{ef} = *60 mm* were used in the tests. Furthermore, reference tests on single anchors were performed in series R9 to ensure that a direct comparison between the test results on single anchors and the groups is possible. The load-displacement curves obtained in the reference tests are depicted in *Figure 8.13a*. The measured mean ultimate load was obtained as 39.5 kN.

The anchor group tests in the case of series G91 and G92 were carried out using the same base plate, however changing the loading position. The tests were carried out in both cases with hinges built-in in the force flow to allow the rotation of the base plate. The load-displacement curves and the typical failure modes are given in *Figure 8.13b,c*, respectively. The curve progression is rather similar. However, the displacement at the ultimate load is slightly higher in series G92 due to the larger base plate rotation. The measured mean ultimate load was 105.4 kN for series G91 and 113.4 kN for series G92. These correspond to 2.66- and 2.87-times the capacity of the reference single anchor R9. A typical concrete breakout body from series G91 is depicted in *Figure 8.13c*. It can be seen that the developed concrete cones of the neighbouring anchors are intersecting and to each anchor, a particular concrete breakout body can be allocated. It is also visible that two corners of the base plate restricted the tensioned concrete area. This is because the base plate rotated due to the eccentric load application and compression forces between the base plate and concrete surface developed, which restricted the tensioned concrete area. These effects must be accounted for while calculating the anchor forces and the ultimate resistance of the group, which is done when using the nonlinear spring modelling approach for determining the group resistance by considering the contact between the base plate and concrete (see Section 5.4). Verification is given in Section 10.

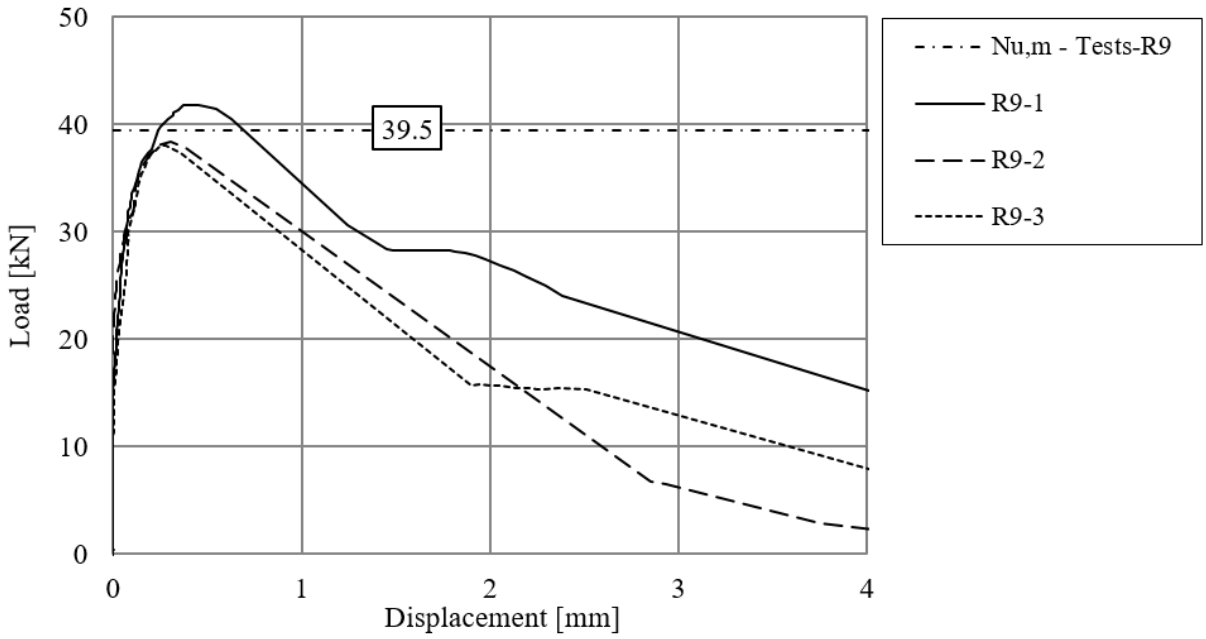

a)

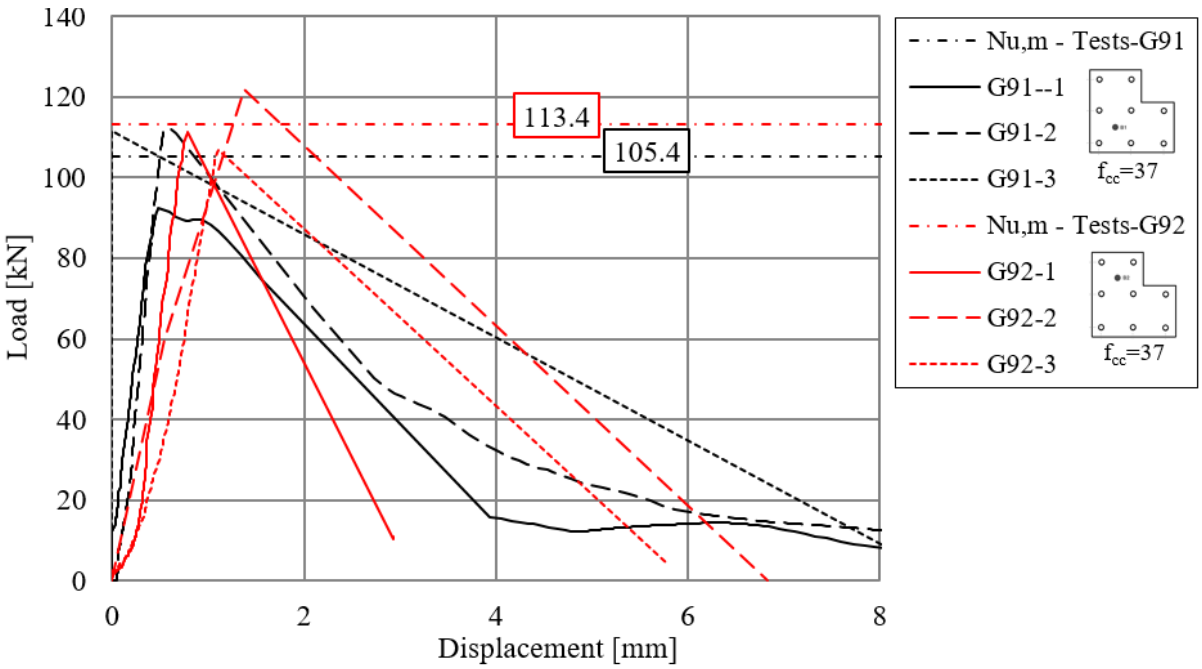

b)

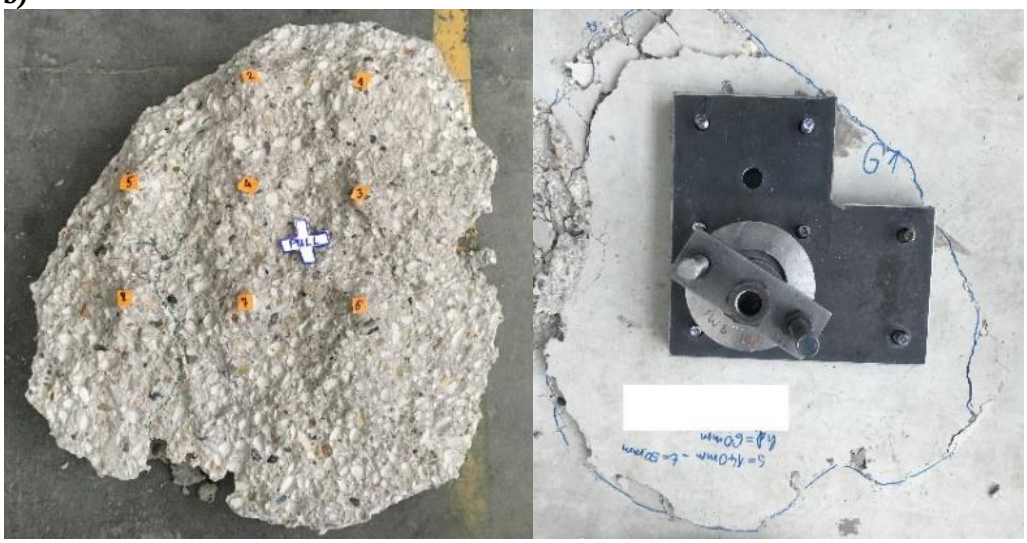

c)

d)

Figure 8.13. a) Load-displacement curves of single anchor test series R9 and R20; b) Load-displacement curves of test series G91-G92; c) Typical failure mode of test series G91; d) Typical failure mode of test series G92

Anchor groups of triangular configuration

Anchor groups of triangular configurations were tested under concentric tension loads in series G101 and G201 in normal and high-strength concrete, respectively. The anchors were arranged at the apexes of an equilateral triangle of side 140 mm using a presumed stiff circular base plate. Bonded anchors of size M16 were used and the anchor embedment depth was 60 mm.

To have a direct comparison for the results obtained on the group tests, reference tests on single anchors in high strength concrete were performed in series R20, while the reference tests of series R9 were considered as reference tests in normal strength concrete (*Figure 8.13a*). *Figure 8.14a* show the load-displacement curves obtained from the reference single anchor series R20. The corresponding mean measured ultimate load in high-strength concrete was obtained as 52.5 kN. The results of the concentric tension tests on triangular anchor groups are summarised in *Table 8.5*, and the corresponding load-displacement curves are shown in *Figure 8.14b*. It can be seen that the load-displacement curves of series G201 in high-strength concrete display a steeper descending branch compared to that in normal strength concrete. The measured mean ultimate load was obtained as 89.8 kN for series G101 and 128.9 kN for series G201. *Figure 8.14c* shows the concrete breakout body from series R101. The breakout body indicates that the same tributary area might be associated with each anchor of the group.

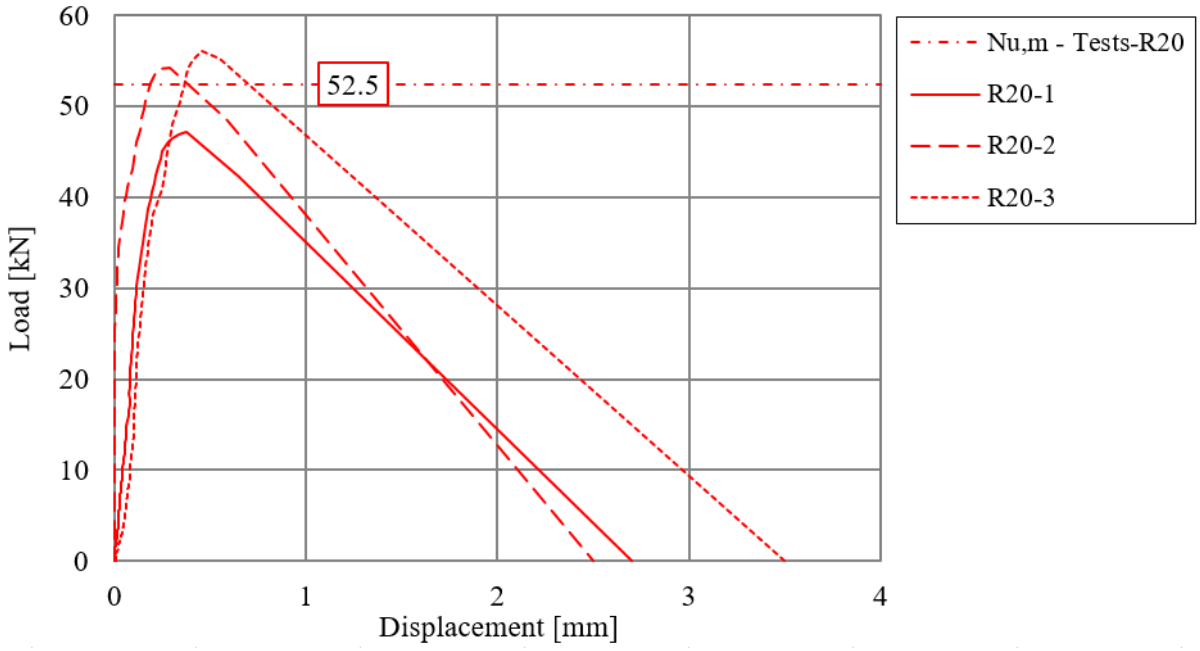

a)

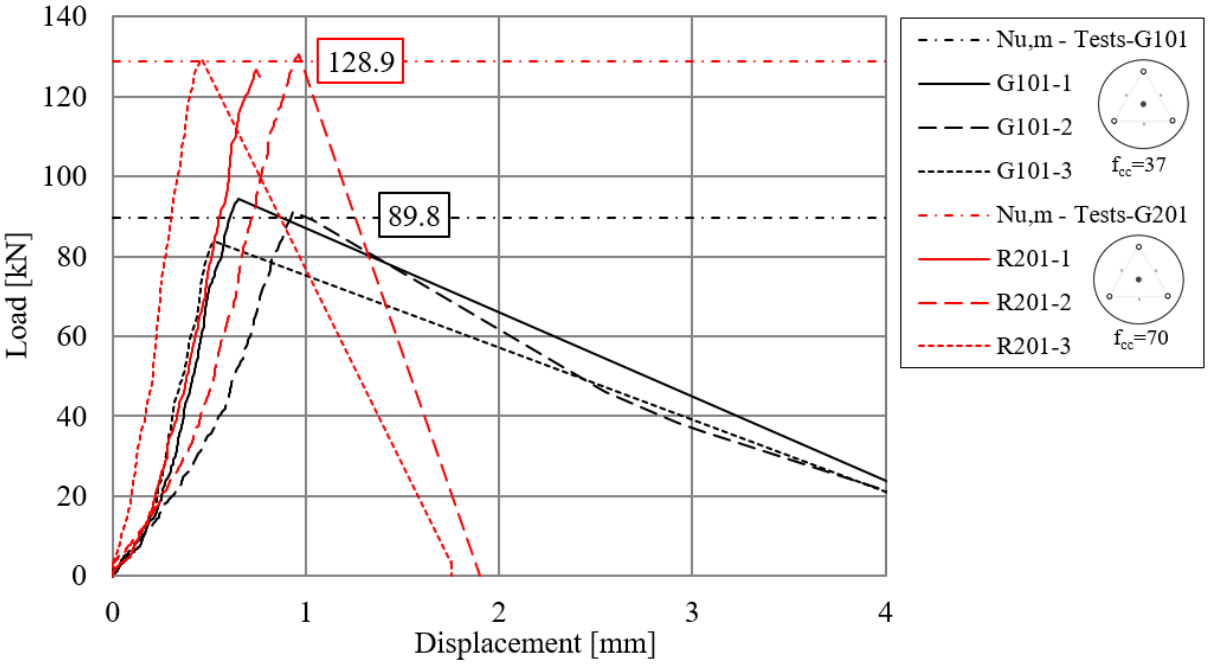

b)

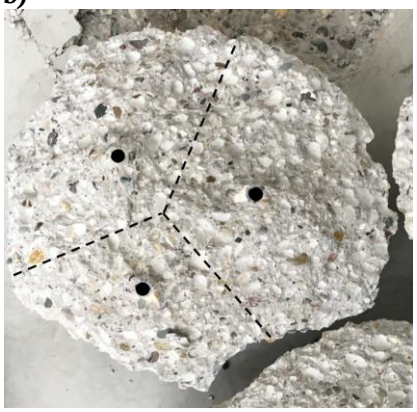

c)

Figure 8.14. Load-displacement curves of test series: a) R20; b) G101 and G201; c) concrete breakout body from series G101

Anchor groups of hexagonal configuration

Anchor groups of hexagonal configuration were tested in series G301. Six anchors were installed in a hexagonal pattern and the concentric tension load was applied on the presumably rigid, circular base plate. The embedment depth of the M12 anchors was $h_{ef} = 60$ *mm* and the spacing between the adjacent anchors was $s = 120$ *mm*. The load-displacement curves are depicted in *Figure 8.15a*, which show that the behaviour of the anchorages was rather brittle. The concrete breakout body of one representative test is depicted in *Figure 8.15b*. It can be seen that the developed concrete cones of the neighbouring anchors are intersecting and to each anchor, a particular concrete breakout body and a certain a tributary area can be allocated. The measured mean ultimate load obtained in series G301 was 127.3 kN. The test results aim to verify the spring model for non-rectangular anchor groups. The verification is discussed in Chapter 10.

Anchor groups of trapezoidal configuration

Test series G401 was carried out by removing two adjacent anchors of the otherwise hexagonal pattern used in series G301 resulting in a trapezoidal anchor group configuration. The other installation parameters were kept the same as for series G301. The tension load was applied at the centre of the circular base plate, which resulted in the trapezoidal anchor group subjected to eccentric tension loading. The measured mean ultimate load was obtained as 70.5 kN, which was 45% lower compared to the series G301. This is attributed to the reduction in the area of the group breakout body and the eccentric loading. The load-displacement curves of series G401 are plotted together with those obtained for series G301 in *Figure 8.15a*. The test results aim to verify the spring model for non-rectangular anchor groups. Furthermore to highlight the necessity to model the contact between the base plate and the concrete surface to evaluate the anchorage behaviour with sufficient accuracy. The verification is discussed in Section 10.

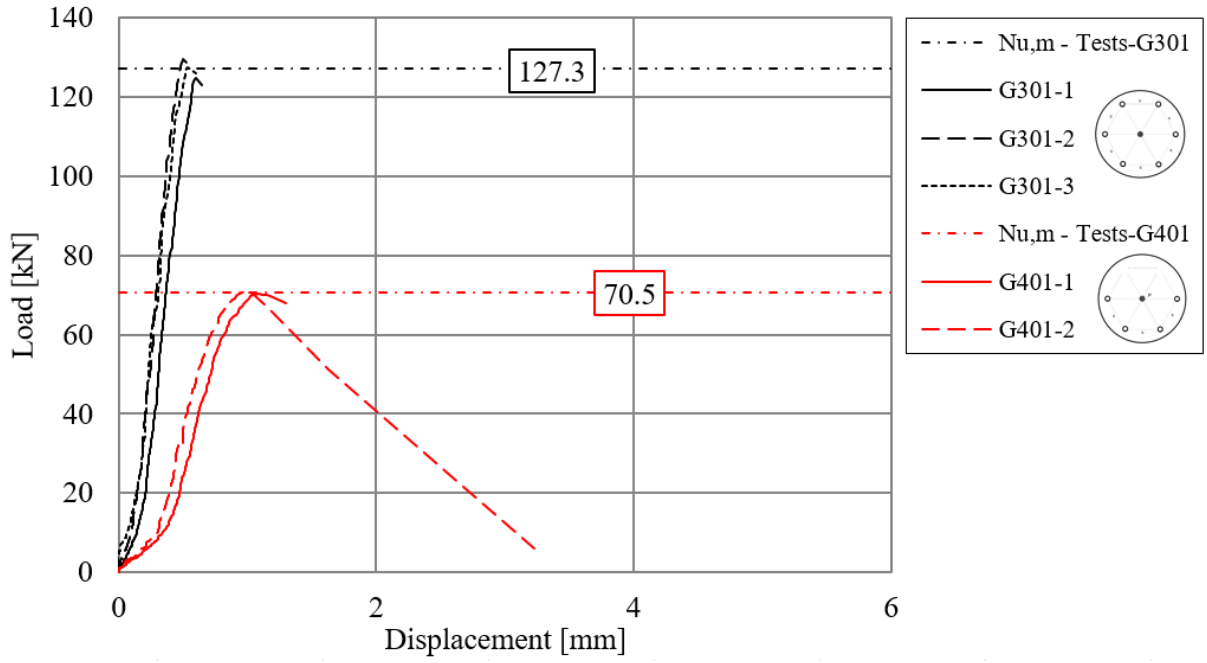

a)

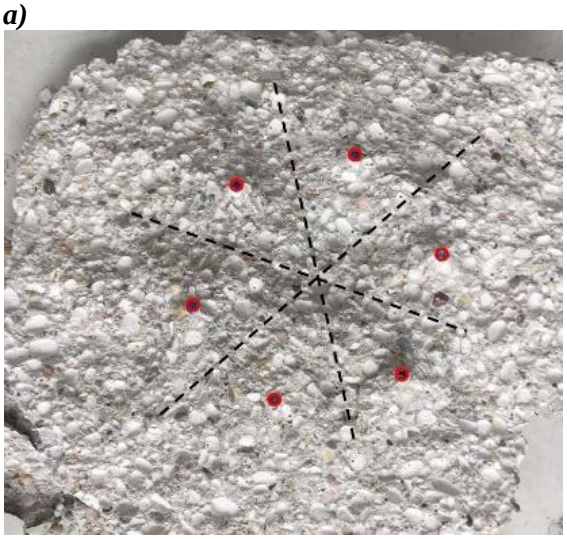

b)

Figure 8.15. a) Load-displacement curves of test series G301 and G401; b) concrete breakout body from series G301

8.3.3 Anchorages in cracked concrete

Tension tests were carried out on anchor groups of 1×3, 2×2 and hexagonal configurations far from the concrete edge in cracked concrete according to the test program given in *Table 8.3*. In addition, single anchor tests were performed in cracked and uncracked concrete, which served to compare the behaviour of a single anchor with the behaviour of an individual anchor of an anchor group. The tests were carried out under concentric and eccentric tension loads with varying crack pattern and the loading point. It was aimed to verify the tension spring model for cracked concrete and for cases with different anchor stiffness within one anchor group.

The anchor installation and testing were carried out according to Section 8.2.3. The load was applied using a hinged loading application in all cases to allow the rotation of the base plate. Furthermore, the ultimate load of the anchorages was calculated based on EN 1992-4. Note that according to EN 1992-4, all the anchors of a group are assumed to be intercepted by a crack and therefore, the calculated group capacity in cracked concrete is taken as 70% of the capacity calculated for the corresponding group in uncracked concrete. The summary of the test results in terms of the mean value of the ultimate tension loads ($N_{u,m}$) and calculated loads ($N_{u,EN1992-4}$) is given in *Table 8.6.* The load-displacement curves of the corresponding series and the failure crack patterns are given in the following sub-sections, in *Figure 8.5 - Figure 8.23*.

Table 8.6. Test results of anchorages of rectangular and non-rectangular configurations in cracked concrete

Anchor system	Test series ID	Test type	Mean ultimate load $N_{u,m}$ [kN]	Calc. mean concrete cone resistance $N_{u,EN1992-4}$ [kN]	$N_{u,m,test}$ / $N_{u,EN1992-4}$ [-]
Bonded anchor – M12	R6-ncr	Ref. single uncracked	27.8	29.1	0.96
	R6-cr	Ref. single cracked	19.2	20.4	0.94
	G61		58.4	67.8	0.86
	G62R		43.1	47.5	0.91
	G62		58.0	47.5	1.22
	G63		41.0	47.5	0.86
	G64		55.3	47.5	1.16
	G65	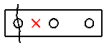	33.8	28.5	1.19
	G66	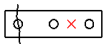	44.3	28.5	1.55
	G67		47.4	47.5	1.00
	G68	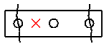	36.6	28.5	1.28

Undercut anchor – M12	R7-ncr	Ref. single uncracked	37.8	39.6	0.95
	R7-cr	Ref. single cracked	27.8	27.7	1.00
	G71		129.6	110.1	1.18
	G72		104.8	77.0	1.36
	G73		80.9	43.3	1.87
	G74		83.2	43.3	1.92
Undercut anchor – M12	R50-ncr	= R7-ncr	37.8	39.6	0.95
	R50-cr	= R7-cr	27.8	27.7	1.00
	G501	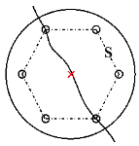	141.4	-	-

8.3.3.1 1×3 anchor groups in cracked concrete

The test series block G6 was performed to investigate the superposed influence of the crack pattern and the influence of eccentricity on anchor groups of 1×3 configuration. The anchor spacing s = 120 mm, the embedment depth h_{ef} = 60 mm, the base plate geometry and the initial crack width $\Delta w = 0.3$ *mm* were kept constant for all the tests. Six different crack patterns, namely (i) uncracked, (ii) middle anchor in the crack, (iii) one outer anchor in the crack, (iv) two outer anchors in the crack, (v) two adjacent anchors in the crack, (vi) all anchors in the crack; and two levels of eccentricity (i) $e = 0$ and (ii) $e = s/2$ were investigated as summarized in *Table 8.6*. Note that considering an equal spacing of the anchors and a relatively regular spacing of the cracks, the possibility of having two neighbouring anchors intercepted by the cracks while the third one remaining in uncracked concrete is rather rare. Nevertheless, this case was also investigated (series G63) for academic reasons.

Reference tests

The reference tests were carried out on single anchors in uncracked and cracked ($\Delta w = 0.3$ *mm*) concrete in the same concrete batch. For single anchors, the mean failure load reduced from 27.8 kN in uncracked concrete to 19.2 kN in cracked concrete, which is a 31% reduction. This corresponds to the assumption of the EN 1992-4 that the concrete cone resistance of the anchor reduces by 30% compared to the concrete cone resistance of the anchors in uncracked concrete. The load-displacement curves *Figure 8.16* display ca. 50% reduction in the initial anchor stiffness for the anchor tested in cracked concrete compared to that in uncracked concrete. The horizontal lines in the figure correspond to the mean value of the test results, which are written

in the boxes. The calculated failure loads are in a reasonably good agreement with the experimental results (*Table 8.6*).

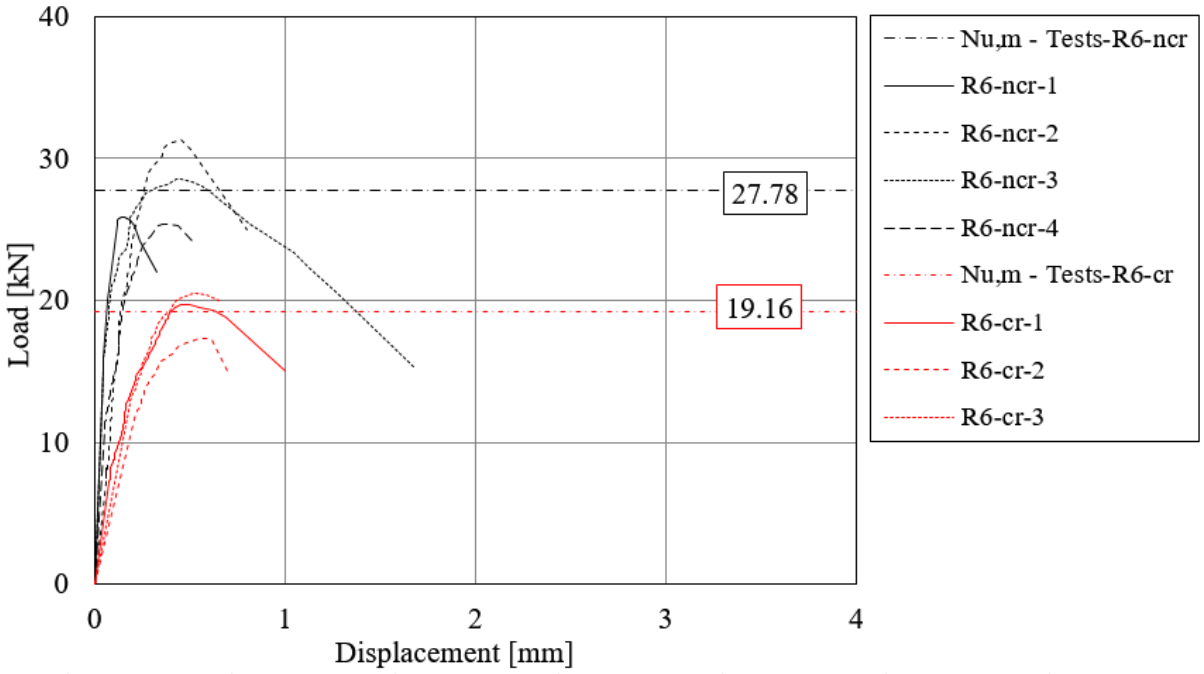

Figure 8.16. Load-displacement curves of test series R6-ncr and R6-cr on single anchors in uncracked and cracked concrete

Influence of crack pattern in case of concentric tension loading

Test series G61 were carried out on 1×3 anchor groups in uncracked concrete under concentric tension loading and series G62R were carried out on the same group configuration in cracked concrete with all three anchors located in a crack. The mean failure load decreased from 58.4 kN to 43.1 kN when all anchors were intercepted by the crack, which corresponds to a reduction of 26%. This again agrees well with the results obtained from the tests on single anchors, where the ultimate load decreased by 30% due to the crack with of $\Delta w = 0.3$ *mm*. *Figure 8.17b* shows that the initial stiffness of the groups (G62R) decreased due to the interception of the anchors by a crack by ca. 50%. In *Figure 8.17b*, the anchor axial forces are plotted as the function of time. It can be seen that all three anchors were activated at the same time. The concrete breakout body of one test of series G61 (uncracked) is depicted in *Figure 8.17c* and the failure pattern of test series G61R showing that the crack intercepts all three anchors is given in *Figure 8.17d*. The shape of the concrete breakout body did not change in cracked concrete compared to the uncracked case.

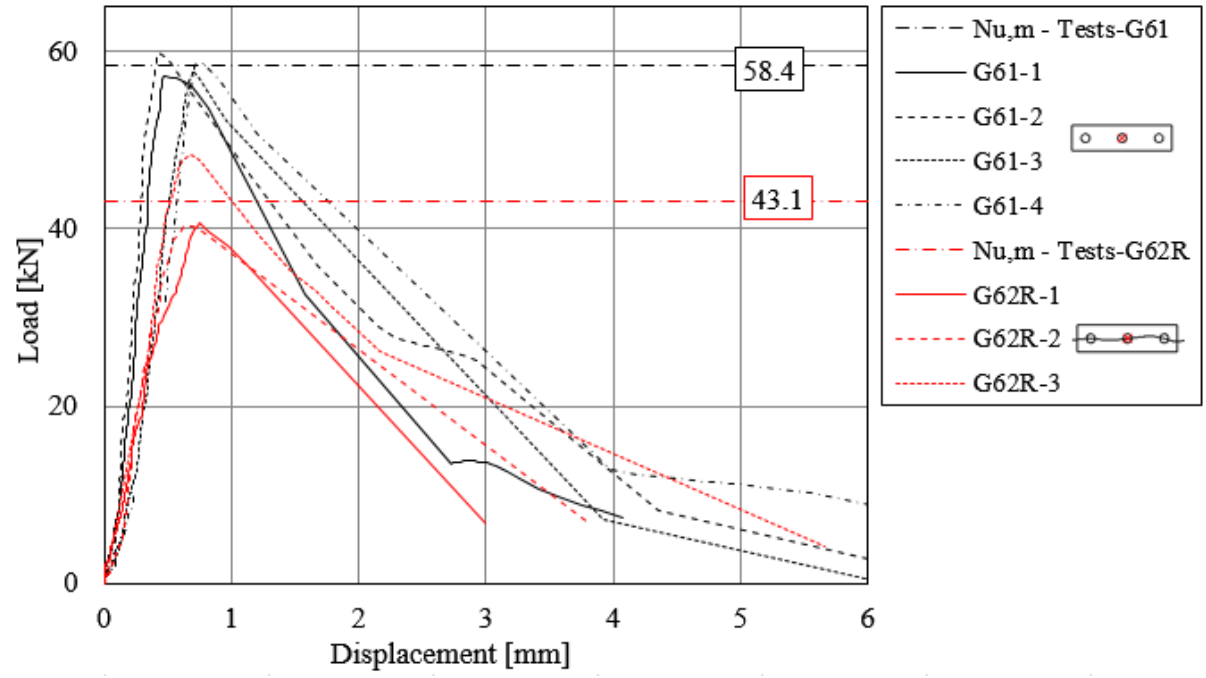

a)

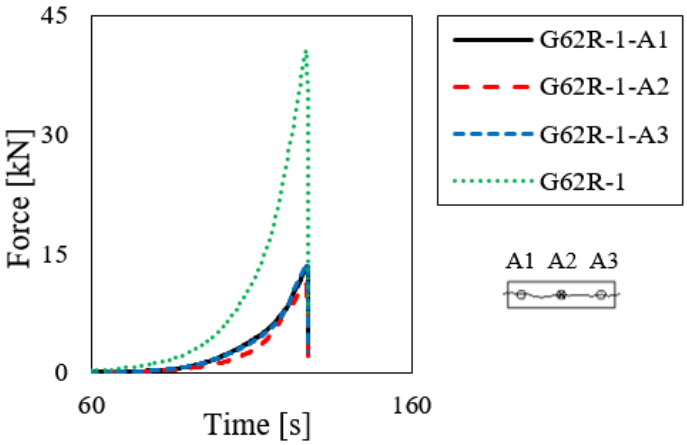

b)

c) *d)*

Figure 8.17. a) Load-displacement curves of test series G61 and G62R, b) Anchor force-time curve of test G62R-1, c) breakout body of one representative test of series G61, d) failure pattern of one representative test of series G62R

The test series G62, G63, G64 and G67 focused on the influence of crack pattern, when the external force is acting at the centre of gravity of the group (on the middle anchor). In series G62 and G64, only one of the anchors of the group was placed in a crack, namely the middle (G62) and the outer anchor (G64). In series G63 and G67, two out of three anchors were intercepted by a crack: for series G63 one outer and the middle and in series G67 the two outer anchors. The corresponding load-displacement curves are depicted in *Figure 8.18a* and *b*. For comparison purposes, the results obtained from series G62R with all anchors intercepted by the crack are also plotted in the graphs.

The results obtained from series G62 with the middle anchor intercepted by a crack showed only a negligible reduction in the mean failure load ($N_{u,m,G62} = 58.0$ *kN*) compared to the series G61 with all the anchors in uncracked concrete ($N_{u,m,G61} = 58.4$ *kN*). The series G64, with one outer anchor in the crack resulted in a mean ultimate load of 55.3 kN, which is 28% higher than in case of series G62R having all anchors in a crack. Furthermore, it can be seen in *Figure 8.18a* that the stiffness of the group is higher when only one anchor was intercepted by crack compared to the case with all anchors in crack.

In series G62, the middle anchor was located in a crack, which had the smallest contribution to the group resistance. This is also visible in the failure pattern in *Figure 8.18d*. It can be seen that the amount of concrete, which was activated by the middle anchor is the smallest. Furthermore, due to symmetry, the loading "remains concentric". In the case of series G64, only the outer anchor is located in a crack. The anchors, which are not intercepted by a crack have a stiffer response than the anchors intercepted by a crack and consequently, the difference in the stiffness causes that the anchors in uncracked concrete are loaded more. This results in an internal eccentricity in the system and therefore, further reduction in the load-carrying capacity of the anchorage is obtained compared to series G62. The failure pattern is shown in *Figure 8.18e*. For the discussed two cases, the assumption of considering all the anchors intercepted by a crack is conservative.

Test results of series G63, where one outer and the middle anchor were intercepted by cracks (not typical crack pattern) pointed out that the cracked concrete assumption can lead to unsafe calculation results. The mean ultimate group capacity was measured to be 5% lower ($N_{u,m,G63} = 41.0$ *kN*), than the resistance obtained assuming all the anchors intercepted by a crack ($N_{u,m,G62R} = 43.1$ *kN*) (see *Figure 8.18b* and *Table 8.6*). This can be explained by the fact that the anchors, which are located in cracks, exhibit a lower stiffness and lower resistance, than those in the uncracked concrete. The external force was applied concentrically; however, the different stiffness conditions within the group resulted in an eccentricity of the internal forces. Consequently, the base plate tends to rotate due to the change of the lever arm of the internal forces and the ultimate group resistance was reached before the anchor in uncracked concrete with the higher stiffness and resistance would have reached its ultimate capacity. This is also shown in *Figure 8.18c*, where the anchor axial forces and the group capacity are plotted as a function of time. First, anchor 3 is activated and then anchor 2 and 1 in the cracked part also took up forces. The failure pattern is shown in *Figure 8.18f*. The stiffness and the progression of the corresponding load-displacement curves are similar to the series G62R with all anchors in cracked concrete.

In test series G67, the two outer anchors were intercepted by cracks and the load was applied at the middle anchor. The measured mean ultimate load (47.3 kN) was 10% higher than for G62R, where all anchors were intercepted by crack. This shows that the most loaded middle anchor, which was not intercepted by a crack, had higher stiffness and higher load capacity (compared to a middle anchor located in the crack) and therefore, higher group capacity could be reached. The group stiffness did not increase considerably compared to series G62R and G63. The developed symmetrical common breakout surface is depicted in *Figure 8.18g*. In this particular case again, the cracked concrete assumption according to EN 1992-4 lead to slightly conservative results (compare *Table 8.6*).

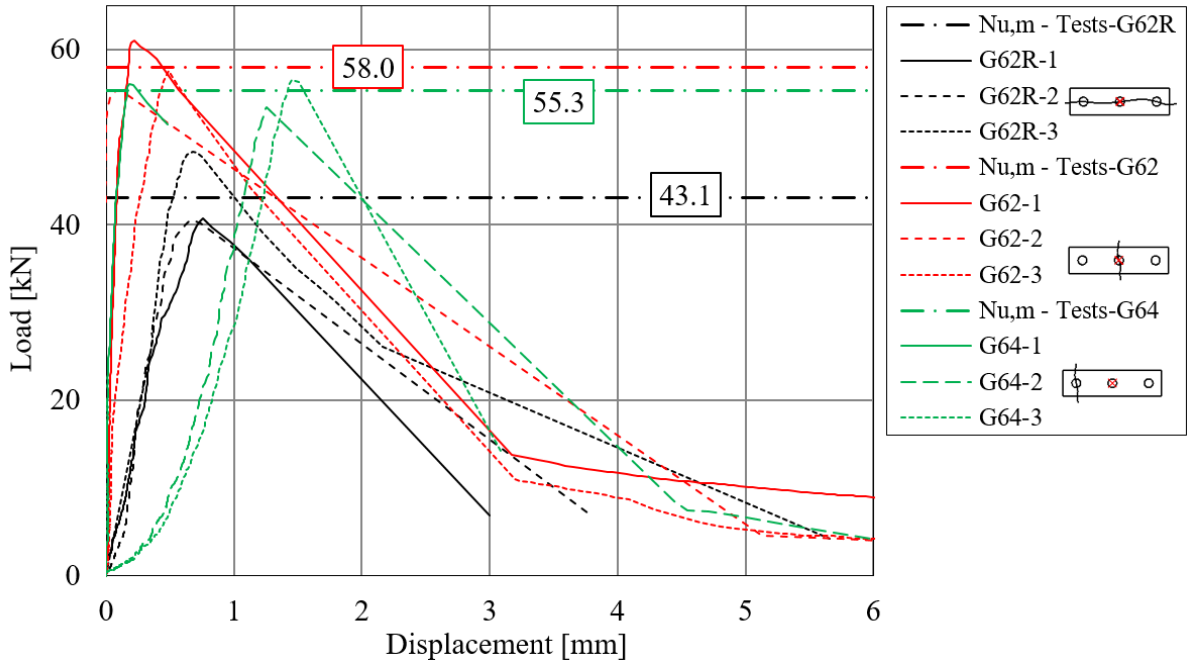

a)

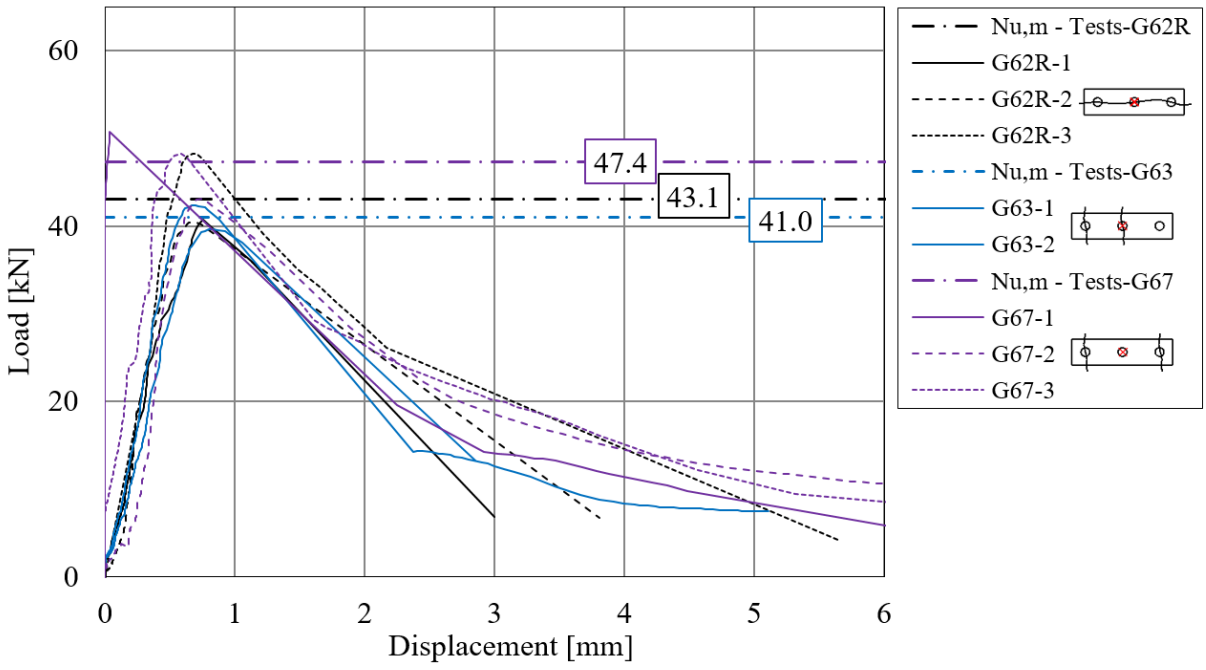

b)

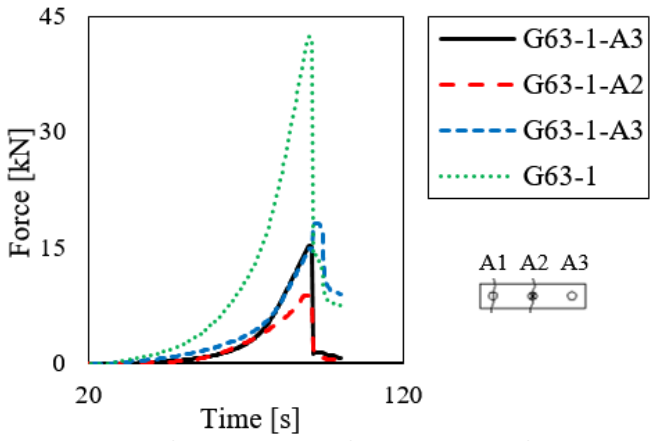

c)

d)

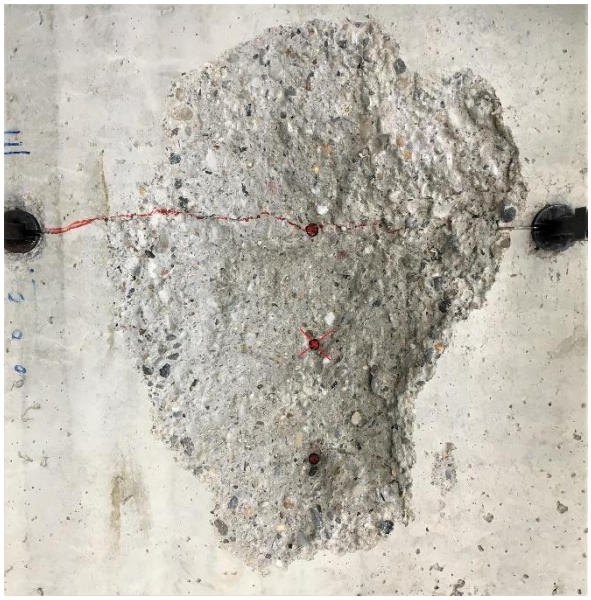

e)

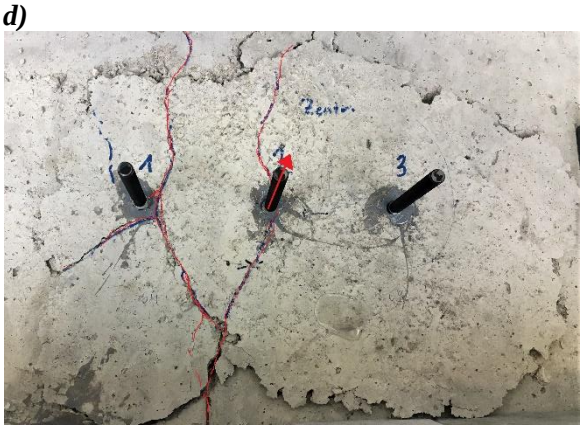

f)

g)

Figure 8.18. a) Load-displacement curves of test series G62R, G62, G64; b) Load-displacement curves of test series G62R, G63, G67; c) Anchor force-time curve of test G63-1; failure pattern of one representative test of series: d) G62, e) G64, f) G63, g) G67

Test series G65, G66 and G68 were targeted to investigate the superposed influence of crack pattern and loading eccentricity. Two different crack patterns, namely (i) one outer anchor in crack, (ii) two outer anchors in crack; and one level of eccentricity (i) $e = s/2$ were investigated according to *Table 8.3*.

In the case of test series G65 and G66, only one outer anchor was intercepted by a crack. However, the load was applied eccentrically with an eccentricity of $e = s/2$ close to the crack in series G65 and far from the crack in series G6, respectively. The results showed that it makes a big difference whether the eccentricity of the load is away or close the anchor, which is intercepted by a crack. For the same value of load eccentricity, the measured mean ultimate load for the group loaded with eccentricity close to the crack (series G65) was obtained as 33.8 kN, while the mean failure load for the group loaded with eccentricity away from the crack (series G66) was 44.3 kN (see *Table 8.6* and *Figure 8.19a*). This means that the concrete cone capacity of the anchor group was 25% lower when the eccentricity was applied close to the crack. This is due to the fact that the cracks in concrete cause a disruption of the stress field, which leads to reduced failure loads (Rehm et al., 1988) and thus, if the load application is closer to the anchor intercepted by a crack, the resistance of this most-loaded anchor is limited and the tension force transfer in this area is reduced. The resistance of the anchors, which are in uncracked concrete cannot be fully utilised, since the ultimate group capacity is reached before the anchors with higher capacity would reach their ultimate loads. On contrary, in series G66, the most loaded anchors were in uncracked concrete and consequently, the influence of the crack was less pronounced (*Figure 8.19a*). The failure patterns are shown in *Figure 8.19b-d*.

The observations from series G65 and G66 are similar to the results on 1×3 anchor groups in uncracked concrete on the influence of eccentricity in the vicinity of concrete edge, which are discussed in Section 8.3.1. Test series G22 and G23 pointed out that when anchor groups are located near the concrete edge and are loaded eccentrically in tension, it makes a considerable difference whether the eccentricity of the load is away or close the edge (21% difference). The similarities in the anchor group behaviour can be explained by the fact that the stress field, which is generated in the concrete by tension loaded anchors close to the concrete edge is comparable with anchors intercepted by cracks. In terms of loads, also the EN 1992-4 considers the vicinity of the concrete edge in a similar way to the cracked concrete condition by applying the factor $\psi_{s,N}$ that takes account of the disturbance of the distribution of stresses in the concrete due to the proximity of an edge of the concrete member and its value is limited to 0.7.

Test series G68 was performed on anchor groups with two outer anchors intercepted by cracks. The load was applied with an eccentricity of $e = s/2$. The measured mean ultimate load was obtained as 36.5 kN, which is in between the above-discussed test series G65 and G66. The obtained results show that the increased number of anchors intercepted by cracks does not implicitly lead to a decrease in the ultimate group capacity. However, the influence of the crack pattern is decisive.

The results of test series block G6 suggest considering the most unfavourable crack pattern in the design when the cracked concrete condition cannot be ruled out in the anchorage zone for the anchor group. The influence of crack pattern can be even more pronounced in case of seismic cracks, which are opening and closing.

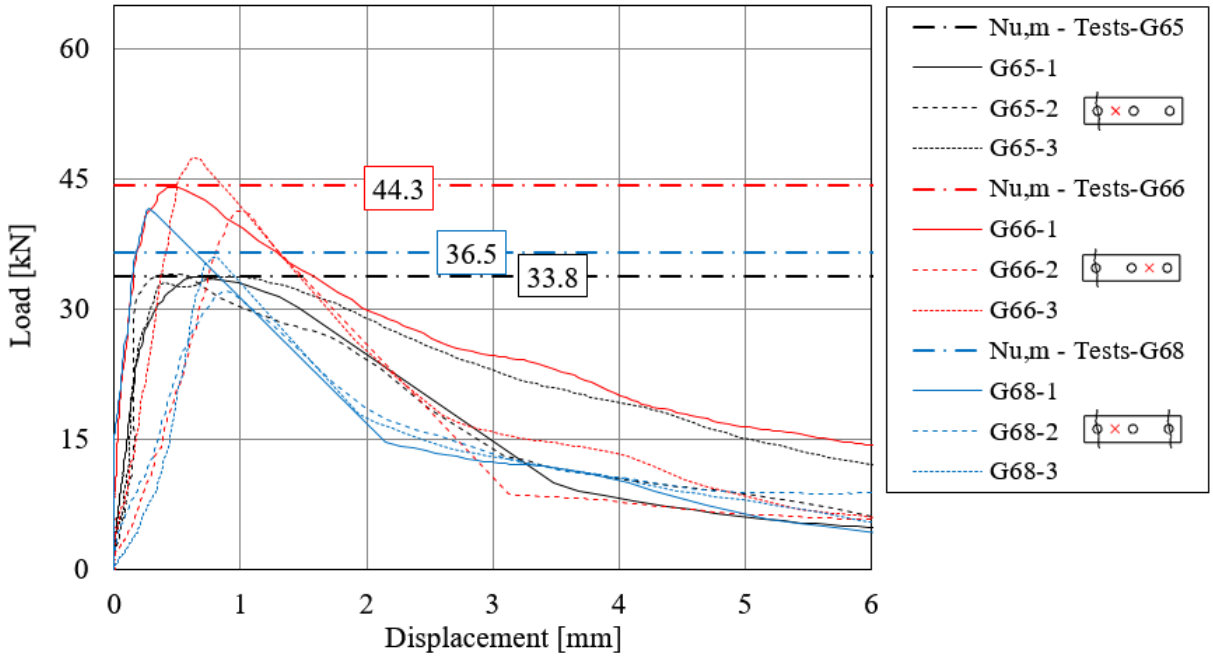

a)

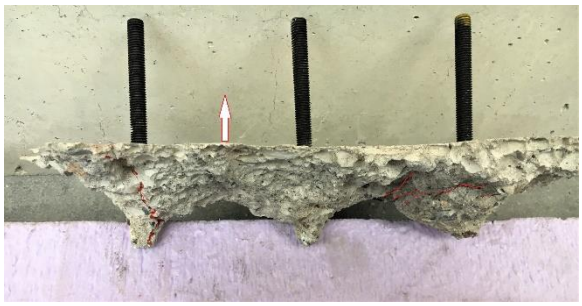

b)

c)

d)

Figure 8.19. a) Load-displacement curves of test series G65, G66, G68; b) breakout body of one representative test of series G65; failure pattern of one representative test of series: c) G66, d) G68

8.3.3.2 2×2 anchor groups in cracked concrete

Test series block G7 was targeted to investigate the influence of the crack pattern in case of concentric tension loading, as well as the superposed influence of crack pattern and biaxial eccentricity. For that, tension tests were carried out on single anchors and anchor groups of quadruple (2×2) configurations with undercut anchors, which have a relatively ductile behaviour and are approved for use in cracked concrete up to a crack width of $\Delta w = 0.8$ *mm* under seismic loads. The reference single anchor tests were performed in uncacked and cracked concrete to enable a comparison of the single anchor results with the group results and served also as input parameters for the spring model for determining the spring properties.

Relatively stiff base plate was used for the experiments. The anchor spacing $s = 140$ *mm*, the embedment depth $h_{ef} = 80$ *mm*, the base plate geometry and the initial crack width $\Delta w = 0.3$ *mm* were kept constant for all tests. The installation torque was applied according to the MII. However, before starting the tests, the torque was reduced to 0 Nm and the nut was only hand tightened to ensure the same initial stiffness conditions to all anchors. Three different crack patterns, namely (i) uncracked, (ii) one anchor row in a crack, (iii) two anchors in diagonal in crack; and two levels of eccentricity (i) $e = 0$ and (ii) $e_1 = e_2 = s/4$ were investigated according to the test program in *Table 8.3*. The test results are given in terms of ultimate loads, load-displacement curves and failure patterns in *Table 8.6* and *Figure 8.20 - Figure 8.22*.

Reference tests

The test series R7-ncr and R7-cr were carried out on single anchors in uncracked (*ncr* = non-racked = uncracked) and cracked (*cr* = cracked) concrete. The load-displacement curves in *Figure 8.20a* show that due to the cracked concrete condition the mean ultimate load and the stiffness decreased by 26% and 27%, respectively. This again corresponds to the assumption of EN 1992-4 that the concrete cone resistance of the anchors reduces by approximately 30% compared to the concrete cone resistance of the anchors in uncracked concrete (for static cracks of limited crack widths).

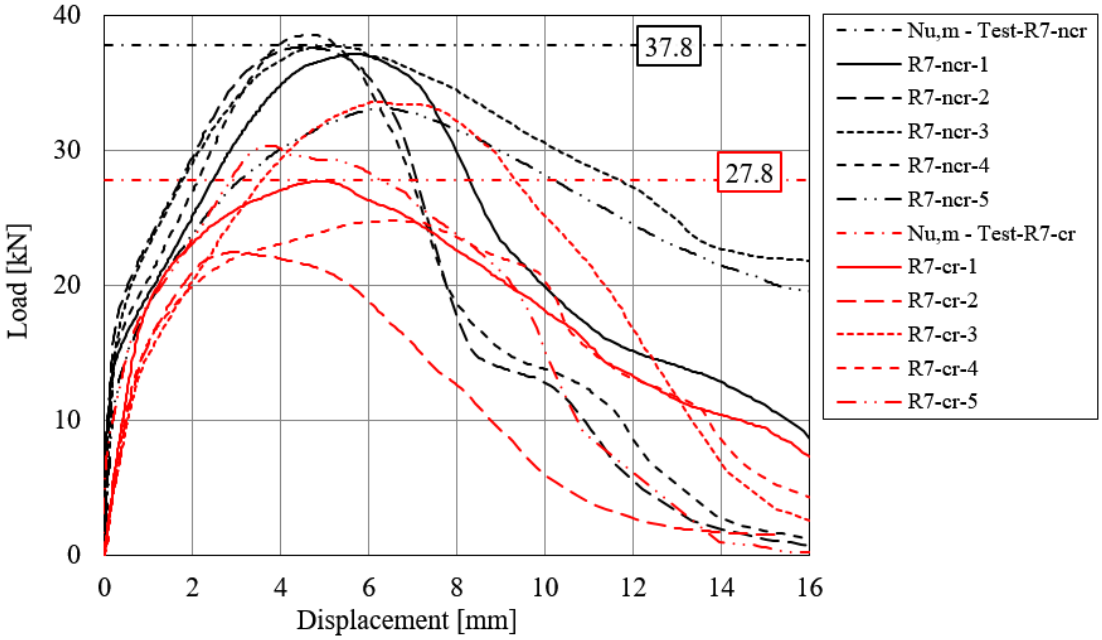

Figure 8.20. Load-displacement curves of test series R7-ncr and R7-cr

Influence of crack pattern in case of concentric tension loading

In test series G71, the anchor group was subjected to concentric tension load in uncracked concrete. The mean ultimate load was obtained as 129.6 kN, which is 3.4-times the load that was measured on the single anchors in uncracked concrete (37.8 kN).

No tests were carried out on the quadruple group configuration with all anchors intercepted by cracks due to the limitations of the predefined crack initiation for the 2×2 anchor configuration. Thus, the influence of the cracked concrete condition, where all anchors are intercepted by cracks could not be investigated directly on the quadruple anchor groups. However, the ultimate load for cracked concrete can be determined following certain assumption:

(1) For anchor groups with all anchors intercepted by a crack, the stiffness of all anchors decreases by the same amount.
(2) Consequently, the ratio of the stiffness of the individual anchors compared to each other does not change in cracked concrete compared to uncracked concrete.
(3) If we assume the same decrease in failure load due to cracks for anchor groups as for single anchors (26%), then an assumed ultimate load for the concentric loaded anchor group in cracked concrete can be calculated as $N_{u,m,G71cracked} = 0.74\ N_{u,m,G71} = 95.9\ kN$.

In test series G72, the load was applied concentrically using a rotationally unrestrained test setup and the crack was intercepting two anchors in a row. This resulted in different stiffness conditions for the two anchor rows. The mean failure load decreased by 19% and the mean initial stiffness by ca. 37 % compared to test series G71 in uncracked concrete as it can be seen in *Figure 8.21a*. However, the measured mean ultimate load is still ca. 10% higher than the ultimate load, which is assumed considering all anchors in crack.

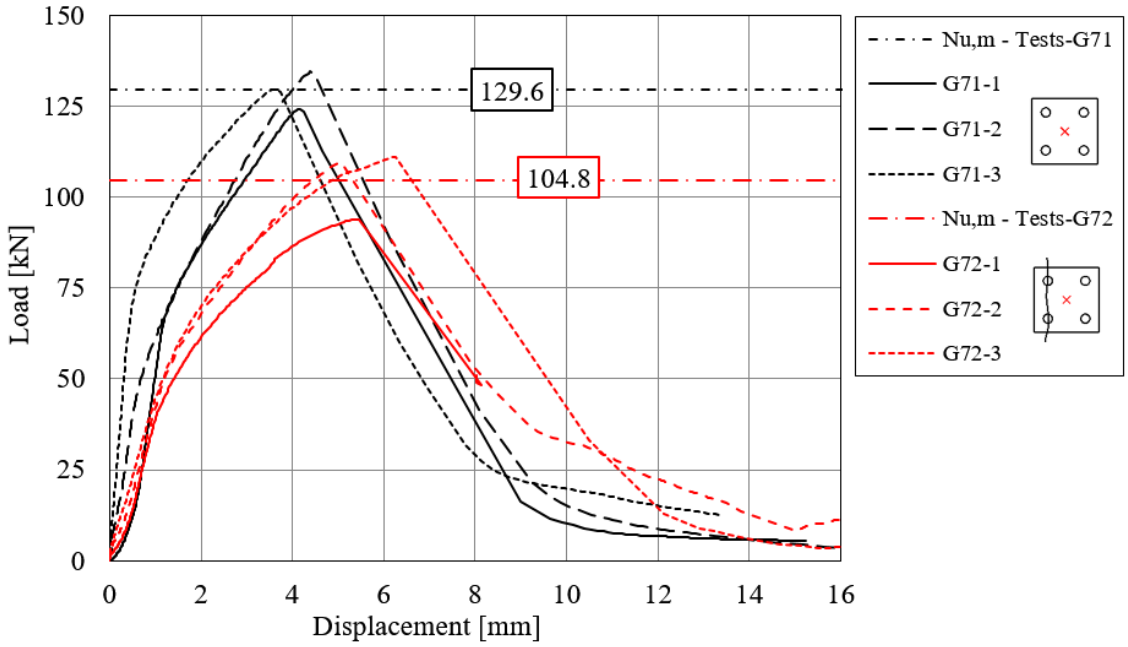

a)

b) ***c)***

Figure 8.21. Influence of the crack pattern: a) Load-displacement curves of test series G71-G72; b) failure pattern of test series G71; c) failure pattern of test series G72

Influence of crack pattern in case of eccentric tension loading

In test series G73 and G74, the crack was intercepting two anchors in diagonal. The load was applied eccentrically close to an anchor in crack in series G73, and away from the crack in series G74 as it is visible in *Figure 8.22b* and *c*. The measured mean ultimate load was obtained as 80.9 kN for series G73 and 83.2 kN for series G74, respectively. This corresponds to only a 3% difference, which is rather negligible. However, the group stiffness was considerably less, when the loading axis coincided with the crack line and consequently, the displacement at ultimate load was larger for series G74. The lower load for series G73 can be explained by the fact that the first loaded anchor, which was located closest to the load application, was intercepted by a crack and had lower resistance and stiffness. The mean ultimate loads of test series block G7 predicted according to EN 1992-4 are underestimated by the calculations in the case of the anchor groups (*Table 8.6*). This is due to the superposed influence of the conservatism in the model for biaxial eccentricity and consideration of cracked concrete in EN 1992-4.

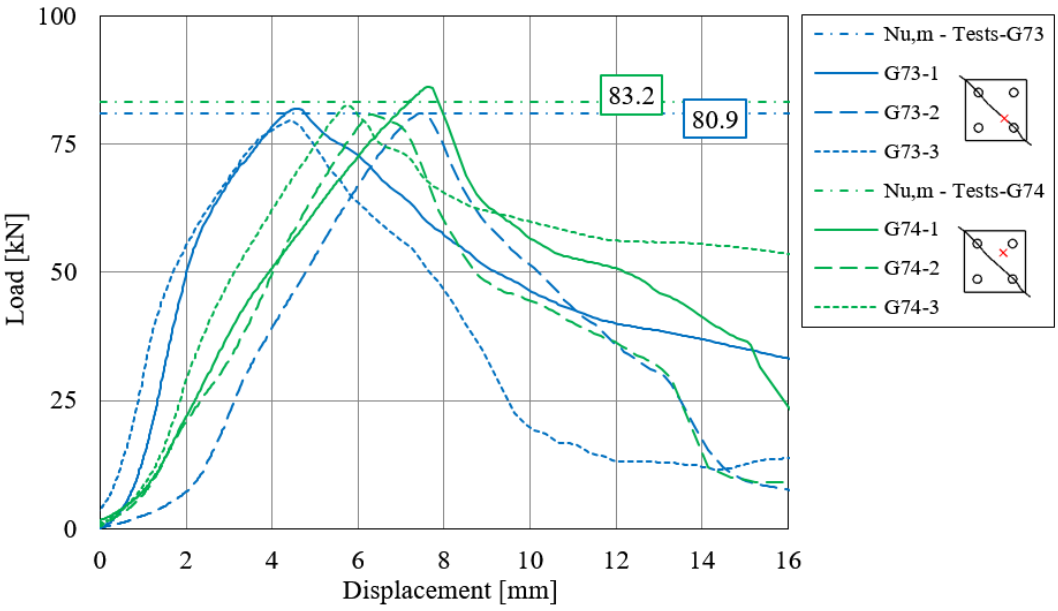

a)

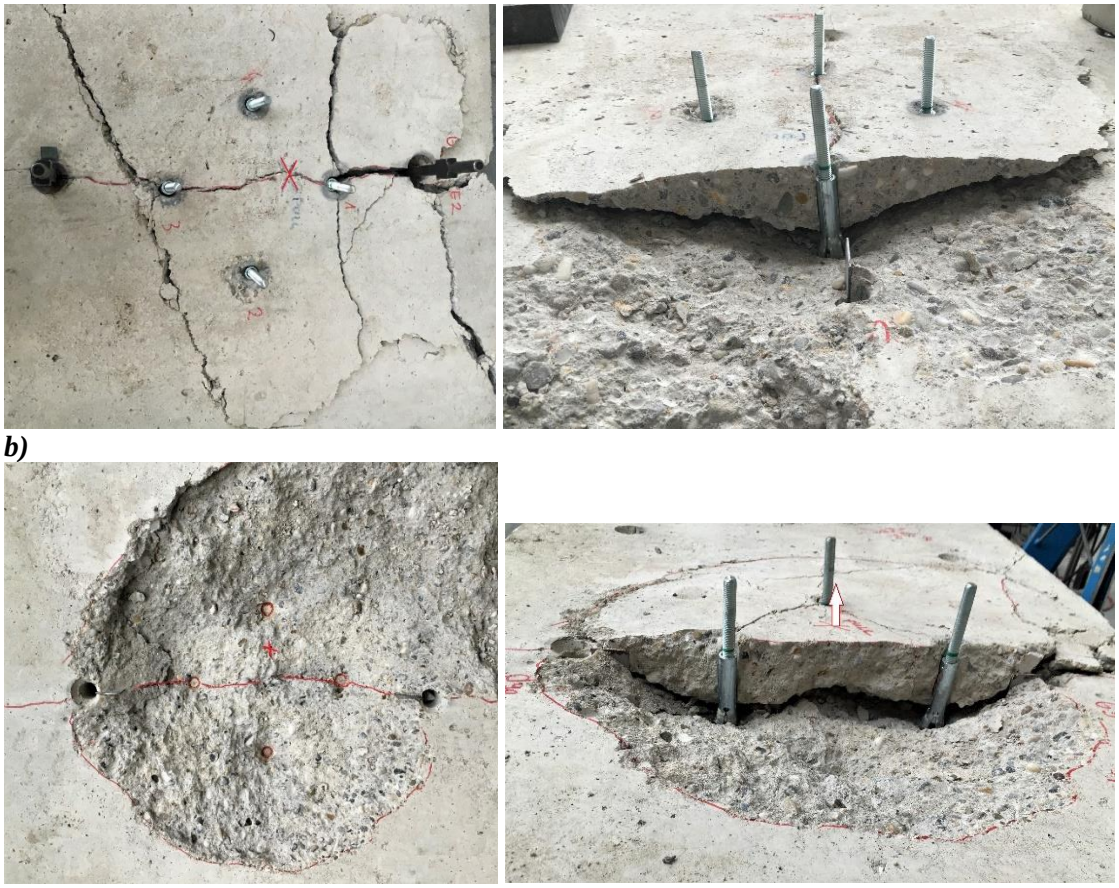

b)

c)

Figure 8.22. Influence of the crack pattern: a) Load-displacement curves of test series G73-G74; b) failure pattern of series G73; c) failure pattern of series G74

8.3.3.3 Anchor groups of hexagonal configuration in cracked concrete

The behaviour of hexagonal anchorages with circular base plate in cracked concrete was investigated with series G50, where two out of six undercut anchors were located in crack ($\Delta w = 0.3$ *mm*) and the load was applied concentrically. The anchor spacing was $s = 120$ *mm* and the embedment depth was 80 mm. In this case, due to symmetry, no rotation of the base plate is expected. The load-displacement curves of the test series are shown in *Figure 8.23a*. *Figure 8.23b* provides information about the individual anchor contribution to the group capacity by plotting the individual anchor forces and the group resistance as the function of time. It can be seen that all anchors were activated ca. at the same time due to the rigid base plate. However, the curves corresponding to the anchors in crack were less steep and the contribution of anchors A1 and A4 was ca. 30% less due to the crack compared to the anchors not intercepted by cracks. The concrete cone body of series G50 is shown in *Figure 8.23c*. It can be seen that each individual anchor of the group developed a concrete cone and these individual cones are intercepting forming a common breakout body. The value of the overlapping depends on the ratio anchor spacing (s) to embedment depth (h_{ef}). The results obtained from these tests serve for the verification of the spring model for anchor groups in "partly" cracked concrete having non-rectangular configuration.

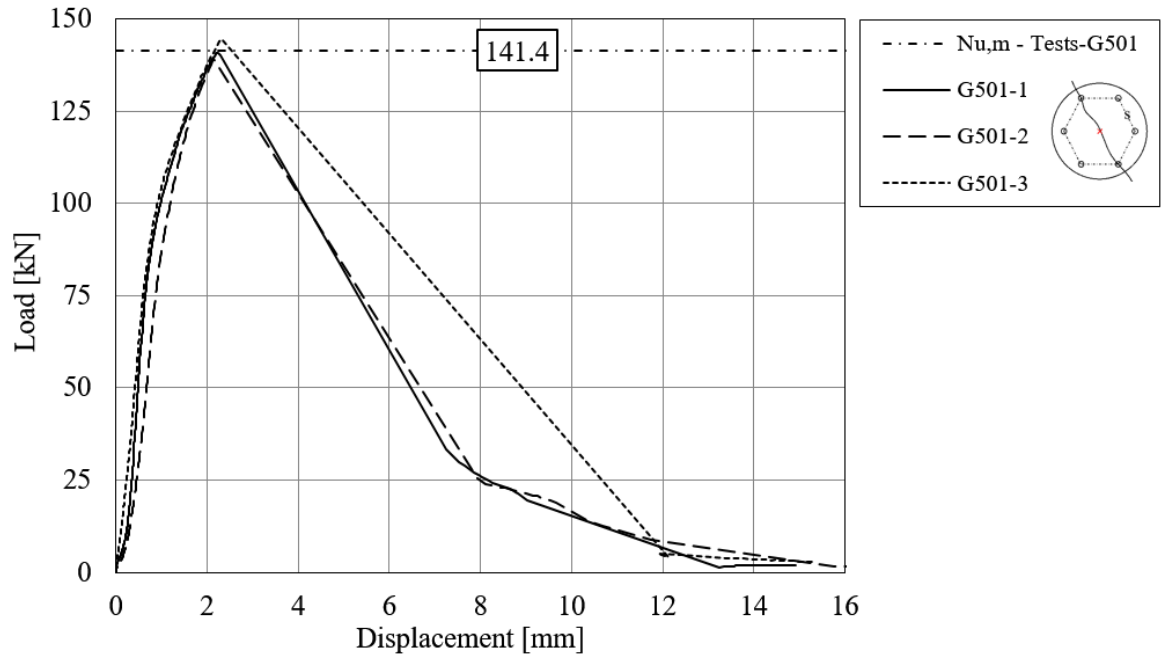
150
125
100
75
50
25
0
Load [kN]
141.4
0
2
4
6
8
10
12
14
16
Displacement [mm]
Nu,m - Tests-G501
G501-1
G501-2
G501-3

a)

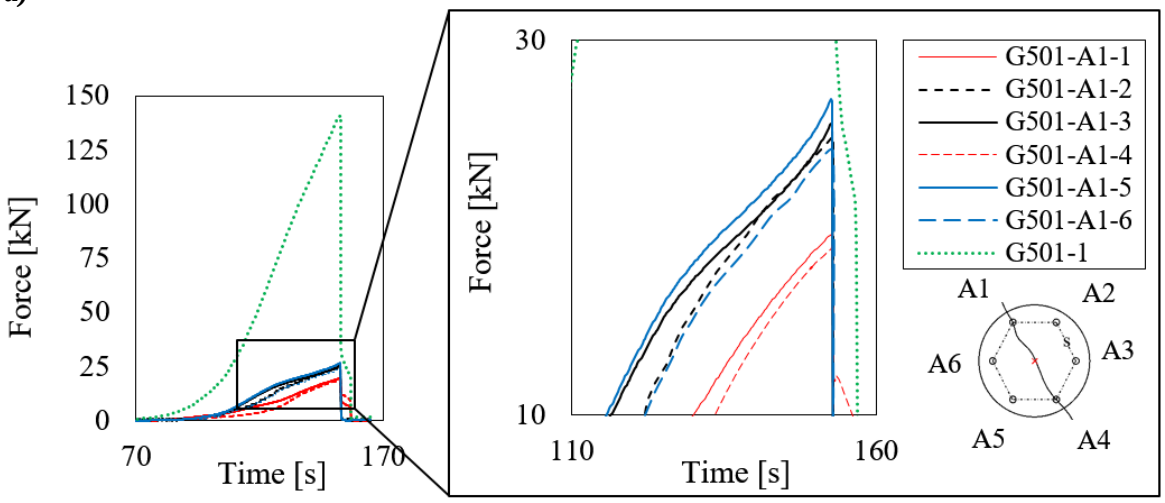
150
125
100
75
50
25
0
Force [kN]
70
Time [s]
170
30
10
Force [kN]
110
Time [s]
160
G501-A1-1
G501-A1-2
G501-A1-3
G501-A1-4
G501-A1-5
G501-A1-6
G501-1
A1
A2
A3
A4
A5
A6

b)

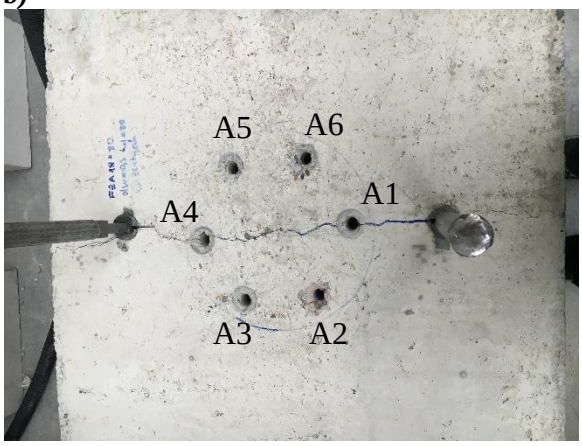
A5
A6
A1
A4
A3
A2

c)

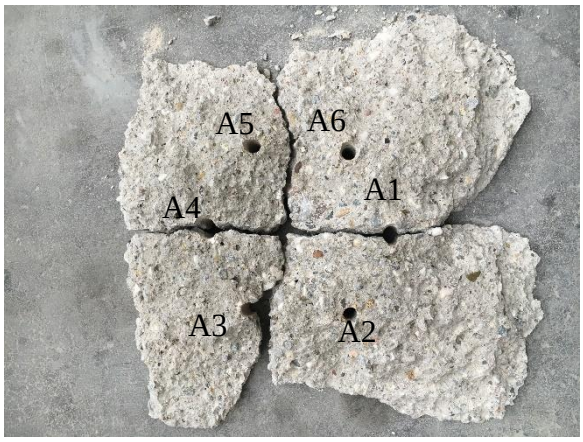
A5
A6
A1
A4
A3
A2

d)

e)

Figure 8.23. a) Load-displacement curves of test series G501; b) Force-time curve of test G501-1; c) anchor group configuration before installation; d) failure breakout body of test G501-1 – bottom view; e) failure breakout body of test G501-1 – front view

8.4 CONCLUSIONS

The experimental investigations discussed in Section 8 aimed to generate an experimental database on the concrete cone failure of anchor groups loaded in tension. For this reason, anchor groups of rectangular (3×1, 2×2, 1×4) and non-rectangular (triangular, hexagonal, trapezoidal, L-shaped) configurations were tested. To allow a comparison of the group behaviour with the behaviour of single anchors, reference tests were carried out with the same installation parameters as for the group tests. Furthermore, the test program and the evaluation of the results aimed to provide the information required for the verification of the spring model to determine the behaviour of anchor groups in case of concrete cone failure mode. A well-instrumented comprehensive experimental program was performed focusing on (i) different geometric configurations, (ii) varying the stiffness of the base plate, (iii) influence of eccentricity, (iv) influence of vicinity of the concrete edge and (v) influence of crack pattern in normal- and high-strength concrete. Based on the detailed evaluation of the test results such as load-displacement curves of the groups and single anchors, individual anchor axial forces and the concrete breakout bodies supported the better understanding of the load-displacement behaviour of anchorages and the load distribution among individual anchors within an anchor group.

The scope of the tests and the test programs are discussed in Section 8.1. Section 8.2 provides the details about the testing, the design of the test specimens, tested fasteners and those installations, and about the test setup and test procedure. In Section 8.3, the experimental tests and the results of the numerical analyses are evaluated. The following main conclusions can be summarised based on the test results:

- The results on the influence of eccentric loading and influence of vicinity of the concrete edge according to Sections 8.3.1.1 and 8.3.1.4 confirmed the well-known phenomena that both influences lead to a reduction in the failure load of anchor groups (Eligehausen et al., 2006). Furthermore, the results showed that the current provisions yield more conservative results with increasing the eccentricity in the case of anchor groups with three anchors in a row.

- When anchor groups are placed near the concrete edge and are loaded in eccentric tension, it makes a considerable difference whether the eccentricity of the load is away or close the edge (see Section 8.3.1.2). The test results suggest that the exact loading position should be considered when determining the concrete cone resistance for anchor groups.
- The experiments on anchor groups subjected to biaxial eccentric loads in 8.3.1.3 highlighted that the calculated failure loads for anchor groups according to the current regulations of EN 1992-4 are rather conservative. In case of biaxial eccentric loading, the factor to account for the influence of eccentric loading ($\psi_{ec,N}$) is determined separately for each direction ($\psi_{ec,N,1}$, $\psi_{ec,N,2}$) and the multiplication of the factors is used as reduction factor. This multiplication leads to conservative results.
- The investigations on anchor groups with varying base plate thickness in Section 8.3.2.1 showed the significant influence of the base plate stiffness on the nonlinear load-displacement behaviour of anchor groups. Furthermore, it was shown that with the current design provisions, it is rather difficult to ensure that a sufficiently rigid base plate is used.
- The evaluation of the test results and the investigation of concrete breakout bodies of the different anchor group configurations in Section 8.3.2.2 showed that even in case of complex breakout bodies, a particular projected area of concrete can be attributed to each individual anchor of a group. This tributary concrete area is a certain percentage of the projected area of the concrete cone that forms in case of a single anchor away from the edge.
- The results obtained from the tests in cracked and partly-cracked concrete in Section 8.3.3 showed that the anchor group behaviour is highly dependent on the load-displacement behaviour and stiffness conditions of the individual anchors within the group. Furthermore, the results suggest to consider the most unfavourable crack pattern in the design, when the cracked concrete condition cannot be ruled out in the anchorage zone for the anchor group.
- The results of the extensive experimental programs performed within the framework of this thesis offer a good basis for the verification of the developed spring model for the design of anchor groups in case of concrete cone breakout failure. The verification is given in Section 10.

9 EXPERIMENTAL AND NUMERICAL INVESTIGATIONS ON SHEAR LOADED ANCHORAGES

9.1 SCOPE

The experimental and numerical investigations performed on shear loaded anchorages are described and discussed in this chapter. The program overview is given in the following Sections 9.1.1 - 9.1.3

The aim to perform new experimental investigations was to generate a test database on anchor groups including reference single anchor tests to provide required information on the load distribution and redistribution and on the displacement behaviour of the anchors to verify the concept of the spring model for shear loaded anchorages. Therefore, all the relevant parameters required for the development and later for the verification of the model was measured and evaluated.

Within the scope of this dissertation, 98 shear loading tests were carried out on single anchors and different anchor group configurations with up to four anchor rows in uncracked and cracked concrete. The tests included rectangular and non-rectangular anchor group configurations within and beyond the scope of the provisions of EN 1992-4. The test parameters included the anchor configuration, anchor spacing, edge distance, eccentricity of the external load and the concrete condition (cracked or uncracked). For each tested configuration, corresponding tests were performed on single anchors to obtain reference load-displacement curves for later comparison with the group results and to understand the load distribution within anchor groups. The results of the single anchor tests are discussed along with the results of the anchor group tests. The test parameters, such as concrete strength, edge distance, anchor diameter, embedment depth and anchor spacing were chosen through pre-calculations in a way that failure modes other than concrete edge failure, i.e. steel failure, pryout failure were not decisive neither in single anchor tests nor in anchor group tests. In the tests, the load was applied towards and perpendicular to the concrete edge. In general, two to four tests were performed for each test configuration. The details about the testing procedure such as the description of the used concrete specimens, anchor type, anchor installation and test setup are described in Section 9.2. The test program is given in *Table 9.1 - Table 9.3*. In the tables, the pictogram of the particular anchor group with the most important installation and test parameters are given.

Furthermore, numerical simulations using 3D finite element analysis were carried out on certain anchor configurations to obtain additional information on the behaviour of shear loaded anchorages. The numerical investigations aimed to support the results obtained from the experimental program and to investigate the corresponding anchor groups without a clearance hole. The failure load and the crack pattern gained from the numerical investigations were compared with the experimental results. Furthermore, the load distribution was analysed. This was necessary because the measurement of the anchor shear forces within anchor groups is challenging to realise in experiments. However, it is crucial to highlight the possible force redistribution

among anchors within anchor groups with multiple rows. The results obtained from the numerical simulations are discussed along with the experimental results in Section 9.4. Details of the numerical simulations and modelling of the anchor groups are given in Section 9.3.

9.1.1 Anchor groups arranged perpendicular to the edge and loaded perpendicular to the free edge

The experimental program presented in this section focuses on the concrete edge failure mode of anchorages loaded in shear perpendicular towards the concrete edge. Additionally to the group tests, reference tests were carried out for every edge distance of a particular anchor group. The reference single anchor tests had the same installation parameters, such as anchor diameter and embedment depth to enable a direct comparison with the group results. The tests were carried out with arbitrary hole clearance, and the actual gap between the anchor rod and base plate was measured before testing.

It was aimed to provide information about the load-displacement behaviour of anchor groups and single anchors with different edge distances and to underline that the anchor group behaviour, as well as the load distribution and redistribution, are strongly dependent on the displacement behaviour of the individual anchors of the corresponding anchor rows. Moreover, through performing the tests with an arbitrary hole clearance pattern, the origination of the failure crack pattern was not aimed to be controlled. It was aimed to show that for normal range of c_1/s_1 ratios (0.5 to 2) and acceptable hole clearances, although the first cracking might limit the design in serviceability limit state, the failure crack always originates from the back anchor row. Whether it is possible to distribute the shear forces further after the first cracking happened, depends on the displacement behaviour of the individual anchors and the clearance hole pattern. In addition, the experimental results were compared to calculations based on the EN 1992-4 and fib Bulletin 58.

Table 9.1 provides with the details of the test program on single anchors and anchor groups of 2×1 and 3×1 configurations arranged perpendicular to the edge and loaded perpendicular towards the edge. These investigations aimed to understand the relation between the load-displacement behaviour of single anchors with a particular edge distance ($c_{1.i}$) and an ith anchor of an anchor group with the same edge distance ($c_{1.i}$) and to verify the assumptions made in the spring model for considering the influence of anchor spacing, namely using the tributary volume approach. *Figure 9.1b* gives an overview of the tested group configurations. In *Table 9.1*, the edge distance for the first, second and third anchor row is represented as $c_{1,1}$, $c_{1,2}$ and $c_{1,3}$, respectively. *Figure 9.1a* shows the parameters of the performed reference tests on single anchors, which were carried out for the individual edge distances of the anchors in the group to enable the evaluation of group behaviour based on the individual anchor load-displacement behaviour. To focus on the force redistribution from one anchor row another, only one anchor per anchor row was installed in this test series.

Furthermore, for better understanding of the behaviour of anchorages undergoing concrete edge failure, two special kinds of tests in special specimens with recess were performed: The first type is the shear loading tests on single anchors to investigate the influence of a “missing”

concrete breakout body of an anchor with $c_{1.1}$ or $c_{1.2}$ edge distance, without the influence of cracks and stress disruption on the behaviour of the tested anchor row ($c_{1.2}$ or $c_{1.3}$). For this reason, special concrete specimens with a recess in front of the investigated anchor row were cast (*Figure 9.1c*, *Figure 9.4*). The shape of the recess corresponded to the theoretical concrete breakout body of a single anchor with an edge distance of $c_{1.1} = 80$ *mm* and $c_{1.1} = 160$ *mm*, respectively. The design of the recess assumed a concrete breakout initiating from the anchor tip, so from the total embedment depth. Further shear loading tests were carried out on single anchors with an edge distance of $c_1 = 240$ *mm*, which were installed after the concrete edge failure of the anchor installed with $c_1 = 160$ *mm* and after the breakout body was removed (*Figure 9.1d*). It may be noted that similar investigations were performed by Unterweger et al. (2008), where the residual capacity of the back anchor was checked. The case investigated within this work simulates an anchor group, where the back anchor can resist forces after the front anchor has already completely failed. Such a configuration and situation is, however, very unlikely in practice, where the second anchor row is only activated when the anchor in the first row cannot bear further forces and no concrete is present. The amount of the redistribution in case of groups, if any, depends on the load-displacement behaviour of the individual anchors. In reality, even after the first anchor has reached its ultimate load, it can still contribute to the group capacity as the resistance drops only gradually due to the quasi-brittle behaviour of the concrete. However, this cannot be accounted for by force-based approaches. The resistance beyond peak can only be considered by taking into account the complete load-displacement behaviour of the anchor.

In addition, numerical investigations were carried out on certain configurations of anchorages that were tested experimentally, however, without hole clearance to investigate the contribution of the individual anchors to the group capacity in case of groups without hole clearance. The details of the numerical investigations are presented in Section 9.3.

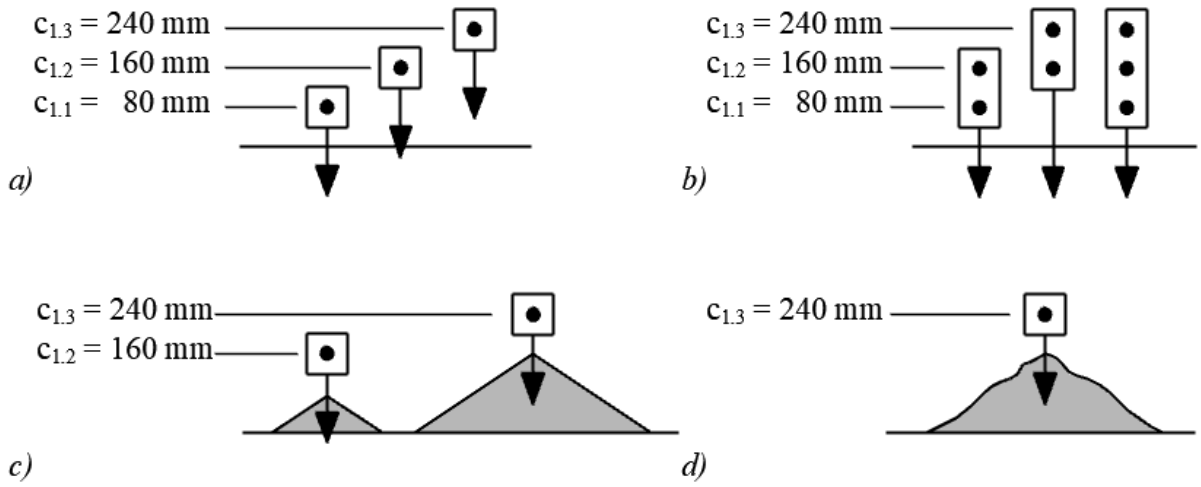

Figure 9.1. Tested configurations for anchor groups arranged perpendicular to the edge and loaded perpendicular towards the free edge: a) single anchors; b) anchor groups with a line of anchors; c) single anchors with concrete recess in the front; d) single anchors with pre-breakout body in the front

Table 9.1. Test program for anchor groups arranged perpendicular to the edge and loaded perpendicular to the edge

Test series ID [a)b)c)d)]	Test type	Edge distance of the corresponding anchor row			Anchor spacing		Edge distance of recess or breakout body	No. of tests	Remarks	Num. analysis
		$c_{1.1}$	$c_{1.2}$	$c_{1.3}$	$s_{1.1}$	$s_{1.2}$				
		[mm]	[mm]	[mm]	[mm]	[mm]	[mm]	[-]	[-]	[Y/N]
SS-80		80	-	-	-	-	-	3	Reference	Y
SS-160		160	-	-	-	-	-	3	Reference	Y
SS-240		240	-	-	-	-	-	3	Reference	Y
GS-3×1-80-80	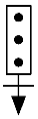	80	160	240	80	80		3	Group	Y
GS-2×1-80-80	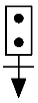	80	160	-	80	80		3	Group	Y
GS-2×1-160-80		160	240	-	80	80		2	Group	Y
SS-160-r80		160	-	-	-	-	80	4	With recess	N
SS-240-r160		240	-	-	-	-	160	4	With recess	N
SS-240-a(SS-160)		240	-	-	-	-	160	1	With pre-breakout	Y
SS-240-a(SS-160-r80)		240	-	-	-	-		2	With pre-breakout	N
SS-240-a(GS-2×1-80-80)		240	-	-	-	-		2	With pre-breakout	N

The mean concrete cube compressive strength fcc,m was 31 N/mm^2 in all tests. The anchor effected embedment depth was 120 mm in all tests.

[a)] Nomenclature for tests on single anchors: **S**ingle **S**hear - tested edge distance c_1 in mm

[b)] Nomenclature for tests on anchor groups: **G**roup **S**hear - configuration - edge distance of front anchor $c_{1.1}$ in mm – spacing s_1 in mm

[c)] Nomenclature for tests on single anchors with recess: **S**ingle **S**hear - tested edge distance c_1 in mm - c_1 of **r**ecess in mm

[d)] Nomenclature for tests on single anchors with pre-breakout: **S**ingle **S**hear - tested edge distance c_1 in mm - **a**fter the failure of (test series)

9.1.2 Anchor groups arranged in a non-rectangular pattern and loaded in shear perpendicular to the free edge

Table 9.2 contains the test program for anchorages with the triangular and hexahedral anchor configurations. These patterns are beyond the scope of the current regulations of EN 1992-4 and fib Bulletin 58. The aim of these tests was to investigate anchor groups of non-rectangular pattern and generate test database because no results were found in the literature on shear loaded anchor groups of hexahedral/circular or triangular pattern. For better evaluation of the test results and to verify the shear spring model for anchor groups of arbitrary configurations, and to show the plausibility of using the tributary volume approach, reference tests on single anchors with corresponding edge distances were also performed.

The tests were carried out on anchorages in uncracked concrete, which were placed close to the concrete edge with random hole clearance and were loaded perpendicular towards the concrete edge. The anchor configuration in the rectangular base plates enabled for both the triangular and hexagonal groups to investigate two different test configurations by rotating the base plate by 180° for the triangular pattern and by 90° for the hexagonal pattern. Note that the edge distance $c_{1.back}$ of the back anchor row was maintained as $c_{1.back} = 240$ *mm* for all cases (see *Figure 9.2*). The anchor diameter and anchor embedment depth were uniform for all tests, namely 20 mm and 120 mm, respectively.

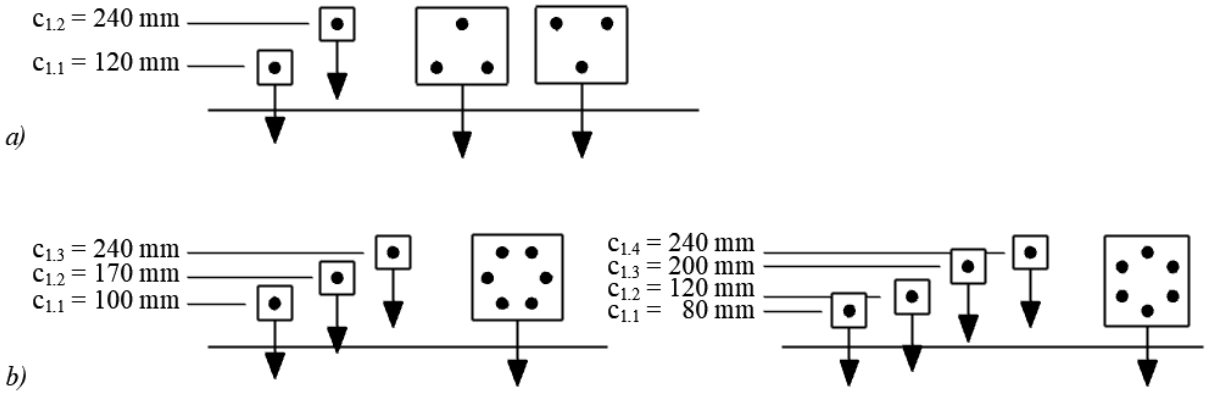

Figure 9.2. Anchorages loaded perpendicular towards the free edge with the corresponding reference single anchor tests: a) anchorage with a triangular pattern; b) anchorages with hexagonal pattern

Table 9.2. Test program for anchor groups of triangular and hexagonal configurations

Test series ID	Test type	Mean concrete cube compressive strength $f_{cc,m}$ [N/mm²]	Embedment depth h_{ef} [mm]	Edge distance of the corresponding anchor row $c_{1.1}$ [mm]	$c_{1.2}$ [mm]	$c_{1.3}$ [mm]	$c_{1.4}$ [mm]	Anchor spacing s [mm]	No.of tests [-]	Num. analysis [Y/N]
SS-100		25.2	120	100				-	3	N
SS-120		27.6	120	120				-	*	N
SS-170		25.2	120	170				-	3	N
SS-200		25.2	120	200				-	2	N
SS-240b		27.6	120	240				-	*	N
GS-TRI-A	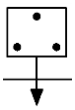	25.2	120	120	240	-	-	139	3	Y
GS-TRI-B	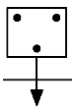	25.2	120	120	240	-	-	139	3	Y
GS-HEX-A	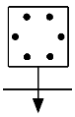	25.2	120	101	171	240	-	80	3	Y
GS-HEX-B	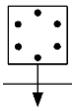	25.2	120	80	120	200	240	80	3	N

* Note that single anchor test series REF-120 and REF-240 are repeated in this table to summarise all tests, which correspond to the test series on triangular and hexagonal anchor groups.

[a)] Nomenclature for tests on single anchors: **S**ingle**S**hear - c_1 in mm

[b)] Nomenclature for tests on anchor groups: **G**roup**S**hear - configuration

9.1.3 Anchorages parallel to the free edge in uncracked and cracked concrete

This section presents the test program for shear loading tests on anchor groups arranged parallel to the concrete edge and loaded perpendicular towards the free edge. Tests were carried out in uncracked and cracked concrete applying the shear load concentrically or with eccentricity. Reference tests on single anchors were carried out in cracked and in uncracked concrete with the corresponding edge distance according to *Table 9.3* to enable a direct comparison and the evaluation of the group behaviour based on the load-displacement behaviour of the single anchors. The comparison was also necessary to verify the assumptions made in the shear spring model. Furthermore, a new test specimen was designed for the tests in cracked concrete (Section 9.2.1).

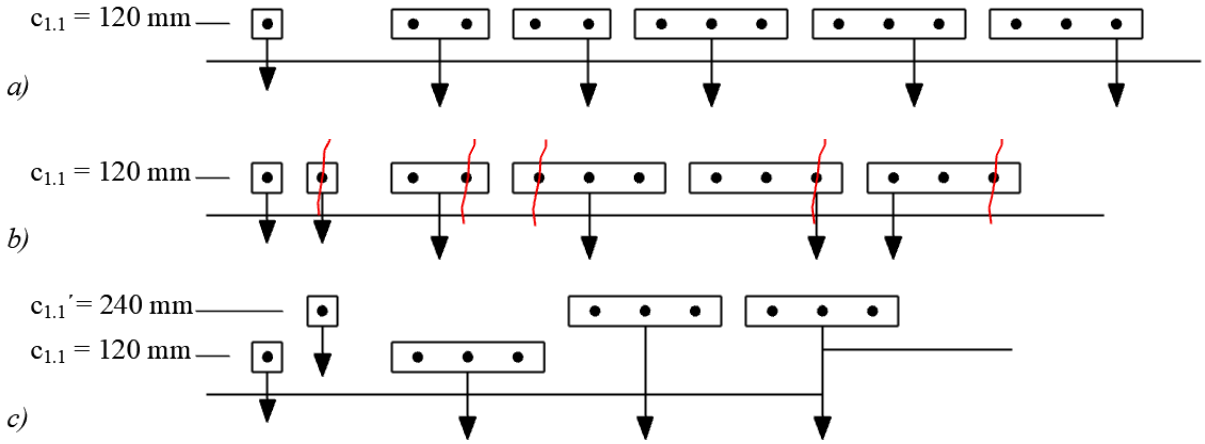

Figure 9.3. Tested configurations for anchor groups arranged parallel to the edge and loaded perpendicular to the free edge with the corresponding reference single anchor tests: a) anchorages in uncracked concrete; b) anchorages in cracked and uncracked concrete; c) different edge distance within an anchor group

In the first test series according to *Figure 9.3a*, the behaviour under concentric and eccentric shear loading was investigated for anchor groups with two or three anchors in a single anchor row arranged parallel to the concrete edge. These tests are required to verify that the spring model for shear loaded anchorages having one anchor row only reduces to tributary area approach (Section 6). This is because, in case of groups with only one anchor row, even the shear loading case towards the concrete edge can be considered as a two-dimensional problem. Furthermore, it was targeted to check the load distribution and mechanism of resistance (including the push-back effect) among the anchors especially for groups subjected to eccentric loading.

The next test series according to *Figure 9.3b* focuses on the influence of the different concrete conditions, namely cracked and uncracked concrete (and consequently different stiffness conditions) within one anchor group and on the influence of load eccentricity without the influence of edge reinforcement. It is aimed to serve as the verification for the fact that the shear spring model can consider different stiffness conditions within an anchor group. Note that there are tests available by Fuchs and Eligehausen (1989) on the concrete edge failure in cracked concrete, however, only on single anchors. They summarised that the ultimate load reduces by ca. 30 - 40 % with placing the anchors in crack widths of Δw = *0.3-0.4 mm*. Although the test results are in accordance with the assumed reduction due to the presence of a crack, the test

specimen was designed with reinforcement close to the edge in front of the anchors and therefore the obtained test results are not perfectly comparable with shear loading tests on anchors close to the concrete edge in unreinforced uncracked concrete. Therefore, a new test specimen was designed and further new tests were performed on single anchors and anchor groups.

The third test series according to *Figure 9.3c* was aimed to investigate a special case, where two different edge distances ($c_{1.1}$ and $c_{1.1}$´) can be assigned to an anchor group having three anchors in a single anchor row. For a better understanding of this problem and comparison, the same 1×3 anchor group was investigated separately with $c_{1.1}$ and $c_{1.1}$´edge distance as well. This configuration underlines why is it important to handle the behaviour of shear loaded anchor groups close to the concrete edge as a 3D problem and why the tributary volume approach proposed in the spring model approach is appropriate for modelling of anchorages under shear loads.

Table 9.3. Test program for anchorages arranged parallel to edge loaded perpendicular to the edge

Test series ID	Test type	Mean concrete cube compr. strength $f_{cc,m}$ [N/mm²]	Embed-ment depth h_{ef} [mm]	Edge dis-tance $c_{1.1}$ [mm]	Anchor spacing s_2 [mm]	Crack width Δw [mm]	No.of tests [-]	Numeri-cal inv. [Y/N]
SS-120		27.6	120	120	-	0	3	N
SS-120-dw03		27.6	120	120	-	0.3	3	N
SS-240b		27.6	120	240	-	0	2	N
GS-1×2-C		27.6	120	120	120	0	3	N
GS-1×2-E60		27.6	120	120	120	0	3	N
GS-1×2-dw03-C		27.6	120	120	120	0.3	3	N
GS-1×3-C	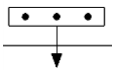	27.6	120	120	120	0	3	Y
GS-1×3-E60	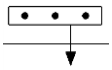	27.6	120	120	120	0	3	N
GS-1×3-E120	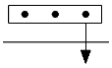	27.6	120	120	120	0	3	N
GS-1×3-dw03-C		27.6	120	120	120	0.3	3	N
GS-1×3-dw03-E120c	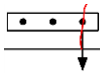	27.6	120	120	120	0.3	2	N
GS-1×3-dw03-E120u		27.6	120	120	120	0.3	2	N
GS-240/1×3-C	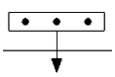	27.6	120	240	120	0	2	Y
GS-1×3-120/240-C	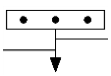	27.6	120	120/240	120	0	4	Y

9.2 TESTING

9.2.1 Test specimens for shear loading tests

Different types of test specimens were designed and used to perform shear loading tests close to the concrete edge (*Figure 9.4*). The aim was to design the specimens in such a way that "pure" concrete edge breakout failure mode is not disturbed or not influenced by premature failure of the specimen or due to the interference by other failure modes. Therefore, all the specimens were provided with sufficient amount of edge reinforcement to avoid the flexural failure of the specimen while applying the shear load perpendicular to the concrete edge and the anchor parameters were selected such that concrete edge breakout would be the dominant failure mode. The dimensions of the concrete specimens and the position of the reinforcement were designed in a way that during the testing, the formation of the full-size concrete edge breakout bodies was ensured without the influence of neighbouring anchor groups or reinforcement. The clear distance between the outermost and closest anchors of the neighbouring groups was kept always greater than 4-times the edge distance of the back anchor row ($c_{1.back}$). Furthermore, the support distance measured from the outermost anchor of the group being tested was kept as $2c_{1.back}$ on both sides. Most of the shear loading tests were carried out using Specimen A, which is a thick concrete specimen of size 163.5×163.5×50 cm^3 (*Figure 9.4*). Special concrete specimens were cast for test series SS-160-r80 (Specimen B) and SS-240-r160 (Specimen C) with a recess in front of the investigated anchor row. The shape of the recess corresponded to the theoretical concrete breakout body of a single anchor with an embedment depth of $h_{ef} = 120\ mm$, edge distance of $c_1 = 80\ mm$ for test series SS-160-r80 and $c_1 = 160\ mm$ for test series SS-240-r160, respectively (see *Figure 9.4*). A failure breakout body was simulated originating from the end of the embedment depth, which propagates towards the concrete edge to a depth of $1.5c_1$ and a width of $3c_1$. The edge distances of the investigated single anchors were $c_1 = 160\ mm$ and $c_1 = 240\ mm$. In *Figure 9.4*, Specimen A-a depicts the schematics of the test specimen with pre-damaged concrete. Before testing, the breakout body of the prior test was removed and the specimen was used for the test series with 240 mm edge distance, namely SS-240-a(SS-160), SS-240-a(SS-160-r80) and SS-240-a(GS-2×1-80-80). Special test specimen (Specimen D) was designed to test a group of anchors in a row with different edge distances. The specimen is shown in *Figure 9.4* and was provided with a step in a way that one of the outer anchors of the group had an edge distance of 120 mm, while the other outer anchor had an edge distance of 240 mm and the middle anchor was located exactly in the line of the step. For the shear loading tests in cracked concrete, a new specimen (Specimen E) was designed, which enabled the anchor testing on the concrete edge without the influence of the reinforcement. Steel plates of 2 mm thickness were used as crack inducers in the design of the specimens that enabled the crack formation by hammering wedges into the pre-formed holes in the concrete members. The specimens were designed in such a way that in each specimen, two tests could be carried out. The thickness of the concrete specimen was 400 mm. The plain concrete depth available for the anchors was 250 mm due to the steel plates cast in the concrete, which is greater than 2-times the edge distance ($c_1 = 120\ mm$) of the corresponding tests (*Table 9.3*).

The dimensions of the concrete specimens enabled the formation of the full-size concrete breakout bodies. Further details about Specimen E are given in Appendix B.

To sum it up, the shear loading tests were carried out in the following types of test specimens:

- Specimen A: thick slab (Appendix B)
- Specimen A-a: thick slab A, pre-damaged specimen, after removing the breakout body of a former test
- Specimen B: thick slab with recess AS1 (Appendix B)
- Specimen C: thick slab with recess AS2 (Appendix B)
- Specimen D: thick slab with 120 mm step (Appendix B)
- Specimen E for cracked concrete (Appendix X)

Note that *Figure 9.4* shows the test specimens schematically. The exact drawings with reinforcement etc. are given in Appendix B.

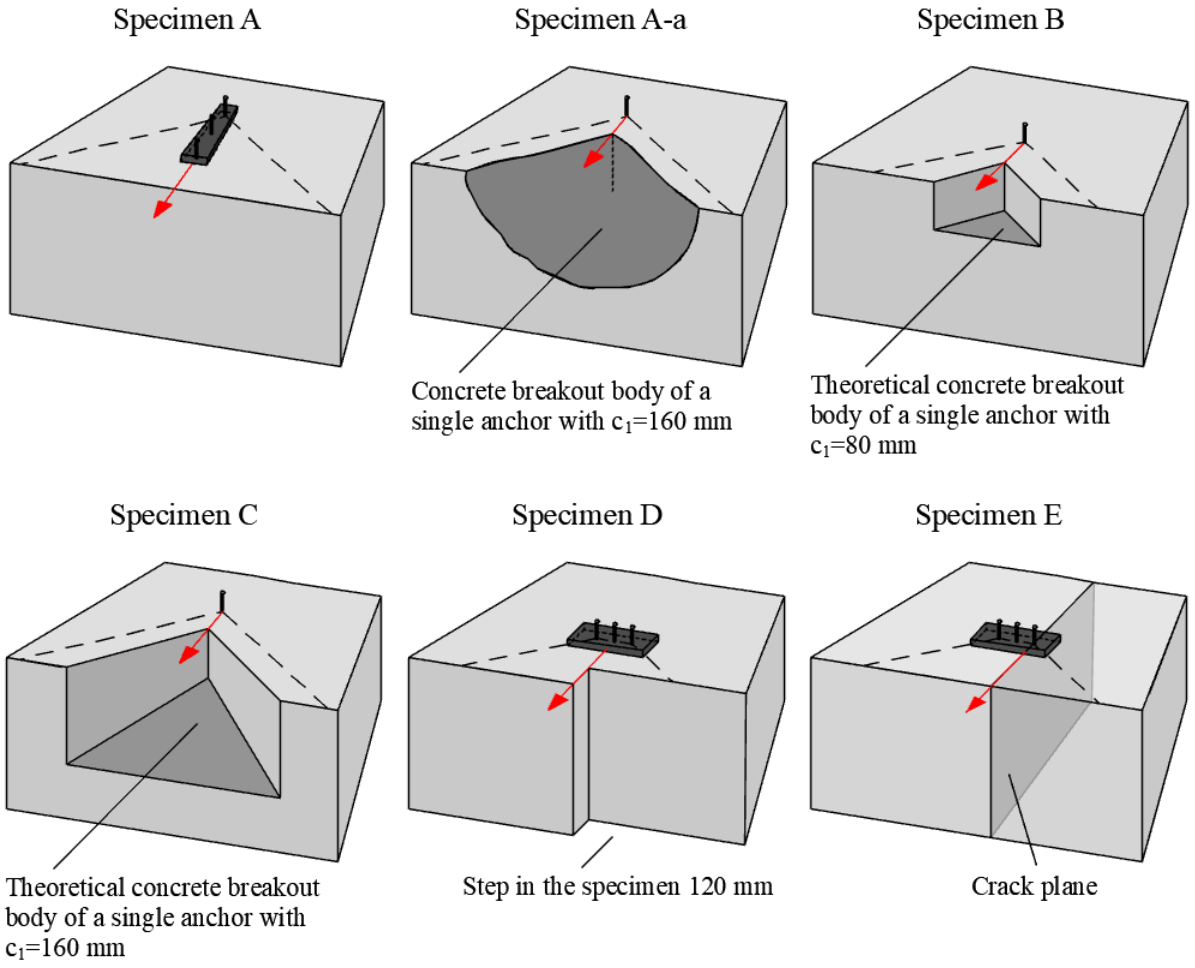

Figure 9.4. Schematic of the test specimens

The concrete mix of the corresponding concrete batches was designed according to DIN EN 206, with a maximum grain size of 16 mm. In all tests, round gravel aggregates were used. The influence of concrete mix composition and aggregate type (crushed or rounded) was beyond the scope of this dissertation. The compressive strength of the concrete batches was

measured on standard concrete cubes of a side length of a = 150 mm according to DIN EN 12390-15. The concrete compressive strength in the performed tests was in the range of $f_{cc,150,m}$ = *25.2 N/mm² – 31.0 N/mm²* (see *Table 9.1-Table 9.3*).

9.2.2 Tested fasteners and installation

The tests were carried out with an epoxy-based adhesive anchor system using M20 (d_{nom} = *20 mm*) steel threaded rods of grade 12.9 ($f_{u,nom}$ = *1200 N/mm²*). The mean bond strength of the used adhesive was approximately τ = 30 N/mm². The effective embedment depth of the anchors was h_{ef} = *120 mm* in all tests. This corresponds to a h_{ef}/d ratio of 6.0. The installation parameters were designed to ensure concrete edge breakout failure as the dominant failure mode. The anchors were installed according to the corresponding Manufacturer´s Installation Instructions (ETA-10/0012). Holes were drilled by hammer drilling perpendicular to the concrete surface using steel templates with pilot-holes to ensure that the anchors within the group are positioned accurately and to provide an accurate edge distance. In case of the tests in cracked concrete (similar to the installation for tension tests), a hairline crack was generated first to ensure that the crack passes the anchor location. After that, the hole was drilled through the crack using steel templates with pilot-holes to ensure accurate positioning of the anchors according to the steps given in *Figure 8.1*. For shear loading tests, maximum one anchor of a group was located in a crack. Then, the holes were cleaned using compressed air and steel brush, and the mortar was injected into the holes and the base plate was positioned on the anchors, respectively. A plastic sheet was placed between the base plate and concrete to avoid that the remaining epoxy on the concrete surface is glued to the base plate. After the prescribed curing time of the epoxy mortar, the base plate was removed and a 1.5 mm Teflon sheet was placed between the base plate and the concrete surface to minimize friction during the tests. After the drilling and cleaning process, the anchors were set and the base plate was positioned on the anchors, respectively. No installation torque was applied on the anchors and the nut was only hand-tightened after the prescribed curing time of the epoxy mortar to ensure the same initial conditions for all anchors of the group. The annular gaps were not filled, thus the anchorages are to be considered as anchor groups with hole clearance.

9.2.3 Test setup and test procedure

This section provides information about the test setups, which were used in the shear loading tests. *Figure 9.5* depicts a schematic drawing of the test setup for anchor groups loaded perpendicular to the concrete edge. The setup can be used for concentric and eccentric tests in cracked and uncracked concrete provided that hinges are built into the force flow to allow rotation (*Figure 9.6)*. The same test setup was used for the reference single anchor tests using the corresponding loading fixture. With minor modifications (e.g. position of supports), the same test setup was used for the tests loaded parallel to the concrete edge (*Figure 14.5*). The tests were performed using rotation unrestrained load application, without using uplift restraint for the base plate.

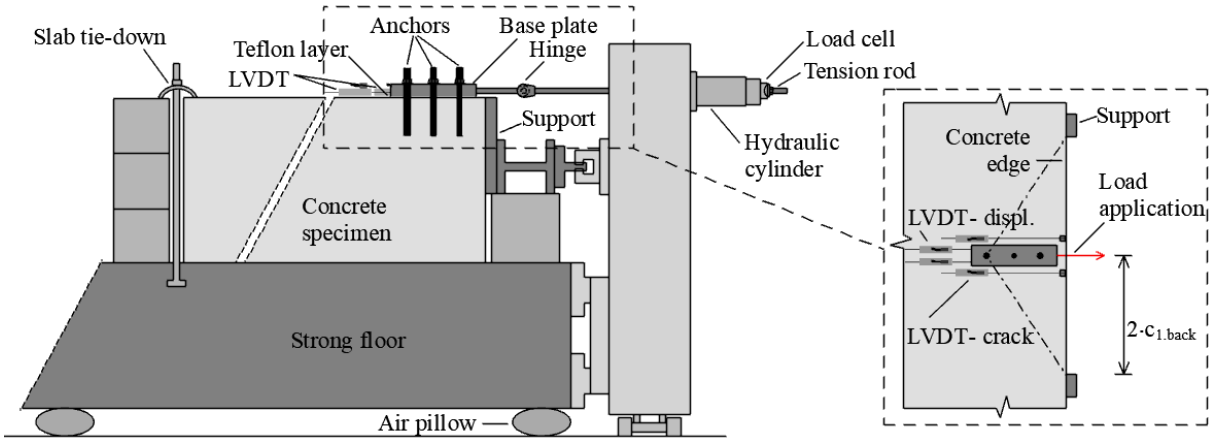

Figure 9.5. Schematic of the setup for shear loading tests – loading perpendicular to the concrete edge

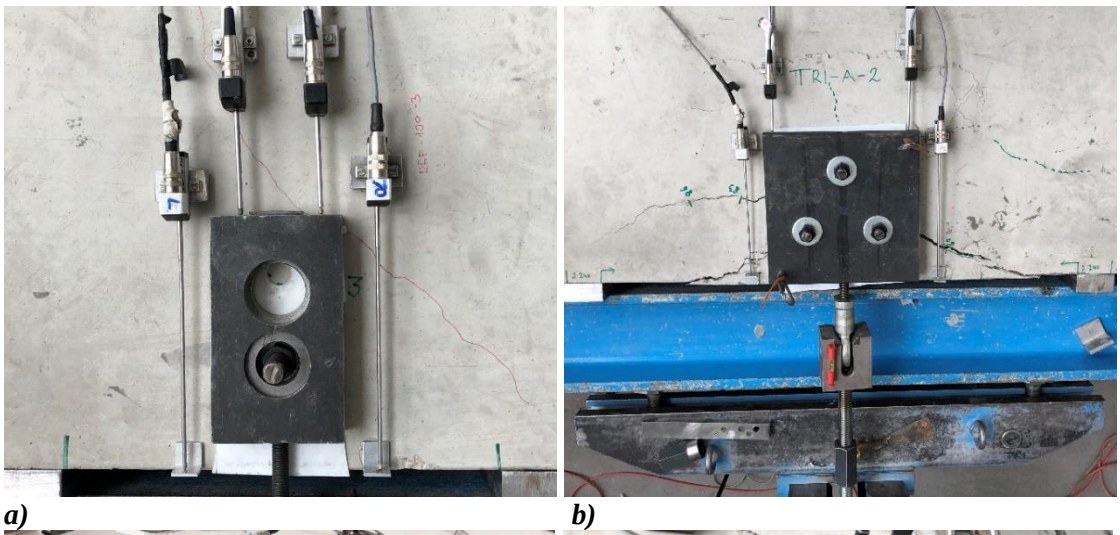

a) *b)*

c) *d)*

Figure 9.6. Typical test setups for shear loading tests – loading perpendicular to concrete edge a) single anchor; b) concentric loaded group; c) group tested in specimen D; d) eccentric loading in cracked concrete

The shear loading tests on anchor groups were performed with hole clearance between the base plate and the anchor rod. The diameter of clearance hole corresponded to the requirements given in Table 6.1 of EN 1992-4, $a_{cl} = 22\ mm$ for nominal anchor diameter of $d_{nom} = 20\ mm$. The actual annular gap was measured before testing. For practical reasons, the measurement was carried out from the top of the base plate. Consequently, a minor misalignment of the anchor rod might slightly falsify the measurement.

The test setup consisted of the following major components:

- steel supports with an adequate distance ($4c_1$ of back row) to allow the formation of an unrestricted concrete breakout body,
- slab tie-down to avoid the uplifting of the specimen,
- a hydraulic cylinder and high strength threaded rod for load application,
- a hinge to allow the free rotation of the base plate,
- a calibrated load cell,
- displacement transducers for measuring anchor and base plate displacement and crack width,
- 1.5 mm thick Teflon layer to minimize friction between the base plate and concrete surface and
- data acquisition system with computer interface.

The shear load was applied to the anchors through the base plate by using the hydraulic cylinder of the expected load range. To transfer the load from the hydraulic cylinder into the base plate, a high strength threaded rod was used with a built-in hinge (hinge capacity up to 120 kN) to allow the free rotation of the base plate. In case of the tests with hexagonal configuration loaded parallel to the concrete edge, a hinge was welded to the base plate to enable the transfer of the expected high loads (*Figure 14.5a*). The load was applied concentrically to the group; however, due to the vicinity of concrete edge, the anchors were not loaded "symmetrically" and large rotation of the base plate at failure and after failure was expected (see *Figure 14.5b*).

The shear load applied on the anchor group was measured using a calibrated load cell (20 – 200 kN and 50 – 500 kN). The horizontal displacement was measured using two displacement transducers (LVDT with a measuring range of 0.01 – 75.00 mm) on the base plate. In the case of tests in cracked concrete, the crack width was measured with LVDT placed perpendicular to the crack close to the anchor located in the crack. Photos of the setups used for the tests in uncracked and cracked concrete are shown in the following.

9.3 NUMERICAL INVESTIGATIONS

9.3.1 General

Nonlinear numerical simulations within the framework of 3D finite element analysis were carried out on certain anchor configurations according to *Table 9.1* - *Table 9.3* to obtain more information on the behaviour of shear loaded anchorages. By means of numerical analysis and appropriate post-processing, the developed stresses and crack patterns can be evaluated at any

monitored loading step at any location within the model. The numerical analysis provides a big advantage over the experimental testing through the fact that the quantities such as stresses, loads among the anchors of a group, crack initiation and propagation inside the concrete etc. can be evaluated from the numerical analysis, which are otherwise rather difficult, if not impossible, to measure in the tests. However, the results of the numerical analysis can be considered reliable if and only if the numerical modelling procedure is able to capture all the features of the real problem in a realistic way. This includes different mechanisms of load transfer, boundary and loading conditions, constitutive laws for the materials, crack initiation and propagation, damage localization, mesh insensitivity and the basic principles of thermodynamics among others. Therefore, the numerical modelling procedure must be validated and proven for its capability to simulate real behaviour. The modelling procedure used in this work has been well-proven to realistically simulate the behaviour of anchorages in concrete by various researchers in the past (Schmid, 2010, Fichtner, 2011, Grosser, 2012, Tóth et al., 2017, Ruta, 2018, Jebara et al., 2019, Tian, 2019). Within the frame of this thesis, the numerical investigations aimed to support and augment the results of the experimental program and to obtain results of the corresponding anchor groups without clearance hole. Furthermore, the force distribution and redistribution among the anchors of the group was analysed by performing nodal-force monitoring.

The finite element Code MASA (IWB and Ožbolt, 1999) was used to perform the 3D nonlinear numerical analyses. The software is capable of performing 3D nonlinear finite element analysis of structural elements made of quasi-brittle materials such as concrete, using microplane model with relaxed kinematic constraint as the constitutive law (Ožbolt et al., 2001). The material is characterized by the relation between the stress and strain components on planes of various orientations (pre-defined directions) in the microplane model. The microplanes may be imagined to represent the damage or weak planes in the microstructure, such as those that exist at the contact between the aggregate and the cement matrix. The microplane strains are the projections of the known macroscopic strain tensor in normal microplane direction (volumetric and deviatoric) and in-plane shear direction (*Figure 9.7*). The microplane stresses are calculated using uniaxial constitutive laws of each microplane component (volumetric, deviatoric, and shear). In the model, the tensorial invariance restrictions do not need to be directly enforced. By employing virtual work approach, the macroscopic stress tensor is obtained as an integral over all predefined 21 microplane directions (symmetric part of the unit sphere). Further details of the model can be found in Ožbolt et al. (2001). Damage and cracking are modelled in the framework of the smeared crack continuum. To assure the objectivity of the analysis with respect to the size of the finite elements, the crack band method is used according to Bažant and Oh (1983). For creating the 3D finite element model and for the evaluation of the numerical results, the commercial pre- and post-processing software FEMAP (Siemens) was used.

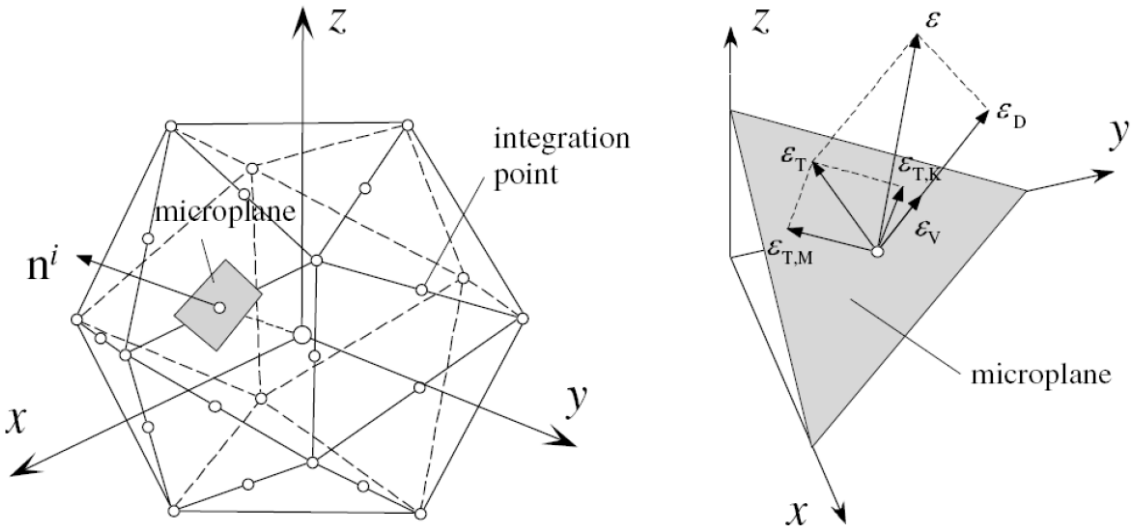

Figure 9.7. Concept of the microplane model: Integration point with microplanes (left) and decomposition of strain vector on the specified microplane (right) – Figure taken from Ožbolt et al. (2001)

9.3.2 Modelling

The geometry and material properties of the numerical model corresponded to the parameters of the experiments. However, in order to minimize the computation time, the size of the concrete block was reduced, since in the experiments four tests per specimen were performed, therefore, a bigger specimen size was required. In the numerical program, only one anchorage was analysed at once, and for this reason, the length and width of the specimen were reduced to $5c_{1.back} + \Sigma s_2$ of the respective test. The height of the concrete block was identical to the height of the concrete block used in the experimental investigations. Furthermore, because the numerical simulations were carried out for groups without hole clearance, the base plate and the anchor were considered to be rigidly connected, and consequently, it was not required to model the nuts. The components of the numerical model are depicted in *Figure 9.8a - f*: concrete specimen modelled using solid 4- node tetrahedral elements, steel base plate and anchors (steel rods) modelled using solid 8-node hexahedral elements, contact layer between anchor and concrete, contact layer between base plate and concrete, and two types of bar elements. The bar elements are implemented in MASA in such a way that, depending on the type, they can only take up compressive and/or shear stresses. Contact bar elements, which can take up only compressive stresses, were used in the interface between the concrete surface and base plate to simulate a Teflon sheet, which was used in the experiments to minimize friction between steel and concrete. Bond type bar elements were applied in the contact layer between concrete and steel rod to model the bond provided by the epoxy mortar realistically. These bar elements can take up both shear and compressive stresses. For the given problem, an element size of 5 - 10 mm is considered as optimal for realistic calculation results. To reduce the calculation time of the models, this element size was only generated in the load application areas i.e.in the area of the anchors. A mesh size of 10-30 mm was used in the regions, where no cracking was expected in the concrete.

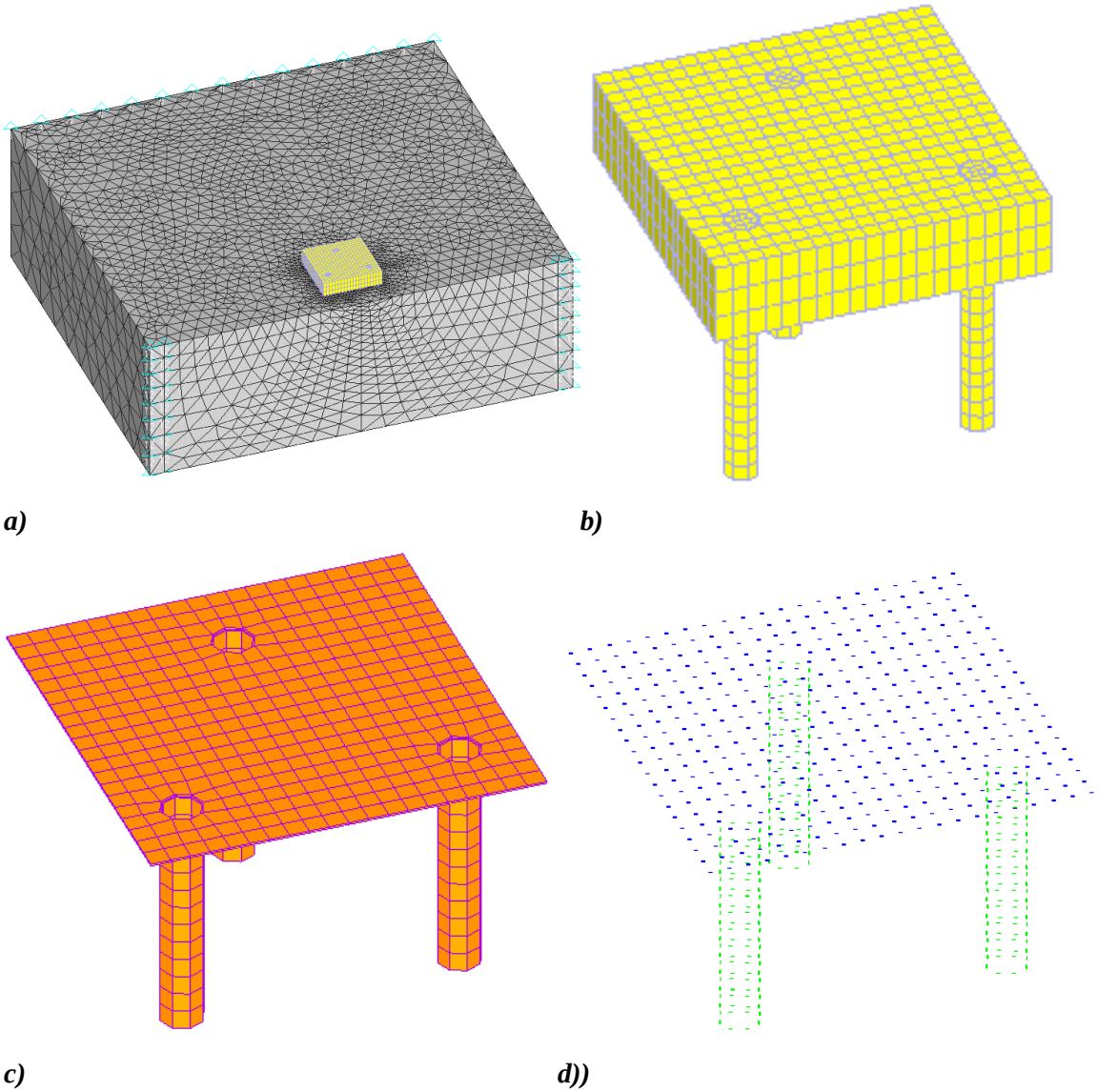

Figure 9.8. a) 3D finite element model of GS-TRI-A; b) base plate and anchors; c) contact between anchor and concrete and contact between the base plate and concrete surface; d) bond type bar elements along the anchor shaft and contact type bar elements below the base plate

The boundary conditions applied during the analyses corresponded to those of the experiments, and are schematically depicted in *Figure 9.9*. At the front side of the concrete block, constraints in x- and y-direction were provided to simulate the front support and were provided at a distance of ($4c_{1.back} + \Sigma s_2$) over the height of the specimen. To prevent the concrete block from overturning, constraints in the z-direction were applied at the rear-upper edge of the specimen. The dimensions of the base plate in the numerical analyses were identical to those of the performed tests.

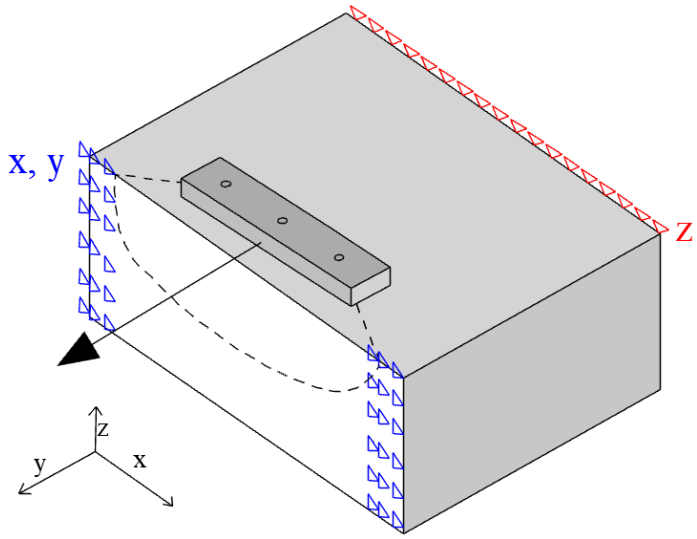

Figure 9.9. Schematic representation of the boundary conditions applied in the model

9.3.3 Material parameters

9.3.3.1 Steel

The behaviour of the base plate and the anchors were assumed to be linear elastic. The modulus of elasticity for steel was assumed to be 210 GPa and the Poisson's ratio was taken as 0.33.

9.3.3.2 Concrete

An example calculation for the concrete material parameters, which are required for the analysis, is given in the following. The calculation is based on the results considering a mean cubic compressive strength of concrete as 31 MPa. However, note that in the cases with different concrete compressive strength, the material parameters were modified correspondingly.

The measured mean cube compressive strength serves as the basis for the calculation of all material parameters. However, for the calculation, the mean cylinder compressive strength is required. The conversion can be done as follows (DIN EN 1992-1-1):

$$f_c = 0.8 \cdot f_{c,cube} = 0.8 \cdot 31 \ {}^{N}/_{mm^2} = 24{,}8 \ {}^{N}/_{mm^2} \qquad \textbf{Eq. 74}$$

The modulus of elasticity of concrete can be calculated according to ACI 318-14 as:

$$E_c = 4730\sqrt{f_c} = 4730\sqrt{24.8 \ {}^{N}/_{mm^2}} = 23555.2 \ {}^{N}/_{mm^2} \qquad \textbf{Eq. 75}$$

The mean tensile strength of the concrete can be calculated according to EN 1992-1-1 as:

$$f_t = 0.3 \cdot {f_c}^{0,67} = 0.3 \cdot 24.8 \ {}^{N}/_{{mm^2}^{0.67}} = 2.58 \ {}^{N}/_{mm^2} \qquad \textbf{Eq. 76}$$

The fracture energy of the concrete can be calculated according to Karihaloo and Bhushan (1995) according to ***Eq. 77***. For a maximum grain size diameter of 16 mm, α_F is assumed to be 7.

$$G_f = \alpha_F \cdot {f_c}^{0.7} = 7 \cdot (24.8 \ {}^{N}/_{mm^2})^{0.7} = 66.25 \ {}^{Nm}/_{m^2} = 0.066 \ {}^{Nmm}/_{mm^2} \qquad \textbf{Eq. 77}$$

The Poisson's ratio of concrete is assumed to be 0.18.

9.3.3.3 Epoxy mortar

For the material parameters of the mortar layer (bond type bar elements), the maximum bond strength τ_{max}, the residual bond stress τ_R and the slip values s_1, s_2 and s_3 (*Figure 9.10*) of the used epoxy mortar are required. The maximum bond stress τ_{max} was determined based on pullout tests on single anchors using a confined test setup as 32.5 N/mm². Furthermore, the following assumptions were made for the displacement values: $s_1 = 0.01$ *mm*, $s_2 = 0.2$ *mm* and $s_3 = 2$ *mm*. The residual bond stress τ_R was assumed to be 8 N/mm². The compression modulus of the mortar was taken as 2500 MPa.

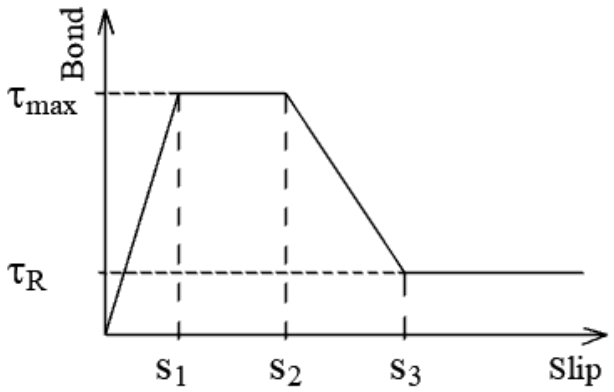

Figure 9.10. Idealised bond stress-displacement relationship used to model bond of epoxy mortar (Sharma et al., 2016)

9.3.4 Displacement controlled nonlinear static analysis

Two types of numerical analyses were performed. In the first type of analysis, the anchorage was modelled as described above, and the anchorage was loaded in displacement control by incrementally applying the displacement in several steps until failure (*Figure 9.11a)*. The second type of analysis was performed to simulate the tests where the rear anchor was installed and tested after the failure of the front anchor. In this type of analysis, two anchors were modelled without connecting them by a common base plate.

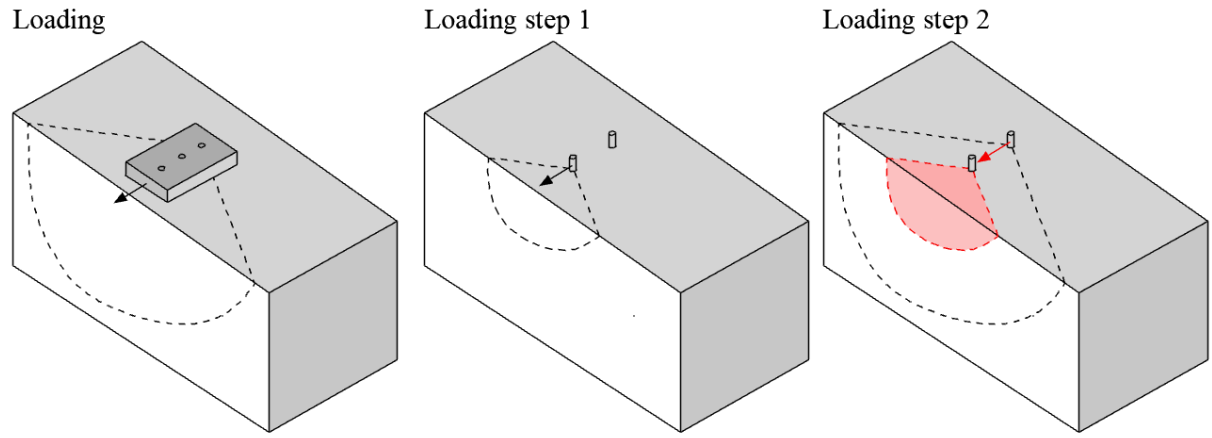

a) ***b)***

Figure 9.11. Loading scenarios: a) loading until failure; b) loading in two steps by applying the load first only on the front anchor until failure, secondly only on the back anchor until failure

In the first loading step, the shear load was applied on the front anchor by incrementally applying the displacement in several steps until failure (*Figure 9.11b left*). In the second loading step, the back anchor was loaded in displacement control until failure, while the stress disturbance and crack pattern caused by the failure of the front anchor remained during the analysis and affected the behaviour of the back anchor (*Figure 9.11b right*). This analysis should simulate the experimental case, where the back anchor was installed after the failure and removal of the breakout body of the front anchor (Series SS-240-a).

9.3.4.1 Evaluation method of the numerical results

As it is mentioned in Section 9.3.1, the aim of the numerical investigations is to support and extend the experimental results. Therefore, within the frame of this dissertation, only the failure loads and in certain cases the force distribution among the anchors of an anchor group are evaluated quantitatively. The developed crack patterns serve solely as a qualitative representation of the results. For the representation of developed crack patters, it is required to perform post-processing in FEMAP. However, for the evaluation of the shear force distribution among the anchors, it is necessary to monitor the shear forces developing in the individual anchors. It was decided to monitor the shear forces at the location just below the base plate, where the shear stresses are highest along the anchor shaft. This location is identified in *Figure 9.12*. The shear forces of all nodes in this layer are summarised in every individual anchor. The plausibility of this method can be confirmed by the fact that the sum of the total shear forces in the anchors at each load step should be equal to the load measured at the point of load application $\Sigma V_1 + \Sigma V_2 + \Sigma V_3 = V_{group}$. Note that reference tests on shear loaded single anchors were performed by means of numerical analysis to verify the used modelling approach and apply it to the anchor groups.

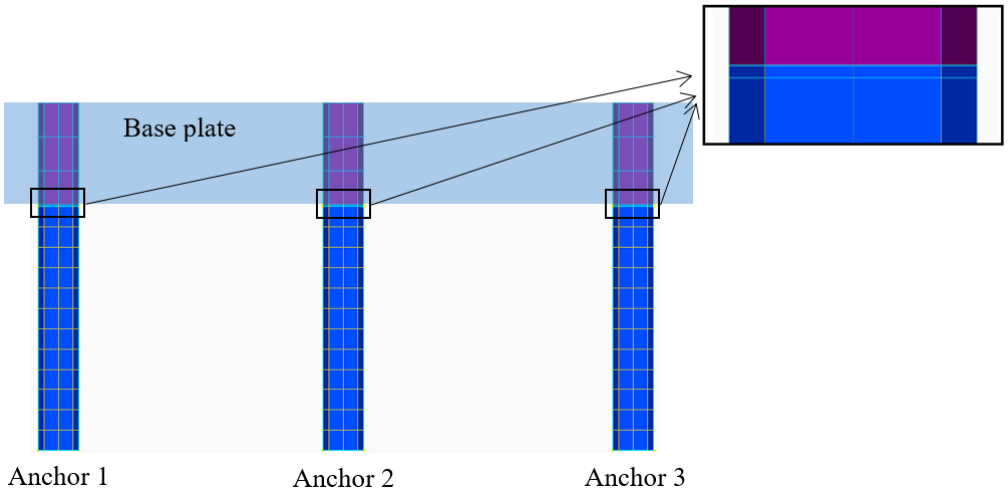

Figure 9.12. Area to monitor the nodal forces to evaluate the shear force distribution within the group

9.4 RESULTS AND DISCUSSION ON SHEAR LOADED ANCHORAGES

This section discusses the results obtained from performing the experimental and numerical investigations on anchorages loaded in shear perpendicular to the concrete edge according to *Table 9.1* - *Table 9.3*. Furthermore, the results are compared with calculations based on the recommendations given in EN 1992-4 and fib Bulletin 58.

The summary of the experimental results in terms of the mean value of the ultimate shear loads $V_{u,m}$, as well as the mean value of the initial shear stiffness $k_{1,m}$ for the particular test series is given in *Table 9.4*, *Table 9.6* and *Table 9.13*. In this thesis, the initial shear stiffness is evaluated as the secant stiffness corresponding to 50% of the ultimate load because the load-displacement curve is practically linear up to this point. Correspondingly, the initial shear stiffness k_1^i was calculated as the ratio of $0.5V_u^i/\delta(0.5V_u^i)$. The load-displacement curves along with the photos of failure patterns are given, in the corresponding sub-sections 9.4.1-9.4.3.

As mentioned in Section 9.3, numerical investigations were carried out on certain anchor configurations to obtain more information on the behaviour of shear loaded anchorages. The 3D finite element modelling and the nonlinear analysis enabled the modelling of the anchorages without the influence of hole clearance, and the evaluation of the force distribution via nodal force monitoring. The obtained crack patterns and information about the anchor force distribution among the individual anchors within a group are evaluated together with the experimental results. This way it is possible to show the influence of hole clearance on the anchorage behaviour and to have a look "into the concrete member" at any cross-section. Note that reference tests on single anchors were also reproduced by means of numerical analysis to verify the used modelling approach (see *Table 9.5*) and apply it to the anchor groups. The numerically obtained results in terms of failure loads are tabulated in *Table 9.5*, *Table 9.7* and Section 9.4.3.3. The anchor shear force distribution and the crack patterns are given in the corresponding subsections.

9.4.1 Anchor groups arranged perpendicular to the edge and loaded perpendicular towards the free edge

To verify the assumptions made for the concept of the spring model for shear loaded anchor groups in case of concrete edge failure, it is essential to investigate the load distribution and load redistribution among the anchors of a group. The best way for understanding the behaviour is to study the anchor groups with multiple anchor rows with one anchor per row. This way, the redistribution of the forces among different anchor rows can be analysed. Note that the experimental tests were performed with a random hole clearance pattern, whereas the numerical investigations were carried out without hole clearance.

According to the test series contained in *Table 9.1*, the relation between the load-displacement behaviour of single anchors with a particular edge distance ($c_{1,i}$) and anchor groups with multiple anchor rows, having the same corresponding edge distance ($c_{1,i}$, $i=1$-3) were investigated. Accordingly, for every edge distance of the investigated anchor groups, reference tests were conducted. The results of the single anchor tests are discussed in Section 9.4.1.1, and together with the group tests for comparison in Sections 9.4.1.3 - 9.4.1.5. The summary of the test results in terms of the mean value of the ultimate shear loads $V_{u,m}$, the mean value of the initial shear stiffness $k_{1,m}$ and the calculated mean concrete edge resistance based on the EN 1992-4 and fib Bulletin 58 are given in *Table 9.4*. The numerically obtained ultimate loads are tabulated in *Table 9.5*. The corresponding load-displacement curves and the experimental and numerical failure crack patterns are discussed in the following sub-sections. Note that the crack pattern

obtained from the numerical investigations correspond to the crack pattern visible in that particular loading step, and the cracks, which were developed during the load distribution from row-to-row may not be visible.

Table 9.4. Test results of anchor groups arranged perpendicular to the edge and loaded perpendicular to the edge

Test series ID	Meas. mean ultimate load [b]	Mean value of initial stiffness	Calc. mean concrete edge res. [c]		Calc. mean concrete edge res. [d]	
	$V_{u,m}$	k_1	$V_{Rm,c,EN}$	$V_{u,m}/V_{Rm,c,EN}$	$V_{Rm,c,fib}$	$V_{u,m}/V_{Rm,c,fib}$
	[kN]	[kN/mm]	[kN]	[-]	[kN]	[-]
SS-80	25.5	29.8	23.6	1.08	23.6	1.08
SS-160	70.1	33.6	57.2	1.23	57.2	1.23
SS-240	106.9	26.3	97.7	1.09	97.7	1.09
GS-3×1-80-80	107.7	61.6	23.6	4.56	97.7	1.10
GS-2×1-80-80	61.9	41.6	23.6	2.62	57.2	1.08
GS-2×1-160-80	113.6	44.8	23.6	4.81	97.7	1.16
SS-160-r80	71.9	27.9	-	-	-	
SS-240-r160	105.0	28.9	-	-	-	-
SS-240-a(160) [a]	54.0	16.2	-	-	-	-

[a] The test series SS-240-a(SS-160), SS-240-a(SS-160-r80) and SS-240-a(GS-2×1-80-80) are evaluated together as test series SS-240-a(160), [b] Crack initiation depends on the actual hole clearance and load distribution, [c] Crack initiation assumed from front anchor row, [d] Crack initiation assumed from back anchor row

Table 9.5. Test results of anchor groups of non-rectangular configurations with hole clearance loaded perpendicular to the edge compared to numerical results obtained on anchorages without hole clearance

Test series ID	Mean ultimate load	Numerically obtained ultimate load	$V_{u,m}/V_{u.num}$
	$V_{u,m}$	$V_{u,num}$	
	[kN]	[kN]	[-]
SS-80	25.5	25.5	1.00
SS-160	70.1	66.7	1.05
SS-240	106.9	105.7	1.01
GS-3×1-80-80	107.7	101.2	1.06
GS-2×1-80-80	61.9	59.0	1.05
GS-2×1-160-80	113.6	100.3	1.13
SS-240-a(160)	54.0	Front anchor 72.5 / Back anchor 24.5	-[a]

[a]The results are not comparable because of the different pre-damage in the experiments

9.4.1.1 Reference tests

The reference tests were carried out on single anchors, with 80, 160 and 240 mm edge distance in test series SS-80, SS-160, SS-240, respectively. As expected and in agreement with the literature available on this topic, the test results display a strong increase in the failure load with increasing edge distance (*Figure 9.13a*). The initial shear stiffness $k_{1,m}$ of the series SS-80, SS160 and SS-240 were obtained as 29.8, 33.6 and 26.3 kN/mm, respectively, which corresponds to a mean value of 29.9 kN/mm. It was found that the initial shear stiffness is practically independent of the edge distance. This agrees well with the findings from the literature (Grosser, 2012, Tian et al., 2018). Having almost the same initial shear stiffness for all anchors means also that all the anchors within an anchor group without hole clearance and loaded in shear should take up load equally in the initial stages. The load-displacement curves of the reference series along with the failure crack pattern of one representative test per series are shown in *Figure 9.13a- d*. The horizontal dashed-dotted lines in the figure correspond to the mean value of the test results, which are written within the corresponding boxes. The calculated mean failure loads on the basis of EN 1992-4 or fib Bulletin 58 are on a slightly conservative side compared to the experimental results (refer to *Table 9.4*). For tests series SS-80 and SS-240, the deviation is less than 10%, which is a good agreement, and it is within the general scatter considered in the CCD Method for concrete edge failure (15%); whereas in the case of the test series SS-160, the measured mean load is 23% higher than the predicted failure load. However, the numerically obtained failure loads are only 0, 5 and 1% lower compared to the experimental values, which verifies the validity of the numerical modelling approach (*Table 9.5)*. A typical failure crack pattern is depicted in *Figure 9.14*, which is in a good agreement with the experimental pattern in *Figure 9.13d.* In the case of Series SS-240, with an edge distance of 240 mm, tensile cracks are visible in the direction opposite to loading in both the tests and numerical investigations. This crack, however, developed in the post-peak phase only and can be attributed to the decreasing c_1/h_{ef} ratio compared to the series SS-80 and SS-160.

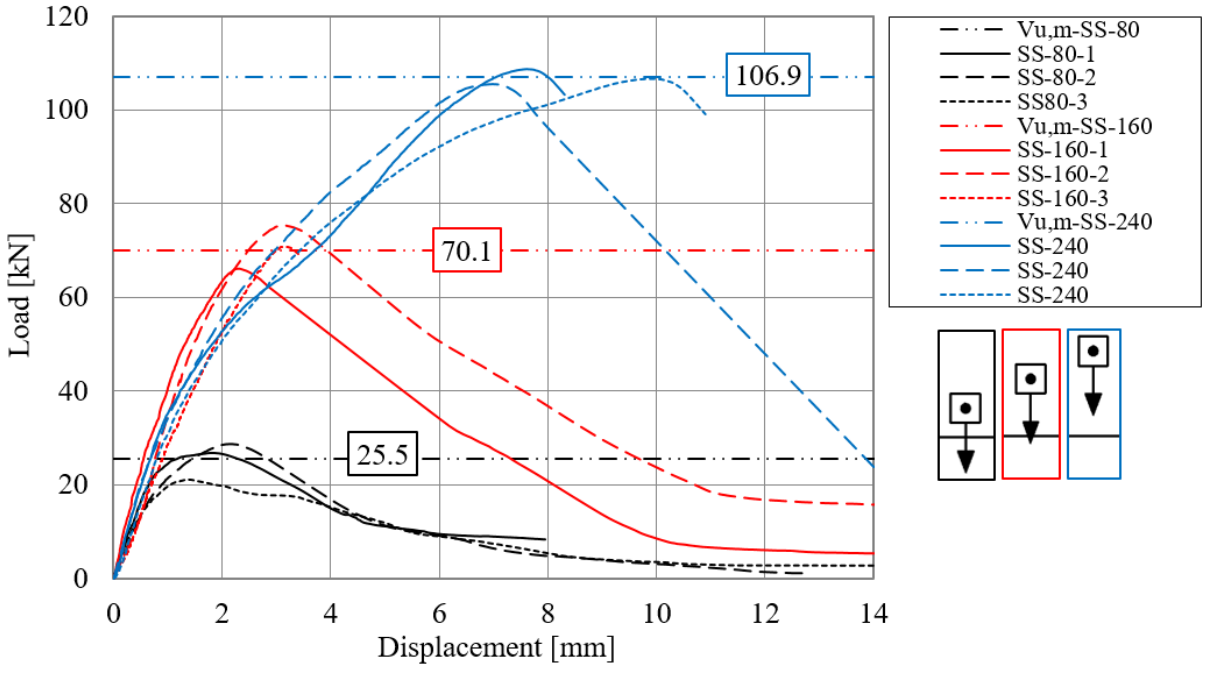

a)

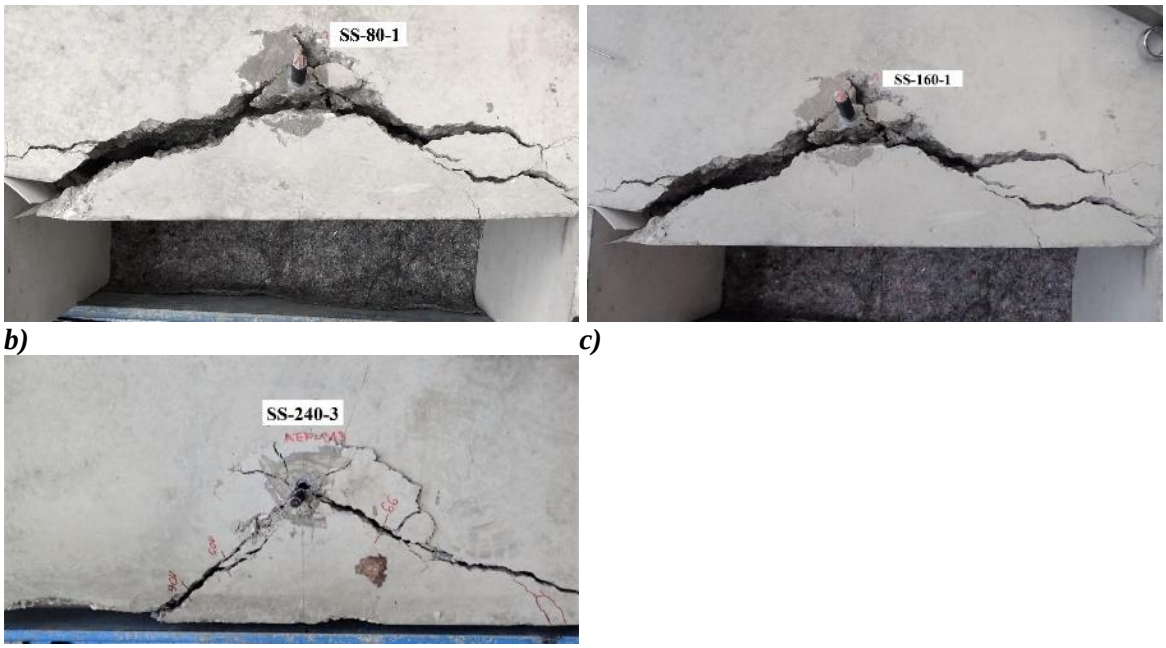

b) *c)*

d)

Figure 9.13. Test series on single anchors: a) load-displacement curves; Failure crack pattern of one representative test: b) SS-80-1, c) SS-160-1, d) SS-240-3

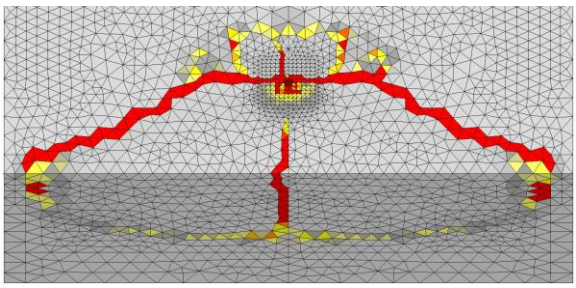

Figure 9.14. Crack pattern obtained from the numerical investigations on SS-240

9.4.1.2 Results of shear tests performed on anchor groups

Tests on groups with the equal edge distance for back anchor row ($c_{1,back}$ = 240 mm)

In the following, test results of anchor groups of 3×1 and 2×1 configurations are discussed. In both configurations, the edge distance for the back anchor row as $c_{1,back} = 240\ mm$. The anchor spacing between the anchors was $s_2 = 80\ mm$ in both cases, which resulted in the edge distance of front anchor row as $c_{11} = 80\ mm$ and $c_{11} = 160\ mm$ for 3×1 (GS-3×1-80-80) and 2×1 (GS-2×1-160-80) groups, respectively. The load-displacement curves along with the reference single anchor series SS-240 are given in *Figure 9.15*. The obtained failure loads for all three series are comparable. This can be attributed to same edge distance for the back anchor. However, it is clear that as the number of anchors in a group is increasing, the initial stiffness increases. With three anchor rows, the stiffness is 2-times, with two anchors, 1.4-times the mean stiffness of the reference series, respectively. With three anchor rows, the stiffness is approx. 2-times, while with two anchors it is, approx. 1.4-times the mean stiffness of the reference series, respectively. Note: Theoretically, the group stiffness should be equal to n times the stiffness of a single anchor, where n is the number of anchors in the group. However, due to the hole clearance and the definition of initial stiffness (secant stiffness corresponding to 50% peak load), the actual group stiffness is less than the theoretical stiffness of the group.

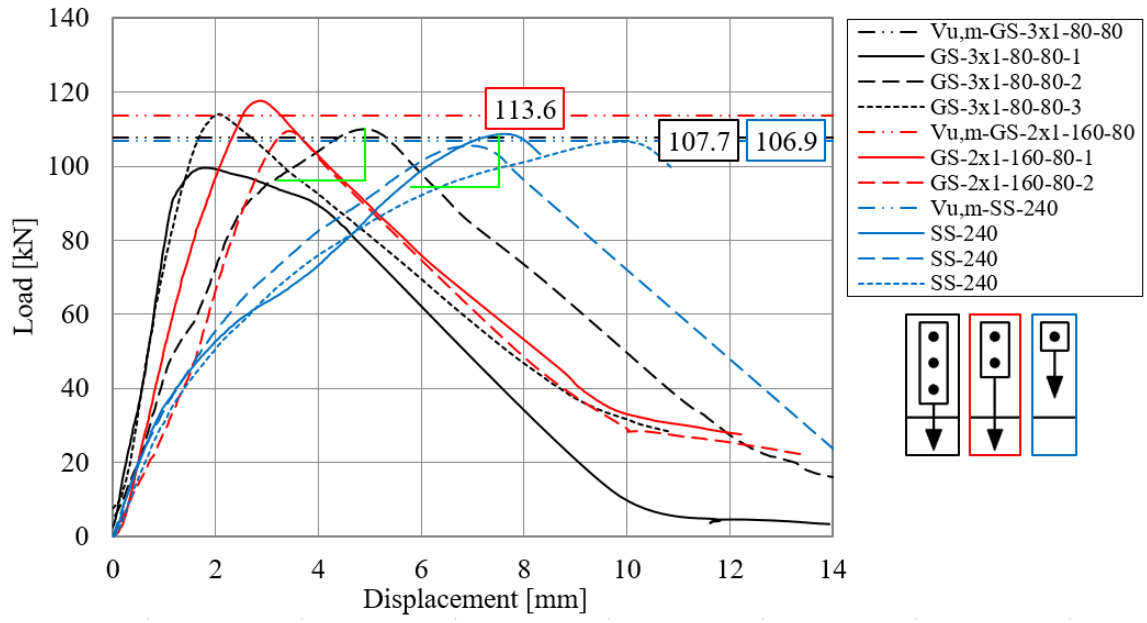

a)

b)

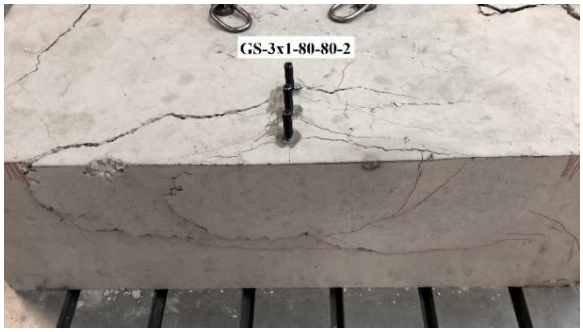

c)

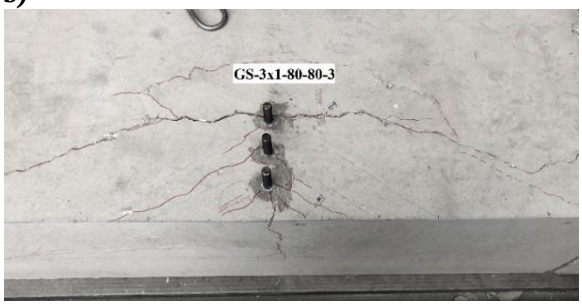

d)

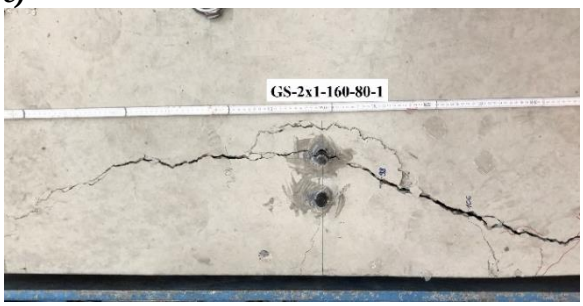

e)

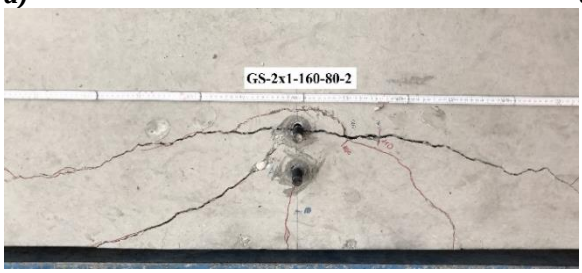

f)

Figure 9.15 a) Load-displacement curves of series GS-3×1-80-80 and GS-2×1-160-80 compared with SS-240; b)-d) failure crack pattern of series GS-3×1-80-80; e)-f) failure crack pattern of series GS-2×1-160-80

Series GS-3×1-80-80

The hole clearance pattern has a significant influence on the force distribution among individual anchors of an anchor group. Therefore, since the tests were performed with random hole clearance, the hole clearance (a gap between base plate and anchor) was measured prior to testing. For practical reasons, the measurement was carried out from the top of the base plate (see details in Section 9.2.3).

Test 1:

The measured hole clearances for anchor 1, 2 and 3 were 0, 0 and 0.7 mm respectively. In test 1, no crack was observed to be formed at the front anchor, only at the middle and back anchors (*Figure 9.15b*). Thus, in the onset of loading, anchor 1 and 2 took up the shear load; and when the applied load reached ca. 50 kN at a displacement of 0.7 mm (= hole clearance of anchor 3), the back anchor started to take up the shear loads as well. Consequently, an increase in the stiffness in the load-displacement curve can be observed. The crack at the middle anchor developed at an applied load of around 90 kN, after which the stiffness of the group reduced. The failure crack at the back anchor was observed at an applied shear load of ca. 99 kN. The ultimate load of the group was measured as 99.6 kN.

Test 2:

The measured hole clearance for anchor 1 was zero, 1 mm for the second anchor and ca. 1.5 mm for the third anchor. It can be seen very clearly from *Figure 9.15c* that in the case of test 2, almost a separate breakout body has formed at the front anchor. This can be explained by the fact that the front anchor was activated at the beginning, and there were relatively large hole clearances at the middle and back anchors, and of course, by the displacement behaviour of the single anchors of the corresponding anchor rows from the reference series. Due to zero hole clearance, the complete shear load is resisted initially by the front anchor only, resulting in a lower stiffness compared to test 1. The load-displacement curve shows a change in stiffness at an applied shear load of ca. 50-55 kN and 1.7 mm displacement. The explanation for that can be found when evaluating the group behaviour together with the load-displacement behaviour of the single anchors tested at different edge distances. The mean failure displacement for the single anchors with $c_1 = 80\ mm$ (series SS-80) was ca. 1.7 mm at the ultimate load $V_{u,m}=25.5\ kN$ (see *Figure 9.13a*). With a hole clearance of 1 mm at the second anchor, which means that when the displacement at the front anchor is 1.8 mm, the displacement at the second anchor would be 0.8 mm, which corresponds to a load of approximately 26 kN resisted by the single anchor in test series SS-160 having the same edge distance, namely 160 mm. With further evaluating the displacement behaviour of the anchorage, we can understand that at an applied displacement of 1.8 mm, anchor 3 reaches only 0.2 mm displacement (1.7 mm- 1.5 mm) due to its hole clearance of 1.5 mm. Anchor 3 has an edge distance of 240 mm, therefore the displacement behaviour of single anchor test series SS-240 is of interests. The 0.2 mm displacement corresponds to approx. 5 kN load in series SS-240. Thus, when we look at the anchor group we can see that at an applied displacement of approximately 1.7 mm, anchor 1 reaches its full capacity, which is around 25 kN, anchor 2 also takes up ca. 25 kN load and anchor 3 resists approximately 5 kN or even less. This helps to explain the first major change in the stiffness on the load-

displacement curve (*Figure 9.13a*). This is due to the failure of the front anchor at a displacement of 1.7 mm and an applied shear load of approximately 50-55 kN. Evaluating further the displacement behaviour, we can see the second loss in stiffness at ca. 91 kN applied load and 2.5 mm group displacement. This can be attributed to the failure of anchor 2, and the redistribution of further forces to the third anchor. This explanation is again possible only by comparing the load-displacement behaviour of the group with the behaviour of single anchors. Therefore, it is essential to perform the single anchor tests with the corresponding edge distances. After this, the third anchor resisted the shear load along with the residual capacity of anchors 1 and 2. The measured ultimate load in case of test 2 was 109.4 kN and the failure displacement was 5 mm. It is interesting to see that secant stiffness of the group at failure was almost identical with the secant stiffness of one single anchor with an edge distance of 240 mm (SS-240), which points out that anchors 1 and 2 had very low stiffness at the time of reaching the ultimate load of the group.

Test 3:

In the case of test 3, the hole clearance pattern was measured as zero at the front anchor, 0.5 mm at the second anchor and ca. 1 mm at the third anchor. The crack formation at all three anchors was only observed at reaching the ultimate load of the group. It can be understood that the load distribution was ideal in this test. This is not just because the highest ultimate load was reached among the tests of this series (*Figure 9.13a*) but there are further explanations. The hole clearance at the second and third anchors was smaller than the displacement at failure for the single anchor series SS-80 and SS-160:

$$a_{cl,160mm} = 0.5 \text{ mm} < \delta(V_{u,c,SS-80}) = 1.8 \text{ mm}$$

$$a_{cl,240mm} = 1.0 \text{ mm} < \delta(V_{u,c,SS-160}) = 2.5 \text{ mm}.$$

This means that the further anchor could be activated before the front or middle anchor would reach its failure displacement. Consequently, the applied shear force is distributed to more anchors. These conditions resulted in an ideal shear force distribution among the anchors so that from 1 mm applied displacement onwards, all the three anchors were loaded together, contributing assumedly with the same amount of force. This can be indicated by the progression of the load-displacement curve.

After evaluating the three tests of series GS-3×1-80-80 with three different crack patterns, we can see that in all three tests, the failure crack originated from the back anchor. However, it is important to note that cracks are also visible originating from the front and middle anchors (*Figure 9.15b-d*). The load redistribution and the crack initiation and propagation depend on the displacement behaviour of the individual anchors of the group, as well as on the actual hole clearance in the fixture. The load-displacement curves of the tests indicate a good agreement with the observed crack pattern. The cracking always causes the loss of stiffness at the particular anchor, which changes the overall stiffness of the group. This is then visible on the load-displacement curves of the anchor groups.

Calculated failure loads

The failure load was calculated according to EN 1992-4 and fib Bulletin 58. According to fib Bulletin 58, the failure crack was assumed to originate from the back row is in a good agreement with the test results. The predicted load is only 10% lower than the experimentally obtained. On the contrary, the calculation based on the EN 1992-4 assuming the failure crack originating from the front row is over-conservative due to neglecting the force redistribution to the further anchor rows and accounting for the capacity of the front anchor only.

Numerical analysis

Numerical analysis was also performed to investigate the behaviour of Series GS-3×1-80-80, however, without the influence of hole clearance. *Figure 9.16* depicts the crack pattern at ultimate load and post-peak phase. From the evaluation of the numerical results it was found that until the group reached its peak load-carrying capacity, all three anchors resisted approximately with the same amount of shear force, confirming the assumption that the shear stiffness of the anchors is independent of the edge distance. In the post-peak phase, however, the back anchor carries less shear force compared to the front anchors. This is attributed to the development of the failure crack from the back anchor row that results in the loss of shear stiffness of the back anchor.

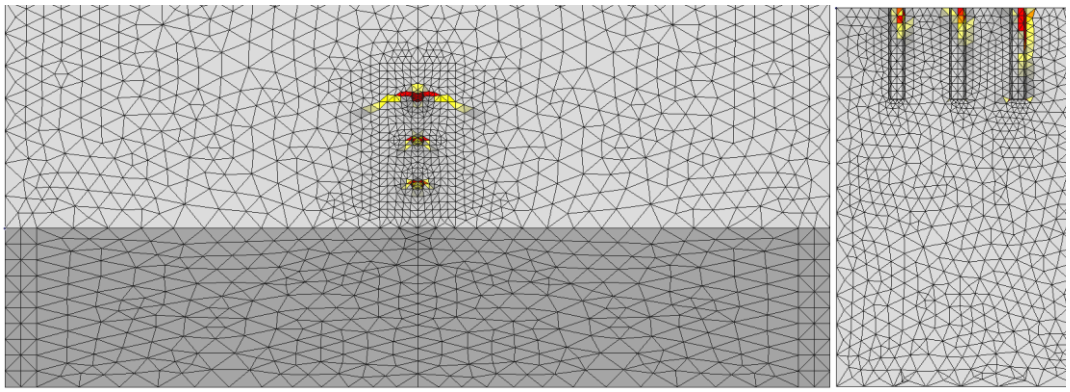

a)

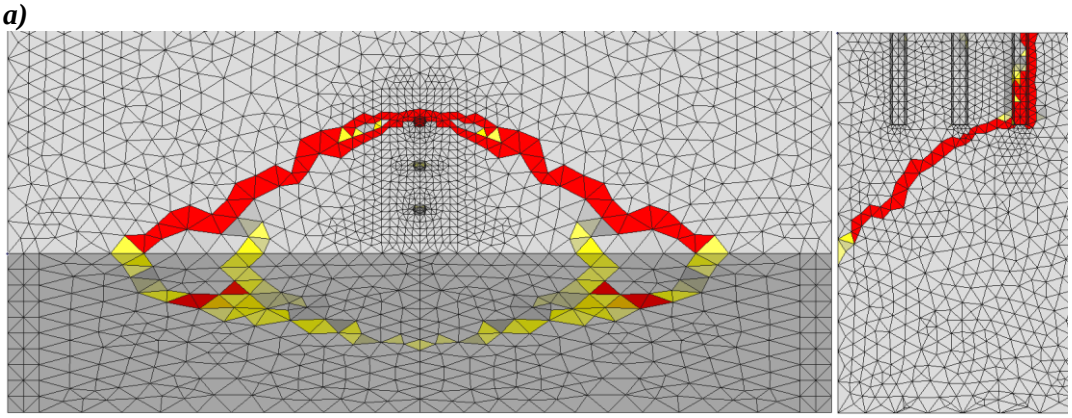

b)

Figure 9.16. Crack pattern obtained from the numerical investigations on GS-3×1-80-80 without hole clearance: a) $V=V_u$, b) Post-peak

Figure 9.16a depicts the crack pattern at ultimate load. Cracks are visible at all three anchors. However, the localization of the failure crack seems to occur at the back anchor. This is confirmed by *Figure 9.16b*, showing the crack pattern in the post-peak phase. Note that in the finite

element analysis, once the crack localizes at a certain location, the earlier formed pre-cracks might not be visible anymore. However, in the tests, once a crack forms, it cannot close. Due to this and the fact that the tests were performed with certain hole clearance, the cracks appeared at different anchor rows (*Figure 9.15b-d*), while in the finite element analysis, the failure crack localizes and propagates from back anchor row only. The numerically obtained ultimate load of the investigated group was 101.2 kN, which is just 4% lower compared to the numerically obtained single anchor result with 240 mm edge distance (105.7 kN). If we compare the measured mean experimental ultimate load (107.7 kN) with the numerically obtained ultimate load (101.2 kN), we can see that although the experiments were carried out with hole clearance and the numerical analysis without, the experimentally obtained load is just slightly (6%) higher. This again shows that for the investigated case, the hole clearance pattern has an influence on the load distribution and the displacement behaviour and that the cracking at the front anchor row(s) might have an influence on the design in SLS, but the failure crack initiates from the back row.

Series GS-2×1-160-80

In the case of test series GS-2×1-160-80 with 160 mm edge distance of the front row and 240 mm of the back row, only two tests were carried out due to limited space in the test specimens. This means that the edge distance of the back anchor is the same as in the case of series GS- 3×1-80-80. Consequently, and as it was expected, the obtained ultimate load was similar in the group tests with 2×1 configuration as that obtained with the groups of 3×1 configuration (*Figure 9.15a*). However, the stiffness was lower since instead of three, only two anchors resisted the shear force. In this series again, the hole clearance pattern was measured before testing to help the evaluation of the load-displacement behaviour of the group.

Test 1:

There was zero hole clearance measured in test 1 at both the front and back anchors. Therefore, this case can be considered as an anchor group without hole clearance and can be directly compared with the numerical analysis. The load-displacement curve in *Figure 9.15a* and the crack pattern in *Figure 9.15e* indicate that the shear force was distributed between both anchors more or less equally up to the failure load.

Test 2:

Approximately 1 mm hole clearance was measured at the front anchor and zero hole clearance at the second anchor in case of test 2. In this test, the hole clearance measured at the front anchor was smaller than the displacement at failure for the corresponding single anchor series SS-160

$$a_{cl,160mm} = 1.0 \text{ mm} < \delta(V_{u,c,SS-160}) = 1.8 \text{ mm}$$

Therefore, the load distribution was optimal. In the beginning, the back anchor was loaded and from ca.1 mm displacement onwards, both anchors were loaded together. This is also visible on the load-displacement curve, which shows an increase in the group stiffness (*Figure 9.15a*) from this point onwards. *Figure 9.15f* depicts the failure crack pattern of the tests, where no cracks are visible originating from the front anchor, and the failure crack originates from the back anchor.

Calculated failure loads

The mean calculated failure load according to fib Bulletin 58, with assuming the failure crack from the back row is 16% lower than the experimental value, which is still close to the typical scatter considered in the CCD Method for concrete edge failure (15%). The calculation based on the EN 1992-4 assuming the failure crack from the front anchor is over-conservative due to neglecting the force redistribution to the back anchor.

Numerical analysis

The numerical analysis was carried out without hole clearance. The numerically obtained crack patterns are given in *Figure 9.17*. We can see in *Figure 9.17a* that the failure crack propagates from the back anchor. First, a horizontal crack is developing to the front anchor (cross-sectional view) and then the inclined crack propagates from the front anchor to the concrete surface (*Figure 9.17b*). The obtained crack pattern is in good agreement with the experimental patterns. The evaluation of the results again showed that until peak load both the anchors carried almost equal amount of shear force. However, in the post-peak phase, the back anchor drops the load carried by it. The assumption regarding the equally distributed shear load agrees with the findings in the literature for groups without hole clearance. According to Hofmann (2004), Grosser & Cook (2009), Anderson & Meinheit (2005), Anderson & Meinheit (2007), when an anchor group is having a ratio of $s_1 / c_{1,1} < 1.0$ and it is loaded in shear perpendicular to the concrete edge, the crack origination from the front row is suppressed by the compression field, which is originating from the back anchor row.

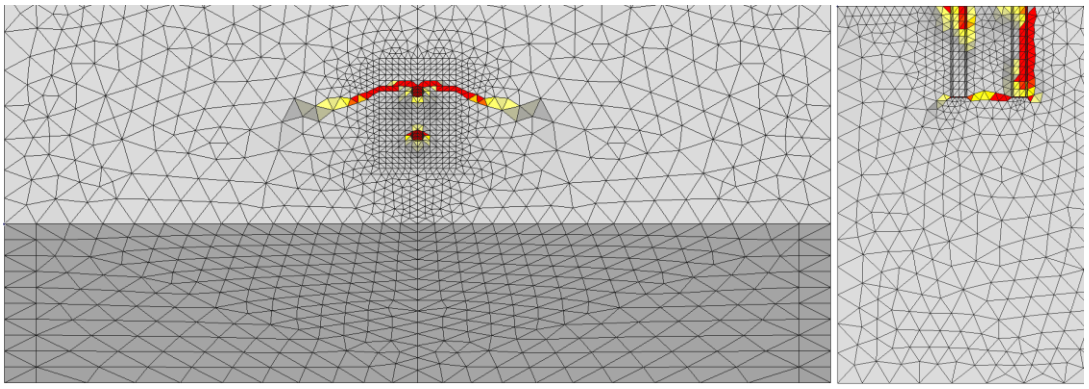

a)

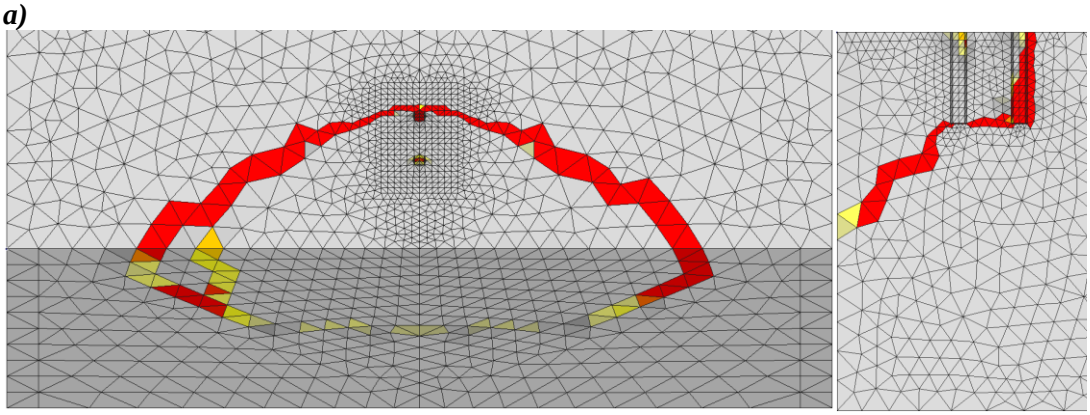

b)

Figure 9.17. Crack pattern obtained from the numerical investigations on GS- 2×1-160-80 without hole clearance: a) V=V_u, b) post-peak

9.4.1.3 Test results on anchor groups with the farthest edge distance of 160 mm Series GS-2×1-80-80

In the following, test results of anchor groups 2×1 configurations having 80 mm edge distance in the front row and 80 mm anchor spacing, resulting in an edge distance of back anchor row as 160 mm are discussed. This corresponds to a $s_1/c_1 = 1$ ratio. The load-displacement curves along with the reference single anchor series SS-160 are given in *Figure 9.18a*. We can see from *Figure 9.18b - d* that in the three performed tests, the failure crack originated from the back anchor row. In general, the stiffness of the groups is higher than the stiffness of single anchors. The mean initial shear stiffness of the groups is ca. 1.5-times the stiffness of the reference series, which is similar to that obtained in Series GS-2×1-160-80 having two anchor rows but with a back edge distance of 240 mm, again confirming the relative independence of the stiffness from the edge distance.

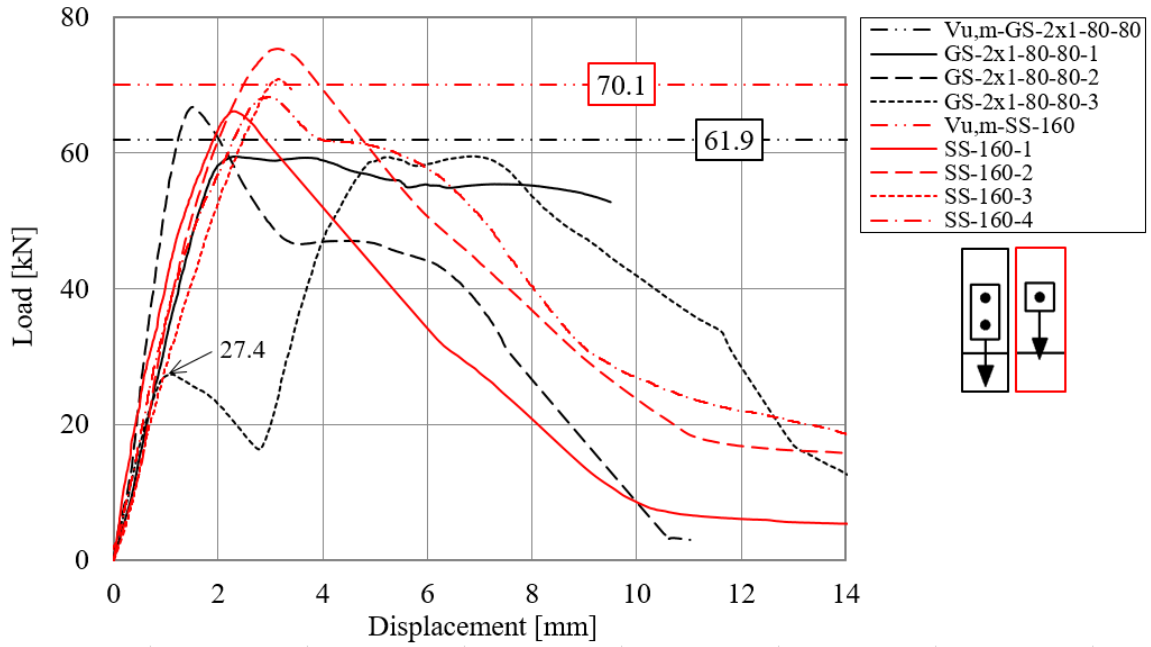

a)

b)

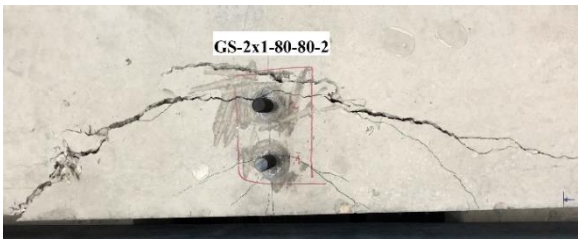

c)

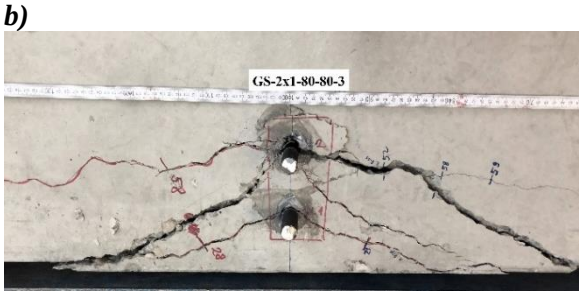

d)

Figure 9.18. a) Load-displacement curves of series GS-2×1-80-80 compared with SS-160; b)-d) failure crack pattern of series GS-2×1-80-80

Test 1:

In test 1, zero hole clearance was measured for anchor 1, and 0.5 mm for anchor 2. The front anchor was activated first and from 0.5 mm displacement, both the anchors took up the shear forces. A crack developed at the front anchor at an applied shear load at ca. 25 kN, which is approximately failure load of the single anchor tested with an edge distance of 80 mm (SS-80), and consequently, its stiffness decreased. From this point onwards, the back anchor started to take up higher forces compared to the front anchor. This is to fulfil the equilibrium: Both anchors had the same displacement because they were loaded with the same base plate and therefore the applied displacement was the same, but due to cracks at the front anchor only, the two anchors had different shear stiffness, which in the end leads to different shear forces in the anchors. The ultimate load corresponds to the failure crack originating from the back anchor. The displacement at the failure of the group was 2.3 mm, which is slightly smaller than the failure displacement measured in the reference series with 160 mm edge distance (mean value 2.7 mm). This can be attributed to the higher stiffness of the group compared to the single anchor. Compared to the mean ultimate load of the series SS-160 on single anchors, the obtained load for this group was just 4% lower, which may be due to the scatter or might be due to the slight influence of cracks at the front anchor.

Test 2:

In test 2, both the anchors were activated simultaneously due to almost zero hole clearance. Consequently, the shear load was initially distributed to both anchors equally up to ca. 80% of the failure load of the front anchor with 80 mm edge distance (compare SS-80 *Figure 9.13a*). It can be attributed to the stiffness reduction of the front anchor upon reaching ca. 80% of its ultimate load. After this, to satisfy the equilibrium, the back anchor could take up slightly higher loads until the failure of the front row was reached. The failure of the anchorage corresponds to the appearance of failure crack from the back anchor row and it is the highest among the tests of this series. This behaviour is also confirmed by the obtained crack pattern.

Test 3:

Comparing the failure pattern depicted in *Figure 9.18c* and the load-displacement curve plotted in *Figure 9.18a* – GS-2×1-80-80-1, we can understand that test 3 is a good example for anchorages having unfavourable hole clearance pattern. Both the crack pattern and the curve progression highlight that due to hole clearance, the entire shear load is taken up initially only by the front anchor. In this test, anchor 1 had zero hole clearance but anchor 2 had a relatively large hole clearance of 2 mm. This caused that initially, only the front anchor took up the shear load. The first peak in the load-displacement curve (27.4 kN and 1 mm) in *Figure 9.18a* corresponds approx. to the failure load of the front anchor (25.5 kN), and intuitively to the first cracking at the front anchor (*Figure 9.18c*). The load of 27.4 kN is just slightly higher compared to the mean failure load obtained from single anchor tests with an edge distance of 80 mm, so it is rather clear that the drop in the curve is caused by the failure of the front anchor without any contribution of anchor 2. Only when the applied shear displacement reached ca. 2 mm, anchor 2 was activated (see *Figure 9.13a*). From this point onwards, the group load corresponds to the shear force taken up by second anchor and the residual capacity of the front anchor. From

2.8 mm group displacement, the shear resistance of the group rises again. Also in this test, the peak load corresponds to the failure crack appearing from the back anchor. It is interesting to see that even if the cracking at the front was significant, the shear forces could be redistributed to the back anchor and a group ultimate load close to that in test 1 was reached. The first cracking/ first peak might limit the design for SLS, however, when the entire load-displacement behaviour of anchor groups is evaluated, a displacement criterion can be worked out.

Calculated failure loads

The calculated mean ultimate load based on the fib Bulletin 58 with assuming the failure crack from the back row is only 8% lower compared to the mean experimental value, which is a good agreement. The calculation based on the EN 1992-4 assuming the failure crack from the front anchor is over-conservative due to neglecting the force redistribution to the back anchor. However, if we see test 3, the calculated failure load according to EN 1992-4 matches well with the first peak of 27.4 kN.

Numerical analysis

The results of the numerical analysis without hole clearance are given in *Figure 9.19* in terms of crack pattern. The crack pattern and the failure load (59 kN) agrees best with the experimentally obtained results for test 2, where almost no hole clearance was measured at both anchors. Similar to the case of GS-2×1-160-80, both the anchor take up equal shear force until the peak, while force taken up by the front anchor is higher than the force taken up by the back anchor in the post-peak phase. We can see in *Figure 9.19a* that the failure crack propagates from the back anchor directly to the concrete surface (*Figure 9.19b*). The failure load obtained from the numerical analysis (no hole clearance) is in a good agreement with the mean experimental ultimate load. This again shows the importance of evaluating the load-displacement behaviour of the anchorages during the experiments. We can see the influence of the hole clearance pattern and the resulting crack pattern on the curve progression.

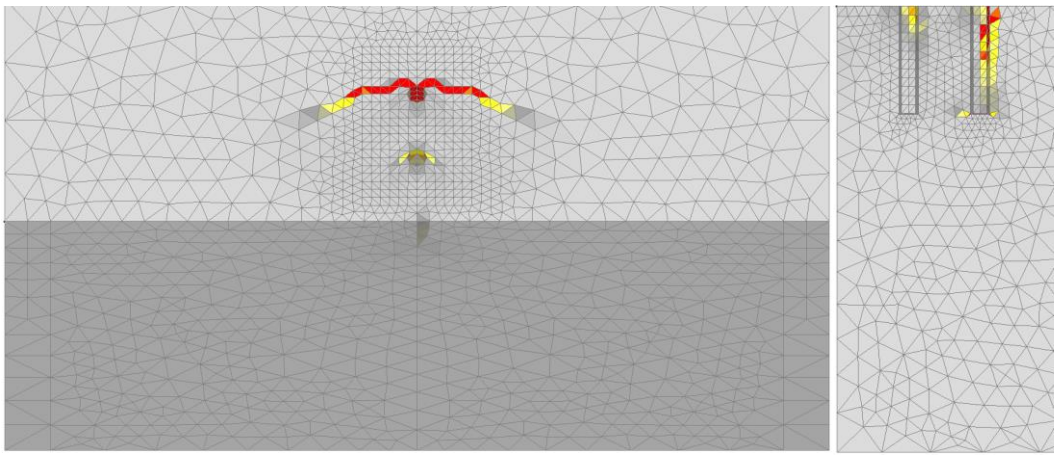

a)

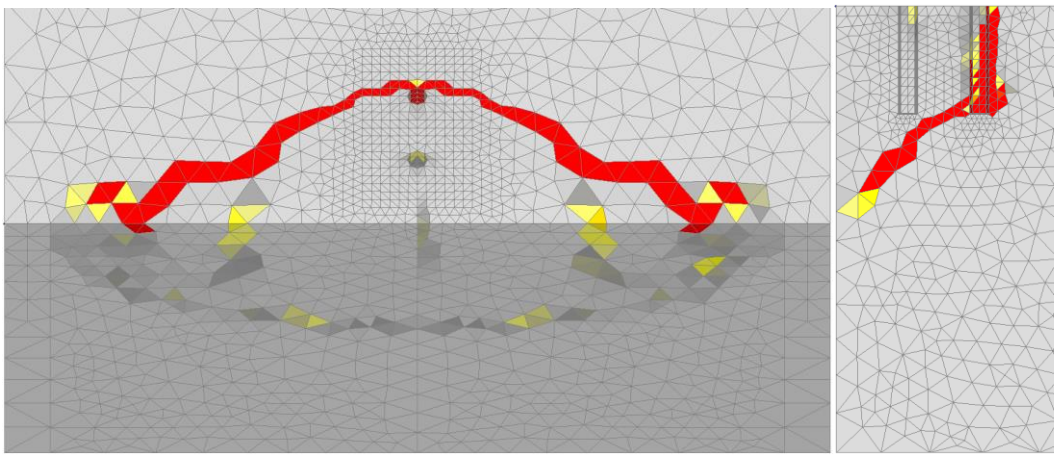

b)

Figure 9.19. Crack pattern obtained from the numerical investigations on GS-2×1-80-80 without hole clearance: a) V=Vu, b) post-peak

9.4.1.4 Test series on single anchors with recess

The tests series on single anchors with recess were carried out to investigate the influence of a "missing" concrete breakout body in front of a single anchor, without the influence of cracks and stress disruption on the behaviour of the tested single anchor. Series SS-160-r80 and SS- 240-r160 correspond to the experiments performed on single anchors at an edge distance of 160 mm and 240 mm, respectively with the corresponding recess of 80 mm and 160 mm in the front according to *Table 9.1* and *Figure 9.1*.

Test series SS-160-r80

The load-displacement curves of series SS-160-r80 are given in *Figure 9.20a*, along with the curves obtained from single anchor tests having the same edge distance but without recess (SS- 160). The test results show that the presence of a recess in front of the anchor has no significant influence on either the ultimate resistance or the stiffness of the single anchor. This can be explained by the fact that the recess in the concrete does not affect the breakout surface of the tested anchor, and the stress distribution in the load transfer area of the tested anchor is not disturbed. However, it can be observed that the displacement at failure is slightly higher compared to the reference tests. Consequently, also the secant stiffness at ultimate load has decreased but not considerably. The failure crack patterns of the four tests are given in *Figure 9.20b-d*. The figures show that in every case, the failure crack propagates to the support, parallel to the recess and the depth of the breakout body was measured as ca. 1.5-times the edge distance of the tested anchor. In principle, the failure crack propagates parallel to the surface of the recess and forms a concrete edge breakout body. Note that in Test 4 (*Figure 9.20e*), cracks parallel to the recess, as well as secondary tension cracks behind the anchor are visible, which developed due to the uplift of the base plate (rotation unrestrained loading). However, these secondary cracks developed in the post-peak phase.

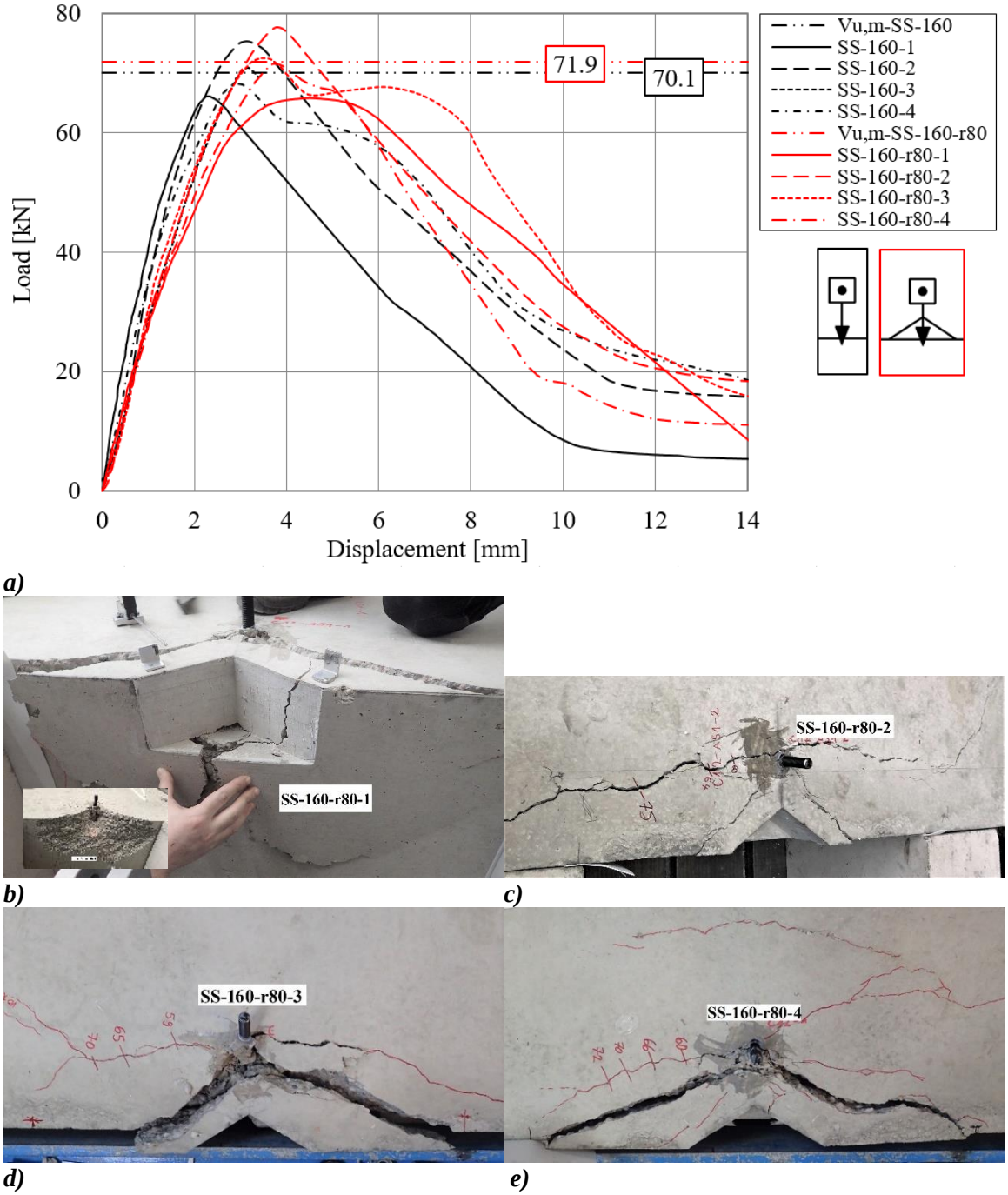

Figure 9.20. Comparison of reference tests on single anchors with tests with recess: a) load-displacement curves; Failure crack pattern of: b) SS-160-r80-1, c) SS-160-r80-2, d) SS-160-r80-3

Test series SS-240-r160

In test series SS-240-r160, no significant influence of the recess is observed on the load-displacement behaviour of the anchors (*Figure 9.21a*). The mean ultimate load is very similar to the ultimate load reached in the reference series with 240 mm edge distance (SS-240). Furthermore, the initial stiffness is in good agreement with the reference tests. This confirms that also in this configuration, at the time when the ultimate load is reached, the stress distribution in the

anchor load transfer zone is not disturbed. The failure pattern of the tests is depicted in *Figure 9.21b-d*. Again, the failure cracks run parallel to the surface of the recess. In series SS-160-r80 and SS-240-r160, single anchor tests were carried out with a recess corresponding to the theoretical breakout body of an anchor in the front ($c_{1,front}$ = 80 mm and $c_{1.front}$ = 160mm) showed that the presence of a recess in front of the anchor has no significant influence on either the ultimate load or the shear stiffness of the investigated single anchor. This can be attributed to the fact that the concrete recess does not affect the breakout surface and the stress distribution in the load transfer area of the anchor is not disturbed.

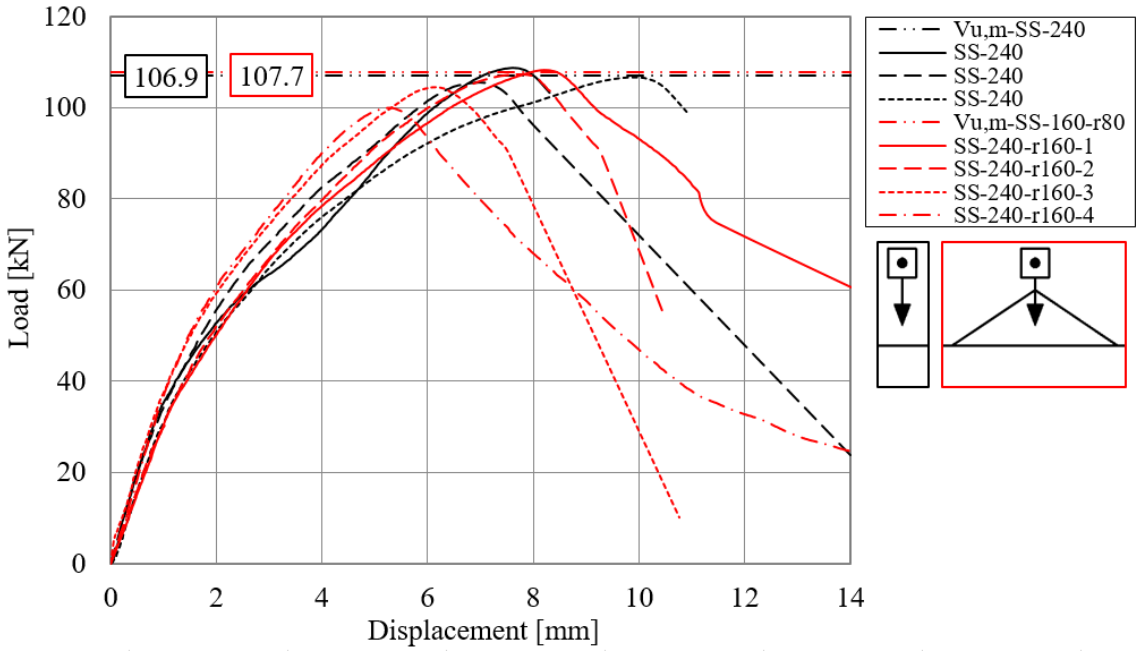

a)

b)

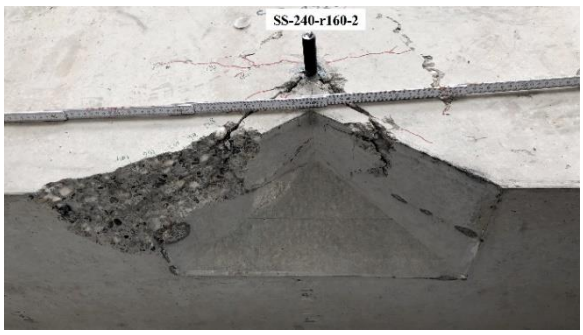

c)

d)

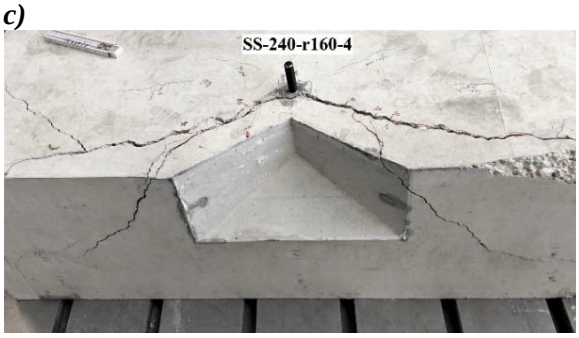

e)

Figure 9.21. Comparison of reference tests on single anchors with tests with recess: a) load-displacement curves; Failure crack pattern of: b) SS-240-r160-1, c) SS-240-r160-2, d) SS-240-r160-3, e) SS-240-r160-4

9.4.1.5 Test series in pre-damaged concrete specimen

The test series in pre-damaged concrete specimens investigated within this work simulates an anchor group, where the back anchor resists forces after the front anchor has already completely failed. Five tests were carried out in test series SS-240-a160 on single anchors with an edge distance of 240 mm. Note that the individual tests in this series are not directly comparable with each other because the initial conditions of both the concrete specimen and the anchorage zone were different, based on the pre-damage of the concrete. Before installing the single anchor at an edge distance of 240 mm, tests with an edge distance of 160 mm have been already carried out. Before the installation and performing the new tests, the breakout body was removed and the anchors were installed only in the location, where no damage was visible at the concrete surface. This has determined basically, after which tests these investigations can be performed. The new tests were carried out after tests on 2×1 anchor groups (GS- 2×1-80-80), single anchors (SS-160) and single anchors with a recess in the front (SS-r80). A typical example is given in *Figure 9.22* showing the pre-damaged condition with a new anchor installed at 240 mm edge distance behind the failure surface of a 2×1 anchor group, namely GS-2x1-80-80-2. We can see that the breakout body of the prior test is completely removed and we can assume the stress disturbance in the load transfer area.

Figure 9.22. Pre-damaged concrete condition with a new anchor installed at 240 mm edge distance behind the failure surface of a 2×1 anchor group, GS-2x1-80-80-2

To enable the comparison of the load-displacement behaviour of the discussed series with the corresponding reference single anchor series (SS-240), the load-displacement curves are plotted in one graph in *Figure 9.23a*. As it was expected, the scatter of the ultimate loads in this series is large. The reached ultimate loads are between 40.7 and 78.1 kN, and the mean value was obtained as 54 kN. To take the two extremes, the lowest value corresponds to $0.38V_{u,m(SS\text{-}240)}$, and the highest value corresponds $0.73V_{u,m(SS\text{-}240)}$. This large scatter in the test results is due to the fact that the "residual" resistance of the anchor depends on the pre-damage in the concrete. Although it is not visible on the concrete surface, the concrete behind the anchor gets certain damage owing to the lateral tensile stresses generated due to the applied loading on the previously tested anchor. The amount of damage varies from case to case and is not quantifiable, only visual assessment was done. As mentioned above, some tests were carried out after a single anchor test, others after a group test or after a single anchor test with recess. It can be inferred that the cases with larger damage to the concrete resulted in lower values of resistance for this series and vice-versa. The failure crack patterns of the investigated anchors are depicted in *Figure 9.23b-f*.

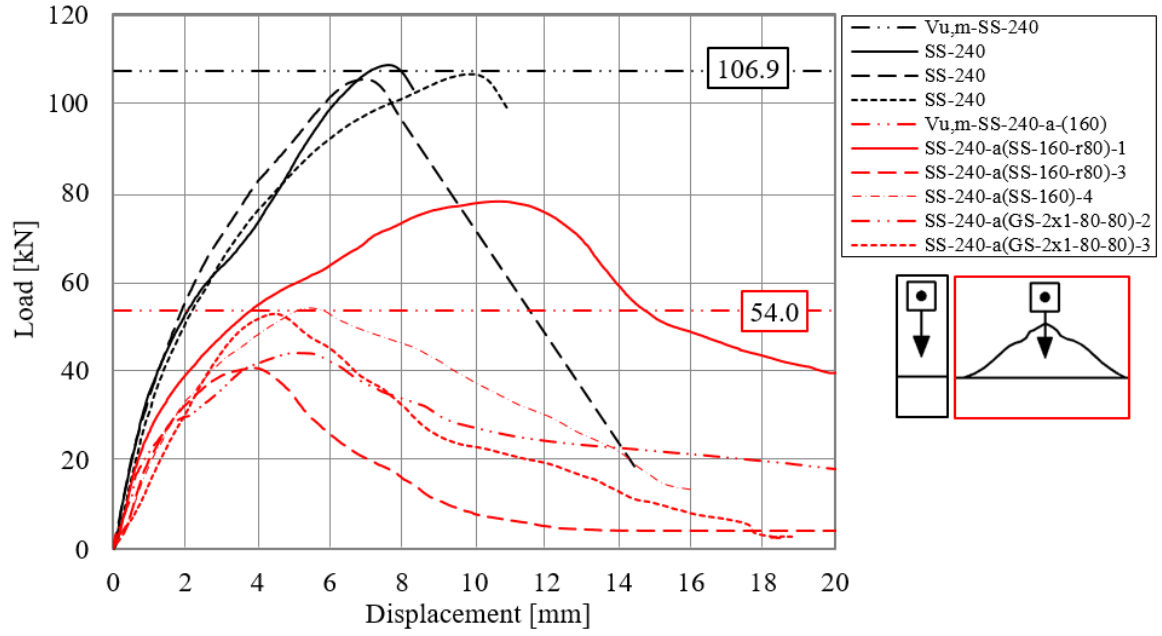

a)

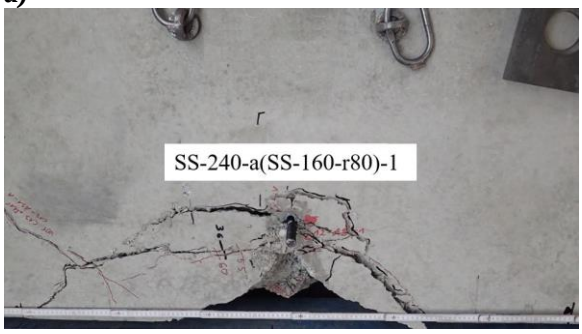

b)

c)

d)

e)

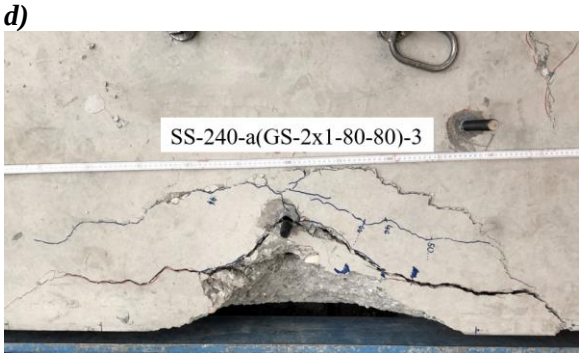

f)

Figure 9.23. Comparison of reference tests on single anchors with tests in pre-damaged concrete: a) load-displacement curves; b)-f) failure crack pattern of series SS-240-a(160)

If we evaluate the distance between the ”new anchor” and the recess, which was created due to pre-damage, it is at least 80 mm in all cases. However, the obtained failure load was in all cases higher than the failure load corresponding to the failure of the anchor with 80 mm edge distance (compare series SS-80). This is attributed to the fact that the concrete breakout surface was larger in this case. The mean initial stiffness in series SS-240-a(160) was obtained as 16.2 kN/mm, which is 62% of the stiffness of the reference series (SS-240). The 38% loss of stiffness can be attributed to the cracked concrete condition since it is assumed that for static cracks of ca. 0.3 mm width, the concrete breakout resistance of the anchors reduces by ca. 30% compared to the resistance of the anchors in uncracked concrete. The results obtained in series SS- 240- a(160) highlight a major difference between the behaviour of anchors with a recess created due to damage of the previously loaded anchor and with a recess created by concrete casting and justify the use of the volume approach for calculating the shear spring characteristics as explained in Chapter 6.

For the calculation of the residual capacity of the back anchor row in case of 2×2 anchor groups, a calculation approach is given in Unterweger et al. (2008). The calculated failure load based on the recommendations given in Unterweger et al. results in 0.55·97.9 kN = 53.8 kN, which is in a good agreement with the mean value of the experimental results; however, higher than the smallest values obtained. Therefore, it is not conservative and cannot be generalised.

Numerical analysis

In addition to the experiments, numerical analysis was carried out according to Section 9.3.4, analysis type 2. Two single anchors were modelled without connecting them by a common base plate and the load was applied in two phases. In the first phase, the shear load was applied on the front anchor only. The front anchor reached a peak load of 72.4 kN. The corresponding crack pattern is depicted in *Figure 9.24a*. Then, it was loaded further in the post-peak phase until 43.6 kN residual capacity (*Figure 9.24b*). This is the “damage level”, after which, in the second phase, the loading point was moved from the front anchor to the back anchor, and it was loaded until failure, while the stress disturbance and crack pattern caused by the failure of the front anchor remained during the analysis, and affected the behaviour of the back anchor. *Figure 9.24c* shows the crack pattern at $V_{u,num}$ of the back anchor and *Figure 9.24d* in the post-peak phase. From the failure crack pattern, we can see that the failure crack could not develop in full size, parallel to the prior crack caused by the failure of the front anchor. Instead, the failure crack merged with the existing prior crack. This is clearly visible not just from the top view but also from the cross-sectional view in *Figure 9.24d.* The crack pattern suggests that the back anchor behaved as if it only had 80 mm edge distance (= anchor spacing). This is one of the reasons why the “residual” load of the back anchor was just 24.6 kN, which is only 60% of the smallest value reached in the experiments. The obtained 24.6 kN is comparable with the failure load reached in the numerical investigation for single anchors having 80 mm edge distance (25.5 kN). The further explanation is that in the numerical analysis, the loading conditions and the supports were perfect as designed, and the breakout body developed at the front anchor was also a fully developed breakout.

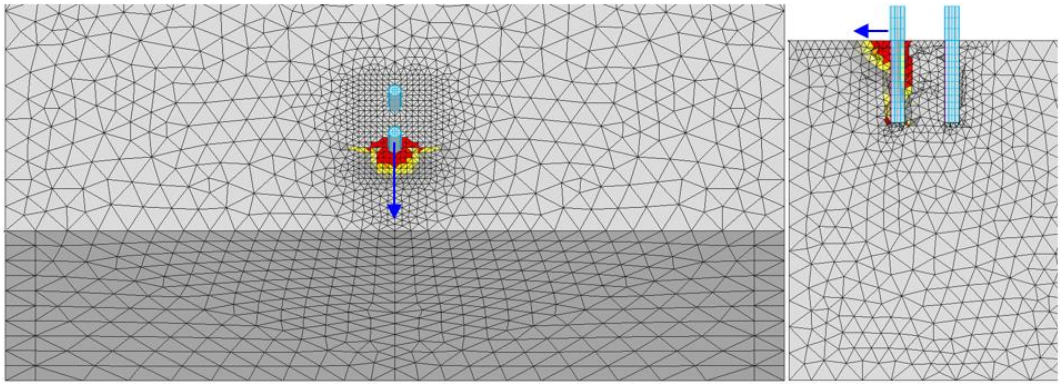

a)

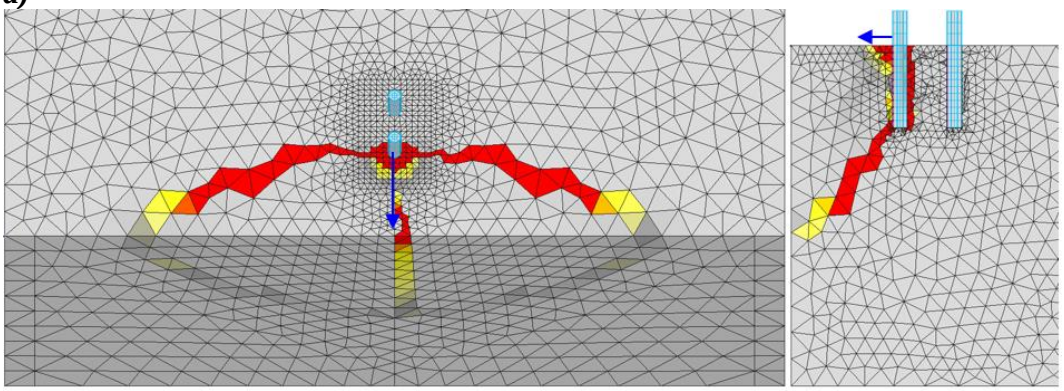

b)

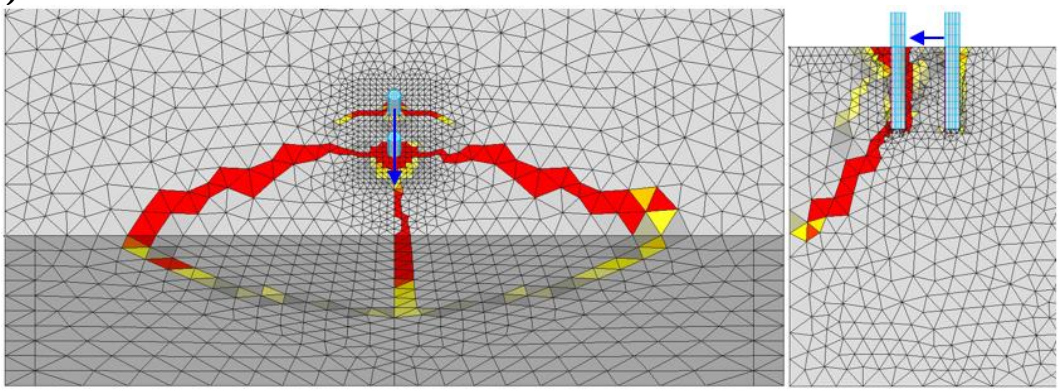

c)

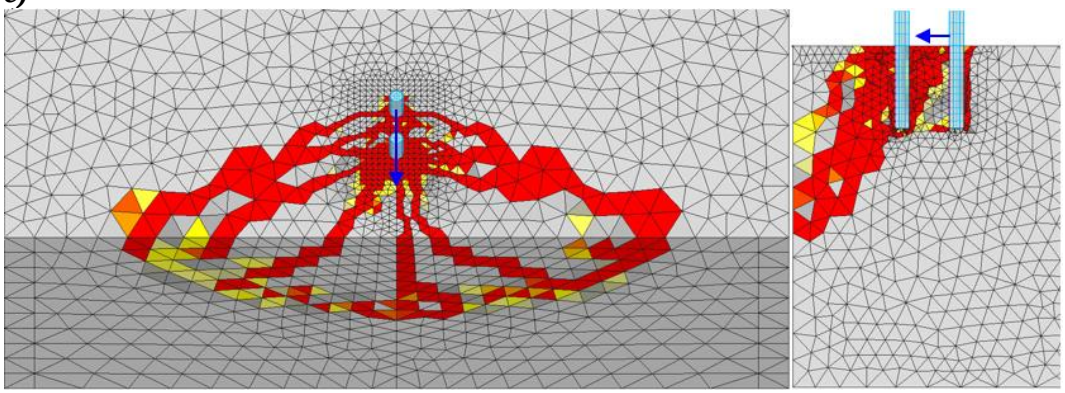

d)

Figure 9.24. Crack pattern obtained from the numerical investigations on single anchor tests in pre-damaged concrete SS-240-a(160): a) $V=V_u$ of front anchor, b) Post-peak of front anchor, c) $V=V_u$ of back anchor, d) Post-peak of back anchor

Note that the obtained 72.4 kN failure load for the front anchor is slightly higher than the failure load obtained for series SS-160 with the same edge distance. This can be attributed to the different mesh because the back anchor was also modelled, and the presence of the back anchor rod might have also slightly influenced the behaviour of the front anchor. However, in the numerical analysis, it was not possible to "install" the back anchor later like in the experiments"

9.4.2 Triangular and hexagonal anchorages in uncracked concrete loaded perpendicular to the concrete edge

Four test series were performed according to *Table 9.2* to investigate the behaviour of anchor groups of triangular and hexagonal configurations. Furthermore, for every edge distance corresponding to each anchor within a particular anchor group, reference tests were carried out to enable the evaluation of the individual anchor contribution based on the single anchor behaviour. In addition, numerical investigations were performed to see the difference between anchorage behaviour with random hole clearance (tests) and without hole clearance (numeric). Furthermore, the ultimate load of the anchorages was calculated by extending the current recommendations given in EN 1992-4 and fib Bulletin 58. The assumed crack initiation is depicted in *Figure 9.25*.

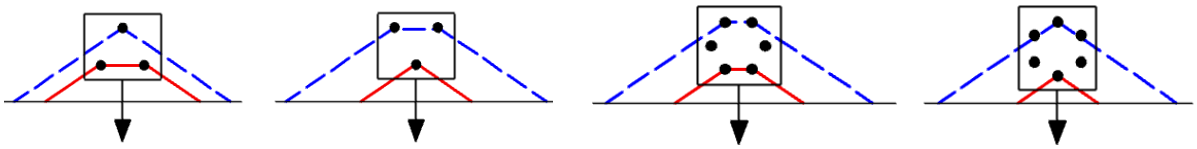

Figure 9.25. Failure crack initiation assumed on the basis of EN 1992-4 (red solid lines), Failure crack initiation considered from back row assumed on the basis of fib Bulletin 58 (blue dashed lines)

It was aimed to show that the current design might yield illogical results in such cases when the number of anchors in a row is different e.g. triangle configuration with one or two anchors in the front row. The summary of the test results in terms of the mean value of the ultimate shear loads ($V_{u,m}$) and the mean value of the initial shear stiffness ($k_{1,m}$) is given in *Table 9.6*. The load-displacement curves corresponding to the discussed series and the failure crack patterns are given in the following sub-sections, in *Figure 9.26* - *Figure 9.30*. The numerically obtained ultimate loads are tabulated in *Table 9.7*. Furthermore, the force distribution among the anchors was analysed in the numerical analysis for a better understanding of the behaviour of anchor groups. The results of the analyses on GS- TRI- A, GS-TRI-B and GS-HEX-A in terms of failure crack patterns are shown in *Figure 9.28*, *Figure 9.29* and *Figure 9.31*. Note that the crack pattern obtained from the numerical investigations correspond to the crack pattern in of that particular loading step, and the cracks, which were developed during the load distribution from row-to-row may not be visible.

Table 9.6. Test results of single anchors and anchor groups of triangular and hexagonal configurations loaded perpendicular to the edge

Test series ID	Meas. mean ultimate load [b]	Normalised mean ultimate load	Mean value of initial stiffness	Calc. mean concrete edge res. [c]		Calc. mean concrete edge res. [d]	
	$V_{u,m}$	$V_{u,m}$* [a]	k_1	$V_{Rm,c,EN}$	$V_{u,m}$*/ $V_{Rm,c,EN}$	$V_{Rm,c,fib}$	$V_{u,m}$*/ $V_{Rm,c,fib}$
	[kN]	[kN]	[kN/mm]	[kN]	[-]	[kN]	[-]
SS-100	36.7	36.7	25.7	28.2	1.30	28.2	1.30
SS-120 [a]	43.4	41.5	31.1	35.5	1.17	35.5	1.17
SS-170	71.0	71.0	37.6	55.8	1.27	55.8	1.27
SS-200	83.6	83.6	31.2	69.2	1.21	69.2	1.21
SS-240b [a]	93.8	89.7	34.9	88.1	1.02	88.1	1.02
GS-TRI-A	80.1	80.1	77.5	49.2	1.63	88.1	0.91
GS-TRI-B	111.3	111.3	69.1	35.5	3.13	105.1	1.06
GS-HEX-A	106.2	106.2	74.2 (91.6)	36.0	2.95	97.9	1.09
GS-HEX-B	92.4	92.4	85.9	21.3	4.34	88.1	1.05

[a] The tests were performed in a different concrete batch compared the other tests, therefore, to allow a direct comparison of the results, the mean ultimate load was normalised with respect to the concrete compressive strength: $V_{u,m}* = V_{u,m}\,(25.2/27.6\,)^{0.5}$.
[b] Crack initiation depends on actual hole clearance and load distribution
[c] Calculation based on EN 1992-4, crack initiation assumed from front anchor row
[d] Calculation based on fib Bulletin 58, crack initiation assumed from back anchor row

Table 9.7. Test results of anchor groups of triangular and hexagonal configurations with hole clearance loaded perpendicular to the edge compared to numerical results obtained on anchorages without hole clearance

Test series ID	Mean ultimate load	Numerically obtained ultimate load	$V_{u,m}/V_{u.num}$
	$V_{u,m}$	$V_{u,num}$	
	[kN]	[kN]	[-]
GS-TRI-A	80.1	105.7	0.76
GS-TRI-B	111.3	120.0	0.93
GS-HEX-A	106.2	113.7	0.93

9.4.2.1 Reference tests

To enable the evaluation of the individual anchor contribution based on the single anchor behaviour, reference tests were carried out on single anchors according to *Table 9.2* with 100, 120, 200 and 240 mm in test series SS-100, SS-120, SS-200 and SS-240b, respectively. The edge distances for the reference tests were selected based on the edge distances of the anchor rows in case of the tested groups. The load-displacement curves of the reference tests are given in *Figure 9.26a*.

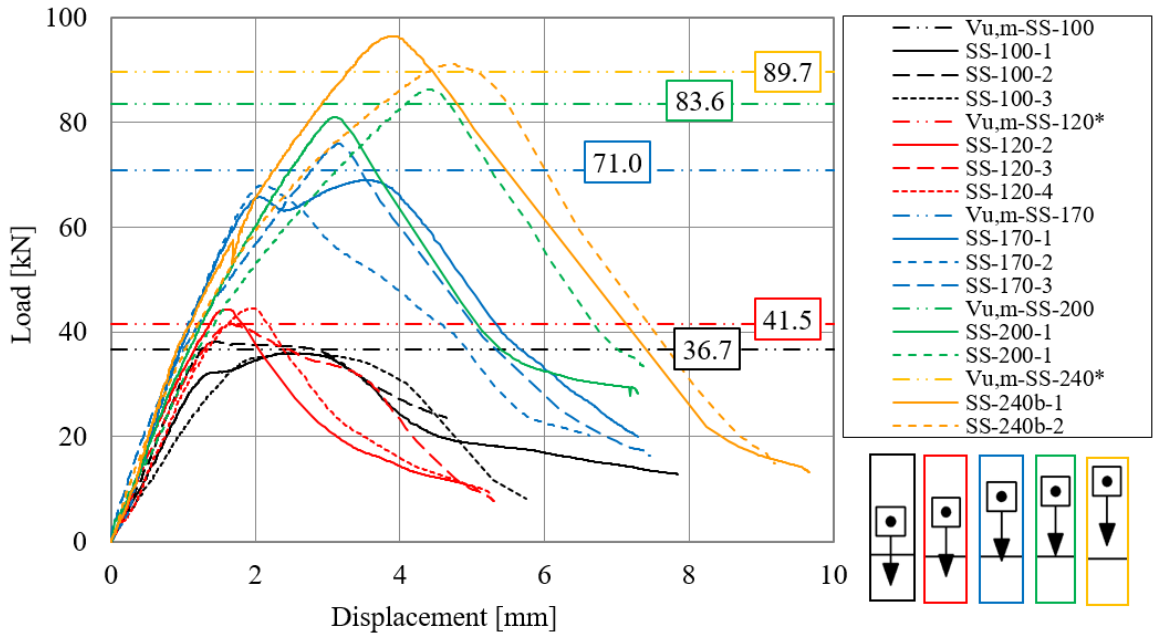

a)

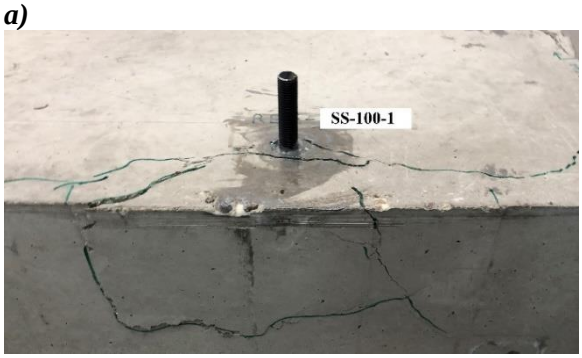

b)

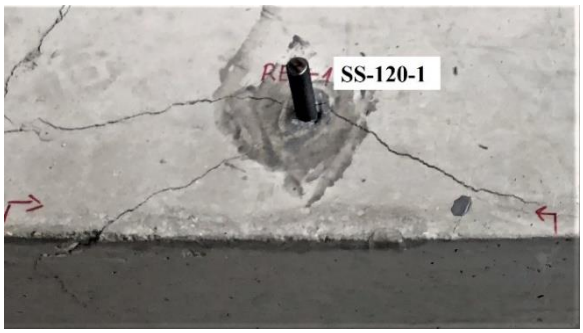

c)

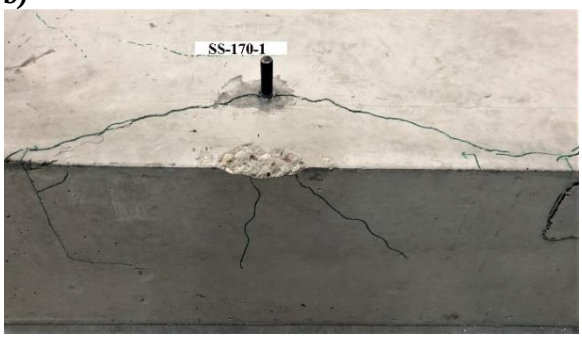

d)

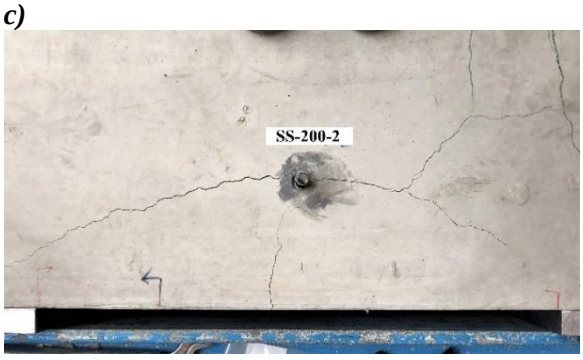

e)

Figure 9.26. Test series on single anchors: a) load-displacement curves; Failure crack pattern of a representative test: b) SS-100, c) SS-120, d) SS-170, e) SS-200

As expected, the ultimate loads increased with increasing edge distance. The initial stiffness $k_{1,m}$ of the corresponding series SS-100, SS-120, SS-200 and SS-240 were obtained as 25.7, 31.1, 37.6, 31.2 and 34.9 kN/mm, respectively, which corresponds to a mean value of 32.1 kN/mm. The value of 32.1 is comparable with 29.9 kN/mm measured in the single anchor test series according to *Table 9.4*. Therefore, again, we can consider the initial shear stiffness as relatively independent of the edge distance. In the case of the reference tests, the failure crack pattern of only one representative test per series is depicted in *Figure 9.26b-e*. The failure cracks correspond to the typical concrete edge breakout crack pattern. The experimental results in terms of mean ultimate loads were always higher than the values calculated according to the EN 1992- 4 and fib Bulletin 58 (for single anchors both the models are essentially the same), however, still in reasonable agreement.

9.4.2.2 Triangular configuration

Shear loading tests and numerical analyses were performed for anchor groups with three anchors arranged in a triangular pattern close to the concrete edge in series GS-TRI-A and GS-TRI- B. The same base plate was used in both the tests and the edge distance of the anchor rows were also maintained the same in both test series. In case of series GS-TRI-A, the arrangement was such that two anchors were installed in the front row and one anchor in the back row; whereas, in the case of series GS-TRI-B, one anchor was installed in the front row and two anchors in the back row (*Figure 9.2*).

These configurations are not covered explicitly in the current design approaches. However, if we extend the current approach of EN 1992-4 by simply considering the failure crack appearing from the front anchor row, the approach results in higher concrete edge breakout resistance for the configuration with two anchors in the front row (Case A) compared to that for Case B. This is because the projected area for case A is higher than case B. According to the approach of fib Bulletin 58, the failure crack can be considered to appear from back anchor row and therefore the calculated failure load for the configuration with two anchors in the back row (case B) results in higher concrete edge resistance than calculated for case A. Furthermore, the failure load calculated according to the approach given in fib Bulletin 58 results in much higher concrete edge resistance (+80%) compared to the approach given in EN 1992-4. The assumption of the appearance of a failure crack from the front ‘or’ back anchor row is necessary due to the projected area approach according to the CCD method and can be rather confusing from the design engineer point of view. However, as will be shown later, by the consideration of the volumes (instead of areas) in the spring model, such a pre-judgement becomes unnecessary.

The corresponding load-displacement curves obtained from the tests for GS-TRI-A and GS- TRI-B and the failure crack patterns are depicted in *Figure 9.27*. It is interesting to see that the initial stiffness of the groups is relatively independent of the arrangement of the anchors. This can be explained by the fact that the total number of anchors is the same for both series, and the shear stiffness is almost independent of the edge distance.

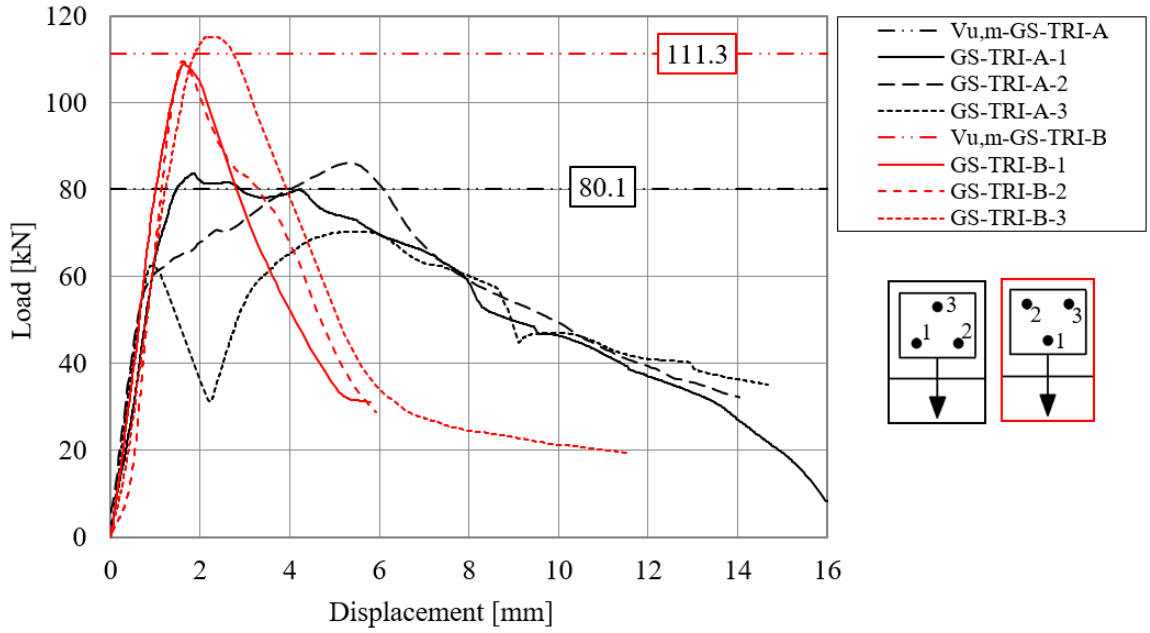

a)

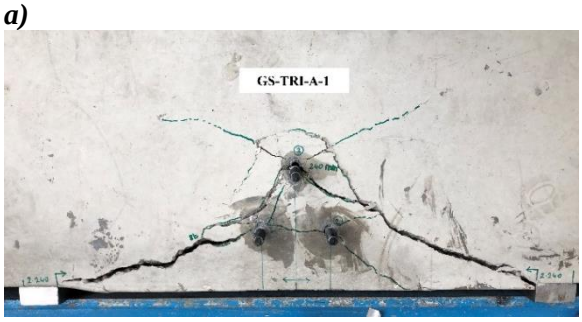

b)

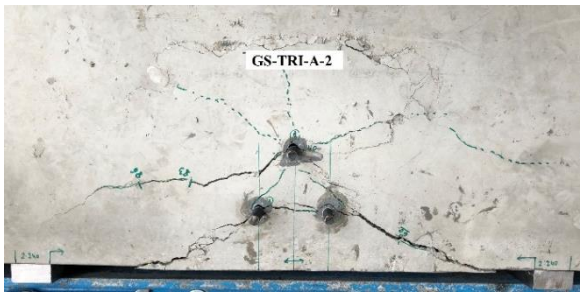

c)

d)

e)

f)

g)

Figure 9.27. Test series with triangular configuration: a) load-displacement curves; Failure crack pattern of test: b) GS-TRI-A-1, c) GS-TRI-A-2, d) GS-TRI-A-3, e) GS-TRI-B-1, f) GS-TRI-B-2, g) GS-TRI-B-3

GS-TRI-A

Test series GS-TRI-A was performed on triangular anchor groups having two anchors in the front row ($c_{1.1} = 120$ *mm*) and one anchor in the back row ($c_{1.2} = 240$ *mm*). The hole clearance configuration was random. The measured hole clearance pattern is tabulated in *Table 9.8*, which should help to evaluate the test results and understand the group behaviour better.

Table 9.8. Hole clearance pattern of series GS-TRI-A

	Test ID	$a_{cl.1}$ mm	$a_{cl.2}$ mm	$a_{cl.3}$ mm
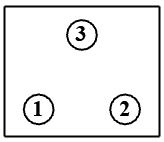	GS-TRI-A-1	1.0	0	0
	GS-TRI-A-2	0	0	1.0
	GS-TRI-A-3	0	0	1.5

Test 1:

The hole clearance pattern was measured as 1 mm for anchor 1, and 0 mm for anchors 2 and 3. This is reflected in the curve progression and crack pattern in *Figure 9.27a* and *b*. During testing, it was observed that initially, the crack originates from anchor 2 and anchor 3, whereas the crack at anchor 1 develops only together with the crack from anchor 3. An increase in the stiffness can be observed in the load-displacement curve at ca. 70 kN applied load and 1.1 mm applied displacement. This suggests that anchor 1 got active after exceeding the hole clearance. The obtained failure load in test 1 is 10% lower compared to the single anchor series SS-240b with 240 mm edge distance. The measured initial shear stiffness is 2.4-times the mean stiffness measured in the single anchor series.

Test 2:

As *Table 9.8* shows, zero hole clearance was measured for the anchors in the front row, and 1 mm for the back anchor in the case of the second test of series GS-TRI-B. Consequently, anchors 1 and 2 in the front row were loaded first and equally, and anchor 3 in the back row had ca. 1 mm gap and it was activated later. The influence of the hole clearance pattern can be indicated both in the load-displacement curve and in the developed crack pattern in *Figure 9.27a* and *c*. The crack at the front row was observed when the group reached ca. 60-65 kN applied load and 1 mm applied displacement. A change in stiffness is also visible on the load-displacement curve. This can be attributed to the fact that when anchor 3 started taking up higher forces, anchors 1 and 2 at the front had already much lower stiffness and were in the post-peak phase. Furthermore, the stiffness of the anchor 3 was strongly influenced by the cracks, which developed prior at the front anchors. *Figure 9.27c* shows that the failure crack from the back anchor went parallel to the previous cracks, and joined partly the cracks developed from the front row. The secondary tensile cracks at the side opposite to loading direction have developed due to the uplift of the base plate, however, only in the post-peak phase of the group. The failure load, as well as displacement at the peak load, are in good agreement with the results of the reference tests on single anchors with 240 mm edge distance (SS-240b).

Test 3:

The third test is a typical example of an unfavourable hole clearance pattern. Anchors 1 and 2 in the front row had zero hole clearance and were activated immediately when the load was applied but anchor 3 was activated only after a displacement of 1.5 mm, due to the hole clearance ($a_{cl.3} = 1.5\ mm$). This is visible also on the curve progression in *Figure 9.27a* and on the crack pattern in *Figure 9.27d*. The first peak of the group was reached when the anchors in the front row failed at ca. 62.5 kN and an applied displacement of 0.9 mm. From this point onwards, crack widening at the front row started $\Delta w = 0.4\ mm$ and reached a value of $\Delta w = 1.4\ mm$ until the third anchor in the back was activated. When anchor 3 started taking up shear force, the group resistance increased again, and the crack widening slowed down. The ultimate load for the group was measured as 70.4 kN, which is considerably less compared to the reference series (SS240b). This can be attributed to the presence of wide cracks at the front row. Furthermore, the failure load is ca. 20% smaller compared to the tests 1 and 2. This is again due to the significant cracking at the front. It is worth noting that the width of the cracks from the front anchor row measured at the failure load was equal to the group displacement. This test highlighted that the pronounced cracking at front anchor had a big influence on the load distribution to the back anchor and the load-displacement behaviour of the entire group. This result shows a good agreement with the findings of Grosser and Cook (2009) that for anchorages with a small edge distance and a ratio spacing to edge distance smaller or equal to one, the failure load of the group may be negatively influenced by the cracks generated at the front anchor row.

Calculated failure loads

The mean failure load obtained from the experiments was 80.1 kN. The load-displacement curves, as well as the photos of the crack pattern, indicate that the displacement behaviour of the individual anchors and the hole clearance pattern have a significant influence on the group behaviour. As expected, the failure load calculated based on EN 1992-4 (47.4 kN) is rather conservative because it neglects the possible load redistribution to the back anchor row with assuming the failure crack originating from front anchors. The failure load calculated based on the fib Bulletin 58 is slightly higher (9%) compared to the mean experimental value. This can be explained again by the influence of hole clearance and by the influence of cracking at the front anchors. However, 9% deviation between the experimental and calculated results lies within the general scatter considered in the CCD Method for concrete edge failure (15%).

Numerical analysis

The influence of the hole clearance pattern on the behaviour of triangular anchorages was shown in the experiments. To investigate the group behaviour without this influence, and to be able to see the load distribution among the anchors if all anchors start to take up the loads together, the numerical investigation was carried out without hole clearance. The numerically obtained failure load of the group GS-TRI-A was 105.7 kN, which is 24% higher than the corresponding mean experimental value. The difference can be attributed to the influence of hole clearance and the caused cracking at the front row in the experiments. The numerically obtained failure crack pattern is shown in *Figure 9.28*. *Figure 9.28a* shows the developed cracking at the ultimate load. We can see that a small crack at the front is visible. However, it is clear that the

failure crack originates from the back anchor and the small damages at the front row do not influence the force distribution significantly at the back anchor. *Figure 9.28b* depicts the crack pattern in the post-peak phase with a significant crack coming from the back anchor and also a secondary tensile crack is visible behind the back anchor just like in test 2.

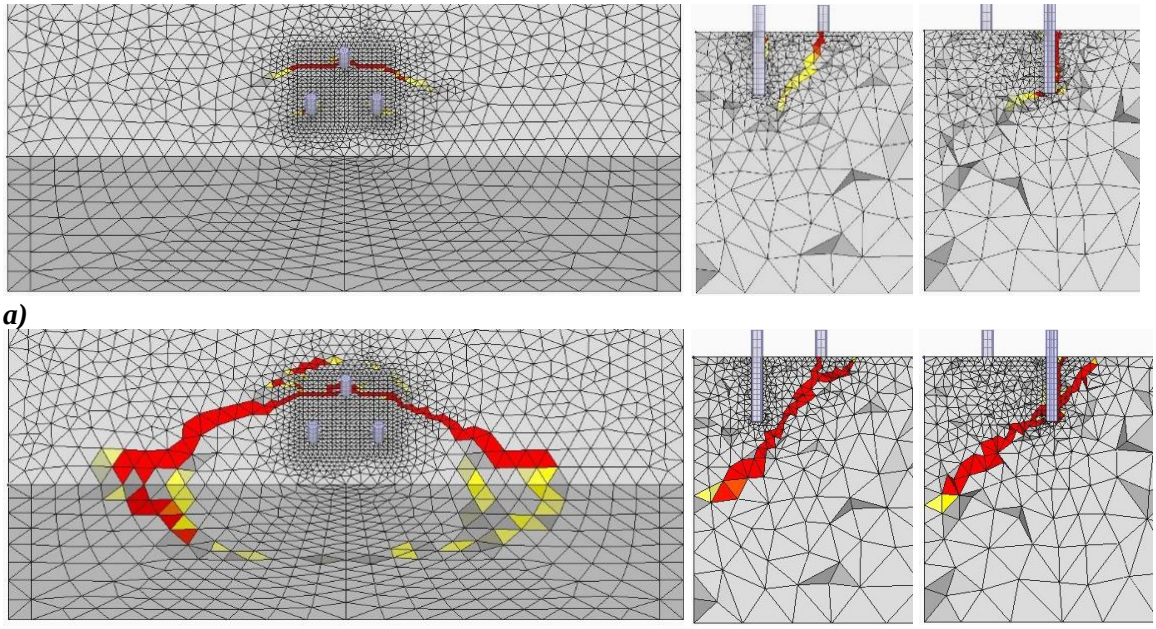

a)

b)

Figure 9.28. Crack pattern obtained from the numerical investigations on GS-TRI-A without hole clearance: a) V=V_u, b) Post-peak

GS-TRI-B

Test series GS-TRI-B was performed on triangular anchor groups having one anchor in the front row ($c_{1.1}$ = *120 mm*) and two anchors in the back row ($c_{1.2}$ = *240 mm*). The hole clearance configuration was random. The measured hole clearance pattern is tabulated in *Table 9.9*, which should help to evaluate the test results and understand the group behaviour better.

Table 9.9. Hole clearance pattern of series GS-TRI-B

	Test ID	$a_{cl.1}$ mm	$a_{cl.2}$ mm	$a_{cl.3}$ mm
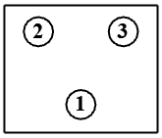	GS-TRI-B-1	0	0.5	0.5
	GS-TRI-B-2	1.0	0	0
	GS-TRI-B-3	0	0.5	0.5

Test 1:

The hole clearance configuration was measured as 0 mm for the front anchor and 0.5 mm for both the back anchors. For this reason, only anchor 1 took up the shear load in the beginning, and then from 0.5 mm applied displacement, the anchors in the back row started also resisting the forces. Note that the measured hole clearance 0.5 mm is much smaller than the failure displacement corresponding to a single anchor with 120 mm edge distance measured in series SS-120. Therefore, the activation of the back anchors was possible before the failure load of the

front anchor would be reached, and so the shear load could be redistributed to the back anchors. This is in agreement with the findings of Grosser (2012). The first crack developed when the group reached an applied load of ca. 80 kN. The failure crack initiated from the back anchor row as it is visible in *Figure 9.27e*.

Test 2:

Test 2 shows a case with favourable hole clearance pattern: the hole clearance of the back anchors was 0 mm, whereas anchor 1 in the front row had ca. 1 mm hole clearance. This way, the anchors in the back row were loaded first and equally. As it can be seen on curve progression in *Figure 9.27a*, group stiffness increases from 1 mm displacement onwards. This suggests that the front anchor gets active. The failure pattern in *Figure 9.27f* shows no cracks originating from the front anchor, and the failure crack originates from the back row.

Test 3:

In the case of test 3, the hole clearance configuration was measured as 0 mm for the front anchor and 0.5 mm for both the back anchors. Consequently, the front anchor was activated first and then at 0.5 mm applied displacement, the back anchors also started taking up forces. This is also indicated by the increase in stiffness in the load-displacement curve (*Figure 9.27a*). Just like in test 1, the hole clearance of the back anchor row is significantly smaller compared to the failure displacement of a single anchor with 120 mm edge distance measured in series SS-120. Although a hairline crack is visible at the front anchor, the failure crack originated from the back anchor row.

Calculated failure loads

The mean failure load obtained from the experimental investigations was 111.3 kN. The curve progression is very similar in all three cases. The failure load calculated based on the EN 1992- 4 was one-third of the mean measured ultimate load, which is very conservative. Assuming the failure crack initiation from the back anchor row based on fib Bulletin 58 resulted in 108.8 kN, which is only 8% lower than the measured value and represents the failure load well.

Numerical analysis

The numerical investigation was carried out without hole clearance. The numerically obtained failure load was 120 kN, which is just 7% higher than the mean value of the experimental results. This small difference can be explained by the fact that in series GS-TRI-B, only one anchor is installed in the front, and therefore, the cracking in the front row has a smaller influence on the group behaviour. This means that the influence of crack pattern was shown to be not that much pronounced in the investigated crack pattern configurations. The crack pattern obtained from the numerical analysis is depicted in *Figure 9.29*. We can see that the failure crack developed from the back anchor row, and there is only a small concrete crushing visible at the front anchor. In addition, a vertical crack has developed from the front anchor in the post-peak, and a secondary crack is visible behind the back anchor in the post-peak phase. The calculated failure load of two anchors at the given configuration with 240 mm edge distance would result in 105.1 kN, which is just 8 % lower than the numerically obtained ultimate load.

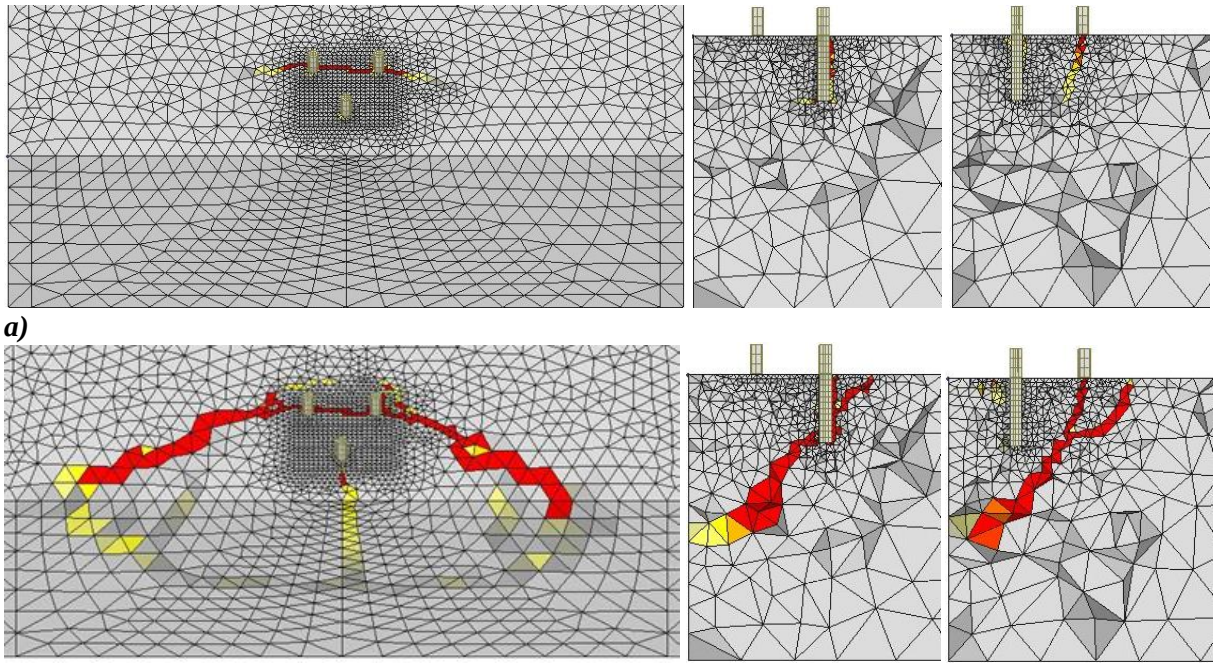

a)

b)

Figure 9.29. Crack pattern obtained from the numerical investigations on GS-TRI-A without hole clearance: a) V=V_u, b) Post-peak

9.4.2.3 Hexagonal configuration

Shear loading tests were carried out close to the concrete edge on anchor groups of hexagonal configuration with random hole clearance pattern in series GS-HEX-A and GS-HEX-B. The hole clearance pattern is, basically depending on the installation accuracy. In test series GS- HEX-A, six anchors were installed in three rows with two anchors per row corresponding to edge distances of 101, 171 and 240 mm. In the case of series GS-HEX-B, the base plate of series GS-HEX-A was rotated by 90°, and the anchors were installed in four rows. For GS-HEX-A, a numerical investigation was carried out in addition to the tests. One anchor was installed at the front with an edge distance of 80 mm, two anchors with 120 mm, two anchors with 200 mm and one anchor with 240 mm edge distance. The measured hole clearance patterns are given in *Table 9.10* and *Table 9.12* for groups GS-HEX-A And GS-HEX-B respectively. The load-displacement curves and the failure crack pattern are given for both series in *Figure 9.30*. The hole clearance pattern as well as the developed crack pattern help to evaluate the tests and to understand the force distribution among the anchors within the groups.

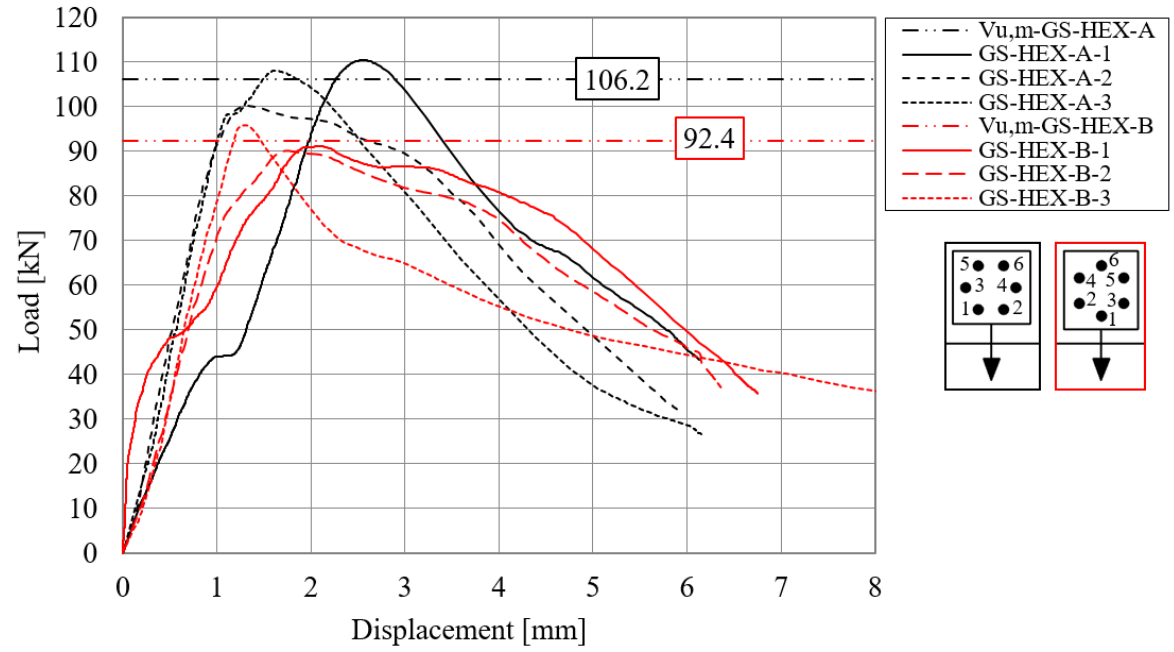
Load [kN]
Displacement [mm]
106.2
92.4
Vu,m-GS-HEX-A
GS-HEX-A-1
GS-HEX-A-2
GS-HEX-A-3
Vu,m-GS-HEX-B
GS-HEX-B-1
GS-HEX-B-2
GS-HEX-B-3

a)


GS-HEX-A-1

b)


GS-HEX-A-2

c)

d)

e)

f)

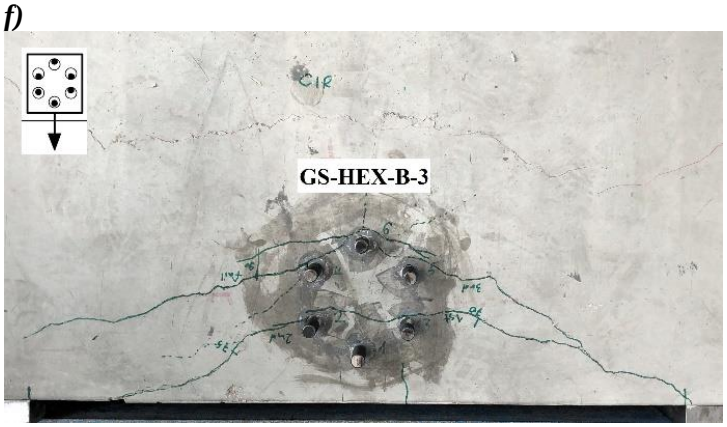

g)

Figure 9.30. Test series with hexagonal configuration: a) load-displacement curves; Failure crack pattern of test: b) GS-HEX-A-1, c) GS-HEX-A-2, d) GS-HEX-A-3, e) GS-HEX-B-1, f) GS-HEX-B-2, g) GS-HEX-B-3

GS-HEX-A

Test series GS-HEX-A was performed on hexagonal anchor groups having three anchor rows with 2 anchors per row. The measured hole clearance pattern is given in *Table 9.10*.

Table 9.10. Hole clearance pattern of series GS-HEX-A

	Test ID	$a_{cl.1}$ mm	$a_{cl.2}$ mm	$a_{cl.3}$ mm	$a_{cl.4}$ mm	$a_{cl.5}$ mm	$a_{cl.6}$ mm
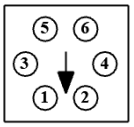	GS-HEX-A-1	0	0	1	0.5	1.5	1.5
	GS-HEX-A-2	0	1	1	0.5	2	1
	GS-HEX-A-3	1.5	0	1	1.5	1.5	1.5

Test 1:

In the case of the first test, it is obvious from the hole clearance pattern that the front anchors get active first. Then, it was possible to further distribute the shear forces to the further anchor rows since the hole clearance of the second row (0.5 mm) was much smaller than the displacement at the failure of the front row. The displacement at front row - ca.1.3 mm – can be related to the reference single anchor tests SS-100 but considering a higher stiffness for two anchors. From the hole clearance pattern and from the crack pattern we can understand that the next anchor 4 of the second row was activated when the applied displacement reached 0.5 mm. Anchor 3 in the second row was active from 1 mm applied displacement. During the test, the cracking was checked visually, and the first crack was observed at an applied load of 45 kN. The crack has opened up to ca. 0.1 mm crack width, and the third anchor row activated after a further 0.5 mm displacement (Σ1.5 mm) due to the hole clearance pattern. The activation of the anchor rows is also reflected in the curve progression in *Figure 9.30a*. We can see that at the end of load plateau at 45 kN the group stiffness increases (the second row activates). The further increase in stiffness happens at ca. 1.5 mm group displacement, which corresponds to the activation of the third row. Finally, the failure crack originated from the back anchor row and the group failed at 110.4 kN. The symmetric crack pattern agrees well with the measured hole clearance pattern *Figure 9.30b*. Note that the cracks visible behind the anchorage are secondary tension cracks due to the uplift of the base plate, which occurred in the post-peak phase only.

It is interesting to see that the first crack appeared at around 45 kN, which corresponds to the theoretical failure load of the front row (46.4 kN). For the second row, it would be 93.0 kN, whereas, for the third row, it would be 103.2 kN, which is very close to the value obtained in the test.

Test 2:

As given in *Table 9.2*, the measured hole clearance pattern in case of test 2 was not symmetric. This is reflected in the developed crack pattern in *Figure 9.30c*. At the beginning anchor 1, followed by anchor 4, then anchors 2, 3 and 6, and finally, anchor 5 was activated. Accordingly, the first cracks originated from anchors 1 and 4. It was observed that an applied shear load of ca. 90 kN, the cracks started widening coming from anchors 1, 4 and 6 at. Finally, the failure crack has developed from anchor 6 from the back row when the group reached the 100.2 kN

ultimate load. The curve progression in *Figure 9.30a* indicates an optimal shear force distribution and that the force redistribution was possible once an anchor was overloaded due to reaching of high forces. This can be explained by the fact that in all cases, the hole clearance was smaller than the failure displacement corresponding to the individual anchor.

Test 3:

The load-displacement behaviour of test 3 is similar to test 2 up to ca. 95 kN applied load. This is due to the same number of anchors, which contribute to the load transfer. According to the hole clearance pattern given in *Table 9.2*, anchor 2 is loaded first, after that anchor 3, and then the other four anchors are contributing to the load transfer. The first cracks were observed at ca. 100 kN applied load as it is visible in *Figure 9.30d*. Furthermore, the cracking can also be indicated in the curve progression by the stiffness reduction of the group. This can be attributed to the failure of anchors 2 and 3, which were loaded first. The ultimate load of the group was reached when the capacity of the back anchors was utilised. The failure crack of the group propagated from the back anchor row. This means that even if cracks at the front and middle rows have developed, the shear forces could be redistributed to the back anchor rows and neglecting the force redistribution would be over-conservative.

Calculated failure loads

The failure load calculated based on the EN 1992-4 was less than one-third the mean measured ultimate load, which was also expected because only the two anchors of the front row were considered to resist the shear loads. The calculation based on fib Bulletin 58 estimated as 97.9 kN assuming the failure crack origination from back anchor row, which is 9% smaller than the measured value. This is a reasonably good agreement with the test results.

Numerical analysis

In addition to the experiments, numerical investigations were carried out on the same GS- HEX-A configuration, however, without hole clearance. The numerically obtained failure crack pattern at the ultimate load of the group and in the post-peak phase is depicted in *Figure 9.31* at the ultimate load of the group and in the post-peak phase. Although some cracks can be observed at the anchors in the front and middle row at ultimate load, it is very clear that the failure crack developed from the back anchor row. The section cuts in post-peak show that the failure crack is running from the back anchor at full anchorage depth and propagates to the front of the specimen to a depth of ca 1.5-times the back edge distance.

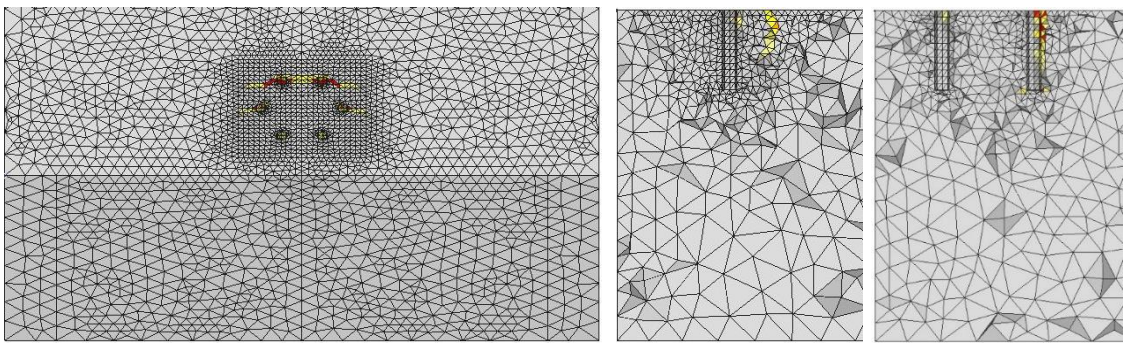

a)

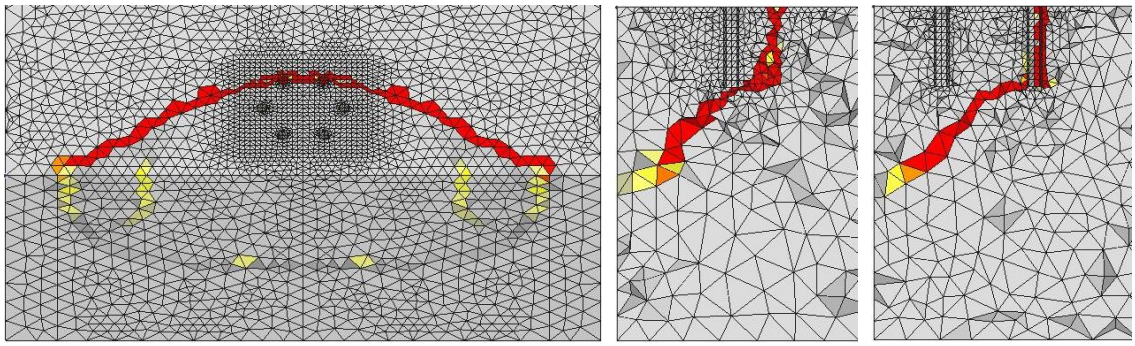

b)

Figure 9.31. Crack pattern obtained from the numerical investigations on GS-HEX-A without hole clearance: a) V=V_u, b) Post-peak

The shear force distribution was monitored during the analyses. *Table 9.11* gives an overview of the results. We can see that up to ca. 50% of the failure load, the anchors are transferring the shear forces relatively equally. However, later, the contribution of the back anchor row is becoming lower. At the failure load, the front anchors are transferring 38%, the middle anchors are transferring 34% and the back row is transferring 28 % of the ultimate load (113.7 kN). This can be explained by the fact that the cracks are developing mostly at the back anchor and the anchors, which are not in cracks are able to carry higher loads compared to those in the crack. Comparing the mean ultimate load from the tests and the numerical investigations, only 7% difference can be observed despite the fact that the tests were done with random hole clearance pattern, whereas the numerical analysis without hole clearance. We can see that if the hole clearance of a given anchor is (much) smaller than the failure displacement of the anchor in the front, then the shear forces can be distributed to back anchors before cracking would occur, leading to results close to those obtained without hole clearance. This shows the importance of the evaluation of the load-displacement behaviour of the anchor group and the load-displacement behaviour of the individual anchors of the group.

Table 9.11. Force distribution among the anchors obtained from the numerical investigations for GS-HEX-A without hole clearance

Load level $V/V_{u,num}$	Anchor 1	Anchor 2	Anchor 3	Anchor 4	Anchor 5	Anchor 6	Sum of anchor forces	Force measured at load application
[-]	[kN]	[kN]	[kN]	[kN]	[kN]	[kN]	[kN]	[kN]
0.34	6.8	6.8	6.5	6.5	6.3	6.3	39.2	39.2
0.52	**10.4**	**10.3**	**9.9**	**9.9**	**9.3**	**9.2**	**59.0**	**59.0**
0.81	16.6	16.5	15.7	15.7	13.9	13.9	92.3	92.4
1.00	**21.6**	**21.4**	**19.4**	**19.5**	**15.8**	**16**	**113.7**	**113.7**
0.79	16	16	15.8	15.8	13	13.1	89.7	89.7

GS-HEX-B

Test series GS-HEX-B was performed on anchor groups of hexagonal configuration with one anchor in the first and fourth rows and two anchors in the second and third anchor rows. The measured hole clearance pattern is given in *Table 9.12.*

Table 9.12. Hole clearance pattern of series GS-HEX-B

	Test ID	$a_{cl.1}$ mm	$a_{cl.2}$ mm	$a_{cl.3}$ mm	$a_{cl.4}$ mm	$a_{cl.5}$ mm	$a_{cl.6}$ mm
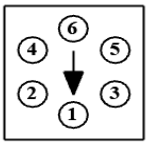	GS-HEX-B-1	0	2	0	1	1.5	1.5
	GS-HEX-B-2	0	1	0.5	1.5	1.5	0.5
	GS-HEX-B-3	1.5	0.5	0	2	2	0

Test 1:

In the case of test 1, the hole clearance was measured to be zero for anchors 1 and 3. This means that in the beginning phase of the loading, only these two anchors were active. The first cracks also appeared to initiate from these anchors at an applied load of ca.50 kN. This is confirmed further not just by the cracking observed during the test but is also clear from the curve progression. The initial stiffness of the load-displacement curve for test 1 is rather low until the displacement of the group reaches a value of approx. 1-1.5 mm and the other anchors get activated. Then, as further anchors started to contribute, the stiffness increases. The third crack originated from anchor 4, which was loaded from 1 mm displacement onwards after overcoming the gap. With further loading, when the group reached 80 kN, cracking was observed originating from anchor 5. Finally, the shear force could be redistributed to anchor 6, and the ultimate load of the group was reached (91.2 kN). This ultimate load corresponds well to the calculations with assuming the failure crack from the back row. However, the failure displacement of the group was ca. half of the failure displacement measured of the corresponding single anchor series SS-240b. This can be explained by the higher stiffness of the group compared to the single anchor stiffness. The load-displacement curve obtained in test 1 (*Figure 9.30a*) reflects the behaviour of the anchor group very well, and it is in a good agreement with the hole clearance pattern and with the developed crack pattern (*Figure 9.30e*).

Test 2:

Anchor 1 was activated first but after 0.5 mm displacement, anchors 3 and 6, and later anchor 2 started resisting the forces. This is also shown by the curve progression and stiffness of the group (*Figure 9.30a*). No cracking occurred at the front anchor because the shear force could be distributed to the further anchors before the failure displacement of the front anchor would be reached ($a_{cl} << \delta V_{u,SS\text{-}80}$). The first loss of stiffness can be indicated at an applied displacement of 1 mm, and applied load of ca. 70 kN. This moment corresponds also to the first cracking at anchor 2. No cracks are visible originating from the third anchor row, which can be explained by the hole clearance pattern of this row ($a_{cl} = 1.5\ mm$). The ultimate load of the group was obtained as 90.1 kN, which corresponds to the calculated theoretical failure load assuming a failure crack from the back anchor row.

Test 3:

Test 3 is a case with favourable hole clearance pattern. This explains that the highest ultimate load of the series could be reached. First, the anchor in the back row and anchor 3 in the second row were activated, followed by anchor 1 and finally by the third row. The displacement behaviour of the group is clearly shown by the crack pattern, which is depicted in *Figure 9.30g*. No cracks have developed from the first and third rows. The first cracking occurred at an applied load of ca. 70 kN, originating from anchor 3, and the second at 75 kN applied load from anchor 2. This can also be seen in the load-displacement curve. However, only a slight loss of stiffness is visible at around 75 kN applied load because a fast redistribution to anchors with higher stiffness was possible. The curve progression shows that more anchors transferred the force at the same time in the case of test 3 compared to tests 1 and 2, which lead to a higher ultimate load and higher stiffness and consequently, smaller displacement at failure.

In all three tests, secondary tension cracks are visible on the opposite side of the loading direction, which occurred due to the uplift of the base plate after the peak.

Calculated failure loads

The mean failure load of series GS-HEX-B was 92.4 kN. This corresponds well to the theoretical failure load calculated based on the fib Bulletin 58 (88.1 kN) assuming the failure crack origination from the back anchor. The calculated failure load based on the EN 1992-4 was 21.3 kN, which is very conservative, less than one-fourth the mean failure load from the tests.

It was observed that with the same number of anchors but different anchor pattern, the mean ultimate load was 15% higher in case of test series GS-HEX-A compared to series GS-HEX-B. This is because in both series, the edge distance of the back row was 240 mm, however, in series GS-HEX-A, two anchors were placed in the back row with a spacing of 80 mm, which increases the activated concrete body.

9.4.3 Anchorages in uncracked and cracked concrete arranged parallel to the concrete edge, loaded perpendicular and towards the concrete edge

Experimental investigations were carried out on anchor groups of 1×2 and 1×3 configurations arranged parallel to the edge and loaded perpendicular to the edge according to the test program given in *Table 9.3*. In addition, single anchor tests were carried out with the corresponding edge distances for comparison. These tests aimed to verify the spring model for the case where all the anchors are located in one single anchor row (anchors arranged parallel to the free edge). Therefore, the anchor group can be considered as a 2D problem like in tension loading case (having the same embedment depth for all anchors). The tests were carried out under concentric and eccentric shear loads, and in four cases, one of the anchors was located in a crack and the shear force was applied either concentrically or eccentrically. With the eccentric loading, it was aimed to verify the assumptions and rules made for the shear springs in Sections 6.2 and 6.3. The cases in cracked concrete targeted to show that the spring model (Section 6.2.3) for concrete edge failure is capable of considering different stiffness conditions within an anchor group in case of concentric and eccentric shear loading. Furthermore, in test series GS- 1×3- 120/240- C, the concrete specimen was cast in such a way that one outer anchor had 120 mm edge distance, the other outer anchor had 240 mm edge distance and the middle anchor had partly 120 mm and partly 240 mm edge distance (see *Figure 9.4*, Specimen D). It was aimed to capture not just different anchor arrangements but also the concrete specimen geometry. This should also represent a case, which is only solvable using the tributary volume approach (Section 6.2.2.2).

All tests were carried out in one concrete batch using bonded anchors with nominal threaded rods of size M20 and an embedment depth of 120 mm. The mean cube concrete strength was 27.6 MPa. The edge distance was taken as 120 mm or 240 mm to avoid having too small edge distances, where the extension of the projected area approach used in the CCD Method might be unconservative (see Grosser, 2012). The anchor installation and testing procedure were carried out as it is explained in Section 9.2. The load was applied using a hinged loading application in all cases. It may be noted that Grosser (2012) has performed shear loading tests on anchor groups arranged parallel to the concrete edge loaded perpendicular to the edge with stiff and hinged load application, and he has shown that in case of shear loading, only a minor difference in ultimate strength can be observed if the load is applied concentrically.

Furthermore, the ultimate load of the anchorages was calculated based on EN 1992-4 and fib Bulletin 58. The summary of the test results in terms of the mean value of the ultimate shear loads ($V_{u,m}$) and the mean value of the initial shear stiffness ($k_{1,m}$) is given in *Table 9.13*. The load-displacement curves of the corresponding series and the failure crack patterns are given in the following sub-sections, in *Figure 9.32 - Figure 9.37*.

Table 9.13. Test results of anchor groups arranged parallel to the edge and loaded perpendicular to the edge

Test series ID	Mean ultimate load	Calculated mean concrete edge resistance based on EN 1992-4	
	$V_{u,m}$	$V_{Rm,c,EN} = V_{Rm,c,fib}$	$V_{u,m}/V_{Rm,c,EN}$
	[kN]	[kN]	[-]
SS-120	43.4	37.2	1.17
SS-120-dw03	34.5	26.4	1.31
SS-240b	94.2	92.2	1.02
GS-1×2-C	56.1	49.6	1.13
GS-1×2-e60	45.8	37.2	1.23
GS-1×2-dw03-C	44.3	35.1	1.26
GS-1×3-C	61.0	62.0	0.98
GS-1×3-e60	57.7	46.5	1.24
GS-1×3-e120	50.6	37.2	1.36
GS-1×3-dw03-C	55.3	43.9	1.26
GS-1×3-dw03-e120c	41.5	26.3	1.60
GS-1×3-dw03-e120u	45.8	26.0	1.74
GS-240/1×3-C	133.9	123.0	1.09
GS-1×3-120/240-C	89.2	-	-

9.4.3.1 Reference tests in uncracked and cracked concrete

Reference shear loading tests were performed on single anchors with 120 mm and 240 mm edge distance in test series SS-120 and SS-240b in uncracked concrete, and on single anchors with 120 mm edge distance in cracked concrete ($\Delta w = 0.3$ *mm*) in series SS-120-dw03. The results confirm that higher ultimate loads are reached with larger edge distance (see *Figure 9.32a*), and lower ultimate loads are obtained in case of tests in cracked concrete. The mean value of the ultimate load was 21% lower in cracked concrete compared to the corresponding tests in uncracked concrete (see *Figure 9.32b*). This reduction is comparable with the reduction factor (0.7) used in the calculations to consider a constant crack width of $\Delta w = 0.3$ *mm* according to EN 1992-4. Furthermore, the initial shear stiffness was calculated: The initial shear stiffness $k_{1,m}$ of the corresponding series SS-120 and SS-240b were 31.0 and 34.9 kN/mm, respectively, which corresponds to a mean value of 33 kN/mm. Thus, the shear stiffness can be considered as relatively independent of the edge distance. In the case of series SS- 120- dw03, a stiffness reduction of 18% was observed compared to the uncracked series SS- 120. This finding agrees well with the loss of stiffness due to cracked concrete condition, which is reported in thy literature by Sharma (2013) and Mahrenholtz (2011).

It can be seen in *Table 9.13* that the experimental results are higher compared to the calculated results according to EN 1992-4 in the case of the tests with 120 mm edge distance. For tests series SS-120, the deviation is 17%, which is just slightly higher than the general scatter considered in the CCD Method for concrete edge failure (15%). However, in test series

SS- 120- dw03, the measured mean ultimate load was obtained 31% higher than the predicted failure load. This can be due to the fact that the influence of cracked concrete had a smaller influence on the anchor behaviour than it is assumed in the calculations.

The failure crack pattern of the experiments is given in *Figure 9.32c-f*. It can be seen that the crack always propagates to the supports, and in the case of the tests in cracked concrete, the crack plane divides the failure breakout body into two parts.

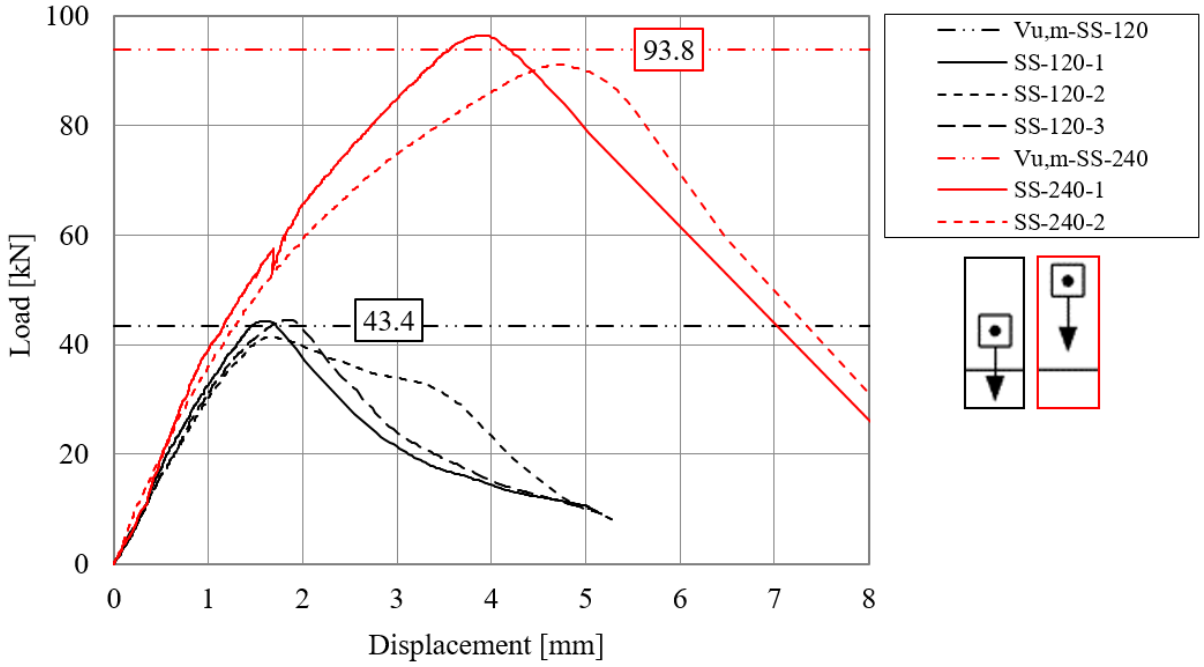

a)

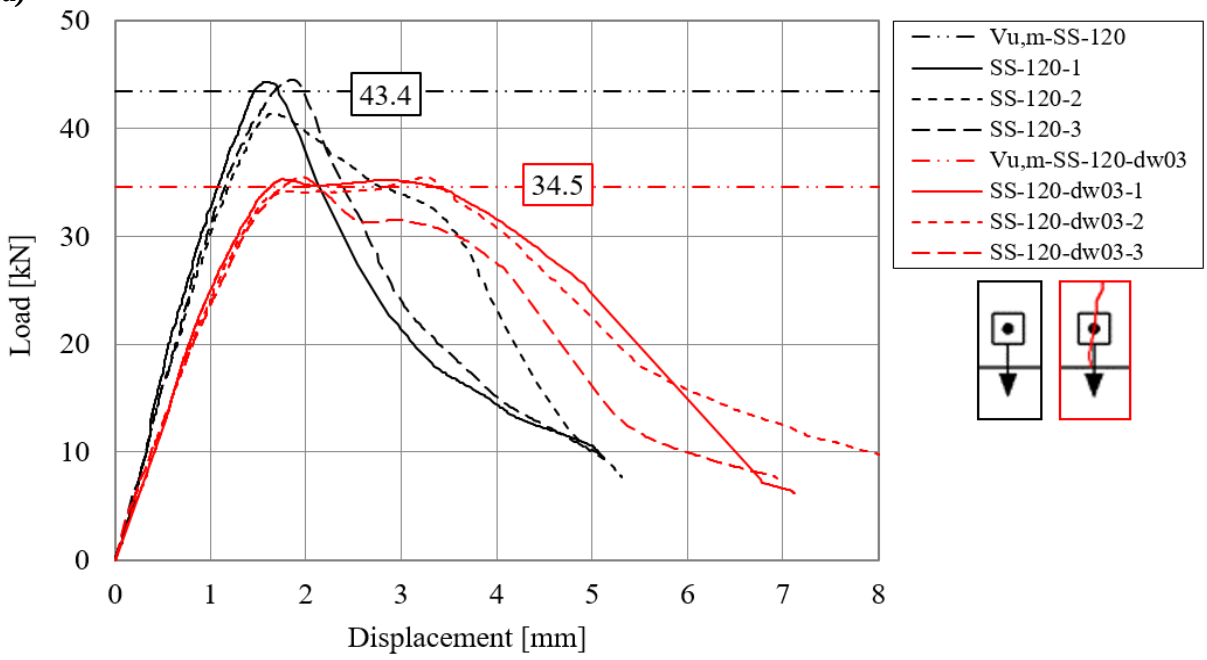

b)

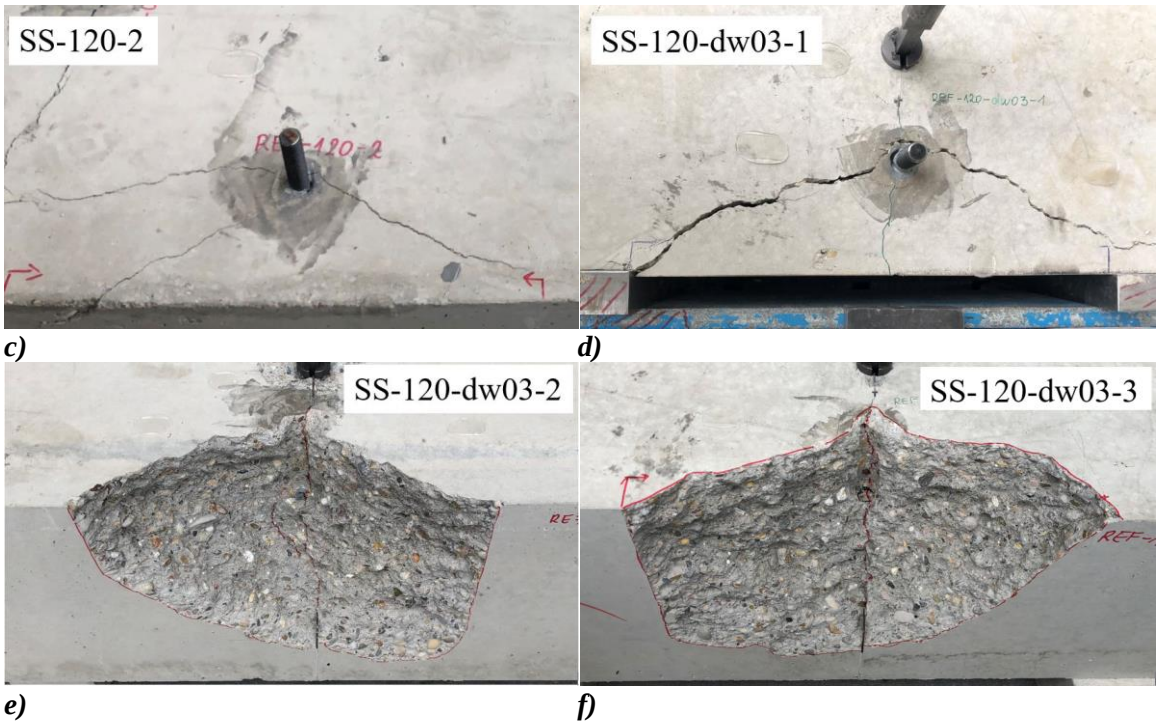

c) *d)*

e) *f)*

Figure 9.32. a) Load-displacement curves of series SS-120 compared with SS-120-dw03 and SS-240b; b)-f) failure crack pattern of series SS-120 and SS-120-dw03

9.4.3.2 Anchor groups of 1×2 configuration

Influence of eccentricity

Test series GS-1×2-C was performed under concentric shear loading and series GS-1×2-e60 was performed under eccentric shear loading. The aim of the tests was the investigation of the influence of eccentric loading, and the verification of the assumptions and rules made for the shear springs in Section 6. The load-displacement curves of the reference series along with the photos of the failure crack pattern are depicted in *Figure 9.33a-h*.

In the case of concentric shear loading in test series GS-1×2-C, a common breakout body developed in all three tests (*Figure 9.33c-e*). The mean measured ultimate load was just 11% higher compared to the calculated mean resistance according to EN 1992-4, which is within the scatter considered typically in case of concrete edge failure.

The results of test series GS-1×2-e60 showed that by applying the shear force eccentrically with the point of load application exactly at one of the right anchors, the mean ultimate load of the group was obtained as 45.8 kN, which is 18% reduction compared to the concentrically loaded identical anchor group. Furthermore, the 45.8 kN is very close to the value obtained in the single anchor series SS-120 (43.4 kN). This is because the load was applied directly on one anchor of the group. *Figure 9.33a* shows that the displacement at failure increased in case of eccentric loading compared to the concentric series. Note that the displacements plotted in *Figure 9.33a* correspond to the displacement at the point of load application, so in case of series GS-1×2- e60, to the left anchor. The higher displacements can be due to the fact that in case of eccentric loading, primarily only one anchor takes up the forces (at the position of load application). This can be confirmed by *Figure 9.33b*, which shows the displacement measured at the left (loaded)

and right anchors in the function of the time, and the applied load in the function of the time. At the onset of loading, only the left anchor displays displacement, which means that at the beginning, all shear forces are resisted by the left anchor, and the right anchor is activated only later. This can also be understood from the slope of the load-time curve: The slope increases when both anchors resist the shear forces. In *Figure 9.33f-h*, the failure patterns of the eccentric case are depicted. In all three cases, a common breakout body has developed. However, a crack perpendicular to the edge occurred at the loaded anchor is visible. When this crack occurred, due to the resulting horizontal tension forces in the concrete member, the loaded anchor started losing stiffness and the right anchor started resisting forces at a higher rate. However, due to the limitations of the setup, the individual anchor shear forces were not measured in the experiments.

According to the calculations based on the EN 1992-4, the ultimate load reduced by 25% compared to the concentric case, and the group resistance is equal to the single anchor resistance loaded concentrically in shear. This is due to the formulations accounting for the load eccentricity and gives a good estimation in case of anchor groups having two anchors in a row.

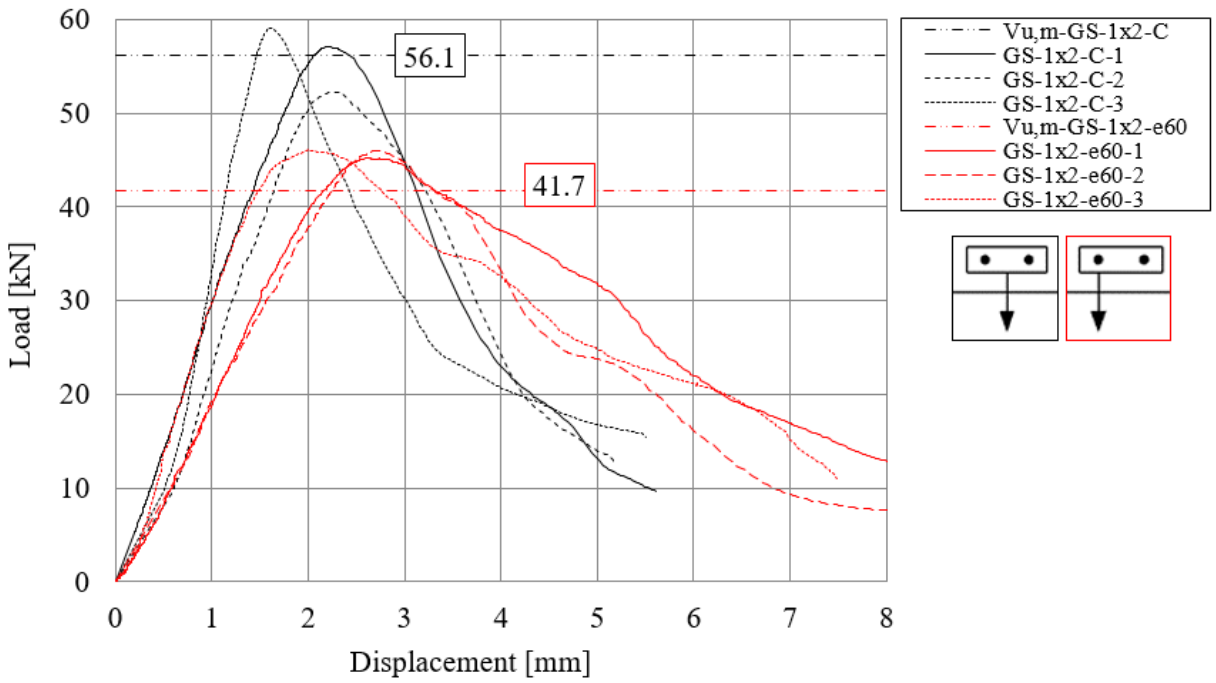

a)

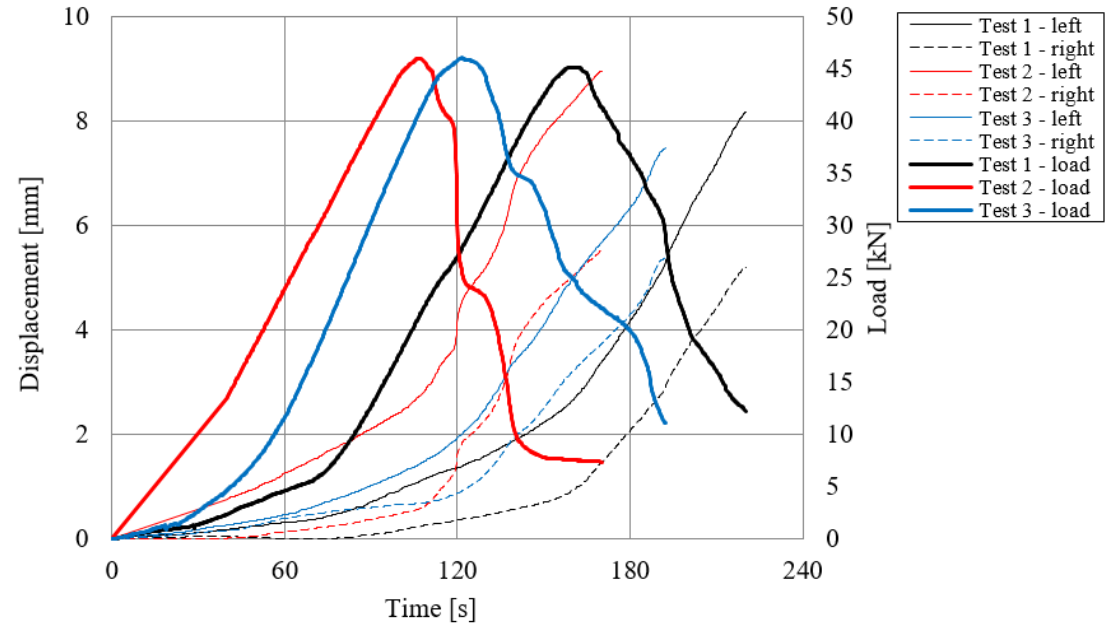

b)

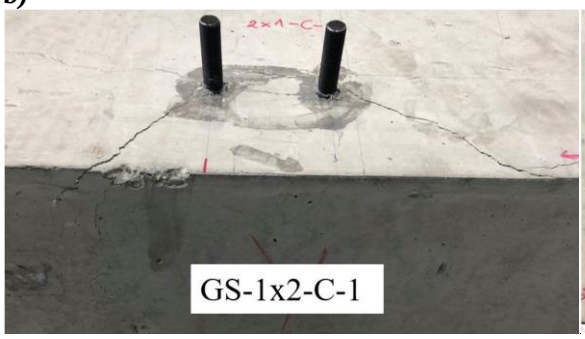

c)

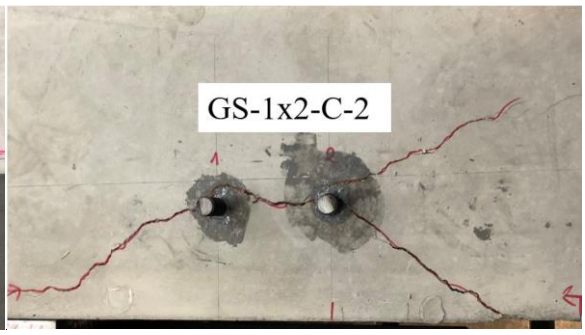

d)

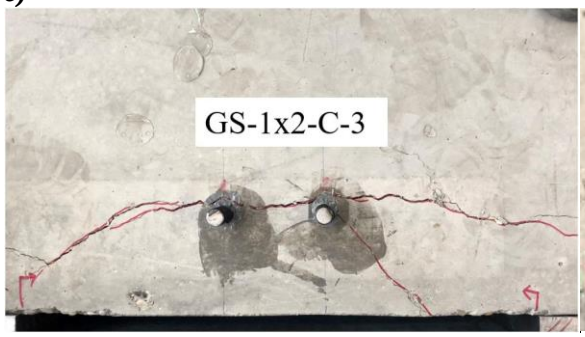

e)

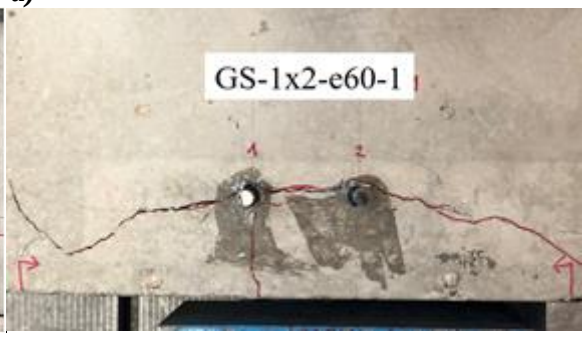

f)

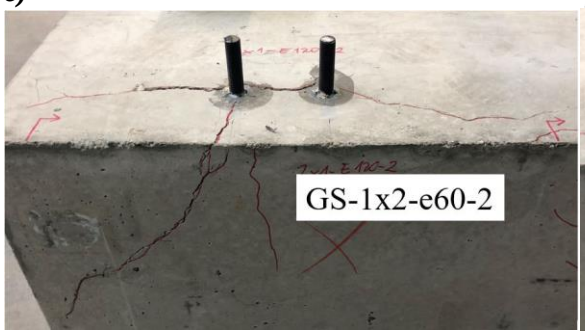

g)

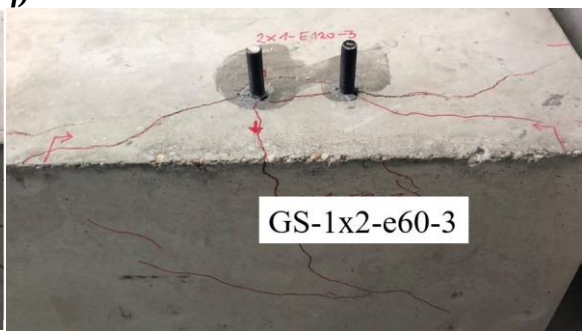

h)

Figure 9.33. a) Load-displacement curves of series GS-1×2-C compared with GS-1×2-e60; b) displacement-time and load-time curves of test series GS-1×2-e60; c)-e) failure crack pattern of series GS-1×2-C; f)-h) failure crack pattern of series GS-1×2-e60

1×2 configuration – Influence of crack pattern

The influence of cracked concrete condition is investigated on 1×2 configurations by series GS- 1×2-C (reference non-cracked) and GS-1×2-dw03-C. In series GS-1×2-dw03-C, one anchor out of two anchors was located in the crack (see *Figure 9.34b-d*). The shear load was applied concentrically; with rotation unrestrained load application to allow the rotation of the base plate based on the stiffness conditions within the group. In *Figure 9.34a*, the group load is plotted in function of the applied displacement at the point of load application. The applied displacement was determined as the mean value of the displacements measured at right and left anchor. The test results given in *Table 9.13* and *Figure 9.34a* show that the ultimate load of the group reduced by 21% due to placing one anchor into crack compared to the uncracked case.

According to the evaluation based on the EN 1992-4 (*Table 9.13)*, it is assumed that both anchors are located in cracks and the ultimate load of anchorages in cracked concrete is considered as 0.7-times the ultimate load of the corresponding anchorage in uncracked concrete.

It can be seen in *Figure 9.34a* that in test 1 and 3, after reaching the ultimate load, the load-displacement curve exhibits further peak(s). This is due to the force redistribution among the anchors within the group. The anchor intercepted by the crack has a lower stiffness compared to the anchor in uncracked concrete. If the plate is perfectly unrestrained against rotation, the force taken up by both the anchors must be equal in an ideal case. An ideally rotationally unrestrained condition may not always be realized in the tests. Therefore, initially, the anchor in uncracked concrete takes up a higher shear load and this leads to the first peak in the load-displacement curve. The second peak results from the residual resistance provided by the anchor installed in the crack.

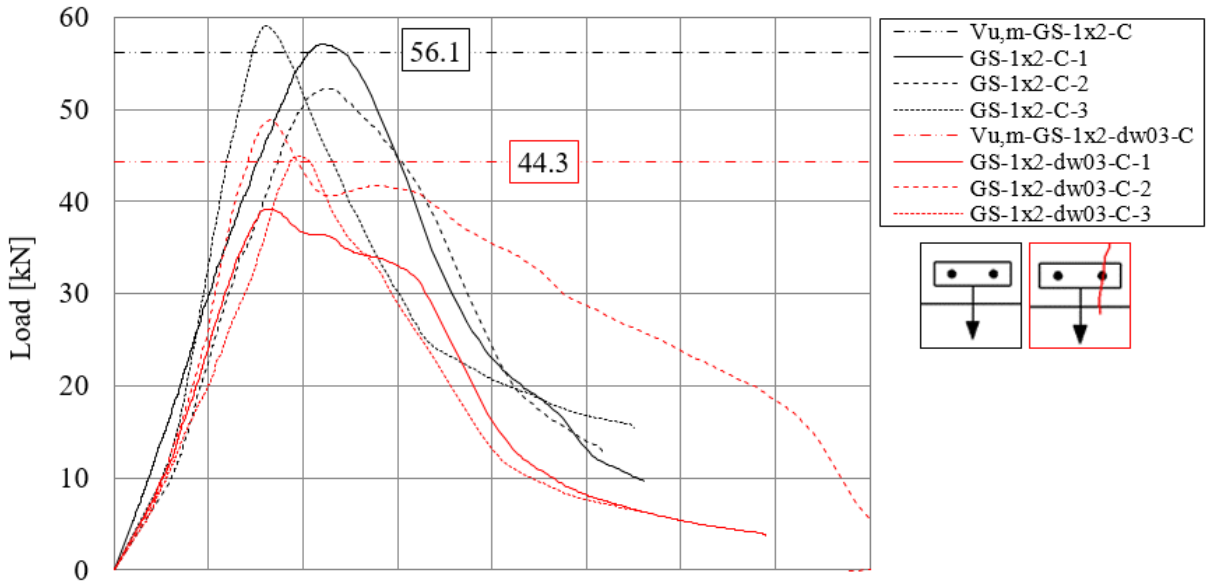

a)

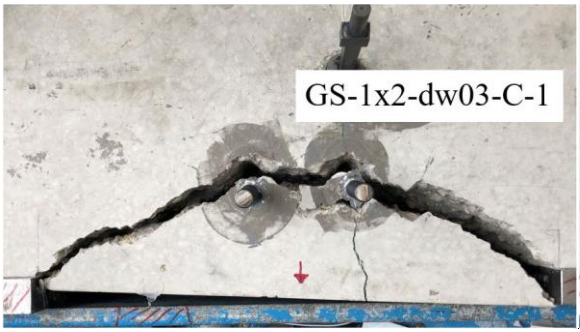

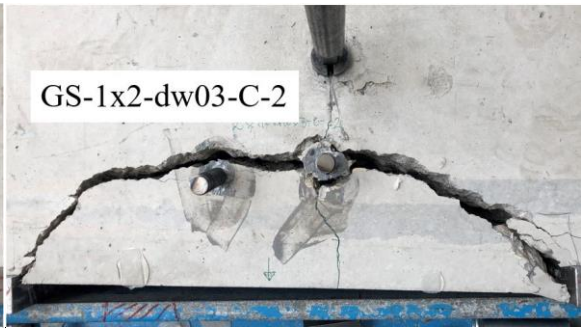

b) *c)*

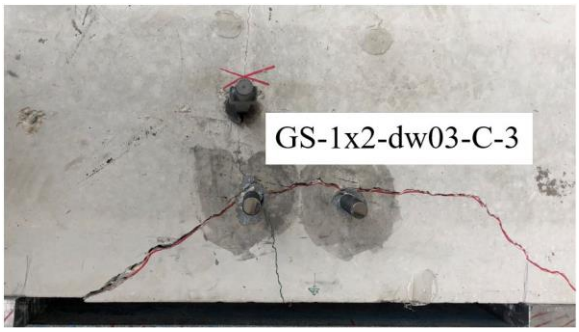

d)

Figure 9.34. a) Load-displacement curves of series GS-1×2-C compared with GS-1×2-dw03-C; b)-d) failure crack pattern of series GS-1×2-dw03-C

9.4.3.3 Anchor groups of 1×3 configuration

1×3 configuration – Influence of eccentricity

Test series GS-1×3-C was carried out under concentric, whereas series GS-1×3-e60 and GS- 1×3- e120 were carried out under eccentric shear loading. The applied eccentricity was 60 mm and 120 mm, respectively. These series aimed to investigate the influence of the eccentric load in case of 1×3 anchor groups and to verify the assumptions and rules made for the shear springs in Section 6. The load-displacement curves of the series along with the failure crack pattern for every 9 tests are given in *Figure 9.35a-j*.

In the concentric series GS-1×3-C, a common breakout body has developed in all three tests as it is depicted in *Figure 9.35b-d*. The measured mean ultimate load is in a good agreement with the calculated mean ultimate load according to EN 1992-4 (see *Table 9.13*). The shear stiffness of the group is ca. two times the mean stiffness measured for the reference single anchor tests. This is lower than expected having three anchors in a row (k_{group} is assumed to be ca. *n*-times the stiffness of the reference single anchor in case of n number of anchors in a row).

In test series GS-1×3-e60, the shear load was applied between the middle and the outer anchor, which did not lead to a significant reduction of the group resistance. Note that if the third anchor is ignored, the group can be considered similar to GS-1×2-C having two anchors only and applying the shear load concentrically. Interestingly, the measured mean ultimate load for series GS-1×3-e60 is comparable with the mean ultimate load obtained in series GS-1×2-C. The crack pattern of this series is given in *Figure 9.35e-g*. In case of tests 1 and 3, a common breakout body developed with an additional vertical crack in front of the outer anchor close to the load application. Note that the anchors were installed in a way that the hole clearance was negligible

at the onset of loading. However, while loading eccentrically, the base plate rotates and not all the anchors might be loaded simultaneously. The crack pattern of test 2 in *Figure 9.35f* suggests that the third anchor (opposite to the loaded side) might not be loaded from the beginning with the other anchors. Anchor 3 is not lying in the failure plane of the group and the ultimate load of the group corresponds to the failure load of series GS-1×2-C having two anchors only and applying concentric shear load. However, the contribution of the third anchor is visible in the post-peak phase on the curve progression (see *Figure 9.35a)*.

In series GS-1×3-e120, the shear load was applied on the base plate at the position of one of the outer anchors. As it was expected, the measured mean ultimate load decreased by 17% compared to the single anchor series GS-1×3-C. *Figure 9.35h-j* depict the crack patterns of the corresponding tests. The crack patterns are similar in all three cases. A vertical crack in the front of the most-loaded anchor is visible, and the developed breakout body includes the most-loaded outer anchor and the middle anchor. The third anchor lies outside of the breakout body. The crack pattern and the load-displacement curves *Figure 9.35a* suggest that while applying the shear load on one of the outermost anchors, the shaft of other outer anchor is pressing the concrete in the direction opposite to the loading direction. This was also shown by the negative displacements measured on that anchor during the test (not plotted). This is also the reason for higher concrete edge breakout resistance of the group compared to the case of GS-1×2-e60. The current design provisions do not capture this effect, and the calculation according to the EN 1992-4 results in a conservative estimation (-26%) compared to the measured values. The mean resistance calculated by the current design is equal to the capacity of a single anchor loaded in concentric shear due to accounting for the eccentricity with the factor $\psi_{ec,V}$ and neglecting the forces acting in the opposite direction. Therefore, it is important to account for this phenomenon in the spring model in a way that based on the displacements and load distribution within the group, the corresponding anchor shear springs are active.

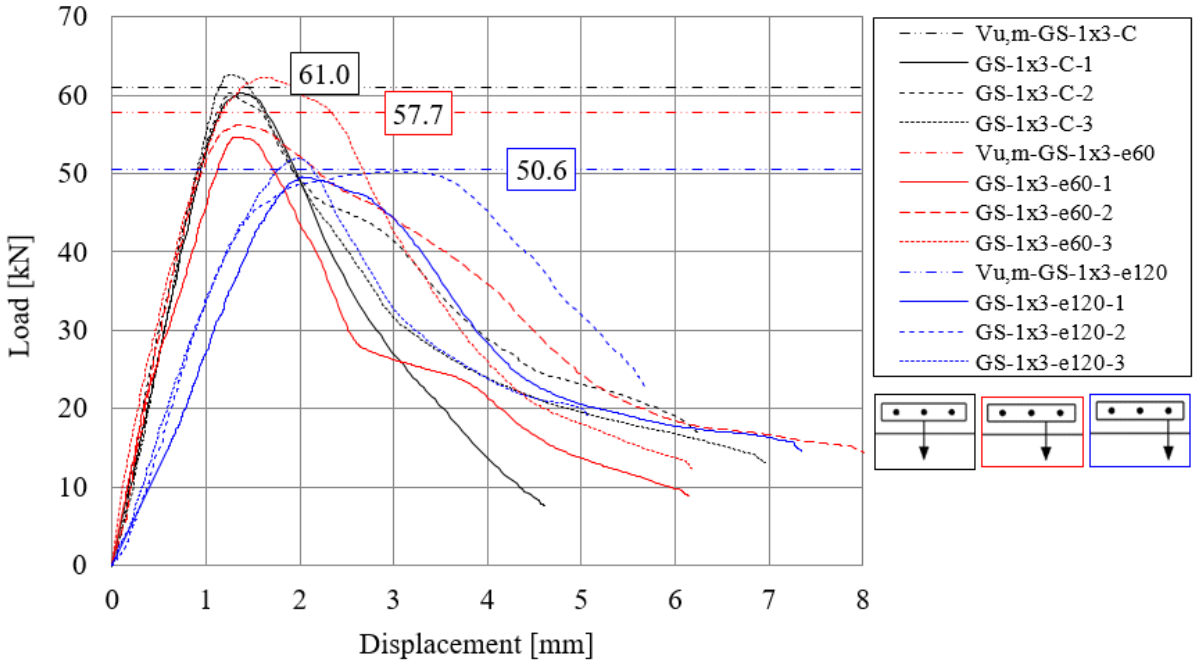

a)

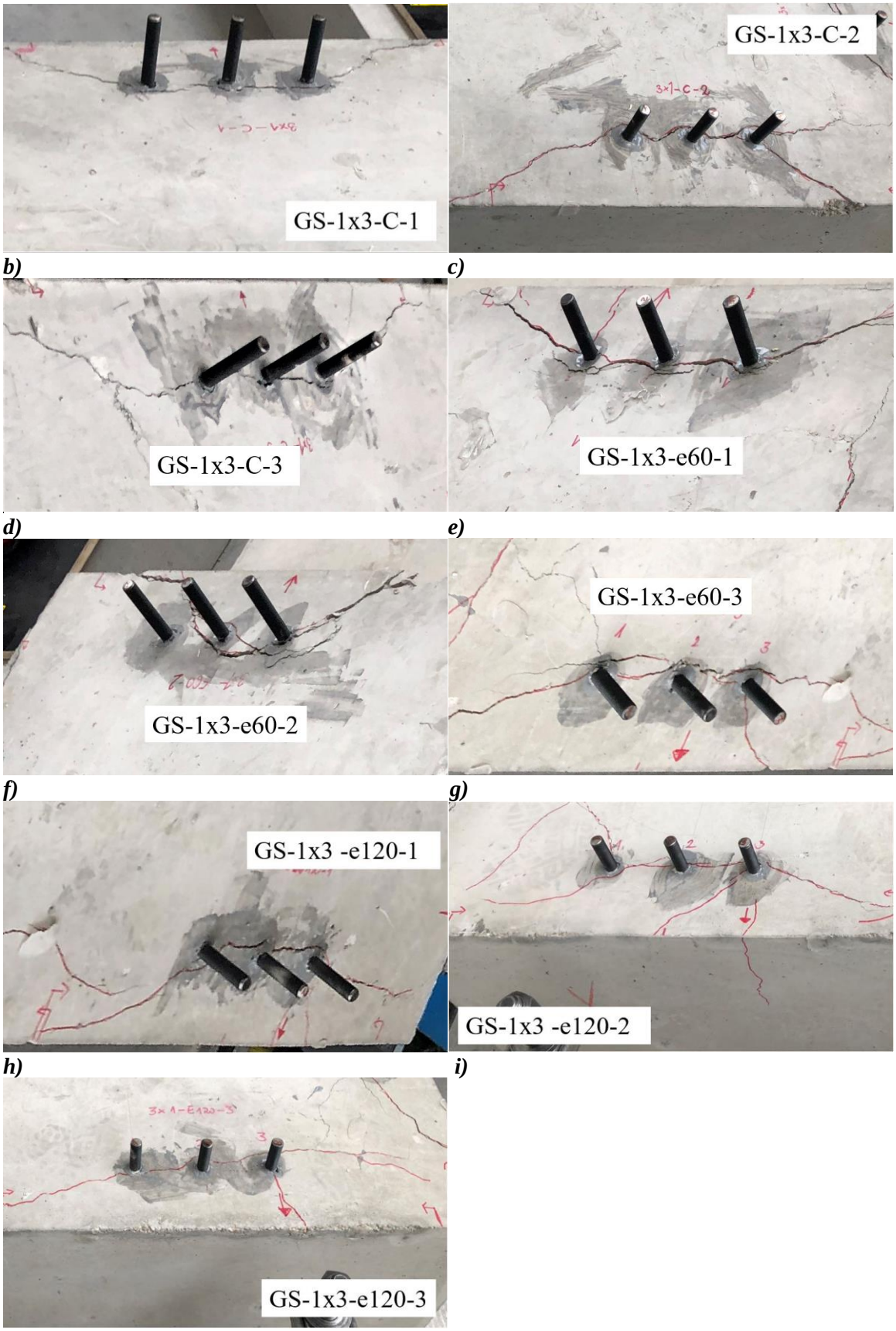

b) c) d) e) f) g) h) i) j)

Figure 9.35. a) Load-displacement curves of series GS-1×3-C compared with GS-1×3-e60 and GS-1×3-e120; Failure crack pattern of series: b)-d) GS-1×3-C, e)-g) GS-1×3-e60 and h)-j) GS-1×3-e120

Superimposed influence of crack pattern and eccentric loading

This section discusses the test results on the superimposed influence of cracked concrete and the influence of the loading eccentricity. The load-displacement curves and the crack patterns are depicted in *Figure 9.36*. The concentric shear loading results obtained on 1×3 group configuration in uncracked concrete (Series GS-1×3-C) are discussed again along with the cracked and eccentric cases for comparison.

Compared to series GS-1×3-C with three anchors in a row in uncracked concrete, the measured mean ultimate load reduced by just 10% and the group shear stiffness reduced by ca. 30% in series GS- 1×3-dw03-C due to installing one anchor out of three into a crack. This reduction of the ultimate load is much lower than that considered according to the current design, where the reduction factor to consider the cracked concrete condition (for $\Delta w = 0.3$ *mm*) is 0.7 irrespectively of the number of anchors located in the crack. If the crack propagation cannot be ruled out from the anchorage zone of one anchor, then the entire group is to be considered as located in the crack. The application of factor 0.7 is considered as conservative for most of the cases but actually, it might even be unconservative in case of certain anchor configurations. Examples for such cases where consideration of all the anchors intercepted by a crack can be found in Bokor et al. (2017), Muccaccia et al. (2019). The crack patterns of the series GS- 1×3-dw03-C are given in *Figure 9.36b-d*. We can see that in all three tests a common breakout body formed and the angle of the failure crack was not influenced by the cracked concrete condition.

The influence of the crack pattern in case of eccentric loading was investigated in series GS- 1×3-dw03-e120c and GS-1×3-dw03-e120u. The applied eccentricity of external forces to the centre of the group was equal to the anchor spacing. However, in tests GS-1×3-dw03-e120c, the eccentric load was applied at the anchor located in the crack, and in tests, GS- 1×3- dw03- e120u, the outer anchor on the opposite side (uncracked) was loaded. As expected, when the load was applied on the anchor in a crack, lower resistance and stiffness were obtained. This can be explained by the fact that the anchor, which is closer to the load application, must take up higher forces compared to the other anchors within the group. However, if the higher loaded anchor is located in a crack, the resistance of this anchor is limited due to the cracked concrete condition and therefore, the group capacity and the stiffness are also lower. The crack patterns of test series GS-1×3-dw03-e120c are given in *Figure 9.36e-f*. In this test series, the most-loaded anchor is intercepted by a crack. However, the further cracks, which developed to loading also originate from the most-loaded anchor. The developed asymmetric breakout body includes the most-loaded outer anchor and a crack propagates in front of the middle and lowest loaded anchor. The cracks originating from the middle anchor are propagating into the main crack of the most-loaded anchor. Furthermore, we can understand from the crack pattern that the outer anchor pressed the concrete in the direction opposite to the loading direction, and with that influenced the group resistance positively. Compared to series GS- 1×3- e120 with the same amount of eccentricity, however, in uncracked concrete, the measured mean ultimate load reduced by 18% and the initial shear stiffness by ca. 30%. This shows that the reduction factor 0.7 for the cracked concrete condition is conservative for this investigated case when only one anchor out of three is intercepted by a crack.

The same anchor and crack pattern were tested in series GS-1×3-dw03-e120u but in this case, the load was applied on the outer anchor in the uncracked concrete part. This means that the anchor with the highest resistance was highest-loaded. This resulted in a higher group resistance. The failure crack patterns in *Figure 9.36g-h* indicate that both the loaded anchor and the middle anchor are included in the failure breakout body. The crack patterns and the load-displacement curves in *Figure 9.36a* suggest that while applying the shear load on the outer anchor, at the beginning of loading, both the anchors resist the applied shear load due to the same stiffness of the outer and middle anchor, while the anchor intercepted by the crack presses against the concrete in the opposite direction. However, this additional resistance is not that pronounced because it is influenced by the crack. Comparing the results with series GS- 1×3- e120, 10% reduction due to the crack was observed and the stiffness remained unchanged.

The calculated concrete edge resistance based on EN 1992-4 is 26 kN for both series GS- 1×3-dw03-e120c and GS-1×3-dw03-e120u, which is equal to the capacity of the corresponding single anchor in cracked concrete. This is a conservative calculation result, which does not take into account the influence of the crack pattern and the anchor forces in the direction opposite to the loading direction.

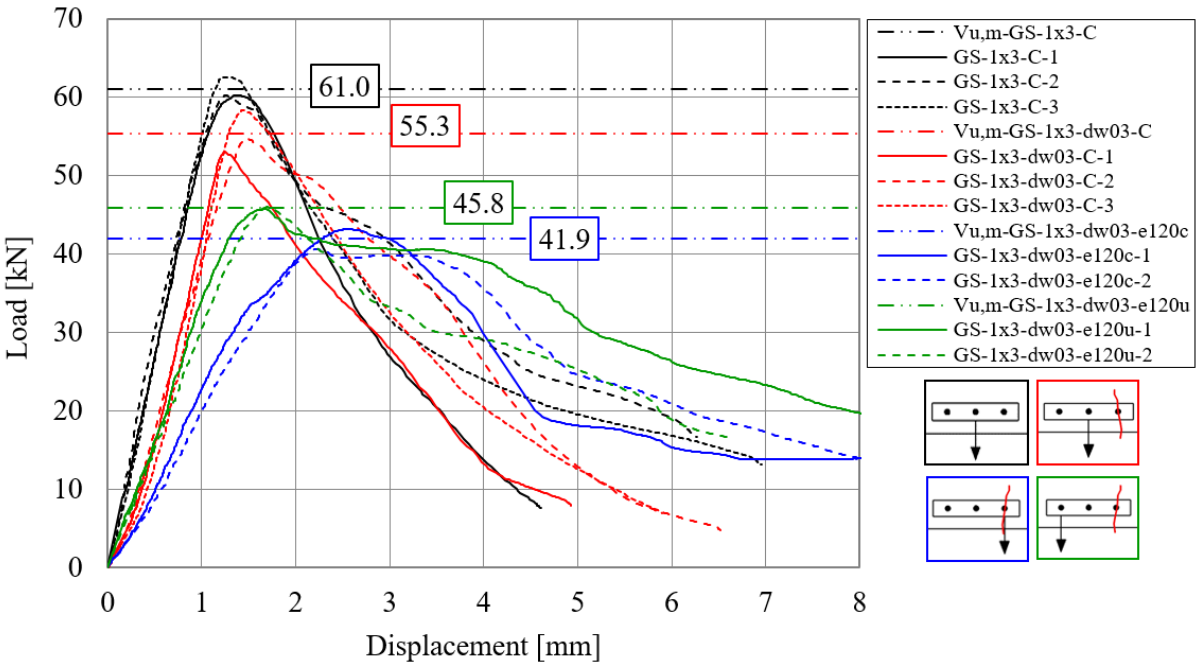

a)

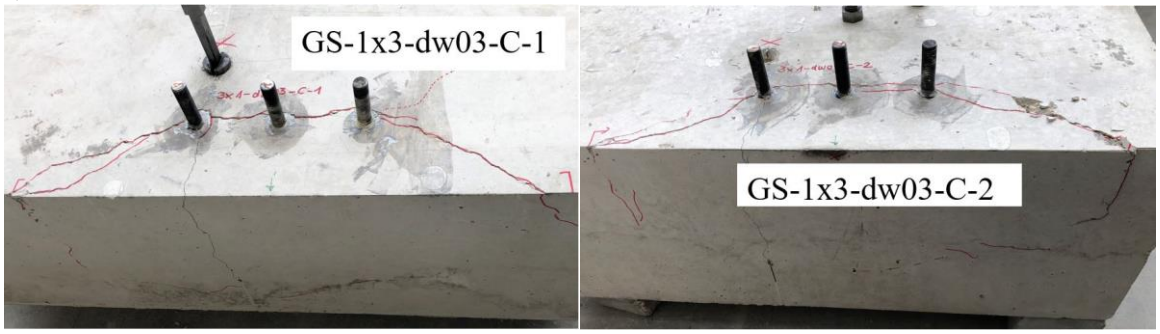

b) ***c)***

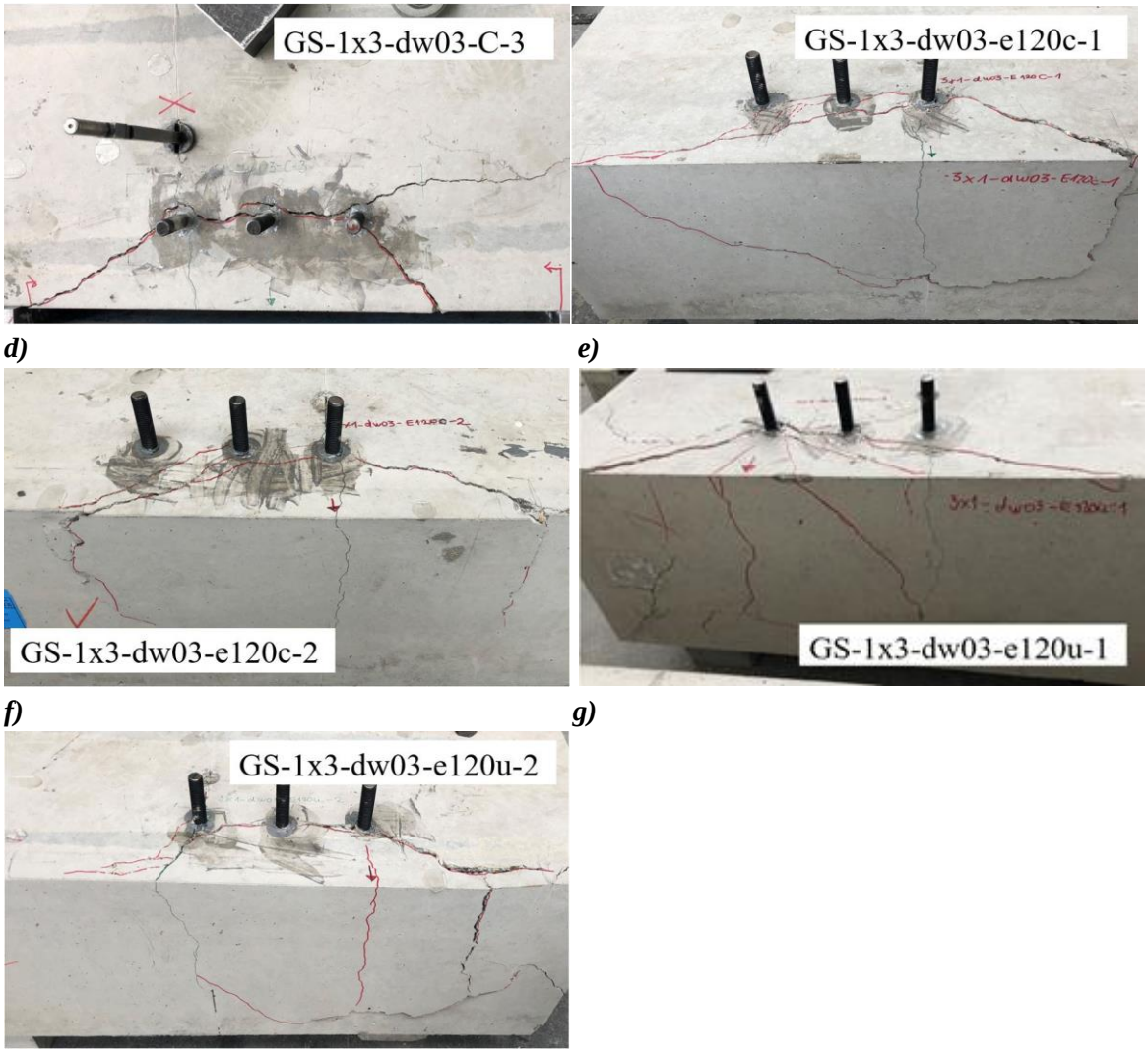

d) ***e)*** ***f)*** ***g)*** ***h)***

Figure 9.36. a) Load-displacement curves of series GS-1×3-C compared with GS-1×3-dw03-C, GS-1×3-dw03-e120c and GS-1×3-dw03-e120u; Failure crack pattern of series: b)-d) GS-1×3-dw03-C, e)-f) GS-1×3-dw03-e120c and g)-h) GS-1×3-dw03-e120u

9.4.3.4 Influence of specimen geometry

Test series GS-1×3-120/240-C was performed to investigate the influence of specimen geometry and to understand the 3D-problem with a single anchor row having more anchors. One of the outer anchors was installed at 120 mm edge distance, the other outer anchor was installed at 240 mm edge distance, and the middle anchor was installed in the plane of the section, where the edge distance changes from 120 to 240 mm. The schematics of the specimen geometry are given in *Figure 9.4*, Specimen D.

The load-displacement curves obtained from the experiments are plotted in *Figure 9.37a.* Furthermore, the same 1×3 anchor group but having 120 mm and 240 mm edge distances are also given in the same graph for comparison. In these tests, the shear load was applied concentrically on the group, at the position of the middle anchor. However, the rotation of the base plate was allowed by using rotation unrestrained load application ensured by a hinge. It can be seen from *Figure 9.37a* that the load-displacement behaviour of this anchor group can be approximated

as the average of the response of the anchor group tested with an edge distance of 120 mm and 240 mm. It is known from the literature that the shear stiffness of the anchors is not influenced by the edge distance (see e.g. in Grosser, 2012, Tian, 2019). Therefore, from the beginning of the loading, all three anchors were loaded. However, due to the different edge distance and corresponding concrete volume, which could be activated by the individual anchors, the anchor with 120 mm edge distance started losing stiffness first, which led to an eccentricity of internal forces and uneven shear load distribution among the anchors of the group. This would explain why the group resistance was 9% lower than the average ultimate load of the series GS-1×3-C and GS-240/1×3-C. Furthermore, note that the clearance hole in the base plate was not filled. This means that even though at the onset of loading all the anchors were loaded together, in case of the rotation of the base plate, it might be a small influence due to the "developed" hole clearance. The crack patterns in *Figure 9.37b-e* show the ratio of the activated concrete by the individual anchors, which suggests that it might be reasonable to consider the volume of activated concrete to consider different concrete geometries when defining the spring properties for shear loaded anchorages.

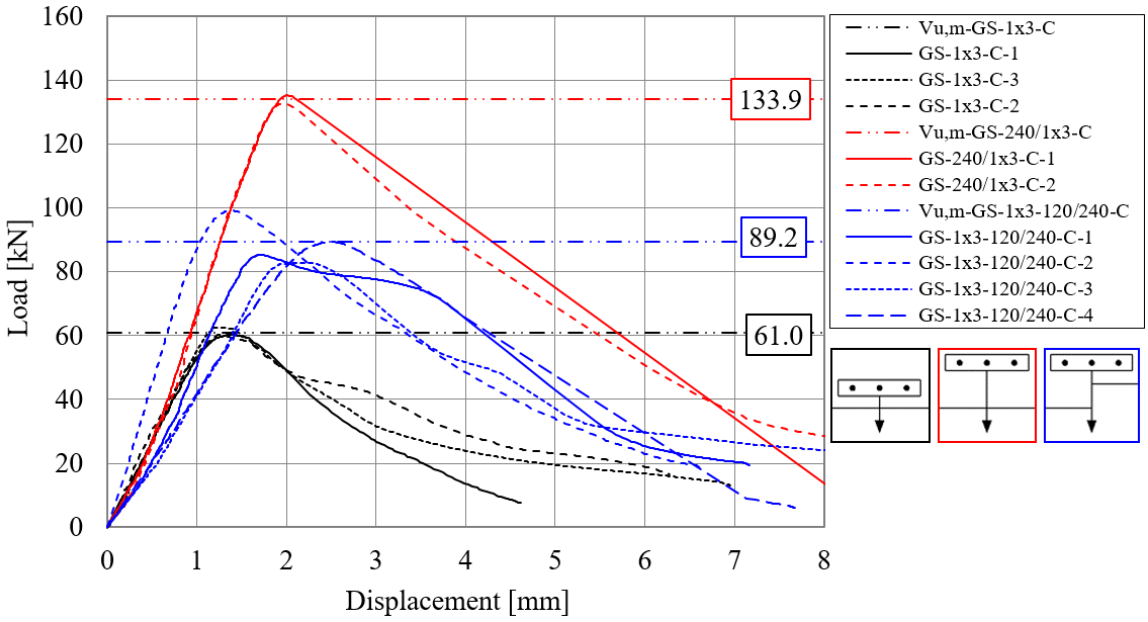

a)

b) ***c)***

d) ***e)***

Figure 9.37. a) Load-displacement curves of series GS-1×3-120/240-C compared with GS-1×3 –C and GS-1×3-240/C; b)-e) failure crack pattern of series GS-1×3-120/240-C

Numerical analysis

The configuration GS-1×3-120/240-C was investigated also numerically. However, without the influence of the hole clearance pattern. The numerically obtained failure load of the group was 94.6 kN, which just 6% higher than the mean measured experimental failure load. The shear force distribution was monitored during the analysis, and the results of certain loading steps are given in *Table 9.14*. We can see that the three anchors are taking up the forces relatively equally up to the peak load. The middle anchor is taking up slightly higher forces. This can be due to the fact that this anchor is closest to the load application. However, this is changing in the post-peak phase from $0.83V_u$, where the middle anchor starts to take up lower forces. This can be attributed to the vertical crack, which developed in the plane of section, where the edge distance changes.

Table 9.14. Force distribution among the anchors obtained from the numerical investigations for series GS-1×3-120/240-C without hole clearance

Load level $V/V_{u,num}$	Anchor 1	Anchor 2	Anchor 3	Sum of anchor forces	Force measured at load application
[-]	[kN]	[kN]	[kN]	[kN]	[kN]
0.32	9.8	10.7	9.8	30.2	30.2
0.53	16.2	17.4	16.2	49.7	49.7
0.85	26.4	27.9	26.4	80.7	80.7
1.00	**31.4**	**31.7**	**31.4**	**94.5**	**94.6**
0.83	26.6	25.4	26.5	78.5	78.5

The numerically obtained failure crack pattern at peak load and in the post-peak phase are depicted in *Figure 9.38a* and *b*, respectively. For both cases, an overall view (top), cross-sectional views in the plane at the anchor sections 1, 2 and 3 (middle), and cross-sectional view in front of the anchors (bottom) are given. We can see from the crack patterns that at peak load, cracks are originating from all three anchors (*Figure 9.38a)*. However, the cracking at anchor 3 (with $c_1 = 120$ *mm*) is slightly more pronounced. This can be due to the smaller edge distance and to the fact that the concrete volume activated by the third anchor is the smallest among the anchors. *Figure 9.38b* depicts the failure crack pattern in the post-peak phase. The developed cracks

agree with the crack pattern expected for the corresponding edge distances. It can be seen in the cross-sectional views at the anchor locations that the initial angle of the crack is the same for the three anchors. Furthermore, the section view in front of the anchors confirms that a common breakout body developed (*Figure 9.38b)*. This example and the obtained results suggest that it is required to consider the shear loaded anchor groups as a 3D problem, and cannot be simplified in every case to a 2D problem so that the CCD Method in the current form would be applicable.

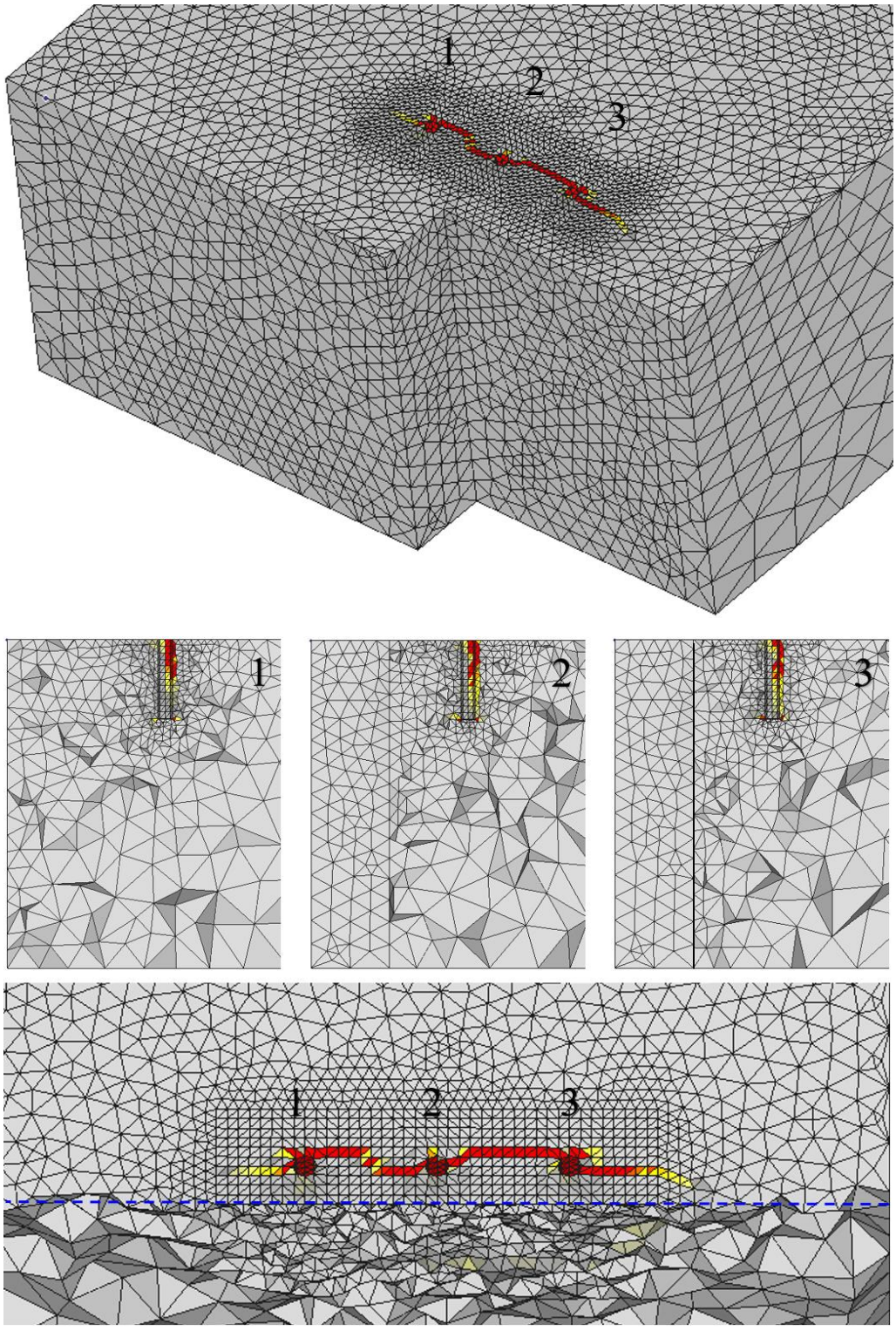

a)

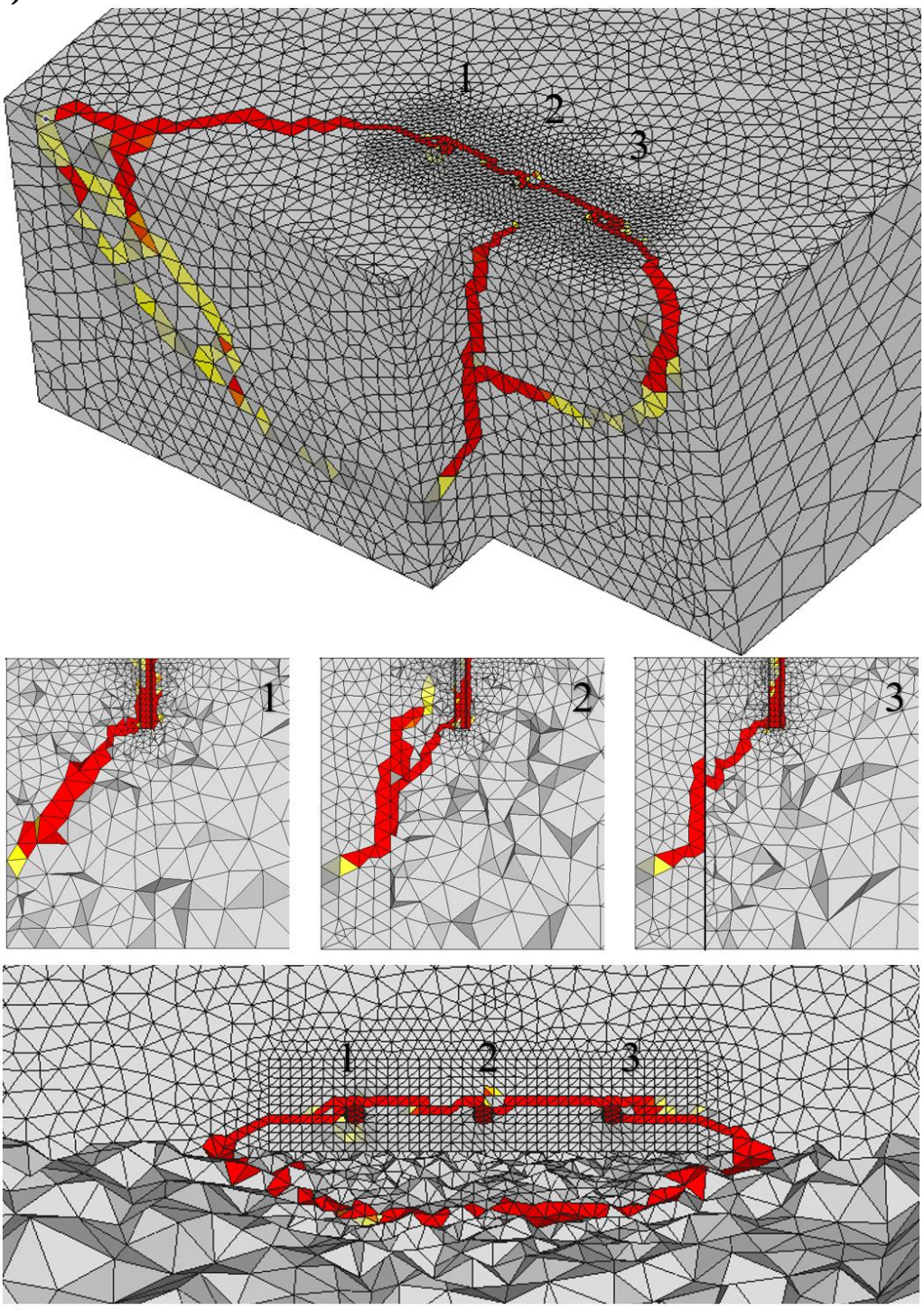

b)

Figure 9.38. Crack pattern obtained from the numerical investigations on GS-1×3-120/240-C, overall view and cross-sectional views: a) $V=V_u$, b) post-peak phase

9.5 CONCLUSIONS OF THE RESULTS OBTAINED FROM SHEAR LOADING TESTS ON ANCHORAGES WITH CONCRETE EDGE BREAKOUT FAILURE

The experimental and numerical investigations reported in Section 9.4 aimed to generate an experimental database on the concrete edge breakout failure of anchor groups loaded in shear perpendicular to the close edge. For this reason, anchor groups of rectangular (3×1, 2×1, 1×3, 1×2) and non-rectangular (triangular, hexagonal) configurations were tested with random hole clearance pattern. To allow a comparison of the group behaviour with the behaviour of single anchors, reference tests were carried out with the edge distance of the corresponding anchor rows. Furthermore, the test program and the evaluation of the results aimed to provide the information required for the verification of the spring model for calculating the resistance of anchor groups in case of concrete edge breakout failure mode considering various anchor and hole clearance configurations, loading and boundary conditions.

The aim of the experiments and the developed test program are intensively discussed in Section 9.1. Section 9.2 gives a detailed overview about the testing inclusive the design of the test specimens, tested fasteners and those installations, and about the test setup and test procedure so that all the experiments are reproducible by following the descriptions. Section 9.3 explains the purpose of the numerical investigations and gives a summary of the modelling and performing the analyses. Through the numerical investigations, the results of the experimental program were supported and the results of the corresponding anchor groups without the influence of clearance hole were investigated. Furthermore, the force distribution and redistribution among the anchors of the group was analysed performing nodal-force monitoring. In Section 9.4, the experimental tests and the results of the numerical analyses are evaluated to obtain the necessary information on

(i) the group behaviour of anchorages,
(ii) the crack origination and propagation in case of anchor groups,
(iii) the influence of the displacement behaviour of single anchors on the behaviour of anchor groups,
(iv) the hole clearance pattern and
(v) the concrete specimen geometry.

The following main conclusions can be summarised based on the results:

- The single anchor tests and numerical investigations with different edge distance according to Sections 9.4.1, 9.4.2 and 9.4.3 confirmed that the failure load increases with increasing edge distance.
- The single anchor tests with different edge distances according to Sections 9.4.1, 9.4.2 and 9.4.3 confirmed the findings from the literature that the initial shear stiffness of single anchors is not dependent on the edge distance if all other parameters such as anchor type, size and embedment depth are kept same.
- The results in cracked concrete confirmed the reduction in failure load and stiffness due to the cracked concrete condition (Section 9.4.3).
- The single anchor tests performed with a recess corresponding to the theoretical breakout body of an anchor in the front showed no significant influence of the presence

of a recess in front of the anchor on either the ultimate resistance or the stiffness of the anchors. This is because the concrete recess does not affect the breakout surface and the stress distribution in the load transfer area of the anchor is not disturbed (Section 9.4.1).

- The single anchor tests carried out in pre-damaged specimen due to the failure of prior tests showed a large scatter in terms of the ultimate load as well as initial shear stiffness and displacement at failure. This is due to the significant influence of the pre-damage in the concrete on the anchor behaviour. The significant influence was also confirmed by numerical investigation (Section 9.4.1).
- The investigations on 3×1 anchor groups showed that the anchor group behaviour is highly dependent on the load-displacement behaviour of the individual anchors within the group. It was found that the failure load is almost independent of the hole clearance pattern. However, the displacement of the anchor group and the activation of the individual anchors and of course, the group stiffness are influenced by the hole clearance pattern (Section 9.4.1).
- In the tests and numerical analyses with one anchor per anchor row (2×1 and 3×1), the ultimate load of the groups was comparable with the reference single anchor series having the edge distance of the back anchor row of the corresponding anchor group. (Section 9.4.1).
- The experimental investigations on the 2×1 group configurations confirmed the findings from the literature regarding the spacing to edge distance of the front row (s_1/c_1) ratios. When the ratio was $s_1/c_1 < 1$, the cracking at the front anchor row was prevented due to the suppression of the cracking in the front row by the compression field, which is originating from the back anchor row. Yet, it is deemed that defining ratios to presume the group behaviour might only be expedient for certain configurations e.g. 1×2, 2×1 or 2×2 and might not be generally applicable (Section 9.4.1).
- The experimental investigations on 1×2 and 1×3 anchor groups in cracked concrete showed that the anchor group behaviour is highly dependent on the load-displacement behaviour and the stiffness conditions of the individual anchors within the group (Section 9.4.3).
- The test results on anchor groups placed parallel to the edge and loaded perpendicular edge showed the importance of considering the actual cack pattern. It was observed that when 1×3 anchor groups are loaded eccentrically in shear and one anchor is located in the crack, it makes a difference whether the eccentricity of the load is away or close to the crack (Section 9.4.3).
- The tests and numerical analyses carried out on triangular and hexagonal configurations and anchor groups placed parallel to edge and loaded perpendicular edge confirmed that the shear stiffness of an anchor group is increasing by n-times, compared to single anchor stiffness, if n number of anchors are installed in an anchor row (in c_2 direction) (Sections 9.4.2 and 9.4.3).
- The experimental and numerical investigations on the hole clearance pattern through the evaluation of the load-displacement curves and crack patterns confirmed the significant influence of the hole clearance configuration on the anchor group behaviour. Furthermore, the results suggest that with controlling the hole clearance pattern, the most

favourable pattern can be found and the best anchor group performance can be achieved. The hole clearance pattern can be controlled either by filling the annular gap with high-strength mortar before loading or by using slotted holes so that only particular anchors are resisting shear forces. (Sections 9.4.1 and 9.4.2)

- The tests on the influence of specimen geometry suggest that it seems reasonable to consider the volume of the activated concrete to consider different concrete geometries. This was confirmed by the crack pattern showing the ratio of the activated concrete by the individual anchors. (Section 9.4.3)
- The different initial stiffness conditions e.g. due to cracks and the changes in the group shear stiffness can automatically be considered when the complete load-displacement behaviour of the individual anchors is considered in an analysis. Due to the loss of stiffness of a particular anchor or due to failure of an anchor, the group stiffness is automatically adjusted (Sections 9.4.1, 9.4.2 and 9.4.3).
- The investigations on anchor groups of different configurations showed that calculating the group resistance with assuming the failure crack originating from the back anchor row (based on fib Bulletin 58) gives a reasonably good agreement with the experimental results. However, it is very important that the information required for a safe design is not ensured without considering the displacement behaviour of the anchorage. The cases investigated within the framework of this dissertation showed that although the failure crack always originates from the back anchor row, the cracks developing at the front anchor row(s) might limit the design in serviceability limit state. (Sections 9.4.1, 9.4.2)
- The results of the extensive experimental and numerical programs performed in this PhD thesis offer a good basis for the verification of the developed spring model for the design of anchor groups in case of concrete edge breakout failure. The verification is given in Section 11.

10 VERIFICATION OF THE NONLINEAR SPRING MODEL FOR CONCRETE CONE FAILURE

The nonlinear spring model for tension loaded anchor groups in the case of concrete cone failure is verified in this chapter. In Section 10.1, the postulates made for the tributary area approach and for the stiffness of the load-displacement curves, which define the spring characteristics, are discussed and verified. The spring model is verified against experiments performed within the framework of this thesis and experiments from the literature in Sections 10.2.1 and 10.2.2, respectively. Section 10.3 gives a summary of the chapter. The load-displacement curves of the corresponding test results are given in Section 8.3. However, for the ease of reading, some of them are reproduced in this chapter to facilitate the comparison with the corresponding load-displacement curves obtained from the analysis using spring model.

10.1 VERIFICATION OF THE POSTULATES MADE FOR THE SPRING MODEL FOR CONCRETE CONE FAILURE

The aim of using the nonlinear spring modelling approach for anchorages failing due to concrete cone failure is to reflect the load-displacement behaviour realistically. In the model, the anchor behaviour is considered by tension-only nonlinear axial springs derived based on the idealised load-displacement curves obtained from tension test on single anchors away from the concrete edge or neighbouring anchors. To consider the group effect and the vicinity of the concrete edge, the tributary area approach is proposed.

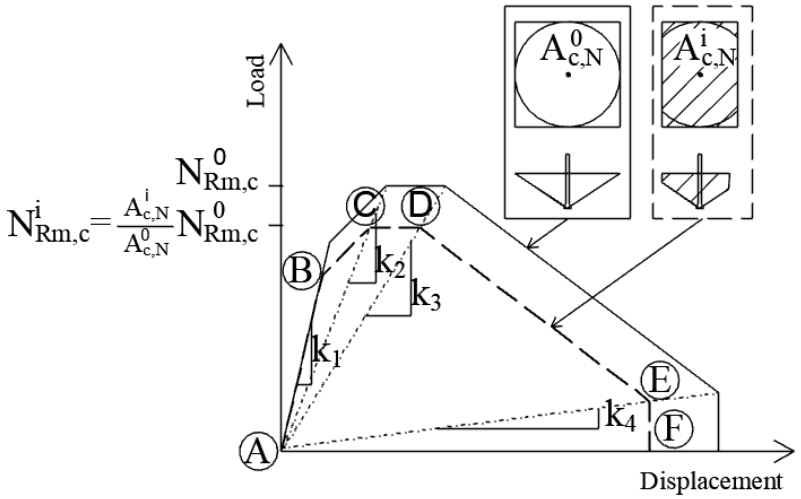

Figure 10.1. Scaling of the idealised curve of a single anchor following postulates 1 and 2 made in Section 5.2.2

In the nonlinear spring model, it is assumed that the failure load of an i^{th} individual anchor of an anchor group (compared to the failure load of a single anchor) is influenced by the neighbouring anchors and/or by a close edge and according to postulate 1, the failure load decreases in proportion to the projected tributary area (Section 5.2.2). The second postulate made in the spring model for the individual properties is that the tributary area assigned to an i^{th} anchor of

the group does not influence the stiffness of the anchor (k_1 - k_4 in *Figure 10.1*) and the stiffness values remain unchanged compared to the stiffness values determined for the corresponding single anchor. These two postulates are aimed to be verified in the following Sections 10.1.1 and 10.1.2.

10.1.1 Tributary area approach – Verification of Postulate 1

In Section 5.2.2, the tributary area approach was proposed to consider the influence of the group effect and the vicinity of the concrete edge. To verify the assumptions made, concrete breakout bodies of different anchor groups and the load distribution within anchor groups were extensively investigated. This was done to understand how to consider the effect of the anchor spacing on the individual anchor behaviour within the group and to define the individual anchor springs. The test results are discussed in Section 8.3 along with photos of typical breakout bodies obtained in the tests. The evaluation of the failure breakout bodies showed that not only in the cases covered by the current design provisions but also in case of relatively complex breakout bodies, a particular projected area of concrete can be attributed to each individual anchor. This tributary concrete area can be understood as a certain percentage of the projected area of the concrete cone that forms in case of the failure of a single anchor away from the edge. In the following, load-displacement curves from the corresponding tests and concrete breakout bodies are evaluated. The assumed theoretical tributary projected areas (red boxes with black lines) and projected cones (black circles) are shown in the corresponding figures (*Figure 10.2 – Figure 10.5*).

Investigations on rectangular configurations

To investigate the behaviour of regular rectangular anchorages, which are covered by the current design provisions and to verify the approach for tributary areas assigned to the individual anchors of a group, concentric and eccentric tension tests were carried out on quadruple (2×2) anchor group configurations. The current design provisions cover these cases and therefore, the direct comparison of the approach of CCD method with considering the projected area of the group and the approach with assigning the tributary projected areas to the individual anchors can be done. To investigate the influence of the anchor spacing on the anchor group behaviour without considering the influences such as the vicinity of concrete edge and eccentricity, the concentric tension tests performed away from the concrete edge, where no redistribution of forces takes place were evaluated. The results of tests showed that in the case of concentric loading, all four anchors within the group contribute equally to the group resistance, with circa one-fourth the total load. In *Figure 10.2a*, the load-displacement curve of one representative group and the corresponding individual anchor curves A1-A4, discussed in Section 8.1.1 are given. The developed concrete fracture surface and concrete breakout body are depicted in *Figure 10.2b*, which verify the contribution of the anchors based on the available concrete. Note that the developed cone shown in *Figure 10.2b* is bigger than the theoretical concrete cone (black circles) and it gets flatter near to the concrete surface. This is because, in reality, the crack always propagates to the support. (The support distance is at least $2h_{ef}$ from the outermost anchor of the group).

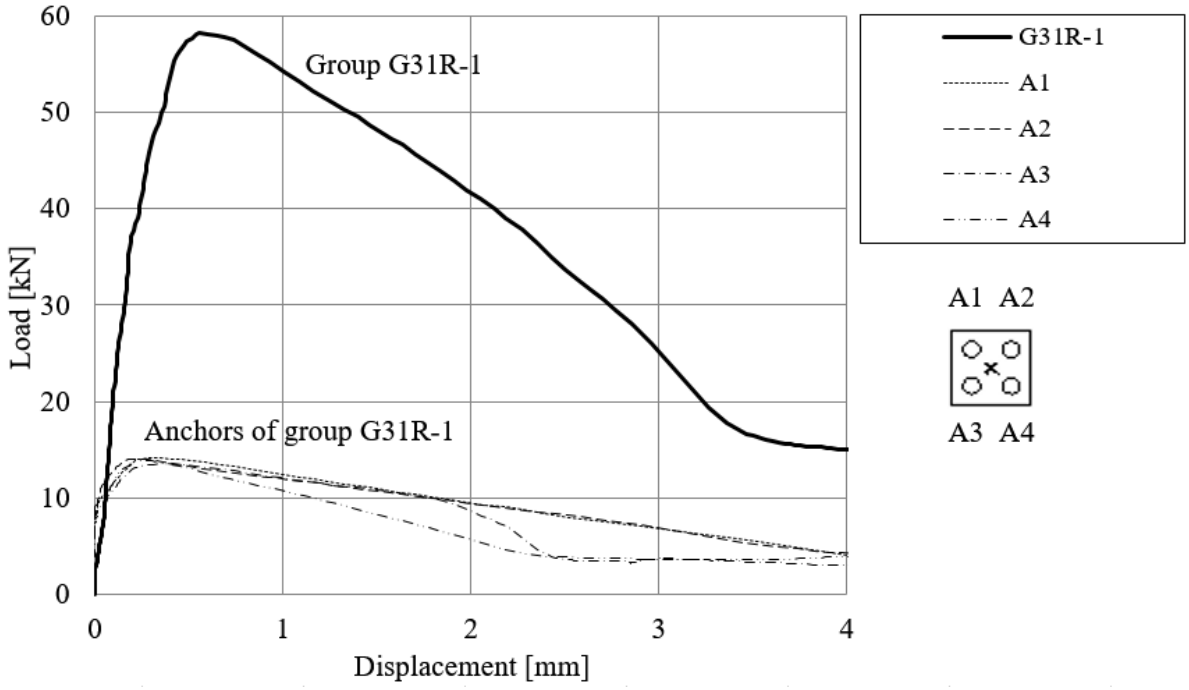

a)

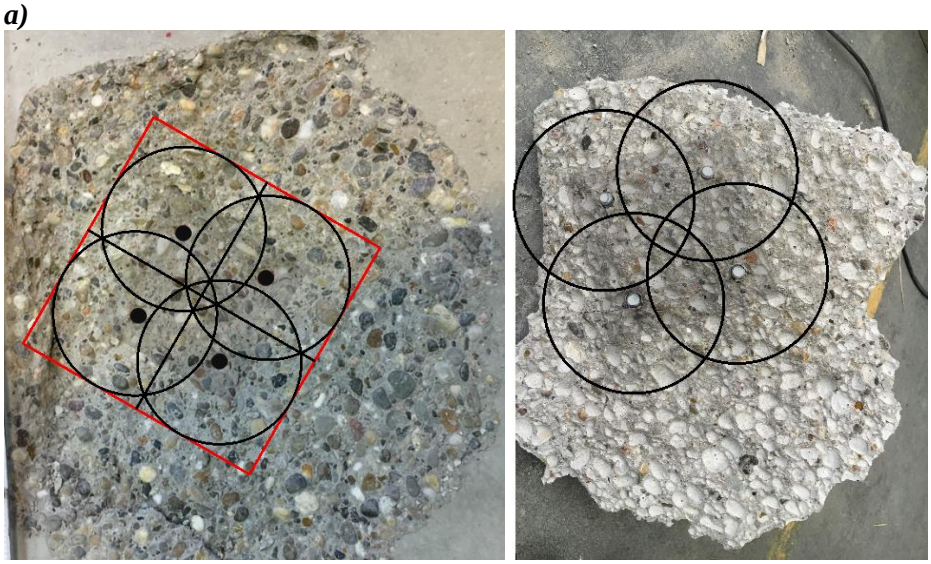

b)

Figure 10.2. Anchor group of 2 x 2 configuration - G31R test 1: a) Load-displacement curves; b) concrete breakout surface and the corresponding breakout body

The next case, which confirmed that the resistance of the individual anchors within the group is in accordance with the amount of concrete, which can be activated during the tests was on anchor group of 1×3 configuration loaded in concentric tension far from the concrete edge (Series G51R). The developed concrete breakout body follows the theoretical consideration of the individual anchor contribution (see *Figure 10.3b*). The graph in *Figure 10.3a* shows the individual anchor contribution during testing by plotting the anchor axial forces in the function of individual anchor displacement in case of test 3 of series G51R, which is in good agreement with the developed breakout body and concrete activated by the individual anchors. It is clear from the graph that the contribution of the middle anchor (A2) is the smallest among the anchors of the group and it is proportional with the calculated tributary projected area. In the depicted

test (test 3), the middle anchor contributed with ca. 25 kN and the outer anchors with 41 and 39 kN, respectively, which corresponds to an anchor contribution of $N_u(A2)/N_u(A1) = 0.64$. In case of test 1, $N_u(A2)/N_u(A1) = 0.75$ and in case of test 2, $N_u(A2)/N_u(A1) = 0.70$. The mean value is 0.7, which is in a good agreement with the ratio (0.72) of the corresponding tributary areas according to ***Eq. 80***

$$A_{c,N}^1 = A_{c,N}^3 = (1.5 \cdot 70 + 120/2) \cdot (3 \cdot 70) = 34650\ mm^2 \qquad \textbf{Eq. 78}$$

$$A_{c,N}^2 = (120) \cdot (3 \cdot 70) = 25200\ mm^2 \qquad \textbf{Eq. 79}$$

$$A_{c,N}^2 / A_{c,N}^1 = 25200/34650 = 0.72 \qquad \textbf{Eq. 80}$$

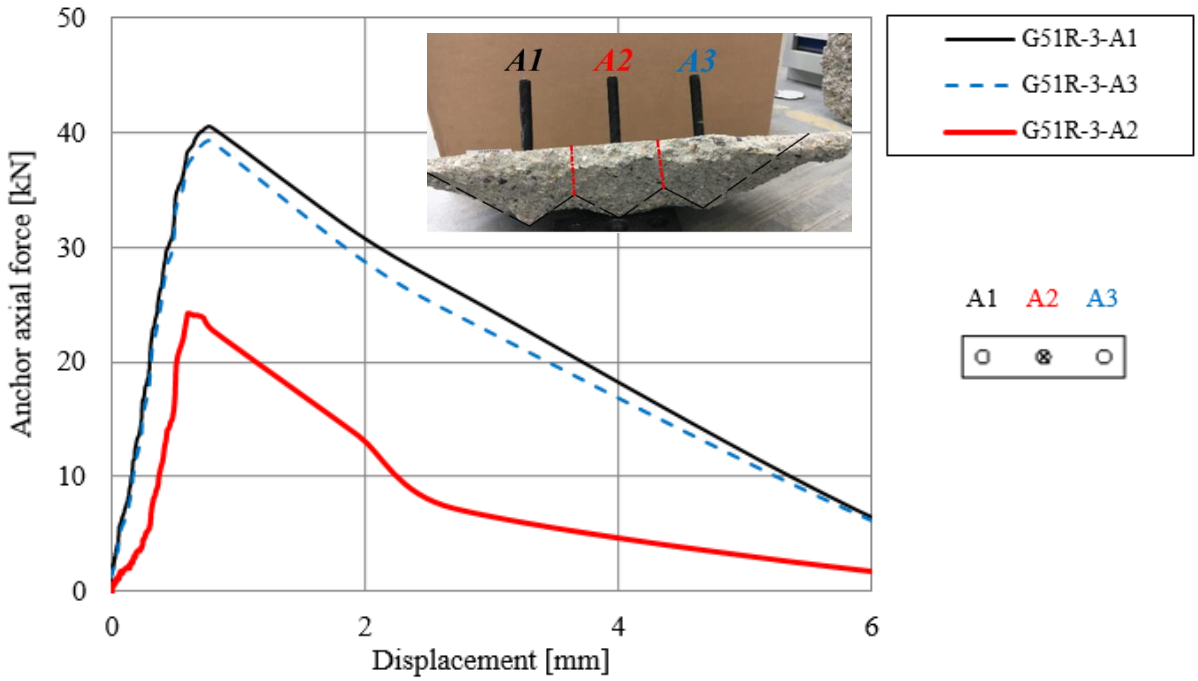

Figure 10.3. Concrete breakout body of G51R and anchor axial force - individual anchor displacement curves of series G51R

Non-rectangular configurations

As described in Section 5.2.2.1, the method for assignment of the tributary area for an anchor was extended for the calculation of non-rectangular anchorages as well. The concept of the assignment of the tributary area for the determination of spring characteristics for the anchors arranged in a non-rectangular pattern is explained with the help of a triangular anchor group in *Figure 5.10.* The concept is verified against tests on triangular, hexagonal, and L-shaped anchor configurations.

The method was verified against the experiments performed on the triangular group as follows: First, the reference tributary area $A_{c,N}^0$ according to ***Eq. 81*** was assigned to each anchor (*Figure 10.4a*). Then, keeping the anchor axis as the axis for rotation, the reference tributary areas $A_{c,N}^0$were rotated until the highest amount of overlap between the reference tributary areas of adjacent anchors $A_{c,N}^1$=$A_{c,N}^2$=$A_{c,N}^3$ was achieved (*Figure 10.4b* and ***Eq. 82***). Once the condition

of the maximum overlap was reached, the individual tributary area was given by the non-overlapping area belonging to the anchor and half of the overlapping area with the neighbouring anchors as it is depicted in *Figure 10.4b*, and which is also confirmed by the experimentally obtained breakout body in *Figure 10.4c*. The triangle configuration corresponds to test series G101 in normal strength concrete. The mean experimental failure load obtained in this series (G101) was 89.8 kN, which is 2.27-times the failure load corresponding to the failure load in series R9 on single anchors (39.5 kN) meaning that the increase due to the group effect was considered by the tributary approach with sufficient accuracy (compare with ***Eq. 84***).

$$A_{c,N}^{0} = (3 \cdot h_{ef})^2 = (3 \cdot 60\ mm)^2 = 32400\ mm^2 \qquad \textbf{Eq. 81}$$

$$A_{c,N}^{1} = A_{c,N}^{2} = A_{c,N}^{3} = (180\ mm \cdot 118.9\ mm) + (180 \cdot 52/2) = 26082\ mm^2 \qquad \textbf{Eq. 82}$$

$$A_{c,N}^{1} + A_{c,N}^{2} + A_{c,N}^{3} = 26082 \cdot 3 = 78246\ mm^2 \qquad \textbf{Eq. 83}$$

$$(A_{c,N}^{1} + A_{c,N}^{2} + A_{c,N}^{3})/A_{c,N}^{0} = 78246/32400 = 2.415 \qquad \textbf{Eq. 84}$$

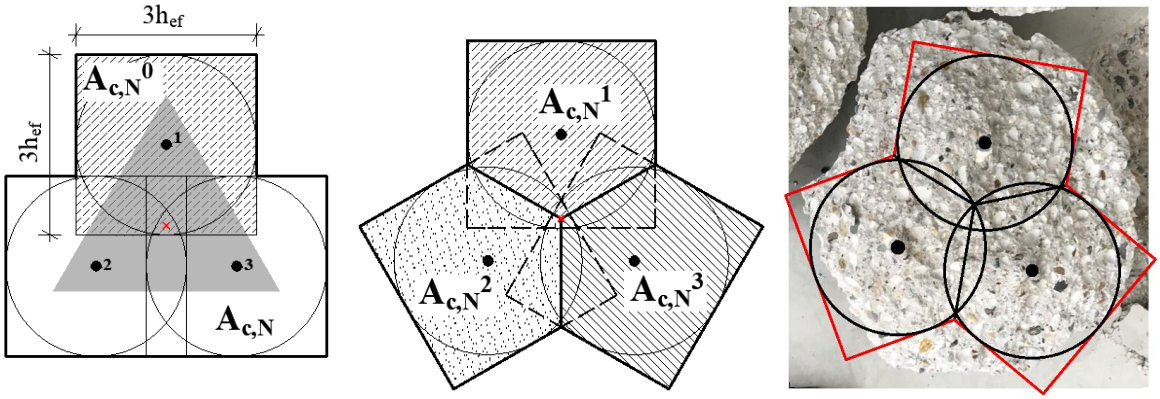

a) ***b)*** ***c)***

Figure 10.4. (a) Possible consideration of the projected area with reference projected area of a single anchor; (b) actual projected area of the group based on the results; (c) concrete breakout body of G101

The method for determination of tributary areas for the individual anchors is also validated against the experiments on hexagonal anchor groups having round base plate (series G301), which were loaded concentrically in tension. The assignment of the tributary areas for individual anchors is shown in *Figure 10.5a*, and the corresponding tributary areas are given in ***Eq. 85*** - ***Eq. 88***. The developed concrete breakout body shown in *Figure 10.5b* suggests that the tributary area associated with each anchor of the group is approximately equal and therefore, all the anchors are expected to contribute with approximately the same amount of force towards the group resistance. This is confirmed by the anchor axial force measurement made during the test (*Figure 10.5c*), where the peak individual anchor force was recorded as 20.8 kN, while the group resistance was recorded as 124.8 kN. The force of 21 kN, which is resisted by each anchor is 61% of the failure load measured on the corresponding single anchor series R30 (34.3 kN), which is comparable to the ratio of the tributary area assigned to the individual anchors and the reference tributary area of the single anchor $A_{c,N}^{1}/A_{c,N}^{0}=0.67$ (see ***Eq. 87***).

$$A_{c,N}^{0} = (3 \cdot h_{ef})^2 = (3 \cdot 60\ mm)^2 = 32400\ mm^2 \qquad \textit{Eq. 85}$$

$$A_{c,N}^{1} = A_{c,N}^{2} = A_{c,N}^{3} = A_{c,N}^{4} = A_{c,N}^{5} = A_{c,N}^{6} = 21810.8\ mm^2 \qquad \textit{Eq. 86}$$

$$A_{c,N}^{1} / A_{c,N}^{0} = 21810.8/32400 = 0.67 \qquad \textit{Eq. 87}$$

$$\sum_{i=1}^{6} A_{c,N}^{i} = 21810.8 \cdot 6 = 130864.8\ mm^2 \qquad \textit{Eq. 88}$$

$$\sum_{i=1}^{6} A_{c,N}^{i} / A_{c,N}^{0} = 130864.8/32400 = 4.04 \qquad \textit{Eq. 89}$$

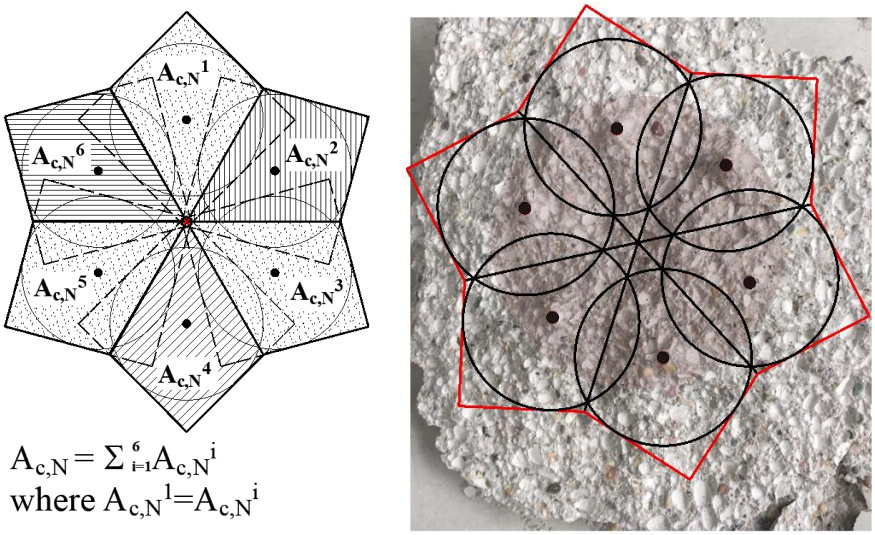

a) *b)*

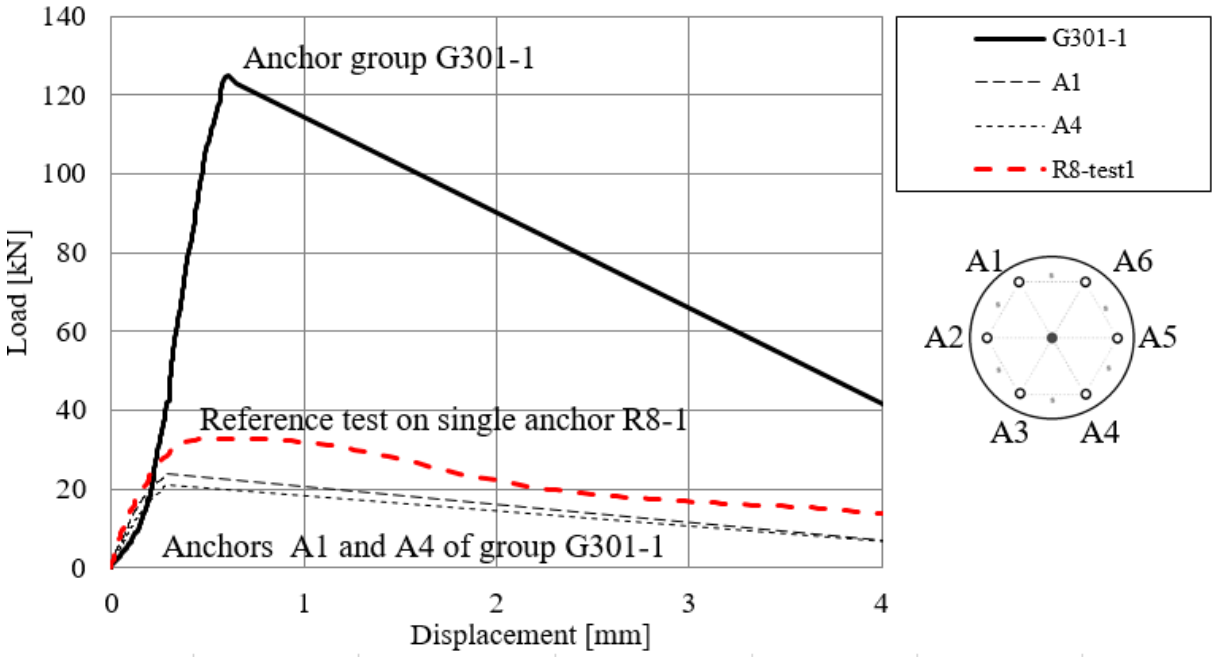

c)

Figure 10.5. a) Actual projected area of the group based on the results, b) concrete breakout body, c) anchor axial force - individual anchor displacement curves of G301-1

Figure 10.6 shows the concrete breakout body of a group of anchors arranged in an L-shaped pattern with a common L-shaped base plate and equal anchor spacing *s* in both directions (series G91). It was observed that the concrete cones of the adjacent anchors are overlapping and the tributary area, which can be allocated to the anchors, can be defined on the basis of the assumptions made for anchor groups of non-rectangular configurations. The failure load of the group reached in this series was 105.4 kN, which is 2.67-times the corresponding single anchor result (series R9). However, this ratio cannot directly be compared with the result of total tributary area for the anchorage since the group was subjected to eccentric tension loading and it is visible that two corners of the base plate restricted the tensioned concrete area. This is because the base plate rotated due to the eccentric load application and compression forces between the base plate and concrete surface developed, which restricted the tensioned concrete area.

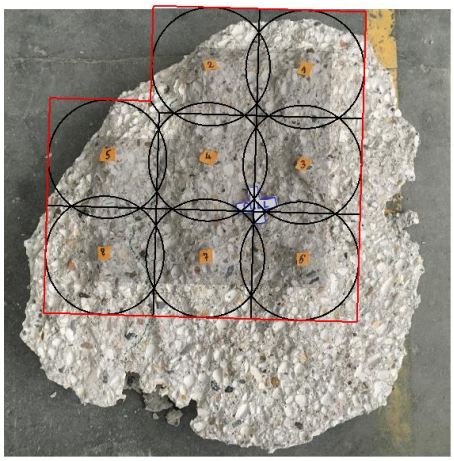

Figure 10.6. Concrete breakout body of the anchor group with L-shaped base plate G91

Investigations on anchor groups in cracked concrete

In the nonlinear spring modelling approach for concrete cone failure, the tributary area approach used for uncracked concrete is applied without any modifications on anchor groups in cracked concrete. The projected area of a single anchor remains unchanged, which is in accordance with the CCD method used for the design of anchorages (EN 1992-4, ACI 318, fib Bulletin 58). The same applies to the tributary projected area, which is assigned to the individual anchors of an anchor group. According to the current design provisions, the reduction in force due to cracked concrete condition is taken into account solely by the factor $k_{cr,N}$ and $k_{ucr,N}$ accounting for a reduction of 30% due to the presence of a crack. Note that according to ACI 318, the basic concrete breakout strength of a single anchor in tension is given in cracked concrete and the uncracked condition is considered by an increase factor $\psi_{c,N} = 1.25$ for cast-in anchors and $\psi_{c,N} = 1.4$ for post-installed anchors.

In the following, two cases are presented on 1×3 anchor groups to verify the assumption of applying the tributary area approach in cracked concrete (G62R) and in the case when only two anchors out of three are located in a crack (G67) as depicted in *Figure 10.7 a* and *b*, respectively. Both cases are loaded concentrically in tension without the influence of (i) a close edge, (ii) asymmetry in crack pattern and (iii) eccentricity of loading so that the tributary approach can be verified based on the area considerations.

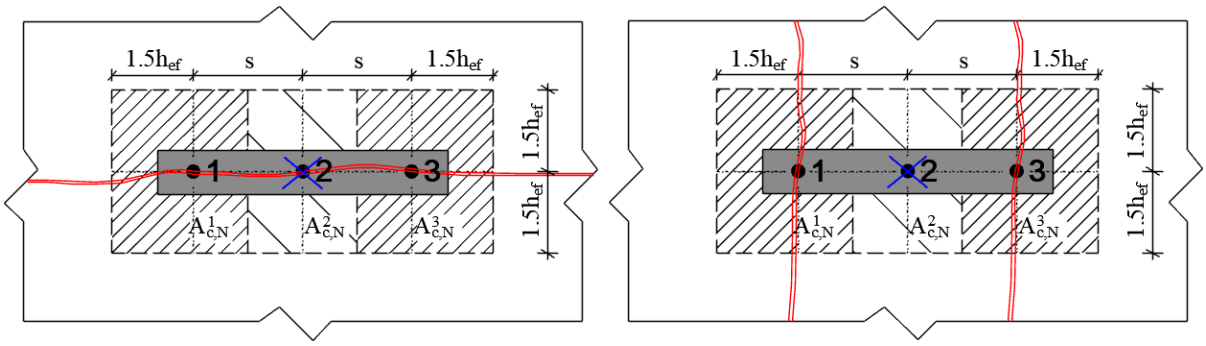

Figure 10.7. Tributary area assigned to 1×3 anchor groups in cracked concrete: a) series G62R, b) series G67

With ***Eq. 90***, the concrete cone resistance of an anchor group can be expressed, which is placed in cracked or uncracked concrete or when only some of the anchors are located in crack. The tributary projected areas should be assigned to the corresponding individual anchors. However, this equation will only deliver accurate results if the base plate is rigid, the load is applied concentrically and the crack pattern is symmetric. The equation is given for demonstration purpose, to show that the tributary area approach can be used without modifying the area that should be assigned to an individual anchor, which is located in a crack. In general, the nonlinear spring model should be used, which includes the tributary area approach but also considers the nonlinear load-displacement behaviour of the anchors in cracked and uncracked concrete, accounts for the influence of base plate stiffness, loading eccentricity, crack pattern and vicinity of the concrete edge. For series G62R and G67, the final equation is given by ***Eq. 94*** and ***Eq. 95***, respectively. The concrete cone resistance of the corresponding single anchors $N^{0}_{Rm,cr}$ and $N^{0}_{Rm,ucr}$ should be taken from *Table 8.6* (series R6-ncr and R6-cr) and applied in the equation.

$$N_{Rm}^{group} = N^{0}_{Rm,cr} \sum_{i=1}^{n_{cr}} \left(\frac{A^{i}_{c,N}}{A^{0}_{c,N}} \right) + N^{0}_{Rm,ucr} \sum_{i=1}^{n_{ucr}} \left(\frac{A^{i}_{c,N}}{A^{0}_{c,N}} \right) \qquad \textbf{Eq. 90}$$

$$A^{0}_{c,N} = (3 \cdot h_{ef})^2 = (3 \cdot 60\ mm)^2 = 32400\ mm^2 \qquad \textbf{Eq. 91}$$

$$A^{1}_{c.N} = A^{3}_{c.N} = \left(0.5 \cdot s + 1.5 \cdot h_{ef}\right) \cdot \left(3 \cdot h_{ef}\right) = (0.5 \cdot 120 + 1.5 \cdot 60) \cdot (3 \cdot 60) = 27000\ mm^2 \qquad \textbf{Eq. 92}$$

$$A^{2}_{c.N} = s\left(3 \cdot h_{ef}\right) = 120 \cdot (3 \cdot 60) = 21600\ mm^2 \qquad \textbf{Eq. 93}$$

$$N_{Rm}^{G62R} = N^{0}_{Rm,cr} \sum_{i=1}^{3} \left(\frac{A^{i}_{c,N}}{A^{0}_{c,N}} \right) = 19.2 \cdot 2.33 = 44.7kN \qquad \textbf{Eq. 94}$$

$$N_{Rm}^{G67} = N^{0}_{Rm,cr} \left(\frac{A^{1}_{c,N}}{A^{0}_{c,N}} \right) + \left(\frac{A^{3}_{c,N}}{A^{0}_{c,N}} \right) + N^{0}_{Rm,uncr} \left(\frac{A^{2}_{c,N}}{A^{0}_{c,N}} \right) = \qquad \textbf{Eq. 95}$$

$$= 19.2 \cdot 1.67 + 27.8 \cdot 0.67 = 50.7\text{kN}$$

The mean measured ultimate load obtained in series G62R was 43.1 kN, which is just 3% lower compared to the calculated value of 44.7 kN (***Eq. 94***). For series G67, the mean measured ultimate load was 47.4 kN, which is 6% lower compared to the calculated value (***Eq. 95***). This

difference can be explained by the fact that calculating the group failure load using ***Eq. 90***, a rigid base plate is assumed. This means also that while loading the group in concentric tension, for symmetric crack pattern, all anchors have equal displacement independently of their load-displacement behaviour. However, in reality, and in the tests, the base plate might not be sufficiently stiff and that way the CCD method cannot be applied directly. The base plate deformations and different stiffness conditions are taken into account automatically by the spring model by applying the corresponding spring characteristics, modelling the base plate realistically and performing a nonlinear static analysis.

10.1.2 Stiffness of the idealised load-displacement curves – Verification of Postulate 2

In the nonlinear spring model for concrete cone failure, even though the load values are scaled down using the reduction factor $A^{i}_{c,N}/A^{0}_{c,N}$ to consider the influence of anchor spacing and vicinity of concrete edge but the stiffness values remain unchanged resulting in smaller displacement values for the salient points on the anchor spring properties as depicted in *Figure 10.1* (more details see Section 5.2). This assumption is based on the evaluation of the results of the experiments discussed in Section 8.3, which showed that the vicinity of concrete edge or the virtual edge (considered at a distance of half the spacing to the neighbouring anchor) influences the individual anchor capacity in the group but not the stiffness of the anchor. Some of the test results supporting this assumption are given in *Figure 10.8* - *Figure 10.9*, with plotting the anchor axial forces and the group load in function of anchor and anchor group displacement.

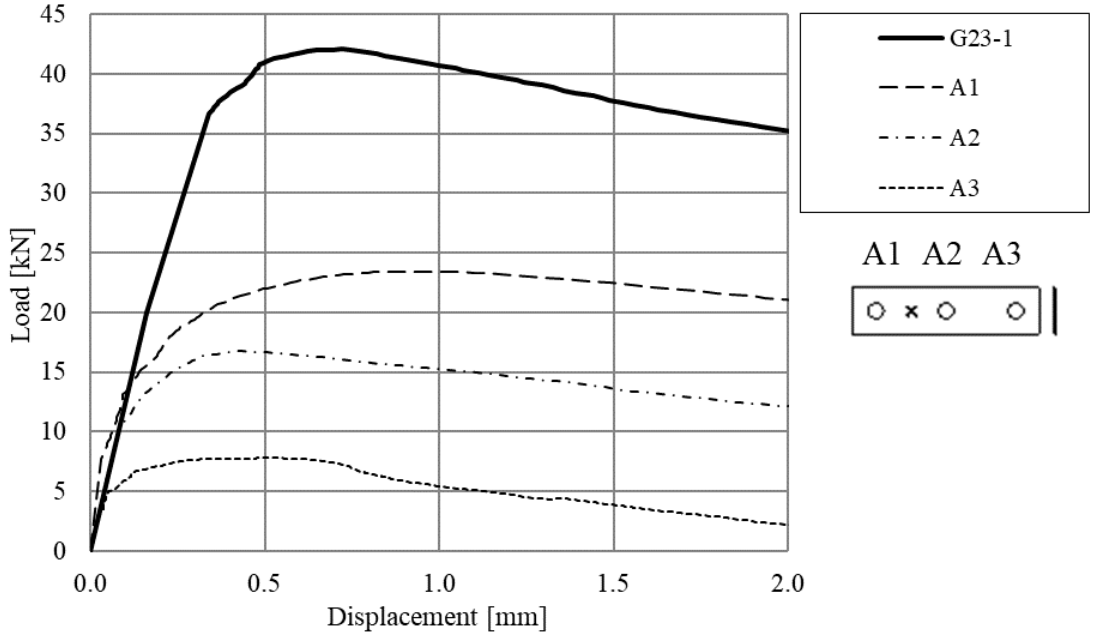

Figure 10.8. Load-displacement behaviour of individual anchors compared to "reference" single anchor Series G23, test 2

Figure 10.8 shows the load-displacement behaviour of an anchor group of 1×3 configuration, which is installed close to the concrete edge (c = 50 mm) and is loaded eccentrically in tension (Series G23). In this case, different projected areas can be assigned to the individual anchors A1, A2 and A3 (21697.5 mm^2, 16170 mm^2 and 16633 mm^2, respectively) but the stiffness of

the individual anchors does not change. The individual anchor axial forces are different due to the amount of concrete, which can be activated by the anchors and due to the uneven loading due to eccentricity, but the initial stiffness k_1 of the corresponding curves remains practically unchanged.

In *Figure 10.9*, the load-displacement curves of an anchor group of 1×4 configuration with 40 mm thick base plate away from the concrete edge are given (series G81, test 2). In this graph, the individual anchor force-displacement curves and the load-displacement curve of the group are compared to one representative reference single anchor curve (series R8, test 3). It can be seen that even though the anchors of the group have unequal load capacity, which is also lower than that of the corresponding single anchor, the initial stiffness k_1 of the individual anchors is equal and the same as that of the corresponding single anchor (series R8). Since the stiffness of the anchors remains unchanged, while the load-carrying capacity reduces due to the group effect considered by the reduction factor $A_{c,N}^{i}/A_{c,N}^{0}$, the anchors of the group reach the peak load at a lower displacement that of the corresponding single anchor away from the edge. This justifies the assumption of reducing the load capacity while maintaining the stiffness to consider the group effect (virtual edge) or edge effect of the anchors as explained in *Figure 10.1*.

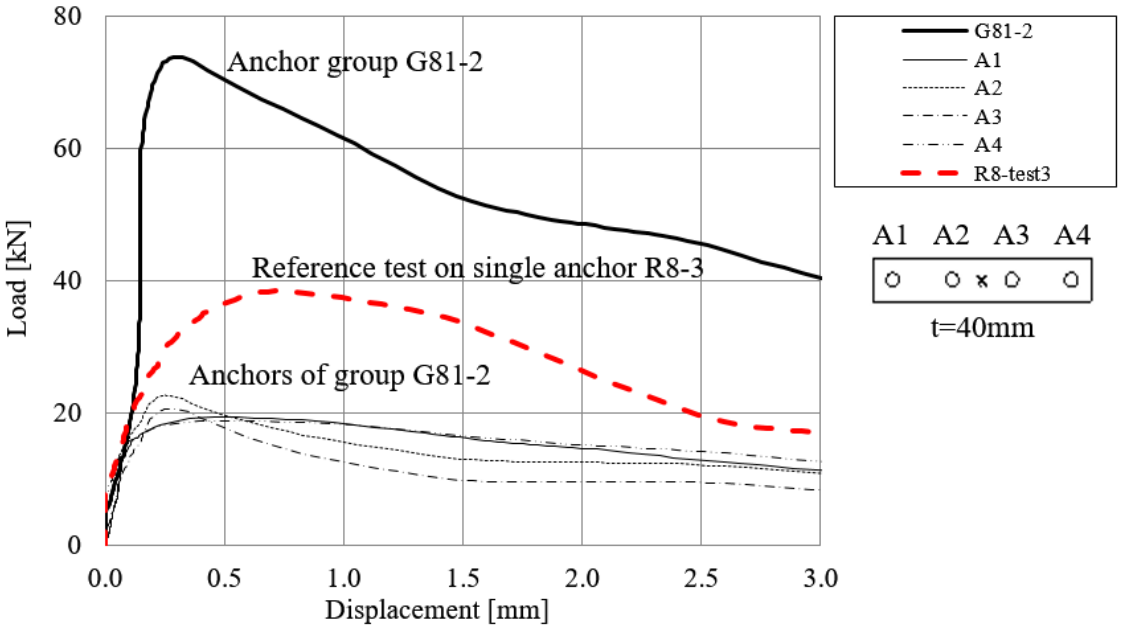

Figure 10.9. Load-displacement behaviour of individual anchors compared to "reference" single anchor Series G81, test 2

The postulate on the stiffness of the reduced curves can also be verified by the test results of non-rectangular anchor configurations. *Figure 10.5* shows the load-displacement curves of a group of six anchors arranged in a hexagonal pattern with a round base plate (series G301). Two representative individual anchor axial force-displacement curves from the group are compared with the reference load-displacement curve from series R8 (test 1). The load, which was reached by the anchors is ca. 67% of the reference single anchor capacity, which corresponds to the factor $A_{c,N}^{i}/A_{c,N}^{0}$, that can be calculated according to ***Eq. 85-Eq. 87***. However, the initial stiffness k_1 of the individual anchors is equal and the same as that of the corresponding single anchor (series R8).

10.2 VERIFICATION OF THE FAILURE LOADS AND LOAD-DISPLACEMENT BEHAVIOUR OBTAINED FROM THE SPRING MODEL AGAINST EXPERIMENTS

In the following, the spring model is verified against test data from this work (Section 10.2.1) and from the literature (Section 10.2.2). The comparison of the failure loads is reported for all investigated case, whereas the load-displacement curves are plotted for representative cases. Furthermore, sample calculations are given in Section 10.2.1.1 to demonstrate how the spring model should be applied and to show how the verification for each test was done.

10.2.1 Verification of the failure loads and load-displacement behaviour obtained from the spring model against test results from this work

10.2.1.1 Sample calculations

Rectangular 1×4 anchor group configuration

In this example, an anchor group of 1×4 configuration subjected to concentric and eccentric tension loading is investigated. The configurations are shown in *Figure 10.10*, which correspond to the test series G81, G82 and G83. In the case of series G81 and G83, the tension load was applied concentrically on the group having 40 mm and 10 mm thick base plates, respectively. In series G82, the same base plate as for series G81 was used, however, applying the tension force eccentrically between anchors 1 and 2.

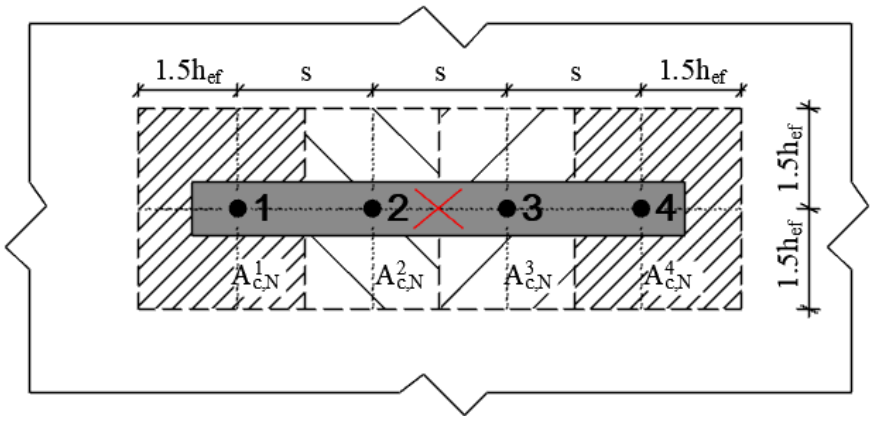

a)

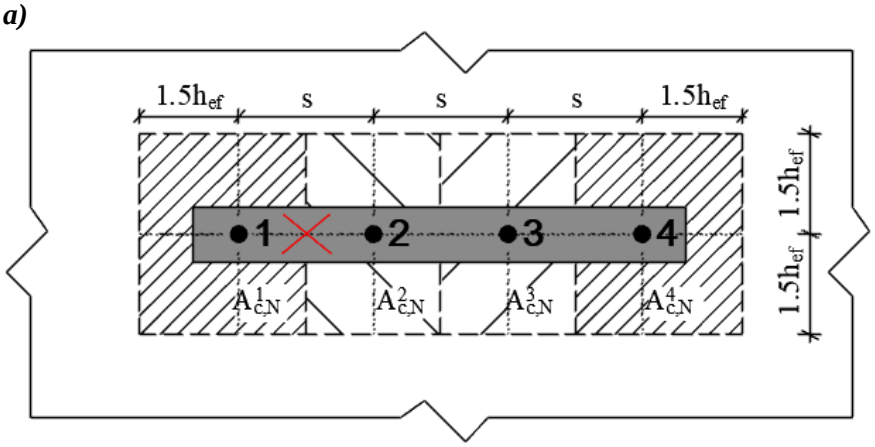

b)

Figure 10.10. Anchor group configuration, tributary projected area and point of load application for a) series G81 and b) series G82

Table 10.1. Test parameters of the groups G81,G82 and G83

Injection system	Bonded anchor (Epoxy $\tau \approx 30$ N/mm^2)
Steel element	Threaded rod M12 12.9
Embedment depth h_{ef}	60 mm
Critical anchor spacing $s_{cr,N}$	180 mm
Anchor spacing s	90 mm
Critical edge distance $c_{cr,N}$	90 mm
Edge distance c	> 90 mm
Concrete compressive strength (cube) $f_{cc,m}$	31.4 N/mm^2
Number of anchors within the group	four in one row
Base plate dimensions $l*w*t$	350 mm×60 mm×40 mm/10 mm
Test type	Centric (G81, G83), eccentric (G82) tension
Failure mode	Concrete cone failure

The parameters of the investigated anchor groups are listed in *Table 10.1*. The results of three tension tests on the corresponding single anchors were taken from section 8.3.2.1 to obtain the basic nonlinear spring characteristics. The load-displacement curves along with the idealised curve are given in *Figure 10.11*. The idealisation was performed according to the method described in Section 5.2.1. The coordinates of the reference curve are listed in *Table 10.2*. Subsequently, the reference curve was scaled down based on the tributary area available for the corresponding individual anchors using the reduction factor $A^i_{c,N}/A^0_{c,N}$ according to ***Eq. 96*** - ***Eq. 100***. The obtained spring characteristics are listed in *Table 10.2*.

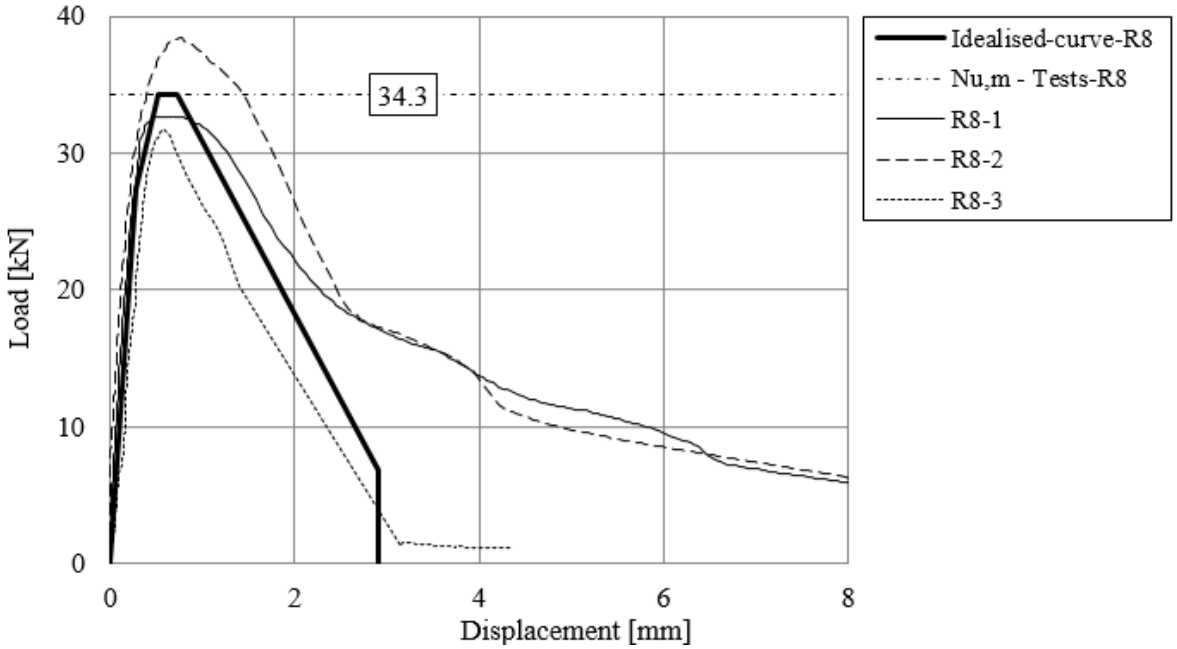

Figure 10.11. Load-displacement curves and idealised curve of tests on single anchor in series R8

$$A^0_{c,N} = (3 \cdot h_{ef})^2 = 32400\ mm^2 \qquad \textbf{Eq. 96}$$

$$A^1_{c,N} = A^4_{c,N} = \left(3 \cdot h_{ef}\right) \cdot \left(1.5 \cdot h_{ef} + 0.5 \cdot s\right) = 24300\ mm^2 \qquad \textbf{Eq. 97}$$

$$A_{c,N}^{2} = A_{c,N}^{3} = \left(3 \cdot h_{ef}\right) \cdot s = 16200\ mm^2 \qquad \textit{Eq. 98}$$

$$N_{Rm,c}^{1} = N_{Rm,c}^{4} = N_{Rm,c}^{0} \cdot \frac{A_{c,N}^{1}}{A_{c,N}^{0}} = 25.7\ kN \qquad \textit{Eq. 99}$$

$$N_{Rm,c}^{2} = N_{Rm,c}^{3} = N_{Rm,c}^{0} \cdot \frac{A_{c,N}^{2}}{A_{c,N}^{0}} = 17.1\ kN \qquad \textit{Eq. 100}$$

Table 10.2. Spring properties of individual springs of the anchor groups G81, G82 and G83

	Load $N_{Rm,c}{}^{i}{}_{A\text{-}F}$ [kN]	Stiffness k_1-k_4 [kN/mm]	Displacement $\delta_{A\text{-}F}$ [mm]
Reference single anchor			
A	0.0	0.0	0.00
B	27.4	97.8	0.28
C	34.3	65.2	0.53
D	34.3	47.1	0.73
E	6.9	2.4	2.91
F	0.0	0.0	2.91
Anchors A1 and A4			
A	0.0	0.0	0.00
B	20.6	97.8	0.21
C	25.7	65.2	0.39
D	25.7	47.1	0.55
E	5.1	2.4	2.18
F	0.0	0.0	2.18
Anchors A2 and A3			
A	0.0	0.0	0.00
B	13.7	97.8	0.14
C	17.1	65.2	0.26
D	17.1	47.1	0.36
E	3.4	2.4	1.46
F	0.0	0.0	1.46

After obtaining the spring characteristics, they were assigned to the tension-only springs representing the nonlinear anchor behaviour in the finite element model, which includes shell elements for modelling of the base plate and compression-only springs simulating the contact between concrete and base plate. For the models G81 and G82, the shell elements were modelled as 40 mm, whereas for the test series G83 the base plate thickness was 10 mm to investigate the influence of base plate thickness. The load was applied on the nodes based on the point of load application (concentric or eccentric) and the nonlinear static analysis was performed in displacement control until the desired displacement.

The load-displacement curve of the concentrically loaded group (G81) obtained as an output from the spring model is shown in *Figure 10.12a*. To verify the results obtained from the analysis with the spring model, the test results are also plotted in *Figure 10.12a*. The comparison shows a very good agreement of test results and the result of the spring model in terms of ultimate load (4% deviation) and curve progression as well.

In series G83, the base plate (shell) thickness was reduced to 10 mm; all other spring and loading parameters remained unchanged compared to G81. The corresponding load-displacement curves from the spring model are plotted in *Figure 10.12b* along with the experimental results. In terms of mean ultimate loads, the spring model delivers slightly conservative results (23%). However, note that the scatter of the test results was large and therefore, to be on the safe side, it is better to consider the lowest test result as decisive, which is test 3 in series G81. In this case, the match in terms of ultimate load and curve progression is satisfactory. The load-displacement behaviour of the anchor group is realistically reflected by using the spring model. The load-displacement curve of the spring model in *Figure 10.12b* follows the same behaviour as in test 3 while activating the two middle anchors first, and after redistribution of the forces activating the outer anchors leading to a second peak. This confirms that the spring model can consider the influence of base plate stiffness on the load-displacement behaviour of anchor groups reasonably well.

Another analysis was carried out on the 1×4 anchor group configuration with 40 mm thick base plate but applying the load with an eccentricity of the external load $e = s = 90$ *mm* (G82). The exact same model as for series G81 was used to carry out this analysis by varying only the point of load application. The spring characteristics for the anchors and concrete remained the same as in the concentric loading case, since the capacity of the individual anchors is not changing by applying the load in another position. Due to the different loading; however, the utilisation of the individual anchor capacity and the load distribution within the group change. The influence of the eccentric loading was not considered by any additional ψ factors. Through the step-by-step nonlinear static analysis, the nonlinear spring model accounts for the effect of eccentricity through the realistic distribution of anchor forces automatically. The load-displacement curve obtained from the spring model and the experimental curves are given in *Figure 10.12c*. The experimental results are again in a good agreement with the results of the spring model ($N_{u,m.test}/N_{u.model} = 1.09$).

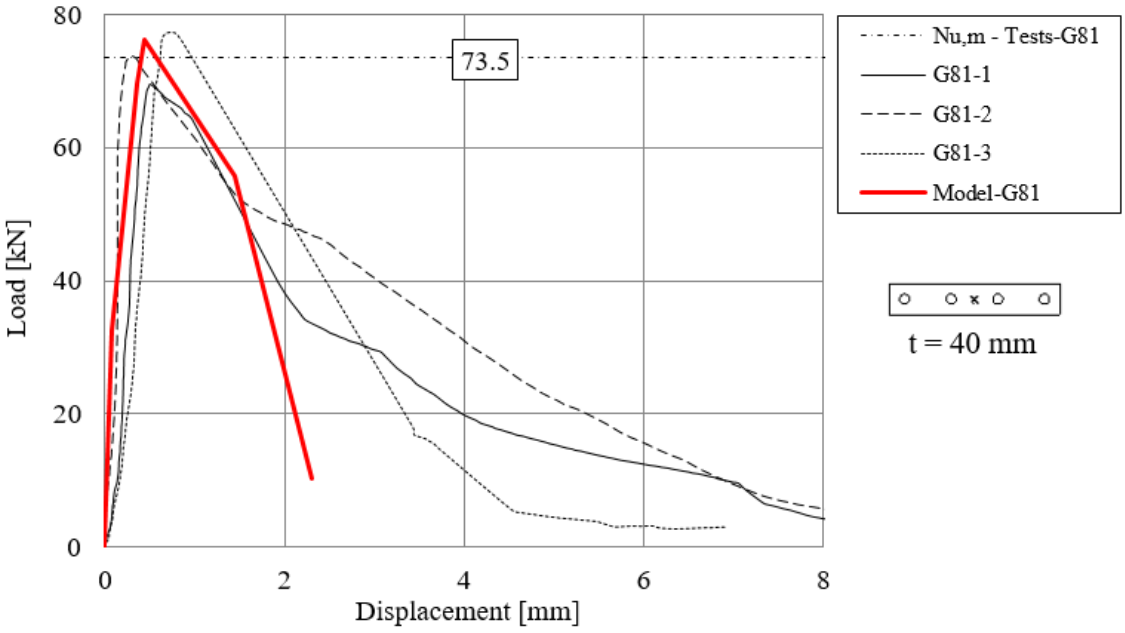

a)

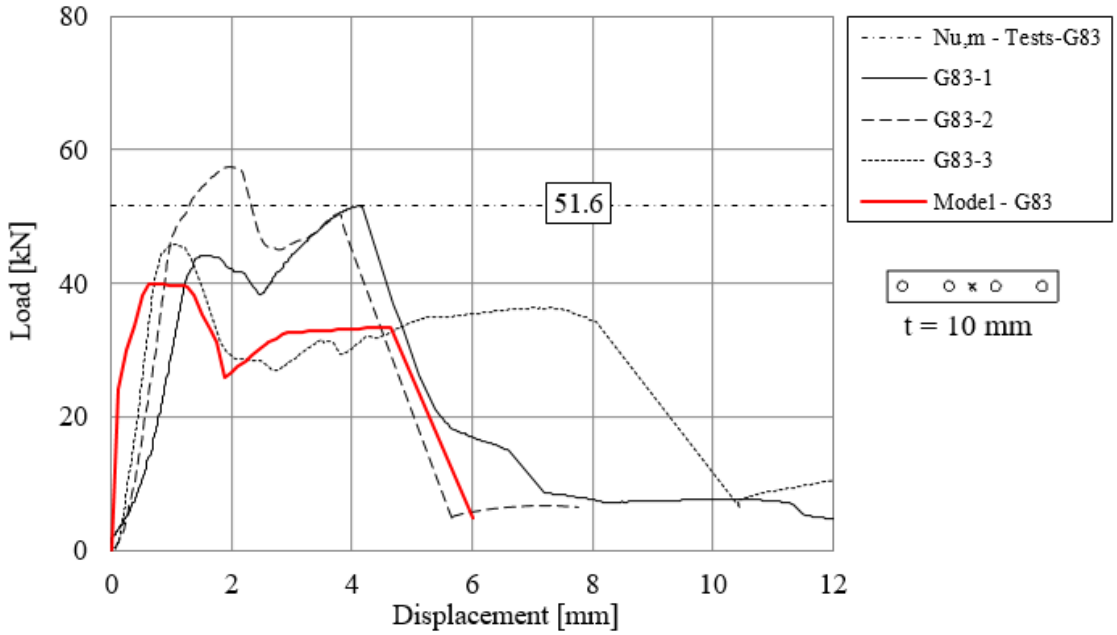

b)

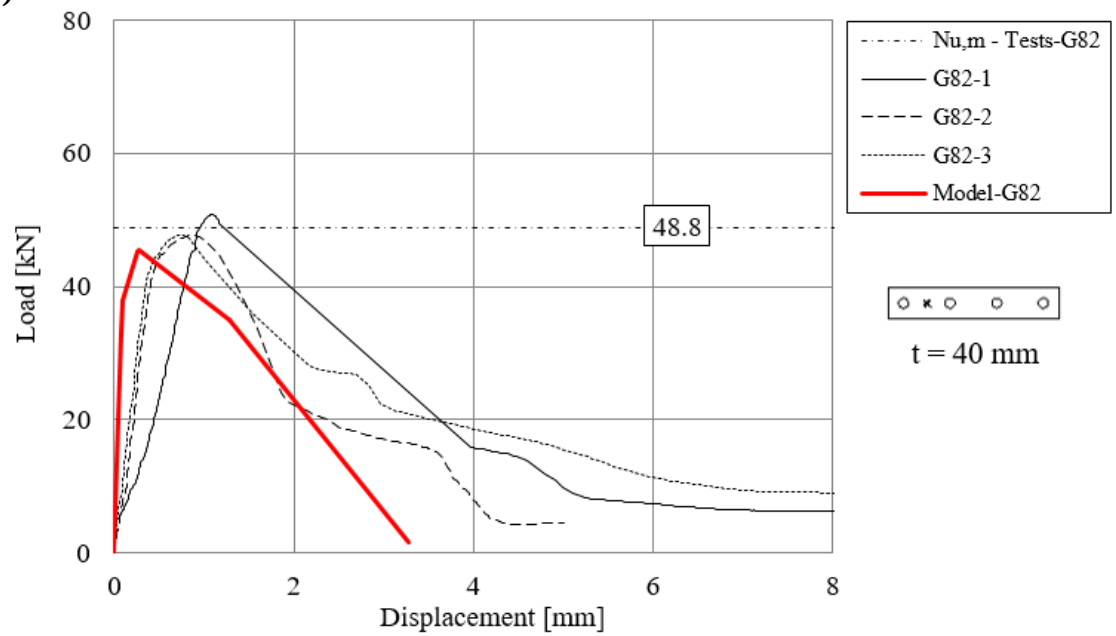

c)

Figure 10.12. Load-displacement curves obtained from tests on anchor groups and the result of the spring model: a) series G81, b) series G83 and c) series G82

Anchor groups in cracked concrete

In the following, the spring model is verified against the results of an anchor group of 1×3 configuration subjected to eccentric tension load, by comparing the results of the spring model and test results from Section 8.3.3.1. In both series G65 and G66, one anchor (A1) out of three was installed in a crack. The investigated configurations are shown in *Figure 10.13a* and *b*, which correspond to the test series G65 and G66, respectively. In the case of series G65, the tension load was applied between the outer anchor located in the crack and middle anchor. In series G66, the tension load was applied between the middle and outer anchors in the uncracked part of the specimen.

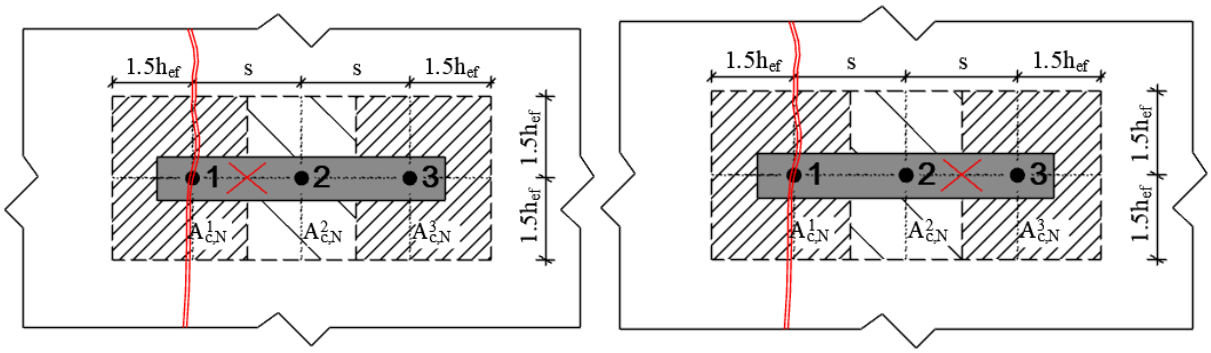

a) ***b)***

Figure 10.13. Anchor group configuration, tributary projected area and point of load application for a) series G65 and b) series G66

The installation parameters of the investigated 1×3 anchor groups are given in *Table 10.3*. Since in the case of series G65 and G66 one anchor out of three was placed in a crack, it was necessary to generate the spring characteristics for single anchors in both uncracked and cracked concrete. For that, the results of tension tests on the corresponding single anchors in uncracked (R6-ncr) and cracked (R6-cr) concrete were taken from Section 8.3.3.1 to obtain the nonlinear spring characteristics (idealised curve).

Table 10.3. Test parameters of the group configurations G65 and G66

Injection system	Bonded anchor (Epoxy $\tau \approx 30$ N/mm^2)
Steel element	Threaded rod M12 12.9
Embedment depth h_{ef}	60 mm
Critical anchor spacing $s_{cr,N}$	180 mm
Anchor spacing s	120 mm
Critical edge distance $c_{cr,N}$	90 mm
Edge distance c	> 90 mm
Concrete compressive strength (cube) $f_{cc,m}$	23.0 N/mm^2
Crack width Δw	0.3 mm (one anchor placed in crack)
Number of anchors within the group	three in one row
Base plate dimensions $l*w*t$	400 mm×120 mm×50 mm
Test type	Eccentric tension test
Failure mode	Concrete cone failure

The load-displacement curves from the single anchor tests along with the idealised curve (spring characteristics of the single anchor) are given in *Figure 10.14*. The coordinates of the idealised curve are listed in *Table 10.4* and *Table 10.5* for uncracked and cracked concrete, respectively. It is clear from the test results that the load and stiffness values are lower for the single anchors in crack concrete than in uncracked, and this is also considered in the spring model with generating the corresponding spring characteristics. Once the data pairs of the idealised curve are available for uncracked and cracked concrete, the curve can be scaled down based on the tributary area available for the corresponding individual anchors using the reduction factor $A^i_{c,N}/A^0_{c,N}$ according to ***Eq. 101*** - ***Eq. 105***. As it was verified in 10.1.1, the tributary area approach used for uncracked concrete can be applied without any modifications on anchor groups in cracked concrete as well.

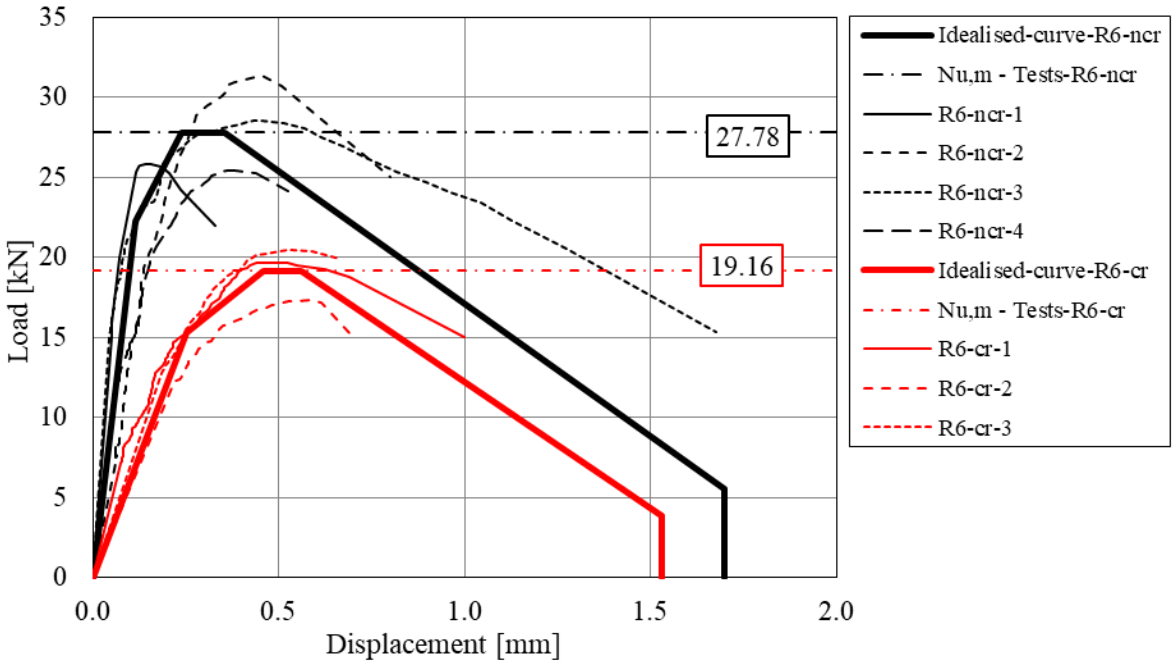

Figure 10.14. Idealised load-displacement curves of single anchors in cracked (R6-cr) and uncracked concrete (R6-ncr)

$$A^0_{c,N} = (3 \cdot h_{ef})^2 = (3 \cdot 60\ mm)^2 = 32400\ mm^2 \qquad \textbf{Eq. 101}$$

$$A^1_{c,N} = A^3_{c,N} = \left(3 \cdot h_{ef}\right) \cdot \left(1.5 \cdot h_{ef} + 0.5 \cdot s\right) = 27000\ mm^2 \qquad \textbf{Eq. 102}$$

$$A^2_{c,N} = \left(3 \cdot h_{ef}\right) \cdot s = 21600\ mm^2 \qquad \textbf{Eq. 103}$$

$N^1_{Rm,c} = N^3_{Rm,c} = N^0_{Rm,c} \cdot A^1_{c,N}/A^0_{c,N} = 23.1\ kN$ for uncracked concrete **Eq. 104**

$N^2_{Rm,c} = N^0_{Rm,c} \cdot A^2_{c,N}/A^0_{c,N} = 18.5\ kN$ for uncracked concrete **Eq. 105**

Table 10.4. Spring properties of individual springs of the anchor groups G65 and G66 in uncracked concrete

	Load $N_{Rm,c}{}^{i}{}_{A\text{-}F}$ [kN]	Stiffness k_1-k_4 [kN/mm]	Displacement $\delta_{A\text{-}F}$ [mm]
Reference single anchor			
A	0.0	0.0	0.00
B	22.2	191.8	0.12
C	27.8	116.3	0.24
D	27.8	78.1	0.36
E	5.6	2.4	2.30
F	0.0	0.0	2.30
Anchors A1 and A3 (outer)			
A	0.0	0.0	0.00
B	18.5	191.8	0.10
C	23.1	116.3	0.20
D	23.1	78.1	0.30
E	4.6	2.4	1.91
F	0.0	0.0	1.91

Anchor 2 (middle)			
A	0.0	0.0	0.00
B	14.8	191.8	0.08
C	18.5	116.3	0.16
D	18.5	78.1	0.24
E	3.7	2.4	1.53
F	0.0	0.0	1.53

Table 10.5. Spring properties of individual springs of the anchor group G65 and G66 in cracked concrete

	Load $N_{Rm,c}{}^{i}{}_{A\text{-}F}$ [kN]	Stiffness k_1-k_4 [kN/mm]	Displacement $\delta_{A\text{-}F}$ [mm]
Reference single anchor			
A	0.0	0.0	0.21
B	15.3	82.1	0.50
C	19.2	38.6	0.63
D	19.2	30.6	3.25
E	3.8	1.2	3.25
F	0.0	0.0	0.21
Anchors A1 and A3 (outer)			
A	0.0	0.0	0.00
B	12.8	82.1	0.17
C	16.0	38.6	0.41
D	16.0	30.6	0.52
E	3.2	1.2	2.71
F	0.0	0.0	2.71
Anchor 2 (middle)			
A	0.00	0.0	0.00
B	10.22	82.1	0.14
C	12.77	38.6	0.33
D	12.77	30.6	0.42
E	2.55	1.2	2.17
F	0.00	0.0	2.17

When the spring characteristics are obtained (see in *Table 10.4* and *Table 10.5*), they should be assigned to the corresponding individual anchors within the group. The modelling is done in the same way as it is described for the 1×4 case above. The load is applied at the point of load application taking into account the configuration and the nonlinear static analysis is performed in displacement control until the desired target displacement.

Figure 10.15a shows the results obtained from the spring model and from the experiments in series G65 when the load was applied close to the crack. This condition was only considered by assigning the corresponding anchor spring characteristics for the anchors A1-A2-A3 as cracked – uncracked – uncracked and by applying the load eccentrically. The comparison of the load-displacement curves shows a very good agreement of results in terms of ultimate load and curve progression. Another analysis was carried out on the same anchor group configuration with applying the eccentric load far from the crack in series G66. The comparison of the

load-displacement curves shows again a good agreement of the obtained results in terms of ultimate load and curve progression as it can be seen in *Figure 10.15b*. With these two cases, it was shown that the nonlinear spring model for concrete cone failure is capable of considering the actual crack pattern, the influence of eccentric loading and their superposition.

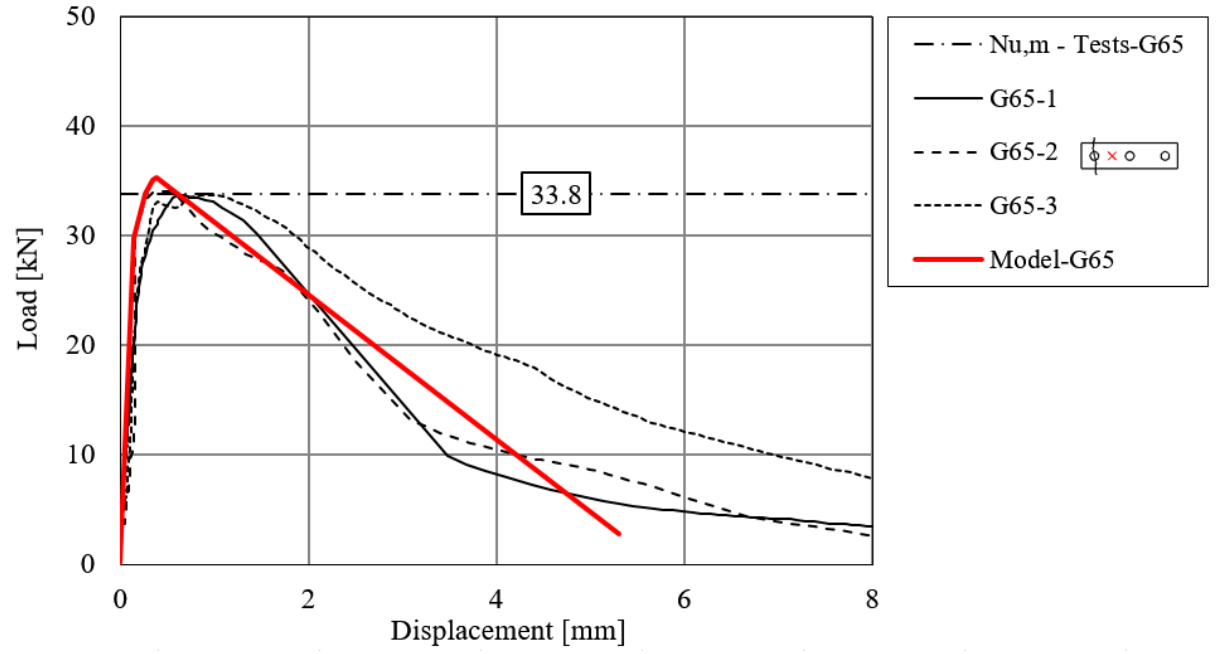

a)

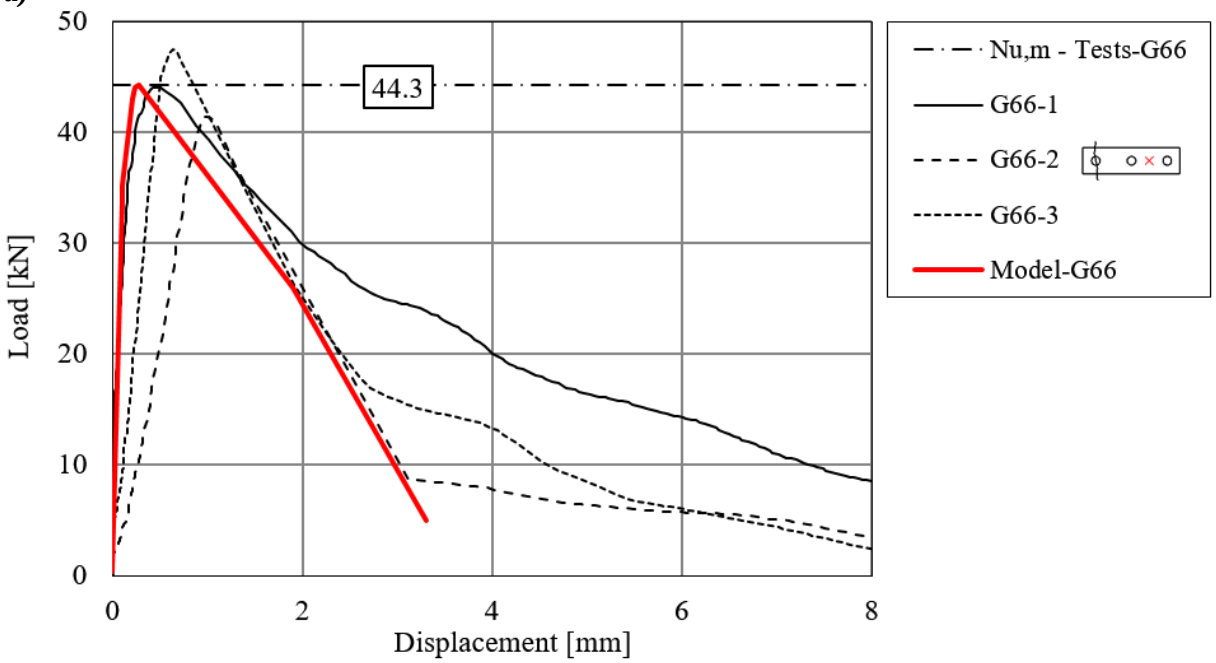

b)

Figure 10.15. Load-displacement curves obtained from tests on anchor groups and the result of the spring model: a) series G65 and b) series G66

10.2.1.2 Comparison of test results with the results of the nonlinear spring model

In the following, the results of the spring model are compared with the results of experimental tests from this thesis. The comparison in terms of the ultimate load of the anchor groups is given in *Table 10.6* - *Table 10.8*. In addition, load-displacement curves from the spring model are plotted against the experimental curves for select cases in *Figure 10.17* - *Figure 10.22* to verify the spring model not just in terms of ultimate loads but also in terms of load-displacement behaviour. Note that the load-displacement curves of the test results are given in Section 8.3. However, for the ease of reading, some of them are reproduced here to facilitate the comparison with the corresponding load-displacement curves obtained from the analysis using spring model in order to verify the spring model as a displacement-based approach.

Anchorages of rectangular configurations in uncracked concrete within the scope of EN 1992-4

Table 10.6 contains the results on anchor groups of rectangular configurations in uncracked concrete within the scope of EN 1992-4, corresponding to anchor groups of 1×3 and 2×2 configurations. The results of the spring model are in good agreement with the experimental results (*Figure 10.16)*. The mean value of $N_{u,test}/N_{u,spring\ model}$ is 0.99 with a coefficient of variation of 7.4%. In addition, for the anchor groups reported in *Table 10.6*, the concrete cone resistance was calculated according to EN 1992-4, and is given in *Table 8.4* along with the experimental results. The calculated values were compared to the corresponding results of the spring model. The mean value of $N_{u,EN1992\text{-}4}/N_{u,spring\ model}$ is 0.94 and the coefficient of variation is 12.5%.

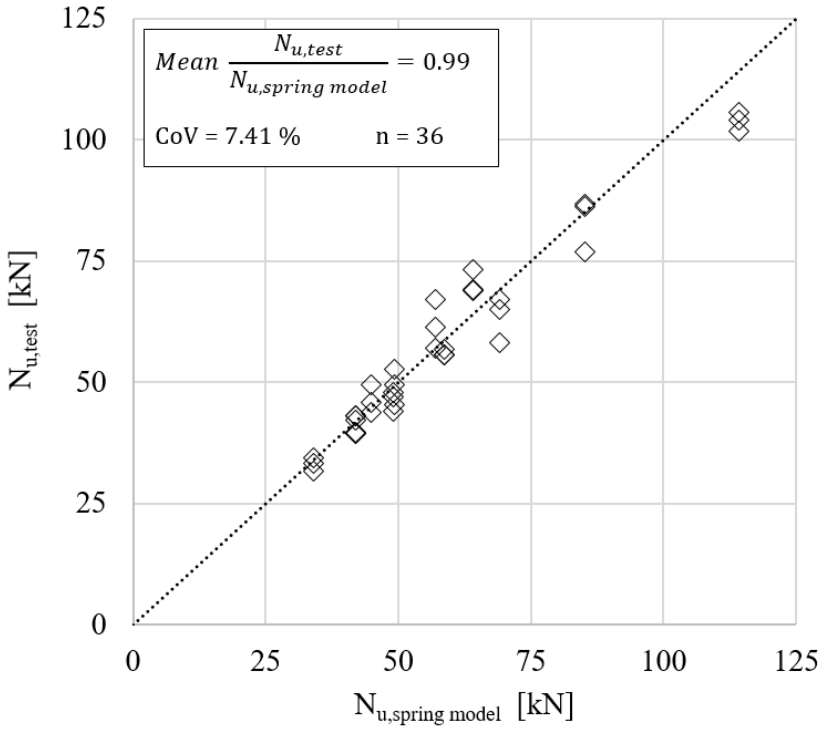

Figure 10.16. Comparison of the failure loads from the tests with the peak loads obtained from the nonlinear spring model: anchorages of rectangular configurations in uncracked concrete within the scope of EN 1992-4

Table 10.6. Verification of the model: anchorages of rectangular configurations in uncracked concrete within the scope of EN 1992-4

Test series ID	Test type	Measured mean ultimate load	Ultimate load obtained from spring model	
		$N_{u,m}$	$N_{u,spring\ model}$	$N_{u,m} / N_{u,spring\ model}$
		[kN]	[kN]	[-]
R1	Ref. single	27.2	27.2	-
G11R		56.1	58.7	0.96
G12	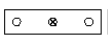	48.1	49.1	0.98
G13	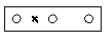	40.7	42.0	0.97
R2	ref. single	29.5	29.5	-
G22	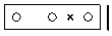	33.1	34.0	0.97
G23	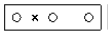	41.6	42.0	0.99
R3	=R1	27.2	27.2	-
G31R		63.4	69.1	0.92
G32		46.4	44.9	1.03
R4	=R2	29.5	29.5	-
G43		49.2	49.2	1.00
R5	Ref. single	58.5	58.5	-
G51R	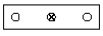	103.9	114.2	0.91
G52	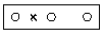	83.3	85.1	0.98
G53	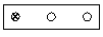	70.4	64.9	1.08
G54		61.8	64.5	0.96

In *Figure 10.17 - Figure 10.19*, load-displacement curves obtained from experimental tests and from the spring model, performed on cases are depicted, which are not considered with sufficient accuracy according to the current design provisions. These include anchor groups close to concrete edge subjected to eccentric tension loading such as series G22 and G23 (*Figure 10.17a,b*), anchor groups with biaxial eccentricity G43 (*Figure 10.18*) and anchor groups with not sufficiently rigid base plates such as the ones shown in *Figure 10.19*. *Figure 10.17a* and *b* confirm that the spring model is capable of accounting for the superposed influence of loading eccentricity and vicinity of concrete edge accurately while considering the exact loading position and performing a nonlinear static analysis to allow a realistic force distribution and redistribution among the anchors. $N_{u,m,test}/N_{u,spring\ model}$ is 0.97 and 0.99 for series G22 and G23, respectively.

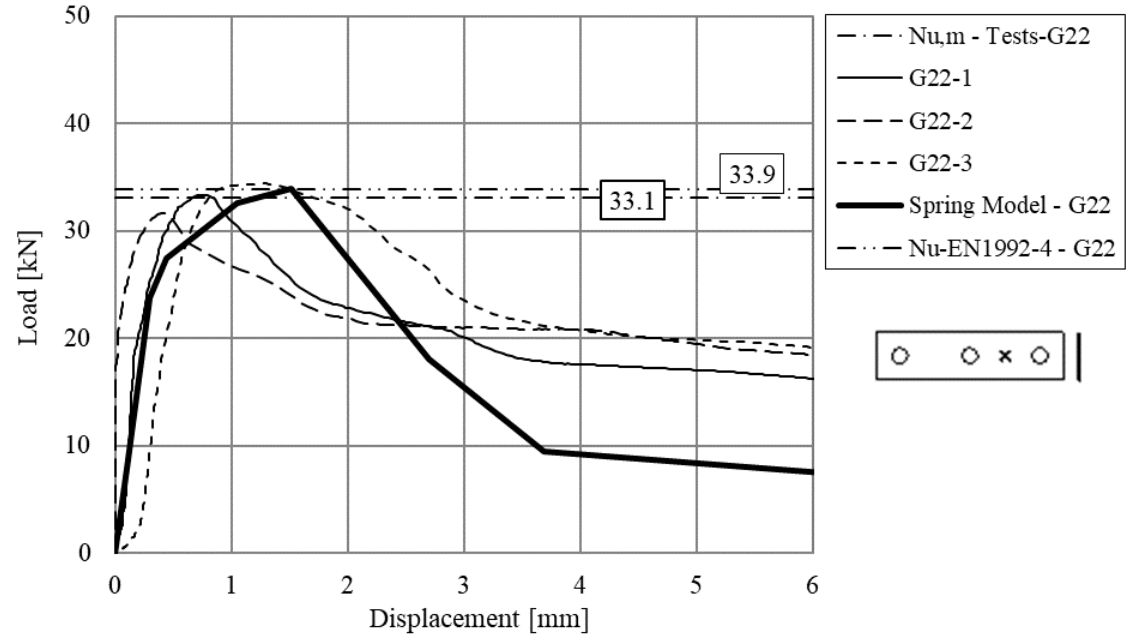

a)

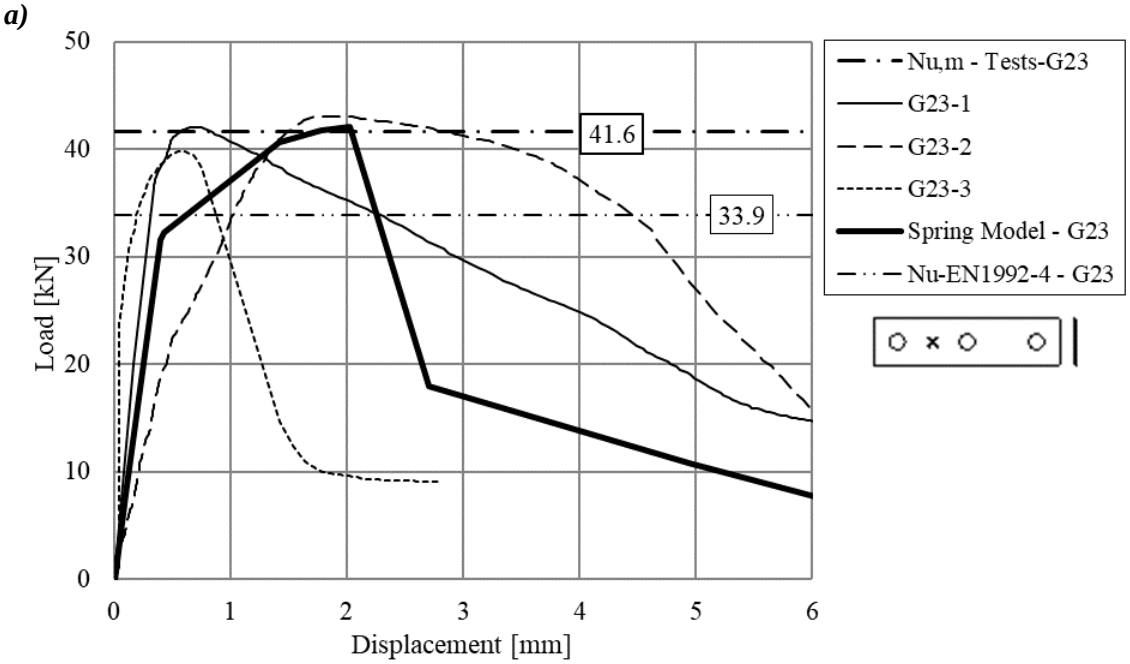

b)

Figure 10.17. Comparison of test results with the results of the nonlinear spring model: a) series G22, b) series G23

Figure 10.18 presents the comparison of the spring model with experimental results from series G43. For this configuration, the anchor group was installed close to the concrete edge, and the tension load was applied eccentrically about two axes. The graph shows that the spring model gives a good match with the experimental tests ($N_{u,m,test}/N_{u,spring\ model} = 1.00$). Note that the highest deviation (31%) between the calculation according to EN 1992-4 and using the spring model was obtained in this case. This highlights that the current provisions are rather conservative for cases with biaxial eccentricity and if anchor groups are loaded eccentrically close to the concrete edge, however, the spring model can capture the anchorage behaviour while applying the corresponding spring characteristics and performing the nonlinear analysis.

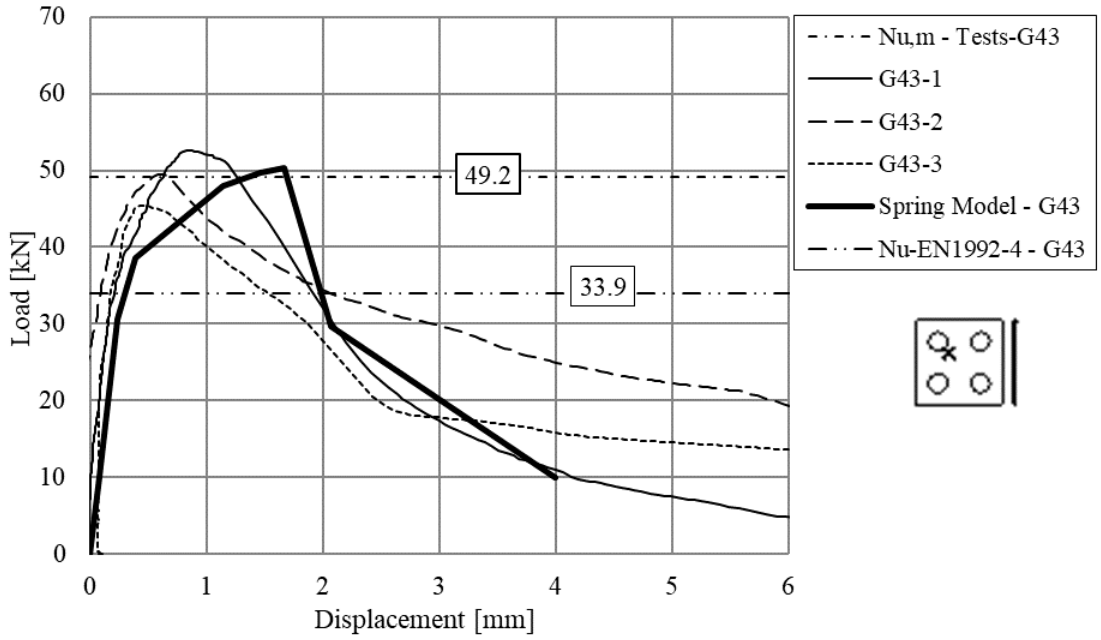

Figure 10.18. Comparison of test results with the results of the nonlinear spring model: series G43

Test results of anchor groups of 1×3 configuration loaded eccentrically in tension with thick and flexible base plates (G53 and G54) are plotted in *Figure 10.19a* and *b* against the load-displacement curve obtained from the analysis using the nonlinear spring model. The graphs show that the spring model can consider the influence of the base plate stiffness, eccentric loading with sufficient accuracy. Both the failure modes and the curve progression agree very well. The graph in *Figure 10.19b* confirms that the analysis using the nonlinear spring model accounts for a realistic force distribution among the anchors and also for the force redistribution in the post-peak phase. The ratio $N_{u,m,test}/N_{u,spring\ model}$ is obtained as 1.08 and 0.96 for test series G53 and G54, respectively.

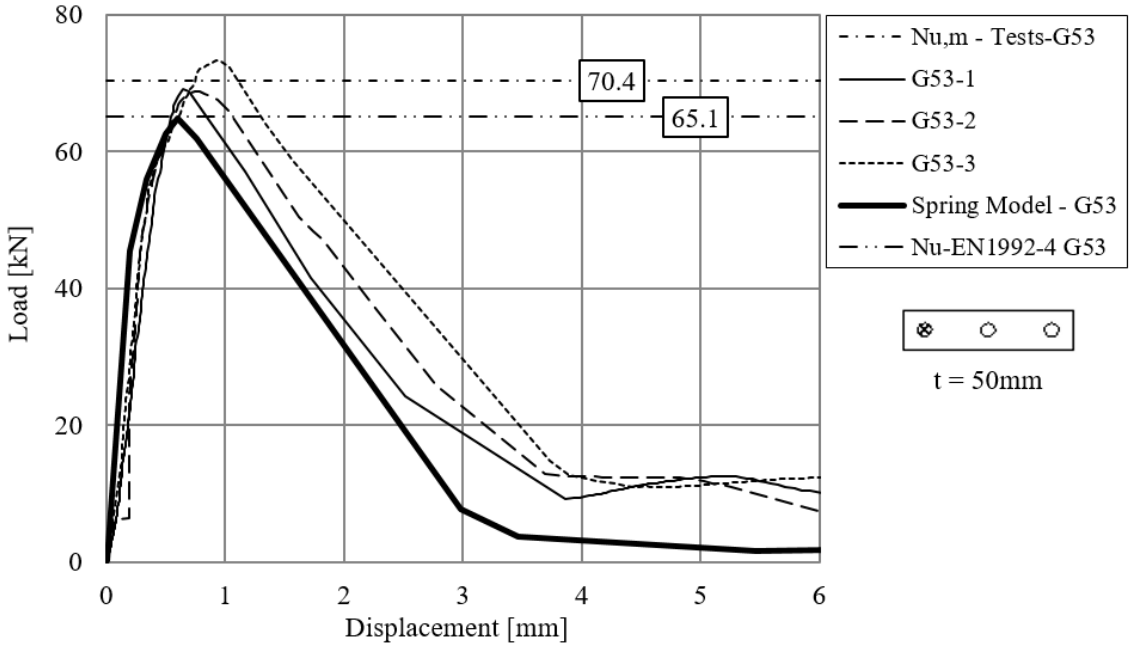

a)

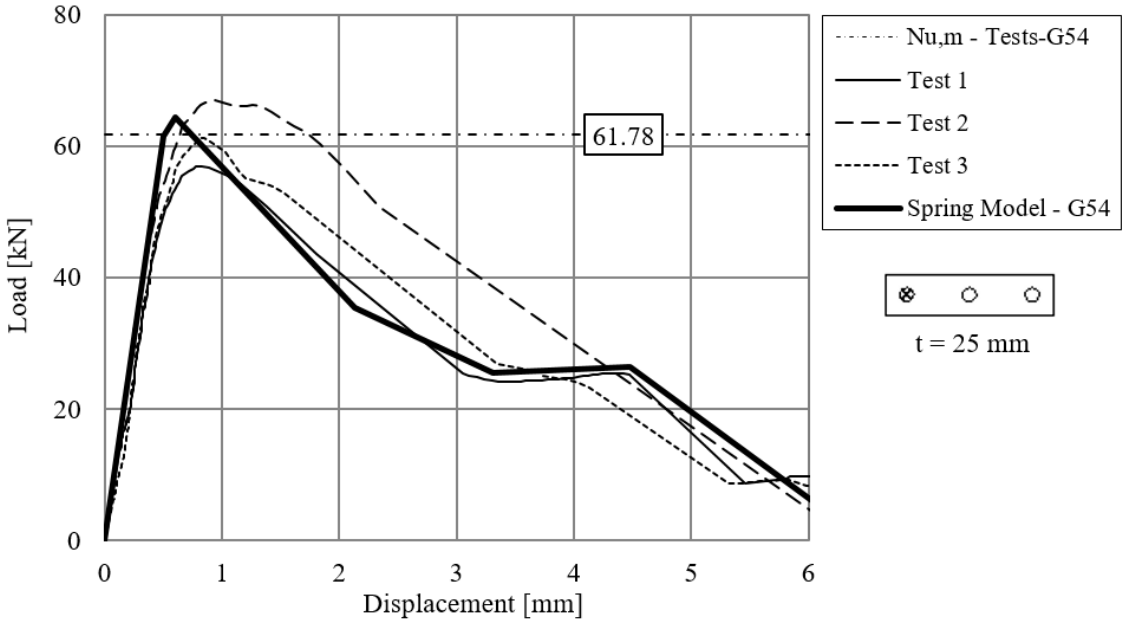

b)

Figure 10.19. Comparison of test results with the results of the nonlinear spring model: a) series G53, b) series G54

Anchorages of rectangular and non-rectangular configurations in uncracked concrete

Figure 10.20 and *Table 10.7* compare the results of a 1×4 anchorage and of non-rectangular anchorages, which are currently not covered by the design provisions. In general, the results of the spring model are in good agreement with the experimental results (mean value of $N_{u,test}/N_{u,spring\ model} = 1.03$). The highest deviation between test results and the results of the spring model ($N_{u,m,test}/N_{u,spring\ model}$) is 1.30, for concentric tension tests on 1×4 anchor groups using a flexible, thin ($t = 5\ mm$) base plate (Series G84). This high deviation can be explained by the fact that in the spring model used in this thesis, the material behaviour of the steel base plate was considered as linear elastic with an elasticity modulus of $E_s = 200\ GPa$, and the anchors failed due to concrete cone failure. However, during the experiments, the failure did not occur due to concrete or anchorage failure rather due to the yielding of the steel base plate, which can be seen in the test results in *Figure 8.10a* in terms of load-displacement behaviour and in *Figure 8.11e* the base plate deformations and yielding are visible. This behaviour was not captured by the model in order to not allow yielding of the base plate of the anchorage. However, if required, a yield criterion e.g. von-Mises may be assigned to consider the nonlinear behaviour of the base plate as well.

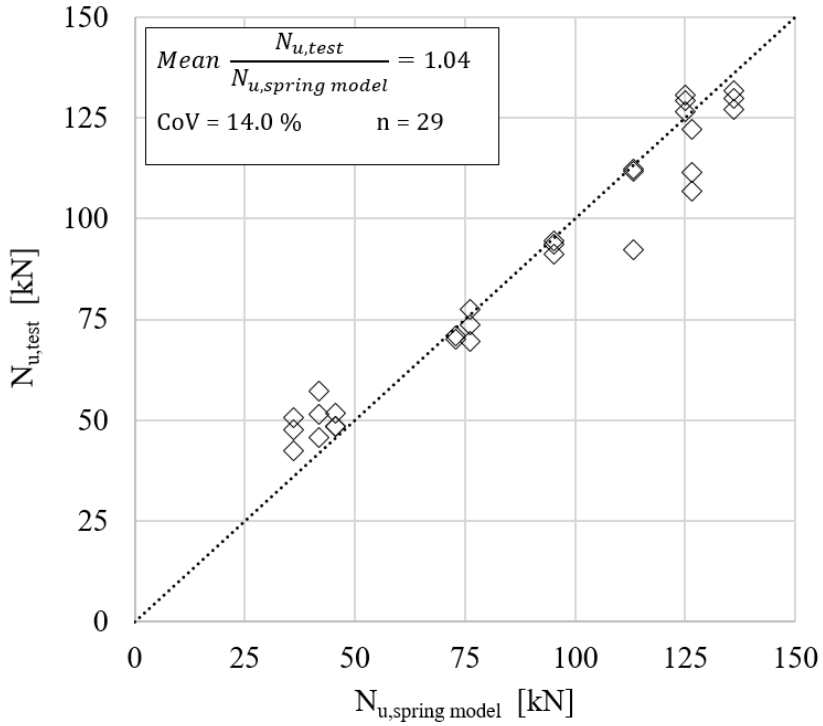

Figure 10.20. Comparison of failure loads from tests with the peak loads obtained from the nonlinear spring model: anchorages of rectangular and non-rectangular configurations in uncracked concrete

Table 10.7. Verification of the model: anchorages of rectangular and non-rectangular configurations in uncracked concrete

Test series ID	Test type	Normalised mean ultimate load	Ultimate load obtained from spring model	
		$N_{u,m*}$	$N_{u,spring\ model}$	$N_{u,m*}/N_{u,spring\ model}$
		[kN]	[kN]	[-]
R8	Ref. single	34.3	34.3	-
G81	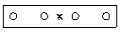	73.5	76.2	0.96
G82		49.7	45.5	1.09
G83	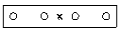	51.6	41.8	1.23
G84	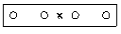	46.9	36.0	1.30
R9	Ref. single	39.5	39.5	-
G91	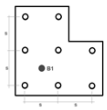	105.4	113.3	0.93
G92	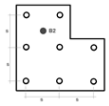	113.4	126.6	0.90
R10	= R9	39.5	39.9	-

G101	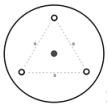	89.8	95.1	0.94
R20	Ref. single	52.5	52.5	-
G201	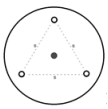	128.9	124.9	1.03
R30	=R8	34.3	34.3	-
G301	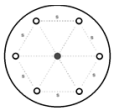	129.6	136.1	0.95
R40	=R8	34.3	34.3	-
G401	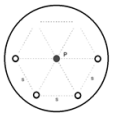	70.6	72.9	0.97

The influence of concrete strength was investigated on anchor groups arranged in a triangular pattern having round and assumedly stiff base plate in series G101 and G201. From the modelling point of view, this means that the exact same finite element model was used, however, different anchor spring and concrete contact spring characteristics accounting for the behaviour in higher concrete strength. The experimental load-displacement curves are given in *Figure 10.21* along with the corresponding load-displacement curves obtained from the analysis using the spring model. The results of the experiments and analysis (spring model) agree very well: The ratio $N_{u,m,test}/N_{u,springmodel}$ was 0.94 and 1.03 for the series G101 and G201, respectively. Moreover, the displacement behaviour could be captured with sufficient accuracy.

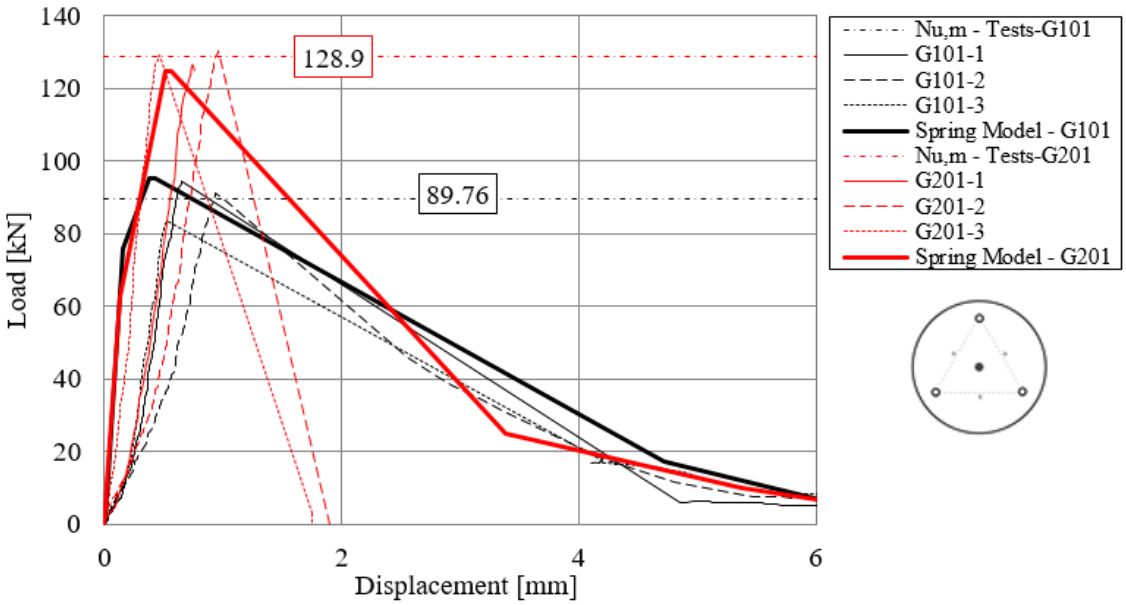

Figure 10.21. Comparison of test results with the results of the nonlinear spring model for series G101 and G201 – influence of concrete strength

In *Figure 10.22*, the experimental results are compared with the results of the nonlinear spring model for series G301 and G401. The influence of the anchor pattern was investigated by using the same base plate and keeping the same loading point. However, due to changing the anchor pattern from hexagonal to trapezoidal by leaving two anchors out of six out, the group is loaded eccentrically in series G401. When modelling, the base plate, the contact springs and the point of load application and the two „bottom“ anchors were the same for the configurations G301 and 401. However, for the spring model of series G401, the two top anchor springs were deleted and the two „middle“ anchors were modified accounting for a bigger tributary area. The comparison of the model with the tests shows a good agreement. The ratio $N_{u,m,test}/N_{u,spring\ model}$ was 0.95 and 0.97 for the series G301 and G401, respectively. Furthermore, the displacement behaviour could be captured with sufficient accuracy.

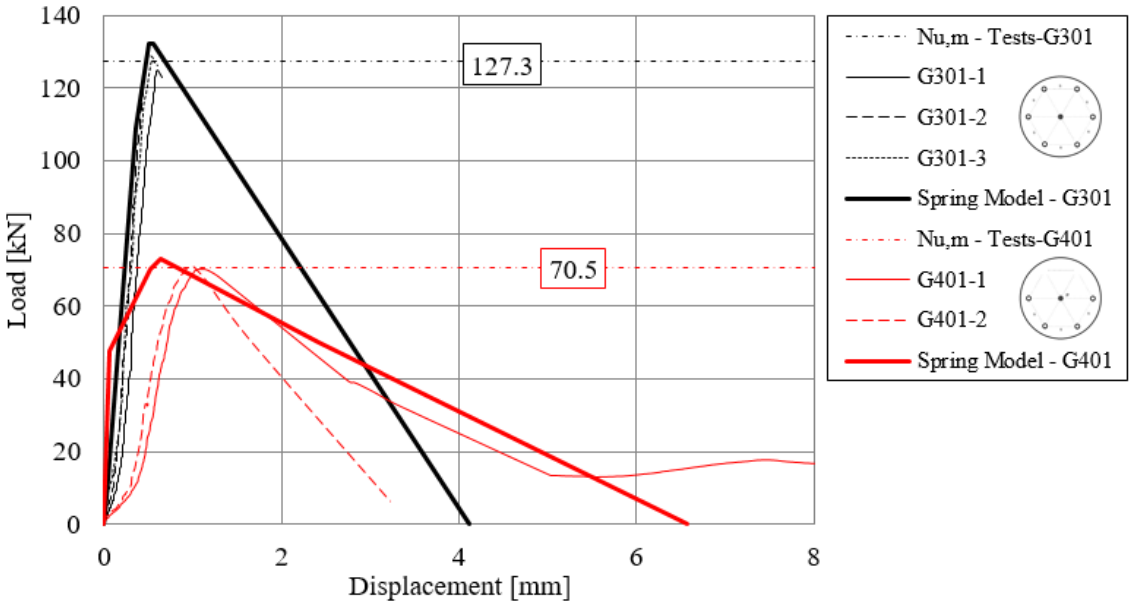

Figure 10.22. Comparison of test results with the results of the nonlinear spring model for series G301 and G401 – influence of anchor pattern

Anchorages of rectangular and non-rectangular configurations in cracked concrete

Table 10.8 summarizes the results on anchor groups of rectangular and non-rectangular configurations in uncracked and cracked concrete. The results of the spring model are in good agreement with the experimental results (*Figure 10.23*). The mean value of $N_{u,test}/N_{u,model}$ is 1.12 with the value ranging from 0.93- 1.43. For test series group G60, the match of experimental and analysis results is very good, $N_{u,m,test}/N_{u,spring\ model}$ corresponds to 1.00. The load-displacement curves of select groups G65 and G66 are compared to the results of the spring model in *Figure 10.15* confirming that the nonlinear spring model for concrete cone failure is capable of considering the actual crack pattern, the influence of eccentric loading and even their superposition. According to the comparison of the experimental results with the spring model in case of group series G70, the spring model seems to yield conservative results. The ratio $N_{u,m,test}/N_{u,spring\ model}$ ranges between 1.23 and 1.43. However, in reality, the large deviation should be explained rather by the anchor performance in the cracked concrete and in the behaviour of the anchors in low strength concrete. The measured mean compressive strength on cubes corresponded to 18 MPa in the tests. In this compressive strength range, the assumed fracture behaviour of the anchorages compared to that in normal strength concrete might not be applicable leading to a concrete cone angle different from 33°, which is assumed in the CCD method and in the tributary area approach. Furthermore, the tests showed that the used undercut anchors are less sensitive to cracks ($\Delta w = 0.3$ *mm*) when installed within a group than as single anchors.

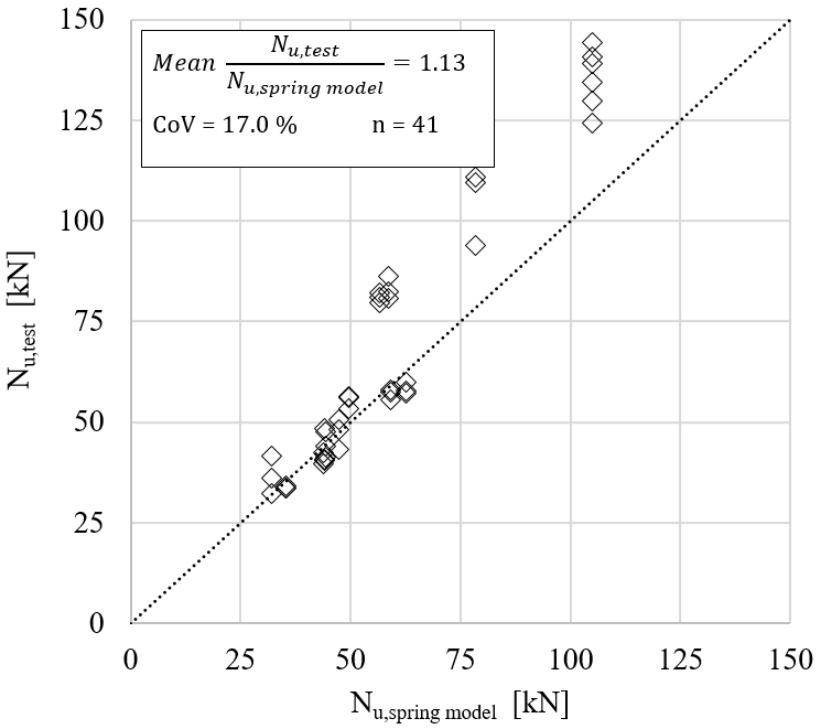

Figure 10.23. Comparison of failure loads from tests with the peak loads obtained from the nonlinear spring model: anchorages of rectangular and non-rectangular configurations in cracked concrete

Table 10.8. Verification of the model: anchorages of rectangular and non-rectangular configurations in cracked concrete

Test series ID	Test type	Measured mean ultimate load	Ultimate load obtained from spring model	
		$N_{u,m}$	$N_{u,spring\ model}$	$N_{u,m}/N_{u,spring\ model}$
		[kN]	[kN]	[-]
R6-ncr	Ref. single uncracked	27.8	27.8	-
R6-cr	Ref. single cracked	19.2	19.2	-
G61		58.4	62.6	0.93
G62R		43.1	44.1	0.98
G62	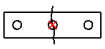	58.0	59.1	0.98
G63		41.0	43.9	0.93
G64		55.3	49.5	1.11
G65		33.8	35.2	0.96
G66	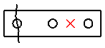	44.3	44.3	1.00
G67		47.4	47.4	1.00
G68	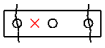	36.6	32.1	1.14
R7-ncr	Ref. single uncracked	37.8	37.8	-
R7-cr	Ref. single cracked	27.8	27.8	-
G71		129.6	104.9	1.23
G72		104.8	78.3	1.33
G73		80.9	56.7	1.43
G74		83.2	58.5	1.42
R50-ncr	= R7-ncr	37.8	37.8	-
R50-cr	= R7-cr	27.8	27.8	-
G501	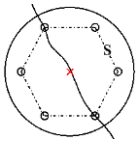	141.4	105.0	1.34

10.2.2 Verification of the spring model against experimental results from the literature

10.2.2.1 Tension tests on anchor groups of 4×4 configurations (Zhao & Dieterle, 1991)

Experimental investigations were carried out in the work of Zhao & Dieterle (1991) on anchor groups of 4×4 configurations using headed studs welded on the base plate (refer to Series 2.2 in the original report) to investigate the behaviour of large anchor groups and the influence of biaxial eccentricity. The embedment depth of the headed studs was $h_{ef} = 160\ mm$ and the anchor spacing $s = 100\ mm$ in both directions. The eccentricity of the external forces was varied but with keeping $e_1 = e_2$ (see *Table 10.9*). The reported material and test parameters, as well as the test results in terms of measured ultimate loads are given in *Table 10.9.* The anchor configuration and dimensions of the base plate are depicted in *Figure 10.24*. The concrete specimens were designed in such a way that an undisturbed concrete breakout body could develop in the tests. The test setup used in the experiments consisted of a tension test rig with adequate support distance to allow the formation of an unrestricted concrete cone ($d = 900\ mm$), a hydraulic cylinder, a load cell, displacement transducers. Furthermore, to allow an unrestrained force transfer into the base plate, an axial hinge was connected in the force flow. Further details about the test setup can be found in Zhao & Dieterle (1991).

In addition, test series on single anchors with the corresponding installation parameters were performed by Zhao (Zhao, 1993). The reported test parameters and the test results in terms of measured ultimate loads are given in *Table 10.9.* The load-displacement curve of one representative test is depicted in *Figure 10.25*, which was used to generate the tension spring characteristics for the nonlinear spring model.

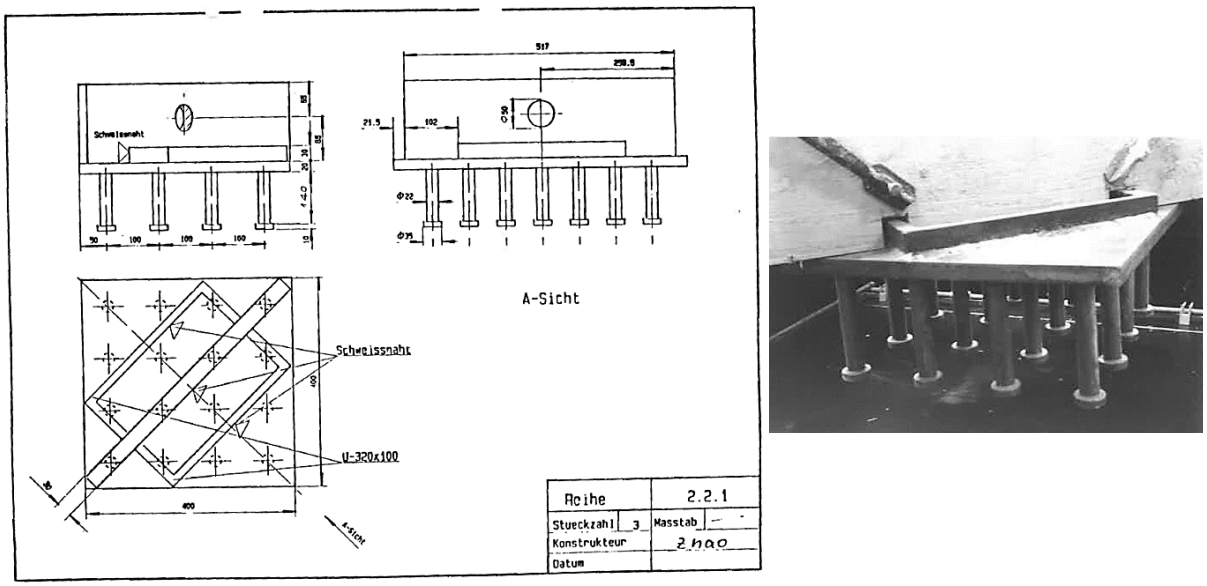

Figure 10.24. Anchorage used in the experiments by Zhao & Dieterle (taken from Zhao & Dieterle, 1991)

Table 10.9. Test program and test results of single anchors and anchor groups of 4×4 configurations (Zhao & Dieterle 1991, Zhao, 1993)

Test ID	Config-uration	Mean meas. concr. cube compr.strength (200 mm)	Mean con-crete cyl. compressive strength	An-chor spac-ing	Eccen-tricity	Meas. ultimate load	Ulti-mate load*	Mean ultimate load*
		$f_{cc,m,200}$	$f_{c,m}$	$s_1 = s_2$	$e_1 = e_2$	N_u	N_u*	$N_{u,m}$*
	[-]	[N/mm²]	[N/mm²]	[mm]	[mm]	[kN]	[kN]	[kN]
R1.1	Single	24.8	20.8	-	0	148.8	165.0	172.4
R1.2	Single	24.8	20.8	-	0	155.8	172.8	
R1.3	Single	24.8	20.8	-	0	161.9	179.5	
2.2.1	4×4	30.5	25.6	100	0	359.5	359.5	353.1
2.2.2	4×4	30.5	25.6	100	0	358.9	358.9	
2.2.3	4×4	30.5	25.6	100	0	340.9	340.9	
2.2.4	4×4	30.5	25.6	100	50	296.5	296.5	315.6
2.2.5	4×4	30.5	25.6	100	50	353.4	353.4	
2.2.6	4×4	30.5	25.6	100	50	296.8	296.8	
2.2.7	4×4	30.5	25.6	100	100	257.0	257.0	258.9
2.2.8	4×4	30.5	25.6	100	100	276.6	276.6	
2.2.9	4×4	30.5	25.6	100	100	243.1	243.1	
2.2.10	4×4	30.5	25.6	100	150	245.6	245.6	240.6
2.2.11	4×4	30.5	25.6	100	150	258.9	258.9	
2.2.12	4×4	30.5	25.6	100	150	217.3	217.3	

*The mean ultimate load was normalised with respect to the concrete compressive strength using the following expression: $N_u^* = N_u \cdot (25.6\ \text{N/mm}^2 / f_{c,m})^{0.5}$

Determination of the anchor spring characteristics and verification of the model

The test results of series R1 on the tension loaded single anchors from Zhao (1993) were used to generate the tension spring characteristics (load-displacement data pairs) for the spring model. The load-displacement curve of one representative test of the series shown in *Figure 10.25* was evaluated and the load and stiffness values for the idealised curve were determined. Note that the idealised curve was then normalised with respect to the compressive strength of the group tests to enable a direct comparison of the spring model on the anchor group with the test results. The corresponding load-displacement-stiffness values are given in *Table 10.10* as "Reference single anchor". The reference projected area of the single anchor $A_{c,N}^0$ and the projected tributary area of the corresponding individual anchors, namely middle, edge and corner anchors of the group were calculated according to ***Eq. 106*** - ***Eq. 109***. The resistance of the individual anchors was calculated according to ***Eq. 110*** - ***Eq. 112*** and the determined tension spring characteristics are tabulated in *Table 10.10* as "Individual anchor - middle", "Individual anchor - edge" and "Individual anchor - corner", respectively.

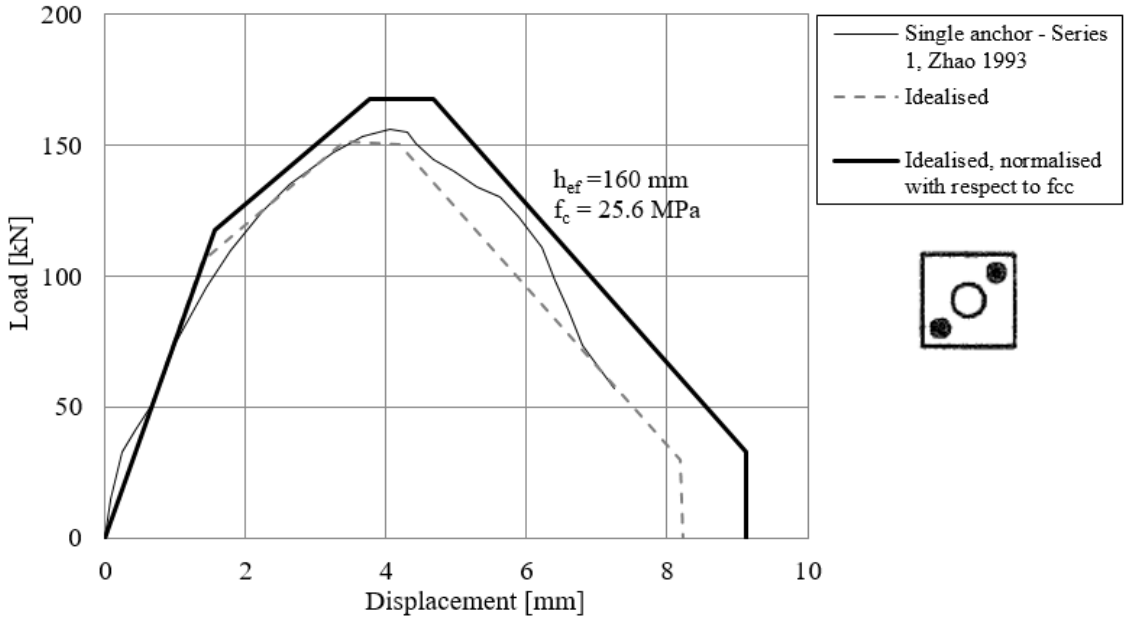

Figure 10.25. Load-displacement curve of a representative test on a single anchor (reproduced from Zhao, 1993), idealised and normalised load-displacement curves used as spring characteristics for a single anchor

$$A_{c,N}^{0} = (3 \cdot h_{ef})^2 = (3 \cdot 160)^2 = 230400\ mm^2 \qquad \textbf{Eq. 106}$$

$$A_{c,N}^{middle} = s^2 = 100^2 = 10000\ mm^2 \qquad \textbf{Eq. 107}$$

$$A_{c,N}^{edge} = \left(1.5 \cdot h_{ef} + s/2\right) \cdot s = (1.5 \cdot 160 + 100/2) \cdot 100 = 29000\ mm^2 \qquad \textbf{Eq. 108}$$

$$A_{c,N}^{corner} = \left(1.5 \cdot h_{ef} + s/2\right)^2 = (1.5 \cdot 160 + 100/2)^2 = 84100\ mm^2 \qquad \textbf{Eq. 109}$$

$$N_{Rm,c}^{middle} = A_{c,N}^{middle} / A_{c,N}^{0} \cdot 168\ kN = 0.04 \cdot 162.3 = 6.7\ kN \qquad \textbf{Eq. 110}$$

$$N_{Rm,c}^{edge} = A_{c,N}^{edge} / A_{c,N}^{0} \cdot 168\ kN = 0.13 \cdot 162.3 = 21.8\ kN \qquad \textbf{Eq. 111}$$

$$N_{Rm,c}^{corner} = A_{c,N}^{corner} / A_{c,N}^{0} \cdot 168\ kN = 0.37 \cdot 162.3 = 62.2\ kN \qquad \textbf{Eq. 112}$$

After obtaining the nonlinear anchor spring characteristics, they were assigned to the tension-only springs representing the nonlinear anchor behaviour in the finite element model, which includes shell elements for modelling of the base plate and compression-only springs simulating the contact between concrete and base plate. The base plate of dimensions 400×400×25 mm^3, the stiffeners using two U-320×100 cross-sections (*h = 30 mm*) and the welded diagonal steel section (to apply the load in the test, *t = 30 mm, h = 150 mm*) were modelled realistically using shell elements orthogonal to the base plate to represent the behaviour of the anchorage as it was in the tests. The load was applied based on the point of load application (concentric or eccentric) and the nonlinear static analysis was performed in displacement control.

It can be seen from *Table 10.11* that even for larger groups (4×4 configuration), the nonlinear spring model is able to predict the behaviour and the capacities of the anchor groups under concentric tension, as well as under biaxial eccentricity with varying levels of eccentricity.

Table 10.10. Spring properties of individual anchors of the 4x4 anchor groups tested by Zhao and Dieterle (1991)

	Load $N_{Rm,c}{}^{i}{}_{A\text{-}F}$ [kN]	Stiffness k_1-k_4 [kN/mm]	Displacement $\delta_{A\text{-}F}$ [mm]
Reference single anchor			
A	0.0	0.0	0.00
B	117.5	75.7	1.55
C	168.0	44.6	3.77
D	168.0	36.0	4.67
E	33.2	3.6	9.12
F	0.0	3.6	9.12
Individual anchor - middle			
A	0.0	0.0	0.00
B	4.7	75.7	0.06
C	6.7	44.6	0.15
D	6.7	36.0	0.19
E	1.3	3.6	0.36
F	0.0	3.6	0.36
Individual anchor - edge			
A	0.0	0.0	0.00
B	15.3	75.7	0.20
C	21.8	44.6	0.49
D	21.8	36.0	0.61
E	4.3	3.6	1.19
F	0.0	3.6	1.19
Individual anchor - corner			
A	0.0	0.0	0.00
B	43.5	75.7	0.57
C	62.2	44.6	1.39
D	62.2	36.0	1.73
E	12.3	3.6	3.37
F	0.0	3.6	3.37

Table 10.11. Results obtained from the spring model compared to mean normalised experimental results from Zhao & Dieterle (1991) on anchor groups of 4×4 configurations

Test ID	Configuration	Eccentricity	Normalised mean ultimate load*	Ultimate load obtained from spring model	
		$e_1 = e_2$	$N_{u,m}$*	$N_{u,spring\ model}$	$N_{u,m}$*/ $N_{u,spring\ model}$
	[-]	[mm]	[kN]	[kN]	[-]
2.2.1-3	4×4	0	353.1	350.9	1.01
2.2.4-6	4×4	50	315.6	277.0	1.14
2.2.7-9	4×4	100	258.9	222.0	1.17
2.2.10-12	4×4	150	240.6	184.5	1.30

10.2.2.2 Tension tests on anchor groups of 2×2 configurations (Sharma et al., 2019)

In the work of Sharma et al. (2019), an experimental program was carried out on anchor groups of 2×2 configurations using headed studs welded on the base plate to study the behaviour of anchorages placed close to the concrete edge and loaded under inclined loads towards the edge (tension-shear interaction). The nonlinear spring model for tension was verified against the tests conducted under pure tension loading (see *Figure 10.26)*. The details of tests and the verification for tension are given in Section 12.1 along with the verification of the model for interaction. The comparison of the tests results (failure loads) with the spring model is given in *Table 12.4* and the load-displacement curves are plotted in *Figure 12.6*.

10.2.2.3 Tension tests on anchor groups of 2×2 configurations placed close to the concrete edge (Lachinger, 2012)

Lachinger (2012) investigated the behaviour of 2×2 anchor groups placed close to the concrete edge and installed with most unfavourable hole clearance pattern under inclined loading using bonded anchors. The comprehensive experimental program also contained tests under pure tension. These tests were used for the verification of the nonlinear spring model for tension (see *Figure 10.26)*. The test details and the verification for tension are given in Section 12.2 along with the verification of the model for interaction.

10.2.2.4 Summary of the literature results

In *Figure 10.26*, the failure loads of various anchor group tests from the literature are compared with the failure loads obtained using the nonlinear spring model.

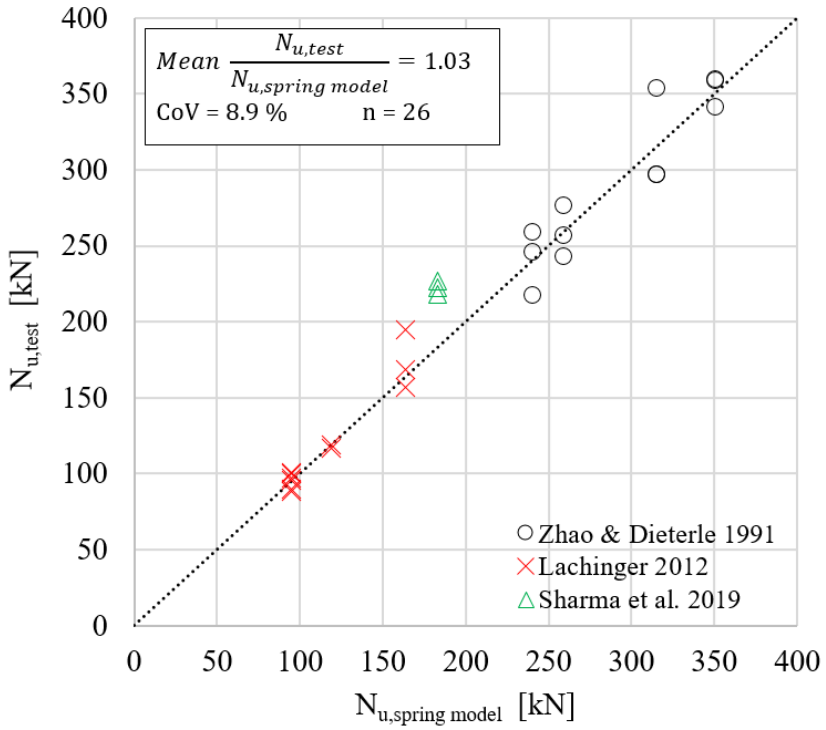

Figure 10.26. Comparison of failure loads from tests with the peak loads obtained from the nonlinear spring model

The comparison of the failure loads shows a very good agreement. The mean value of $N_{u,test}/N_{u,spring\ model}$ is 1.03 with a coefficient of variation of 8.9 %. Note that in the case of the evaluation of tests from the literature, not in every case reference tension tests were available to generate the spring characteristics. Therefore, the spring characteristics were generated by calculating the mean concrete cone resistance of the corresponding individual anchors based on the CCD method and the stiffness values were derived from group tests while assuming a stiffness for the individual anchors $k_{1-4} = k_{group,1-4}/n$ (n = number of anchors within a group). The good match of the results of test and spring model proves the reliability of the model

10.3 SUMMARY

In Chapter 10, the nonlinear spring model for tension loaded anchorages in case of concrete cone breakout failure is verified.

In Section 10.1, the postulates made for the spring model are verified against experimental data from this thesis. It was shown that the tributary area approach can be applied to anchor groups of rectangular and non-rectangular configurations. Furthermore, it was verified that the tributary area approach used for uncracked concrete can be applied without any modifications on anchor groups in cracked concrete. It was confirmed by tests on rectangular and non-rectangular anchor groups that the vicinity of concrete edge or the virtual edge (considered at a distance of half the spacing to the neighbouring anchor) influences the individual anchor capacity in the group but not the stiffness of the anchor.

In Section 10.2, the analyses performed by using the nonlinear spring model were verified against 106 experiments conducted on post-installed anchors within the framework of this thesis and against test results on welded headed studs (15 tests) and post-installed anchors (11 tests) from the literature. In addition, sample calculations are given in Section 10.2.1.1 to demonstrate the application and verification of the spring model . A total of 132 experimental results were compared with the results of the corresponding spring models. Considering all investigated cases in uncracked and cracked concrete on post-installed and cast-in anchor groups having three to sixteen anchors within a group, the mean value of $N_{u,test}/N_{u,spring\ model}$ is 1.05, and the coefficient of variation is 14.2 %. The graph in *Figure 10.27* confirms that the spring model is able to predict the concrete cone resistance of various anchorage configurations (rectangular and non-rectangular anchorages) in uncracked and cracked concrete very well.

The comparison of the results obtained from the spring model with the experiments clearly shows that the spring model can capture the load-displacement behaviour of the anchorages while applying the corresponding spring characteristics for the anchors and concrete contact, modelling the base plate with the attached profile and possible stiffeners realistically and performing the nonlinear static analysis. Due to this, the model considers both the distribution as well as the redistribution of forces among the anchors within the anchor group. Using the model does not require any definition of the rigid or stiff base plate, instead, it considers the real stiffness of the base plate in the analysis automatically. Furthermore, there are no requirements for additional factors to consider the influence of the vicinity of the concrete edge or the influence

of eccentricity. It provides the results in terms of the complete load-displacement behaviour of the anchorage that may be used in the performance-based approaches.

It was verified that the nonlinear spring model for concrete cone failure is capable of realistic consideration of anchor groups of rectangular and non-rectangular configurations, the actual crack pattern, influence of eccentric loading, the vicinity of concrete edge and their superposition. Through this approach, a reliable solution can be obtained even for the anchor groups, which are not considered with sufficient accuracy according to the current design provisions.

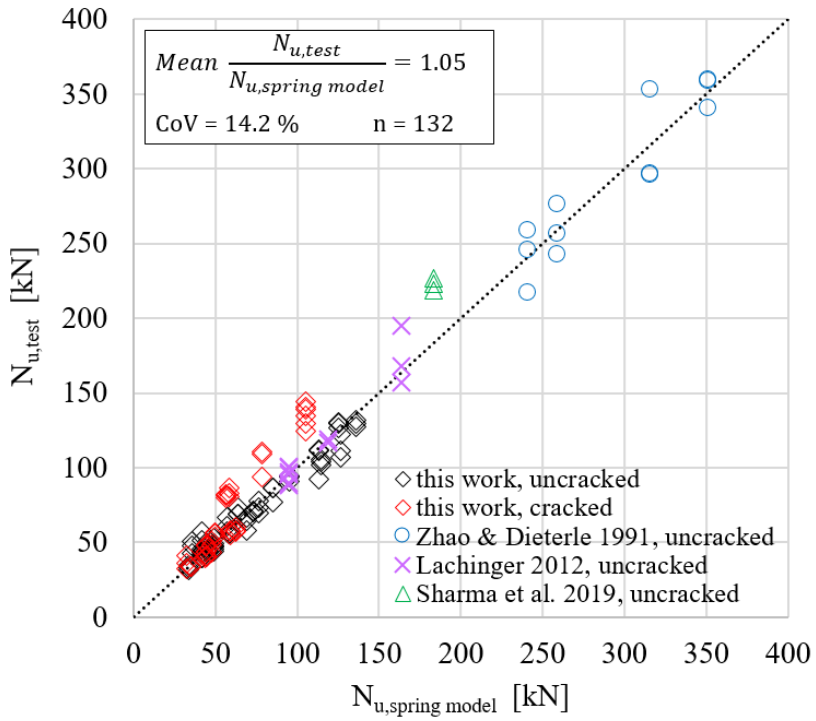

Figure 10.27. Summary of the comparison of tension test results (failure loads) from this work and from the literature with the results obtained from the nonlinear spring model: anchorages of rectangular and non-rectangular configurations in uncracked and cracked concrete

11 VERIFICATION OF THE NONLINEAR SPRING MODEL FOR CONCRETE EDGE FAILURE

The nonlinear spring model is verified in this chapter for anchor groups loaded in pure shear in the case of concrete edge failure mode. In Section 11.1, the postulate regarding the stiffness of the load-displacement curves defining the spring characteristics is verified. In Section 11.2, the approach is verified by comparing results obtained from the spring model with the corresponding test results on anchor groups having one anchor row arranged parallel to the concrete edge. The verification of applying the nonlinear spring modelling approach on anchorages having multiple anchor rows and using the tributary volume approach against experiments is given in Section 11.3 The spring model is verified against experiments from the literature in Section 11.4. Finally, Section 11.5 summarizes the chapter. Note that the load-displacement curves of the corresponding test results are given in Section 9.4. However, for the ease of reading, some of them are reproduced in this chapter to facilitate the comparison with the corresponding load-displacement curves obtained from the analysis using spring model in order to verify the spring model as a displacement-based approach.

11.1 STIFFNESS OF THE IDEALISED LOAD-DISPLACEMENT CURVES – SPRING PROPERTIES

In the nonlinear spring model for concrete edge failure of shear loaded anchorages, the failure load of an ith individual anchor of j^{th} row of an anchor group is influenced by the neighbouring anchors in both orthogonal directions (Chapter 6). The resistance of this particular i^{th} anchor of j^{th} row decreases in proportion to its tributary volume compared to the tributary volume of a single anchor having the same edge distance. It is taken into account by the factor $V_{c,V}^{i,j}/V_{c,V}^{0,j}$. However, the tributary volume assigned to an i^{th} anchor of a j^{th} row of the group does not influence the stiffness of the anchor (k_1 - k_4 in *Figure 11.1*) and the stiffness values remain unchanged compared to the stiffness values determined for the corresponding single anchor (refer to Section 6.2.2). Furthermore, since the initial shear stiffness of single anchors is independent of the edge distance, the stiffness determined for a particular edge distance is considered valid for all edge distances in the spring model.

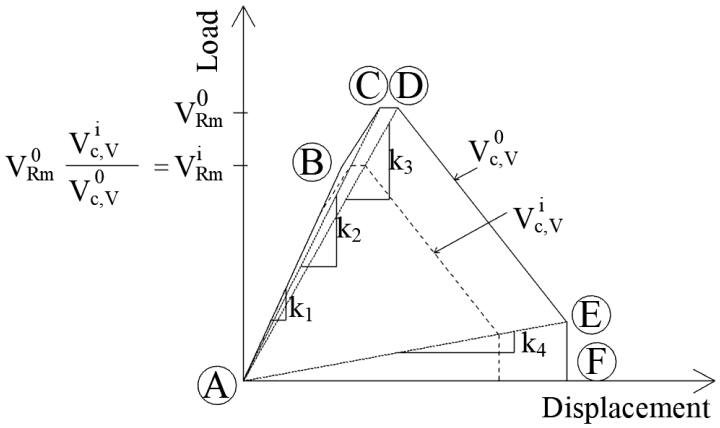

Figure 11.1. Scaling of the idealised curve of a single anchor failed by concrete edge breakout considering tributary volumes

The single anchor tests with different edge distances according to Sections 9.4.1.1, 9.4.2.1 and 9.4.3.1 showed, and confirmed the findings from the literature (Grosser, 2012, Tian et al., 2018, Bokor et al., 2020), that the initial shear stiffness of single anchors is independent of the edge distance. It is mostly dependent on the anchor diameter, provided that all other parameters such as anchor type, size and embedment depth are kept same, (which is a requirement for the anchors of an anchor group according to the current regulations). This means that the initial shear stiffness of an anchor can be assumed not to change with increasing or decreasing the edge distance, and so with changing the concrete volume, which is activated by the anchor. Furthermore, the tests series discussed in Section 9.4.1.4, carried out on single anchors, having a recess in front of the anchor also confirmed that the presence of a recess – missing concrete body – does not have an influence on the shear stiffness of the single anchors. The corresponding load-displacement curves ($k_{1.m}$ = *28.4 kN/mm*) compared to the curves of single anchors ($k_{1.m}$ = *29.9 kN/mm*) without recess verify that the shear stiffness remains unchanged (see *Figure 9.20* and *Figure 9.21*). The above considerations and the comparison of the load-displacement curves obtained from the spring model and from the corresponding tests on anchor groups confirm that in the nonlinear spring model, although a smaller concrete tributary volume can be assigned to an i^{th} individual anchor of j^{th} row of an anchor group compared to the corresponding single anchor, the stiffness of the individual anchors of the group should be kept unchanged. The comparison is given for select cases in the following sections.

11.2 VERIFICATION OF THE SPRING MODEL FOR ANCHORAGES WITH ONE ANCHOR ROW

In this section, the spring model is verified against tests carried out on anchor groups arranged parallel to the concrete edge in one anchor row and loaded in shear towards and perpendicular to the free edge (refer to test program in *Table 9.3*). With analysing anchorages having one anchor row only, it is possible to show directly that the spring model is capable of considering (i) the anchor spacing in the direction perpendicular to the loading, (ii) the influence of loading eccentricity, (iii) the influence of crack pattern and the superposed influence of (i), (ii) and (iii).

The verification of the model on anchor groups arranged parallel to the edge and loaded perpendicular towards the edge in terms of ultimate loads is given in *Table 11.2*. Furthermore, a sample calculation for the spring model for shear is given in the following Section 11.2.1.

11.2.1 Sample calculation – 1×3 anchor group configuration

In this example, an anchor group of 1×3 configuration subjected to eccentric shear loading in cracked concrete is calculated with the nonlinear spring model for shear. The configuration is shown in *Figure 11.2*, which corresponds to the test series GS-1×3-dw03-e120c applying the shear load eccentrically at the position of the anchor in cracked concrete (anchor 3). The anchor spacing s_2 and edge distance c_1 were 120 mm in the tests and considered accordingly in the analysis. The further installation parameters of the anchor group GS-1×3-dw03-e120c can be taken from *Table 9.3*. Load-displacement curves of shear loading tests on single anchors were

evaluated to get information on the displacement behaviour, and the stiffness values were determined for both cracked and uncracked concrete. For the given case, using bonded anchors of size M20, 30% reduction in shear stiffness and failure load was considered with the spring characteristics. The mean ultimate load of the corresponding single anchor was determined based on the corresponding single anchor series SS-120 and SS-120dw03. The load-displacement data pairs and stiffness values of the reference curve of the single anchor are listed in *Table 11.1*. Then, the reference curve was scaled based on the tributary volume (or tributary area in case of anchor group of one row) available for the corresponding individual anchors using the reduction factor $V^i_{c,V}/V^0_{c,V} = A^i_{c,V}/A^0_{c,V}$ according to ***Eq. 113*** - ***Eq. 115***.

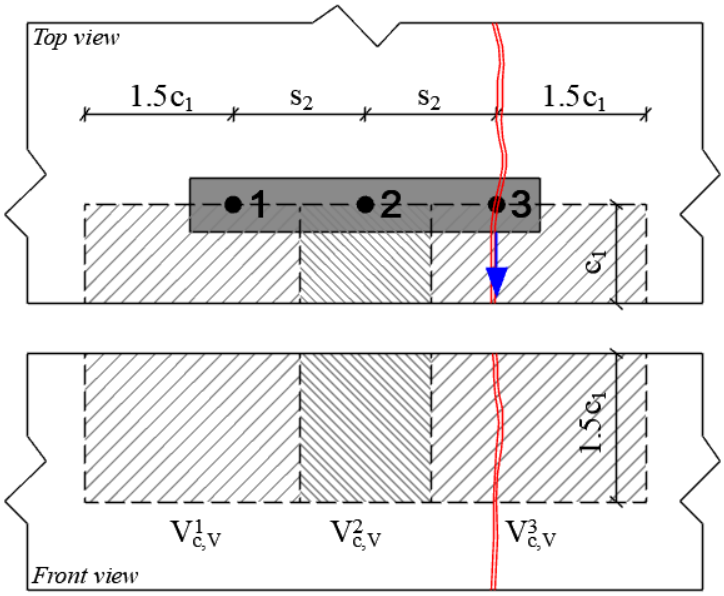

Figure 11.2. Anchor group configuration, tributary volume and point of load application for series GS-1×3-dw03-e120c

The obtained spring characteristics are listed on the right side of *Table 11.1*. Note that the tributary area of the anchor in crack remains unchanged compared to that in uncracked concrete, and the tributary area approach used for uncracked concrete is applied without any modifications on anchor groups in cracked concrete. The reduced stiffness and resistance due to the presence of the crack is considered in the reference single anchor spring characteristics (see *Table 11.1, anchor 3)*.

$$V^1_{Rm,c} = V^0_{Rm,c,ucr} \cdot \frac{A^1_{c,V}}{A^0_{c,V}} = 43.4\ kN \cdot \frac{43200\ mm^3}{64800\ mm^3} = 28.9 kN \qquad \textbf{Eq. 113}$$

$$V^2_{Rm,c} = V^0_{Rm,c,ucr} \cdot \frac{A^2_{c,V}}{A^0_{c,V}} = 43.4\ kN \cdot \frac{21600\ mm^3}{64800\ mm^3} = 14.5\ kN \qquad \textbf{Eq. 114}$$

$$V^3_{Rm,c} = 0.7 \cdot V^0_{Rm,c,ucr} \cdot \frac{A^3_{c,V}}{A^0_{c,V}} = 30.4 kN \cdot \frac{43200\ mm^3}{64800\ mm^3} = 20.3\ kN \qquad \textbf{Eq. 115}$$

Table 11.1. Spring characteristics of individual anchors of the anchor group series GS-1×3-dw03-e120c (to be considered in loading direction and direction opposite to loading)

	Load $V_{Rm,c}{}^{i}{}_{A\text{-}F}$ [kN]	Stiffness k_1-k_4 [kN/mm]	Displacement $\delta_{A\text{-}F}$ [mm]	Load $V_{Rm,c}{}^{i}{}_{A\text{-}F}$ [kN]	Stiffness k_1-k_4 [kN/mm]	Displacement $\delta_{A\text{-}F}$ [mm]
Reference single anchor				***Anchor A1***		
A	0.0	0.0	0.0	0.0	0.0	0.0
B	34.7	33.0	1.1	23.1	33.0	0.7
C	43.4	24.7	1.8	28.9	24.7	1.2
D	43.4	19.9	2.2	28.9	19.9	1.5
E	8.7	2.1	4.1	5.8	2.1	2.8
F	0.0	0.0	4.1	0.0	0.0	2.8
Reference single anchor				***Anchor A2***		
A	0.0	0.0	0.0	0.0	0.0	0.0
B	34.7	33.0	1.1	11.6	33.0	0.4
C	43.4	24.7	1.8	14.5	24.7	0.6
D	43.4	19.9	2.2	14.5	19.9	0.7
E	8.7	2.1	4.1	2.9	2.1	1.4
F	0.0	0.0	4.1	0.0	0.0	1.4
Reference single anchor (in cracked concrete)				***Anchor A3 (in cracked concrete)***		
A	0.0	0.0	0.0	0.0	0.0	0.0
B	24.3	23.1	1.1	16.2	23.1	0.7
C	30.4	17.3	1.8	20.3	17.3	1.2
D	30.4	13.9	2.2	20.3	13.9	1.5
E	6.1	1.5	4.1	4.1	1.5	2.8
F	0.0	0.0	4.1	0.0	0.0	2.8

The spring characteristics given in *Table 11.1* were assigned to the anchor springs (as uni-directional shear springs active in the loading direction and uni-directional shear springs active in the direction opposite to loading) representing the nonlinear anchor behaviour under shear in the finite element model. The load was applied at the anchor position 3 on the base plate (modelled with shell elements), and the nonlinear static analysis was performed in displacement control until the desired displacement. The base plate was considered as rigid in the analysis.

The load-displacement curve obtained as an output from the spring model is plotted in *Figure 11.3* along with the test results to verify the results obtained from the analysis. The comparison shows a very good agreement of test results and the result of the spring model ($V_{u,m} / V_{u,spring\ model} = 0.99$). This example confirms that the nonlinear spring model is capable of considering the exact crack pattern and furthermore, the influence of loading eccentricity is captured due to accounting for the "push-back effect" with the anchor spring characteristics.

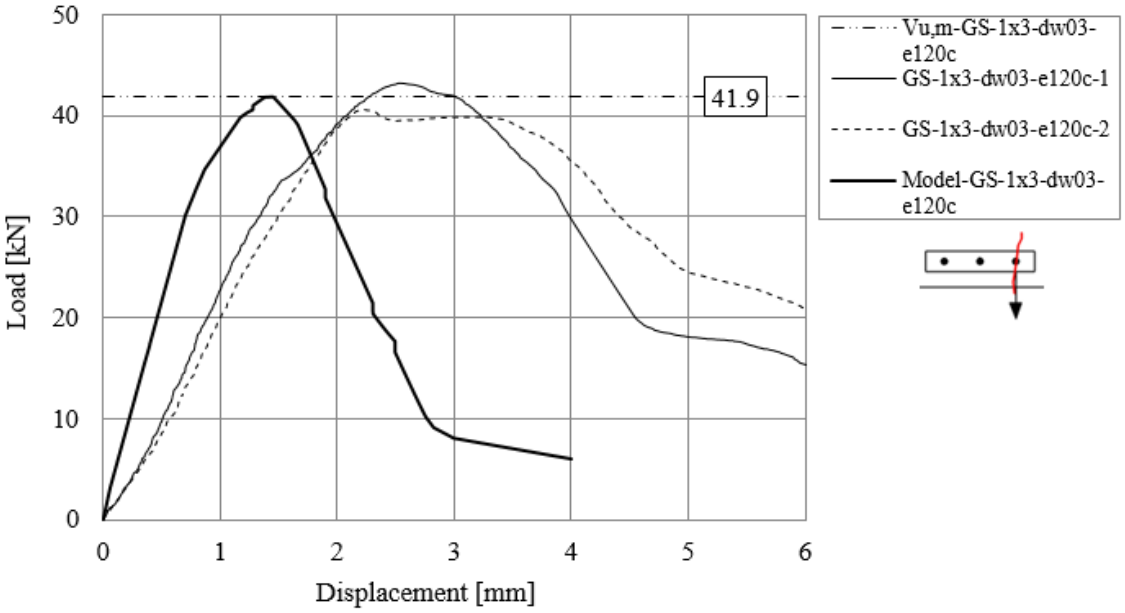

Figure 11.3. Load-displacement curves obtained from tests on anchor groups and result of the spring model for series GS-1×3-dw03-e120c

11.2.2 Comparison of test results with the results of the nonlinear spring model

Results of 11 nonlinear static analyses performed using the spring model on anchor groups are compared with the corresponding experimental results (31 tests) in the following. The mean value of the ratio of ultimate loads, $V_{u,,test}/V_{u,spring\ model}$ is 1.04, and the coefficient of variation is 15.9% (*Figure 11.4*).

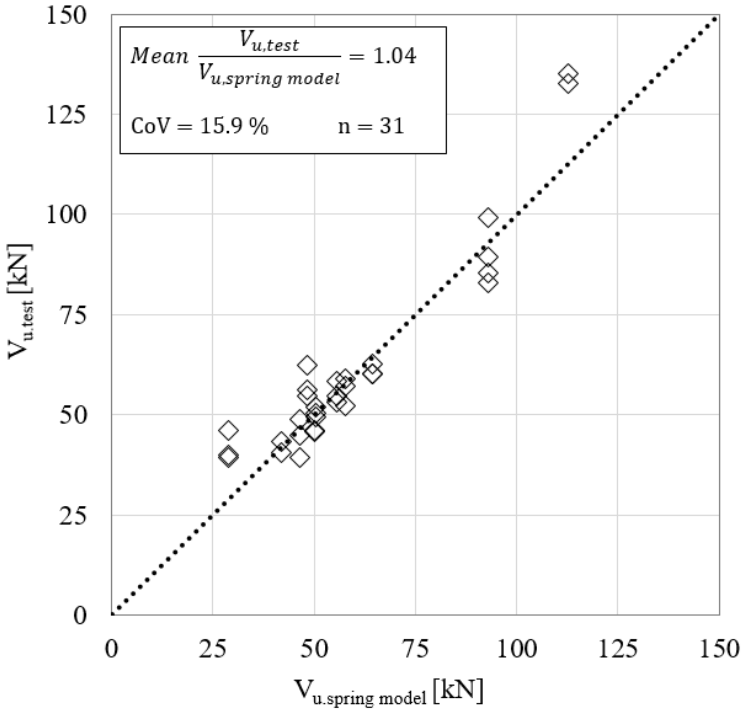

Figure 11.4. Comparison of failure loads from tests with the peak loads obtained from the nonlinear spring model: anchor groups arranged parallel to the edge and loaded perpendicular to the edge

Table 11.2. Verification of the model: anchor groups arranged parallel to the edge and loaded perpendicular to the edge

Test series ID	Mean measured ultimate load	Ultimate load obtained from spring model	
	$V_{u,m}$	$V_{u,spring\ model}$	$V_{u,m} / V_{u,spring\ model}$
	[kN]	[kN]	[-]
GS-1×2-C	56.1	57.8	0.97
GS-1×2-e60	45.8	28.9	1.58
GS-1×2-dw03-C	44.3	46.6	0.95
GS-1×3-C	61.0	64.4	0.95
GS-1×3-e60	57.7	48.4	1.19
GS-1×3-e120	50.6	50.5	1.00
GS-1×3-dw03-C	55.3	55.6	0.99
GS-1×3-dw03-e120c	41.5	41.8	0.99
GS-1×3-dw03-e120u	45.8	50.2	0.91
GS-240/1×3-C	133.9	112.8	1.19
GS-1×3-120/240-C	89.2	92.9	0.96

In general, the spring model delivers accurate results compared to the test results for the configurations given in *Table 11.2*, which confirms that the spring model is able to predict the behaviour of anchorages having one anchor row arranged parallel to the concrete edge in uncracked and cracked concrete very well. Through this approach, it is possible to consider the exact or worst possible crack pattern and the superposed influence of eccentric loading and crack pattern. The highest difference between test results and result of the spring model was obtained in test series GS-1×2-e60 ($V_{u,m,test} / V_{u,spring\ model} = 1.58$), which corresponds to the 1×2 anchor group with the eccentric shear load applied at the position of one anchor. Neglecting this series from the evaluation, the mean value would result in 1.01, while the CoV is 9.7%.

According to the CCD method (approach followed by EN 1992-4), in the case of an 1×2 anchor group, if the loading is applied directly in line with one anchor, the failure load of the group corresponds to the failure load of a single anchor irrespective of the spacing ($V_{Rm,c,EN} = V^0_{Rm,c,EN}$=*37.2 kN*, refer to *Table 9.13*). This can be explained by the formulations in the current design approach (***Eq. 116*** - ***Eq. 118***), where the factor to account for loading eccentricity, $\psi_{ec,V}$, becomes equal to $A^0_{c,V}/A_{c,V}$ if e_v=*s/2*. According to this consideration, the tributary area of the group is equal to the projected area of one single anchor as it is depicted in *Figure 11.5*, and the single anchor is loaded in concentric shear. This behaviour was also confirmed by the test results on single anchor series SS-120 and anchor group series GS-1×2-e60, with the mean measured ultimate loads 43.4 kN and 45.8 kN, respectively.

$$V_{Rm,c} = V^0_{Rm,c} \cdot \frac{A_{c,V}}{A^0_{c,V}} \cdot \Psi_{ec,V} = V^0_{Rm,c} \cdot \frac{A_{c,V}}{A^0_{c,V}} \cdot \frac{A^0_{c,V}}{A_{c,V}} = V^0_{Rm,c} \qquad \textbf{Eq. 116}$$

$$\frac{A_{c,V}}{A^0_{c,V}} = \frac{(s + 3 \cdot c_1) \cdot 1.5 \cdot c_1}{4.5 \cdot {c_1}^2} \qquad \textbf{Eq. 117}$$

$$\psi_{ec,V} = \frac{1}{1 + 2 \cdot e_v/(3 \cdot c_1)} = \frac{1}{1 + 2 \cdot \frac{s}{2}/(3 \cdot c_1)} = \frac{3 \cdot c_1}{3 \cdot c_1 + s} = \frac{A^0_{c,V}}{A_{c,V}} \qquad \textbf{Eq. 118}$$

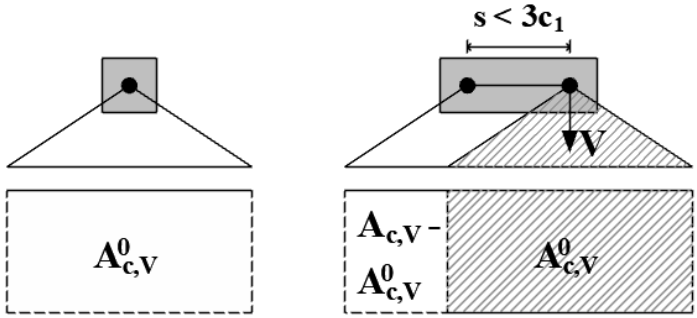

Figure 11.5. Tributary area considered for the group derived from Eq. 116 - Eq. 118 (GS-1×2-e60)

In the nonlinear spring model, the reduction in resistance of any individual anchor of the group compared to the corresponding single anchor resistance is considered by the ratio of the tributary areas $A^i_{c,V}/A^0_{c,V}$ (***Eq. 119*** **-** ***Eq. 120***). This means that in the case of a 1×2 anchor configuration with having an anchor spacing smaller than $3c_1$, to each anchor, a tributary area according to ***Eq. 119*** can be assigned. For the discussed case, series GS-1×2-e60, $A^i_{c,V}/A^0_{c,V}$ corresponds to 0.67. When using the nonlinear spring model to calculate the resistance of a 1×2 anchor group, if the shear load is applied directly in line with one anchor (anchor 2) and the loading is rotationally unrestrained, the centre of rotation is the position of the loaded anchor and the failure load of the group corresponds to ***Eq. 120***. This failure load and load-displacement behaviour correspond to the spring characteristics, which are assigned to the anchor (anchor 2). Consequently, if $s < 3c_1$, the failure load is always smaller than the failure load of the corresponding single anchor, and the conservatism of the model to the test results increases with decreasing anchor spacing. This is due to the tributary area (or volume) approach used in the spring model for the individual anchors of a group. However, this effect is only pronounced in the case of 1×2 anchor configuration, where the load is applied on one anchor and no redistribution can take place due to the centre of rotation at the loaded anchor.

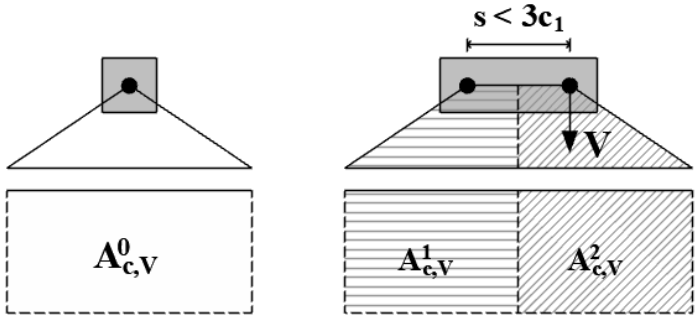

Figure 11.6. Tributary area considered for the group in the nonlinear spring model (GS-1×2-e60)

$$A^1_{c,V} = A^2_{c,V} = (\frac{s}{2} + 1.5 \cdot c_1) \cdot 1.5 \cdot c_1 \leq A^0_{c,V} \qquad \textbf{Eq. 119}$$

$$V^1_{Rm,c} = V^0_{Rm,c} \cdot \frac{A^1_{c,V}}{A^0_{c,V}} \leq V^0_{Rm,c} \qquad \text{if } s = 3 \cdot c_1 \;\rightarrow\; V_{Rm,c} = V^0_{Rm,c} \qquad \textbf{Eq. 120}$$

1×2 anchor group in cracked concrete

In the test program according to *Table 9.3*, i.a., the influence of crack pattern was investigated on anchor groups having one anchor row arranged parallel to the concrete edge and loaded perpendicular towards the free edge. Series GS-1×2-dw03-C, GS-1×3-dw03-C, GS-1×3-dw03-e120c and GS-1×3-dw03-e120u confirmed that the nonlinear spring model is capable of considering the exact crack pattern and the influence of loading eccentricity is captured. However, no tests were carried out, where all anchors were located in crack. In such cases, all anchors have the same stiffness, so the behaviour is directly comparable with a case in uncracked concrete but with reduced stiffness and resistance. When the reduction of the resistance is taken into account as observed in the single anchor tests series, $V_{u,m}(SS - 120- dw03) / V_{u,m}(SS - 120) = 0.79$, the group resistance in cracked concrete should result in $V_{u,m}(GS\text{-}1\times2\text{-}C)\cdot0.79=44.3$ *kN*.

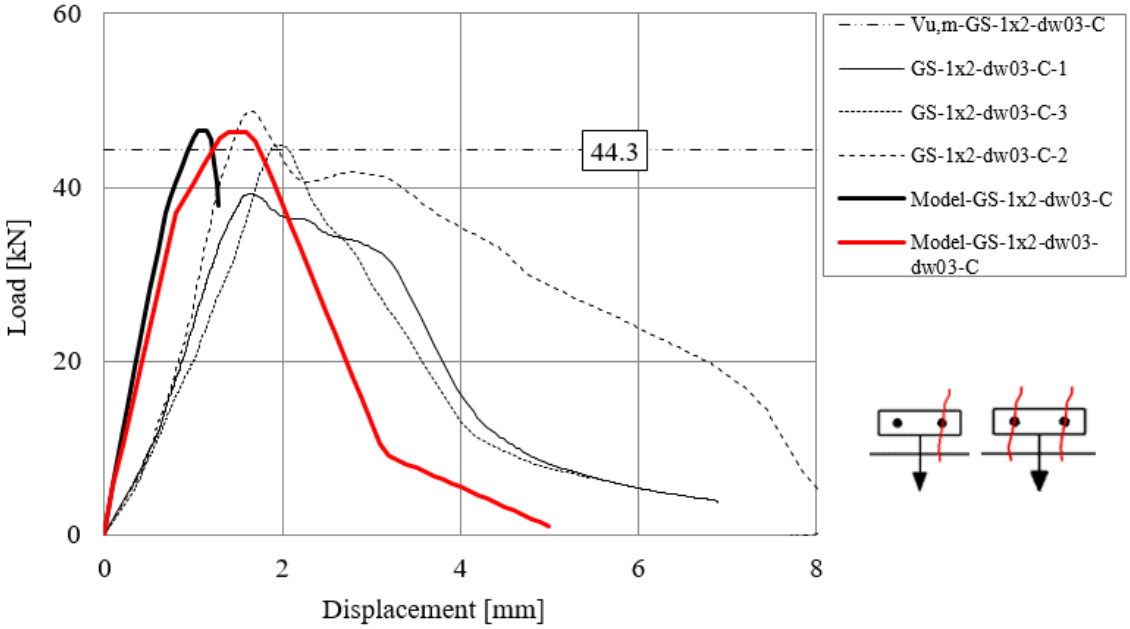

Figure 11.7. Load-displacement curves obtained from tests on anchor groups and result of the spring model for series GS-1×2-dw03-C

The case with both anchors of the group located in crack and loaded in concentric shear was analysed using the nonlinear spring model in Model-GS-1x2-dw03-dw03-C (red line in *Figure 11.7)*. The ultimate load was obtained as 46.3 kN, which corresponds to the result of Model- GS-1x2-dw03- C (46.6 kN) carried out with one anchor intercepted by crack. The stiffness is slightly lower when two anchors are located by the crack, which is intuitive.

Figure 11.8 gives the explanation why the 1×2 groups with either only one anchor or two anchors in crack, and consequently different spring characteristics (in terms of resistance and stiffness) result in the same group resistance. In *Figure 11.8a*, the displacement behaviour and the force equilibrium for the case with two anchors in crack are shown. In case of rotation unrestrained load application, at any loading step, the forces in both anchors are equal, and since the stiffness, k_{cr}, of both anchors is the same, this results in the same displacement, δ, for

the anchors and in zero rotation for the base plate ($tan\theta = 0$). In the second case, in *Figure 11.8b*, the displacement behaviour and the force equilibrium for the case with only one anchor in crack are shown for the 1×2 anchor group with rotation unrestrained load application. Once the shear load is applied, the base plate starts to rotate, and the angle θ is changing in every loading step. Due to the rotation unrestrained load application, the force taken up by the anchors is the same; however, the displacement of the anchors is different because of the different stiffness conditions of the anchors (k_{ucr} and k_{cr}). Even if anchor 2 could theoretically reach a higher load due to the uncracked condition compared to anchor 1, the resistance of anchor 2 cannot be fully utilised because once anchor 1 fails, to satisfy the equilibrium, anchor 2 also has to drop the load. With this, the assumed behaviour, and the result of the spring model for the 1×2 group with two anchors in crack (Model-GS-1x2-dw03-dw03-C) is confirmed in the case of concentric shear loading and rotation unrestrained load application.

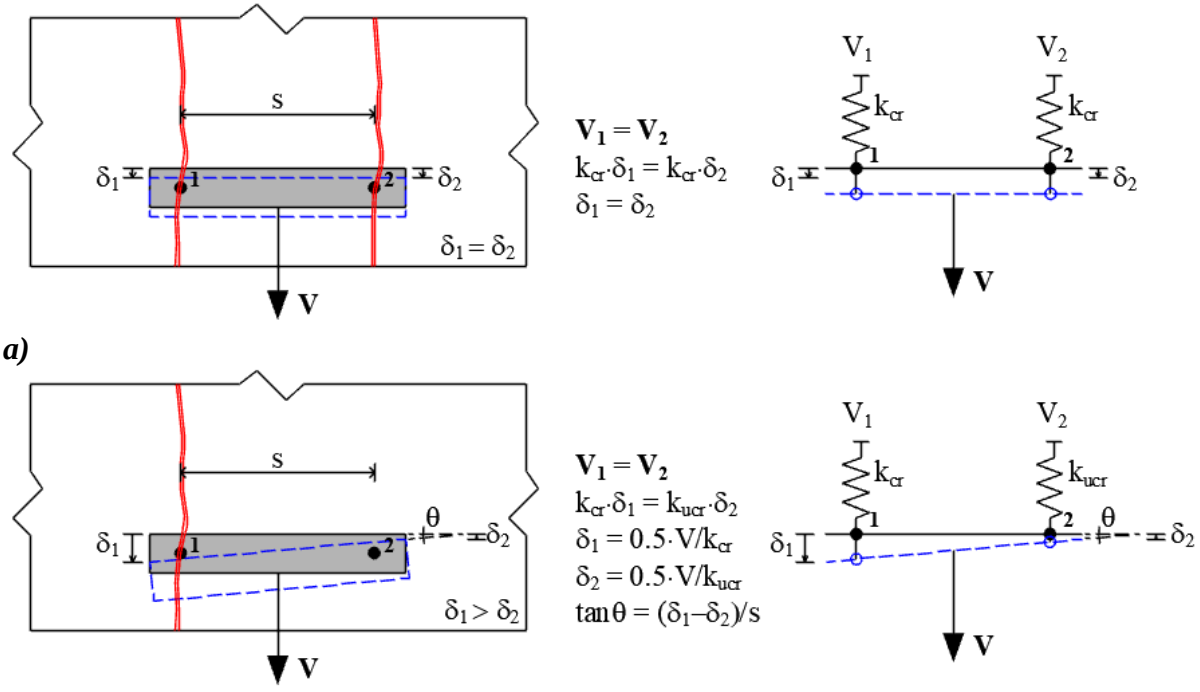

Figure 11.8. Displacement behaviour of a 1×2 anchor group subjected to concentric shear in cracked concrete

11.3 VERIFICATION OF THE SPRING MODEL FOR ANCHORAGES WITH MULTIPLE ANCHOR ROWS

In this section, the results of the spring model on anchorages with multiple anchor rows are discussed. The tributary volume approach is verified for multiple anchor rows and it is shown that the total force and volume of the group without hole clearance cannot be more than the volume of the corresponding last anchor row. Furthermore, the spring model is verified to capture the hole clearance pattern, for rectangular and non-rectangular anchor groups up to four anchor rows.

11.3.1 Nonlinear spring model for rectangular anchorages having multiple anchor rows

11.3.1.1 Sample calculation of 3×1 anchor group

In the following example, an anchor group of 3×1 configuration subjected to concentric shear loading is calculated with the nonlinear spring model for shear. The investigated configuration GS-3×1-80-80 is shown in *Figure 11.9*.

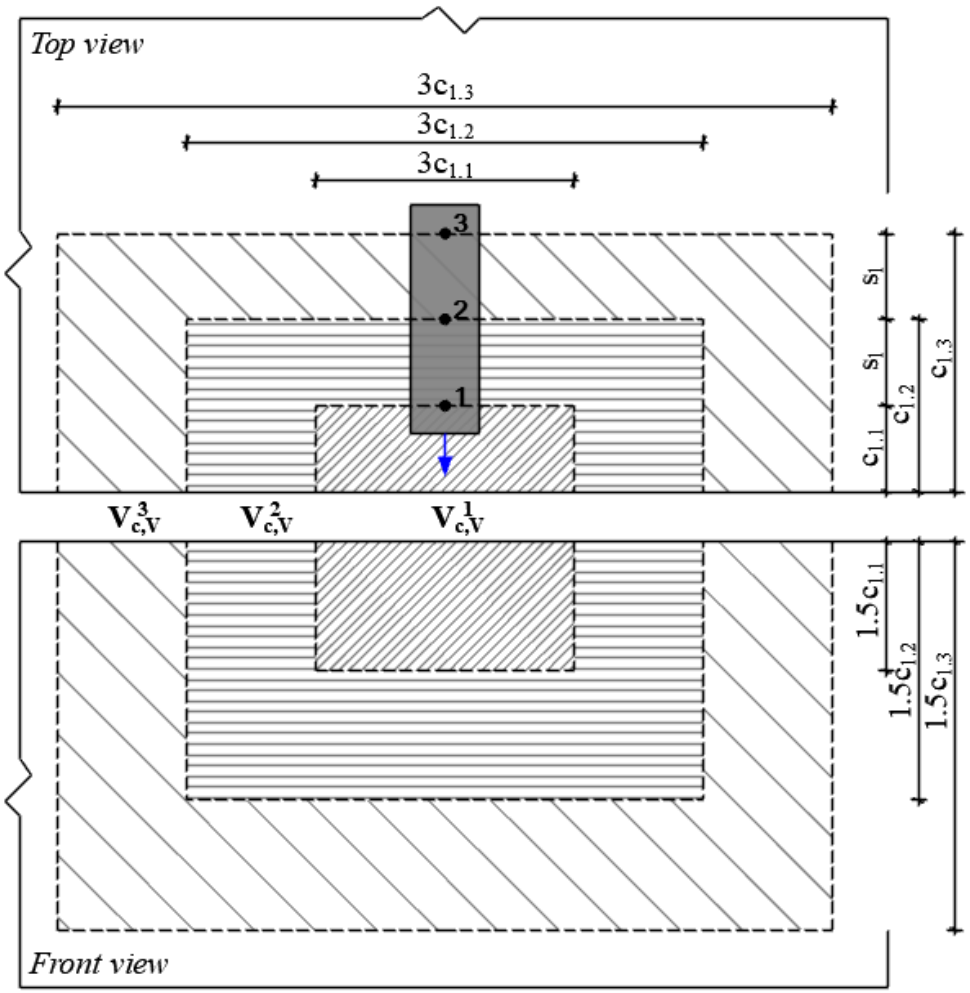

Figure 11.9. Anchor group configuration, tributary volume for series GS-3×1-80-80

The hole clearance (a_{cl}) pattern, which was measured in the three performed tests, was considered in the analyses. In addition, the configuration without the influence of hole clearance and with the most favourable hole clearance pattern was analysed. The anchor spacing and the edge distance were 80 mm. The further installation parameters of the anchor group GS-3×1-80-80 can be taken from *Table 9.1*, *Table 9.2*. The load-displacement curves of the shear-loading tests on single anchors with 80, 160 and 240 mm edge distance were evaluated to determine the spring properties for the single anchors, which are listed in *Table 11.3*. After that, the reference curve was scaled down based on the tributary volume available for the corresponding individual anchors using the reduction factor $V_{c,V}^{i,j}/V_{c,V}^{0,j}$ according to ***Eq. 121*** - ***Eq. 125***.

$$V_{c.V}^{0,1} = V_{c.V}^{1,1} = 4.5 \cdot {c_{1.1}}^3 = 2304000\ mm^3 \qquad \textbf{Eq. 121}$$

$$V_{c.V}^{0,2} = 4.5 \cdot {c_{1.2}}^3 = 18432000\ mm^3 \qquad \textbf{Eq. 122}$$

$$V_{c.V}^{1,2} = 4.5 \cdot {c_{1.2}}^3 - V_{c.V}^{1,1} = 15128000\ \ mm^3 \qquad \textbf{Eq. 123}$$

$$V_{c.V}^{0,3} = 4.5 \cdot {c_{1.3}}^3 = 62208000\ mm^3 \qquad \textbf{Eq. 124}$$

$$V_{c.V}^{1,3} = 4.5 \cdot {c_{1.3}}^3 - V_{c.V}^{1,1} - V_{c.V}^{1,2} = 43776000\ \ mm^3 \qquad \textbf{Eq. 125}$$

Table 11.3. Spring properties of individual anchors of the anchor group series GS-3×1-80-80

	Load $V_{Rm,c}{}^{i}{}_{A\text{-}F}$ [kN]	Stiffness k_1-k_4 [kN/mm]	Displacement $\delta_{A\text{-}F}$ [mm]	Load $V_{Rm,c}{}^{i}{}_{A\text{-}F}$ [kN]	Stiffness k_1-k_4 [kN/mm]	Displacement $\delta_{A\text{-}F}$ [mm]
Reference single anchor $c_{1.1}$				***Anchor A1 $c_{1.1}$***		
A	0.0	0.0	0.0	0.0	0.0	0.0
B	18.9	35.1	0.5	18.9	35.1	0.5
C	23.6	26.7	0.9	23.6	26.7	0.9
D	23.6	21.4	1.1	23.6	21.4	1.1
E	4.7	1.6	2.9	4.7	1.6	2.9
F	0.0	0.0	2.9	0.0	0.0	2.9
Reference single anchor $c_{1.2}$				***Anchor A2 $c_{1.2}$***		
A	0.0	0.0	0.0	0.0	0.0	0.0
B	45.8	35.1	1.3	40.0	35.1	1.1
C	57.2	26.7	2.1	50.1	26.7	1.9
D	57.2	21.4	2.7	50.1	21.4	2.3
E	11.4	1.6	7.1	10.0	1.6	6.2
F	0.0	0.0	7.1	0.0	0.0	6.2
Reference single anchor $c_{1.3}$				***Anchor A3 $c_{1.3}$***		
A	0.0	0.0	0.0	0.0	0.0	0.0
B	58.6	35.1	1.7	41.3	35.1	1.2
C	97.7	26.7	3.7	68.8	26.7	2.6
D	97.7	21.4	4.6	68.8	21.4	3.2
E	19.5	1.6	12.2	13.8	1.6	8.6
F	0.0	0.0	12.2	0.0	0.0	8.6

The spring properties given in *Table 11.3* were assigned to the anchor springs representing the nonlinear anchor behaviour under shear. Note that for the anchors with hole clearance, an additional horizontal segment was added at zero load level into the idealised load-displacement curve so that point of the curve moved horizontally by the corresponding a_{cl} (a_{cl} values are given directly in the legend of *Figure 11.10*). The load was applied concentrically on the base plate and the nonlinear static analysis was performed in displacement control until the desired displacement. The base plate was considered as rigid in the analysis. The load-displacement curves obtained from the spring model considering the exact hole clearance pattern measured in the tests are plotted in *Figure 11.10* along with the test results. The load-displacement curves show a very good agreement in terms of ultimate loads (*mv of* V_u / $V_{u,spring\ model}$ is 0.97) and curve progression (see *Figure 11.10*, *Table 11.4*).

Using the same spring properties of anchors A1 and A2, the analysis was performed for the 2×1 anchor group having the same edge distance and spacing, which was also tested with hole clearance. The corresponding results and hole clearance pattern are given in *Figure 11.11*, which again show that the nonlinear spring model can calculate the load-displacement curves for the anchor groups with arbitrary hole clearance pattern. The test GS-2×1-80-80-3 is a typical example for anchorages having unfavourable hole clearance pattern. The spring model replicates the behaviour very well that due to hole clearance, the entire shear load is distributed initially only to the front anchor (compare spring properties in *Table 11.4* and first peak in *Figure 11.11*).

In addition, for both configurations, analyses were performed on the same configuration without hole clearance and with the most favourable hole clearance pattern to show that the anchor group behaviour can be improved by controlling the hole clearance pattern and to highlight the importance of using displacement-based approach for the design.

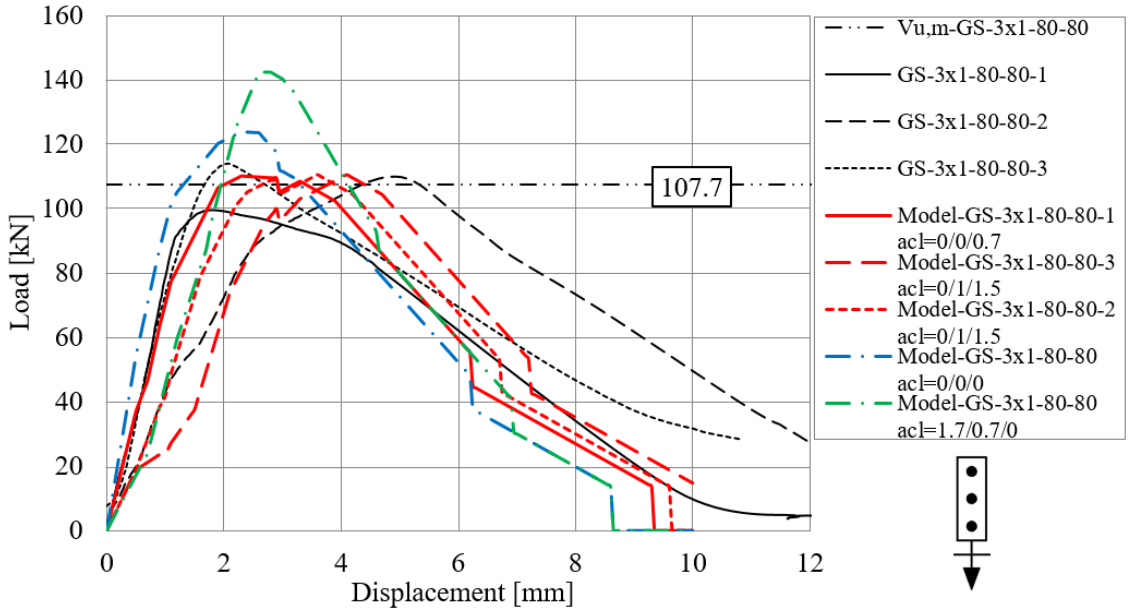

Figure 11.10. Load-displacement curves obtained from tests on anchor groups and result of the spring model for series GS-3×1-80-80

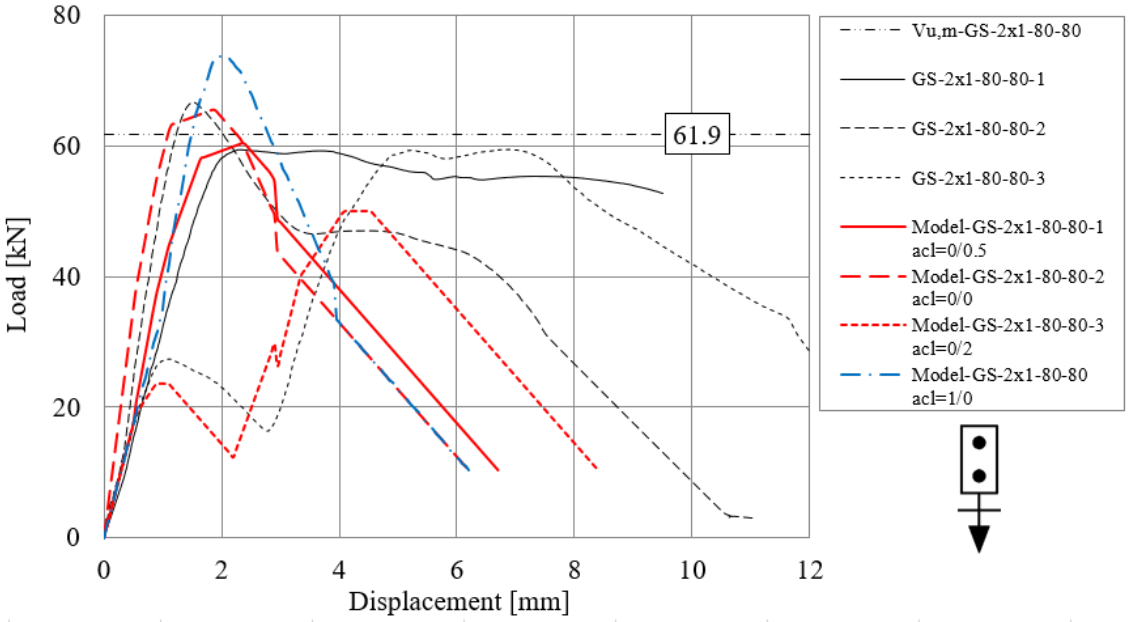

Figure 11.11. Load-displacement curves obtained from tests on anchor groups and result of the spring model for series GS-2×1-80-80

11.3.1.2 Comparison of test results with the results of the nonlinear spring model for rectangular anchorages having multiple anchor rows

To verify the tributary volume approach for anchor groups of rectangular configurations having multiple anchor rows, the results of the performed analyses and tests on series GS-3×1-80-80, GS-2×1-80-80, GS-2×1-160-80 were compared in *Table 11.4* in terms of ultimate loads.

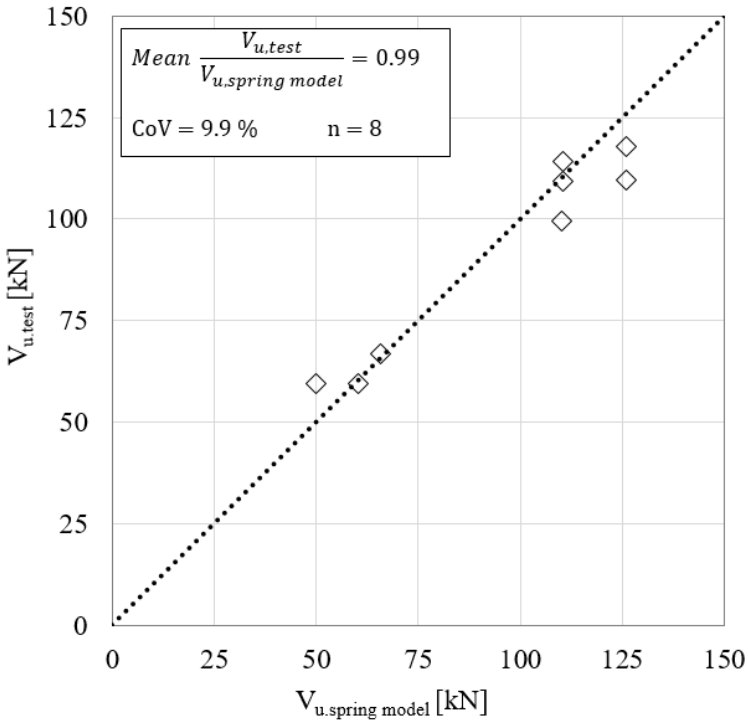

Figure 11.12. Comparison of failure loads from tests with the peak loads obtained from the nonlinear spring model: anchor groups arranged perpendicular to the edge and loaded perpendicular to the edge

The mean value of the ratio of ultimate loads, $V_{u,test}/V_{u,spring\ model}$ is 0.99, and the coefficient of variation is 9.9% (*Figure 11.12*). The spring model delivers accurate results compared to the test results for the analysed cases, confirming that the spring model can predict the behaviour of anchor groups with multiple anchor rows considering hole clearance pattern very well.

Table 11.4. Verification of the model: anchor groups arranged perpendicular to the edge and loaded perpendicular to the edge

Test series ID	Hole clearance pattern	Meas. ultimate load	Measured mean ultimate load	Ultimate load obtained from spring model	
	$a_{cl1/2/3/4}$	V_u	$V_{u,m}$	$V_{u,spring\ model}$	$V_u/V_{u,spring\ model}$
	[mm]	[kN]	[kN]	[kN]	[-]
GS-3×1-80-80	0/0/0.7	99.57	107.7	110.2	0.90
	0/1/1.5	109.35	-	110.6	0.99
	0/0.5/1	114.03	-	110.6	1.03
	0/0/0	-	-	*123.9*	-
	1.7/0.7/0	-	-	*142.4*	-
GS-2×1-80-80	0/0.5	59.5	61.9	60.4	0.99
	0/0	66.8	-	65.6	1.02
	0/2	59.5	-	50.0	1.19
	1/0	-	-	*73.7*	-
GS-2×1-160-80	0/0	117.7	113.6	125.9	0.93
	0/1	109.55	-	125.9	0.87
	0.5/0	-	-	*125.9*	-

11.3.2 Nonlinear spring model to consider non-rectangular anchor pattern

11.3.2.1 Sample calculation of a triangular anchor group

In the case of anchor groups of non-rectangular configurations, the influence of anchor spacing in both parallel to and perpendicular to the concrete edge must be considered. This can be done by following the tributary volume approach. In *Figure 11.13*, the tributary volumes assigned to the anchors of a triangular anchor group configuration (GS-TRI-A) are shown. The hole clearance (a_{cl}) pattern measured in the tests was considered in the analyses using the spring model (see *Table 9.8*). The further installation parameters can be taken from *Table 9.2*. To determine the spring characteristics, load-displacement curves of the shear-loading tests on single anchors with 120 and 240 mm edge distance were evaluated. The stiffness values were derived from the curves and the force values were calculated. Then, the reference curve was scaled down based on the tributary volume available for the corresponding individual anchors (***Eq. 126*** - ***Eq. 129***) using the reduction factor $V_{c,V}^{i,j}/V_{c,V}^{0,j}$.

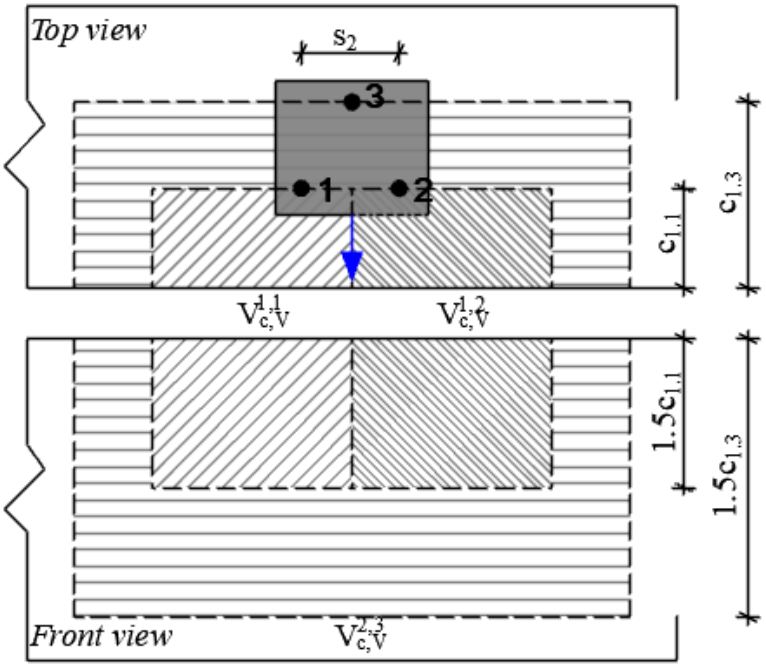

Figure 11.13. Anchor group configuration, tributary volume for series GS-TRI-A

$$V_{c.V}^{0,1} = 4.5 \cdot {c_{1.1}}^3 = 4.5 \cdot 118.8^3 = 7545045\ mm^3 \qquad \textbf{Eq. 126}$$

$$V_{c.V}^{0,2} = 4.5 \cdot {c_{1.2}}^3 = 4.5 \cdot 240^3 = 62208000\ mm^3 \qquad \textbf{Eq. 127}$$

$$V_{c.V}^{1,1} = V_{c.V}^{1,2} = (1.5 \cdot c_{1.1} + \frac{s_2}{2}) \cdot c_{1.1} = 5254433.7\ mm^3 \qquad \textbf{Eq. 128}$$

$$V_{c.V}^{2,3} = V_{c.V}^{0,2} - V_{c.V}^{1,1} - V_{c.V}^{1,2} = 51699132.6\ mm^3 \qquad \textbf{Eq. 129}$$

Table 11.5. Spring properties of individual anchors of the anchor group series GS-TRI-A

	Load $V_{Rm,c}{}^{i}{}_{A\text{-}F}$ [kN]	Stiffness k_1-k_4 [kN/mm]	Displace-ment $\delta_{A\text{-}F}$ [mm]	Load $V_{Rm,c}{}^{i}{}_{A\text{-}F}$ [kN]	Stiffness k_1-k_4 [kN/mm]	Displace-ment $\delta_{A\text{-}F}$ [mm]
Reference single anchor $c_{1.1}$				***Anchor A1 $c_{1.1}$ A2 $c_{1.1}$***		
A	0.0	0.0	0.0	0.0	0.0	0.0
B	28.0	37.5	0.7	19.5	37.5	0.5
C	35.0	28.1	1.2	24.4	28.1	0.9
D	35.0	22.6	1.5	24.4	22.6	1.1
E	7.0	2.4	2.9	4.9	2.4	2.1
F	0.0	0.0	2.9	0.0	0.0	2.1
Reference single anchor $c_{1.3}$				***Anchor A3 $c_{1.3}$***		
A	0.0	0.0	0.0	0.0	0.0	0.0
B	52.9	37.5	1.4	43.9	37.5	1.2
C	88.1	28.1	3.1	73.2	28.1	2.6
D	88.1	22.6	3.9	73.2	22.6	3.2
E	17.6	2.4	7.4	14.6	2.4	6.2
F	0.0	0.0	7.4	0.0	0.0	6.2

The spring characteristics of the corresponding individual anchors given in *Table 11.5* were assigned to the anchor springs extended with an additional horizontal segment at zero load level to consider the hole clearance. The load was applied concentrically on the rigid base plate, however, the influence of the hole clearance pattern leads to the uneven force distribution, which is automatically considered by performing nonlinear static analysis. For each hole clearance pattern (=for each test), a new analysis was carried out. Consequently, to each load-displacement curve obtained from the tests, the corresponding curve from the spring model considering the exact hole clearance pattern is plotted (*Figure 11.14*). The load-displacement curves represent the anchor group behaviour very well (mv of $V_u/V_{u,spring\ model}$ is 1.02).

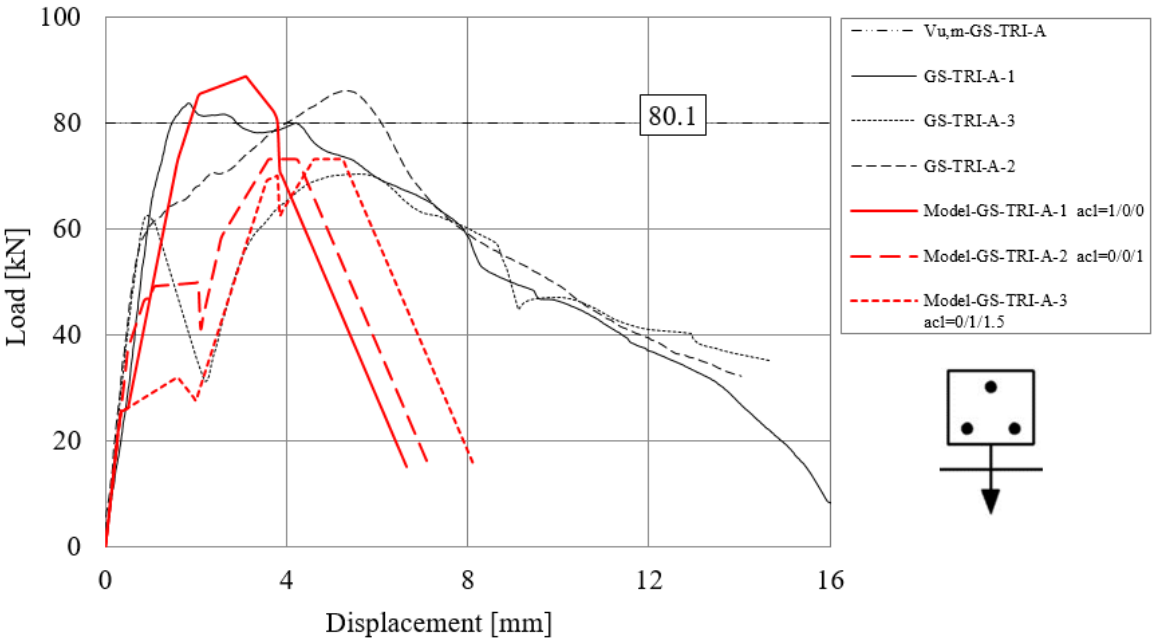

Figure 11.14. Load-displacement curves obtained from tests on anchor groups and result of the spring model for series GS-TRI-A

11.3.2.2 Comparison of test results with the results of the nonlinear spring model for non-rectangular anchorages having multiple anchor rows

Results of 12 nonlinear static analyses performed using the spring model on anchor groups of triangular and hexagonal configurations are compared with the corresponding experimental results in the following. The mean value of the ratio of ultimate loads, $V_{u,test}/V_{u,spring\ model}$ is 1.0 and the coefficient of variation is 8.1% (refer *to Figure 11.15*). The corresponding load-displacement curves, to verify the model in terms of curve progression as well, are depicted in *Figure 11.14* - *Figure 11.18*. The spring model delivers accurate results compared to the test results for the analysed triangular and hexagonal cases with arbitrary hole clearance pattern, which again confirms that the nonlinear spring model with using the tributary volume approach can predict the behaviour of non-rectangular anchor groups with multiple anchor rows considering hole clearance pattern very well. Note that it is required to evaluate the displacement behaviour of the anchor groups to provide the design for SLS (refer to Section 13.7.2) that is not unnecessarily conservative for anchor groups having multiple anchor rows.

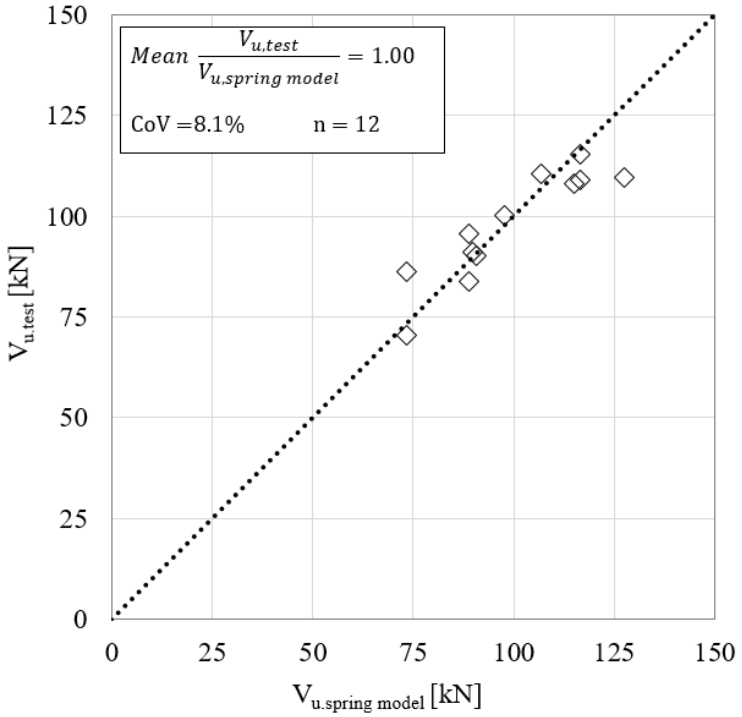

Figure 11.15. Comparison of test results with the results from the nonlinear spring model (failure loads): anchor groups of non-rectangular configurations loaded perpendicular to the edge

Table 11.6. Verification of the model: anchor groups of triangular and hexagonal configurations loaded perpendicular to the edge

Test series ID	Hole clearance pattern	Meas. ultimate load	Meas. mean ultimate load	Ultimate load obtained from spring model	
	$a_{cl.1/2/3/4/5/6}$	V_u	$V_{u,m}$	$V_{u,spring\ model}$	V_u / $V_{u,spring\ model}$
	[mm]	[kN]	[kN]	[kN]	[-]
GS-TRI-A	1/0/0	83.8	80.1	88.8	0.94
	0/0/1	86.1		73.2	1.18
	0/1/1.5	70.4		73.2	0.96
GS-TRI-B	0/0.5/0.5	108.9	111.3	116.6	0.93
	1/0/0	109.6		127.6	0.86
	0/0.5/0.5	115.3		116.6	0.99
GS-HEX-A	0/0/1/0.5/1.5/1.5	110.4	106.2	106.9	1.03
	0/1/1/0.5/2/1	100.2		97.6	1.02
	1.5/0/1/1.5/1.5/1.5	108.1		115.0	0.94
GS-HEX-B	0/2/0/1/1.5/1.5	91.2	92.4	89.8	1.02
	0/1/0.5/1.5/1.5/0.5	90.1		90.7	0.99
	1.5/0.5/0/2/2/0	95.8		88.8	1.08

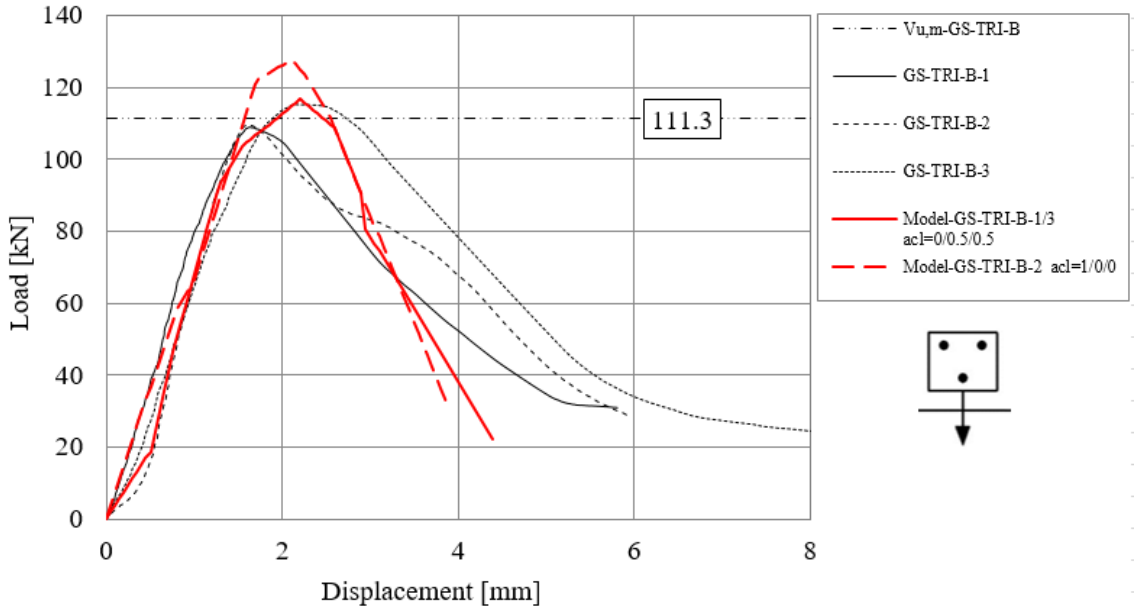

Figure 11.16. Load-displacement curves obtained from tests on anchor groups and result of the spring model for series GS-TRI-B

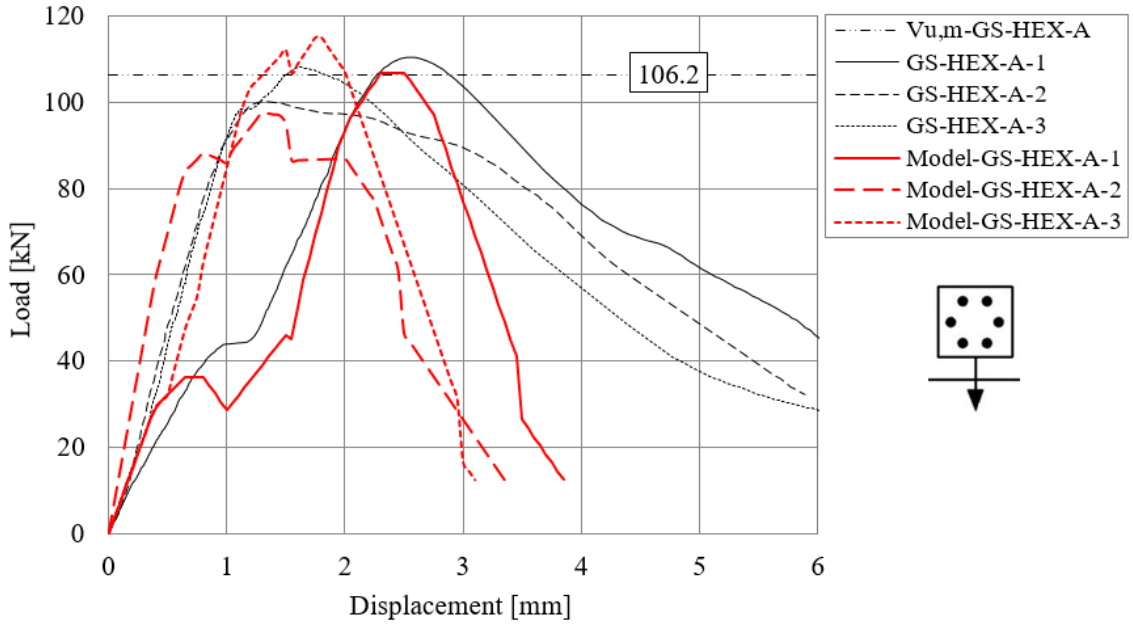

Figure 11.17. Load-displacement curves obtained from tests on anchor groups and result of the spring model for series GS-HEX-A

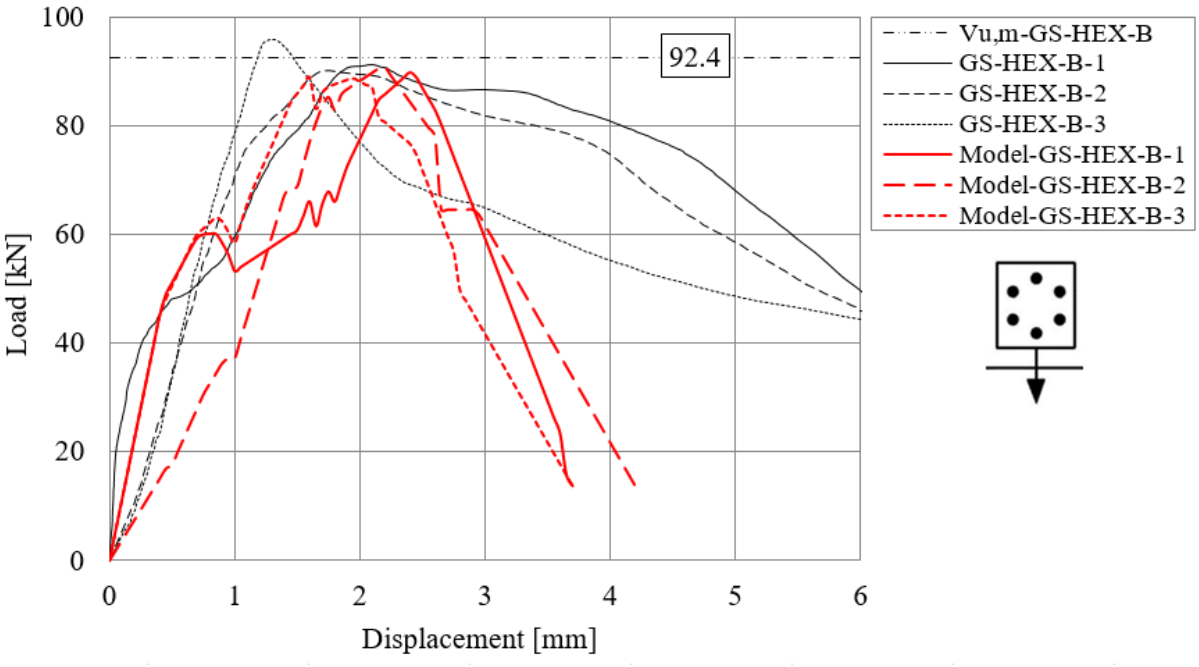

Figure 11.18. Load-displacement curves obtained from tests on anchor groups and result of the spring model for series GS-HEX-B

11.4 VERIFICATION OF THE SPRING MODEL AGAINST EXPERIMENTS FROM THE LITERATURE

11.4.1 Shear loading tests on anchor groups of 2×2, 1×2, 2×1 configurations (Hofmann, 2005)

The shear behaviour of anchorages was investigated extensively by Hofmann (2005). To verify the nonlinear spring model for concrete edge failure, anchor groups of 2×2, 1×2, 2×1 configurations placed close to the concrete edge and loaded perpendicular and towards the edge are evaluated from the work of Hofmann (see evaluated configurations in *Figure 11.19*). Of particular interest was the evaluation of the tests series with the influence of a further edge on the concrete edge failure load since this case was not tested in this work.

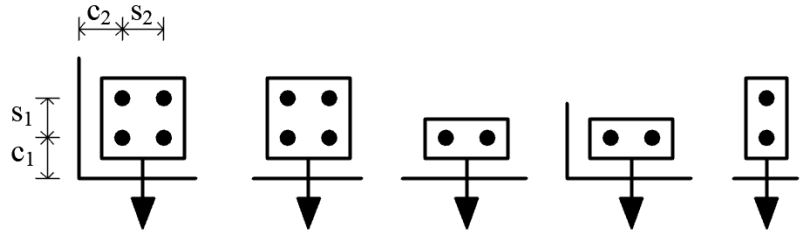

Figure 11.19. Anchor group configurations tested in the work of Hofmann by varying the parameters c_1, c_2, s_1, s_2

The test parameters, the anchor configurations as well as the test results in terms of the measured ultimate loads normalised to a concrete compressive strength (cylinder) of 25 N/mm^2 are given in *Table 11.7*. The test parameters can be read from the nomenclature of the test ID as anchor size (d_{nom}) – edge distance in the loading direction (c_1) – further edge distance in the

direction parallel to the loading (c_2) – anchor spacing perpendicular to loading direction (s_2) – anchor spacing in the loading direction (s_1) – loading angle. Further details on the material and test parameters can be taken from Hofmann (2005), Tabelle A11-1 – A11-6.

Determination of the anchor spring characteristics and verification of the model

The test results of series M16-70-0-0-0° on the shear loaded single anchors with 130 mm embedment depth, and 70 mm edge distance were used to generate the shear spring characteristics (load-displacement data pairs) for the spring model (*Figure 11.20*). The stiffness values for the idealised load-displacement curve of a single anchor were obtained from the load-displacement curves as $k_1 – k_4$ = *13.0, 10.7, 8.6* and *0.8 kN/mm,* and the same values were used for all edge distances. The corresponding ultimate loads ($V^0_{Rm,c}$) for the edge distances 70, 100, 140, 170 and 210 mm and for embedment depths 130 and 80 mm were calculated according to ***Eq. 54***. Then, the individual anchor spring characteristics were determined for all cases applying the tributary volume approach as described in Section 6.2.2.2. The resistance against concrete edge failure of i^{th} anchor of j^{th} row of a group ($V^{i,j}_{Rm,c}$) was calculated according to ***Eq. 63***.

A total of 58 test results from Hofmann were compared with the spring model (*Table 11.7*). The mean value of $V_{u,test}/V_{u,spring\ model}$ is 1.02 with a coefficient of variation of 11.0 %. Through the evaluation of the series with the influence of a further close edge, the nonlinear spring model for concrete edge failure is applicable for such applications as well.

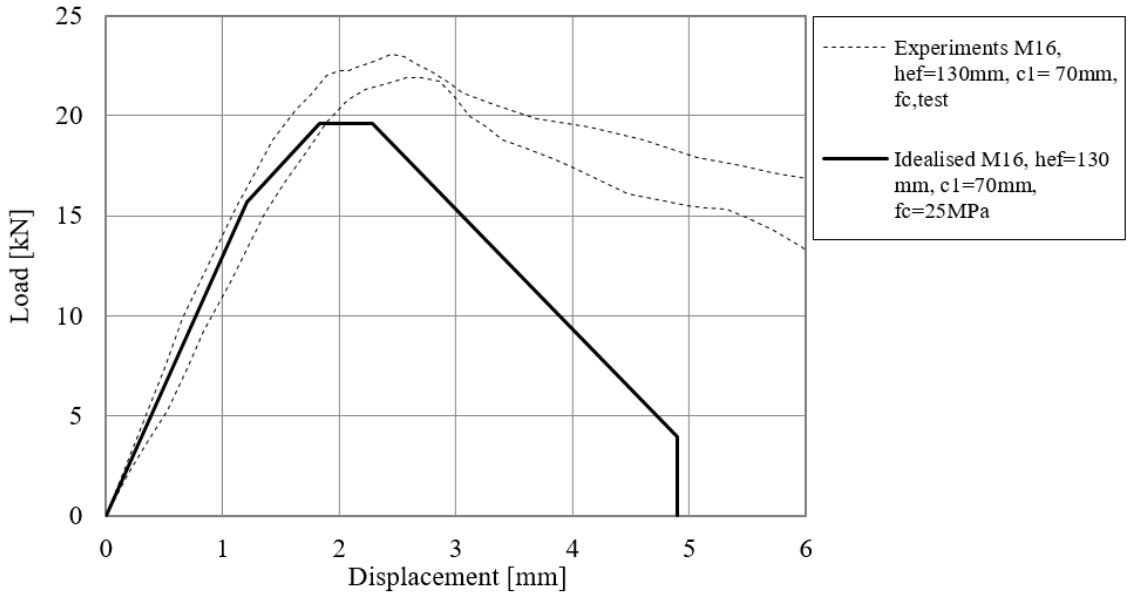

Figure 11.20. Load-displacement curves from series M16-70-0-0-0° (reproduced from Hofmann, 2005), idealised and normalised load-displacement curve used as spring characteristics for a single anchor with 70 mm edge distance

Table 11.7. Verification of the spring model against test results from Hofmann (2005)

Tested configuration	Test series ID	Meas. ultimate load*	Meas. mean ultimate load*	Ultimate load obtained from spring model	
		V_u	$V_{u,m}$	$V_{u,spring\ model}$	$V_u/V_{u,spring\ m.}$
		[kN]	[kN]	[kN]	[-]
Single anchor h_{ef} = 130 mm	M16-70-0-0-0°	-	34.1	-	-
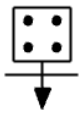 h_{ef} = 130 mm	M16-70-70-70-0°	59.3	59.2	58.8	1.01
		59.0		58.8	1.00
		60.0		58.8	1.02
		58.6		58.8	1.00
	M16-100-70-70-0°	96.1	97.8	84.4	1.14
		105.5		84.4	1.25
		98.6		84.4	1.17
		91.1		84.4	1.08
	M16-70-140-70-0°	69.0	69.5	58.8	1.18
		72.5		58.8	1.23
		66.9		58.8	1.14
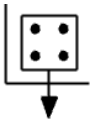 h_{ef} = 80 mm	M16-70-70-70-70-0°	35.0	34.3	37.3	0.94
		33.1		37.3	0.89
		34.4		37.3	0.92
		34.5		37.3	0.93
	M16-70-70-140-70-0°	37.2	37.9	39.3	0.94
		37.0		39.3	0.94
		39.6		39.3	1.01
	M16-100-100-70-70-0°	48.9	49.4	46.7	1.05
		50.0		46.7	1.07
		49.3		46.7	1.06
 h_{ef} = 130 mm	M16-140-70-0-0°	60.7	58.7	55.2	1.10
		56.1		55.2	1.02
		59.0		55.2	1.07
		59.2		55.2	1.07
	M16-100-100-0-0°	39.6	44.0	40.9	0.97
		45.7		40.9	1.12
		43.9		40.9	1.07
		46.7		40.9	1.14
	M16-70-140-0-0°	30.7	31.1	32.7	0.94
		33.8		32.7	1.04
		27.9		32.7	0.85
		32.0		32.7	0.98
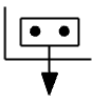 h_{ef} = 130 mm	M16-70-70-70-0-0°	18.2	19.1	21.8	0.83
		18.4		21.8	0.84
		21.8		21.8	1.00
		18.2		21.8	0.83

	M16-100-70-70-0-0°	24.8	26.9	23.9	1.04
		28.7		23.9	1.20
		27.0		23.9	1.13
	M16-100-100-100-0-0°	31.8	30.3	34.1	0.93
		30.0		34.1	0.88
		29.1		34.1	0.85
	M16-70-70-140-0-0°	22.4	22.6	26.1	0.86
		21.6		26.1	0.83
		24.0		26.1	0.92
	M16-70-70-70-0-0°	18.5	19.9	21.8	0.85
		20.4		21.8	0.94
		20.7		21.8	0.95
	M16-70-0-0-70-0°	57.1	56.0	51.5	1.11
		57.9		51.5	1.12
		53.0		51.5	1.03
	M16-70-0-0-100-0°	64.3	65.4	58.2	1.11
		68.0		58.2	1.17
		63.9		58.2	1.10
h_{ef} = 130 mm	M16-70-0-0-100-0°	83.3	86.3	77.8	1.07
		93.0		77.8	1.20
		82.5	59.2	77.8	1.06

*The ultimate load reported by Hofmann (2005) was normalised with respect to the concrete compressive strength to a value of f_{cm} = 25 N/mm^2, Nomenclature of the test ID: d_{nom} – c_1 - c_2 - s_2 - s_1 – loading angle

11.4.2 Shear loading tests on anchor groups of 2×2 configurations (Lachinger, 2012)

Lachinger (2012) investigated the behaviour of 2×2 anchor groups placed close to the concrete edge and installed with most unfavourable hole clearance pattern under inclined loading using bonded anchors. As a part of the comprehensive experimental program, tests under pure shear loads were also carried out. These tests were used for the verification of the nonlinear spring model for shear (see *Figure 11.23).* The test details and the verification for shear are given in Section 12.2 along with the verification of the model for interaction.

11.4.3 Shear loading tests on anchor groups multiple anchor rows (Grosser, 2012)

Results on 2×1 and 3×1 anchor configurations from Grosser (2012) were used to verify the spring model by performing the analyses on the corresponding configurations with and without the influence of hole clearance (see *Table 11.8*). For the cases with the influence of hole clearance, the installation was reported to be done by randomly locating the anchors in the drilled hole. The most unfavourable hole clearance pattern ($a_{cl.front}$ *= 0,* $a_{cl,mid}$ *= 2mm* and $a_{cl,back}$ *= 2mm*) was assumed for the evaluated cases. To obtain the stiffness values for the anchor spring characteristics, load-displacement curves reproduced from Grosser for single anchors of sizes M16 and M24, with h_{ef} *= 130 mm* and c_1 *= 100 mm* were evaluated (*Figure 11.21*). The following stiffness values of a single anchor were used to generate the idealised load-displacement curves: $k_1 – k_4$ *= 20, 17.6, 15.5* and *1.3 kN/mm* for M16 and $k_1 – k_4$ *= 40.0, 32, 26* and *1.7 kN/mm* for

M24. Note that the same stiffness values were used for all edge distances. The corresponding ultimate loads ($V^{0}_{Rm,c}$) for the edge distances 2" (50.8 mm), 3" (76.2 mm), 4" (101.6 mm) and 8" (203.2 mm) were calculated according to ***Eq. 54***. Then, the individual anchor spring characteristics were determined for all the cases applying the tributary volume approach as described in Section 6.2.2.2. The resistance against concrete edge failure of ith anchor of jth row of a group ($V^{i,j}_{Rm,c}$) was calculated according to ***Eq. 63***. The comparison of the test results and the spring model shows a good agreement. The mean value of $V_{u,test}/V_{u,spring\ model}$ is 1.18 with a coefficient of variation of 14.2 %.

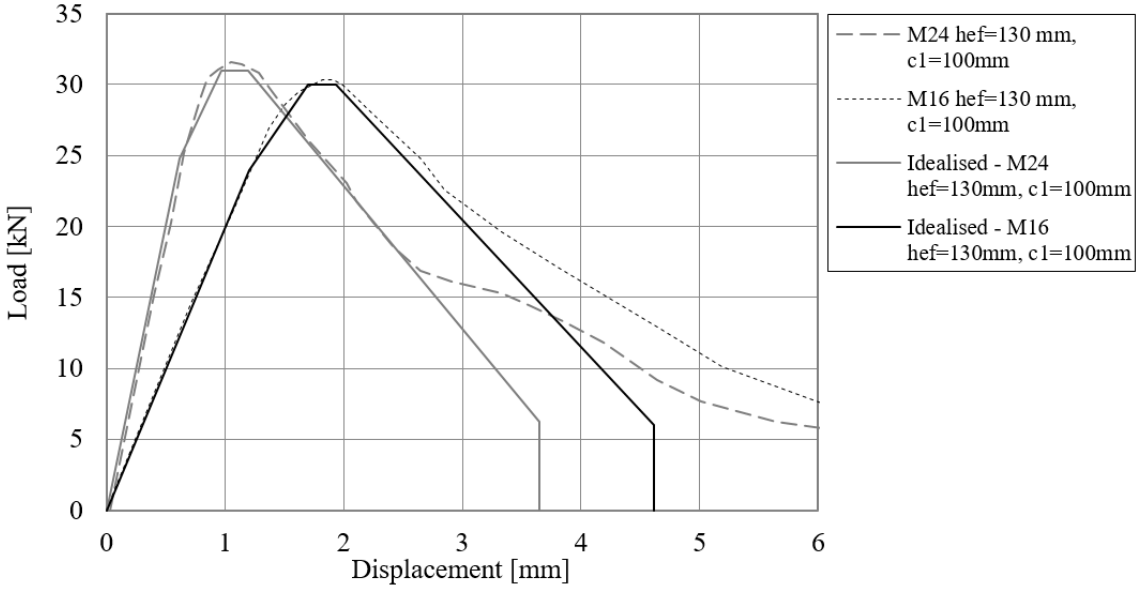

Figure 11.21. Load-displacement curves on single anchors (reproduced from Grosser, 2012) and idealised load-displacement curves used as spring characteristics for single anchors (M16 and M24)

Table 11.8. Verification of the spring model against test results from Grosser (2012): anchor groups arranged perpendicular to the edge and loaded perpendicular to the edge

Source	Test series ID	Hole clearance pattern	Meas. ultimate load	Ultimate load from spring model	
		$a_{cl1/2/3}$	V_u	$V_{u,spring\ model}$	$N_u/V_{u,spring\ model}$
		[mm]	[kN]	[kN]	[-]
Grosser 2012	2×1-5/8"-4"-2"-1	*0/0*	81.8	73.4	1.11
	2×1-7/8"-4"-4"-2	*0/0*	125.9	101.8	1.24
	3×1-7/8"-4"-2"-2"-1	*0/0/0*	125.0	126.4	0.99
	3×1-7/8"-3"-4"-4"-2	*0/0/0*	183.7	196.1	0.94
	2×1-7/8"-8"-2"-1	*0/2*	171.3	141.2	1.21
	2×1-7/8"-4"-2"-2	*0/2*	66.3	58.1	1.14
	2×1-7/8"-4"-4"-3	*0/2*	83.6	79.6	1.05
	2×1-7/8"-2"-4"-4	*0/2*	78.3	57.5	1.36
	3×1-7/8"-4"-2"-2"-1	*0/2/2*	121.0	85.4	1.42
	3×1-7/8"-3"-4"-4"-1	*0/2/2*	188.6	136.0	1.39

The test results were taken from Grosser (2012) *Figures 3.97-3.100*, *Table B-5* and *Table B-6*

11.4.4 Shear loading tests on anchor groups of 2×2 and 4×2 configurations (Sharma et al., 2017, 2019)

In the work of Sharma et al. (2017 and 2019), an experimental program was carried out on anchor groups of 2×2 and 4×2 configurations using headed studs welded on the base plate to investigate the behaviour of anchorages placed close to the concrete edge and loaded under inclined loads towards the edge (tension-shear interaction). Due to the fact that the headed studs were welded on the base plate, the anchorages are without the influence of hole clearance.

The nonlinear spring model for concrete edge failure was verified against the tests conducted under pure shear loading up to 4 anchor rows considering the influence of member thickness for the back rows. The details of tests, a detailed discussion of the results and the verification for shear are given in Section 12.1 along with the verification of the model for interaction. The comparison of the test results with the spring model is given in *Table 12.4* and the load-displacement curves are plotted in *Figure 12.9* and *Figure 12.10* to highlight that not only the ultimate loads but also the load-displacement behaviour can be captured by the nonlinear spring model even for larger anchor groups.

11.4.5 Summary of the literature results

In *Figure 11.23*, the failure loads of various anchor group tests from the literature are compared with the failure loads obtained using the nonlinear spring model.

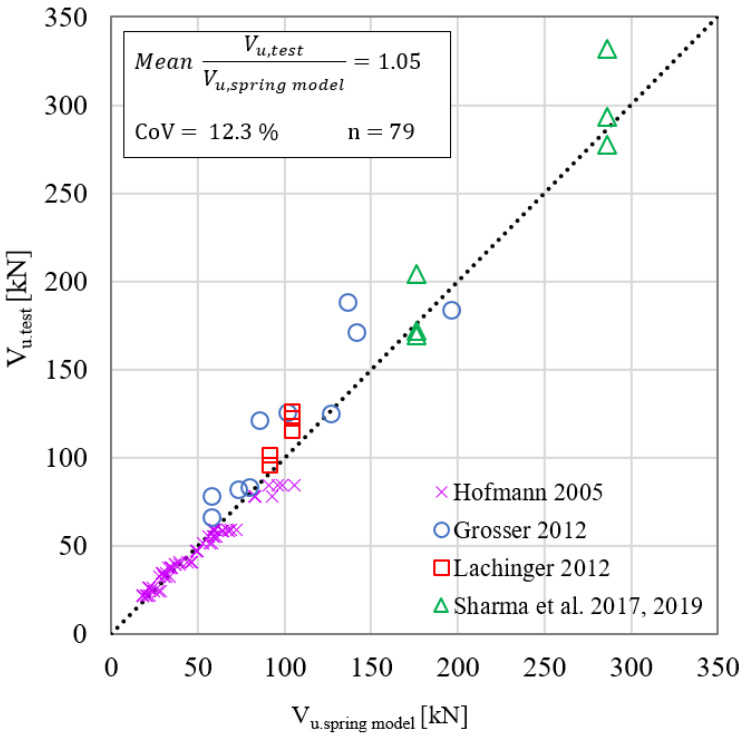

Figure 11.22. Comparison of test results from the literature with the results obtained from the nonlinear spring model (failure loads)

The comparison of the results shows a very good agreement. The mean value of $V_{u,test}/V_{u,spring\ model}$ is 1.05 with a coefficient of variation of 12.3 % for a total of 79 tests. Note

that in the case of the evaluation of tests from the literature, not in every case reference tests on single anchors were available to generate the spring characteristics. Therefore, the spring characteristics were generated by calculating the mean concrete edge resistance of the corresponding individual anchors based on the CCD method, whereas the stiffness values were derived from either tests on single anchors (if reported) or from group tests while assuming stiffness values for the individual anchors $k_{1-4} = k_{group,1-4}/n$ (n = number of anchors within an anchor row). The good match of the results of tests from the literature and spring model proves the reliability of the model for anchor groups of rectangular configurations with up to four anchor rows, anchorages with or without hole clearance and for anchorages influenced by a further close edge.

11.5 SUMMARY

In Chapter 11, the nonlinear spring model for shear loaded anchorages for concrete edge breakout failure is verified.

In Section 11.1, the postulate made for the nonlinear spring model regarding the stiffness of the individual anchor springs is verified with test results. It was confirmed by tests that the edge distance and the anchor spacing influence the individual anchor capacity within the group but not the stiffness of the individual anchors.

Section 11.2 gives the verification of the spring model for anchor groups placed in a single row parallel to the concrete edge, and to verify the tributary area and volume approach considering the anchor spacing in the direction perpendicular to the loading direction. For anchorages with a single anchor row, using the tributary area or tributary volume approach leads to identical results. The spring model was verified against 31 tests, and the mean value of $V_{u,test}/V_{u,spring\ model}$ is 1.05, and the coefficient of variation is 15.9%. With the spring model, the crack pattern of the anchorage and the superposed influence of crack pattern and eccentric loading can be accounted for reasonably well.

Section 11.3 presents the verification of the spring model for the anchorages with multiple anchor rows utilising the tributary volume approach for rectangular and non-rectangular anchorages. Evaluating the results obtained in this work (20 tests), the mean value of $V_{u,test}/V_{u,spring\ model}$ is 0.99, and the coefficient of variation is 8.6%.

Considering 79 further tests from the literature performed on anchor groups of rectangular configurations with up to four anchor rows, anchorages with or without hole clearance and for anchorages influenced by a further close edge, the mean value of $V_{u,test}/V_{u,spring\ model}$ is 1.05, and the coefficient of variation is 12.3%.

A total of 130 experimental results were compared with the corresponding spring models. Considering all investigated cases in uncracked and cracked concrete on post-installed and cast-in anchor groups having two to eight anchors within a group, the mean value of $V_{u,test}/V_{u,spring\ model}$ is 1.04, and the coefficient of variation is 12.9 %. The graph in *Figure 11.23* confirms that the spring model is able to predict the concrete edge resistance of various anchorage configurations

(rectangular and non-rectangular anchorages) in uncracked and cracked with or without hole clearance concrete very well.

Furthermore, the comparison of the experimental load-displacement curves with the result obtained using the nonlinear spring model proves that the spring model can capture the load-displacement behaviour of the anchorages while applying the corresponding spring characteristics for the anchors, considering the exact hole clearance pattern, modelling the base plate accordingly and performing the nonlinear static analysis in displacement control. Due to this, the model considers realistic force distribution and force redistribution among the anchors within the anchor group. Using the model does not require any pre-decision on the crack initiation. The nonlinear spring model for concrete edge failure provides the results in terms of the complete load-displacement behaviour of the anchorage that may be used in the performance-based approaches.

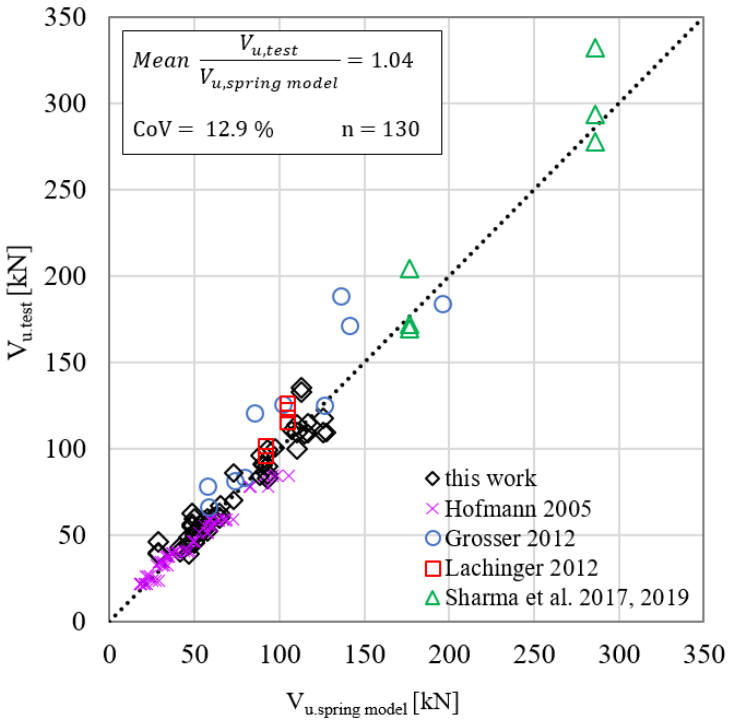

Figure 11.23. Summary of comparison of test results with the results obtained from the nonlinear spring model (failure loads)

12 VERIFICATION OF THE NONLINEAR SPRING MODEL FOR TENSION-SHEAR INTERACTION FOR CONCRETE BREAKOUT FAILURE

In this chapter, the nonlinear spring model for tension-shear interaction in case of concrete breakout failure is verified. In other words, only failure combinations "concrete cone failure - concrete edge breakout failure" of an anchorage placed close to the concrete edge is covered. Within the framework of this thesis, no tests were carried out under combined tension and shear, (interaction) and therefore, the spring model is verified through test data from the literature. Test results from Sharma et al. (2019) on anchor groups of 2×2 configuration with welded headed studs without the influence of hole clearance pattern under inclined loads and test results from Lachinger 2012 on anchor groups of 2×2 configurations using bonded anchors with most unfavourable hole clearance pattern loaded under inclined loads were used to verify the model.

In Section 12.1, the nonlinear spring model is verified for applications without hole clearance and Section 12.2 gives the verification of the model for anchorages with unfavourable hole clearance pattern.

12.1 VERIFICATION OF THE MODEL USING TEST RESULTS ON ANCHOR GROUPS WITH WELDED HEADED STUDS WITHOUT HOLE CLEARANCE

12.1.1 Interaction tests on anchor groups of 2×2 and 1×2 configurations

Experimental investigations were carried out in the work of Sharma et al. (2017 and 2019) on anchor groups of 2×2 and 1×2 configurations using headed studs welded on the base plate (WELDA® anchor plates from Peikko Group Corp.), which was cast flush with the concrete surface. The anchorages were subjected to pure tension (0°) on groups away from the edge and close to the concrete edge, pure shear (90°) perpendicular and towards the concrete edge and tension-shear interaction P at a loading angle of θ (= 30° and 60° with the vertical) close to the concrete edge with the shear component of the load towards the edge.

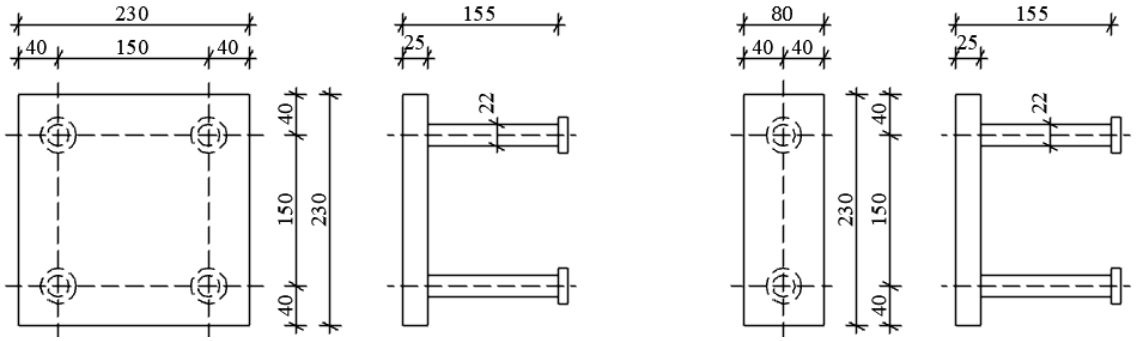

a) *b)*

Figure 12.1. Anchorages used in the experiments by Sharma et al. (2017, 2019) a) 2×2 configuration; b) 1×2 configuration

The reported material and test parameters, as well as the test results in terms of the mean measured ultimate loads are given *Table 12.1*, and the anchor configuration and dimensions of the base plate are depicted in *Figure 12.1*. Note that reference tests on single anchors have not been carried out either for the tension loading or for the shear loading case within the scope of the reported experimental work.

Table 12.1. Test program and test results of anchor groups of 2×2 and 1×2 configurations tested by Sharma et al. (2017, 2019)

Test ID[#]	Loading angle	Configuration	Mean concrete cube compressive strength	Edge distance of the corresponding anchor row		Anchor spacing		Measured mean ultimate load	Ultimate load normalised*
	θ		$f_{cc,m}$	$c_{1.1}$	$c_{1.2}$	s_1	s_2	P_u	P_u*
	[°]	[-]	[N/mm^2]	[mm]	[mm]	[mm]	[mm]	[kN]	[kN]
17-0-2×2	0	2×2	33.5	>3·h_{ef}	>3·h_{ef}	150	150	256.9	247.1
17-90-2×2-120	90	2×2	31.0	120	270	150	150	74.1	74.1
17-90-1×2-120	90	1×2	31.0	120	-	-	150	161.7	161.7
19-0-2×2-120	0	2×2	31.0	120	270	150	150	222.6	222.6
19-30-2×2-120	30	2×2	31.0	120	270	150	150	180.2	180.2
19-60-2×2-120	60	2×2	31.0	120	270	150	150	161.1	161.1
19-90-2×2-120	90	2×2	31.0	120	270	150	150	181.9	181.9

[#]Nomenclature of the Test ID used in this thesis: year of publication - angle of loading – configuration – edge distance of front row; *The mean ultimate load was normalised with respect to the concrete compressive strength using the following expression: $P_u^* = P_u \cdot (31\ \text{N/mm}^2 / f_{cc,m})^{0.5}$

12.1.2 Determination of the anchor spring characteristics

To verify the spring model for tension-shear interaction for anchorages without the influence of hole clearance pattern, the anchor group of 2×2 configuration was chosen as shown in *Figure 12.2a* because this configuration was tested under pure tension, pure shear, and under interaction at load angles of 30° and 60°. The load-displacement curves (with the permission of Peikko Group Corp.) are given along with the load-displacement curves from the nonlinear spring model for interaction in *Figure 12.6 – Figure 12.9*.

For application and verification of the spring model, in the first step, it is necessary to derive the spring properties for the corresponding single anchors. To each anchor, one tension and one uni-directional two-way shear springs are assigned considering the installation parameters and geometric conditions. Since no reference tests on single anchors were carried out either in tension or in shear, results on anchor groups were used to derive the spring characteristics by applying the postulates laid in Chapters 5 and 6 for tension and shear springs, respectively.

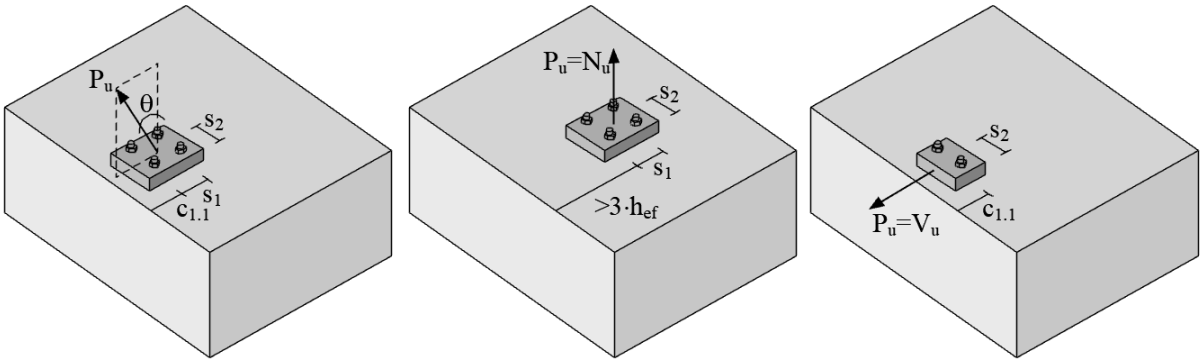

a) ***b)*** ***c)***

Figure 12.2. Anchorage configuration a) used to verify the interaction model, b) used to generate tension spring characteristics, c) used to generate shear spring characteristics

12.1.2.1 Tension spring characteristics

The test series 17-0-2×2 on the tension loaded anchor groups placed far from the concrete edge as shown in *Figure 12.2b* and the corresponding test results were used to generate the tension spring characteristics. The mean measured ultimate load of the series was reported as 256.9 kN, which was normalised with respect to the compressive strength of all other tests (31 MPa) to enable a direct comparison. The normalised mean ultimate tension load is 247.1 kN, which is 13% lower than the value calculated according to EN 1992-4 (295.2 kN) considering a concrete cube strength of 31 MPa (= 24.8 MPa cylinder strength), an embedment depth of 155 mm and anchor spacing of 150 mm. It was, therefore, decided to calculate the concrete cone resistance of a single anchor $N^0_{Rm,c}$ according to EN 1992-4 and not to derive the value from the experiments on groups to generate the spring properties of the single anchor, since the validity of ***Eq. 130*** has been proven by numerous experiments and authors in the past.

$$N^0_{Rm,c} = 16.9 \cdot 155^{1.5} \cdot \sqrt{0.8 \cdot 31} = 162.3\ kN \qquad \textbf{Eq. 130}$$

However, to obtain the stiffness values and then to derive the idealised load-displacement curve, the load-displacement curves reported from the experiments were used (see *Figure 12.3* - Note that the influence of prestressing was eliminated from the test results). The stiffness values of the 2×2 anchor group are k_1 - k_4 = 400, 312, 227 and 22.7 kN/mm, respectively. To take into account that higher stiffness values were obtained in the group tests by simultaneously loading four headed studs, the stiffness values obtained from series 17-0-2×2 were divided by four and used as stiffness values of a single anchor. Note that according to the postulates presented in Chapter 5, the stiffness values are considered independent of any influence of neighbouring anchors or vicinity of the concrete edge. The corresponding load-displacement-stiffness values (spring characteristics of a single anchor) are given in *Table 12.2* as “Reference single anchor”.

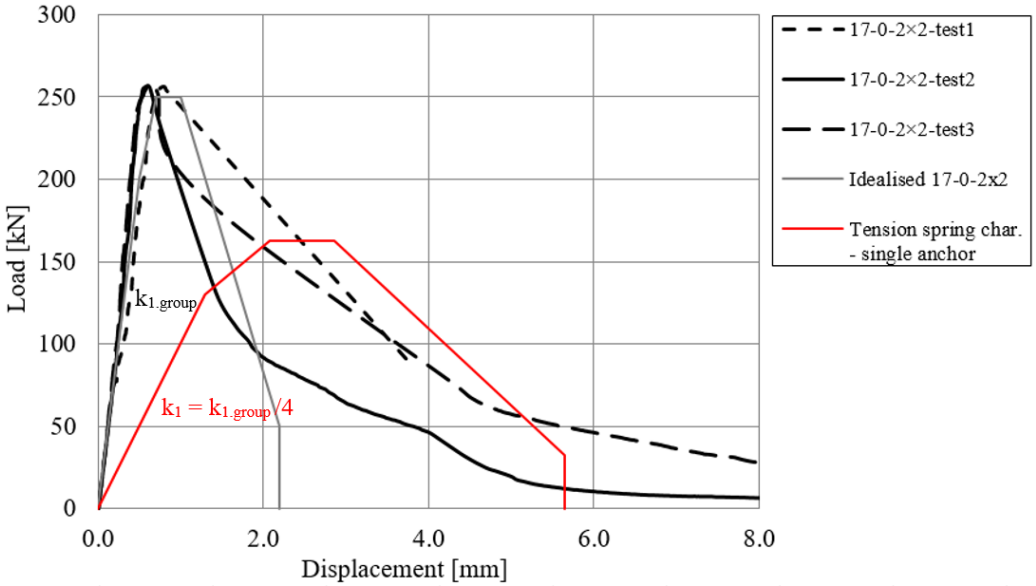

Figure 12.3. Load-displacement curves of series 17-0-2×2 on the tension loaded anchor groups (reproduced from Sharma et al., 2017) and idealised load-displacement curve (Tension spring char. – single anchor) at mean level

The geometric parameters such as embedment depth h_{ef} = 155 mm, edge distance c_1 = 120 mm and anchor spacing $s_1 = s_2$ = 150 mm of the anchor group of 2×2 configuration (*Figure 12.2a)* were considered while generating the spring curves. The resistance of the individual anchors was calculated according to ***Eq. 131*** and ***Eq. 132***. The tension spring characteristics are given in *Table 12.2* as "Individual anchor of front row" and "Individual anchor of back row".

$$N_{Rm,c}^{front} = A_{c,N}^{front} / A_{c,N}^{0} \cdot N_{Rm,c}^{0} = 0.28 \cdot 162.3 = 45\ kN \qquad \textbf{Eq. 131}$$

$$N_{Rm,c}^{back} = A_{c,N}^{back} / A_{c,N}^{0} \cdot N_{Rm,c}^{0} = 0.44 \cdot 162.3 = 71\ kN \qquad \textbf{Eq. 132}$$

Table 12.2. Tension spring properties of individual anchors of the anchor groups tested by Sharma et al. (2017, 2019)

	Load $N_{Rm,c}{}^{i}{}_{A\text{-}F}$ [kN]	Stiffness k_1-k_4 [kN/mm]	Displacement $\delta_{A\text{-}F}$ [mm]
Reference single anchor			
A	0.0	0.0	0.0
B	129.8	100.0	1.3
C	162.3	78.0	2.1
D	162.3	56.8	2.9
E	32.5	5.8	5.6
F	0.0	0.0	5.6
Individual anchor of front row			
A	0.0	0.0	0.0
B	36.0	100.0	0.4
C	45.0	78.0	0.6
D	45.0	56.8	0.8
E	9.0	5.8	1.6
F	0.0	0.0	1.6

Individual anchor of back row			
A	0.0	0.0	0.0
B	56.8	100.0	0.6
C	71.0	78.0	0.9
D	71.0	56.8	1.3
E	14.2	5.8	2.5
F	0.0	0.0	2.5

12.1.2.2 Shear spring characteristics

To determine the shear spring characteristics, the test results of series 17-90-1×2-120 were utilized (*Figure 12.2c)*. The tests were performed on anchor groups of 1×2 configuration placed close to the concrete edge with an edge distance of 120 mm loaded in pure shear perpendicular to and towards the free edge. The mean measured ultimate load of the series was reported as 74.1 kN, which is 23% higher than the value calculated according to EN 1992-4 (60.2 kN) considering a concrete cube strength of 31 MPa, edge distance of 120 mm, anchor diameter of 22 mm and embedment depth of 155 mm. Therefore, the concrete edge resistance of the single anchor $V^0_{Rm,c}$ was calculated according to EN 1992-4 (***Eq. 133***) and not derived from the results of the experiments on groups. The load-displacement curves from the tests were, however, used for obtaining the stiffness values for the spring characteristics.

$$V_{Rm,c}^{0,front} = 1.33 \cdot 2.4 \cdot {d_{nom}}^{\alpha} \cdot {l_f}^{\beta} \cdot \sqrt{f_{cm}} \cdot {c_1}^{1.5} \qquad \textbf{Eq. 133}$$
$$= 1.33 \cdot 2.4 \cdot 22^{0.11} \cdot 155^{0.07} \cdot \sqrt{24.8} \cdot 120^{1.5} = 42.5 \text{ kN}$$

The calculated concrete edge breakout resistance corresponds to 42.5 kN and 121 kN for the single anchors with 120 mm and 270 mm edge distance, respectively. These values were taken as basis for the further calculations.

The geometric conditions such as edge distance $c_{1.1}$ = 120 mm, $c_{1.2}$ = 270 mm and anchor spacing $s_1 = s_2$ = 150 mm were considered while defining the shear spring characteristics. The resistance of the individual anchors of the front row and back row were calculated according to ***Eq. 134*** and ***Eq. 135***, respectively.

$$V_{Rm,c}^{front} = V_{c,V}^{front} / V_{c,V}^{0,front} \cdot V_{Rm,c}^{0,front} = 0.71 \cdot 42.5 = 30.1\ kN \qquad \textbf{Eq. 134}$$

$$V_{Rm,c}^{back} = V_{c,V}^{back} / V_{c,V}^{0,back} \cdot V_{Rm,c}^{0,back} = 0.53 \cdot 121.0 = 64.1\ kN \qquad \textbf{Eq. 135}$$

To determine the stiffness values and define the idealised load-displacement curves (shear spring characteristics), the load-displacement curve from the series 17-90-1×2-120 was used (see *Figure 12.4*). The edge distance of the anchorage was 120 mm, which also corresponds to the edge distance of the front row of the 2×2 configuration of the interaction tests. The load-displacement curve of the 1×2 configuration in *Figure 12.4* was idealised and the stiffness values were obtained. However, these values correspond to the group stiffness k_{group}, which according to the postulates laid in Chapter 6 is assumed to be n-times the stiffness of the reference single anchor in case of n number of anchors in a row (in this case, n = 2). Therefore, the

stiffness values k_1-k_4 of the dashed curve in *Figure 12.4* were divided by two. The stiffness values k_1-k_4 determined for the front row were applied for the anchors of the back row as well. This is because the shear stiffness of the single anchors is assumed to be independent of the edge distance, provided all other parameters such as anchor type, size and embedment depth remain the same. The shear spring characteristics, thus determined, are given in *Table 12.3* as "Individual anchor of front row" and "Individual anchor of back row", respectively.

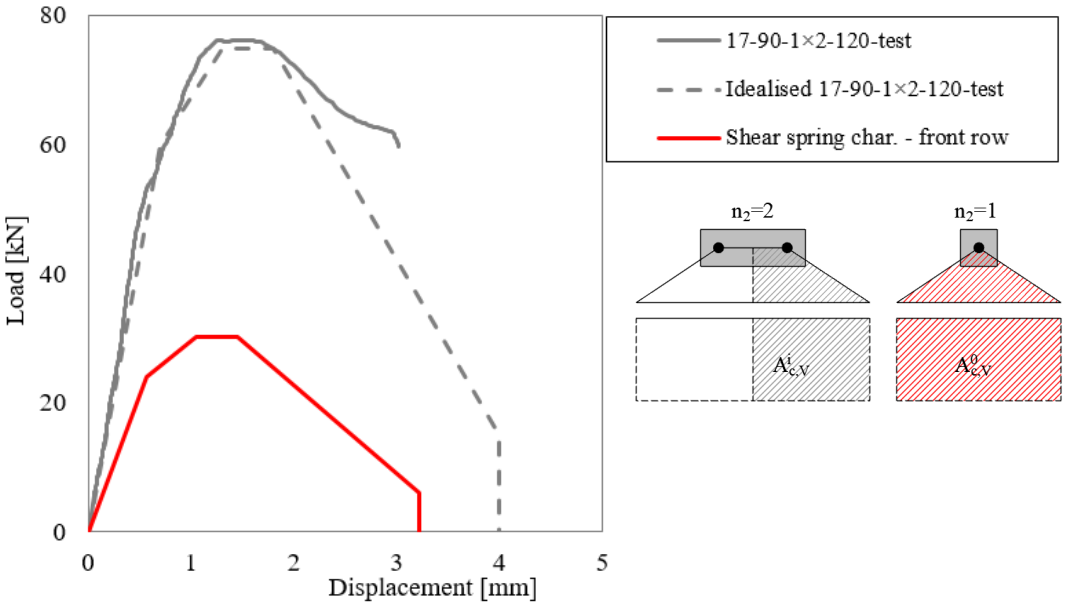

Figure 12.4. Load-displacement curve of a shear loaded anchor group from series 17-90-1×2-120 (reproduced from Sharma et al., 2017), idealised curve and shear spring characteristics of a single anchor loaded in shear towards the edge with c_1 = 120mm

Table 12.3. Shear spring characteristics of individual anchors of the anchor groups

	Load $V_{Rm,c}{}^{i}{}_{A\text{-}F}$ [kN]	Stiffness k_1-k_4 [kN/mm]	Displace-ment $\delta_{A\text{-}F}$ [mm]	Load $V_{Rm,c}{}^{i}{}_{A\text{-}F}$ [kN]	Stiffness k_1-k_4 [kN/mm]	Displace-ment $\delta_{A\text{-}F}$ [mm]
Reference single anchor of front row				***Individual anchor of front row***		
A	0.0	0.0	0.0	0.0	0.0	0.0
B	34.0	42.9	0.8	24.1	42.9	0.6
C	42.5	28.8	1.5	30.1	28.8	1.0
D	42.5	20.8	2.0	30.1	20.8	1.4
E	8.5	1.9	4.5	6.0	1.9	3.2
F	0.0	0.0	4.5	0.0	0.0	3.2
Reference single anchor of back row				***Individual anchor of back row***		
A	0.0	0.0	0.0	0.0	0.0	0.0
B	72.6	42.9	1.7	38.4	42.9	0.9
C	121.0	28.8	4.2	64.1	28.8	2.2
D	121.0	20.8	5.8	64.1	20.8	3.1
E	24.2	1.9	12.9	12.8	1.9	6.9
F	0.0	0.0	12.9	0.0	0.0	6.9

12.1.3 Evaluation and verification of the spring model for interaction for anchorages without hole clearance

The verification of the nonlinear spring model for combined tension-shear in case of concrete breakout failure for anchorages without hole clearance was performed by comparing the results on headed studs welded on the base plate and the results obtained from the nonlinear analyses.

The series 19-0-2×2-120, 19-30-2×2-120, 19-60-2×2-120 and 19-90-2×2-120 correspond to the same 2×2 group arrangement close to the concrete edge as it is shown in *Figure 12.2a*, only the loading angle θ is varied as 0°, 30°, 60° and 90°, respectively. Correspondingly, the same model as shown in *Figure 12.5* was used in all four analyses and only the loading angle θ was changed. The spring characteristics for tension and shear were taken from *Table 12.2* and *Table 12.3* and were used as input in the model, respectively.

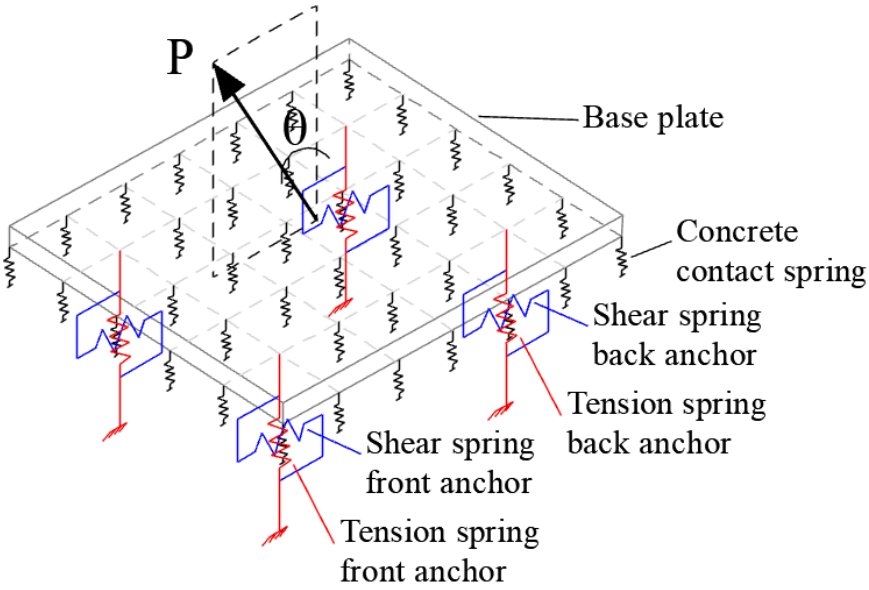

Figure 12.5. Spring model of the 2×2 group subjected to combined tension and shear loads

The evaluation of the results and the verification of the spring model for interaction for anchorages without hole clearance was done according to the following methodology:

1. The nonlinear static analyses were performed in displacement control utilising the nonlinear spring modelling approach for tension-shear interaction at loading angles θ = 0°, 30°, 60° and 90°.
2. The results of the spring model were obtained as load-displacement curves of the 2×2 anchor group loaded at an angle of θ, and are compared with the corresponding experimental curves in *Figure 12.6 - Figure 12.9*.
3. The ultimate loads obtained from the spring model $P_{u,spring}$ for the case of loading angle of θ are listed in *Table 12.4*.
4. The "theoretical" ultimate load of the group $P_{u,th}$ at a given loading angle θ was calculated according to the interaction equation ***Eq. 136*** applying the pure tension $N_{u,spring}$ (0°) and pure shear $V_{u,spring}$ (90°) results in the equation, which were obtained

from the spring model. The exponent α was taken as 1.5 for concrete breakout modes, in accordance with EN 1992-4.

$$P_{u,th} = \left[\left(\frac{Cos\theta}{N_{u,spring}}\right)^{\alpha} + \left(\frac{Sin\theta}{V_{u,spring}}\right)^{\alpha}\right]^{\frac{1}{\alpha}} \qquad \textit{Eq. 136}$$

5. The resistance of the anchor group loaded at an angle of θ was calculated analytically according to the models given in EN 1992-4 and fib Bulletin 58 ($P_{u,EN1992-4}$ and $P_{u,fib,B58}$), and are listed in *Table 12.4.*
6. The failure loads reported from the experiments, the failure loads of the spring model, the theoretical failure load according to ***Eq. 136*** and the calculated mean failure loads according to EN 1992-4 and fib Bulletin 58 were plotted in function of loading angle in *Figure 12.11* for comparison.
7. The interaction curve was generated using experimental failure load values from Sharma et al. (2019), using the spring model directly and acc. to ***Eq. 136*** and the calculated mean failure loads according to EN 1992-4 and fib Bulletin 58.

Table 12.4. Test results of anchor groups of 2×2 configurations reported in Sharma et al. (2019), obtained from the spring model and calculated acc. to EN 1992-4 and fib Bulletin 58

Test ID	Loading angle	Measured mean ultimate load	Ultimate load obtained from the spring model	Calculated resistance – Theoretical using spring model	Calculated resistance acc. to EN 1992-4	Calculated resistance acc. to fib Bulletin 58
	θ	$P_{u,exp,m}$	$P_{u,spring}$	$P_{u,th}$	$P_{u,EN1992-4}$	$P_{u,fib,B58}$
	[°]	[kN]	[kN]	[kN]	[kN]	[kN]
19-0-2×2-120	0	222.6	183.2	183.2	198.3	198.3
19-30-2×2-120	30	180.2	183.2	164.1	97.1	159.5
19-60-2×2-120	60	161.1	167.9	161.7	66.3	140.5
19-90-2×2-120	90	181.9	176.5	176.5	60.2	142.5

Results on the tension loaded anchorage θ = 0°

Figure 12.6 shows the comparison of the load-displacement curves of the anchorage from the spring model and from the experiments under pure tension loading (Series 19-0-2×2-120). The ultimate load obtained from the spring model, $P_{u,spring}$ = 183.2 kN, is 18% lower compared to the mean value of the tests $P_{u,exp,m}$ = 222.6 kN. However, the failure load from the spring model is just 9% lower than the analytical value $P_{u,EN1992-4}$ = 198.3 kN according to EN 1992-4 and fib Bulletin 58, and so it is within the typical scatter (15%) considered in the CCD method for concrete-related failure modes. Furthermore, the initial stiffness of the curve obtained from the spring model is in a good agreement with the experimentally obtained stiffness.

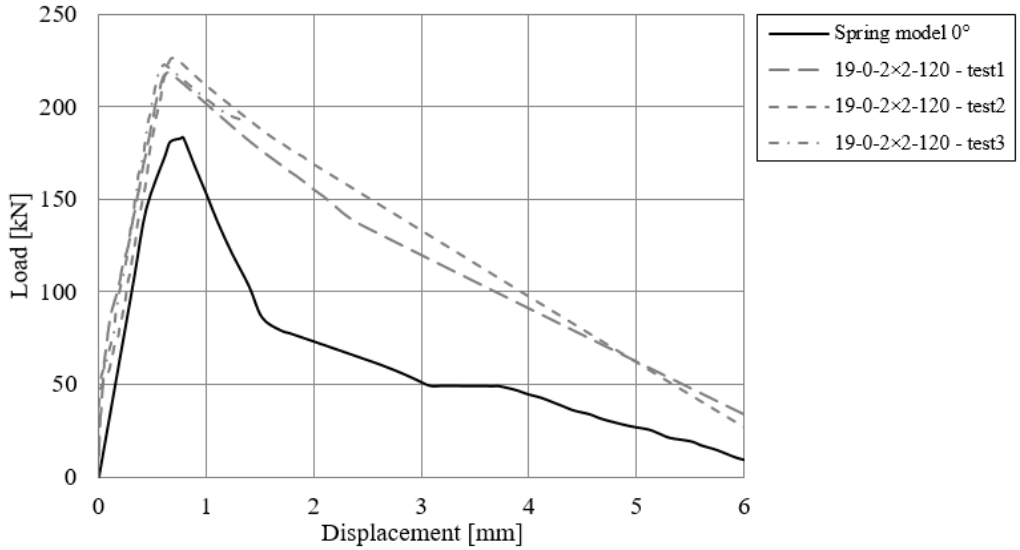

Figure 12.6. Load-displacement curves for the series 19-0-2×2-120 from the spring model for interaction and comparison with test results (exp. curves reproduced with permission from Peikko)

Results on the anchorage loaded under combined tension and shear θ = 30°

The load-displacement curve obtained from the spring model and the reported experimental results for combined tension-shear loading at 30° angle (series 19-30-2×2-120) are plotted in *Figure 12.7.* Due to a relatively low angle of loading with the vertical, the behaviour of the group is primarily dominated by the tension behaviour. The calculated load-displacement curves correspond very closely to the experimentally obtained load-displacement curves and in terms of failure loads (~ 2% difference). This indicates that the nonlinear spring model for interaction is capable of describing the complete non-linear load-displacement behaviour of the anchorage loaded at an angle of θ if the corresponding springs for tension, shear and contact are applied and the nonlinear static analysis is carried out.

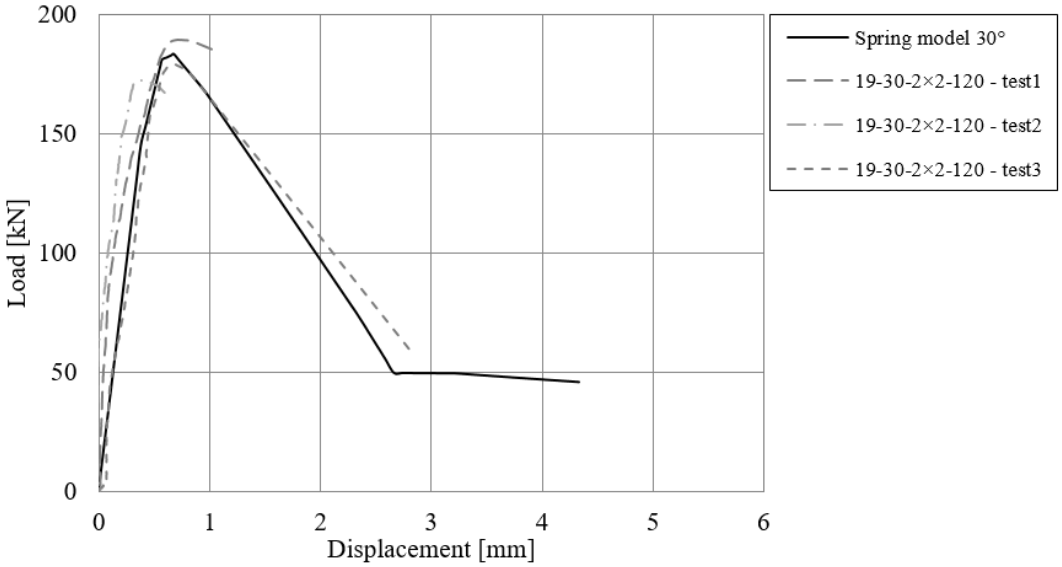

Figure 12.7. Load-displacement curves for the series 19-30-2×2-120 obtained from the spring model for interaction and comparison with test result (exp. curves reproduced with permission from Peikko)

Results on the anchorage loaded under combined tension and shear θ = 60°

In *Figure 12.8,* the load-displacement curve obtained from the spring model and the reported experimental results for combined tension-shear loading at 60° angle are plotted (series 19-60-2×2-120). At 60° loading angle, the shear component is dominant, causing the slippage of the base plate in the tests, which is reflected by the slip of the displacements, characterized by an almost horizontal branch in the initial part of the curve progression. However, as the displacement monitoring in the spring model was done directly at the loading angle of 60°, therefore, there is no slip in the curve progression. To allow a better comparison of the results, the curve from the spring model was shifted by 2.9 mm on the x-axis. Apart from the slip of the displacements, the results are in a very good agreement with respect to the failure loads (4%) and curve progression. This again shows that the nonlinear spring model for interaction is capable of describing the complete non-linear load-displacement behaviour of the anchorage.

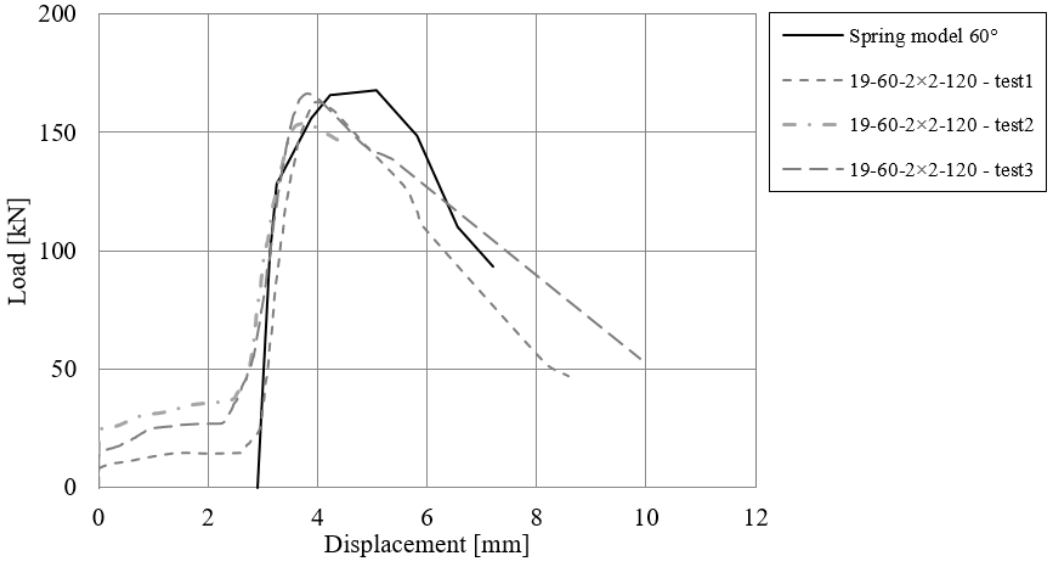

Figure 12.8. Load-displacement curves for the series 19-60-2×2-120 obtained from the spring model for interaction and comparison with tests (exp. curves reproduced with permission from Peikko)

Results on the anchorages loaded under pure shear θ = 90°

In *Figure 12.9,* the load-displacement curve obtained from the spring model and the reported experimental curves under pure shear loading are presented (series 19-90-2×2-120). The displacement slip in the experimental curve can be attributed to the slippage of the base plate, which happens after the applied shear load exceeds the friction resistance of the base plate (and prestressing forces) in the shear tests. However, there is no slip of displacements in the analysis using the spring model, since the frictional effects are not explicitly modelled. Therefore, to allow the comparison of the results, the spring model curve was shifted by 0.6 mm. The initial stiffness and the curve progression show a good match and the failure load obtained by the spring model is just 3% lower compared to the mean value of the experimental results.

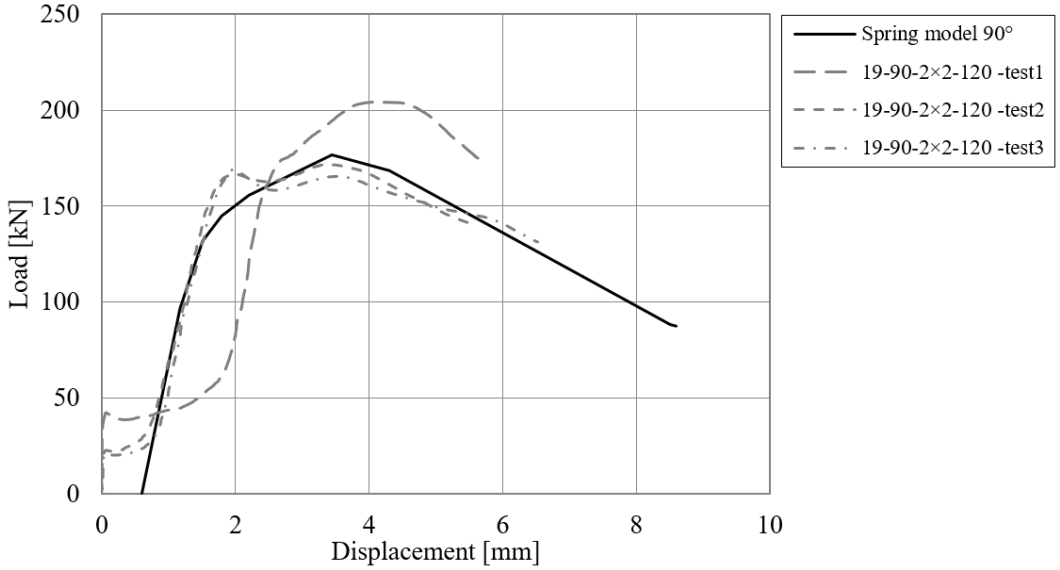

Figure 12.9. Load-displacement curves for the series 19-90-2×2-120 obtained from the spring model for interaction and comparison with tests (exp. curves reproduced with permission from Peikko)

In addition, a further case with 4×2 anchor configuration was considered from the literature (Sharma et al., 2017). The load-displacement curve for the series 17-90-4×2-120 obtained from the spring model for interaction and comparison with test results are plotted in *Figure 12.10*. It can be seen that the spring model is capable to capture the behaviour of even large anchor groups.

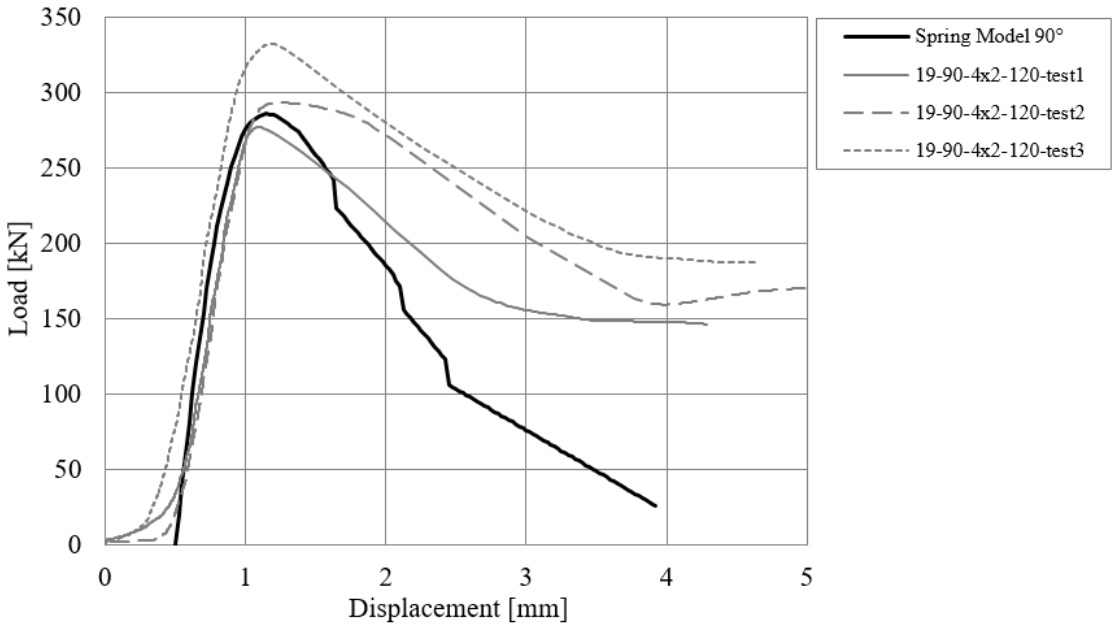

Figure 12.10. Load-displacement curves for the series 17-90-4×2-120 obtained from the spring model for interaction and comparison with tests (exp. curves reproduced with permission from Peikko)

Comparison of the failure loads using different approaches and experimental results

The failure loads reported from the experiments, the failure loads obtained from the spring model, the failure loads according to ***Eq. 136*** and the calculated mean failure loads according to EN 1992-4 and fib Bulletin 58 are plotted in the function of the loading angle in *Figure 12.11* for comparison. In addition, the corresponding tension and shear components are plotted in form of interaction curve in *Figure 12.12*.

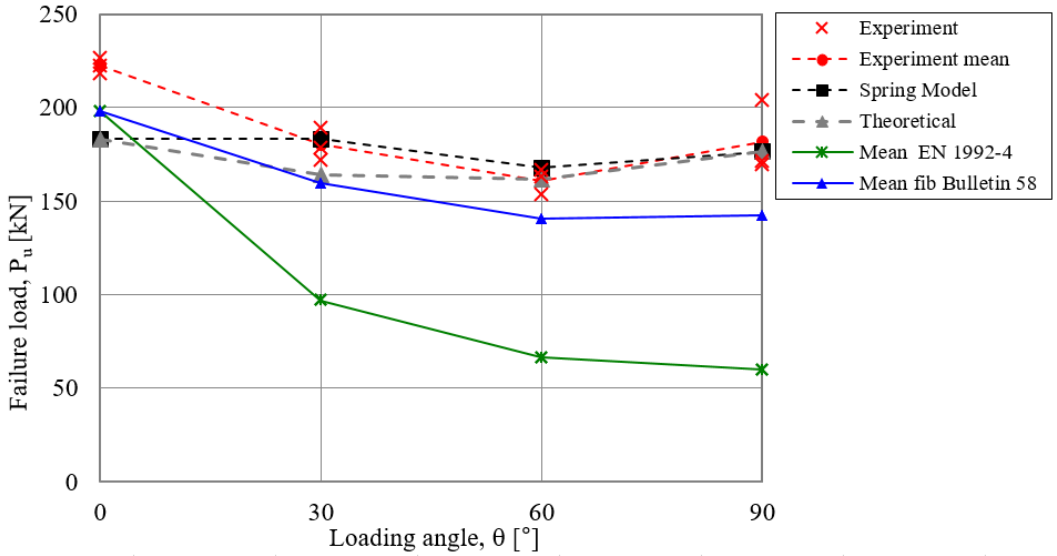

Figure 12.11. Comparison of the failure loads obtained using the spring model directly, failure loads obtained applying Eq. 136 (Theoretical) with the experimental failure loads and with the calculated mean failure loads

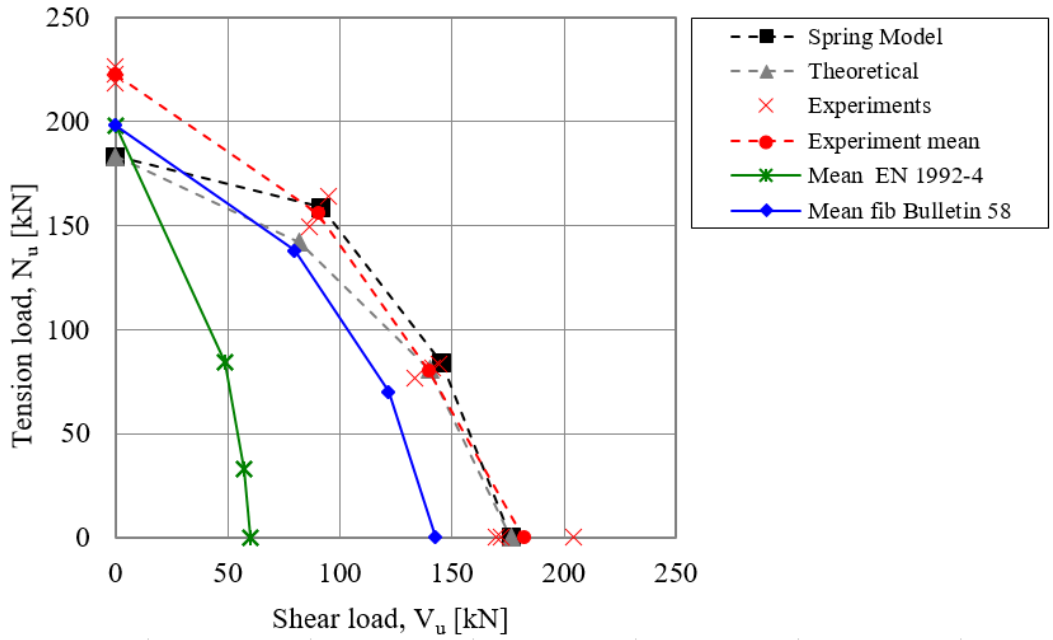

Figure 12.12. Comparison of the interaction curves generated using the spring model, applying Eq. 136 (Theoretical), using experimental failure load values and using the procedure of EN 1992-4 and fib Bulletin 58

When the results from the pure tension and pure shear analyses of the spring model are used to generate the theoretical curve according to ***Eq. 136*** (grey dashed line), the match is still rather reasonably close to the experimental curve. However, note that the evaluation using ***Eq. 136*** is only recommended if it can be ensured that a sufficiently stiff base plate is used. In the calculation according to ***Eq. 136***, the possible base plate deformations and prying actions are not considered in the shear model. Consequently, they are neglected from the interaction equation, which might lead to unconservative results in certain cases and thus, the safety margin of the concept might differ from case to case.

Under shear loading, the calculated mean failure load according to EN 1992-4 is significantly lower compared to the mean experimental failure load and result of the spring model (see *Figure 12.11)*. This is due to the fact that the EN 1992-4 assumes the failure crack initiating from the front anchor row, while in reality, the failure crack appears from the back anchor row. This conservatism can be observed also in the interaction model. The conservatism of the model increases with increasing shear component (θ close to 90°). The calculated mean failure loads for interaction and shear obtained using the model given in fib Bulletin 58 are lower than the experimental results and the results of the spring model. Nevertheless, due to considering the failure crack originating from the back anchor row in the shear model, the conservatism of the model seems reasonable for the case analysed here.

In summary, the comparison given in *Figure 12.11* and *Figure 12.12* verifies that compared to the existing models, the nonlinear spring modelling approach can estimate the failure loads for anchorages without hole clearance rather accurately and realistically. Moreover, the comparison of the load-displacement curves reported from the experiments and obtained from the spring model for interaction confirm the suitability of the spring model not just to calculate the ultimate loads but also to estimate the complete load-displacement behaviour (*Figure 12.6 – Figure 12.9*). Note that the use of the nonlinear spring model precludes the requirement of a stiff base plate for the anchorage and is equally applicable for stiff or flexible base plates. Therefore, it is strongly recommended to use the nonlinear spring model for interaction for the evaluation of anchorages without hole clearance loaded under combined tension and shear failing due to concrete breakout.

12.2 VERIFICATION OF THE MODEL FOR ANCHOR GROUPS OF 2×2 CONFIGURATION WITH THE INFLUENCE OF UNFAVOURABLE HOLE CLEARANCE PATTERN

12.2.1 Interaction tests on anchor groups of 2×2 configurations (Lachinger, 2012)

Lachinger (2012) investigated the behaviour of 2×2 anchor groups placed close to the concrete edge and installed with most unfavourable hole clearance pattern under inclined loading using bonded anchors (*Figure 12.13a*). The anchorages were subjected to pure tension ($\theta = 0°$) on groups close to the concrete edge, pure shear ($\theta = 90°$) close to and towards the concrete edge and tension-shear interaction P at a loading angle of θ (= 30°, 45°, 60° and 75°with the vertical) close to the concrete edge with the shear component of the load towards the edge.

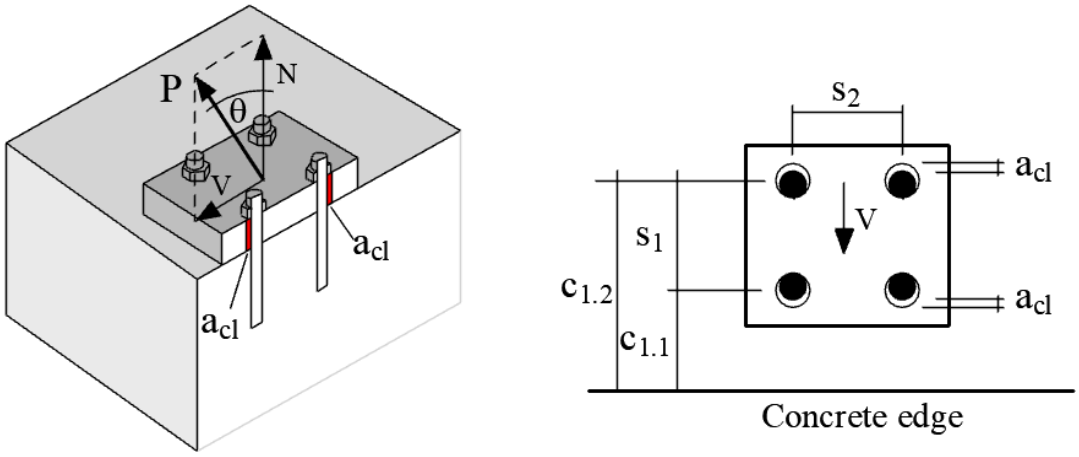

a) ***b)***

Figure 12.13. a) Section cut of the anchorage configuration used to verify the interaction model with unfavourable hole clearance pattern; b) most unfavourable hole clearance pattern of a shear loaded anchorage

The edge distance of the front row and the anchor spacing in both orthogonal directions were kept constant as $c_{1.1} = s_1 = s_2 = 120$ *mm* and the anchor diameter was $d_{nom} = 12$ *mm*. The hole clearance was maintained in all tests as $a_{cl} = 2$ *mm* (in the front for front anchors and at the back for back anchor row) ensured by careful installation and the hole clearance pattern. This anchor installation corresponds to the most unfavourable hole clearance pattern as depicted in *Figure 12.13b.* According to the most unfavourable hole clearance pattern, in case of pure shear loading, at the onset of loading only the front anchor row takes up the shear force, whereas the second row starts to take up forces only after a horizontal displacement of 2 mm. Another variable parameter, besides the loading angle, was the embedment depth ($h_{ef} = 70$, *100, 120 and 180 mm*) and in one series of tests, a bonded anchor system with lower bond properties was used.

Within the framework of this thesis, only tests results with the higher bond strength anchor system, with embedment depths of 70, 120 and 180 mm are investigated from Lachinger (2012). Furthermore, the series with 120 mm embedment depth and pure tension loading (Test, h_{ef} = 120 mm – 0°) was used to generate the tension spring characteristics of the anchors.

The reported test parameters, as well as the test results in terms of the mean measured ultimate loads normalised to a concrete cube strength of a 25 N/mm^2 are given in *Table 12.5*.

Note that reference tests on single anchors were not carried out either for the tension loading or for the shear loading case within the scope of the reported experimental work. Furthermore, no tests were conducted without the influence of the hole clearance pattern.

Table 12.5. Test program and test results of anchor groups of 2×2 configurations with hole clearance tested by Lachinger (2012)

Test ID[#]	Embedment depth	Loading angle	Edge distance of the corresponding anchor row		Anchor spacing	Mean meas. ultimate load normalised*
	h_{ef} [mm]	θ [°]	$c_{1.1}$ [mm]	$c_{1.2}$ [mm]	$s_1=s_2$ [mm]	P_u* [kN]
Test, h_{ef} = 70 mm – 0°	70	0	120	240	120	95.4
Test, h_{ef} = 70 mm – 30°	70	30	120	240	120	76.4
Test, h_{ef} = 70 mm – 45°	70	45	120	240	120	64.8
Test, h_{ef} = 70 mm – 60°	70	60	120	240	120	65.0
Test, h_{ef} = 70 mm – 75°	70	75	120	240	120	74.2
Test, h_{ef} = 100 mm – 0°	100	0	120	240	120	118.1
Test, h_{ef} = 100 mm – 30°	100	30	120	240	120	79.5
Test, h_{ef} = 100 mm – 45°	100	45	120	240	120	72.5
Test, h_{ef} = 100 mm – 60°	100	60	120	240	120	79.7
Test, h_{ef} = 100 mm – 90°	100	90	120	240	120	98.9
Test, h_{ef} = 120 mm – 0°	120	0	120	240	120	154.1
Test, h_{ef} = 180 mm – 0°	180	0	120	240	120	173.4
Test, h_{ef} = 180 mm – 30°	180	30	120	240	120	103.1
Test, h_{ef} = 180 mm – 45°	180	45	120	240	120	111.9
Test, h_{ef} = 180 mm – 60°	180	60	120	240	120	102.0
Test, h_{ef} = 180 mm – 75°	180	75	120	240	120	118.2
Test, h_{ef} = 180 mm – 90°	180	90	120	240	120	121.4

[#]Nomenclature of the Test ID used in this thesis: Test, embedment depth – angle of loading; *The mean ultimate load was normalised with respect to the concrete compressive strength in the work of Lachinger using the following expression: $P_u^* = P_u \cdot (25\ \text{N/mm}^2 / f_{cm,150})^{0.5}$

12.2.2 Determination of the anchor spring characteristics

To verify the spring model for tension-shear interaction for anchor group of 2×2 configurations with the influence of most unfavourable hole clearance pattern, the test database of Lachinger (2012) was used. The same way, as it is described in Section 12.1.2 for anchorages without hole clearance, one tension and one shear spring is assigned to each anchor considering the installation parameters and geometric conditions including the hole clearance in the shear spring (refer to *Figure 6.6*). In addition, for this case, further aspects should be considered due to the hole clearance and its effect on the anchorage behaviour.

The test results of Lachinger highlighted that the behaviour of 2×2 anchor groups placed close to the concrete edge with unfavourable hole clearance pattern under inclined loads is significantly affected by the formation of the cracks at the front row. When the crack at the front row develops due to inclined loading, the resulting shear forces are taken up by the front row only and the tension forces are taken up by all anchors. The damage at the front row depends on the ratio of anchor embedment depth to edge distance of the front anchor row. In the case of anchor groups with relatively short embedment depth, the failure crack developing from the front anchor row showed a much stronger negative influence on the tension capacity of the anchorage compared to the corresponding anchorage with larger embedment depth in his tests (see *Figure 2.16)*. After overcoming the hole clearance of $a_{cl} = 2\ mm$ in the shear direction, the back row takes up shear forces due to force redistribution. How much tension force the anchors can take up depends on the damage at the front row. In any case, the tension loading becomes eccentric due to the loss of stiffness and loss of resistance due to the cracking at the front anchor row. Therefore, the consideration of the hole clearance pattern is essential for the assessment of anchorages under inclined loads.

To account for the discussed considerations, in the nonlinear spring model for anchor groups with most unfavourable hole clearance pattern, in every case the hole clearance of the back row is considered in the shear spring characteristics (12.2.2.2). Furthermore, to account for the crack development at the front row that influences the tension resistance of the anchorage, cracked concrete condition is assumed at the front row for tension. This is done by assuming a 30% reduction in strength and a 50% reduction in stiffness in the tension spring characteristics (see details in Section 12.2.2.1). This way, the developing eccentricity of loading is taken into account automatically due to the different stiffness and resistance of the tensioned anchors of the group. Note that an even higher reduction in strength and stiffness might be considered.

No reference tests on single anchors were reported to be carried out either in tension or in shear in the work of Lachinger. Therefore, results on anchor groups were used to derive the spring characteristics by applying the postulates laid in Chapters 5 and 6 for tension and shear springs, respectively.

12.2.2.1 Tension spring characteristics

The results of the series with 120 mm embedment depth and pure tension loading (Test, h_{ef} = 120 mm – 0°) were used to derive the stiffness values for the anchor tension spring characteristics. The load-displacement data pairs from *Figure 12.3* were used to determine the stiffness values of the 2×2 anchor group, which are k_1-k_4 = 521, 428, 300 and 50 kN/mm, respectively. To take into account that higher stiffness values were obtained in the group tests by simultaneously loading four anchors, the stiffness values obtained from the group test were divided by four and were used as stiffness values of a single anchor (k_1-k_4 = 130, 107, 75, 12.5 kN/mm). These values are used when generating the spring curves for the series with 70, 100 and 180 mm embedment depth in uncracked concrete with the assumption that the embedment depth does not influence the anchor stiffness considerably in this embedment depth range. The stiffness values used for cracked concrete correspond to 50% of those in uncracked concrete, namely $k_{1,cr}$ - $k_{4,cr}$ = 65, 53.5, 37.5 and 6.25 kN/mm.

The corresponding mean concrete cone resistance of a single anchor $N^{0}_{Rm,c}$ was calculated for the investigated embedment depths (70, 100 and 180 mm) for uncracked and cracked concrete condition according to EN 1992-4. These values were taken then as basis for the further calculations to generate the spring characteristics for the individual anchors of the group. The determined tension spring characteristics are tabulated in *Table 12.6 - Table 12.8.*

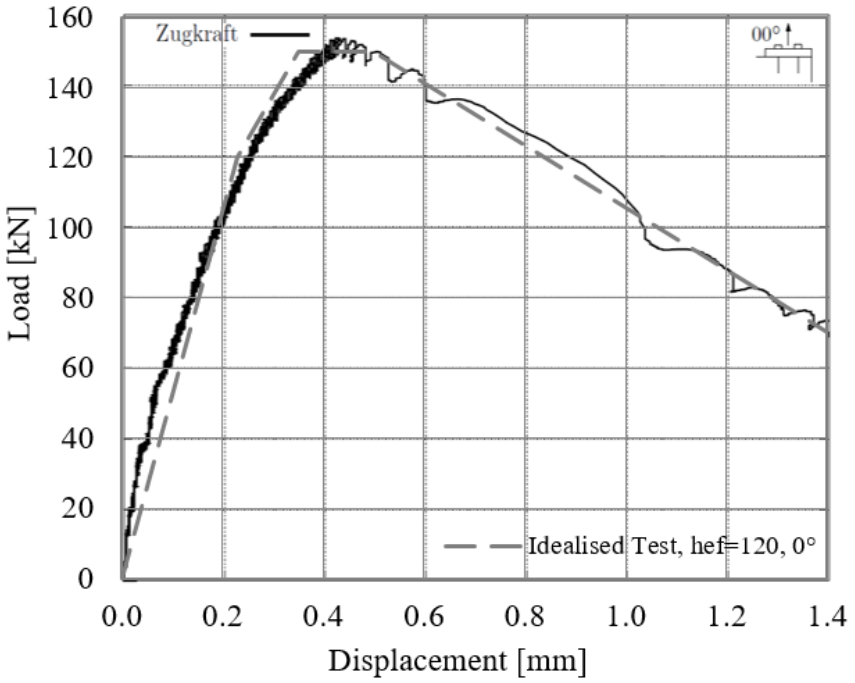

Figure 12.14. Load-displacement curve of one representative test on anchor groups from series Test, hef=120 mm, 0° (reproduced from Lachinger 2012) and idealised load-displacement curve (Tension spring characteristics – single anchor) at mean level

Table 12.6. Tension spring characteristics for anchors with h_{ef} = 70 mm

	Load $N_{Rm,c}{}^{i}{}_{A\text{-}F}$ [kN]	Stiffness k_1-k_4 [kN/mm]	Displacement $\delta_{A\text{-}F}$ [mm]	Load $N_{Rm,c,cr}{}^{i}{}_{A\text{-}F}$ [kN]	Stiffness $k_{1,cr}$-$k_{4,cr}$ [kN/mm]	Displacement $\delta_{A\text{-}F}$ [mm]
Individual anchor of front row (uncracked)				***Individual anchor of front row (cracked)***		
A	0.0	0.0	0.00	0.0	0.0	0.00
B	18.9	130.4	0.15	13.2	65.2	0.20
C	23.6	107.1	0.22	16.6	53.6	0.31
D	23.6	75.0	0.32	16.6	37.5	0.44
E	4.7	12.5	0.38	3.3	6.3	0.53
F	0.0	0.0	0.38	0.0	0.0	0.53
Individual anchor of back row (uncracked)						
A	0.0	0.0	0.00			
B	18.9	130.4	0.15			
C	23.6	107.1	0.22			
D	23.6	75.0	0.32			
E	4.7	12.5	0.38			
F	0.0	0.0	0.38			

Table 12.7. Tension spring characteristics for anchors with h_{ef} = 100 mm

	Load $N_{Rm,c}{}^{i}{}_{A\text{-}F}$ [kN]	Stiffness k_1-k_4 [kN/mm]	Displacement $\delta_{A\text{-}F}$ [mm]	Load $N_{Rm,c,cr}{}^{i}{}_{A\text{-}F}$ [kN]	Stiffness $k_{1,cr}$-$k_{4,cr}$ [kN/mm]	Displacement $\delta_{A\text{-}F}$ [mm]
Individual anchor of front row (uncracked)				***Individual anchor of front row (cracked)***		
A	0.0	0.0	0.00	0.0	0.0	0.00
B	22.0	130.4	0.17	15.4	65.2	0.24
C	27.5	107.1	0.26	19.2	53.6	0.36
D	27.5	75.0	0.37	19.2	37.5	0.51
E	5.5	12.5	0.44	3.8	6.3	0.62
F	0.0	0.0	0.44	0.0	0.0	0.62
Individual anchor of back row (uncracked)						
A	0.0	0.0	0.00			
B	25.6	130.4	0.20			
C	32.0	107.1	0.30			
D	32.0	75.0	0.43			
E	6.4	12.5	0.51			
F	0.0	0.0	0.51			

Table 12.8. Tension spring characteristics for anchors with h_{ef} = 180 mm

	Load $N_{Rm,c}{}^{i}{}_{A\text{-}F}$ [kN]	Stiffness k_1-k_4 [kN/mm]	Displacement $\delta_{A\text{-}F}$ [mm]	Load $N_{Rm,c,cr}{}^{i}{}_{A\text{-}F}$ [kN]	Stiffness $k_{1,cr}$-$k_{4,cr}$ [kN/mm]	Displacement $\delta_{A\text{-}F}$ [mm]
Individual anchor of front row (uncracked)				***Individual anchor of front row (cracked)***		
A	0.0	0.0	0.00	0.00	0.0	0.00
B	25.7	130.4	0.20	18.02	65.2	0.28
C	32.2	107.1	0.30	22.53	53.6	0.42
D	32.2	75.0	0.43	22.53	37.5	0.60
E	6.4	12.5	0.51	4.51	6.3	0.72
F	0.0	0.0	0.51	0.00	0.0	0.72
Individual anchor of back row (uncracked)						
A	0.0	0.0	0.00			
B	47.2	130.4	0.36			
C	59.0	107.1	0.55			
D	59.0	75.0	0.79			
E	11.8	12.5	0.94			
F	0.0	0.0	0.94			

12.2.2.2 Shear spring characteristics

No reference tests on single anchors or anchor groups without hole clearance were reported in the work of Lachinger on shear loaded anchorages. Therefore, to generate the shear spring characteristics, the concrete edge resistances of the single anchor for the front anchor row ($V_{Rm,c}^{0,front}$) and back anchor row ($V_{Rm,c}^{0,back}$) were calculated according to EN 1992-4 for the embedment depths 70, 100 and 180 mm, respectively. The stiffness values were taken as k_1-k_4 = 20.0, 13.0,

9.0, 1.0 kN/mm based on the evaluation of similar tests from the literature. These load and stiffness values were taken as the basis for further calculations for the individual anchors of the group. The determined shear spring characteristics are tabulated in *Table 12.9* - *Table 12.11* as "Individual anchor of front row" and "Individual anchor of back row". To account for the hole clearance a_{cl} = *2 mm* at the back anchor row in shear direction, an extra segment (A-A´) with zero force and 2 mm displacement is considered in the spring characteristics for the back anchor row (refer to *Figure 6.6*).

Table 12.9. Shear spring characteristics for anchors with h_{ef} = 70 mm

	Load $V_{Rm,c}{}^{i}{}_{A\text{-}F}$ [kN]	Stiffness k_1-k_4 [kN/mm]	Displacement $\delta_{A\text{-}F}$ [mm]
Individual anchor of front row			
A	0.0	0.0	0.00
B	15.8	20.0	0.79
C	19.8	13.0	1.52
D	19.8	9.0	2.20
E	4.0	1.0	3.96
F	0.0	0.0	3.96
Individual anchor of back row			
A	0.0	0.0	0.00
A´	0.0	0.0	2.00
B	27.6	20.0	3.38
C	34.5	13.0	4.65
D	34.5	9.0	5.83
E	6.9	1.0	8.89
F	0.0	0.0	8.89

Table 12.10. Shear spring characteristics for anchors with h_{ef} = 100 mm

	Load $V_{Rm,c}{}^{i}{}_{A\text{-}F}$ [kN]	Stiffness k_1-k_4 [kN/mm]	Displacement $\delta_{A\text{-}F}$ [mm]
Individual anchor of front row			
A	0.0	0.0	0.00
B	16.8	20.0	0.84
C	21.0	13.0	1.62
D	21.0	9.0	2.33
E	4.2	1.0	4.20
F	0.0	0.0	4.20
Individual anchor of back row			
A	0.0	0.0	0.00
A´	0.0	0.0	2.00
B	28.9	20.0	3.44
C	36.1	13.0	4.78
D	36.1	9.0	6.01
E	7.2	1.0	9.22
F	0.0	0.0	9.22

Table 12.11. Shear spring characteristics for anchors with h_{ef} = 180 mm

	Load $V_{Rm,c}{}^{i}{}_{A\text{-}F}$ [kN]	Stiffness k_1-k_4 [kN/mm]	Displacement $\delta_{A\text{-}F}$ [mm]
Individual anchor of front row			
A	0.0	0.0	0.00
B	17.3	20.0	0.87
C	21.7	13.0	1.67
D	21.7	9.0	2.41
E	4.3	1.0	4.33
F	0.0	0.0	4.3
Individual anchor of back row			
A	0.0	0.0	0.00
A´	0.0	0.0	2.00
B	29.6	20.0	3.48
C	37.0	13.0	4.85
D	37.0	9.0	6.12
E	7.4	1.0	9.41
F	0.0	0.0	9.41

12.2.3 Evaluation and verification of the spring model for interaction for anchorages of 2×2 configuration with hole clearance

The verification of the nonlinear spring model for combined tension-shear in case of concrete breakout failure for 2×2 anchorages with the most unfavourable hole clearance pattern was performed by comparing the test results on post-installed bonded anchors and the results obtained from the nonlinear analyses. The modelling concept as shown in *Figure 12.5* was used in the analyses with anchor spacing equal to 120 mm, with a rigid base plate and only the loading angle θ was varied. The embedment depth and the edge distance are considered with the spring characteristics. The spring characteristics for tension and shear were taken from *Table 12.6* - *Table 12.11* and were used as input in the model. The obtained failure loads from the spring model correspond directly to the failure load at the given loading angle θ. Since the load-displacement curves for the interaction tests are not given in the thesis of Lachinger, only the reported failure loads of the tests are compared with the results of the nonlinear spring model.

The evaluation of the results of the spring model for interaction for anchorages with most unfavourable hole clearance pattern was performed according to the following methodology:

1. The nonlinear static analyses were performed in displacement control utilising the nonlinear spring modelling approach for tension-shear interaction at loading angles θ = *0°, 30°, 45°, 60°, 75°* and *90°*. For the case with pure tension (θ = *0°*), all anchors were assumed to be in uncracked concrete, therefore the tension spring characteristics for uncracked concrete were used for the front and back anchors. For all other cases, cracked concrete condition was assumed for the front anchors in tension. Therefore, the corresponding tension spring characteristics in cracked concrete were assigned to the

front anchors and the corresponding tension spring characteristics in uncracked concrete were assigned to the back anchors.

2. The results of the spring model were obtained as load-displacement curves of the anchor group loaded at an angle of θ. The ultimate loads $P_{u,spring}$ for the corresponding loading angles θ are listed in *Table 12.12*.
3. The "theoretical" ultimate load of the group $P_{u,th}$ at a given loading angle θ was calculated according to the interaction equation ***Eq. 136*** using the peak load values of pure tension $N_{u,spring}$ (0°) and pure shear $V_{u,spring}$ (90°) cases from the spring model in the equation. The exponent α was taken as 1.5 for concrete breakout modes. Note that the ultimate load of the spring model for pure tension $N_{u,spring}$ (0°) corresponds to uncracked concrete condition. For shear, both anchor rows are considered with a_{cl} = 2 mm at the back row.
4. The resistance of the anchor group loaded at an angle θ was calculated analytically according to the model given in EN 1992-4 ($P_{u,EN1992-4}$) and fib Bulletin 58 ($P_{u,fib,B58}$), and is listed in *Table 12.12.*
5. The failure loads reported from the experiments, the failure loads of the spring model, the theoretical failure load according to ***Eq. 136*** were plotted as a function of loading angle in *Figure 12.15* for comparison.
6. The interaction curves were generated using experimental failure load values from Lachinger, using the spring model and the calculated mean failure loads according to EN 1992-4 and fib Bulletin 58. In the calculation according to EN 1992-4 and fib Bulletin 58, all anchors were considered to take up tension forces. To take up for shear forces, only the front anchor row is considered according to EN 1992-4 and the back anchor row is considered according to fib Bulletin 58 (*Figure 12.16 - Figure 12.18*).

Table 12.12. Test results of anchor groups of 2×2 configurations reported in Lachinger (2012)and calculated according to different approaches

Test ID[#]	Loading angle	Meas. mean ultimate load	Ultimate load from spring model	Calculated resistance acc. to EN 1992-4	Calculated resistance acc. to fib Bulletin 58
	θ	$P_{u,exp,m}$	$P_{u,spring}$	$P_{u,EN1992-4}$	$P_{u,fib,B58}$
	[°]	[kN]	[kN]	[kN]	[kN]
Test, h_{ef} = 70 mm – 0°	0	95.4	94.6	94.6	94.6
Test, h_{ef} = 70 mm – 30°	30	76.4	76.0	57.5	76.5
Test, h_{ef} = 70 mm – 45°	45	64.8	67.7	47.4	70.6
Test, h_{ef} = 70 mm – 60°	60	65.0	67.6	42.4	67.7
Test, h_{ef} = 70 mm – 75°	75	74.2	74.7	40.0	67.5
Test, h_{ef} = 100 mm – 0°	0	118.1	119.0	111.9	111.9
Test, h_{ef} = 100 mm – 30°	30	79.5	86.4	63.4	85.9
Test, h_{ef} = 100 mm – 45°	45	72.5	73.0	51.7	77.3
Test, h_{ef} = 100 mm – 60°	60	79.7	84.5	45.5	72.7
Test, h_{ef} = 100 mm – 90°	90	98.9	91.5	42.0	72.2
Test, h_{ef} = 180 mm – 0°	0	173.4	163.5	152.0	152.0
Test, h_{ef} = 180 mm – 30°	30	103.1	104.0	71.1	101.1
Test, h_{ef} = 180 mm – 45°	45	111.9	120.0	55.8	86.2
Test, h_{ef} = 180 mm – 60°	60	102.0	117.1	48.0	78.0
Test, h_{ef} = 180 mm – 75°	75	118.2	105.0	44.4	74.4
Test, h_{ef} = 180 mm – 90°	90	121.4	104.4	43.4	74.1

Comparison of the failure loads using different approaches and experimental results

The failure loads reported from the experiments, the failure loads obtained from the spring model and the failure loads according to ***Eq. 136*** (Theoretical) are plotted in the function of the loading angle in *Figure 12.15* for comparison. In addition, the corresponding tension and shear components are plotted in form of interaction curve in *Figure 12.16 - Figure 12.18*.

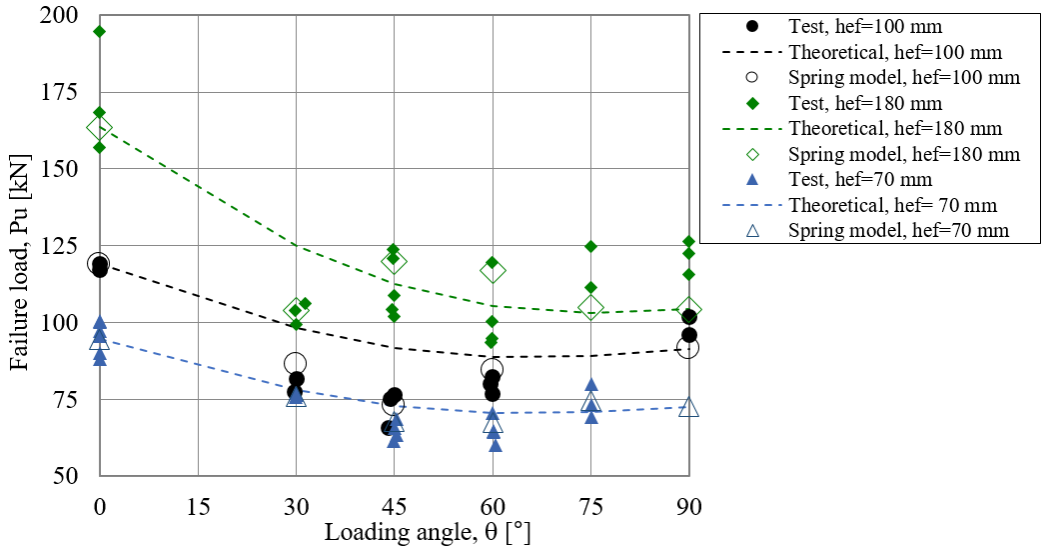

Figure 12.15. Comparison of the failure loads obtained using the spring model directly, failure loads obtained applying Eq. 136 (Theoretical) with the experimental failure loads

Figure 12.15 and *Table 12.12* show that the spring model can describe the anchorage behaviour reasonably well for the investigated cases. The ratio of the experimentally obtained failure loads to failure loads calculated by the spring model is 0.99 with a coefficient of variation of 9% considering 52 test results from Lachinger. The good agreement of the results confirms the fact that in the spring model, realistic load distribution and redistribution is considered. Initially, the shear force is taken up entirely by the front anchors. The shear force is redistributed to the back anchor row after 2 mm hole clearance is considered through the nonlinear displacement controlled analysis. The behaviour of the anchors under tension and inclined loading is accounted for by considering different stiffness and strength conditions among the anchors and by automatically considering the influence of the developing eccentricity by performing the nonlinear analysis. When the results from the pure tension and pure shear analyses of the spring model are used to plot the theoretical curve according to ***Eq. 136*** (dashed lines), the curve generally overestimates the resistance of the group in case of inclined loading. This is due to the fact that for pure tension, all anchors were assumed to be in uncracked concrete in the spring model. Consequently, using ***Eq. 136*** leads to a higher contribution in tension than in reality due to neglecting the cracking/breakout at the front anchor row caused by the shear component. Therefore, it is not recommended to calculate the resistance of anchorages with unfavourable hole clearance configuration by simply applying the $N_{u,spring}$ (0°) and $V_{u,spring}$ (90°) values in the interaction equation to avoid unconservative results. For further evaluation of the results, the corresponding tension and shear components are plotted in the form of interaction curves in *Figure 12.16 - Figure 12.18* following different approaches.

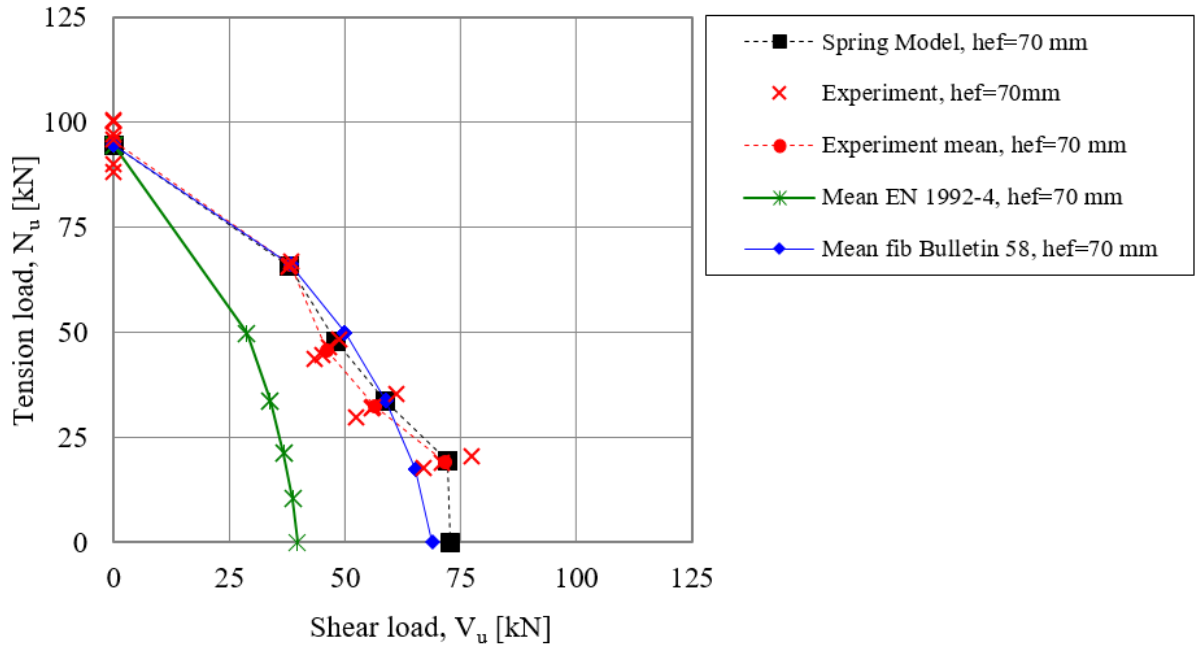

Figure 12.16. Comparison of the interaction curves obtained by the tests with the curves generated using various approaches for the case with h_{ef} = 70 mm

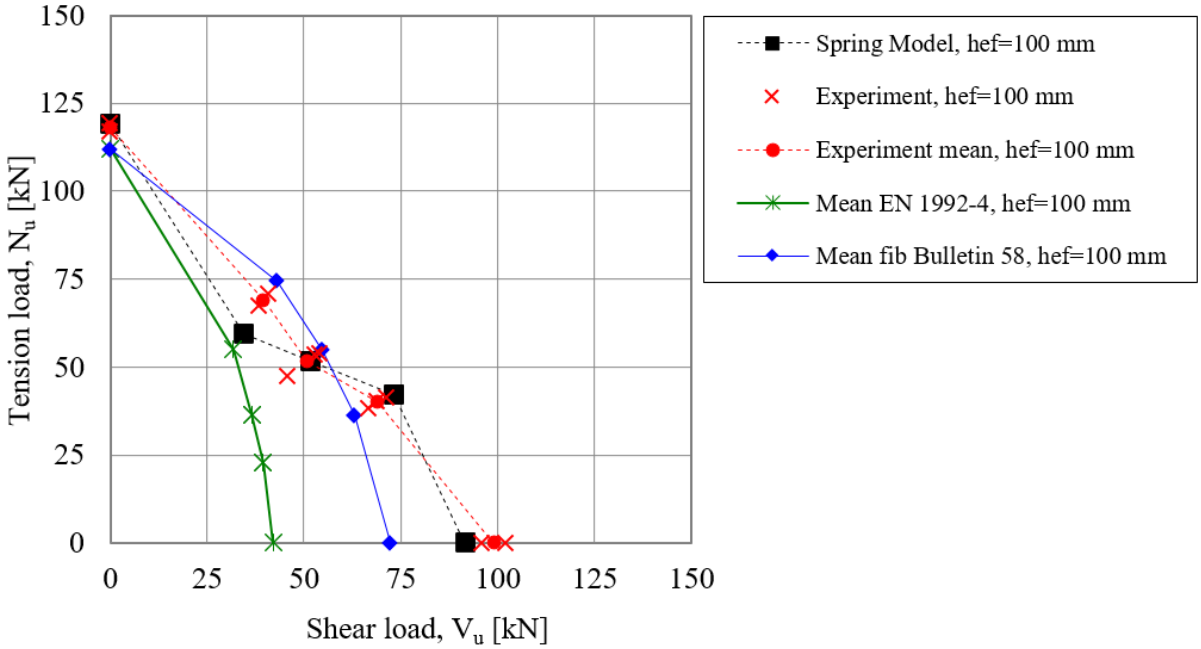

Figure 12.17. Comparison of the interaction curves obtained by the tests with the curves generated using various approaches for the case with h_{ef} = 100 mm

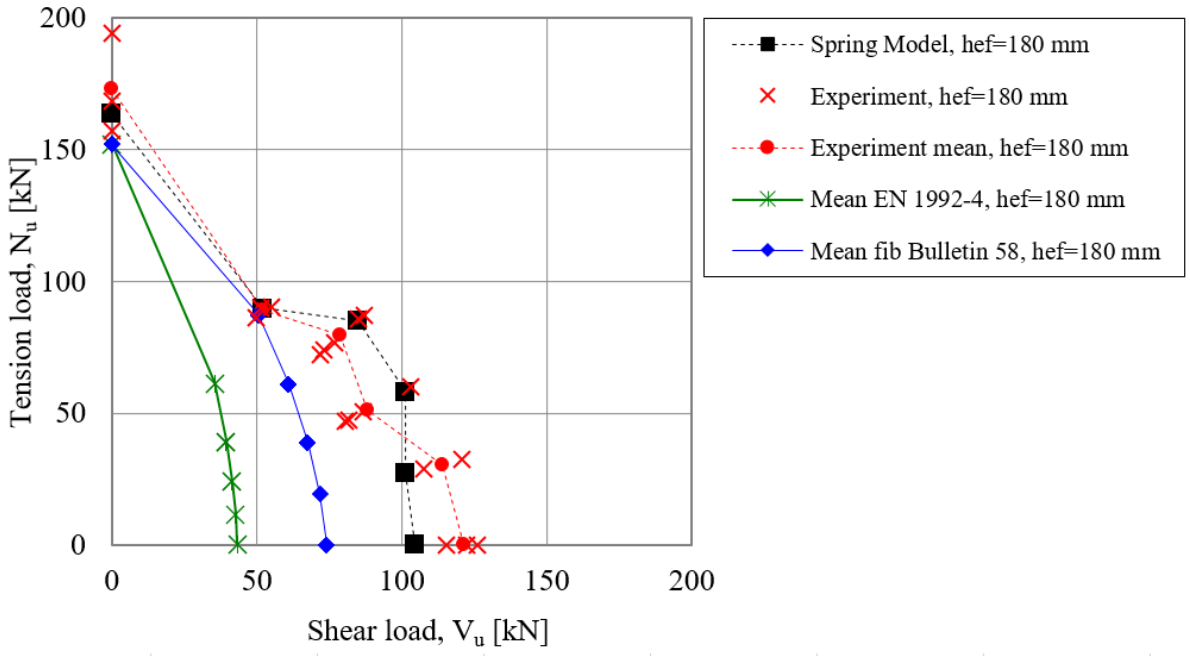

Figure 12.18. Comparison of the interaction curves obtained by the tests with the curves generated using various approaches for the case with h_{ef} = 180 mm

In the calculation according to EN 1992-4, only the front anchor row is considered for shear load, whereas for tension both anchor rows were assumed to be in uncracked concrete. For the cases investigated, the interaction equation according to the EN 1992-4 generally underestimates the failure loads, especially when the loading is shear dominated and seems to be rather conservative. However, it does not describe the realistic behaviour of the anchorage and might be unconservative for certain anchorages with small edge distance to embedment depth ratios in case of tension-dominant inclined loading (loading angles less than 45 degrees).

In the calculation according to fib Bulletin 58, assuming failure crack originating from the back anchor row the shear resistance against concrete edge breakout was calculated from the back anchor row, whereas for tension all anchors were taken into account in uncracked concrete. *Figure 12.16* shows that for 70 mm embedment depth, the calculation based on this concept delivers results close to the experimentally obtained points. In case of loading angles 45 and 60°, the calculated failure loads slightly overestimate the real capacity. From *Figure 12.17* it can be understood that considering the failure crack from back anchor row in the calculations leads to unconservative results under inclined loading with dominating tension for the cases with embedment depth 100 mm. In this case, the embedment depth to edge distance of the front anchor row ratio is small, and the tension behaviour is also influenced by the vicinity of an edge. Consequently, the damages due to the shear cracks at the front row significantly influence the tensile behaviour. *Figure 12.18* depicts the interaction curves generated for the case with 180 mm embedment depth. In this case, the failure loads calculated assuming failure crack from back anchor row under shear loading are conservative if the loading angle is greater than 30° and is equal to the test results for $\theta = 30°$. However, this does not verify the model to use for anchorages with most unfavourable hole clearance pattern but it rather shows that the safety margin may not remain uniform with this approach and, may change on case to case basis. This

is due to the fact that the anchorage behaviour taking into account the hole clearance cannot be considered realistically by the force-based approach.

The failure loads calculated using the spring model confirm that the nonlinear spring model is capable of simulating the behaviour of the investigated anchorages reasonably well provided all aspects such as considering the hole clearance pattern and the cracking at the front anchor row are taken into account in the model. Although the nonlinear spring model considering the most unfavourable hole clearance pattern was only verified against anchor groups of 2×2 configurations, it's concept is easily extendable and applicable to other anchor configurations as well. Nevertheless, it is recommended that the gap be filled to eliminate the influence of hole clearance.

12.3 SUMMARY

In Chapter 12, the nonlinear spring model for tension-shear interaction in case of concrete breakout failure is verified. Only failure combinations "concrete cone failure - concrete edge breakout failure" of an anchorage which is placed close to the concrete edge was investigated with the spring model, and consequently, only this is covered by the scope of application of the model. Within the framework of this thesis, no tests were carried out under combined tension and shear, (interaction) and therefore, the spring model is verified solely through test data from the literature. Test results from Sharma et al. (2019) on anchor groups of 2×2 configuration of welded headed studs without the influence of hole clearance pattern under inclined loads and test results from Lachinger (2012) on anchor groups of 2×2 configurations using bonded anchors with most unfavourable hole clearance pattern loaded under inclined loads were used.

In Section 12.1, the nonlinear spring model is verified for applications without hole clearance and in Section 12.2, for anchor groups of 2×2 configurations with most unfavourable hole clearance pattern. The information on the determination of the anchor spring characteristics for tension and shear for the applications without and with hole clearance is detailed in the corresponding Sections 12.1.2 and 12.2.2, respectively.

The evaluation of the obtained results is discussed in Sections 12.1.3 and 12.2.3. In *Figure 12.19,* a comparison of the test results against the results obtained using the nonlinear spring model for interaction is shown. Altogether 64 tests from the literature were compared with the spring model. The mean value of $P_{u,test}/P_{u,spring}$ is 1.0, and the coefficient of variation is 9.7%. This proves the capability of the spring model to simulate the behaviour of anchorages under inclined loads.

The evaluation in Section 12.1.3 indicates that for anchorages without hole clearance loaded under combined tension and shear and failing due to combined concrete cone – concrete edge failure, the nonlinear spring model is a strong tool to predict not just the failure loads but also the complete load-displacement behaviour. For applications with hole clearance under inclined loading, the scope of application of the nonlinear spring model is recommended only for rec-

tangular anchorages of 2×2 configurations. This is because the nonlinear spring model considering the most unfavourable hole clearance pattern was only verified against anchor groups of 2×2 configurations (Section 12.2.3). To overcome the restrictions, alternatively, the gap in the base plate can be filled to eliminate the influence of hole clearance.

The interaction model is deemed applicable equally for welded headed anchors and post-installed anchors provided the nonlinear spring characteristics for the anchors under tension and shear are well-evaluated and the restrictions for the applications are considered.

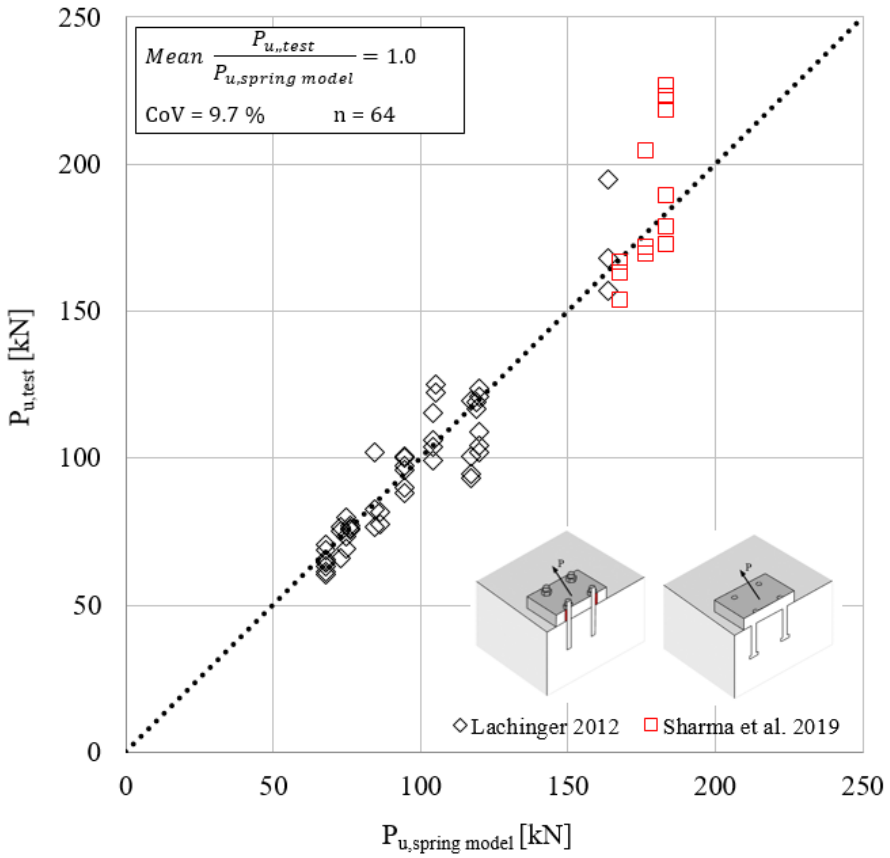

Figure 12.19. Comparison of test results with the results obtained from the nonlinear spring model for anchor groups subjected to combined tension and shear loads

13 RECOMMENDATIONS FOR THE CALCULATION OF RESISTANCES

This chapter gives the recommendations for the calculation of anchorage resistances using the nonlinear spring modelling approach, discussing the field of application, the safety concept, the modelling rules and the verification of the results for Ultimate Limit State (ULS) and Serviceability Limit State (SLS) in case of concrete cone and concrete breakout failure.

13.1 FIELD OF APPLICATION

13.1.1 Failure modes

The proposed nonlinear spring modelling approach is applicable to calculate the resistances for anchor groups undergoing concrete cone failure under tension, concrete edge breakout failure under shear or concrete breakout failure in the case of tension-shear interaction.

In principle, the approach should be extendable to anchor steel failure, anchor pullout failure and combined concrete cone and pullout failure under tension loading, and to steel failure and pryout failure under shear loading but this has not been verified within the framework of this thesis and therefore, it is not addressed among the design recommendations.

The approach is not applicable to calculate the resistance of tension loaded anchorages in the case of splitting failure and side face blowout failure.

13.1.2 Concrete strength classes

The nonlinear spring modelling approach is valid for anchorages installed in concrete members made of compacted normal weight concrete without fibres with strength classes in the range C12/15 to C90/105 in accordance with EN 206. The range of concrete strength classes in which particular anchors may be used is given in the relevant technical product specifications.

Note that the nonlinear spring modelling approach has been verified against experiments performed on anchor groups in a concrete strength range of C12/15 - C50/60.

13.1.3 Anchor group configurations

The approach has been verified against experiments carried out on rectangular and non-rectangular configurations up to sixteen anchors (4 anchor rows with 4 anchors per row) within a group. However, as the approach is capable of simulating the behavior of anchorages in general rather well, the permissible anchor configurations are not restricted to rectangular anchor groups when applying the nonlinear spring modelling approach. Furthermore, the number of anchor rows or number of anchors in a row is not limited.

13.1.4 Concrete condition

The nonlinear spring modelling approach is applicable to anchorages placed in uncracked or cracked concrete. The condition of concrete for the service life of the anchorage shall be determined by the designer. According to forced-based approaches, considering cracked concrete condition for all anchors of a group over its service life is assumed to be conservative. However, in reality, there is a high chance that not all the anchors of a group are intercepted by a crack leading to a significant difference in the stiffness of the anchors of the same group. Therefore, considering cracked concrete condition for all anchors might not always be conservative because the crack pattern has an influence on the load distribution among the anchors of the group and on the load-displacement behaviour of the anchorage. With the nonlinear spring modelling approach, the influence of different crack patterns on the behaviour of the anchorage can be automatically accounted for by assigning the corresponding spring characteristics to the anchors and performing nonlinear analysis. The spring model should be used to determine the worst possible crack pattern and the design should be performed for that case. In this thesis, only crack widths $\Delta w = 0$ *mm* (uncracked) and $\Delta w = 0.3$ *mm* (referred to as cracked concrete) are covered. In case of larger crack widths, the spring characteristics should be determined based on the crack width correspondingly.

13.1.5 Hole clearance

When anchorages are loaded in shear, the force distribution depends on the effectiveness of the anchors resisting shear loads, which is strongly influenced by the hole clearance pattern. The hole clearance pattern is accounted for by the nonlinear spring model via the anchor spring characteristics. The spring model should be used to determine the worst possible hole clearance pattern and the design should be performed for that case. Analogous to EN 1992-4, only anchors with no hole clearance or hole clearance in the direction of the shear load according to EN 1992- 4, Table 6.1 are covered.

13.1.6 Base plate stiffness

Unlike CCD method, using the nonlinear spring modelling approach does not require the base plate to be sufficiently stiff. The geometry of the base plate, including stiffeners and attachment (if any) should be modelled realistically (Section 13.4.3).

13.2 CALCULATION OF DESIGN ACTIONS

The nonlinear spring modelling approach requires the analysis to be performed within displacement domain. Therefore, the actions are not considered explicitly as design forces, rather both the actions and the resistances of the anchorage are calculated in a single calculation.

The method is applicable for all kind of static actions. The dynamic actions such as earthquake or fatigue loading are currently not covered.

13.3 CALCULATION OF DESIGN LOAD-DISPLACEMENT CURVES (RESISTANCE)

13.3.1 Guidance on performing the tests on single anchors

Tests on single anchors should be performed in order to determine the nonlinear spring characteristics - for tension and shear - as accurately as possible for reference cases without influence of the (further) edge or neighbouring anchors. The tests should ideally be carried out in displacement-control. Alternatively, the tests can be performed using oil pressure control while measuring sufficient number of load-displacement data pairs for ascending branch, plateau and descending branch. The tests should be carried out by maintaining the support distance of $2h_{ef}$ on each side of the anchor for tension tests, and $2c_1$ on each side of the anchor for the shear loading tests on the concrete edge according to EOTA TR 048. The tests should be designed in such a way that concrete cone failure under tension or concrete edge failure under shear dominates. This should be ensured by adequate combination of the test parameters. A minimum of five tests should be performed for each series. However, the required number of tests may need to be increased based on the requirements on scatter.

A reliable measurement of anchor displacements is essential for the reliable assessment of the anchorages using the nonlinear spring modelling approach. For tension loaded single anchors, direct displacement measurement relative to the concrete specimen should be performed. For shear loading, it is reasonable to measure the horizontal displacement of the loading fixture provided the friction between the concrete surface and the fixture is minimized (e.g. by using as Teflon sheet) and the slip of the fixture relative to the anchor shaft is negligible. The influence of prestressing force and uncontrolled slip should be considered as per the requirements laid out in EAD 330232-00-0601.

13.3.2 Development of the idealised mean anchor spring properties

13.3.2.1 Idealisation of the load-displacement curves for mean level

The idealisation of the load-displacement curves for mean level is represented for tension loaded anchors in this section. Note, however, that the same rules apply for idealizing the load-displacement curves of shear loaded single anchors as well.

The load-displacement curves obtained from tension tests on single anchors should be idealised to describe the load-displacement behaviour of a single anchor with a limited number of parameters in order to obtain the secant stiffness values k_1-k_4 of the load-displacement curve (*Figure 13.1*). It is recommended to characterize the nonlinear anchor behaviour using a penta-linear format *Figure 13.1a*. However, more or less number of segments may be used for the idealisation of the load-displacement curve if required. A minimum of tri-linear curve should be used. An example is given in *Figure 13.1b*. *Figure 13.1c* shows an example using the penta-linear format for cases when only limited measuring points in the descending branch are available. Note that the idealisation should be performed for each individual curve and the mean value of the secant stiffness values k_1-k_4 should be taken.

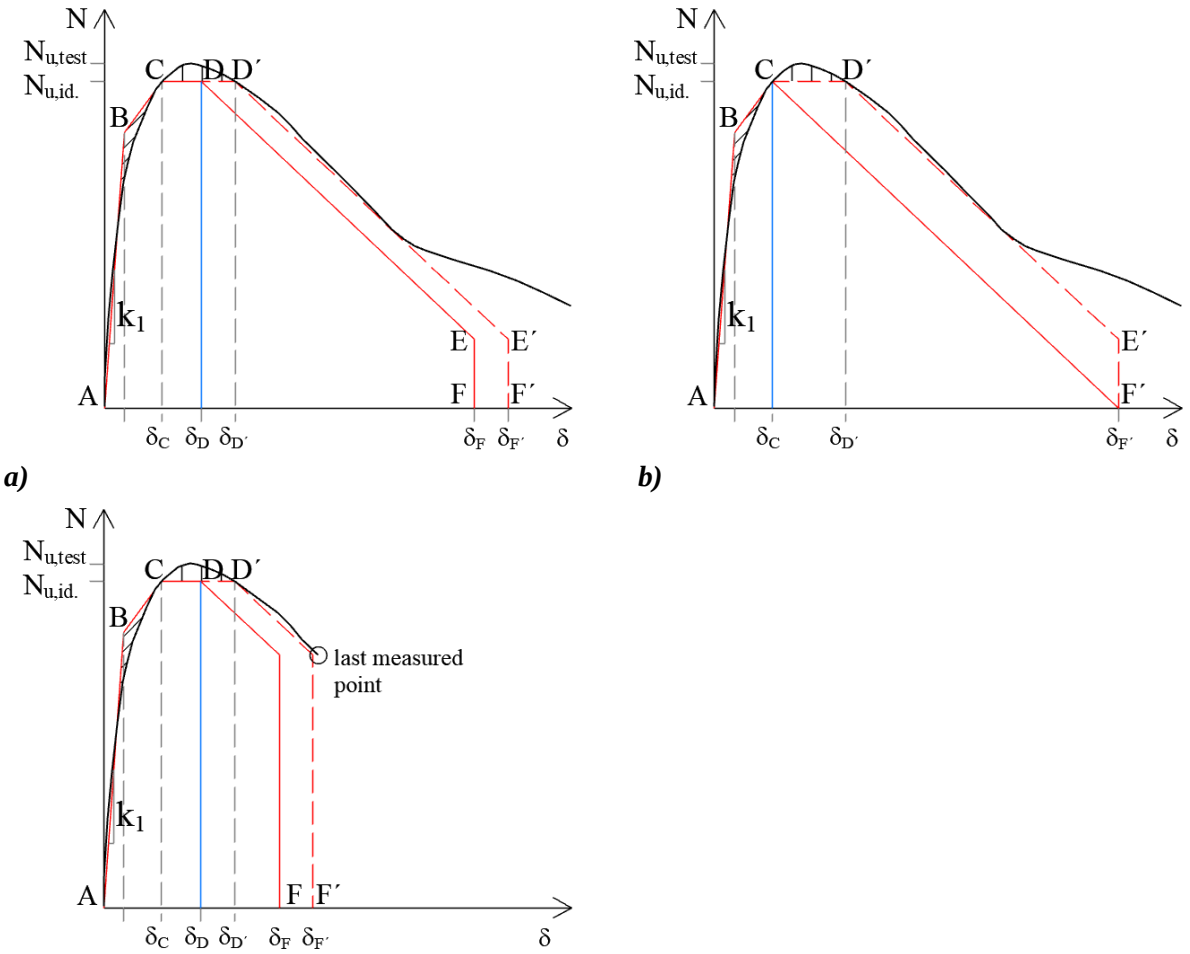

Figure 13.1. Principle of idealisation of a load-displacement curve: a) penta-linear format; b) tri-linear format; c) penta-linear format in cases when limited measuring points in the descending branch are available

The following method is used for the idealisation of the curves:

1. The initial stiffness line is ascertained by joining the point corresponding to 50% of peak load (N_u) on the ascending branch of the curve with the origin.
   $k_1 = k(0.5N_u)$ is the secant stiffness corresponding to a load of $0.5N_u$ on the ascending branch.

$$k_1 = \frac{0.5 \cdot N_u}{\delta(0.5 \cdot N_u)} \qquad \textit{Eq. 137}$$

   (i) The initial stiffness, k_1, is valid until point B of the format (*Figure 13.1a,b,c*).

   (ii) The value of the initial stiffnes k_1 to be used in the anchor spring properties to model the nonlinear load-displacement behaviour of anchors depends on the scatter of the stiffness values obtained from the idealised individual load-displacement curves. In general, the coefficient of variation of initial anchor stiffness, cv_{k1}, should be limited to 40%,

for $cv_{k1} \leq 40\%$, $k_1 = k_{1(mean)}$

for $cv_{k1} > 40\%$, more tests should be performed.

$$k_{1(mean)} = \left(\sum_{i=1}^{n} k_1^i\right)/n \qquad \textit{Eq. 138}$$

2. The horizontal segment of the idealised curve is ascertained by making the areas enclosed by the real curve and its idealisation approximately equal algebraically.
3. The descending branch of the idealised curve should realistically simulate the descending branch of the actual curve.
4. To avoid unrealistically large plateau of the curve, the following restrictions apply to δ_D:

   (i) $\delta_D = min\ \{(2\delta_B + \delta_C); (2.5\delta_C); (\delta_D')\}$

5. The following restrictions apply to δ_F:

   (i) If sufficient number of points are measured for the descending branch (minimum 10 measured points) between $N_{u,test}$ and $0.5N_{u,test}$, then $\delta_F \leq 2.5\delta_D$

   (ii) Otherwise, $\delta_F = \delta_D$ (see *Figure 13.1a,c*, blue line) and $\delta_F = \delta_C$ (see *Figure 13.1b*, blue line)

   (iii) Alternatively, the curve can be idealised as shown in the example in *Figure 13.1c*

Note that in case of shear loaded anchorages, the actual hole clearance of the anchor (gap between the anchor rod and base plate) is considered by the anchor spring properties. This is done by adding an additional horizontal segment at zero load level into the idealised load-displacement curve so that point of the curve moves horizontally by a_{cl} (refer to *Figure 6.6*).

Table 13.1. Salient points of the idealised load-displacement curve: spring properties

Point	Load	Stiffness	Displacement
A	0	0	$\delta_A = 0$
B	$\alpha \cdot N_u$*	k_1 *	$\delta_B = \alpha \cdot N_u/k_1$*
C	N_u	k_2	$\delta_C = N_u/k_2$
D	N_u	k_3	$\delta_D = N_u/k_3$
E	$\beta \cdot N_u$*	k_4 *	$\delta_E = \beta\ N_u/k_4$*
F	0	0	$\delta_F = \delta_E$

**Note that different anchor systems may display a different load-displacement behaviour. Therefore, the definition of points A- F of the idealised curve may be altered depending on the shape of the load-displacement curve. For example the factors α and β can take a value of 0.8 and 0.2, or 0.6 and 0.2 depending on the used anchor system.*

13.3.2.2 Calculation of the resistance for the idealised mean anchor spring properties

To develop the idealised mean anchor spring properties, first, the mean resistance of the single anchor for concrete breakout failure modes should be determined. This can be obtained from the technical product assessment. Alternatively, for concrete cone failure, ***Eq. 139*** and for concrete edge breakout failure ***Eq. 140*** apply. The stiffness values (secant stiffness), k_1-k_4, should be taken from the idealised load-displacement curves obtained from test results as described in Section 13.3.2.1. Finally, the salient points of the mean spring properties using a penta-linear format are given in *Table 13.2*. Note: The idealised load-displacement curves are used only to ascertain the values of stiffnesses k_1-k_4 while the mean resistance of the single anchor (not influenced by other factors) undergoing concrete cone breakout or concrete edge breakout is obtained using ***Eq. 139*** (tension) or ***Eq. 140*** (shear).

$$N_{Rm,c}^{0} = 1.33 \cdot k_1 \cdot \sqrt{f_{cm}} \cdot {h_{ef}}^{1.5} \qquad \textbf{Eq. 139}$$

$k_1 = k_{cr,N}$ for cracked concrete, $k_1 = k_{ucr,N}$ for uncracked concrete

$k_{cr,N}$ and $k_{ucr,N}$ should be taken from the corresponding European Technical Product Specification

$$V_{Rm,c}^{0} = 1.33 \cdot k_9 \cdot {d_{nom}}^{\alpha} \cdot {l_f}^{\beta} \cdot \sqrt{f_{cm}} \cdot {c_1}^{1.5} \qquad \textbf{Eq. 140}$$

$k_9 = 1.7$ for cracked concrete, $k_9 = 2.4$ for uncracked concrete

$\alpha = 0.1 \cdot \left(l_f / c_1\right)^{0.5}$

$\beta = 0.1 \cdot (d_{nom}/c_1)^{0.2}$

Table 13.2. Salient points of the idealised load-displacement curve: mean anchor spring properties

Point	Load	Stiffness	Displacement
A	0	0	$\delta_A = 0$
B	$0.8 \cdot N_{Rm,c}^{0}$	k_1	$\delta_B = 0.8 \cdot N_{Rm,c}^{0}/k_1$
C	$N_{Rm,c}^{0}$	k_2	$\delta_C = N_{Rm,c}^{0}/k_2$
D	$N_{Rm,c}^{0}$	k_3	$\delta_D = N_{Rm,c}^{0}/k_3$
E	$0.2 \cdot N_{Rm,c}^{0}$	k_4	$\delta_E = 0.2 \cdot N_{Rm,c}^{0}/k_4$
F	0	0	$\delta_F = \delta_E$

Note that the stiffness values k_1 - k_4 are taken from Table 13.1 and correspond to the idealisation of the load-displacement curve of the same product.

Consideration of the anchor spacing and edge distance in the anchor spring properties:

Tension loading: Due to the vicinity of concrete edge or neighbouring anchors (group effect in case of anchor spacing, $s < 3h_{ef}$), the anchor spring properties should be modified taking into account the actual configuration of the anchorage (*Figure 13.2*). This is done by following the tributary area approach as described in Section 5.2.2. The mean concrete cone resistance of the i^{th} anchor, $N_{Rm,c}^{i}$ influenced by the neighbouring anchors or a close edge is calculated as:

$$N^{i}_{Rm,c} = N^{0}_{Rm,c} \cdot \frac{A^{i}_{c,N}}{A^{0}_{c,N}}$$ ***Eq. 141***

Where,

$N^{0}_{Rm,c}$ is the mean resistance of a single anchor not influenced by the neighbouring anchors or close edge (***Eq. 139***)

$A^{i}_{c,N}$ is the tributary projected area assigned to the anchor considering the distance from the adjacent anchors and the edge distance (see *Figure 5.8*)

$A^{0}_{c.N}$ is the reference projected area of a single anchor with a distance from all the edges equal to or greater than the critical edge distance $c_{cr,N} = 1.5h_{ef}$

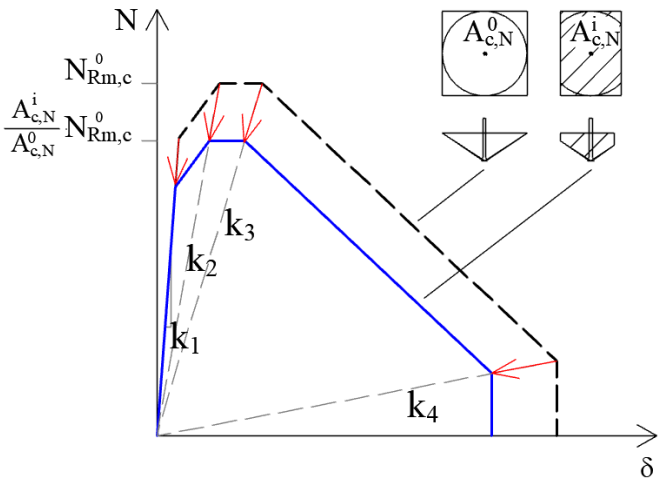

Figure 13.2. Derivation of the mean anchor spring properties of an i-th anchor of a group from the anchor spring properties of a single anchor not influenced by other factors

Shear loading: To consider the influence of anchor spacing in both orthogonal directions s_1 and s_2 on the individual anchor resistance compared to the single anchor resistance (with the same edge distance), the anchor spring properties should be modified. This is done by following the tributary volume approach as described in Section 6.2.2. The mean concrete edge breakout resistance of ith anchor of jth row, $V^{i,j}_{Rm,c}$, influenced by neighbouring anchors or an edge or limited member thickness can be calculated as:

$$V^{i,j}_{Rm,c} = V^{0,j}_{Rm,c} \cdot \frac{V^{i,j}_{c,V}}{V^{0,j}_{c,V}} \cdot \Psi_{h,V}$$ ***Eq. 142***

Where,

$V^{0,j}_{Rm,c}$ is the mean concrete edge breakout resistance of the anchor not influenced by the neighbouring anchors or further edge or member thickness

$V^{i,j}_{c,V}$ is the tributary volume assigned to ith anchor of jth row considering the distance from the adjacent anchors, close edge and thin member when applicable

$V_{c,V}^{0,j}$ is the reference tributary volume of a single anchor of j[th] row

$\Psi_{h,V}$ to account for the fact that the concrete edge resistance does not decrease proportionally to the member thickness (h) as assumed by the ratio $V_{c,V}^{i,j}/V_{c,V}^{0,j}$

13.4 MODELLING RULES

13.4.1 Modelling of anchor springs

The anchor springs for tension loading should be modelled as tension-only uni-directional springs in the numerical model and the anchor springs for shear loading should be modelled as uni-directional shear springs active in both the loading direction and in the direction opposite to the loading.

Ideally, the springs can be modelled as physical springs with only uniaxial degree of freedom. If the numerical modelling and the analysis is performed using a software where the nonlinear spring properties are assigned within a frame element, the other degrees of freedom (shear, torsion and moment components) should be released so that the spring (frame) does not transfer shear and moment forces.

13.4.2 Modelling of compression-only contact springs

The compression forces, which may develop between the baseplate and the concrete surface, should be accounted for by modelling an elastic bedding below the baseplate using compression-only uni-directional springs. The compression-only springs may be calculated according to Winkler spring characteristics assuming a modulus of elasticity E_{cm} = *30,000 MPa*. More details can be found in Section 5.4.

13.4.3 Modelling of the base plate and attachment

The model should replicate the behaviour of the base plate considering the influence of the attachment and stiffeners (if any) so that a realistic load transfer, load distribution and redistribution among the anchors of the anchor group is ensured. The base plate along with the attachment and stiffeners may be modelled by using solid elements or shell elements applying thick-plate formulation following the Mindlin-Reissner plate theory. Alternatively, the influence of stiffeners and attachment may be modelled by applying constraints, provided it is justified by the application. The material behaviour of the steel base plate may be considered as linear elastic with an elasticity modulus of E_s = *200,000 MPa*. Alternatively, if required, a yield criterion e.g. von-Mises may be assigned to consider the nonlinear behaviour of the baseplate as well. The meshing of the base plate should appropriately consider the shape of the attached profile and the anchor location. Further details about the modelling are given in Section 5.3.

13.5 ANALYSIS

13.5.1 Calculation procedure

Non-linear static analysis should be performed on the model of the anchorage in displacement-control using sufficiently small step size by incrementally applying the displacement until failure or at least until 20% of the ultimate load in post-peak is reached. During the analysis, a step-by-step verification and updation of the stiffness matrix is performed. To account for the non-linear anchor behaviour and realistic distribution and redistribution of forces among the anchors, secant stiffness method or tangent stiffness method may be used for the analysis. It is recommended to use the secant stiffness method due to its robustness and relatively high stability. Furthermore, it is recommended to define a tolerance or convergence criterion (< 1%) for the non-linear analysis. More details are given in sections 5.5 and 7.6.

13.5.2 Anchorage capacity curve at mean level

The load-displacement curve obtained for the anchorage by performing the nonlinear analysis following the procedure as described above gives the mean anchorage capacity curve (load-displacement curve of the anchor group at mean level). From the evaluation of the results, at any stage of the global output (L-d curve for the anchor group), the following further information can be obtained at mean level:

(i) load-displacement behaviour of individual anchors
(ii) force distribution and redistribution among the anchors of a group
(iii) extent of nonlinear excursion
(iv) deformed shape of the base plate, attachment and stiffener (if any)
(v) stresses developed in the base plate, attachment and stiffener (if any)
(vi) step-by-step performance check for the anchorage.

13.6 DETERMINATION OF THE CHARACTERISTIC CAPACITY CURVE OF THE ANCHORAGE

The mean load-displacement curve obtained for the anchor group after performing the nonlinear analysis should be converted to the characteristic level to obtain the characteristic capacity curve of the anchorage. An example of derivation of characteristic anchor group behavior from the mean anchor load-displacement response is depicted in *Figure 13.3*.

The characteristic capacity curve of the anchorage can be derived from the anchorage capacity curve at mean level obtained as output of the analysis using the nonlinear spring model. The characteristic resistance of the anchorage $N_{Rk,c}$ is obtained from the mean resistance of the anchorage $N_{Rm,c}$ as

$$N_{Rk,c} = \frac{N_{Rm,c}}{1.33} \cdot \sqrt{\frac{f_{ck}}{f_{cm}}} \qquad \textit{Eq. 143}$$

The stiffness values for each point of the curve should be maintained (see *Figure 13.3*).

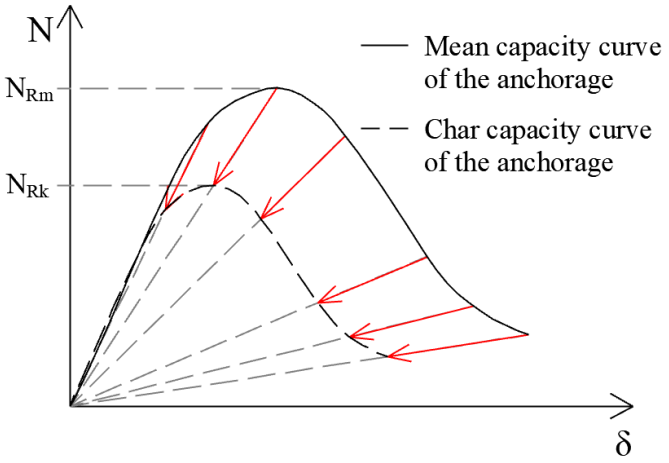

Figure 13.3. Example: Derivation of the characteristic capacity curve from the mean capacity curve

13.7 DESIGN CAPACITY OF THE ANCHORAGE

13.7.1 Design capacity curve of the anchorage and verification for ultimate limit state (ULS)

The design capacity curve of the anchorage can be derived from the characteristic capacity curve of the anchorage (Section 13.6). For each point of the characteristic capacity curve, the force value should be divided by the partial factor for concrete cone and concrete edge failure, $\gamma_{Mc} = 1.5$ in accordance with EN 1992-4 (see *Figure 13.4*). Note that the characteristic capacity curve is reduced only in the vertical direction and no modification to the displacements are made. This is in accordance with the EN 1992-1-1, where the design stress-strain curve for concrete is obtained from the characteristic stress-strain curve by following a similar approach (*Figure 13.5*).

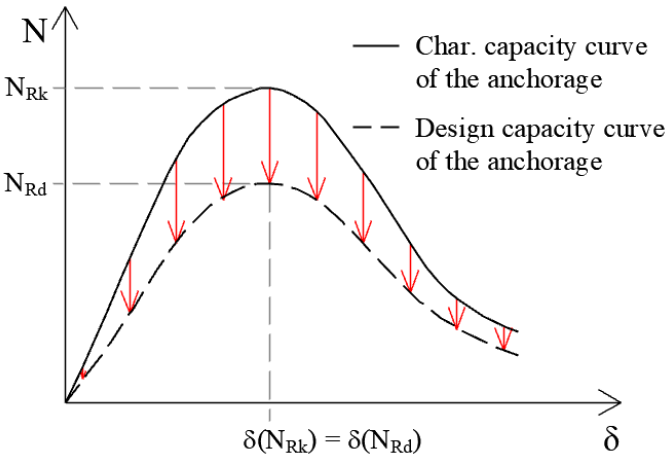

Figure 13.4. Derivation of design capacity curve of the anchorage from the characteristic capacity curve of the anchorage (example for tension loading)

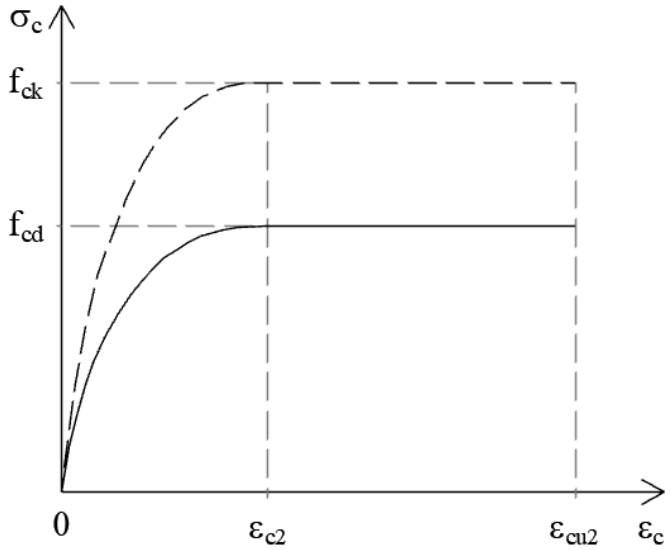

Figure 13.5. Parabola-rectangle diagram for the characteristic and design stress-strain curve of concrete under compression (reproduced from EN 1992-1-1, Figure 3.3)

For the ULS verification in terms of forces, the following equations should be satisfied:

(1) For tension loading in the case of concrete cone failure: $N_{Ed} \leq N_{Rd,c} = \frac{N_{Rk,c}}{\gamma_{Mc}}$

(2) For shear loading in the case of concrete edge breakout failure: $V_{Ed} \leq V_{Rd,c} = \frac{V_{Rk,c}}{\gamma_{Mc}}$

(3) For inclined loading in the case of concrete breakout failure (tension-shear interaction): $P_{Ed}(\theta) \leq P_{Rd}(\theta) = \frac{P_{Rk,c}(\theta)}{\gamma_{Mc}}$

Note that when using the nonlinear spring model for calculating the group resistance for inclined loading at an angle, θ, the results are directly obtained for the group loaded at the corresponding angle, θ.

13.7.2 Verification for serviceability limit state (SLS)

For the SLS verification in terms of forces, the following equations should be satisfied:

(1) For tension loading in the case of concrete cone failure: $N_{Ed} \leq N_{Cd,c}$

(2) For shear loading in the case of concrete edge breakout failure: $V_{Ed} \leq V_{Cd,c}$

(3) For inclined loading in the case of concrete breakout failure (tension-shear interaction): $P_{Ed}(\theta) \leq P_{Cd}(\theta)$

The serviceability limit state is governed by

(1) displacement limits

(2) crack control

(3) stress limitation

13.7.2.1 Displacement limits

The limiting displacement might arise due to the displacement of the anchors and/or deformation of the base plate. The limiting displacements may vary from one application to the other

as governed by the functional requirements of the attachment. In the serviceability limit state, it should be shown that the displacements occurring under the relevant actions are not larger than the admissible displacement. For example, if the admissible displacement is δ_{SLS}, then the design resistance of the anchorage corresponding to SLS is given as the load corresponding to δ_{SLS} in the ascending branch of the design capacity curve (see *Figure 13.6*).

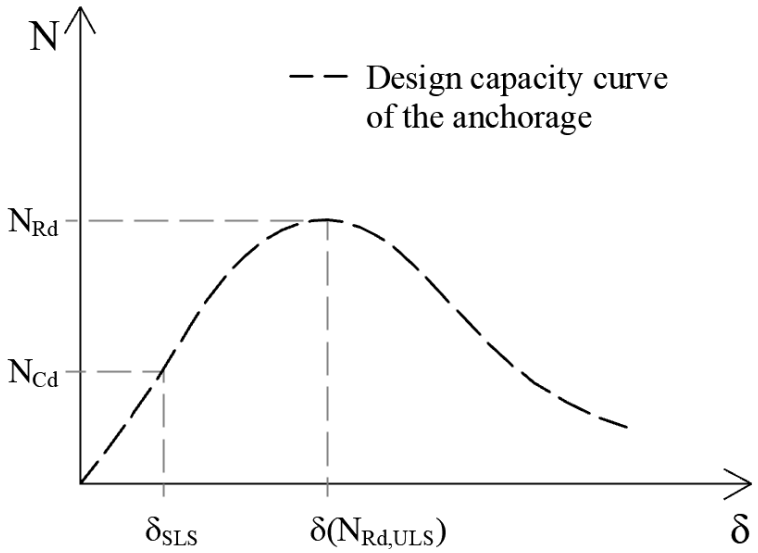

Figure 13.6. Design capacity curve of the anchorage and verification against SLS for displacement limits (example for tension loading)

13.7.2.2 Crack control

For anchorages under tension loads, the cracking may occur due to concrete cone breakout or due to splitting failure (in non-cracked concrete). Investigations by Sawade and Eligehausen (see Section 2.1.2) showed that for concrete cone breakout, the crack is initiated at the level of the embedment depth of the anchor and when the failure load is reached the crack length is relatively small and far from the surface. Under service loads, the length of the crack would be even smaller (refer to *Figure 2.6*) and farther from the concrete surface to affect serviceability in any way. Therefore, for concrete cone breakout, an additional check for SLS for crack control is considered redundant. This approach is also followed in the current norms such as EN 1992-4. However, it is essential to prevent the loss of serviceability due to the occurrence of splitting cracks, which is deemed satisfied provided any of the following requirements is fulfilled:

(i) sufficient amount of surface reinforcement/ is provided to prevent the splitting failure of the concrete member under tension loads
(ii) the design is performed using the spring characteristics valid for cracked concrete for all the anchors within a group

If none of the above conditions is fulfilled, the verification for splitting failure should be performed. However, the splitting failure mode is not covered by the proposed nonlinear spring modelling approach.

For anchorages under shear loads failing due to concrete edge breakout, if the failure crack appears from the front anchor row either due to hole clearance or due to large spacing (s_1) to edge distance ratio (c_1), then the SLS might be governed by the cracking of the front anchor

row (see example in *Figure 13.7*). The definition of SLS design capacity in the case of favourable hole clearance pattern considering crack and displacement control in case of anchor groups is shown with an example in *Figure 13.8.*

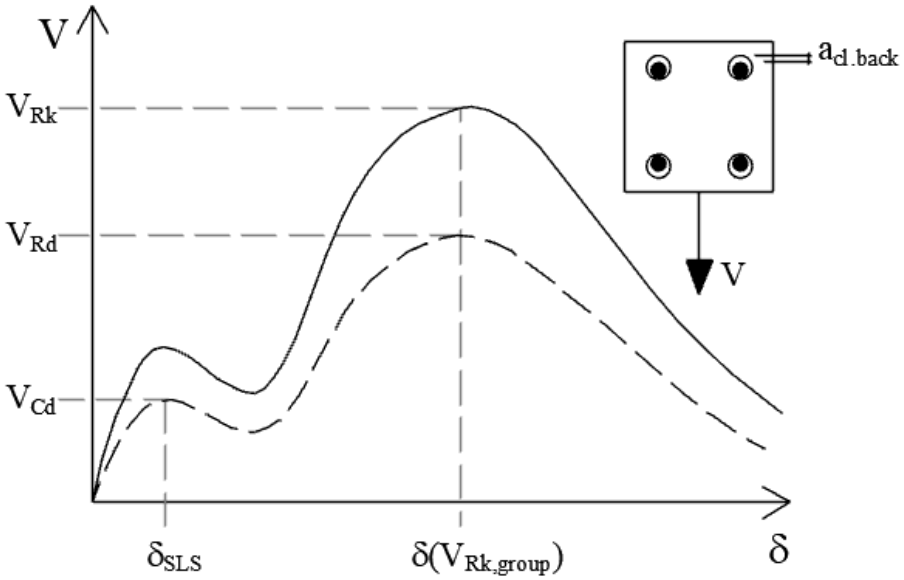

Figure 13.7. Definition of SLS design capacity in the case of unfavourable hole clearance pattern considering crack control

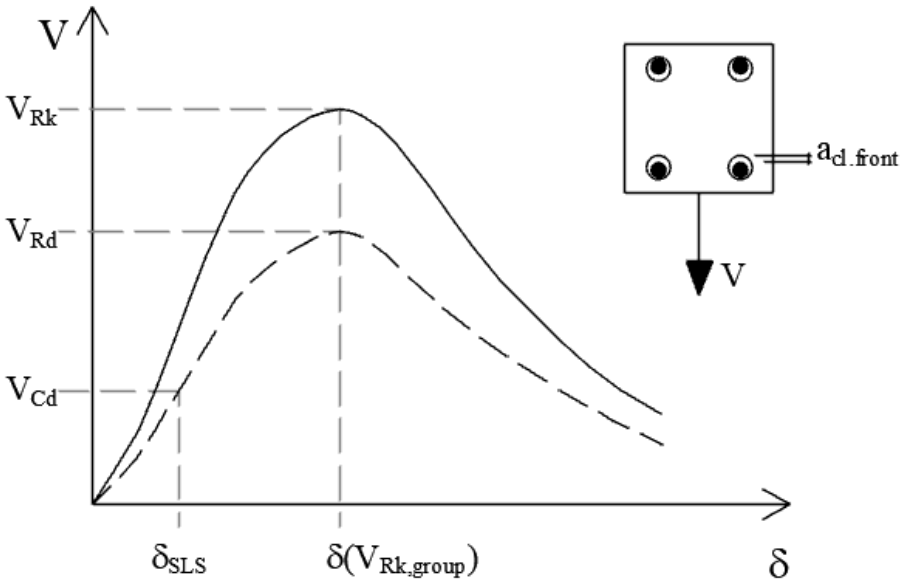

Figure 13.8. Definition of SLS design capacity in the case of favourable hole clearance pattern considering crack and displacement control

13.7.2.3 Stress limitation

The stresses in the base plate and the anchors under service loads shall be limited to the allowable service stresses. Typically, for base plate $\sigma_{sd,base\ plate} \leq f_{yd,base\ plate}$ is valid. For anchors, the steel stresses in the highest loaded anchor shall be limited to the allowable values that are typically based on the characteristic ultimate stress and depend on the loading direction ($\sigma_{Ns} \leq f_{Ns,\text{allowable}}$; $\sigma_{Vs} \leq f_{Vs,\text{allowable}}$). Note: The spring model proposed here is valid for

concrete breakout failure modes for the anchorage as a whole but the steel stresses in individual anchors of the group should not exceed permissible values for the method to be valid.

13.8 SUMMARY

In this chapter, the recommendations for the design of anchorages using the nonlinear spring modelling approach, including the field of application, the safety concept, the modelling rules and the verification of the results for ULS and SLS are given for concrete breakout failure modes. The design concept is in accordance with the generally accepted approach included in EN 1992-1-1 and EN 1992-4.

14 CONCLUSIONS AND RECOMMENDATIONS FOR FUTURE RESEARCH

14.1 CONCLUSIONS

The current approaches for the design of anchorages in concrete are limited in applicability due to the semi-empirical nature of the concepts and force-based methods. These limitations restrict the design to a maximum of 3×3 anchor group with anchors arranged in rectangular pattern and connected with a sufficiently stiff base plate. Furthermore, the considerations such as the crack pattern and the hole clearance pattern is not explicitly considered in the current design approaches.

In this thesis, a new displacement-based approach referred to as the nonlinear spring model is developed, verified and proposed for the calculation of anchorages in the case of concrete breakout failure modes under tension, shear and interaction thereof. The approach is valid irrespective of the arrangement of the anchors, the stiffness of the base plate and can explicitly consider the influence of crack pattern and the hole clearance pattern.

A nonlinear spring model for tension loaded anchorages undergoing concrete cone failure includes explicit modelling of the nonlinear anchor behaviour, the base plate, attachments, and the contact between the base plate and the concrete surface. The main principles followed in the model are the consideration of virtual edges between the neighbouring anchors through the tributary area approach and the consideration of realistic distribution and redistribution of forces among the anchors through performing nonlinear analysis in displacement control.

The nonlinear spring model for shear loaded anchorages for concrete edge breakout failure is analogous to the model for anchorages under tension loads. To consider different anchor rows with different edge distances, and thereby enabling a realistic force distribution and redistribution of shear forces among the anchors, the tributary area approach is extended to a tributary volume approach. With the spring model for shear, it is possible to account for the hole clearance pattern of the anchorage in a rather straightforward way by considering the hole clearance of the individual anchors through the anchor spring properties.

The nonlinear spring model for anchorages failing due to concrete breakout failure under inclined loads (interaction) is the combination of the nonlinear spring model for tension and shear. No further considerations are needed to perform an analysis for anchorages loaded under inclined loads in case of anchorages without hole clearance. For applications with unfavourable hole clearance pattern under inclined loading, the scope of application of the nonlinear spring model is recommended only for rectangular anchorages with up to two anchors in a row because the verification was performed only for such cases. The interaction model is deemed applicable equally for welded headed anchors and post-installed anchors provided the nonlinear spring characteristics for the anchors under tension and shear are well-evaluated and the restrictions for the applications are considered.

Well-designed and well-instrumented experimental tests were performed on anchor groups of different configurations and on single anchors under tension and shear loading to verify the postulates made for the spring model and to obtain the information required for the development

and verification of the spring model. The tests were carried out on various anchor groups with different rectangular and non-rectangular configurations, variable the base plate stiffness, crack pattern, loading case (concentric/eccentric), hole clearance pattern and the combination of the investigated parameters.

The nonlinear spring model for tension, shear and interaction was verified against a total of 304 experiments carried out within the framework of this thesis (157) and from the literature (147). The results of experiments and the spring model display excellent agreement in terms of ultimate loads (mean value of $P_{u,test}/P_{u,spring\ model}$ = *1.04*, *CoV = 13.3%*) as well as load-displacement behaviour due to considering the change in stiffness and the corresponding redistribution of forces among the anchors of a group (see *Figure 14.1*).

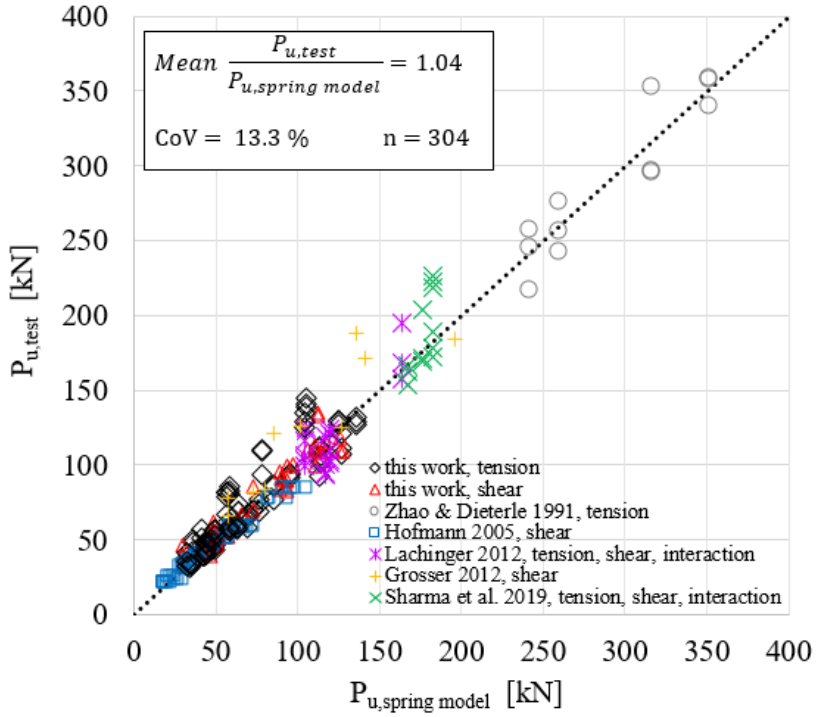

Figure 14.1. Comparison of the test results of this work and from the literature with the results obtained using the nonlinear spring model

Recommendations for the design of anchorages are given for using the nonlinear spring modelling approach including the field of application, the safety concept, the modelling rules and the verification of the results for Ultimate Limit State (ULS) and Serviceability Limit State (SLS) for concrete cone and concrete edge breakout failures.

Although the nonlinear spring model for tension, shear and interaction is verified for concrete breakout failure modes, several questions remain open. Some of the open questions and recommendations for future work are discussed in Sections 14.2 and 14.3.

14.2 RECOMMENDATIONS FOR FUTURE RESEARCH

14.2.1 Spring model for tension loaded anchorages – Consideration of failures modes other than concrete cone failure

In this thesis, a nonlinear spring modelling approach is proposed to simulate the behaviour of tension loaded anchor groups failing due to concrete cone failure mode. However, in principle, the model is extendable to other failure modes as well. The general modelling rules described in Chapter 5, including modelling of the base plate, modelling the anchors as springs and modelling of the contact elements are valid for all failure modes. However, the derivation of spring properties might require different considerations for different failure modes. In the following, certain recommendations are given that might be useful to extend the spring modelling approach for other failure modes. Further investigations are needed to extend the applicability of the nonlinear spring model.

Steel failure

According to the current design, when a tension loaded anchorage fails due to steel failure, the resistance of the anchors is not influenced by the adjacent anchors or by the vicinity of the concrete edge. Therefore, the verification of the steel failure mode for anchor groups has to be carried out only for the most loaded single anchor. This aspect is considered automatically in the nonlinear spring model. However, in the nonlinear spring model, the additional benefit due to the redistribution of forces is also accounted for. The spring properties, which are determined for the steel failure of a single anchor not affected by edges or by adjacent anchors, can directly be assigned to one individual anchor of an anchor group irrespective of the anchor spacing. Trautner and Hutchinson (2018) used nonlinear tension-only springs to model the anchor behaviour for steel failure in moment frame column baseplate connections subjected to combined axial and moment loads. The “steel springs” of the used headed anchors were calibrated using the results of a testing program on different anchor materials, where the nonlinear force-deformation response of the anchors was measured using a tensile test specimen. Furthermore, in order to extend the applicability of his results, scaling relationships were proposed in Trautner et al. (2017) to extrapolate force-deformation relationships to larger anchor diameters than the tested diameter. The scaling was done by multiplying the discretised force data obtained from tests by the ratio of the stress area of the (larger) anchor to the stress area of the tested anchor. In contrast to cast-in-place headed studs, which have uniform diameter and strength over the length, post-installed anchors may have non-constant cross-sections along the anchor length, and due to the manufacturing methods, the different parts might exhibit different steel strengths. Therefore, the idealised load-displacement curves (spring characteristics) for steel failure of the anchors can be obtained from testing of a single anchor, which is embedded into concrete.

Pullout failure

Similar to the steel failure mode, when a tension loaded anchorage fails due to pullout failure (but not a combination of pullout and concrete cone, which is valid only for adhesive anchors), the resistance of the individual anchors of the group is not influenced by the adjacent anchors or by the vicinity of the concrete edge. To use the nonlinear spring model, the nonlinear spring

properties shall be determined for the pullout failure mode. Then, the spring properties, which are determined for the pullout failure of a single anchor, can directly be assigned to one individual anchor of an anchor group irrespective of the anchor spacing. The load-displacement curves can be obtained from approval testing of anchors or pullout tests shall be performed

Combined pullout and concrete cone failure (for adhesive anchors only)

The nonlinear spring model proposed for concrete cone failure mode should be extendable to use for calculation of anchor groups failing due to combined pullout and concrete cone failure. However, this requires the modification of the tributary area approach used in the model.

Splitting failure

The nonlinear spring model in the current format is not directly applicable to consider the splitting failure. However, splitting failure of the concrete member can be precluded in the following situations: (i) cracked concrete condition for the anchorage is considered in the design, or (ii) sufficient amount of reinforcement is provided to prevent splitting failure of the concrete member.

Concrete blow-out failure

Concrete blow-out failure is a special case usually associated with anchors with small edge distance and relatively deep embedment depth. The concrete breakout occurs on the side without any major breakout at the top concrete surface. The nonlinear spring model in the current format is not directly applicable to consider the concrete blow-out failure.

14.2.2 Spring model for shear loaded anchorages – Consideration of failures modes other than concrete edge breakout failure

The nonlinear spring model for shear proposed in this work is applicable for concrete edge breakout failure mode (Chapter 6). The other failure modes possible in shear include anchor steel failure and pryout failure. The general modelling rules described in Chapter 6, including the modelling of the base plate, modelling the anchors, as springs are valid for steel failure and pryout failure as well. Due to an indirect influence of concrete strength on steel strength of the anchor, for steel failure, the spring curves for anchors should be obtained based on tests performed with the same installation parameters and concrete grade as considered in the design.

Note that in the case of shear loaded anchorages it is possible to have different failure modes of different anchors within one anchor group depending on certain parameter combinations. One such example with the application of the spring model for a 3×1 anchor group undergoing “concrete edge – steel - steel” failure is presented in Section 14.2.2.1.

The concrete pryout failure occurs due to the tension forces developing in the anchor under shear loading. This failure mode is dominant for anchors with small embedment depth to anchor diameter ratios. To extend the spring model to capture this failure mode, special considerations might be needed. Further research in this regard is highly recommended.

14.2.2.1 Consideration of different failure modes within one anchor group

Preliminary tests on shear loaded anchor groups were carried out in Bokor (2019) to investigate the application of the nonlinear spring model for anchor groups, where the anchors in different rows fail due to different failure modes. Tests were performed on 3×1 anchor groups loaded in shear perpendicular to the free concrete edge. The tests were designed in such a way that the targeted failure mode of the front row was concrete edge breakout, whereas the second and third rows fail due to steel failure of the anchor rod. To obtain the corresponding spring properties, single anchor tests were carried out with the edge distance of the corresponding anchor rows for concrete edge failure (front row) and steel failure (middle and back row). Details about the testing and results are reported in Bokor (2019). The determined springs were assigned to the anchors in the model and a nonlinear static analysis was carried out in displacement control.

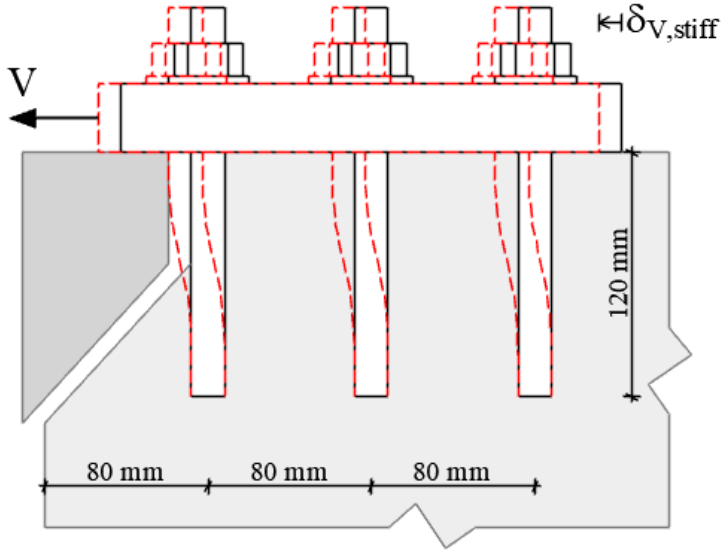

Figure 14.2. 3×1 anchor group loaded in shear perpendicular to the edge with different failure modes for individual anchors

The theoretical behaviour of the investigated anchor group configuration is explained in *Figure 14.2:* At the onset of loading all three anchors carry almost equal amount of shear force due to equal shear stiffness independent of the edge distance. The first damage (concrete edge cracking) is seen at the front anchor row, however, the front anchor is still capable of resisting further shear forces due to the steel capacity of the anchor and the fact that the part of the anchor is still embedded in concrete. Ultimately, the anchorage fails due to anchor steel failure. This behaviour is clearly reflected in the load-displacement curves obtained from the tests. The experimental curves reproduced from Bokor (2019), are plotted in *Figure 14.3* along with the load-displacement curve obtained from the nonlinear spring model. It can be seen that the spring model is able to predict the behaviour of the investigated anchor group in terms of failure load and curve progression very well. The first peak in the load-displacement curve corresponds to the cracking at the front row, whereas the second peak can be attributed to reaching the steel capacity of the anchors. The obtained results are promising, however, using the spring model for different failure modes within an anchor groups needs further verification.

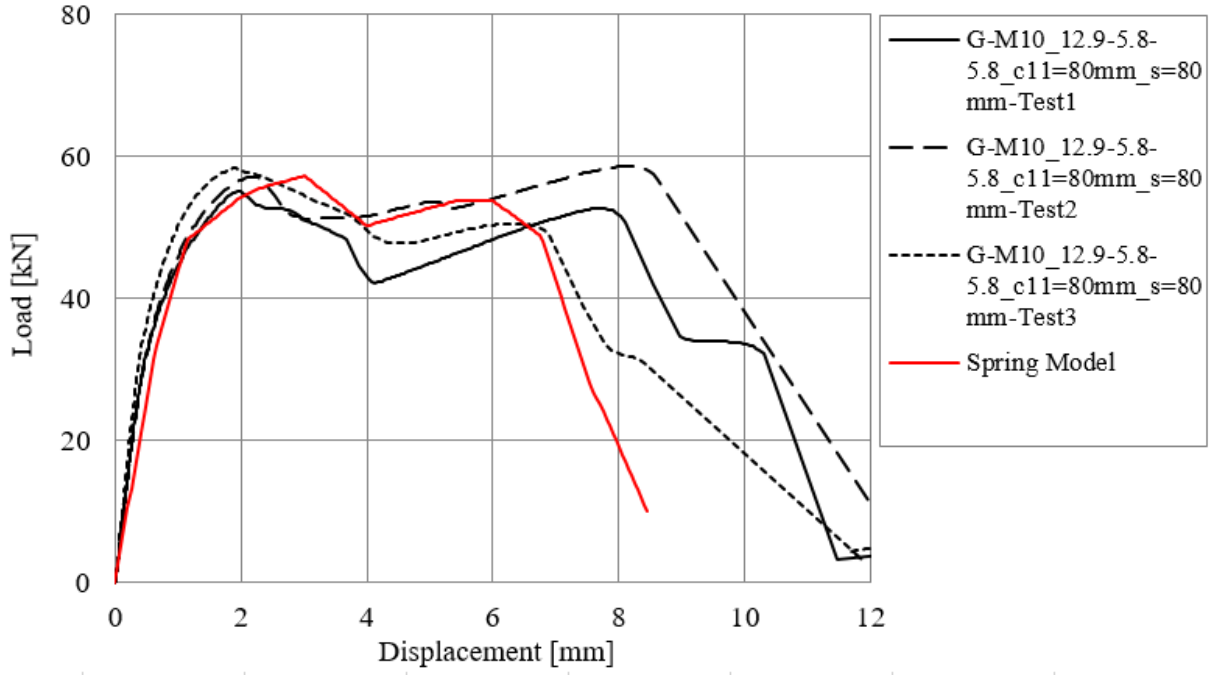

a)

b)

Figure 14.3. a) Load-displacement curves on 3×1 anchor groups with different failure modes for the anchors reproduced from Bokor (2019) and result of the spring model; b) failure mode

14.2.3 Shear loading - Concrete edge breakout failure in the case of anchor groups placed close to the concrete edge and loaded parallel or inclined to the edge

Preliminary tests were carried out on anchor groups of hexagonal configuration to investigate the behaviour of anchorages with such non-rectangular configurations and possibly extend the applicability of the nonlinear spring model for concrete edge breakout failure to anchorages loaded parallel to the free concrete edge (*Figure 14.4*, *Figure 14.5*).

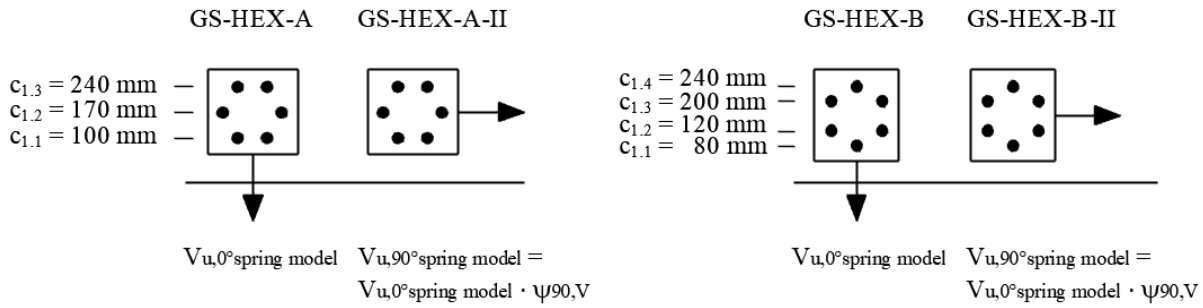

Figure 14.4. Anchorages with hexagonal anchor pattern loaded perpendicular or parallel to the free edge

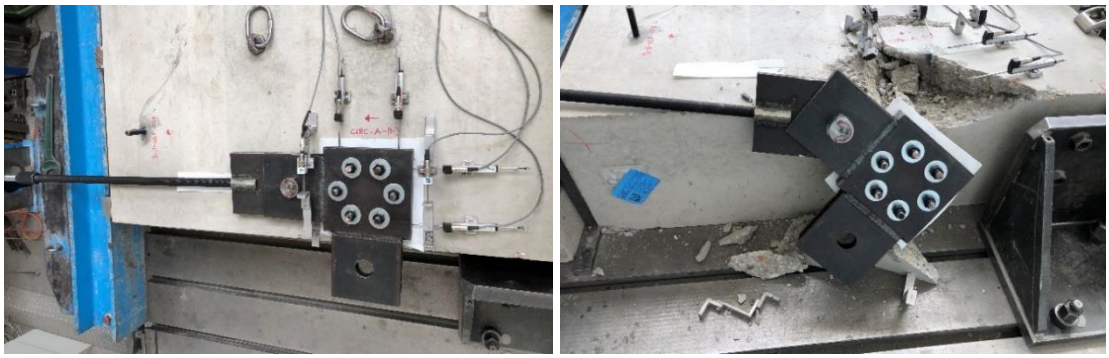

a) ***b)***

Figure 14.5. Test setup for shear loading tests – loading parallel to concrete edge a) during loading; b) after failure

The anchor group configurations GS-HEX-A and GS-HEX-B, against which the spring model was verified (refer to Section 11.3.2.2) for loading perpendicular to the free edge, were tested under shear load in the direction parallel to the free edge while keeping all other parameters the same. The ratio of failure loads obtained for parallel loading to the values valid for perpendicular loading ($V_{u,90°}/V_{u,0°}$) corresponded to 2.3 and 2.5 in the case of the group configuration HEX-A and HEX-B, respectively. The current approach given in EN 1992-4, which is based on the work of Hofmann (2005), recommends that the capacity of anchorages loaded in shear inclined to the edge be calculated by multiplying the capacity valid for the anchorage loaded in shear perpendicular to the edge with the factor $\psi_{\alpha,V}$ according to ***Eq. 144***.

$$\psi_{\alpha,V} = \sqrt{\frac{1}{(cos\alpha_V)^2 + (0.5sin\alpha_V)^2}} \qquad \textbf{Eq. 144}$$

Where, α_V is the angle of direction of loading with the direction perpendicular to the edge ($\alpha_V = 0°$ referring to loading perpendicular to the edge). Note that for $\alpha_V = 90°$, $\psi_{\alpha,V} = 2.0$. This corresponds well with the results of tests performed on anchorages with hexagonal configurations. Therefore, the test results indicate that the capacity of the anchorage loaded inclined to the free edge can be obtained by multiplying the failure load obtained from the spring model for the case with loading perpendicular to the concrete edge with the factor, $\psi_{\alpha,V}$.

Alternatively, the behaviour of the anchorage may be simulated by modelling each anchor with two decoupled springs, one in each the directions “perpendicular and towards the edge (⊥)” and “parallel to the edge (∥)”. The anchor spring characteristics for the springs used to model the

behaviour of anchors perpendicular to the edge is obtained as explained in *Figure 6.5*. Based on the assumption that the stiffness of the anchor is independent of the edge distance, and the concrete edge resistance of the anchor loaded parallel to the edge is twice the resistance when loaded perpendicular to the edge, the anchor spring characteristics for the parallel loading can be determined as shown in *Figure 14.6*.

The behaviour of the anchorage under shear loading in any direction ($-90 \leq \alpha_V \leq 90$) should be then automatically considered through the components of forces carried individually by the decoupled springs in two directions. This method should be, however, verified through experiments on different anchor group configurations, loaded under different loading angles.

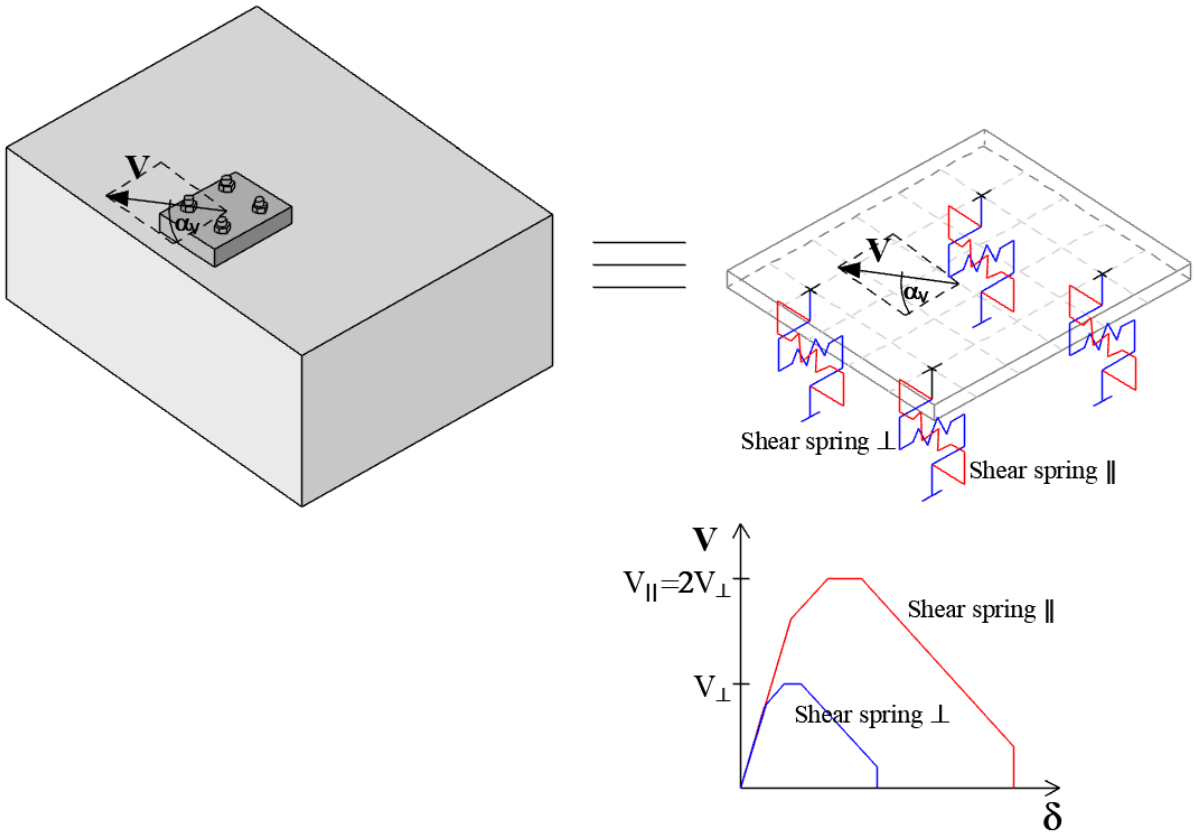

Figure 14.6. Spring model for an anchorage under shear loading – considering different loading angles

14.3 FURTHER POSSIBLE APPLICATIONS OF THE NONLINEAR SPRING MODELLING APPROACH

14.3.1 Anchorages in SFRC

Addition of steel fibres to the concrete mix improves the fracture behaviour of the concrete, and leads to an improved flexural tensile strength, residual flexural tensile strength and post-peak cracking behaviour compared to plain concrete (Balagaru & Shah, 1992, Mechtcherine, 2010, Døssland, 2008). It was shown in Tóth et al. (2019) that in the case of concrete breakout failure modes, with maintaining certain parameter combinations of the anchorage (fibre length, embedment depth, edge distance), the load-displacement behaviour of anchorages is improved if they are installed into steel fibre reinforced concrete (SFRC) compared to normal strength plain concrete (NPC). This is attributed to the crack bridging mechanism of the fibres and due to less brittle concrete breakout failure mode in SFRC. Based on the evaluation of test results on single anchors and anchor groups under tension and shear loads, design recommendations for concrete cone and concrete edge breakout failure modes were developed and are published in the same work. To account for the beneficial effect of the steel fibres on concrete cone or concrete edge resistance of the anchorages in SFRC, an increase factor, γ_{fibre}, was proposed (***Eq. 145***), with which the corresponding concrete cone or concrete edge resistance in plain concrete should be multiplied.

$$\gamma_{fiber} = \frac{k_{fib}}{300} + 1 < 1.25 \qquad \textit{Eq. 145}$$

The factor should be applicable for fibre contents of 30 - 80 kg/m^3 provided that hooked-end type steel fibres that fulfil certain requirements for fibre length (as a function of aggregate size and embedment depth or edge distance) are used and the anchor is approved for use in SFRC. Further details and requirements to apply the factor γ_{fibre} can be taken from Tóth et al. (2019a).

Since the increase factor, γ_{fiber}, might be applied to increase the single anchor resistance, it should be also applicable on the resistance of the individual anchors of an anchor group ($N^i_{Rm,c,SFRC}$ or $V^i_{Rm,c,SFRC}$) and can be used to generate the spring properties (***Eq. 146***). Note that the approach can only be used if the assumed angle of the concrete cone is ca. 33° with the horizontal and the tributary area approach remains valid. Literature results (Nilforoush et al., 2017, Tóth et al., 2019, Vita et al., 2020) show that the angle of the concrete cone is not changing compared to normal plain concrete if the anchor is installed in conventional SFRC and a full concrete breakout body develops.

$$N^i_{Rm,c,SFRC} = N^0_{Rm,c} \cdot \gamma_{fibre} \cdot \frac{A^i_{c,N}}{A^0_{c,N}} \qquad \textit{Eq. 146}$$

To generate the spring properties for the individual anchors of a group (e.g. as shown in *Figure 14.7*), the resistance of the individual anchors should be calculated according to ***Eq. 146***. Literature results (Nilforoush et al., 2017, Tóth et al., 2019a, Vita et al., 2020) show that the initial stiffness of the anchor embedded in SFRC in the case of concrete breakout failure modes (tensile failure of the concrete) can be considered equal to the initial stiffness in the corresponding plain concrete. However, the post-cracking stiffness, the length of the plateau (if any) and

the stiffness of the descending branch might be different for anchors in SFRC compared to NPC depending on the type and amount of fibres. Once the spring properties are generated, the spring model can directly be applied as described in Chapters 5-7. In *Figure 14.7*, a verification of this approach for a group of three anchors installed in SFRC and subjected to eccentric tension load is provided. The concept of the nonlinear spring model extended to SFRC is given in *Figure 14.7a*, and the comparison of test results in terms of load-displacement curves reproduced from Tóth et al. (2019) and obtained from the spring model are shown in *Figure 14.7b*. The preliminary results indicate that the spring model is extendable for anchorages in SFRC. However, the approach should be verified further on anchorages of different configurations, under various loading cases and crack patterns.

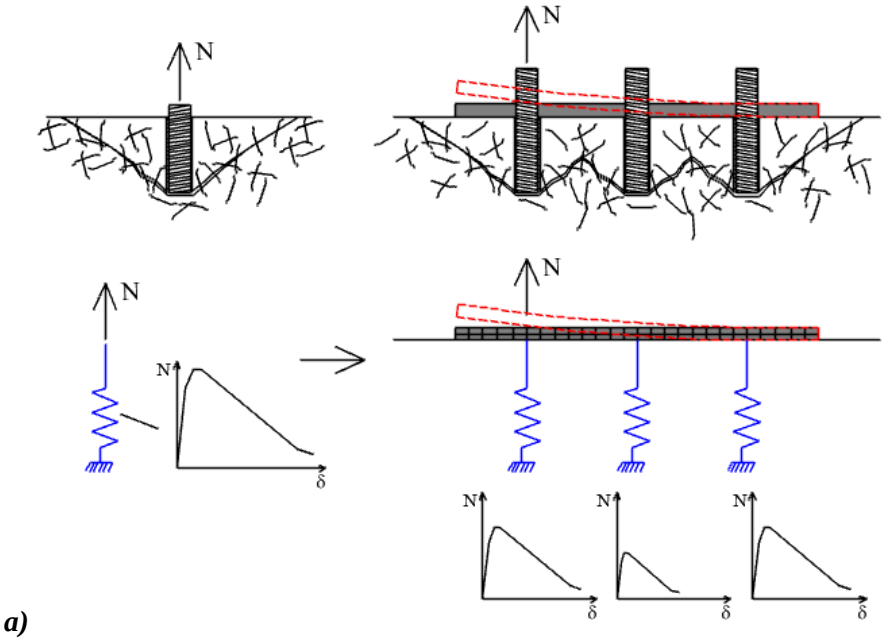

a)

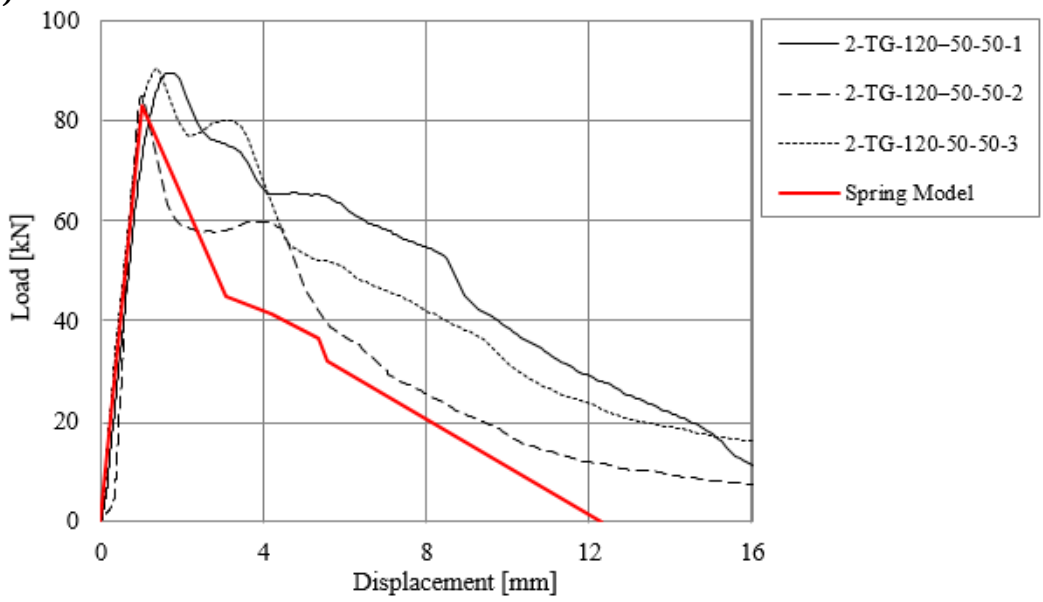

b)

Figure 14.7. a) Spring model for applications in SFRC; b) load-displacement curves reproduced from Tóth et al. (2019) compared with the spring model

14.3.2 Extension of the spring model to seismic applications

Under seismic actions, the anchorages in concrete are subjected to cyclic tension and shear loads and opening and closing of cracks, which intercept the anchors. These cracks open and close depending on the amplitude and frequency of the earthquake and the structural characteristics of the building etc. It is well known that the anchor performance is negatively influenced by the cracks, crack width and by the crack opening and closing (Eligehausen et al., 2006). Therefore, specific testing programs and evaluation requirements are necessary to evaluate the performance of an anchor subjected to seismic actions. For using anchors under seismic conditions, it is required to have design provisions and qualified anchor products with specific prequalification and approval document.

For the application of the spring model for seismic cases, the spring characteristics valid for the estimated crack width under seismic loads need to be used. Additionally, to consider the effect of cyclic loads, a hysteretic rule must be associated with the spring characteristics. One possible approach was demonstrated by Sharma (2013) utilizing the pivot hysteretic model to describe the cyclic load-displacement behaviour of the anchors. Such an approach is necessary, in particular, for the assessment and design of anchorages, which form structural connections. When the structure exceeds its elastic limit, forces acting on the structural connections and thus on the anchors become less important, while the displacement and hysteretic behaviour of the anchors become relevant. For this reason, a performance-based approach is necessary to include in seismic assessment procedure by performing seismic tests on anchors in displacement control (Sharma, 2019). The hysteretic behaviour of the anchorages can be best evaluated based on displacement based tests on anchors under cyclic loads (Stehle & Sharma, 2019).

Once the load-displacement and the hysteretic behaviour of the anchors are available based on results of adequate performance-based testing, the nonlinear seismic springs can be derived, and the nonlinear spring model can be used to calculate the resistance of anchor groups for seismic applications. The concept discussed in Chapters 5, 6, 7 including the modelling of the base plate, modelling of the contact elements, the tributary area approach, the scaling of the idealised curves and the performed nonlinear static analysis might remain the same. An approach for indirect consideration of the influence of opening and closing of cracks is given in Dwenger (2019). However, an extension of the spring model for seismic applications requires a thorough verification against tests on anchorages carried out following displacement based seismic tests.

REFERENCES

American Concrete Institute Committee 318 (ACI) (2002). Building Code Requirements for Structural Concrete (ACI 318-02) and Commentary (ACI 318R-02), American Concrete Institute, Farmington Hills, Michigan

American Concrete Institute, ACI 318-14 (2014) Building Code Requirements for Structural Concrete and Commentary, ACI Committee 318, American Concrete Institute

American Concrete Institute, ACI 318-19 (2019) Building Code Requirements for Structural Concrete and Commentary, ACI Committee 318, American Concrete Institute

American Concrete Institute Committee 349 (ACI) (1980): Code Requirements for Nuclear Safety Related Concrete Structures (ACI 349-85), American Concrete Institute, Farmington Hills, Michigan

American Concrete Institute, ACI Standard 349–90 (1990): Code Requirements for Nuclear Safety Related Concrete Structures, Appendix B – Steel Embedments, American Concrete Institute, Farmington Hills, Michigan

Anderson, N. S.; Meinheit D. F. (2007): A review of headed-stud design criteria in the sixth edition of the PCI design handbook. PCI Journal, V. 52, No. 1, 2007, pp. 2-20. 2007

Anderson, N. S.; Meinheit D. F. (2007): PCI's headed stud design redefined. Structure Magazine, April 2005, pp. 26-29

Appl, J.J. (2009): Tragverhalten von Verbunddübeln unter Zugbelastung, 2009, PhD Thesis, University of Stuttgart, Germany (in German)

Armstrong, K. S.; Klingner, R. E., Steves, M. A. (1985): Response of Highway Barriers to Repeated Impact Loads: Steel Post Barriers, Research Report 382-1, Center for Transportation Research, the University of Texas at Austin, November 1985

Asmus, J. (1999): Verhalten von Befestigungen bei der Versagensart Spalten des Betons. PhD thesis, University of Stuttgart, 1999 (in German)

Bailely, J. W.; Burdette, E.G. (1977): Edge effects on Anchorage to Concrete. Civil Engineering Series No. 31, The University of Tenessee at Knoxville, August, 1977

Bažant, Z. P. (1984): Size Effect in Blunt Fracture: Concrete, Rock, Metal. Journal of Engineering Mechanics, ASCE, 110, No. 4, April 1984, pp. 518–535

Bažant, Z.P.; Oh, B. (1983): Crackband theory of concrete. Matériaux et Construction 1983, Vol. 16, No. 93

Bažant, Z.P.; Lin, F.B. (1988): Nonlocal smeared cracking model for concrete fracture. Journal of Engineering Mechanics, ASCE, 114:2493–2510,

Bede, N.; Grosser, P.; Ožbolt, J. (2018). Shear breakout capacity of various fastening systems in concrete elements. Građevinar. 2018, 69, pp. 1093-1100, 10.14256/JCE.2168.2017

Bode, H.; Hanenkamp, W. (1985): Zur Tragfähigkeit von Kopfbolzen bei Zugbeanspruchung. Bauingenieur,1985, pp. 361–367 (in German).

Bode, H.; Roik, K. (1987): Headed Studs – Embedded In Concrete And Loaded InTension, American Concrete Institute SP 103-4, American Concrete Institute, Farmington Hills, Michigan, pp. 61-88

Bokor, B.; Sharma, A.; Hofmann, J. (2017): On the limitations of the current provisions of PREN 1992-4 for design of anchor groups subjected to tension loads. Proceedings of 3rd International Symposium on Connections between Steel and Concrete, 27th - 29th September 2017, Stuttgart, Germany, pp 118-129

Bokor, B.; Sharma, A.; Hofmann, J. (2018): Experimental Investigations on tension loaded anchor groups of arbitrary configurations. The International Federation for Structural Concrete 5th International fib Congress, Melbourne, Australia 7 – 11 October 2018

Bokor, B.; Sharma, A.; Hofmann, J. (2019/1): Experimental investigations on concrete cone failure of rectangular and nonrectangular anchor groups, Engineering Structures, 188, 2019, pp. 202–217, https://doi.org/10.1016/j.engstruct.2019.03.019

Bokor, B.; Sharma, A.; Hofmann, J. (2019/2): Spring modelling approach for evaluation and design of tension loaded anchor groups in case of concrete cone failure, Engineering Structures 197, 2019: 109414, https://doi.org/10.1016/j.engstruct.2019.109414

Bokor, B.; Sharma, A.; Hofmann, J. (2019/3): Experimental and numerical investigations on the concrete edge failure of anchor groups of arbitrary configurations. 7th International Conference of Euro Asia Civil Engineering Forum 30.09.2019 – 02.10.2019, Stuttgart, Germany EACEF

Bokor, B. (2019): Shear loading tests on single anchors and anchor groups targeting a combined failure. Test report FI489/01-19/20, Institute of Construction Materials, University of Stuttgart, (not published)

Bokor, B.; Sharma, A.; Hofmann, J. (2020): Experimental investigations on the concrete edge failure of shear loaded anchor groups of rectangular and non-rectangular configurations. Engineering Structures, Volume 222, 1 November 2020, 111153, DOI:10.1016/j.engstruct.2020.111153

Bokor, B.; Sharma, A.; Hofmann, J. (2021): Concrete edge failure of anchor groups placed parallel to an edge. ACI Structural Journal, Volume 118, Issue 2, pp. 237-248, DOI: 10.14359/51728193

Braestrup, M. W.; Nielsen, M. P.; Jensen, B. C.; Bach, F. (1976): Axisymmetric punching of plain and reinforced concrete. Report R. 75. Technical University of Denmark. Structural Research Laboratory, Copenhagen

Bui, T.T; Limam, A.W.; Nana, S.A.; Arrieta, B.; Roure T. (2018): Cast-in-place Headed Anchor Groups Under Shear: Experimental and Numerical Modelling. Structures, 2018; 14, pp 178-196, https://doi.org/10.1016/j.istruc.2018.03.008

Cervenka, V.; Pukl, R.: Eligehausen, R. (1990): Computer Simulation of Anchoring Technique in Reinforced Concrete Beams. In Bicanic, N., Mang, H. (Editor): Computer Aided Analysis and Design of Concrete Structures, Pineridge Press, Swansea, 1990, pp. 1–19

Cannon, R. W.; Godfrey, D. A.; Moreadith, F. L. (1981): Guide to the Design of Anchor Bolts and Other Steel Embedments, Concrete International, Vol. 3, No. 7, pp. 28-41

Cannon, R. W. (1995): Straight Talk About Anchorage to Concrete – Part I, ACI Structural Journal, Vol. 92, No. 6, pp. 581-586.

Cook, R.A. (1989): Behavior and design of ductile multiple-anchor steel-to-concrete connections. Phd Thesis, The University of Texas at Austin, USA

Cook, R.A., Klingner, R.E. (1992): Ductile Multiple-Anchor Steel-to-Concrete Connections. Journal of Structural Engineering, ASCE, 1992, V. 118, No. 6, pp. 1645-1665

Courtois, P. (1969): Industrial Research on Connections for Precast and in Situ Concrete," American Concrete Institute SP-22, Paper SP 22-10, American Concrete Institute, Farmington Hills, Michigan, pp. 123-188

Cruz, R.D. (1987): Effect of Edge Distance on Stud Groups Loaded in Shear and Torsion. Stillwater, Oklahoma State University, School of Civil and Environmental Engineering, Master Thesis, 1987

DIN EN 12390-1:2012-12 Prüfung von Festbeton – Teil 1: Form, Maße und andere Anforderungen für Probekörper und Formen; Deutsche Fassung EN 12390-1:2012. (in German)

Di Nunzio, G.; Muciaccia, G. (2019): Safety reduction in anchor groups due to uneven crack distribution. IOP Conference Series: Materials Science and Engineering. 615. 012087. 10.1088/1757-899X/615/1/012087

Dwenger, F. (2019): Einfluss des Tragverhaltens von Dübelbefestigungen auf die Bauwerk-Komponenten-Wechselwirkungen bei Erdbebenbeanspruchung, PhD Thesis, University of Stuttgart, Germany (in German)

Dwenger, F.; Kerkhof, K.; Mahadik, V.; Sharma, A. (2016): Numerical studies describing the interactions of the coupled system "building-post installed anchor-piping" at seismic loading. 27th International Conference on Noise and Vibration engineering - ISMA2016, Leuven, Belgium, September 2016

Elfgren, L.; Ohlsson, U.; Gylltoft, K. (1989): Anchor Bolts Analysed with Fracture Mechanics. Fracture of Concrete and Rock 10.1007/978-1-4612-3578-1_27.

Eligehausen, R.; Fuchs, W. (1988): Tragverhalten von Dübelbefestigungen unter Querzug-, Schrägzug- und Biegezugbeanspruchung. Beton + Fertigteil-Technik, 1988, No. 2, pp. 48–56 (in German)

Eligehausen, R.; Sawade, G. (1989): A Fracture Mechanics based Description of the Pull-Out Behaviour of headed Studs embedded in Concrete. Fracture Mechanics of Concrete Structures. From Theory to Applications. Editors: Elfgren, L., Chapman and Hall, London, New York, 1989, pp. 281–299

Eligehausen, R. (1990): Bemessung von Befestigungen in Beton mit Teilsicherheitsbeiwerten (Design of fastenings to concrete with partial safety factors). Bauingenieur 65,1990, pp. 295–305 (in German)

Eligehausen, R.; Pusill-Wachtsmuth, P. (1982): Stand der Befestigungstechnik im Stahlbetonbau. IVBH Report S-19/82, IVBH-Periodica 1/1982, February 1982 (in German).

Eligehausen, R.; Ožbolt, J. (1990): Size effect in anchorage behavior. Proceedings, ECF8, Fracture Behavior and Design of Materials and Structures, Turin, October 1990.

Eligehausen, R.; Bouska; P.; Cervenka; V.; Pukl; R. (1992): Size Effect of the Concrete Cone Failure Load of Anchor Bolts. In: Bazant, Z. P. (Editor), Fracture Mechanics of Concrete Structures, pp. 517–525, Elsevier Applied Science, London, New York

Eligehausen, R.; Fuchs, W.; Ick, U.; Mallée, R.; Reuter, M.; Schimmelpfennig, K.; Schmal, B. (1992): Tragverhalten von Kopfbolzenverankerungen bei zentrischer Zugbeanspruchung. Bauingenieur 67, pp. 183–196 (in German)

Eligehausen, R.; Okelo, R. (1996): Design of group fastenings for pull-out or pull-through failure modes of the individual anchors of a group. Report No. 18/1-96/20, Institut für Werkstoffe im Bauwesen, Universität Stuttgart, 1996, not published

Eligehausen, R.; Mallée, R.; Rehm, G. (1997): Befestigungstechnik. Betonkalender 1997, Part II, Ernst & Sohn, 1997, pp. 609–753 (in German)

Eligehausen, R.; Hofmann, J. (2003): Experimentelle und numerische Untersuchungen an Befestigungen am Bauteilrand unter Querlast Report, Institut für Werkstoffe im Bauwesen, Universität Stuttgart, for the Deutsche Forschungsgemeinschaft, (in German).

Eligehausen, R., Mallée, R., Silva J.F. (2006) Anchorage in Concrete Construction. Berlin: Ernst & Sohn, 2006, ISBN-13: 978-3-433-01143-0

Eligehausen, R.; Sharma, A. (2014): Seismic safety of anchorages in concrete construction – the latest perspective, 2nd European conference on earthquake engineering and seismology, Istanbul, 24-29 August, 2014

EN 1990: Eurocode 0 Basis of structural design, European committee for standardization, Brussels, EN 1990:2002

EN 1992-1-1 Eurocode 2 Design of concrete structures - Part 1-1 General rules and rules for buildings, European committee for standardization, Brussels, EN1992-1-1:2004

EN 1992-4 Eurocode 2 Design of concrete structures - Part 4 Design of fastenings for use in concrete, European committee for standardization, Brussels, July 2018 EN 1992-4:2018

EN 206:2014-07 Beton – Festlegung, Eigenschaften, Herstellung und Konformität; Deutsche Fassung EN 206:2013 (in German)

Epackachi, S.; Esmaili, O.; Mirghaderi, S.R.; Behbahani, A.A.T. (2015): Behavior of adhesive bonded anchors under tension and shear loads. Journal of Constructional Steel Research, 2015 Vol. 114, pp 269-280, https://doi.org/10.1016/j.jcsr.2015.07.022

ETAG 001 Guideline for European Technical Approval of Metal Anchors for Use in Concrete. Edition 1997, Annex A: Details of tests, Brussels, EOTA, 3rd Amended April 2013.

Fédération Internationale du Béton: Design of Anchorages in Concrete: Part I-V. Lausanne: International Federation for Structural Concrete (fib), 2011. (fib Bulletin 58)

Fichtner, S. (2011): Untersuchungen zum Tragverhalten von Gruppenbefestigungen unter Berücksichtigung der Ankerplattendicke und einer Mörtelschicht", PhD Thesis, University of Stuttgart, Germany, 2011, (in German)

Fuchs, W.; Eligehausen, R. (1986/1): Tragverhalten und Bemessung von Befestigungen ohne Randeinfluß unter Querzugbelastung. Report No. 10/8-86/12, Institut für Werkstoffe im Bauwesen, Universität Stuttgart, October 1986, not published (in German)

Fuchs, W.; Eligehausen, R. (1986/2): Tragverhalten und Bemessung von auf Querzug beanspruchten Dübelbefestigungen mit Randeinfluß im ungerissenen Beton. Report No. 10/9-86/13, Institut für Werkstoffe im Bauwesen, Universität Stuttgart, October 1986, not published (in German)

Fuchs, W.; Eligehausen, R. (1986): Tragverhalten von Dübeln bei Querzug-, Schrägzug- und Biegebeanspruchung: Auswertung von Querzugversuchen an Einzel- und Mehrfachbefestigungen. Stuttgart, University of Stuttgart, Institute of Construction Materials, 1986, Report No. 10/7 - 86/4, not published (in German)

Fuchs, W.; Eligehausen, R. (1989): Tragverhalten von Befestigungsmitteln im gerissenen Beton bei Querzugbeanspruchung. Report No. 1/41-89/15, Institut für Werkstoffe im Bauwesen, Universität Stuttgart, July 1989, not published (in German)

Fuchs, W. (1990): Tragverhalten von Befestigungen unter Querlast in ungerissenem Beton. Stuttgart, University of Stuttgart, Dissertation, 1990 (in German)

Fuchs, W.; Eligehausen, R.; Breen, J. E. (1995): Concrete Capacity Design (CCD) Approach for Fastening to Concrete. ACI Structural Journal, Vol. 92 (1995), No. 1, pp. 73–94

Furche, J.; Eligehausen, R. (1991): Lateral Blowout Failure of Headed Studs Near the Free Edge. In: Senkiw, G. A.; Lancelot, H. B. (Editor), SP-130, Anchors in Concrete, Design and Behaviour. American Concrete Institute, Detroit, 1991, pp. 235–252

Furche, J. (1994): Zum Trag- und Verschiebungsverhalten von Kopfbolzen bei zentrischem Zug. PhD thesis, University of Stuttgart, 1994

Grosser, P.; Cook, R. (2009): Load-bearing Behavior of Anchor Groups Arranged Perpen-dicular to the Edge and Loaded by Shear Towards the Free Edge. Florida, USA: Department of Civil and Coastal Engineering, University of Florida, UF Structures Report 2009-1, 2009.

Grosser, P. (2012): Load-bearing behavior and design of anchorages subjected to shear and torsion loading in uncracked concrete, PhD Thesis, University of Stuttgart, Stuttgart, Germany, July 2012.

Hofmann, J. (2005): Tragverhalten und Bemessung von Befestigungen unter beliebiger Querbelastung in ungerissenem Beton Stuttgart, University of Stuttgart, Dissertation, 2005, (in German)

Hofmann, J.; Mahadik, V.; Sharma, A. (2015): Modelling structure-anchor-component interaction for nuclear safety related structures under seismic loads – part 2: development of numerical model. Transactions, SMiRT-23, August 10-14, 2015, Manchester, United Kingdom

Hofmann, J.; Dwenger, F.; Sharma, A.; Kerkhof, K. (2020): Verschiebungsverhalten von Hinterschnittdübeln unter Zuglast bei Rissöffnen und -schließen: Vergleich von Einzeldübelversuchen und großmaßstäblichen Erdbebenversuchen. Beton- und Stahlbetonbau, 115. 54-61. 10.1002/best.201900044

Jebara, K.; Ožbolt, J.; Sharma, A. (2019): Pryout capacity of headed stud anchor groups with stiff base plate: 3D finite element analysis. Structural Concrete, Volume 21, Issue3, June 2020, pp. 905-916, 10.1002/suco.201900241

Karihaloo, Bhushan L. (1995): Fracture Mechanics and Structural Concrete (Concrete Design and Construction Series) Longman Pub Group, 1995, ISBN 10: 058221582X

Klingner, R.; Mendonca, J.; Malik, J. (1982): Effect of Reinforcing Details on the Shear Resistance of Anchor Bolts under Reversed Cyclic Loading, Journal of the American Concrete Institute, V. 79, No. 1, Jan.-Feb., pp. 3-12

Kunz, J.; Cook, R. A.; Fuchs, W.; Spieth, H. (1998): Tragverhalten und Bemessung von chemischen Befestigungen. Beton- und Stahlbetonbau, 93,1998, No. 1

Lachinger, S. (2012): Randnahe Mehrfachbefestigungen Unter Kombinierter Belastung. PhD Thesis, 2012, BOKU Vienna, Austria, (in German)

Lachinger, S.; Bergmeister, K. (2014): Randnahe Mehrfachbefestigungen unter kombinierter Belastung. Beton- und Stahlbetonbau. Volume109, Issue5, May 2014, pp. 334-343, 109. 10.1002/best.201300091

Lehr, B.; Eligehausen, R. (1998): Vorschlag eines Bemessungskonzeptes für Vebundanker. Report No. 20/25-98/6, Institut für Werkstoffe im Bauwesen, Universität Stuttgart, 1998, not published (in German).

Li, L. (2017): Required Thickness of Flexurally Rigid Baseplate for Anchor Fastenings. Proceedings of the 2017 fib Symposium, Maastricht, The Netherlands, June 12-14, 2017

McMakin, P. J.; Slutter, R. G.; Fisher, J. W. (1973): Headed Steel Anchor Under Combined Loading, Engineering Journal, AISC, Second Quarter, pp.43-52

Mahrenholtz, P. (2011): Anchor ductility – Development of ductility parameters and evaluation of database. HS III/08-11/02, Report, Institute of Construction Materials, University of Stuttgart, not published

Mahrenholtz, P. (2013) Experimental performance and recommendations for qualification of post-installed anchors for seismic applications, 2013. (IWB-Mitteilungen; 2013,1), PhD Thesis, University of Stuttgart, Germany

Mallée, R. (2004/1): Bericht über Versuche mit Ankerplatten mit exzentrisch aufgeschweißtem Profil unter exzentrischer Druckbeanspruchung, Report, fischerwerke, April 2004, not published (in German)

Mallée, R. (2004/2): Versuche mit Ankerplatten und unterschiedlichen Dübeln, Report, fischerwerke, April 2004, not published (in German)

Marsh, M.L.; Burdette, E.G. (1985): Multiple anchorages: Method for Determining the Effective Projected Area of Overlapping Stress Cones, Engineering Journal, AISC, Vol 22.; No. 1, 1985

Mayer, B.; Eligehausen, R. (1984): Ankergruppen mit Dübeln in der Betonzugzone. In: Werkstoffe und Konstruktion. Institut für Werkstoffe im Bauwesen, Universität Stuttgart and Forschungs- und Materialprüfungsanstalt Baden-Württemberg, October 1984, pp. 167–180 (in German)

Meszaros, J. (1999): Tragverhalten von Verbunddübeln im ungerissenen und gerissenen Beton. PhD thesis, Universität Stuttgart, 1999 (in German)

Morgan, R. T. (2018): Base Plate Design for Post-Installed Anchors. Structural Design, Structure Magazine, September 2018

Nilforoush, R. (2017): Anchorage in Concrete Structures: Numerical and Experimental Evaluations of Load-Carrying Capacity of Cast-in-Place Headed Anchors and Post-Installed Adhesive Anchors. Doctoral thesis, Luleå University of Technology, Sweden

Nilforoush, R.; Nilsson, M.; Elfgren, L. (2017): Experimental evaluation of tensile behaviour of single cast-in-place anchor bolts in plain and steel fibre-reinforced normal- and high-strength concrete. Engineering Structures, Vol. 147. pp. 195-206, 10.1016/j.engstruct.2017.05.062

Nilson, A.H. (1968): Nonlinear Analysis of Reinforced Concrete by the Finite Element Method. Journal of ACI, 65(9), pp. 757-766

Ngo, D.; Scordelis, A. C. (1967): Finite Element Analysis of Reinforced Concrete Beams,"ACI Journal, Vol. 64, 1967, pp. 152-163

Okelo, R. (1996): The influence of the scatter of the load-displacement curves of individual anchors on the bearing capacity of a quadruple anchor group. Report No. 20/29-96/34. IWB, University of Stuttgart

Oktavianus, Y.; Chang, H.; Goldsworthy, H.;Gad, E. (2017): Component model for pull-out behaviour of headed anchored blind bolt within concrete filled circular hollow section. Engineering Structures. 148. 210-224. 10.1016/j.engstruct.2017.06.056

Ožbolt, J.; Eligehausen, R. (1990): Numerical Analysis of headed studs embedded in large plain concrete blocks. In: Bicanic, N.; Mang, H. Computer Aided Analysis and Design of Concrete Structures. Pinerdige Press, London, 1990

Ožbolt, J. (1995): Maßstabseffekt und Duktilität von Beton- und Stahlbetonkonstruktionen). Thesis - Habilitation, Universität Stuttgart, 1995, published in: Mitteilungen des IWB, No. 1995/2 (in German)

Ožbolt, J.; Tonkovic, Z.; Lackovic, L. (2015): Microplane Model for Steel and Application on Static and Dynamic Fracture. Journal of Engineering Mechanics. 142. 04015086. 10.1061/(ASCE)EM.1943-7889.0000993

Pallares, L.; Hajjar, J. F. (2009): Headed Steel Stud Anchors in Composite Structures: Part II - Tension and Interaction. Newmark Structural Engineering Laboratory Report Series 014, Newmark Structural Engineering Laboratory. University of Illinois at Urbana-Champaign., ISSN:1940-9826, 2009-04-24

Paschen, H.; Schönhoff, T. (1983): Untersuchungen über in Beton eingelassene Scherbolzen aus Betonstahl. Schriftenreihe des Deutschen Ausschusses für Stahlbeton, No. 346, Ernst & Sohn, Berlin, 1983 (in German)

Periškić, G. (2006): Einzel- und Zweifachbefestigungen mit Verbunddübel senkrecht zum Rand unter Querlast zum Rand im ungerissenen Beton, Report No. E06/01-E01301/1, University of Stuttgart, Stuttgart, 2006 (in German)

Periskic, G (2009): Numerical investigations of multiple anchors connected by a common, rigid plate (flexible or hinged) with anchor spacing s ≥ scr under seismic loading conditions, Research Report, Institute of Construction Materials, University of Stuttgart

Pregartner, T. (2009): Bemessung von Befestigungen in Beton Einführung mit Beispielen, Berlin, Germany: Ernst & Sohn, 2009

Pusill-Wachtsmuth, P. (1982): Tragverhalten von Metallspreizdübeln unter zentrischer Zugbeanspruchung bei den Versagensarten Betonausbruch und Spalten des Betons. PhD thesis, Universität Stuttgart, 1982 (in German)

Rashid, Y: R. (1968): Analysis of prestressed concrete pressure vessels. Nuclear Engineering and Design, 7(4), 334-344

Rehm, G.; Eligehausen, R.; Mallée, R. (1988): Befestigungstechnik. Betonkalender 1988, Part II, Ernst & Sohn, Berlin, 1988, pp. 569–663 (in German)

Rehm, G.; Eligehausen, R.; Mallée, R. (1992): Befestigungstechnik. Betonkalender 1992, Part II, Ernst & Sohn, Berlin, 1992, pp. 597–715 (in German)

Riemann, H. (1985): Das "erweiterte κ-Verfahren" für Befestigungsmittel, Bemessung an Beispielen von Kopfbolzenverankerungen. Betonwerk + Fertigteil-Technik, 1985, No. 12, pp. 808–815 (in German)

Ruopp, J.; Kuhlmann, U. (2017) Steel-to-Concrete joints with large anchor plates under shear loading. Proceedings 3rd International Symposium on Connections between Steel and Concrete, Stuttgart, Germany 27th - 29th September 2017

Ruopp, J.; Kuhlmann, U. (2017): Steel-to-Concrete joints with large anchor plates under shear loading. Steel Construction, 2017, 10, pp. 115-124, DOI: 10.1002/stco.201710015

Ruta, D. (2018) Numerical and experimental study of concrete structures exposed to impact and fire, PhD Thesis, 2018, University of Stuttgart, Stuttgart, Germany

Scheer, J.; Peil, U.; Nölle, P. (1987): Schrauben mit planmäßiger Biegebeanspruchung. Report 366 References No. 6079, Institut für Stahlbau, TU Braunschweig, 1987 (in German)

Schmid, K. (2010): Tragverhalten und Bemessung von Befestigungen am Bauteilrand mit Rückhängebewehrung unter Querlasten rechtwenklig zum Rand, PhD Thesis, 2010, University of Stuttgart (in German)

Sharma, A. (2013): Seismic Behavior and Retrofitting of RC Frame Structures with Emphasis on Beam-Column Joints – Experiments and Numerical Modeling. PhD Thesis, University of Stuttgart, Germany, 2013

Sharma, A.; Eligehausen, R.; Hofmann J. (2014): Numerical modeling of joints retrofitted with haunch retrofit solution. ACI Structural Journal, 2014; 111(4), pp 861-872

Sharma, A.; Bosnjak, J.; Ožbolt, J.; Hofmann, J. (2016): Numerical modeling of reinforcement pull-out and cover splitting in fire-exposed beam-end specimens. Engineering Structures, 111. pp. 217-232. 10.1016/j.engstruct.2015.12.017.

Sharma, A. (2017): Performance based approach for anchorage in concrete construction. Proceedings of 3rd International Symposium on Connections between Steel and Concrete, 27th-29th September 2017, Stuttgart, Germany, pp 663-673

Sharma, A.; Eligehausen, R.; Asmus, J. (2017): Experimental investigation of concrete edge failure of multiple-row anchorages with supplementary reinforcement. Structural Concrete 2017, 18, pp 153–163, https://doi.org/10.1002/suco.201600015

Sharma, A. (2019): Urgent Need for a Performance-Based Approach for Seismic Assessment and Design of Fastenings Used in Structural Applications. Advancements in Civil Engineering & Technology. 3. 10.31031/ACET.2019.03.000555

Sharma, A; Eligehausen, R.; Asmus, J; Bujnak, J. (2019): Anchorages with supplementary reinforcement under tension, shear and interaction loads – experimental database, fib symposium 2019, Concrete – Innovations in materials, design and structures, May 27-29, 2019, Krakow, Poland

Siddiqui, M.A.; Beseler, J.W. (1989): Computing Concrete Pullout Strength, Concrete International, 1989

Sippel, T.; Ignatiadis, A. (2017): Design of Fastenings for use in Concrete Construction: NEW EN 1992-4 – Current status, Commentary and background. Proceedings of 3rd International Symposium on Connections between Steel and Concrete, 27th-29th September 2017, Stuttgart, Germany, pp 40-46

Stichting Bouwresearch (1971): Uit beton stekende ankers. Report of the Studienkommission B 7, No. 29, 1971

Stork, J. (1998): Zur Berechnung von Dübel-Mehrfachbefestigungen unter Zugbelastung bei Versagen durch Betonausbruch, PhD Thesis, Darmstadt: 1998

Swirsky R.A.; Dusel, J.P.; Crozier W.F.; Stoker, J.R.; Nordlin, E.F. (1977): Lateral Resistance of Anchor Bolts Installed in Concrete, Report No. FHWA-CA-ST-4167-77-12, California Department of Transportation, Sacramento, May 1977

Tian, K. (2019) Concrete failure of headed stud fasteners exposed to fire and loaded in shear: experimental and numerical study. PhD Thesis, 2019, University of Stuttgart, Stuttgart, Germany

Tóth, M.; Bokor, B.; Sharma, A. (2019): Anchorage in steel fiber reinforced concrete – concept, experimental evidence and design recommendations for concrete cone and concrete edge breakout failure modes. Engineering Structures 2019, 181, pp 60-75, DOI:10.1016/j.engstruct.2018.12.007

Tóth, M. (2020): Fatigue Behaviour of Fasteners: Numerical and Experimental Investigations on the Concrete Cone Failure Mode PhD Thesis, 2020, University of Stuttgart, Stuttgart, Germany

Tóth, M.; Bokor, B.; Sharma, A. (2020): Numerical study on closely spaced anchor groups of identical configurations under centric tension loading, Engineering Structures 2020, Accepted 21.08.2020

Trautner, C.; Hutchinson, T., Piccinin, R. (2017): An automated pre- and post-processor for the analysis of steel column baseplate connections. Proceedings of 3rd International Symposium on Connections between Steel and Concrete, 27th-29th September 2017, Stuttgart, Germany pp 1201-1212

Trautner, C.; Hutchinson, T. (2018): Parametric Finite-Element Modeling for Exposed Steel Moment Frame Column Baseplate Connections Subjected to Lateral Loads. Journal of Structural Engineering, 2018, 144(6): 04018049

Unterweger, A. (2008): Randnahe Anker unter Querlast: mechanische Modellierung und Bemessung, PhD Thesis, Vienna, Austria Universität für Bodenkultur, 2008 (in German)

Unterweger, A.; Spyridis, P.; Mihala, R.; Bergmeister, K. (2008): Shear Loaded Quadruple Fastenings Close to edge - Experimental and Numerical Analysis. Beton- und Stahlbetonbau 2008, 1013 Heft 11, pp. 741-747. https://doi.org/10.1002/best.200800644

Vintzeleou, E.; Eligehausen, R. (1991): Behavior of fasteners under monotonic or cyclic shear displacements. In: Senkiw, G.A.; Lancelot, H.B. (Editor): SP-130 "Anchors in Concrete – Design and Behaviour". American Concrete Institute, Detroit, 1991, pp. 181–204

Wald, F.; Sokol, Z.; Jaspart, J. P. (2008a): Base plate in bending and anchor bolts in tension. Heron, 53 (1/2), pp. 21-50, 2008

Wald, F.; Sokol, Z.; Steenhuis, M.; Jaspart, J. P. (2008b): Component method for steel column bases. Heron, 53(1/2), pp. 3-20. 2008

Wong, T.L.; Donahey, R.C.; Lloyd, J.P. (1988): Stud Groups Loaded in Shear Near a Free Edge. Stillwater: Oklahoma State University, Draft Paper, to be submitted to PCI in 1998

Zhao, G.; Fuchs, W.; Eligehausen, R. (1989): Einfluß der Bauteildicke auf das Tragverhalten von Dübelbefestigungen im ungerissenen Beton unter Querzugbeanspruchung. Report No. 10/12A-89/5, Institut für Werkstoffe im Bauwesen, Universität Stuttgart, March 1989, not published (in German).

Zhao, G.; Eligehausen, R. (1992): Tragfähigkeit von Befestigungen unter kombinierter 370 References Zug- und Querlast. Report No. 10/17-92/2, Institut für Werkstoffe im Bauwesen, Universität Stuttgart, 1992, not published, (in German)

Zhao, G.; Eligehausen, R. (1992/2): Vorschläge zur Modifikation des CC-Verfahrens Report No. 12/20-92/11, Institut für Werkstoffe im Bauwesen, Universität Stuttgart, 1992, not published (in German)

Zhao, G. (1993): Tragverhalten von randfernen Kopfbolzenverankerungen bei Betonbruch, PhD Thesis, University of Stuttgart, Stuttgart, Germany, 1993

APPENDIX A

CONCRETE SPECIMENS USED FOR TENSION LOADING TESTS

Concrete specimen for tests in uncracked concrete far from edge:

Specimen I.

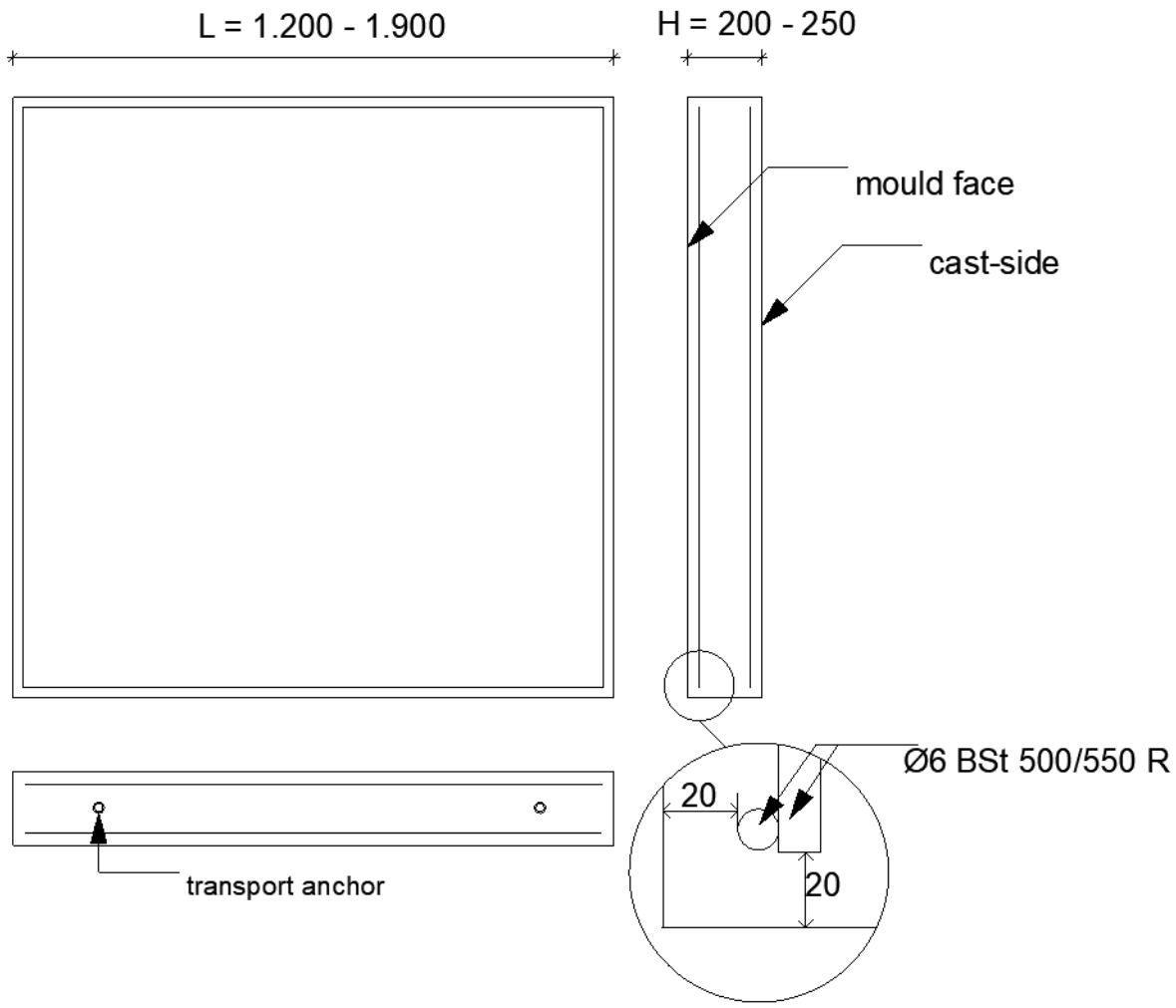

Concrete specimen for tests in uncracked concrete close to concrete edge:

Specimen II.

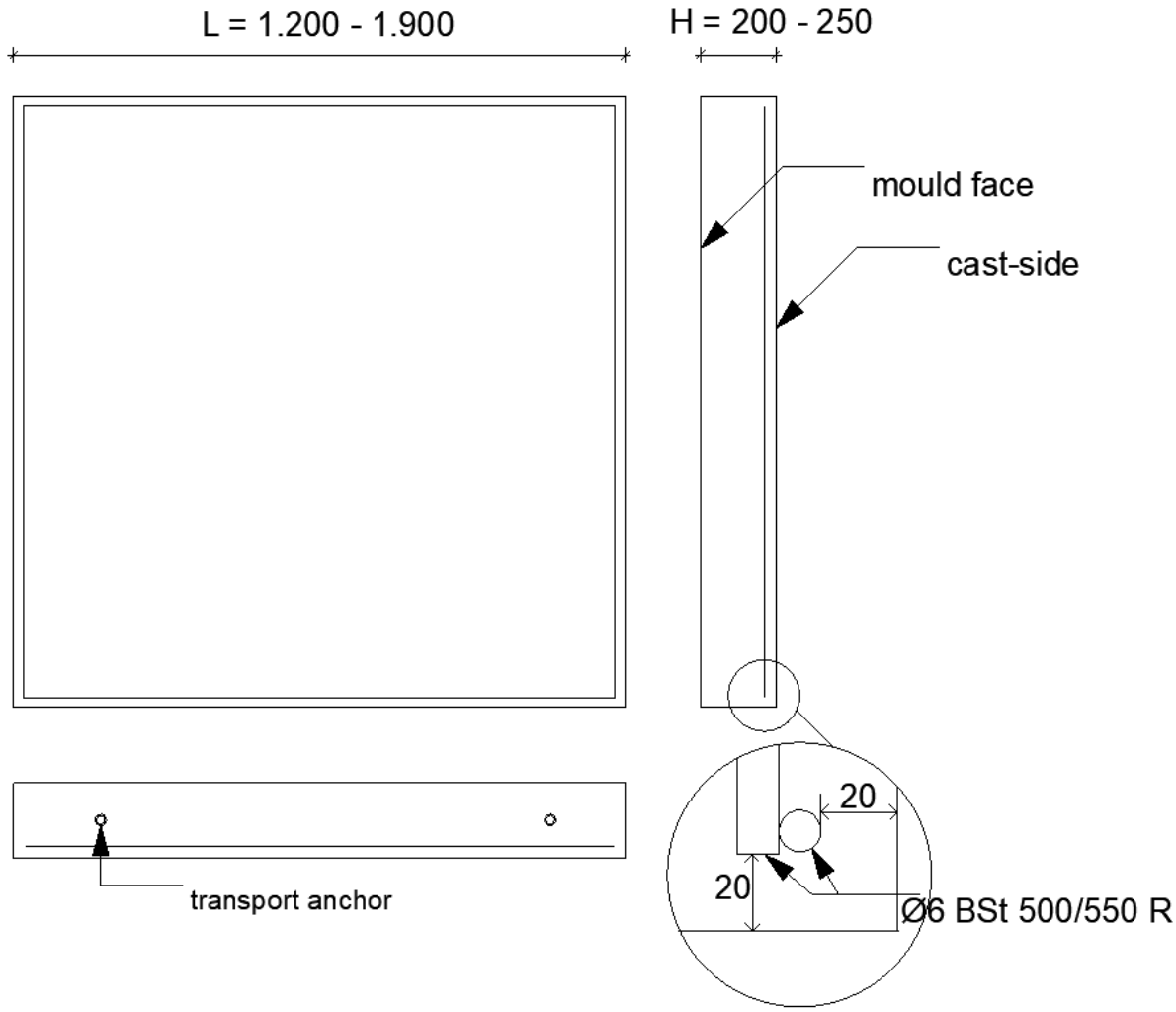

Concrete specimen for tests in cracked concrete:

Specimen III.

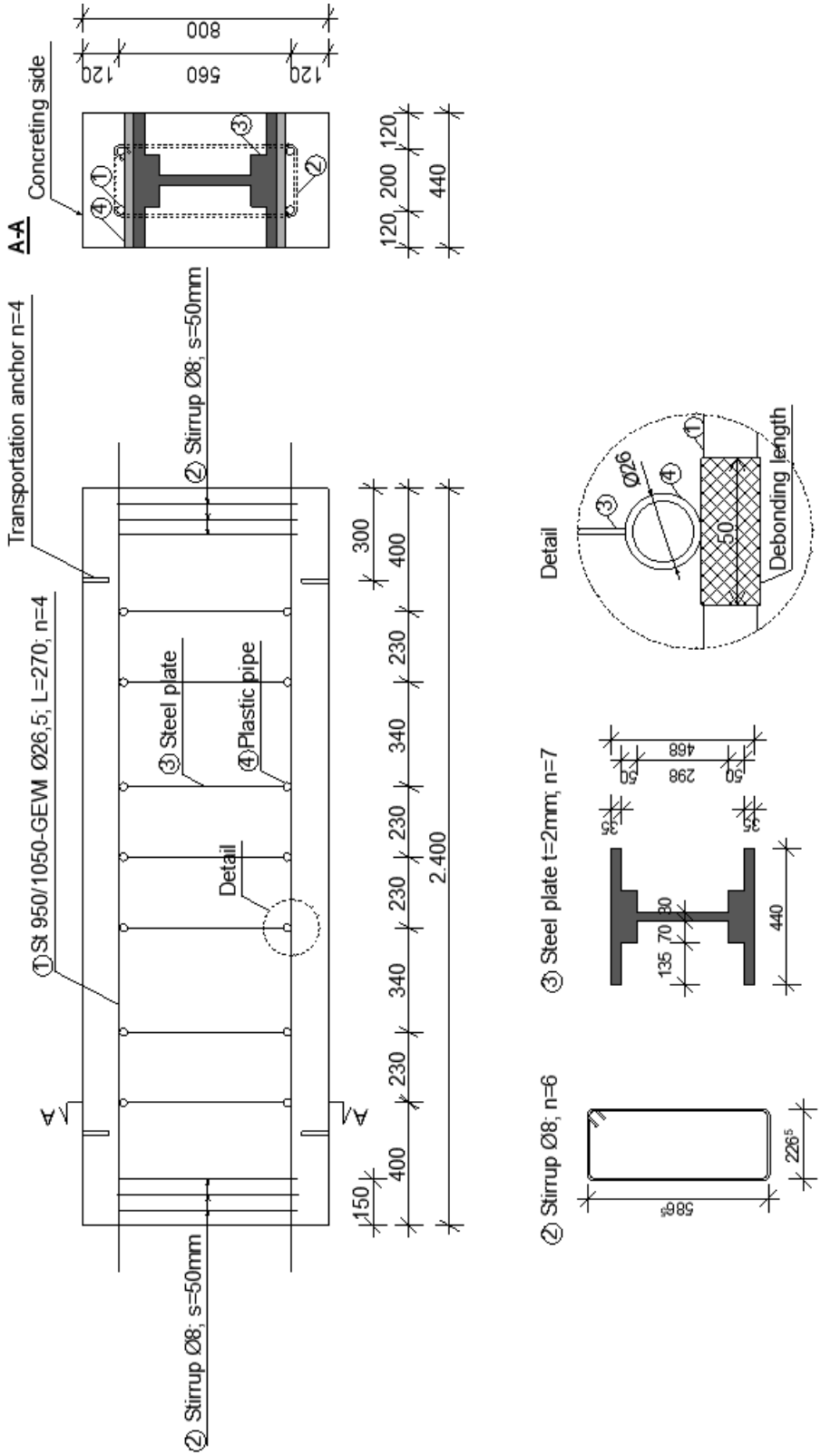

APPENDIX B

CONCRETE SPECIMENS USED FOR SHEAR LOADING TESTS

Concrete specimens for tests in uncracked concrete:

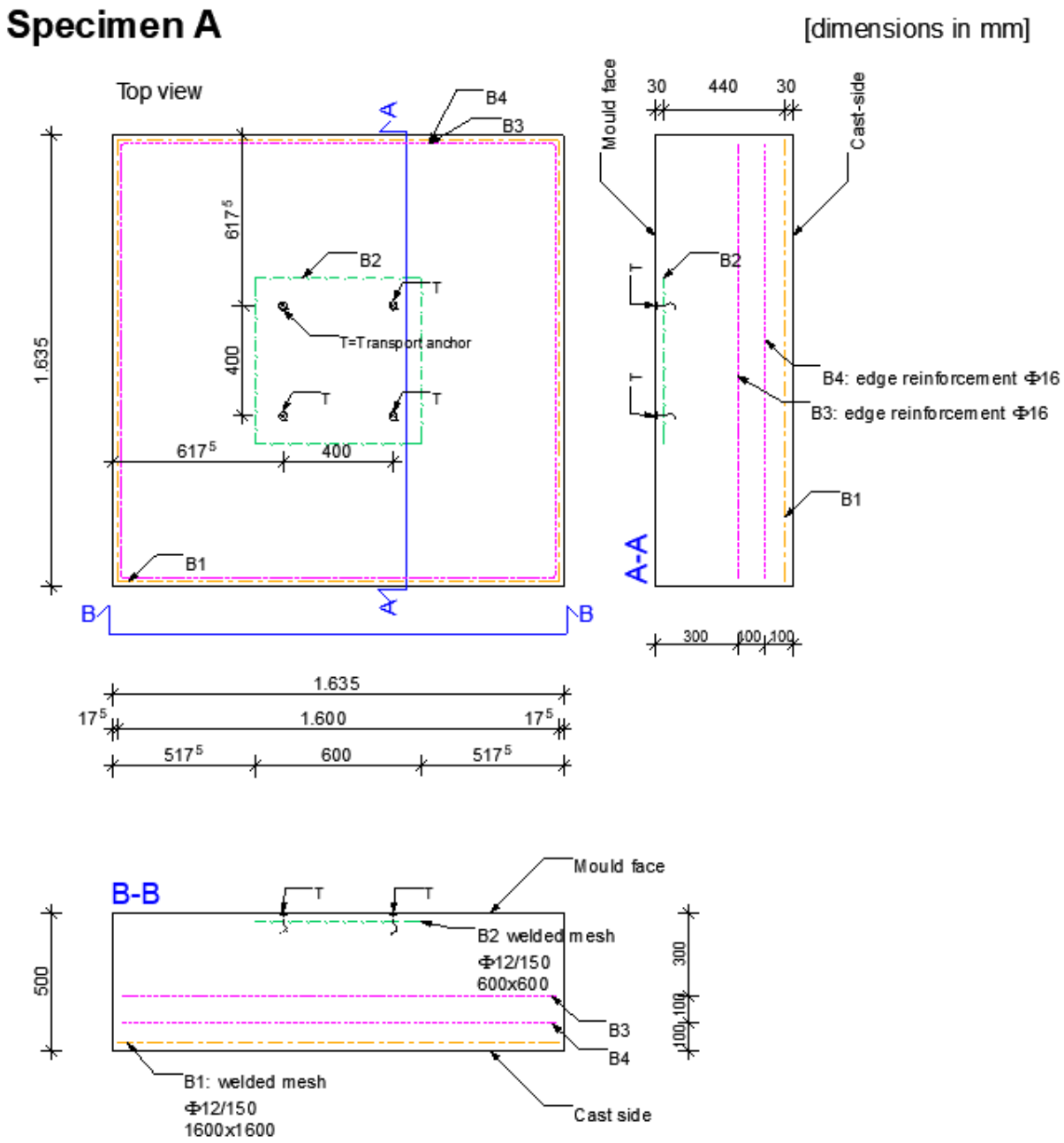

Specimen B

[dimensions in mm]

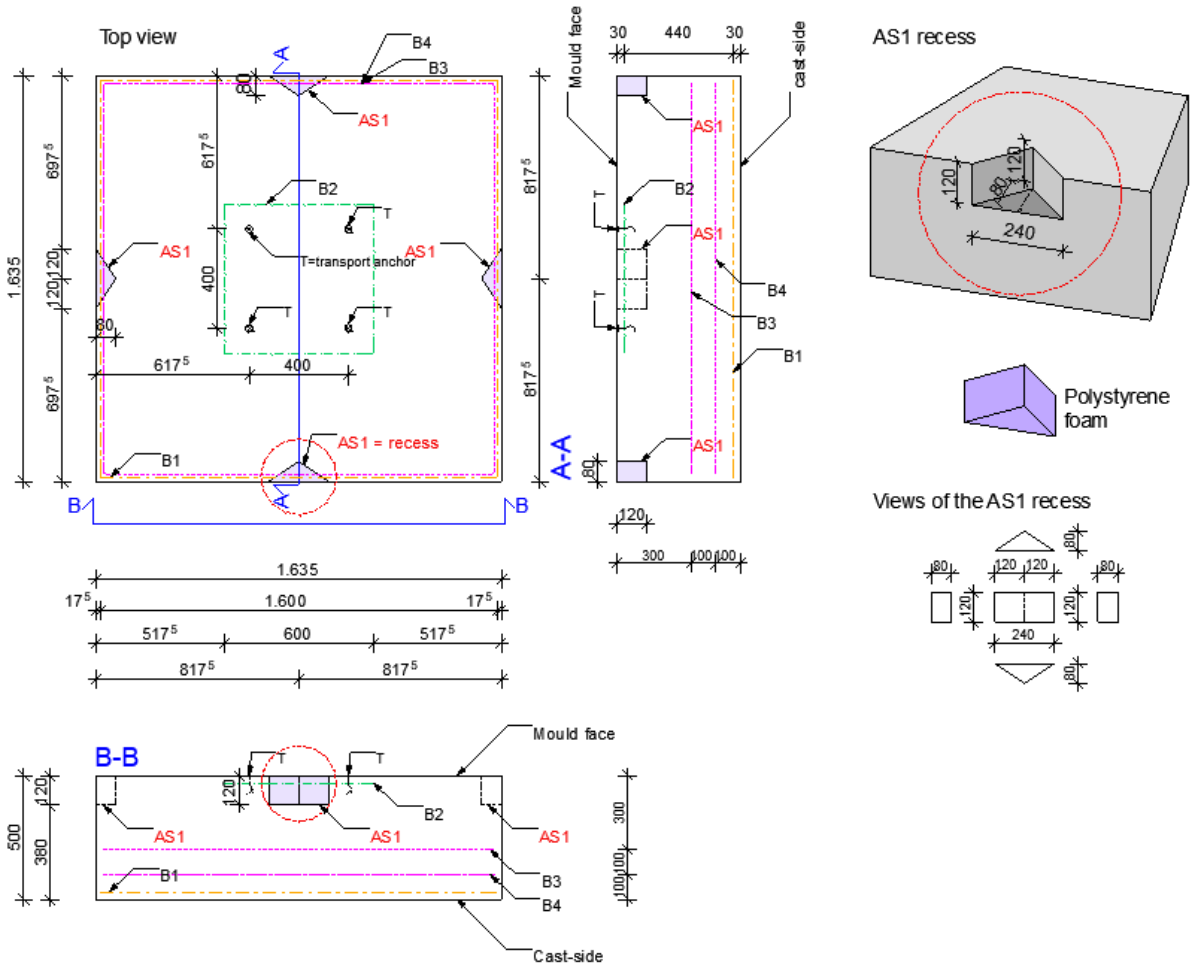

Specimen C

[dimensions in mm]

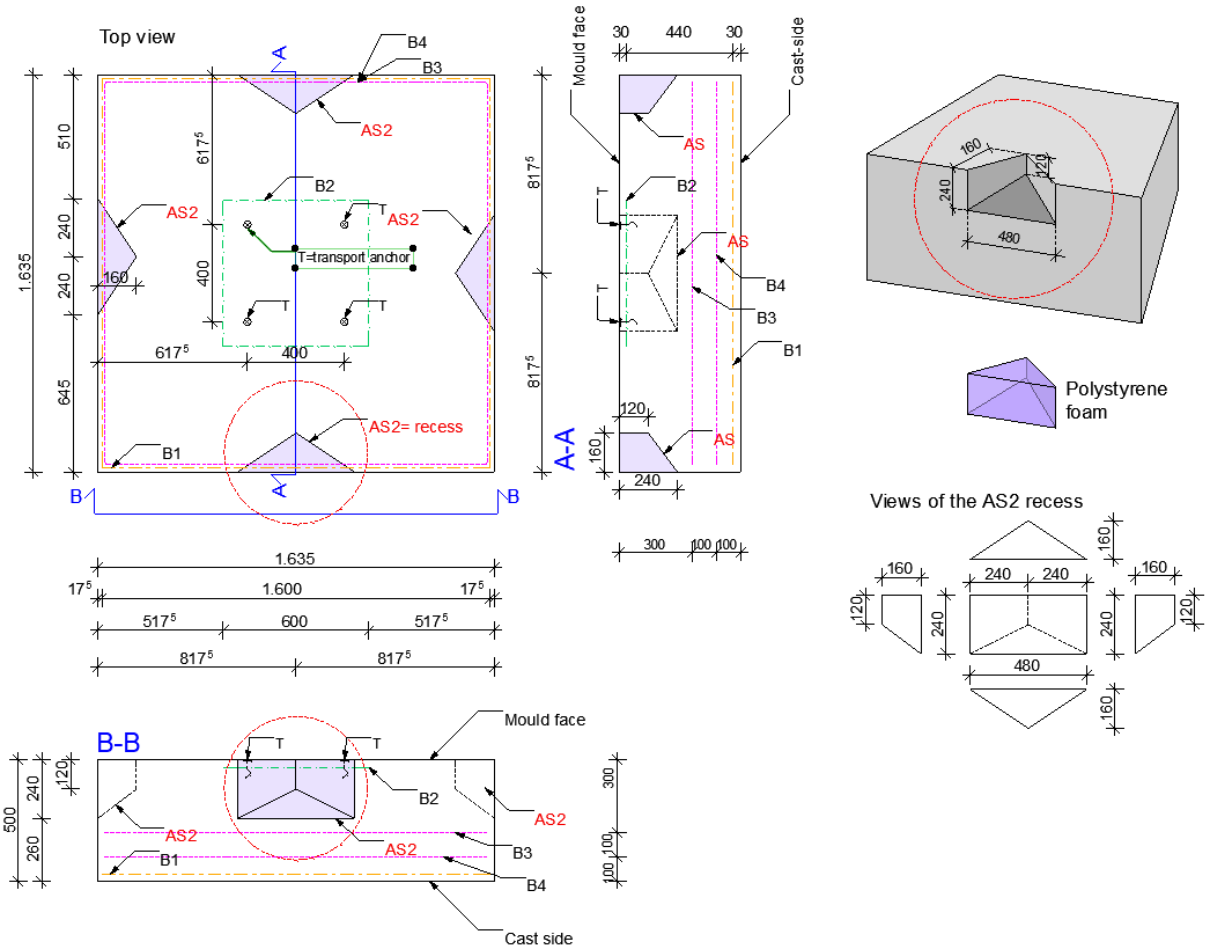

Specimen D

[dimensions in mm]

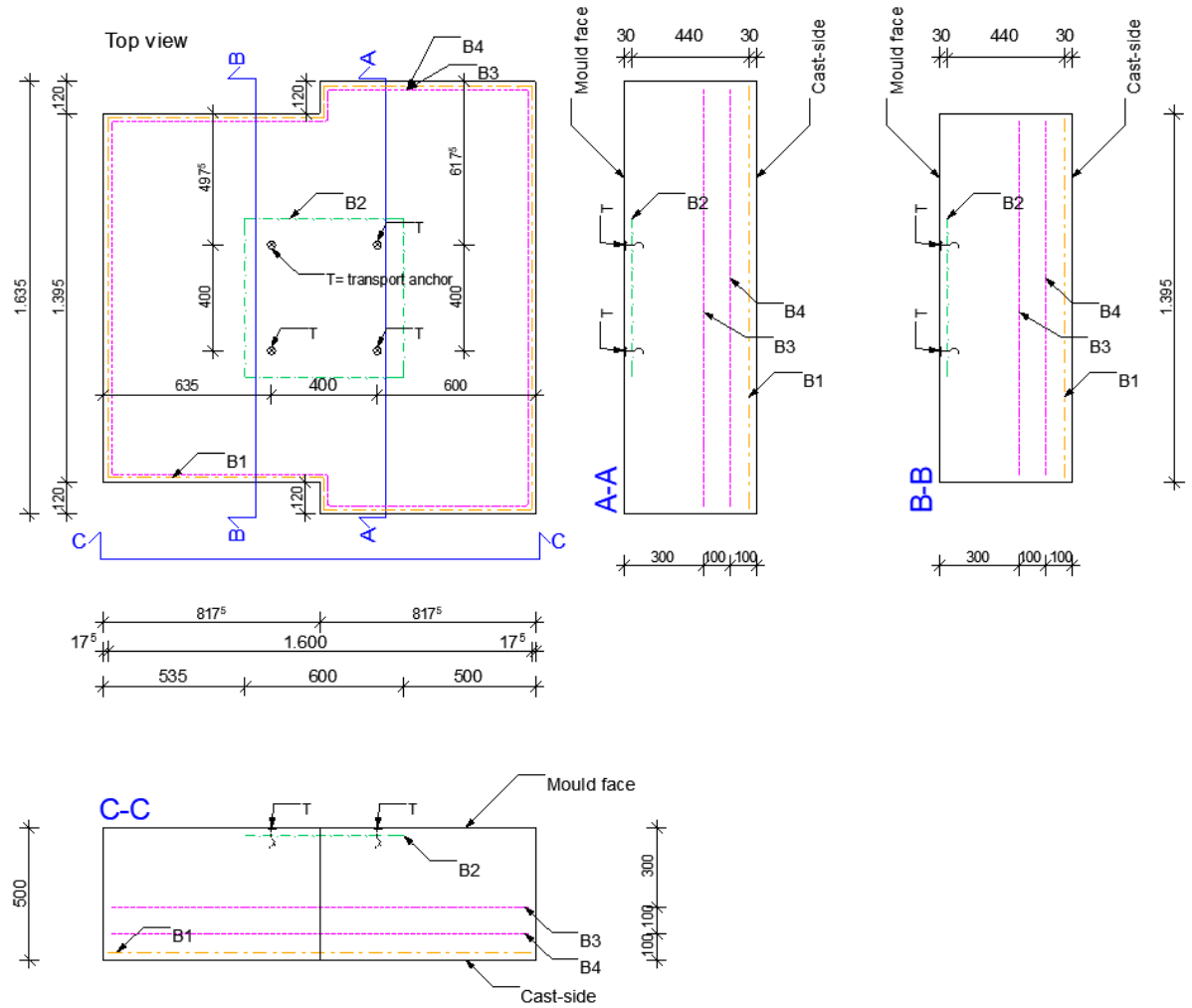

Concrete specimen for tests in cracked concrete:

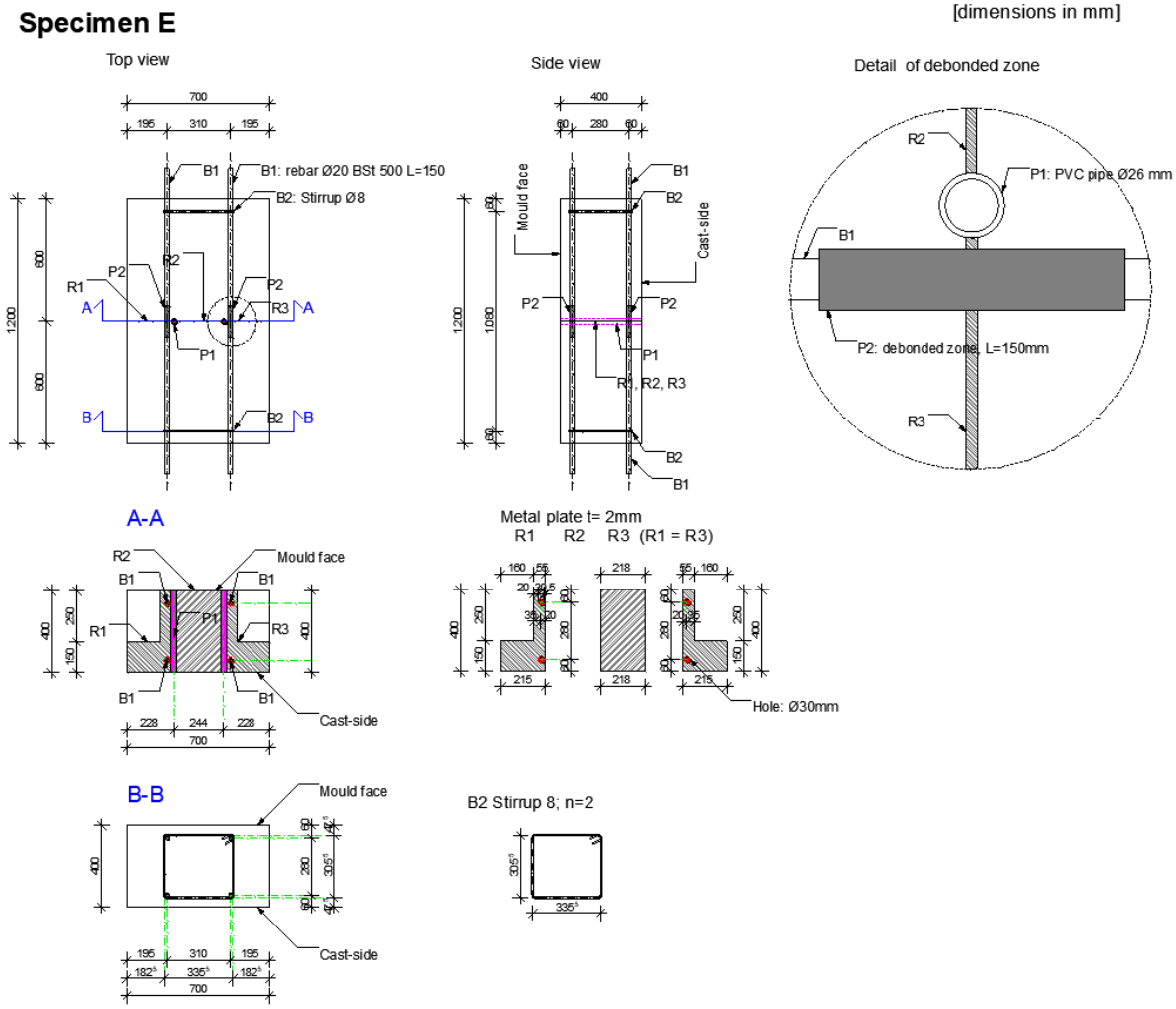

CURRICULUM VITAE

Personal Data

Boglárka Bokor

1989, Sopron, Hungary

Education

1996 – 2004	Primary and Secondary School, Fertőszentmiklós, Hungary
2004 – 2008	Dániel Berzsenyi Lutheran High School (Lyceum), Sopron, Hungary
2008 – 2012	Budapest University of Technology and Economics, Hungary
2012	Bachelor of Science in Civil Engineering
2014 – 2016	Technische Universität Dresden, Germany
2017	Diplom-Ingenieurin (M.Sc.) in Structural Engineering
2013 – 2020	University of Stuttgart, Germany
2021	Doktor-Ingenieurin (Ph.D.)

Experience

2013 – 2020	University of Stuttgart, Germany Research Associate, Institute of Construction Materials
since 2020	fischerwerke GmbH & Co. KG, Waldachtal, Germany Senior Expert

List of publications

Peer Reviewed Journals

Boglárka Bokor, A. Sharma, J. Hofmann, Concrete edge failure of anchor groups placed parallel to an edge. ACI Structural Journal, Vol. 118, Issue 2, March 2021, pp. 237-248

M. Tóth, **Boglárka Bokor**, A. Sharma, Numerical study on closely spaced anchor groups of identical configurations under centric tension loading. Engineering Structures, Vol. 224, December 2020, 111245

Boglárka Bokor, A. Sharma, J. Hofmann, Experimental investigations on the concrete edge failure of shear loaded anchor groups of rectangular and non-rectangular configurations. Engineering Structures, Vol. 222, November 2020, 111153

Boglárka Bokor, A. Sharma, J. Hofmann, Spring modelling approach for evaluation and design of tension loaded anchor groups in case of concrete cone failure, Engineering Structures, Vol. 197, October 2019, 109414

Boglárka Bokor, A. Sharma, J. Hofmann, A new spring model for concrete cone failure of anchorages under tension, Otto-Graf-Journal, Vol. 18, 2019

Boglárka Bokor, T. Pregartner, A. Sharma, J. Hofmann, Bemessung von zugbeanspruchten Befestigungen in Beton mit einem nicht-linearen Federmodell - Hintergrund und Softwarelösung für die Versagensart Betonausbruch, Bauingenieur, September 2019, Vol. 94

Boglárka Bokor, A. Sharma, J. Hofmann, Experimental investigations on concrete cone failure of rectangular and nonrectangular anchor groups, Engineering Structures, Vol. 188, June 2019, pp. 202–217

M. Tóth, **Boglárka Bokor**, A. Sharma, Anchorage in steel fiber reinforced concrete – concept, experimental evidence and design recommendations for concrete cone and concrete edge breakout failure modes, Engineering Structures, Vol. 181, February 2019, pp. 60-75

Boglárka Bokor, M. Tóth, A. Sharma, Fasteners in steel fiber reinforced concrete subjected to increased loading rates, MDPI Journal Fibers – Special Issue: Recent advancements in steel fiber reinforced concrete and its applications, December 2018, 6, 93

Conferences

M. Tóth, **Boglárka Bokor**, A. Sharma, Closely spaced anchor groups under centric tension loading – A numerical study. fib Symposium 2020 Shanghai - Concrete structures for resilient society, Nov 2020

Boglárka Bokor, A. Sharma, J. Hofmann, Experimental and numerical investigations on the concrete edge failure of anchor groups of arbitrary configurations, 7th International Conference of Euro Asia Civil Engineering Forum 30.09.2019 – 02.10.2019, Stuttgart, Germany

M. Tóth, **Boglárka Bokor**, A. Sharma, Design recommendations for fasteners for use in steel fiber reinforced concrete, fib Symposium 2019, Concrete Innovations in Materials, Design and Structures, 27-29 May 2019, Krakow, Poland

Boglárka Bokor, A. Sharma, J. Hofmann, Experimental Investigations on tension loaded anchor groups of arbitrary configurations, The International Federation for Structural Concrete 5th International fib Congress 7 – 11 October 2018, Melbourne, Australia

Boglárka Bokor, A. Sharma, J. Hofmann, On the limitations of the current design provisions prEN 1992-4 for design of anchor groups subjected to tension loads, Connections between Steel and Concrete 2017, 27-29 September 2017, Stuttgart, Germany

Boglárka Bokor, M. Tóth, A. Sharma, Influence of steel fiber content on the load-bearing capacity of anchorages in concrete, Connections between Steel and Concrete 2017, 27-29 September 2017, Stuttgart, Germany

Boglárka Bokor, M. Tóth, A. Sharma, Zugtragfähigkeit von Befestigungen in stahlfaserverstärkten Betonen, DAfStb 5. Jahrestagung / 58. Forschungskolloquium, TU Kaiserslautern, 20-21 September 2017, Kaiserslautern, Germany

Book contribution

Boglárka Bokor, J. Hofmann, Load distribution under shear load, in: Commentary to EN 1992- 4 Design of Festenings for use in Concrete, Heft 615(en), Deutscher Ausschuss für Stahlbeton e.V. – DAfStb (German Committee for Structural Concrete), Beuth Verlag GmbH, Berlin, 1st edition 2019, ISBN 978-3-410-65823-8

Boglárka Bokor, Zugtragverhalten von Befestigungen im stahlfaserverstärkten Beton - Experimentelle Untersuchungen, In: Werkstoffe, Denkmalschutz und… Festschrift zum 60. Geburtstag Prof. Dr.-Ing. Harald Garrecht, IWB, Stuttgart 2017, ISBN 978-3-945773-05-5